# Characterising the astrocyte responses to oligomeric and fibrillary $A\beta_{1-42}$ in Alzheimer's disease

By

**Martyna Maria Matuszyk**


Sheffield Institute for Translational Neuroscience

The University of Sheffield

Submitted for the degree of Doctor of Philosophy (PhD)

**October 2022**

# Acknowledgments

First and foremost, I would like to thank my supervisor, Professor Stephen Wharton, for his incredible support, guidance, and patience over the course of my PhD. I would also like to thank my secondary supervisors, Dr Julie Simpson and Professor Laura Ferraiuolo, for their input, advice, and mentorship throughout my PhD. I am incredibly grateful to Dr Claire Garwood for providing me with both academic and personal support throughout my studies.

I would like to extend acknowledgements to the Alzheimer's Society for funding my project; and I would especially like to thank my Alzheimer's Society Research Mentors, Sandra Barker, Geoff Redman, and Janet Farr. Their ongoing support, real-life experience with dementia, and valuable advice kept me focused on my work, and fuelled me with positive encouragement throughout the years.

Thank you to my incredible parents, Krzysztof and Violetta, for always supporting and encouraging me; and to my wonderful sisters, Ewa and Magdalena, for always being there for me through everything. You have been my biggest supporters and fans; I truly would not have made it without you.

Thank you to all my friends, but especially to 'The Best Row in SITraN' girls, Bridget, Katy, Rachel, and Sarah. We made it through to the other side. You have seen me laugh, cry, and panic; and for that, I will be forever grateful. Finally, a special thank you to Michael for encouraging me, supporting me, keeping me sane, and supplying me with endless cups of tea.

This PhD has been equally challenging and rewarding. I could not have done it alone. From the bottom of my heart, thank you all.

# Abstract

**Background:** Alzheimer's disease is a devastating disease, and the most common cause of dementia. Alzheimer's disease is characterised by the formation of neurofibrillary tangles (NFTs) composed of tau protein, and senile plaques composed mainly of Aβ fibrils. Small and soluble Aβ oligomers have also been implicated in disease, however the exact mechanism of how Aβ oligomers and fibrils modulate Alzheimer's disease pathology remains elusive.

Astrocytes are the most abundant glial cells, which function to provide essential metabolic and trophic support for neurons. Astrocytes are implicated in Alzheimer's disease and change early in disease. The mechanisms of the interplay of astrocytes and Aβ fibrils and oligomers in Alzheimer's disease are unclear.

**Hypothesis:** Different forms of $A\beta_{1-42}$ (oligomers vs fibrils) elicit a varying response in astrocytes, driving astrocytes to a neurodegenerative or neuroprotective phenotypes in Alzheimer's disease.

**Results:** Stable monomeric $A\beta_{1-42}$ preparations were generated *in vitro* and were confirmed using asymmetric flow field flow fractionation and transmission electron microscopy. $A\beta_{1-42}$ was aggregated into oligomers and fibrils *in vitro.* The morphology of the preparations was confirmed using transmission electron microscopy, size exclusion chromatography with multi-angle light scattering, Thioflavin T assay, and immunoblotting.

The highest physiological concentration of $A\beta_{1-42}$ oligomers and fibrils (1 µM) does not cause any significant cell death, DNA damage, or cell morphology changes in human fetal astrocytes or iAstrocytes. However, the individual iAstrocyte cell lines could have a varying response to different Aβ aggregation species, suggesting a small degree astrocyte heterogeneity. As a confirmation of the model, and to characterise the astrocyte responses to disease-related stressors, human fetal astrocytes were treated with 100 µM of hydrogen peroxide to induce oxidative stress. Acute oxidative stress caused a rapid upregulation of DNA damage response markers and formation of γH2AX-positive DNA foci, which indicate double stranded DNA breaks. Furthermore, acute oxidative stress causes a significant cell death in human fetal astrocytes after 24h of treatment.

Finally, RNAseq analysis, followed by differential gene expression pathway analyses showed that Aβ can elicit heterogeneous responses in iAstrocytes, resulting in differential expression of many cellular pathways, and corresponding genes. Furthermore, the astrocytes showed a heterogenic response to different types of Aβ (oligomers, fibrils, extracts). The gene changes identified imply Aβ-mediated astrocyte changes in inflammation (*MIRLET7I, MMP9, IL1A, IL32, CXCL8, SAA1*), increased Aβ production (*MIRLET7I*), breakdown of the extracellular matrix (*MMP1, MMP9, MMP13*), loss of tight

junctions (*CLDN2, CLDN18, MARVELD3*), and impairment in neurotransmitter signalling (*EPHB2, EPHB6, GRIN2C, GABRA1, GABRAP, SHISA7*).

**Conclusions:** Well-characterised $A\beta_{1-42}$ preparations were generated and optimised, which allowed for reliable and reproducible treatment of astrocytes. Astrocytes show a rapid DNA damage response to oxidative stress, which is not seen as a response to Aβ treatments in fetal astrocytes or iAstrocytes. This implies that astrocytes could display a heterogenic response to different types of stress and injury in disease (Aβ vs oxidative stress). Both younger and aged astrocytes appear resistant to various forms of Aβ, which differs from neuronal responses in disease.

Treatment of iAstrocytes with Aβ shows a differential expression of genes, suggesting that Aβ-modulated astrocytes may play a role in neuroinflammation, breakdown of BBB, oxidative stress, and impairment in neurotransmitter signalling. However, different types of Aβ (oligomers, fibrils, extracts) can elicit varying gene expression responses in astrocytes, implying that Aβ can induce heterogenic changes to astrocytes based on their final conformation. This may alter astrocyte function, which could be relevant to Alzheimer's disease progression. Dysregulation of these astrocytic functions could show potential mechanisms behind Alzheimer's disease pathology and should be investigated further.

# Table of contents

# List of Figures

# List of Tables

# Abbreviations

| | |
|---|---|
| aCSFb | Artificial cerebrospinal fluid buffer |
| AD | Alzheimer's disease |
| AF4 | Asymmetric Flow Field Flow Fractionation |
| ALS | Amyotrophic lateral sclerosis |
| ANOVA | Analysis of variance |
| ApoE4 | Apolipoprotein E4 |
| APP | Amyloid Precursor Protein |
| APS | Ammonium Persulphate |
| ATM | Ataxia telangiectasia mutated |
| ATR | ATM-Rad3-related |
| Aβ | Amyloid-beta |
| BACE1 | Beta-site amyloid precursor protein cleaving enzyme 1 |
| BBB | Blood brain barrier |
| BCA | Bicinchoninic acid |
| BP | Biological process |
| bPGM | Biophosphoglycerate mutase |
| BSA | Bovine Serum Albumin |
| CC | Cellular component |
| cdc2 | Cyclin-dependent kinase 2 |
| CDK1 | Cyclin dependent kinase 1 |
| CNS | Central Nervous System |
| CSF | Cerebrospinal fluid |
| DDR | DNA damage response |
| DEG | Differentially expressed gene |
| DMEM | Dulbecco's Modified Eagle Medium |
| DNA-PK | DNA-dependent protein kinase |
| DO | Disease ontology |
| DSBs | Double stranded breaks |
| EAAT1 | Excitatory amino acid transporter 1 |
| EAAT2 | Excitatory amino acid transporter 2 |
| EDTA | Ethylenediaminetetraacetic acid |
| EDTA | Ethylenediaminetetraacetic acid |
| EGTA | Ethylene glycol-bis (β-aminoethyl ether)-N,N,N',N'-tetraacetic acid |
| ELISA | Enzyme-linked immunosorbent assay |
| EOAD | Early-onset Alzheimer's disease |
| fAD | Familial Alzheimer's disease |
| FBS | Fetal Bovine Serum |
| GFAP | Glial Fibrillar Acidic Protein |
| GO | Gene ontology |
| GSEA | Gene Set Enrichment Analysis |
| GWAS | Genome-wide association studies |
| $H_2O_2$ | Hydrogen Peroxide |
| HFIP | Hexafluoroisopropanol |
| iAstrocytes | Induced Astrocytes |
| ICC | Immunocytochemistry |

| | |
|---|---|
| IDE | Insulin-degrading enzyme |
| IL- | Interleukin- |
| INF | Interferon |
| iNPCs | Induced Neural Progenitor Cells |
| JAK | Janus kinase |
| KEGG | Kyoto Encyclopedia of Genes and Genomes |
| LDH | Lactate dehydrogenase |
| LOAD | Late-onset Alzheimer's disease |
| LRP1 | Lipoprotein receptor-related protein |
| MALS | Multi-Angle Light Scattering |
| MCI | Mild cognitive impairment |
| MF | Molecular function |
| Mn | Number average molecular weight |
| Mw | Weight average molecular weight |
| NFTs | Neurofibrillary Tau Tangles |
| NFκB | Nuclear factor kappa B |
| NMR | Nuclear magnetic resonance |
| PBS | Phosphate-buffered saline |
| pChk1 | Phosphorylated checkpoint kinase 1 |
| pChk2 | Phosphorylated checkpoint kinase 2 |
| PDI | Polydispersity Index |
| PEN-2 | Presenilin enhancer-2 |
| PICUP | Photo-induced cross-linking |
| pSTAT3 | phosphorylated signal transducer and activator of transcription 3 |
| ROS | Reactive Oxygen Species |
| sAD | Sporadic Alzheimer's disease |
| sAPP | Soluble Amyloid Precursor Protein |
| SDS-PAGE | Sodium Dodecyl Sulphate- Polyacrylamide Gel Electrophoresis |
| SEC-MALS | Size Exclusion Chromatography |
| STAT | signal transducer and activator |
| TBS | Tris-buffered saline |
| TEM | Transmission Electron Microscopy |
| TEMED | N,N,N',N'-Tetramethylethylenediamine |
| ThT | Thioflavin T |
| TREM2 | Triggering receptor expressed on myeloid cells 2 |
| XSLB | Extra strong lysis buffer |
| β-CTF | βC-terminal fragment |
| γH2AX | Gamma-H2A histone family member X |

# Chapter 1 – Introduction

## 1.1 Introduction to Alzheimer's disease

The term 'dementia' refers to a chronic, severe loss of cognition, affecting individual's day-to-day life. Alzheimer's disease is the most prevalent type of dementia; other common dementias include vascular dementia, frontotemporal dementia, and Lewy body dementia. Clinically, dementia is associated with memory impairments, cognitive decline, executive dysfunction, language problems, and difficulties carrying out daily activities (Grontvedt *et al.*, 2018). In an individual's daily life, this could manifest as a gradually progressive loss of memory, inability to learn new information, and inability to recall information about oneself including recent life events. The episodic memory is affected in AD, for example, it could present itself as forgetting to pay bills or forgetting about appointments. However, there are different stages of cognitive decline, which largely depend on both pathological and symptomatic severity of a case. For example, AD could begin with a mild cognitive impairment (MCI), which can be defined as a very early stage of dementia, or predementia. MCI is characterised by a greater cognitive decline than expected for the individual's age and education level, without interrupting the individual's daily life (Gauthier *et al.*, 2006). MCI can be categorised as amnestic or non-amnestic. Amnestic MCI is associated with a higher risk of developing AD in the future, whilst non-amnestic MCI is associated with the development of other dementia types, such as dementia with Lewy bodies (Csukly *et al.*, 2016). Furthermore, not all MCI converts to dementia. With AD progression, further symptoms become apparent, such as executive dysfunction, problems with language, and further difficulties carrying out daily activities, however symptoms can vary between affected individuals (Grontvedt *et al.*, 2018). There are a range of further manifestations of dementia beyond the cognitive symptoms. These include depressive symptoms, apathy, aggregation, wandering, sleep disorders, and repetitive movements (such as fidgeting) (Arvanitakis, Shah and Bennett, 2019).

Alzheimer's disease (AD) was first described by Alois Alzheimer as a "singular disease of the cerebral cortex", which was described by the presence of "neurofibrils" within cortical neurones and "minute milary foci" (Alzheimer *et al.*, 1995). These are now widely known as neurofibrillary tau tangles (NFTs) and amyloid-beta (Aβ) plaques, which are the main neuropathological hallmarks of AD (Hardy and Higgins, 1992). The accumulation of intraneuronal NFTs formed from the microtubule-associated protein tau, and extracellular amyloid plaques composed mainly of aggregated amyloid-beta (Aβ) are predominately localised to medial temporal lobe and cortical areas of the brain (Aleksis *et al.*, 2017). The neuropathological hallmarks may be present more than 10 years before the clinical presentation of AD (Jack Jr. *et al.*, 2010; Jack *et al.*, 2013). Further neuropathological features of Alzheimer's disease can include loss of synapses, axonal degeneration and neuronal loss, which can take place in the pre-clinical disease stage, and can later correlate with MCI and AD (DeKosky and Scheff, 1990; Terry *et al.*, 1991; Serrano-Pozo *et al.*, 2011; Goel *et al.*, 2022).

Age is a big risk factor contributing to AD and dementia, and the disease prevalence increases exponentially after 65 years of age, hence most cases are in an older age group (Isik, 2010). The World Health Organisation reported 47 million to be affected by dementia worldwide in 2015, a number predicted to increase to 132 million by 2050 (World Health Organization (WHO), 2017), as many countries are facing the ageing of their populations. AD cases can be classified as early onset AD (EOAD) or late onset AD (LOAD). The cut-off ages defining these cases are only arbitrary, however the classification system suggests that EOAD cases affect people below the age of 65 (van der Flier *et al.*, 2011). Amongst these AD cases, familial (fAD) and sporadic (sAD) AD can be distinguished. Majority of fAD cases are early- onset, however they account for less than 1% of all AD cases. fAD cases have a distinct genetic background and specific disease-related genetic mutations that can be inherited. These mutations include mutations in the *APP* (Goate *et al.*, 1991), *PSEN1* (Sherrington *et al.*, 1995) and *PSEN2* (Levy-Lahad *et al.*, 1995) genes, which all result in an abnormal production of Aβ. fAD is typically inherited in an autosomal dominant pattern (Schellenberg and Montine, 2012). Additionally, 35 to 65% of all early onset AD patients have been reported to have at least one first-degree relative affected by AD (van der Flier *et al.*, 2011; Cacace, Sleegers and Van Broeckhoven, 2016), further suggesting a strong association between the genetic background of an individual and the AD onset.

Point mutations in the *APP* gene are reported to be one of the causative mutations responsible for the onset of fAD (Goate *et al.*, 1991). Such mutations may lead to altered Aβ metabolism in the brain (Weggen and Beher, 2012). Namely, *APP* genetic variants, for example D678H, A673V and E682K, have been associated with increased Aβ production and AD pathogenesis (Di Fede *et al.*, 2009; Zhou *et al.*, 2011; W.-T. Chen *et al.*, 2012). Other *APP* variants however, such as A673T, have been found to reduce Aβ production and may be protective against AD (Jonsson *et al.*, 2012). This suggests the importance of *APP* in the pathology of AD, as it plays an important role in modulating the levels of Aβ in the brain. Other causative mutations include *PSEN1* (Sherrington *et al.*, 1995) and *PSEN2* (Levy-Lahad *et al.*, 1995). These mutations result in an abnormal production of Aβ (Liu *et al.*, 2013). For example, loss of-function mutations in the *PSEN* genes may lead to an increased *in vitro* and *in vivo* production of Aβ. Though not always, these mutations could also cause an increase of $A\beta_{1-42}$ production, which is thought to be a more toxic Aβ variant (Cacquevel *et al.*, 2012; Potter *et al.*, 2013). Possession of familial genetic mutations in *PSEN1* and *APP* may correlate with early-onset AD, whilst mutations in *PSEN2* may correlate with a late onset of the disease (Gao *et al.*, 2019). Both *PSEN* and *APP* mutations could promote formation of toxic Aβ aggregates, which further contributes to the hypothesis that Aβ is central to AD pathogenesis (Weggen and Beher, 2012).

The majority of AD cases are sporadic, and occur later in life (~above 65 years of age) (Isik, 2010). There are several risk factors associated with the development of sAD, such as the possession of the

E4 allele of apolipoprotein (ApoE4) (Liu *et al.*, 2013). Homozygous *APOE4* carriers have a lower average age of AD onset, as well as, an increased chance of developing AD, compared to homozygous *APOE3* carriers (Tzioras *et al.*, 2019). The role of the APOE4 in AD has been studies over the years, and it has been suggested to be involved in altered Aβ clearance, aggregation and plaque formation (Hunsberger *et al.*, 2019).

Moreover, genome-wide association studies (GWAS) furthered the discovery of new genetic risk factors, such as *PICALM* (encoding Phosphatidylinositol Binding Clathrin Assembly Protein), and *CLU* (encoding clusterin) (Harold *et al.*, 2009). Clusterin, also known as apolipoprotein J, has been proposed to be a facilitator of Aβ aggregation, which might lead to neurotoxicity in AD. In mice clusterin knockout leads to a reduction in fibrillar Aβ, suggesting that clusterin may play a role in Aβ metabolism and processing (DeMattos *et al.*, 2002). Furthermore, point mutations in the gene encoding the triggering receptor expressed on myeloid cells 2 (TREM2) have been implicated in AD pathogenesis. TREM2 is a protein expressed on microglial cell membranes, which prompted a hypothesis that TREM2 may affect inflammatory processes in the brain, in turn modulating AD pathogenesis (Guerreiro *et al.*, 2013; Jonsson *et al.*, 2013; Qin *et al.*, 2021). However, as GWAS progresses, further characterisation of new AD variants will be required, including large sequencing studies to complement GWAS results. This will allow further discovery and thorough investigation of possible genetic factors underlying the mechanisms behind the onset of sporadic (as well as familial) AD cases.

## 1.2 Amyloid-beta peptide

### 1.2.1 Introduction to Amyloid-beta

Aβ is a small peptide of ~4 kDa in size. Aβ is the main component of amyloid plaques present neuropathologically in an AD brain (Hardy and Higgins, 1992; Selkoe and Hardy, 2016). Most reports investigating Aβ focus on its role in disease.

Amyloid proteins are a group of proteins found to be present naturally in many functional processes. These include processes essential to normal cell and tissue physiology. For example, amyloid fibrils can be used as scaffolds, or more compact aggregates can act as storage. Thus, functional amyloids exist, such as amyloid-bodies (for protein stores), protegrin-1 (as an antimicrobial peptide), and peptide hormones (for hormone storage), amongst others (Jackson and Hewitt, 2017; Almeida and Brito, 2020).

Aβ is a type of amyloid protein, however the role of Aβ in a healthy system remains to be elucidated. It has been suggested that Aβ may have functional roles in the brain, including antimicrobial, antifungal and antiviral properties (Soscia *et al.*, 2010; Bourgade *et al.*, 2015). Furthermore, evidence suggests that Aβ may also play a role in tumour suppression, and also in maintenance of the blood brain barrier and regulation of synapses (Driver *et al.*, 2012; Brothers, Gosztyla and Robinson, 2018). However, the physiological function of Aβ in the brain remains unclear. Aβ peptide is usually studied in the context of disease, and therefore most knowledge about its function relates to its adverse effects in the CNS. In Alzheimer's disease, Aβ aggregation is a crucial disease-related and/or disease-modifying process.

### 1.2.2 Amyloid cascade hypothesis

The Aβ depositions characteristic of Alzheimer's disease have been at the forefront of many research avenues in the context of disease. Almost 40 years ago the amino acid sequence of the main component of senile plaques has been reported by Glenner and Wong (Glenner and Wong, 1984). The report revealed an accumulation of a small peptide in AD plaques, which they termed as Aβ, and this initiated the amyloid cascade hypothesis. The amyloid cascade hypothesis was first proposed in 1992 (Hardy and Higgins, 1992), and stated that Aβ deposition into plaques might be causative of AD pathology. The abnormal production and aggregation of Aβ in the brain has been proposed as a trigger for a cascade of events, including tau aggregation, inflammation, activation of glial cells, disturbance of ion homeostasis, and increased oxidative stress, which ultimately lead to synaptic and neuronal loss resulting in the onset of dementia (Selkoe and Hardy, 2016). Certainly, as mentioned earlier, the impact of genetic mutations modulating Aβ production on AD development supports the amyloid cascade hypothesis. Moreover, it has been reported *post mortem,* that an increase in both $A\beta_{1\text{-}40}$ and

$A\beta_{1-42}$ is observed in the frontal cortex of the brain of patients with dementia, and this increase correlates with cognitive decline (Naslund *et al.*, 2000).

Aβ can have profound effects on the brain and neuronal loss. It has been shown that injecting fibrillary Aβ into rhesus monkey brains can cause neuronal loss, as well as activation of microglia (Geula *et al.*, 1998). Furthermore, aggregation of Aβ might be the initiating step in activating neuroinflammatory responses, which also include activating microglia (Nagele *et al.*, 2003; Nagele *et al.*, 2004; Streit *et al.*, 2018). Activated microglia might be able to promote the conversion of oligomeric Aβ to fibrillar Aβ, contributing further to the Aβ plaque problem (Nagele *et al.*, 2004). Additionally, neuronal and axonal loss can be observed in the vicinity of plaques, containing fibrillary Aβ. This is observed in aged primates, as well as in humans. Interestingly, diffuse and non-fibrillary plaques are not associated with the loss of neurones (Shah *et al.*, 2010; Reiss *et al.*, 2018).

Evidence to date overwhelmingly suggests that Aβ aggregation is an important component of toxicity in AD (Hardy and Higgins, 1992; Hardy and Selkoe, 2002; Selkoe and Hardy, 2016), therefore targeting polymerisation events might prove to be a successful AD therapy. One approach could be to prevent the formation of toxic Aβ oligomers by inhibiting the catalytic processes on the surface of Aβ fibrils, for example by inhibiting the protein-protein interactions of Aβ fibrils and monomers. Protein chaperones have been proposed to have inhibitory effects on Aβ nucleation processes, and therefore may be promising therapeutic agents. The molecular chaperone clusterin has been shown to interfere with the kinetics of Aβ fibrillogenesis (Beeg *et al.*, 2016). Furthermore, clusterin can regulate Aβ fibril formation (Miners, Clarke and Love, 2017), and therefore may be an interesting therapeutic target for AD. *In vivo* clusterin treatments of *Caenorhabditis elegans* dose-dependently reversed toxic effects of oligomeric $A\beta_{1-42}$ (Beeg *et al.*, 2016).

Brichos is a protein chaperone domain, identified in Bri proteins, which have been identified from isolated amyloid fibrils in familial British dementia patients (Vidal *et al.*, 1999). Brichos has been found to delay formation of $A\beta_{1-40/42}$ fibrils in a concentration-dependent manner (Willander *et al.*, 2012). Brichos inhibits secondary nucleation as it blocks the catalytic effect of Aβ fibrils by binding to their surface with a high affinity, hindering the positive feedback loop and generation of oligomers (Cohen *et al.*, 2015), although studies show that it may not completely abrogate fibril formation (Willander *et al.*, 2012).

There has been a number of clinical trials looking at targeting Aβ as a potential therapeutic option for AD. Some clinical trials have been of BACE inhibitors, which could modulate and decrease Aβ production in the brain (Vassar, 2014). Such therapeutic options are designed to specifically target and interfere with the starting events and processes of the amyloid cascade hypothesis, inhibiting Aβ

production. However, BACE inhibitors, such as Verubecestat, Atabecestat, Lanabecestat and CNP520, targeting participants in the prodromal, preclinical and mild to moderate AD, have all failed phase 3 clinical trials due to lack of efficacy, or, in the case of Atabecestat, toxicity (Huang, Chao and Hu, 2020).

Another approach to treating AD is to target Aβ removal using passive immunisation approaches. Early studies showed that immunisation of AD mice overexpressing human APP with $A\beta_{42}$ can prevent formation of plaques, induction of reactive astrocytes, and neuritic dystrophy (Schenk *et al.*, 1999). Recently, the United States Food and Drug Administration approved Aducanumab as a treatment of mild cognitive impairment and early stages of AD. Aducanumab is a human IgG1 anti-Aβ monoclonal antibody, which specifically targets Aβ plaque formation and removal in AD. However, the approval of this disease-modifying therapy has not come without controversy. Aducanumab has previously failed phase 3 clinical trials for lack of efficacy (Huang, Chao and Hu, 2020). Further AD therapies, which specifically target Aβ are currently being developed and investigated (Huang, Chao and Hu, 2020; Tampi, Forester and Agronin, 2021). However, targeting Aβ aggregation, especially at later stages of the disease may not be as effective as once thought. It is possible that at the later stages of AD, when there is a high plaque burden in the brain, the majority of Aβ could be found as fibrils in the plaques. This would also mean that more downstream effects of amyloid cascade hypothesis have already been triggered, and that targeting the peptide at this stage would be futile. It could also suggest that clearance of Aβ fibrils is not the most efficient treatment option available. Perhaps, it would be more beneficial to target smaller and intermediate Aβ species, which could be present at the earlier stages of the disease, rather than Aβ fibrils and plaques themselves.

The amyloid cascade hypothesis states that Aβ aggregation and deposition into fibril-rich amyloid plaques influences the start of downstream effects, such as glial activation, and tau phosphorylation, which in turn leads to synaptic dysfunction and neuronal loss (Hardy and Higgins, 1992; Selkoe and Hardy, 2016). However, since the original Aβ hypothesis has been published, a new idea emerged. This stated that the Aβ oligomers are the more toxic form of Aβ. The Aβ oligomer hypothesis implicates the smaller, soluble, intermediate species of Aβ as more neurotoxic (Selkoe and Hardy, 2016; Cline *et al.*, 2018). The idea of Aβ oligomers being the more toxic species than Aβ fibrils may be the reason for the failure of clinical trials that have targeted Aβ in the past.

Indeed, accumulation of $A\beta_{1\text{-}42}$ may be an early event occurring in AD, preceding the formation of plaques, neuronal death, astrogliosis and cognitive impairment (DaRocha-Souto *et al.*, 2011). *In vivo* evidence has supported this idea and shown that oligomeric $A\beta_{1\text{-}42}$ can cause greater memory deficits in rat brain, as well as increased neuronal loss and neuroinflammation, than fibrillary $A\beta_{1\text{-}42}$. Oligomeric Aβ has been widely studied in the field, and it is clear, that its role in AD pathology is important. For

example, it has been shown to constrict blood vessels in early AD brains (Nortley *et al.*, 2019); facilitate excitotoxicity contributing to neurodegeneration (Arbel-Ornath *et al.*, 2017); increase baseline neuronal calcium levels (Resende *et al.*, 2008); and cause a loss of functional synapses (Lacor *et al.*, 2007).

Direct administration of oligomeric $A\beta_{1-42}$ can induce significant neuronal loss, whereas administration of fibrillary $A\beta_{1-42}$ does not (Yukiko Doi *et al.*, 2009). Administration of Aβ oligomers has adverse effects on rat memory function and cognitive abilities, even at low concentrations (Cleary *et al.*, 2005; Karthick *et al.*, 2018). Moreover, oligomeric Aβ and not fibrillary or monomeric Aβ can inhibit long-term potentiation in the hippocampus (Walsh *et al.*, 2002; Shankar *et al.*, 2008). This indicates that oligomeric Aβ is more responsible for the decline of cognitive abilities in AD. Oligomeric Aβ reduces the activity and number of excitatory synapses in organotypic slices of rat hippocampus (Shankar *et al.*, 2007) mediating synapse loss and dysfunction. A significant reduction in excitatory synapses has also been found in AD transgenic mice, compared to wild type. This synapse loss increases near Aβ plaques, however most synapse loss is found near halos of oligomeric Aβ (Koffie *et al.*, 2009), suggesting the involvement of oligomeric Aβ in mediating cognitive decline in AD.

It has been suggested, that tau hyperphosphorylation and formation of NFTs is necessary for AD progression; and according to the amyloid cascade hypothesis, such events take place downstream of Aβ aggregation (Bloom, 2014). In vivo studies have shown that oligomeric Aβ can colocalise and interact with non-phosphorylated tau (Oddo *et al.*, 2006) and that oligomers alone, in the absence of fibrillary Aβ, can induce tau phosphorylation (Jin *et al.*, 2011). This might suggest Aβ oligomers as a starting point of the toxic events leading to AD pathology.

Furthermore, oligomeric $A\beta_{1-42}$ can cause increased neuroinflammation, as well as neuronal loss, when compared to fibrillar $A\beta_{1-42}$ (Y Doi *et al.*, 2009; He *et al.*, 2012). Aβ oligomers can also affect the inflammatory profile of glial cells in AD. In the presence of oligomeric Aβ, microglia increase their pro-inflammatory profile and aggravate Aβ-induced neuronal death (C M Sondag, Dhawan and Combs, 2009; Maezawa *et al.*, 2011). Oligomeric Aβ can induce the pro-inflammatory microglial phenotype at a higher level than fibrillary Aβ (Michelucci *et al.*, 2009). Aβ can also affect astrocytes. Oligomeric Aβ has been shown to induce a higher release of pro-inflammatory cytokines, as well as increased levels of oxidative stress in astrocytes, than fibrillary Aβ (White *et al.*, 2005). Astrocytes may mediate Aβ toxicity in primary neurons through increased secretion of proinflammatory molecules (Garwood *et al.*, 2011). Oligomeric Aβ can also induce astrocytic release of pro-inflammatory cytokines, increased oxidative stress and induce reactive astrocytes, which can contribute to neurodegeneration in AD (Lian *et al.*, 2015, 2016).

According to the amyloid hypothesis, APP processing leads to the formation of toxic Aβ species, which in turn may modulate protein kinases that regulate tau phosphorylation. This leads to tau hyperphosphorylation and misfolding, generating NFTs. Further downstream, events characteristic of AD pathology take place, such as neuron death, synaptic dysfunction and cognitive deficits, suggesting that Aβ-mediated toxicity also requires tau pathology to elicit the onset of AD (Bloom, 2014). In AD synaptic terminals, there is a co-localisation of Aβ and phosphorylated tau. However, phosphorylated tau can be found at higher levels in the hippocampus, while Aβ plaques can be seen in neocortex (Fein *et al.*, 2008). It has been shown *in vivo* that oligomeric Aβ can co-localise and interact with non-phosphorylated tau (Oddo *et al.*, 2006). Additionally, oligomers in the absence of fibrillar Aβ can induce tau hyperphosphorylation (Jin *et al.*, 2011). However, other studies contradict this by showing that fibrillary Aβ can induce tau phosphorylation leading to loss of microtubule binding (Busciglio *et al.*, 1995). Therefore, AD might not be caused by only one pathology, but rather several pathologies actively interacting with each other. This would also further suggest how important Aβ pathology is in the downstream effects leading to a more profound adverse effects in the brain.

Even though all the above evidence suggests that Aβ plays an important role in AD, it is important to highlight that it is still unclear through what mechanisms Aβ induces such adverse effects in AD brains. It is also important to suggest that Aβ may act upon many different systems and pathways in the CNS, disrupting its delicate environment, leading to neuronal loss and dementia. The exact roles of Aβ oligomers and fibrils should therefore be carefully investigated.

### 1.2.3 Amyloid-beta peptide production

Aβ is produced by an enzymatic cleavage of a larger membrane-bound protein called amyloid precursor protein (APP) (Glenner and Wong, 1984) (fig.1.1.). APP is a transmembrane protein with a large extracellular domain, and it is coded for by the *APP* gene located on chromosome 21. In development, *APP* is expressed in the neural tube, developing motor neurons and neural crest cells, as well as the retina and cranial ganglia. Whilst in adult systems, APP is ubiquitously expressed in the nervous tissue (Murphy and LeVine, 2010; O'Brien and Wong, 2011; Zhang *et al.*, 2011; Müller, Deller and Korte, 2017). The precise physiological function of APP in the brain remains unclear, however APP has been suggested to promote the formation of synapses and their activity, as well as dendritic spine formation (Hoe, Lee and Pak, 2012). Moreover, APP is highly expressed in neurons of the CNS and can be internalised and trafficked by the endosomes (Lee *et al.*, 2008).

APP can be processed via amyloidogenic or non-amyloidogenic pathways. Non-amyloidogenic cleavage of APP occurs by the action of the α-secretase and γ-secretase enzymes, of which the cleavage sites are situated within the Aβ sequence. α-secretase cleaves APP between positions 16 and

17 of the Aβ domain. Hence, this precludes Aβ production (Thinakaran and Koo, 2008; Zhang *et al.*, 2011). This enzymatic cleavage results in the release of a large soluble domain called soluble amyloid precursor protein (sAPP) α, which plays a role in neuronal plasticity and/or survival. For example, sAPPα has been shown to have a protective role towards hippocampal neurons against excitotoxicity (Furukawa *et al.*, 1996), as well as to have a role in enhancing the proliferation of neural stem cells (Ohsawa *et al.*, 1999). Moreover, there are reports stating that sAPPα might be beneficial to differentiated neurons, protecting them from glutamate neurotoxicity and reactive oxygen species (ROS) (Chow *et al.*, 2010; Habib, Sawmiller and Tan, 2017).

The amyloidogenic pathway occurs via the action of β-secretase, particularly the enzyme called beta-secretase 1, also known as beta-site amyloid precursor protein cleaving enzyme 1, (BACE1) (Sinha *et al.*, 1999), which releases a C-terminally truncated sAPP, namely sAPPβ. In turn, the sequential enzymatic activity of γ-secretase results in the production of Aβ (O'Brien and Wong, 2011). BACE1 cleaves APP to yield soluble sAPPβ and a βC-terminal fragment (β-CTF) (Chow *et al.*, 2010; O'Brien and Wong, 2011; Zhang *et al.*, 2011). β-CTF is then cleaved by γ-secretase to generate Aβ. γ-secretase is an enzyme complex, which is made of APH-1 (anterior pharynx defective 1 homolog A), PEN-2 (presenilin enhancer-2), nicastrin, presenilin-1 and presenilin-2 proteins. Presenilin-1 and -2 are essential components of the catalytic domain in γ-secretase (Edbauer *et al.*, 2003; Kummer and Heneka, 2014).

Due to the non-specific proteolytic activity of γ-secretase, the amyloidogenic cleavage of APP produces Aβ isoforms of varied sizes at the N- and C-termini of the peptide (Näslund *et al.*, 1994; Bibl *et al.*, 2012; Haass *et al.*, 2012). The resulting Aβ can vary in length; however, the isoforms $A\beta_{1-40}$ and $A\beta_{1-42}$ are the most abundant Aβ isoforms in the central nervous system. The $A\beta_{1-40}$ peptide processing route may be more predominant (Qi-Takahara *et al.*, 2005). Meanwhile, $A\beta_{1-42}$ is the most neurotoxic variant and is the primary isoform found in neuritic plaques in AD. $A\beta_{1-42}$ also has more propensity to aggregate than other isoforms of Aβ (Iwatsubo *et al.*, 1996; Bartolini *et al.*, 2011).

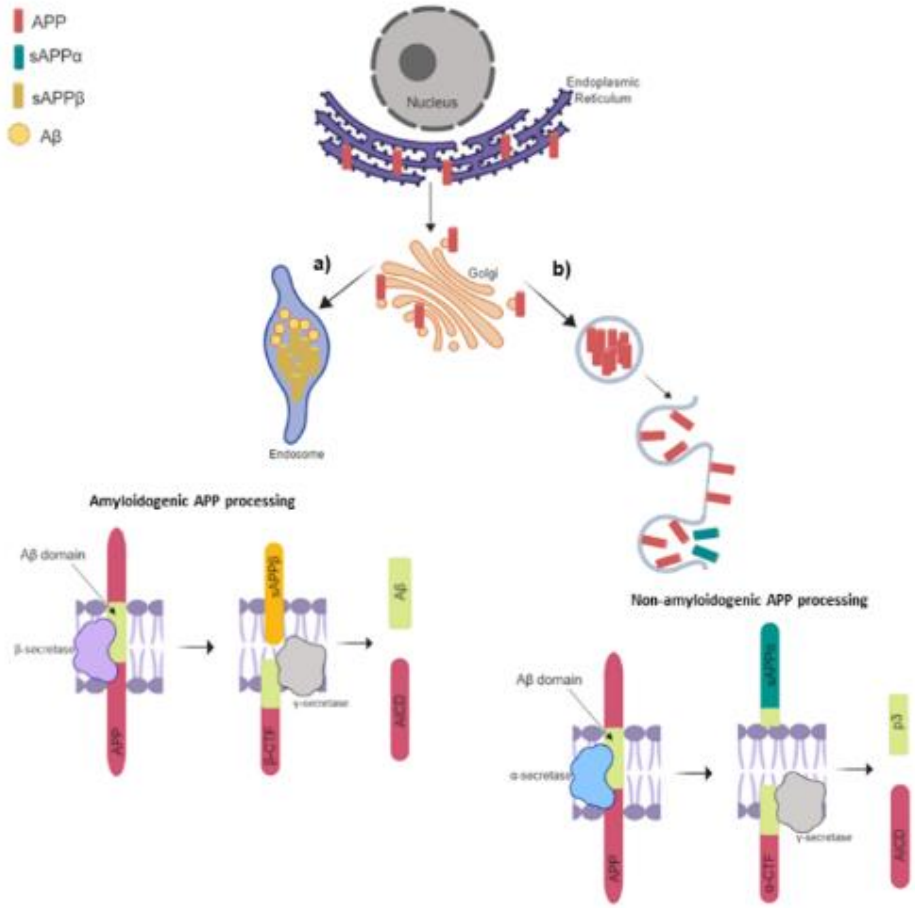


**Figure 1.1** Amyloid Precursor Protein trafficking and processing

Synthesised APP (red) is transported from the Endoplasmic Reticulum into Golgi, from where it travels further down the axon. APP is then processed in two separate ways. **a)** APP can internalise into an endosome, from where it undergoes amyloidogenic APP processing and Aβ production. This involves proteolysis by β-secretase, namely BACE1, and then γ-secretase. This generates a stable domain sAPPβ, and β-secretase derived fragment (β-CTF) and leads to a production of Aβ and APP intracellular domain (AICD). **b)** APP can internalise into an endosomal compartment, and insert into a cell surface, followed by non-amyloidogenic processing. This involves APP cleavage with αsecretase, producing sAPPα and α-CTF. This leads to final products of p3 and AICD (Images produced using BioRender).

### 1.2.4 Forms of Amyloid-beta and associated toxicity

As mentioned above, the formation of Aβ relies on the enzymatic cleavage of APP via the amyloidogenic pathway (fig.1.1.), and the generation of Aβ is dependent on γ-secretase activity, as inhibiting γ-secretase prevents amyloidogenesis (Beher *et al.*, 2002; O'Brien and Wong, 2011). However, the proteolytic activity of γ-secretase is non-specific, thus it is not restricted to a single cleavage site (fig.1.2.). APP can therefore be cleaved at multiple sites within its transmembrane domain, which can generate Aβ peptides of various sizes (Aβ isoforms) (Haass *et al.*, 2012). Studies suggest that there might be two distinct product lines of APP processing, resulting in either $Aβ_{1-40}$ or $Aβ_{1-42}$ peptide (fig.1.2.) (Qi-Takahara *et al.*, 2005; Takami *et al.*, 2009). $Aβ_{1-40}$ processing starts with a cleavage at $Aβ_{49}$, and continues through $Aβ_{46}$, $Aβ_{43}$, and eventually $Aβ_{40}$. The second processing line starts with $Aβ_{48}$, to $Aβ_{45}$ and $Aβ_{42}$ cleavage. γ-secretase has been shown to cleave APP at no less than two cleavage sites, called γ-site and ε-site, which may be regulated sequentially. ε-cleavage site could regulate APP cleavage further upstream (49 amino acids) to the γ-cleavage site (40 and 42 amino acids), and ε-cleavage site could be an important step preceding Aβ generation (Funamoto *et al.*, 2004; Kametani, 2008). This could therefore result in generation of various Aβ isoforms.

In AD, and in a healthy brain, different Aβ variants can be detected. These predominantly include $Aβ_{1-40/42}$, however other variants, such as $Aβ_{4-42}$, $Aβ_{8-42}$ and $Aβ_{9-42}$ can be detected (Naslund *et al.*, 1994). In the cerebrospinal fluid of AD patients, Aβ peptide variants such as $Aβ_{1-37}$, $Aβ_{1-38}$ and $Aβ_{1-39}$ can also be detected (Bibl *et al.*, 2012). Although $Aβ_{1-40}$ is the most predominant isoform in the brain, $Aβ_{1-42}$ is the primary isoform found in senile plaques in AD. $Aβ_{1-40}$ and $Aβ_{1-42}$ isoforms differ largely due to their ability to form aggregates, as $Aβ_{1-42}$ is more prone to aggregation (Iwatsubo *et al.*, 1996).

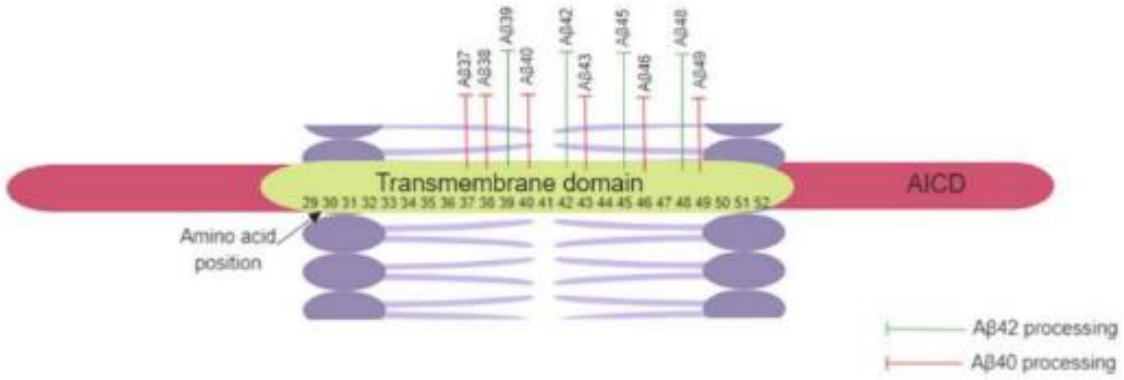


**Figure 1.2.** Amyloid Precursor Protein processing, generating Aβ peptides of varying sizes.

Binding of APP to γ-secretase triggers the proteolytic activities of the enzyme, which starts with APP cleavage at amino acid positions 49 or 48. This leads to cleavage further down. Two distinctive cleavage pathways are recognised, where one leads to generation of the $A\beta_{40}$ peptide and the other to $A\beta_{42}$. These peptides can be cleaved further down the distinct pathways. (Adapted from: figure 3 of Haass et al., 2012)

### 1.2.5 Amyloid-beta clearance

Aβ can be cleared via enzymatic action. Neprilysin proteolysis is considered one of the most important enzymatic routes for clearing cerebral Aβ (Marr and Hafez, 2014). It has been found, that neprilysin can degrade both $Aβ_{1-40}$ and $Aβ_{1-42}$; however enzyme kinetics show that $Aβ_{1-40}$ is degraded at a higher rate *in vitro* (Shirotani *et al.*, 2001). Overexpression of human neprilysin in transgenic AD mice significantly reduces the Aβ plaque burden, suggesting neprilysin as a key player in Aβ clearance (Marr *et al.*, 2003). Another important regulator of Aβ levels in the brain is insulin-degrading enzyme (IDE), which can also be involved in AD pathology (Farris *et al.*, 2003). An overexpression of IDE in mammalian cells leads to a reduction of Aβ (Vekrellis *et al.*, 2000). A genetic link between IDE and late-onset AD has been suggested, where missense mutations in IDE can lead to decreased Aβ degradation in rat brains (Farris *et al.*, 2004). Moreover, IDE knockout causes Aβ accumulation in the brain, as well as decreased Aβ degeneration in neurons (Farris *et al.*, 2003). Aβ can accumulate in capillary and arterial walls, leading to cerebral amyloid angiopathy often present in AD patients (Yoon and Jo, 2012). The accumulation of Aβ in the walls of cerebral blood vessels can take place before the onset of amyloid plaques in the brain. This cerebral amyloid angiopathy can correlate with dementia and could take place due to the decreased activity of Aβ-clearing enzymes, such as neprilysin, or ageing of artery walls. As a result, failure to clear Aβ from the interstitial fluid, a type of extracellular fluid linked to the CNS (Weller *et al.*, 2008; Yoon and Jo, 2012), promotes accumulation of senile plaques in the brain. This can alter brain homeostasis, and cause AD-associated cognitive decline and neurotoxicity (Weller *et al.*, 2008).

Aβ can also be cleared from the brain via the vascular endothelium, which involves low-density lipoprotein receptor-related protein-1 (LRP1) (Storck *et al.*, 2016). Inhibiting LRP1 *in vitro* decreases $Aβ_{1-42}$ clearance (Storck *et al.*, 2018). Moreover, *Lrp1* knockout increases the levels of Aβ in the brain, leading to cognitive deficits in mouse models of AD (Storck *et al.*, 2016). Mouse studies also suggest that LRP1-mediated clearance of Aβ can decrease with age (Shibata *et al.*, 2000). Age is an important risk factor of AD, and the levels of Aβ often increase in aged brains, even in individuals who remain cognitively healthy.

Kinetic studies on AD patients and control individuals revealed that in a healthy system, there is an effective $Aβ_{1-40/42}$ clearance from the brain, whilst in AD, this clearance appears to be hindered (Mawuenyega *et al.*, 2010). This suggests that an impaired Aβ clearance mechanism could be one of the main components in AD pathology and progression, particularly for sporadic cases. Moreover, an imbalance between clearance and production of Aβ in the brain could be one of the factors associated with the increased levels of Aβ in AD brains. An impaired proteasome system could also be one of the key factors involved in the insufficient Aβ clearance from AD brains. Proteasome clearance is the main

protein clearance mechanism within cells. However, conflicting results exist, where $A\beta_{1-42}$ has been found to increase the proteasome activity, rather than hindering it (Orre *et al.*, 2013).

Glial cells, such as astrocytes and microglia are also involved in Aβ clearance. Astrocytes are the most abundant cells in the brain and have many key functions, including providing trophic and metabolic support to neurons (Garwood *et al.*, 2017). During AD, astrocytes can become progressively more reactive (Kamphuis *et al.*, 2014). Astrocytes can function to clear away Aβ from the CNS, in order to protect neurons from its toxic effects (Thal *et al.*, 2000; Wyss-Coray *et al.*, 2003). Furthermore, adult mouse astrocytes have been shown to degrade Aβ aggregates *in vitro* (Wyss-Coray *et al.*, 2003; Pihlaja *et al.*, 2008).

Microglia, the macrophage cells of the brain, play a key role in the phagocytosis of apoptotic cells, unfolded proteins, such as Aβ, and pathogens, including bacteria and viruses (Janda, Boi and Carta, 2018). It has been found, that fibrillar Aβ can increase microglial phagocytosis, whilst oligomeric Aβ inhibits phagocytosis, leading to an increase in pro-inflammatory pathways and reactive oxygen species (Pan *et al.*, 2011). Furthermore, increasing Aβ load might correlate with microglial dystrophy. This effect could occur due to microglia no longer being able to remove the high levels of insoluble Aβ. In turn, this could lead to further activation of pro-inflammatory pathways, ending with neurodegeneration (Streit *et al.*, 2018).

## 1.3 Introduction to astrocytes

Over one hundred years ago, the significance of astrocytes and their function was highlighted by Ramon y Cajal. Cajal produced pioneering studies describing the physiological significance of glial cells and contributed to our understanding of glia in the human brain (Navarrete and Araque, 2014). Astrocytes are the most abundant glial cells of the CNS. They are heterogenous cells, which demonstrate adaptive plasticity, helping in the maintenance of the CNS as well as acting as defence mechanisms of the CNS (Verkhratsky and Nedergaard, 2018). Astrocytes have a wide variety of roles in the CNS, ranging from their homeostatic roles to CNS defence and immune responses. However, astrocytes are also important in disease and injury, and have been implicated in neurodegenerative diseases such as Alzheimer's disease and Parkinson's disease (Bouvier *et al.*, 2022).

Astrocytes are tightly integrated in the neural networks, and they control the homeostasis of the CNS (Verkhratsky and Nedergaard, 2018). Astrocytes are widely distributed throughout the CNS. The morphology of mature astrocytes includes very dense ramification of fine processes, causing astrocytes to adopt a 'spongiform' morphology. The astrocytes can be described to have a 'star-shaped' morphology, with their cytoskeleton usually highlighted by the presence of the intermediate filament called the glial fibrillar acidic protein (GFAP) (Bushong, Martone and Ellisman, 2004; Bouvier *et al.*, 2022).

The complex morphology of astrocytes facilitates them to extend their ramified processes into the neuropil, establishing wider connections on cellular levels. Furthermore, the widespread distribution of astrocytes throughout the CNS provides them with an ideal position to provide local and global support to neuronal networks and synapses. The widespread distribution of astrocytes not only facilitates the formation of such connections between astrocytes and neurons via tripartite synapses, but also facilitates the formation of intricate networks with blood vessels (via astrocytic end-feet) and other astrocytes via connexins and gap junctions (Bushong, Martone and Ellisman, 2004; Agarwal *et al.*, 2017; Bouvier *et al.*, 2022).

It is therefore clear that astrocytes are an essential component to the CNS, and that astrocytes have a wide variety of roles in the CNS (fig.1.3). Astrocytes are essential for neuronal health and CNS homeostasis. Astrocytes can act as regulators in the CNS, maintaining homeostasis by facilitating the transport of ions, movement of neurotransmitters, and by regulating the levels of ROS in the CNS (fig.1.3). However, their functions are vast. These astrocyte functions are essential in physiological and pathological conditions. Any changes to the delicate environment of the CNS, and astrocytes in particular, may have detrimental effects on the overall brain health and activity, as well as neuronal survival (Verkhratsky and Nedergaard, 2018).

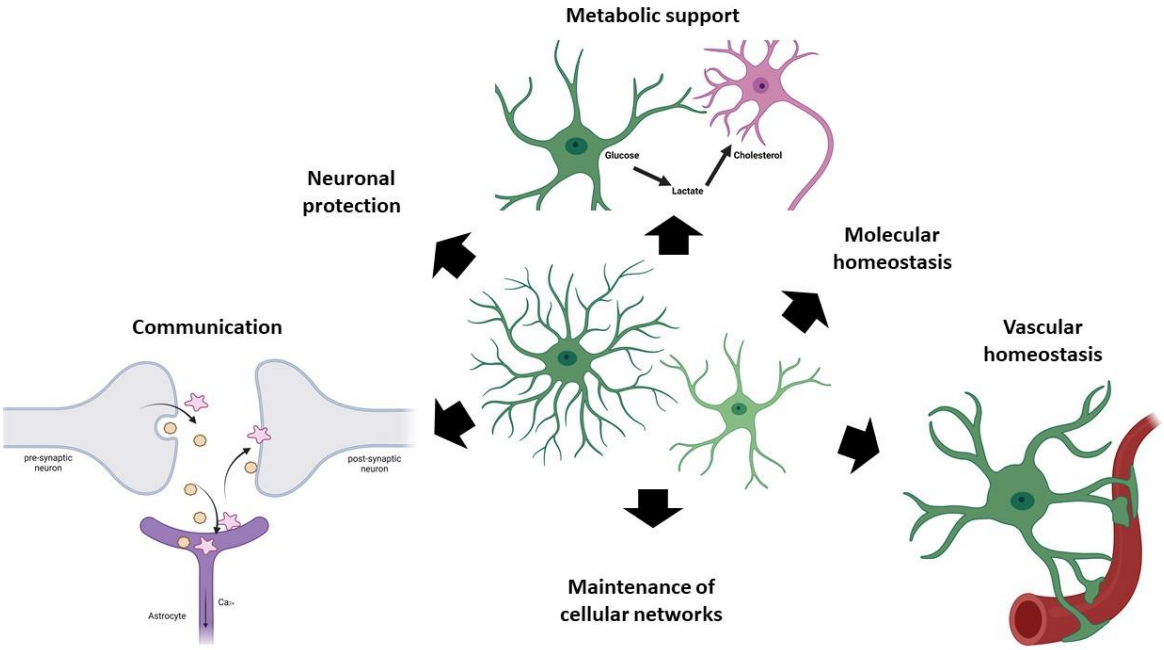


**Figure 1.3** The roles of astrocytes in the central nervous system.

Astrocytes provide metabolic support to neurons through lactate shuttle, and they are a major energy source in the brain due to their roles in glycogen synthesis and storage. Astrocytes facilitate communication between neurons through tripartite synapses and can communicate with each other through gap junctions. They are also involved in neuronal protection, regulation of molecular and vascular homeostasis, and maintenance of cellular networks, particularly through regulation of synaptic plasticity. (Images generated using BioRender. Adapted from: Garwood et al. (2017)).

### 1.3.1 The role of astrocytes in homeostasis

The homeostatic roles of astrocytes include functional maintenance of the CNS where astrocytes play a role in the transport of ions and neurotransmitters, as well as removing and utilising neurotransmitters due to their role in maintaining tripartite synapses (Garwood *et al.*, 2017; Verkhratsky and Nedergaard, 2018). At the synapses, the astrocytes are involved in modulating and facilitating the synaptic activity. For example, astrocytes express glutamate transporters, Excitatory amino acid transporter 1 (EAAT1) and Excitatory amino acid transporter 2 (EAAT2), which help to regulate the amount of neurotransmitters at the synaptic cleft, and allows the neurotransmitters to be recycled and recirculated. As well as the recycling of the neurotransmitters, astrocytes can also release neurotransmitters directly into the synaptic cleft, modulating its activity (Bouvier *et al.*, 2022).

Regulation of calcium homeostasis is an important role of astrocytes in the CNS. The lack of calcium regulation could have detrimental effects on neurons, as it can lead to neuronal hyperexcitability and, as a consequence, neuronal cell death. Astrocytes are equipped with glial microdomains, which consist of thin membrane sheets and a few mitochondria. Such glial microdomains can wrap around synapses and facilitate synaptic efficacy, increase neurotransmitter availability and influence neuronal communication based on the calcium signals in the CNS (Grosche *et al.*, 1999). In disease, astrocytes may interact with CNS pathology, such as senile amyloid plaques in AD, increasing astrocytic resting calcium levels. The impact of such event could mean changes to astrocytic intra and inter cellular signalling, causing the astrocytes to exhibit a global network-based response to focal pathology (Kuchibhotla *et al.*, 2009). Apart from regulating the calcium levels in the CNS, astrocytes are also responsible for the control of extracellular neurotransmitters. This includes the control and regulation of glutamate levels. This takes place via the high-affinity excitatory amino acid transporters 1 and 2. The glutamate uptake and homeostasis by astrocytes is crucial for the delicate CNS environment, as high levels of glutamate can be toxic to neurons through a process of excitotoxicity (van Putten *et al.*, 2021).

### 1.3.2 The role of astrocytes in metabolic support

Astrocytes are mediators of metabolic support to neurons, mainly through the lactate shuttle. The astrocyte-neurone lactate shuttle hypothesis states that astrocytes are essential players in metabolising glucose to lactate, and lactate is a key resource taken up by neurons as source of energy (Newington, Harris and Cumming, 2013). Moreover, astrocytes are the main cells in the CNS capable of storing glycogen for further use in the lactate shuttle processes, and astrocytic glycogen is essential for the support of axon function and for meeting the high energy demands of the brain (Brown, Tekkök and Ransom, 2004; Newman, Korol and Gold, 2011). Astrocyte morphology equips astrocytes with tools needed for an effective uptake of glucose. The spatial orientation of astrocytes permits them to

extend their perivascular end-feet and to form connections with the brain vasculature. This further facilitates the energy supply to the brain by connecting astrocytes to the blood vessels (Kacem *et al.*, 1998; Garwood *et al.*, 2017; Verkhratsky and Nedergaard, 2018). Glucose uptake by astrocytes and the consequent metabolism of lactate is essential for memory processing as shown in rat studies (Newman, Korol and Gold, 2011). Inhibition of glycogen in astrocytes can cause synaptic changes as well as impaired learning (Vezzoli *et al.*, 2020). Impaired lactate shuttle system can be detrimental to the health and survival of neurons. In Alzheimer's disease, there are defects in the astrocyte-neuron lactate shuttle system in both *in vitro* and *in vivo* models. Rescuing such deficits with growth factors can positively modulate the astrocyte-neurone lactate shuttle system, alleviating memory dysfunction, decreasing Aβ-associated cytotoxicity and improving brain metabolism (Sun *et al.*, 2020).

### 1.3.3 Astrocytes and neurons

Additionally, astrocyte coupling to neurons is essential and beneficial not only for the correct energy metabolism for neurons, but it also protects neurons from toxic by-products. These can include toxic fatty acids produced by hyperactive neurons. These fatty acids can be actively consumed by astrocytes, which switch on their detoxifying pathways to protect active neurons (Ioannou *et al.*, 2019).

Astrocytes have important roles in synaptic communication, via their role in the formation, maintenance, and involvement in tripartite synapses (Garwood *et al.*, 2017). Hence, astrocytes can modulate the synaptic function. It has been shown that astrocytes can show plasticity in the CNS, and that the interplay between glia and neurons, and the associated structural changes, can contribute to the synaptic plasticity of the hippocampus (Haber, Zhou and Murai, 2006). Furthermore, the presence of astrocytes can enhance synaptic activity, and can provide essential signals to neurons which may facilitate efficient synaptic function (Chung, Allen and Eroglu, 2015).

## 1.4 Astrocyte reactivity

One of the roles of astrocytes in the CNS is to respond to injury and disease through a process commonly referred to as astrogliosis or reactive astrogliosis. Reactive astrogliosis is a well-observed phenomenon, present in many neurological conditions, which include, but are not limited to, traumatic injury (Faulkner *et al.*, 2004) and neurodegeneration (Vargas *et al.*, 2008). Reactive astrogliosis is an essential process which allows astrocytes to perform their supportive functions, such as neuronal support, synaptic remodelling, regulation of the blood brain barrier, and neurite outgrowth (Anderson, Ao and Sofroniew, 2014; Moulson *et al.*, 2021). Reactive astrocytes also release pro-inflammatory signals and display altered gene expression profiles, which can alter the astrocyte function (Pekny, Wilhelmsson and Pekna, 2014; Li *et al.*, 2019). This phenomenon can result in gain of function or loss of function regarding astrocyte homeostasis (Escartin *et al.*, 2021). Even though astrogliosis can sometimes initially be protective, prolonged astrogliosis may lead to the formation of astroglial scarring in the CNS. This scar formation may hinder axonal regrowth and CNS healing. Such scarring can be observed in a plethora of neurodegenerative diseases (Blackburn *et al.*, 2009).

Additionally, there are reports of astrocyte reactivity during ageing. Astrocytes can display region-specific differences in their transcription profiles, and these can change with age. The astrogliosis response may change as we age, as aged brains have been found to express more neurotoxic astrocytes in response to neuroinflammatory signals (Clarke *et al.*, 2018).

Reactive astrocytes which play a role in the CNS scar formation, have also been suggested to be detrimental to the process of CNS healing, especially after traumatic injury. Ablation of reactive astrocytes has been shown to be the cause of failed BBB repair, leukocyte infiltration, tissue disruptions, demyelination, as well as neuronal death (Faulkner *et al.*, 2004). Preventing the formation of glial scar by astrocytes, or deleting the astrocyte-formed scars in the CNS, significantly reduces axonal regrowth (Anderson *et al.*, 2016). Furthermore, the disruption of glial scar formation can cause an increased inflammatory processes, as well as decreased neuronal survival (Wanner *et al.*, 2013). Reactive astrocytes may therefore play an essential protective role in the CNS.

The onset of reactive astrogliosis has led to a proposal of the term ‘A1’ and ‘A2’ astrocytes, where astrocytes can be either toxic (A1), upregulating complement cascade genes, disrupting synapses and promoting inflammation; or protective (A2), upregulating neurotrophic factors (Liddelow *et al.*, 2017).

Many different definitions of what it means for astrocytes to be ‘reactive’ have been published. Recently, it has been suggested that a more standardised nomenclature should be used to define such population of astrocytes responding to CNS injury and disease (Escartin *et al.*, 2021). Therefore, ‘reactive astrogliosis’ is the preferred nomenclature defining a process where astrocytes engage in

specific molecular changes resulting in the regulation of transcription, as well as resulting in changes to the astrocytic biochemistry, morphology, physiology and metabolism (Escartin *et al.*, 2021).

Compelling evidence over the years has suggested that reactive astrogliosis is not an all-or-nothing phenomenon, and that there is a spectrum of responses dependent on the different stimuli the astrocytes are exposed to. This observable varying response of astrocytes resulted in a proposed hypothesis describing astrogliosis, which states that there is a high degree of heterogeneity within astrocytic populations, and that there is a spectrum of molecular, cellular, and functional changes to astrocyte biology. Astrogliosis-related molecular changes to astrocytes happen due to the changes of the CNS environment as a general response to disease and/ or injury (Anderson, Ao and Sofroniew, 2014). Indeed, accumulating evidence suggests that there is a high degree of heterogeneity displayed by astrocytes in terms of their pathological responses (Liddelow *et al.,* 2017). It is clear that astrocyte responses are very heterogenous and expand beyond the proposed simplicity of A1/A2 reactive phenotypes.

### 1.4.1 Astrocyte response to injury

It is widely known that as a response to an acute traumatic injury or disease, reactive astrocytes can form a protective scar in the CNS, which closes off the injured areas, and may promote the healing of CNS environment (Campbell *et al.*, 2020). After CNS injury, mature glial scar borders are mainly composed of newly proliferated astrocytes, and during scar formation astrocytic processes of various astrocytes overlap forming a mesh-like arrangement (Wanner *et al.*, 2013). Pioneering research by Cajal describing astrocyte changes suggested that scar forming astrocytes can have harmful effects on the regeneration of the injured CNS, particularly in the context of axon regrowth (Cregg *et al.*, 2014). Chronic reactive astrogliosis can cause impairments in glutamate homeostasis and neuronal hyperexcitability (Robel *et al.*, 2015). Moreover, neurons in the vicinity of reactive astrocytes can display reduced inhibitory synaptic currents, and this suggests that reactive astrocytes can play a role in synaptic dysfunction (Ortinski *et al.*, 2010). Reactive astrocytes do not just respond to signals from injury, in disease such as amyotrophic lateral sclerosis (ALS), astrocytes can be activated due to signals from injured neurons. In healthy systems, these astrocytes exhibit a beneficial response. However, in disease, the pro-inflammatory and anti-inflammatory pathways are inadequately activated in reactive astrocytes (Tyzack *et al.*, 2017). Indeed, disease astrocytes can exhibit dysregulated cargo processes, and can release micro-RNAs which in turn can cause neuronal loss (Varcianna *et al.*, 2019). This could suggest that in certain neurodegenerative diseases, reactive astrocytes can exhibit a toxic loss of function.

The reactive astrogliosis response can be dependent on the type of injury the brain is exposed to. For example, rather than focal injury, diffuse injury causing tissue shearing may produce atypical astrogliosis. Such astrocytes do not express increased levels of GFAP and do not show any glial scarring. However, such astrocytes have been found to downregulate homeostatic proteins and exhibit impaired astrocytic coupling, which can have profound adverse effects in the brain (Shandra *et al.*, 2019). Not only do reactive astrocytes vary as a response to different types of injury, but these astrocytes can also exhibit heterogeneous morphology with regards to the distance from the site of injury.

It has been suggested that there are at least two broadly defined categories of reactive astrocytes as a response to injury. Firstly, there are astrocytes that are newly proliferated which overlap with each other forming networks and inter-cellular interactions leading to glial scar formation. There are also non-proliferative mature astrocytes, which are derived from local astrocytes, and these do not extend their processes but rather remain in their original territory (Wanner *et al.*, 2013). Furthermore, reactive astrocytes can organise themselves into heterogenous populations with one population retaining their original morphology and other population being more proliferative (Bardehle *et al.*, 2013). It is therefore clear that there is a great heterogeneity regarding reactive astrocytes responding to CNS trauma, even in neighbouring areas. Astrocytes are highly dynamic, displaying a varying degree of plasticity in the changing CNS environment (Moulson *et al.*, 2021). The onset of reactive astrogliosis is a quick process, associated with gene expression changes which are specific to a given injury. Moreover, depending on the injury and associated astrocytic response, the effects in the CNS may be either beneficial and protective or they might be neurotoxic instead. During ischemic conditions, reactive astrocytes can display a beneficial molecular phenotype. Meanwhile, during an increased inflammation, the related response of reactive astrocytes shows a more detrimental molecular profile (Zamanian *et al.*, 2012).

### 1.4.2 Astrocyte response in disease

Astrocytes can become progressively reactive in disease, which includes AD. Interestingly, in Alzheimer's disease, reactive astrocytes that are found in the vicinity to Aβ plaques may display more neuroprotective roles. Astrogliosis identified near plaques has been shown to correlate with lower cognitive impairment in Alzheimer's disease (Mathur *et al.*, 2015). On the other hand, astrocyte reactivity can induce neuroinflammation via the release of pro-inflammatory cytokines, and other pro-inflammatory mediators. Example of this being the release of the nuclear factor kappa B (NFκB) (Kamphuis *et al.*, 2014). NFκB has been suggested as both neuroprotective and neurotoxic agent in various neurodegenerative diseases, including AD (Lian *et al.*, 2015, 2016). NFκB can be responsible for mediating oxidative stress-induced toxicity in astrocytes (Choi *et al.*, 2007). Activated microglia

releasing pro-inflammatory factors such as IL-1α, TNF and C1q, are capable of in turn activating astrocytes and promoting reactive astrogliosis (which has formerly been associated with the A1 astrocyte phenotype). Such reactive astrocytes can be abundantly found in many neurodegenerative diseases, including Alzheimer's disease. These pro-inflammatory reactive astrocytes display changes in their molecular profile, losing their supportive roles towards neurons, as well as losing the ability to promote synaptogenesis and contributing to neuronal cell death (Liddelow *et al.*, 2017). This further suggests that a population of pro-inflammatory astrocytes can have detrimental effects on their role and function in the CNS.

Furthermore, as a response to disease, astrocytes can display impaired ion channels, and deficits in ion regulatory processes. These could contribute to neuronal dysfunction and neuronal excitability in disease, which are mediated by the altered homeostatic properties of astrocytes (Tong *et al.*, 2014). Additionally, potassium and glutamate transport may be impaired in reactive astrocytes. Under healthy, physiological conditions, astrocytes express glutamate transporters, aiding in the removal of excess extracellular glutamate, supporting the survival on neurons. During disease or injury, the formation of reactive astrocytes can impair the glutamate transport, leading to neuronal hyperexcitability and neuronal death (Campbell *et al.*, 2020).

Reactive astrocytes that are found in the vicinity of gliomas express higher levels of GFAP, which is a marker for reactive astrogliosis. Furthermore, such astrocytes have a changed molecular signature, as reactive astrocytes closer to the tumour site upregulate a phosphorylated signal transducer and activator of transcription 3 (pSTAT3), which in turn regulates genes involved in astrogliosis. This includes *GFAP*. There are also morphological changes associated with scar-forming astrocytes found around the tumour borders (Campbell *et al.*, 2020). This strengthens the idea that there is a wide variety of astrocyte responses to injury and disease, and that the potential responses might be highly dependent on the type and severity of the injury to the CNS. The precise factors and mechanisms governing such heterogenous astrocyte responses to various diseases and varying types of injury are still unclear.

### 1.4.3 The role of astrocytes in Alzheimer's disease

Astrocytes play an important role in a number of neurodegenerative diseases, including AD. Changes in astrocyte function have been demonstrated in human brain and using *in vitro* and *in vivo* AD models (Gonzalez-Reyes *et al.*, 2017). As mentioned previously, depending on the type and severity of the CNS stress, reactive astrocytes may act on a spectrum of molecular, cellular, and functional processes. Astrocytes may display a high level of heterogeneity, which is important in their responses to the dynamic brain environment. In neurological disorders, A1 and A2 astrocyte phenotypes can be distinguished, where A1 astrocytes might promote neurodegeneration and reactive phenotype. A2 astrocytes might promote neuronal survival and non-reactive phenotype (Liddelow and Barres, 2017; Liddelow *et al.*, 2017).

There is a correlation between increased levels of GFAP, which is a marker of astrogliosis, and AD duration and astrocytes can become progressively reactive in AD (Ingelsson *et al.*, 2004; Kamphuis *et al.*, 2014). Compared with healthy controls, AD brains have an increased number of detectable GFAP positive astrocytes, without a significant change in overall astrocyte numbers. This concludes that reactive astrocytes in AD are not proliferative (Serrano-Pozo *et al.*, 2013).

Astrocytes in AD could become dysfunctional as the disease progresses, leading to exacerbated symptoms seen in the later stages of the disease. Interestingly, a microarray study identified significant gene expression changes in genes associated with cytoskeleton, immune and stress responses, and apoptosis. Progression of AD can be associated with dysregulation of the astrocyte cytoskeleton, which can affect the morphology and signalling of astrocytes (Simpson *et al.*, 2011).

Astrocytes can become reactive as a response to Aβ, this may be associated with changes to their molecular profiles, and ultimately with neuronal loss (Pike *et al.*, 1994; Garwood *et al.*, 2011). Exposing astrocytes to Aβ can cause the production of reactive oxygen species and nitric oxide and can induce the activation of pro-inflammatory pathways as well. The upregulation of reactive oxygen species and nitric oxide may in turn induce or enhance oxidative stress in AD (Akama *et al.*, 1998; Singh *et al.*, 2020). Interestingly, the conditioned media from oligomer-treated astrocytes can induce neuronal cell death. This may suggest that astrocytes in AD may react to disease stressors (Aβ oligomers) by changing their secretome, and in turn causing neuronal loss. Changes to astrocyte secretome in a state of astrogliosis has been implicated in other neurodegenerative diseases, such as ALS (Haidet-Phillips *et al.*, 2011).

Reactive astrocytes can associate with amyloid plaques in AD, and this can correlate with improved cognitive scores (Mathur *et al.*, 2015). Astrocytes have been reported to surround and engulf

dystrophic neurites independently of microglial clearance mechanisms, suggesting phagocytic properties of astrocytes in disease (Gomez-Arboledas *et al.*, 2018).

However, even though astrocytes in Alzheimer's disease might be involved in phagocytosis, they can also exhibit impaired autophagy mechanisms. This has been evident in ApoE4-expressing astrocytes, which could not clear away Aβ and amyloid plaques as effectively as ApoE3 astrocytes (Simonovitch *et al.*, 2016). This suggests that genetic background of Alzheimer's disease may modulate the pathways by which astrocytes are involved in toxic downstream events leading to dementia. It further suggests that an impaired clearance mechanism may be a factor in disease pathology and perhaps severity. Indeed, impaired proteasome mechanisms in astrocytes may further glial dysfunction as well as enhance neuroinflammation in Alzheimer's disease (Orre *et al.*, 2013). Furthermore, reactive astrocytes can function to clear away Aβ from the CNS, in order to protect neurons from its toxic effects (Thal *et al.*, 2000; Wyss-Coray *et al.*, 2003). Astrocytes near plaques demonstrate increased GFAP expression, suggesting that fibrillary Aβ modulates astrocyte reactivity (Pike *et al.*, 1994). Plaque type and astrocyte proximity to plaques may be important in AD since it has been shown that reactive astrocytes located close to diffuse or compact plaques may be neuroprotective (Mathur *et al.*, 2015). Remarkably, the ablation of reactive astrocytes in amyloid models can result in an increase of Aβ production and a decrease in Aβ clearance. This is associated with increased inflammation, decreased synaptic activity and exacerbated memory impairments in mice (Katsouri *et al.*, 2020). Reactive astrogliosis in AD has been suggested as beneficial as it could limit the growth of amyloid plaques (Kraft *et al.*, 2013).

However, astrocytes could be a site of Aβ production, as reactive astrocytes may also act on BACE1 and APP, through pro-inflammatory cytokines, to stimulate generation and secretion of Aβ (Zhao, O'Connor and Vassar, 2011). Moreover, astrocytes can contribute to the formation of Aβ plaques (Robert G. Nagele *et al.*, 2003). It has also been suggested that astrocytes may not only promote aggregation, but also promote the spread of toxic Aβ oligomers, furthering neuronal loss in AD (Wang *et al.*, 2019). Astrocytes may also be implicated in the induction of oxidative stress in the brain, as a result of Aβ (Akama *et al.*, 1998).

Additionally, in a mouse model of AD, it has been shown that astrocytes can respond to the disease by modulating calcium levels, facilitating calcium transients independently of neuronal networks. Neuronal calcium homeostasis has been found to be severely impacted near amyloid senile plaques, whereas the distance from the plaques does not impact how active the astrocytes are. Instead, astrocytes display increased levels of resting calcium globally.

Aβ plaques have been found to have no effect on astrocytic cell viability, even though they could have detrimental effects on neurotoxicity and synaptotoxicity, inducing neuronal cell death. However, such Aβ plaque deposits may increase the resting calcium levels. This calcium increase could in turn have an effect on the intra- and inter- cellular signalling events in astrocytes (Kuchibhotla *et al.*, 2009).

Neurovascular coupling and cerebral vasoregulation may be impaired in AD (Rosengarten *et al.*, 2009). Increased levels of Aβ in the brains of AD patients correlate with decreased cerebral blood flow and volume (Mattsson *et al.*, 2013). Furthermore, oligomeric Aβ has been found to constrict brain blood vessels in AD (Nortley *et al.*, 2019). Amyloid deposition can be associated with the endothelial blood vessel walls, and it has been shown to be deposited between the astrocytic end feet. Amyloid deposition can therefore hinder the astrocytic regulation of brain vasculature (Kimbrough *et al.*, 2015). As astrocytes are implicated in the regulation of blood supply to the brain, they may therefore be implicated in early changes to the brain vasculature associated AD, particularly as a response to Aβ. This can have detrimental effects on brain health and can further contribute to disease pathology.

Overall, astrocytes clearly play a role in AD pathology. Astrocytes have been shown to interact with Aβ in Alzheimer's disease and become reactive. However, this reactivity may be either neuroprotective or neurotoxic. The exact mechanisms governing these astrocyte changes in the context of Aβ are still unclear.

### 1.4.3 Oxidative stress

The human brain is the largest source of energy and oxygen consumption in the body. Oxygen usage and cellular metabolism can give rise to toxic by-products, namely ROS. This is especially true in the CNS due to the intense metabolic requirements and high energy demands of the brain (Cobley, Fiorello and Bailey, 2018; Rizor *et al.*, 2019). Reactive oxygen species are free radicals of free reactive oxygen produced by cells as a by-product of their usual aerobic activities, during respiration. Most of the free oxygen can be dismutated into hydrogen peroxide ($H_2O_2$) by superoxide dismutase. In turn, $H_2O_2$ can form highly reactive hydroxyl ions which are capable of reacting with cell membranes and proteins (Liguori *et al.*, 2018). The ageing brain is very vulnerable to oxidative stress, and this can be seen in many neurodegenerative diseases including AD.

In general, cells are well-equipped for such event via the release and actions of antioxidants. Antioxidants function to neutralise and remove ROS. However, during disease, other pathological conditions, as well as ageing, a state of imbalance between antioxidants and ROS can occur. This results in oxidative stress (Pizzino *et al.*, 2017). Oxidative stress is therefore defined as accumulation of high levels ROS, due to insufficient ROS clearance or increased ROS production (Cheignon *et al.*,

2018). As mentioned previously, the role of astrocytes in the CNS is to promote the correct function and environment of the CNS by regulating the CNS homeostasis. Astrocytes are therefore involved in regulating oxidative stress in the CNS. It has been suggested that astrocytes can act both as a clearance mechanism for oxidative stress and ROS, but they can also be a source of ROS and can promote microglial activity and neuronal cell death (Chen *et al.*, 2020). For example, are equipped with an antioxidant glutathione, promoting the clearance of ROS, namely nitric oxide. Ablation of glutathione in astrocytes causes significant increase in neuronal cell death, highlighting the importance of astrocytes in protecting the neurons from oxidative stress (Chen *et al.*, 2001). The sub-population of astrocytes seemingly promoting the release of ROS and therefore oxidative stress is reactive astrocytes. Astrocytes stimulated with proinflammatory factors can cause astrocytes to release ROS via an increased superoxide production in the mitochondria. In turn, this for example, can cause lipid peroxidation, potentially having adverse effects on the surrounding cells and tissue (Sheng *et al.*, 2013). However, recently it has been proposed that ROS generated by astrocytes could have an important regulatory role in the CNS, where astrocytic ROS could regulate the use of glucose to promote neuronal survival (Vicente-Gutierrez *et al.*, 2019).

Oxidative stress has been implicated in DNA damage and DNA mutations, disruption of cellular membrane bilayer, and changes to protein structures (Birben *et al.*, 2012). The aetiology of AD is multifactorial, and oxidative stress has been implicated as one of the key players in the disease (Huang, Zhang and Chen, 2016). Evidence suggests there is increased oxidative stress in the brains of people with Alzheimer's disease, which may hinder the crosstalk communication between astrocytes and neurons (Gonzalez-Reyes *et al.*, 2017). This in turn can have detrimental effects on neuronal survival and neuronal function and homeostasis (Butterfield, Swomley and Sultana, 2013a; Gonzalez-Reyes *et al.*, 2017). Previous studies have shown that Aβ aggregation can lead to increased levels of ROS, particularly in neurons, which could contribute to neurotoxicity and AD pathology (Drake, Link and Butterfield, 2003; Butterfield, Swomley and Sultana, 2013a). Moreover, oxidative stress in AD could arise due to changes in neurotransmitter, lipid and energy metabolism. These include mitochondrial and synaptic dysfunction (Tönnies and Trushina, 2017). Oxidative stress could also lead to astrocyte senescence and may be the mechanism by which neurodegeneration in many diseases might take place (Garwood *et al.*, 2017).

## 1.5 Overall aims and objectives

Evidence suggests a heterogeneity in astrocyte responses to disease, and this includes Alzheimer's disease. Despite the controversies surrounding it, Aβ is one of the key players modulating the cellular responses in Alzheimer's disease, as well as modulating disease pathology and/or progression. Current evidence suggests that oligomeric and fibrillary Aβ may elicit differential responses in Alzheimer's disease. Reactive astrocytes are a key feature of Alzheimer's disease, and the molecular and/or functional profile of astrocytes can change early in the disease. Changes in astrocytes have also been implicated in the downstream events of the amyloid cascade hypothesis. Therefore, astrocytes may play an important role in Alzheimer's disease in the context of Aβ.

We hypothesise that astrocytes can react with different molecular profiles when exposed to different stressors in Alzheimer's disease. This includes oligomeric and fibrillary Aβ. We further hypothesise that this effect will drive astrocytes into a reactive astrogliosis state, and that the astrocytes may display a neurodegenerative or neuroprotective molecular phenotype dependent on which Aβ aggregation species they are exposed to. Due to the idea that oligomeric Aβ may be the more neurotoxic species of Aβ, we hypothesise that Aβ oligomers will elicit a more neurotoxic phenotype in astrocytes when compared to fibrillary Aβ.

The project aims are as follows:

i. To prepare and characterise stable monomeric $A\beta_{1-42}$, from which distinctive oligomeric and fibrillary $A\beta_{1-42}$ preparations will be derived;
ii. To assess the effects of oligomeric and fibrillary $A\beta_{1-42}$ treatments on astrocyte morphology;
iii. To assess the effects of oligomeric and fibrillary $A\beta_{1-42}$ on astrocyte viability;
iv. To characterise the DNA damage response in astrocytes as a response to oligomeric and fibrillary $A\beta_{1-42}$ treatments;
v. To compare and contrast the fetal astrocyte *in vitro* model to the induced astrocyte *in vitro* model in the context of Alzheimer's disease and Aβ toxicity;
vi. To extract $A\beta_{1-42}$ from human Alzheimer's disease brain tissue for the comparison of the effects of *in vitro* and *ex vivo* Aβ on astrocytes;
vii. To assess and determine the molecular and genetic differences in astrocyte phenotypes after treatment with various forms of $A\beta_{1-42}$ (oligomeric, fibrillary and brain extracts) using RNAseq.

# Chapter 2 - Preparation and characterisation of Amyloid-beta aggregates

## 2.1 Introduction

### 2.1.1 Amyloid-beta aggregation

Amyloid proteins are central to many diseases, and it is well known that protein misfolding plays a key role in disease pathology of many neurodegenerative diseases. These include alpha-synuclein in Parkinson's disease, huntingtin in Huntington disease, and most importantly for the context of the current work, Aβ and tau in Alzheimer's disease. Protein misfolding can happen as a result of genetic mutations, transcription or translation errors, errors in post-translational modifications, structural errors due to environmental changes, and seeding of proteins by pre-formed aggregates or surfaces. Protein misfolding causes formation of an altered protein compared to its native structure, which in turn leads to protein aggregation. This is often observed in amyloid diseases (Almeida and Brito, 2020).

Aggregation of Aβ monomers into oligomers and fibrils is a complex process involving protein nucleation and Aβ polymerisation. Nucleation is a mechanism of ordered polymerisation of proteins. Protein nucleation occurs in normal cellular processes, for example actin polymerisation or in pathological events, such as prion aggregate formation. Protein nucleation is a key event facilitating Aβ aggregation and toxicity, and this includes primary and secondary nucleation (Jan *et al.*, 2011; Cohen *et al.*, 2013). Primary nucleation refers to an initial event during which monomers self-aggregate. Secondary nucleation takes place further along the amyloid aggregation pathway, after the initial formation of nucleation 'seeds' from monomers. Both nucleation events are needed during the amyloid aggregation pathway to produce mature fibrils, as well as lower-molecular weight intermediate species such as oligomers and protofibrils.

Due to the aggregating nature of Aβ, the peptide can exist in different aggregation states. These include monomers (smallest species of Aβ), small and large molecular weight oligomers, protofibrils and fibrils. The heterogeneity of the Aβ peptides *in vitro* and *in vivo* makes it difficult to establish which aggregation species elicits the biggest neurotoxic effects, triggering the downstream effects posited by the amyloid cascade hypothesis described in chapter 1. However, monomeric Aβ has been regarded as a benign peptide, which does not appear to be directly involved in disease pathology. Indeed, monomeric Aβ might be essential in normal physiological functions of the central nervous system (CNS), however its role(s) in the healthy system remain unclear. Instead, the disease-relevant species have been proposed to be the aggregated Aβ peptides, and it has been suggested that Aβ oligomers are the more neurotoxic species of Aβ (Benilova, Karran and De Strooper, 2012). The mechanisms of this toxicity are yet to be elucidated.

Aβ monomers are crucial to the formation of oligomers and fibrils, as monomeric Aβ is the initiator for further Aβ aggregation steps (fig.2.1.) (Jan *et al.*, 2011; Linse, 2017). Monomers can spontaneously

associate into oligomers or fibrils. This association process depends on their stability, which can be determined by their environment, as well as the amount of monomers available in the environment (Nichols *et al.*, 2005; Tornquist *et al.*, 2018). *In vitro*, it is crucial that a careful preparation of monomers as the starting material takes place. This requires the starting monomers to be stable, pure, and free of any contaminants, in order to achieve efficient Aβ aggregation (Faller and Hureau, 2021).

Monomer self-aggregation is a kinetically unfavourable process, where formation of an initial nucleus, or a 'seed', creates a kinetic 'barrier'. During the process of Aβ aggregation, the primary nucleation and, as a result, the formation of the initial monomer seed, are therefore a rate-limiting step. This can result in a long lag-phase (Xue, Homans and Radford, 2008; Ghosh *et al.*, 2016). Insufficient amounts of Aβ monomers can hinder peptide aggregation and assembly into mature fibrils (Jeong *et al.*, 2013; Ghosh *et al.*, 2016). Also, the concentration of Aβ peptides at the start of the aggregation process influences the rate of aggregation, further suggesting that the amount of monomers present is crucial (Tougu, Tiiman and Palumaa, 2011). The monomer self-assembly into a nucleus drives the formation of further aggregates, which include low and high molecular weight Aβ oligomers, intermediate species such as protofibrils, and finally mature fibrils (Jarrett, Berger and Lansbury Jr., 1993; Cohen *et al.*, 2013; Linse, 2017). After the initial nucleus formation, and subsequent Aβ aggregation, the growth of amyloid aggregates is more thermodynamically favourable (Jarrett, Berger and Lansbury Jr., 1993). Aβ fibrils can act as a catalyst for further monomeric self-assembly, creating a rapid growth phase and a positive feedback loop for the aggregation of Aβ oligomers and fibrils, with oligomers being the smaller and intermediate Aβ species in the aggregation pathway. This rapid oligomer and fibril aggregation can be referred to as 'secondary nucleation' (Jan *et al.*, 2011; Cohen *et al.*, 2013; Linse, 2017). Secondary nucleation is the main contributor to the rapid growth phase of Aβ aggregates (Faller and Hureau, 2021). The aggregation process continues until a fibril growth plateau is reached, when all free monomers have aggregated into Aβ fibrils.

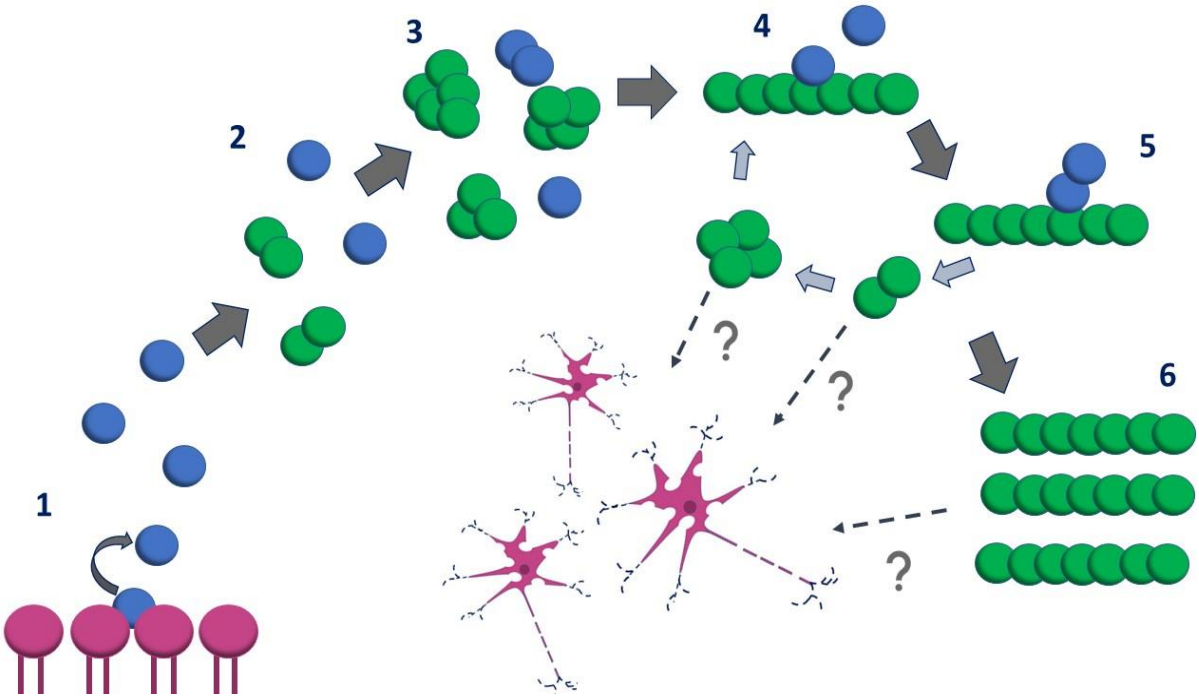


**Figure 2.1.** The aggregation of Amyloid-beta.

**1)** Aβ monomers are formed by the amyloidogenic processing of transmembrane APP. The monomers are liberated and enter a kinetically unfavourable lag phase. **2)** Monomers self-aggregate to produce nucleation seeds (Aβ aggregation nuclei). **3)** The self-seeding of monomers and formation of the initial aggregation nuclei is needed to produce small, then large oligomers. **4)** The oligomers aggregate further to become elongated fibrils. The surface of these fibrils acts as a catalyst for monomers to self-aggregate. **5)** This results in a rapid growth phase (secondary nucleation) and creates a positive feedback loop of aggregation, where a large amount of small and large oligomers is formed. **6)** The process continues until the population of monomers is depleted, and all oligomers have progressed on to become fibrils. The aggregation reaches a plateau. There is currently no consensus regarding which Aβ aggregation species, if any, is causative of neuronal loss in Alzheimer's disease, and what mechanisms would govern this effect.

### 2.1.2 Modelling amyloid-beta aggregation *in vitro*

Oligomeric and/ or fibrillary Aβ can be prepared *in vitro* through a careful manipulation of the Aβ peptide environment, which can be achieved through a careful experimental design. The final structure of Aβ aggregates depends on the conditions in which the peptide was allowed to self-assemble and aggregate. This includes controlling the temperature, pH and ionic strength of the buffers the peptide is dissolved in, as well as the concentration of the starting monomeric Aβ and its purity (Stine Jr. *et al.*, 2003; Faller and Hureau, 2021; Matuszyk *et al.*, 2022).

However, a careful experimental design may also include more subtle factors. For example, a gentle agitation of peptide samples can cause a faster rate of aggregation, as well as a different fibril morphology. This is also true for intermediate Aβ aggregation species, such as oligomers (Lee, Fernandez and Good, 2007). *In vitro* Aβ aggregation can also depend on the storage conditions of the stock peptides, as well as the type of plasticware, plates and vials used (Faller and Hureau, 2021). Furthermore, the presence of hydrophilic or hydrophobic nanoparticles, such as silica and polystyrene respectively, can have an impact on the fibrilization process. Hydrophobic polystyrene can show both acceleratory and inhibitory properties, whilst hydrophilic silica accelerates Aβ aggregation into fibrils (Ghavami *et al.*, 2013). As such factors can impact the rate of Aβ aggregation and final morphology, they are important to take into consideration during experimental design. Aβ aggregates are highly heterogenous, and this means that they could also have differing disease-related properties. We can assume, that not every Aβ structure formed will have a comparable toxic effect in AD brains. Therefore, varying Aβ species may have different disease-modifying roles and effects in AD. By ensuring that the Aβ species in question undergo the same aggregation conditions, one can minimise such peptide heterogeneity. This increases the confidence in the peptide preparation and ensures that any effect seen during experimental investigations is true for that specific Aβ conformation. This is especially important when studying the roles of Aβ in disease, as well as when developing potential therapeutic option for AD (Matuszyk *et al.*, 2022).

Due to inherent nature of Aβ, the peptides are highly unstable and aggregation prone *in vitro,* and many factors can impact the rate, and process of Aβ aggregation (Klement *et al.*, 2007). Incubation of the Aβ peptide at lower temperatures can lead to oligomerisation, whilst higher temperatures can lead to fibrilization of Aβ (Tiiman *et al.*, 2015). Increasing the temperature, for example from 37°C to 42°C, can result in a faster aggregation process, faster fibrillation, and a faster formation of Aβ oligomers (Ghavami *et al.*, 2013). Furthermore, different temperature ranges can impact the final structure and properties of Aβ aggregates. Gursky and Aleshkov have reported that peptide incubation at 37°C can lead to a slow and reversible aggregation into β-sheet structures; whilst even higher temperatures of 85°C can induce further folding into β-sheets, as well as oligomerisation (Gursky and

Aleshkov, 2000). However, such high temperatures are certainly not physiological. However, increased temperatures have been shown to impact AD pathology *in vivo*. For example, higher internal temperatures can induce neuronal death, inflammation, activation of glial cells, and interestingly maturation of amyloid plaques and formation of tau tangles in a rat brain (Sinigaglia-Coimbra, Cavalheiro and Coimbra, 2002). On a molecular and protein levels, high temperatures (39$^{o}$C) can increase the expression of heat shock protein 90, which in turn is associated with a γ-secretase complex. This increases Aβ production in the brain (Noorani *et al.*, 2020). As well as an increased rate of Aβ aggregation, high temperatures can also facilitate structural changes in the Aβ peptide structure. For example, certain epitopes of Aβ can elicit temperature-dependent conformational changes. These conformational changes can impact the rate, and the process of Aβ aggregation and deposition into plaques, as well as structural changes regarding the formation of a β-sheet (Hatip *et al.*, 2009). Such reports indicate the importance of a controlled temperature setting when preparing Aβ aggregates *in vitro*, as even the smallest of changes in the peptide environment may have a significant impact on the final morphology and structure of the Aβ preparations.

Another important factor to consider when preparing Aβ *in vitro* is the pH level of its environment. Aβ aggregation takes place at pH levels of below 10. Even though Aβ aggregation can take place under acidic and basic conditions, the greatest level of aggregation has been shown to occur at pH 6-8 (Kobayashi *et al.*, 2015; Tiiman *et al.*, 2015). Additionally, it has also been suggested that the Aβ aggregates are more neurotoxic when formed in more acidic conditions, as opposed to more neutral pH levels. As with temperature changes, changes in pH levels can result in structurally different aggregates. These changes depend on the acidic/ basic conditions of the peptide environment (Su and Chang, 2001). Therefore, a careful manipulation of the pH levels of the environment that the peptide is found in is crucial for ensuring that a reproducible Aβ peptide structure has been formed. The slightest changes in the peptide environment can have drastic effects on the final structure, characteristics, properties and potentially toxicity of Aβ. These could be detrimental when investigating the role of Aβ in disease, especially when investigating which Aβ structures elicit the most toxic effects in AD brains.

The formation of amyloid aggregates can be further influenced by the presence and concentration of salt ions in the peptide's environment. In the presence of salt ions, the aggregation of Aβ into fibrils is faster, as the time taken to enter the peptide growth phase is significantly reduced (Klement *et al.*, 2007). It has been suggested that $A\beta_{1\text{-}40}$ directly interacts with salt ions, which in turn can induce changes of the surface tension. There are structural changes associated with the fibrils formed in the presence of salt ions. In the absence of salt ions, $A\beta_{1\text{-}40}$ fibrils are longer, more regular, and well-

separated. Meanwhile, once salt ions are added, the fibrils can associate into bundles, with the fibrils being less regular and shorter with a smaller diameter (Klement *et al.*, 2007).

It is clear that there is an array of conditions that need to be carefully controlled when preparing the peptide, as every parameter that is changed will result in the formation of structurally and/or functionally different Aβ aggregate. When studying these peptides in a disease context, reproducibility is of high importance, to allow the correct conclusions to be drawn.

Even with a careful experimental design, the structural and functional variation of Aβ aggregates can still be observed. The Aβ isoforms used in experiments will also have an impact on the aggregation rate and final structure of the Aβ formed. Due to the non-specific enzymatic cleavage of APP to form Aβ, the resulting Aβ peptide includes isoforms ranging from 37-49 amino acid residues (Qi-Takahara *et al.*, 2005; Takami *et al.*, 2009; Haass *et al.*, 2012). The different Aβ isoforms can have an impact on the final morphology and structural changes of the aggregated peptides, as well as can impact the aggregation rate. Longer Aβ peptides at the C-terminal ($Aβ_{1-42}$ and $Aβ_{1-43}$) have an increased propensity to aggregate when compared to shorter Aβ peptides ($Aβ_{1-37}$, $Aβ_{1-38}$, and $Aβ_{1-40}$). This could be due to the differences in the content of amino acids present in the peptide structure (Vandersteen *et al.*, 2012a). Recent findings suggest that, for example, $Aβ_{40}$ and $Aβ_{42}$ isoforms can assemble into fibrils via varying aggregation processes, resulting in the formation of structurally and morphologically different fibrils (Wang, Eom and Kwon, 2021). Moreover, longer Aβ peptides have a higher propensity to form oligomers than shorter Aβ peptides, and these oligomers are morphologically and structurally different. Interestingly, when comparing the structure of longer and shorter Aβ isoforms, the latter form extended fibrils, whilst longer Aβ peptides form heavily intertwined fibril networks (Vandersteen *et al.*, 2012a). However, $Aβ_{1-40}$ and $Aβ_{1-42}$ are the most abundant and widely studied isoforms in the context of AD. The ratio of $Aβ_{42}/Aβ_{40}$ is significantly elevated in AD as compared to healthy controls (Kim *et al.*, 2015). Furthermore, it has been suggested that $Aβ_{42}$ is the main isoform present in amyloid plaques in AD, initiating the plaque pathology (Gouras *et al.*, 2000; R G Nagele *et al.*, 2003), and that it is the more neurotoxic isoform in AD, compared to $Aβ_{40}$ (Klein, Kowall and Ferrante, 1999). Therefore, $Aβ_{42}$ is considered as the most disease-relevant isoform, and it is the focus of this project.

## 2.2 Aims and Objectives

Careful preparation of well-characterised Aβ aggregates is essential to study the roles of Aβ in AD. There are many inconsistencies in Aβ preparations described in the literature and resulting Aβ preparations are not extensively analysed (Matuszyk *et al.*, 2022). Therefore, the aim of the work in this chapter was to develop robust methods for preparing oligomeric and fibrillary $Aβ_{1-42}$, as well as extracting Aβ from human brain tissue for comparison.

The objectives of this chapter were:

i. To prepare stable monomeric $Aβ_{1-42}$ by manipulating the pH levels and temperature of a commercially available recombinant $Aβ_{1-42}$.
ii. To characterise and validate monomeric $Aβ_{1-42}$ preparations using Asymmetric Flow Field Flow Fractionation analysis and Transmission Electron Microscopy.
iii. To derive distinct oligomeric and fibrillary preparations of $Aβ_{1-42}$ from the previously characterised monomeric $Aβ_{1-42}$.
iv. To characterise and validate oligomeric $Aβ_{1-42}$ preparations using Transmission Electron Microscopy, immunoblotting, and Size Exclusion Chromatography with Multiangle Light Scattering.
v. To characterise and validate fibrillary $Aβ_{1-42}$ preparations using Transmission Electron Microscopy, and Thioflavin T assay.
vi. To extract Aβ from AD brain tissue for comparison with *in vitro* synthesis Aβ.

## 2.3 Materials

### 2.3.1 Amyloid-beta chemistry

| | |
|---|---|
| $A\beta_{(1-42)}$ HFIP (Hexafluoroisopropanol) (0.5 mg) | rPeptide, A-1163-1 |
| $A\beta_{(1-42)}$ HFIP (1 mg) | rPeptide, A-1163-2 |
| $A\beta_{(1-42)}$ Scrambled (1.0 mg) | rPeptide, A-1004-2 |
| 0.75% Uranyl Formate stain | *0.0375 g uranyl formate; 5 mL boiling $ddH_2O$; add 5M NaOH until a slight change of colour; filtered through a 0.2 µm filter* |
| 10 mM HCl | |
| 2x Tris-buffered saline (TBS) (pre-adjusted) | *40 mM Tris base; 155 mM NaCl adjusted to pH 7.4; then add 45 mM HCl* |
| Low binding Eppendorf tubes (1.5 mL) | Eppendorf® LoBind, 022431081 |
| NaOH | *50 mM in $ddH_2O$* |
| Thioflavin T (ThT) | Sigma-Aldrich, T3516-5G |
| Tris-buffered saline (TBS) | *20 mM Tris/HCl, pH 7.4; 100 mM NaCl* |

### 2.3.2 Sodium dodecyl sulphate-polyacrylamide gel electrophoresis (SDS-PAGE)

| | |
|---|---|
| 10x Running Buffer | *144 g glycine; 30.2 g Tris Base; 10 g SDS; 0.9 L $H_2O$* |
| 10x Transfer Buffer | *144 g glycine; 30.2 g Tris Base; 0.9 L $H_2O$* |
| 1x PBS | *137 mM NaCl; 2.7 mM KCl; 10 mM $Na_2HPO_4$; $KH_2PO_4$; pH 7.4* |
| 1x PBS-Tween (PBS-T) | *1x PBS; 0.05% Tween-20* |
| 6x Laemmli Sample Buffer | *2.4 g SDS; 9.4 mL glycerol; 2.4 mL Tris 0.5M - pH 6.8; 4.2 mL dd$H_2O$; 24 mg bromophenol blue; 1.86 DTT* |
| Bovine Serum Albumin (BSA) | Sigma, 05482-100G |
| Novex™ 4-20% Tris-Glycine Mini Gels, WedgeWell™ format, (Gradient gels) | ThermoFisher Scientific, Invitrogen™, XP04202BOX |
| Ponceau stain | *0.1% (w/w) Ponceau S dye; 1% v/v acetic acid; in 500 mL dd$H_2O$* |

#### *Protein molecular weight marker*

Precision Plus Protein™ Dual Xtra Prestained Protein Standards protein ladder (Bio-Rad, 1610377) was used when immunoblotting Aβ detection. The protein markers range from 2 kDa to 250 kDa.

### 2.3.3 Immunoblotting antibodies

**Table 2.1.** Primary antibodies used for immunoblotting detection of Amyloid-beta.

| Antibody | Specificity | Species / type | Dilution | Source and catalogue number |
|---|---|---|---|---|
| 6e10, Purified anti-β-Amyloid, 1-16 Antibody | Reactive to amino acid residue 1-16 of Aβ and APP | Mouse / Monoclonal | 1:1000 | Biolegend, SIG-39320 |
| Oligomer A11 | Synthetic molecular mimic of soluble oligomers | Rabbit/ Polyclonal | 1:500 | Thermofisher Scientific, AHB0052 |

**Table 2.2.** Secondary antibodies used for immunoblotting detection of Amyloid-beta.

| Antibody | Raised species | Dilution | Source and catalogue number |
|---|---|---|---|
| Anti-rabbit IgG, HRP- linked antibody | Goat | 1:2000 | Cell Signalling Technology, 7074 |
| Anti-mouse IgG, HRP- linked antibody | Horse | 1:2000 | Cell Signalling Technology, 7076 |

## 2.4 Methods

The experimental procedures regarding the preparations of $A\beta_{1-42}$ monomers, oligomers and fibrils, as well as subsequent data analysis of $A\beta_{1-42}$ preparations were carried out with the help and supervision of Dr Rosemary Staniforth's group (Molecular Biology and Biotechnology, The University of Sheffield).

### 2.4.1 Monomeric amyloid-beta

#### *Preparation*

Human recombinant $A\beta_{1-42}$ (rPeptide®, cat: A-1163-1, A-1163-2) was dissolved in 50 mM sterile NaOH using a Hamilton syringe, to prepare a 1 mg/ml $A\beta_{1-42}$ monomeric solution. The peptide solution was further dissolved using a waterbath sonicator, at room temperature for 5 minutes. The prepared monomeric $A\beta_{1-42}$ stock solution was aliquoted into low-bind Eppendorf tubes, to ensure that the peptide does not interact with plastic material of standard Eppendorf tubes. Monomeric $A\beta_{1-42}$ aliquots were flash- frozen in liquid nitrogen and stored at -80$^{o}$C until further experiments. The pH level of the prepared monomeric $A\beta_{1-42}$ stock solution was checked using a pH strip, and a pH level of ~11 was achieved.

#### Asymmetric Flow Field Flow Fractionation

The prepared monomeric $A\beta_{1-42}$ was analysed using Asymmetric Flow Field Flow Fractionation (AF4) (AF2000 Multiflow, Postnova), coupled with multi-angle light scattering (MALS), allowing the determination of size and mass of eluted particles. The AF4 column was firstly washed with 50 mM NaOH buffer, then the peptide sample was loaded and allowed to elute.

When performing AF4 analysis, a sample is passed through the column channel by a laminar flow with a parabolic flow profile (fig.2.2). Forces inside the channel, which are perpendicular to this flow, allow particles to arrange themselves in different layers of thickness. The perpendicular flow inside the channel transports these particles through the column at different velocities. There is also a cross flow inside the channel, where particles can diffuse out through a semi-permeable membrane. However, particles also diffuse back into the channel, based on the principles of the Brownian motion. Smaller particles are then situated further away from the membrane, meeting the fastest part of the flow. Therefore, smaller particles move through the channel at higher velocities than larger particles, and elute out of the column first (Wagner *et al.*, 2014). At the end of the elution process, the particles encounter light scattering and UV detectors, which are used to further determine the parameters and characteristics of the eluted peptide.

The results were analysed using AF200 analysis software (Postnova), where distinct peaks corresponding to the eluting particles, can be observed. Based on the light scattering and

concentration detector data, information about molecular weight and size of eluting particles can be calculated, which is then used to predict and evaluate the final morphology of the peptide.

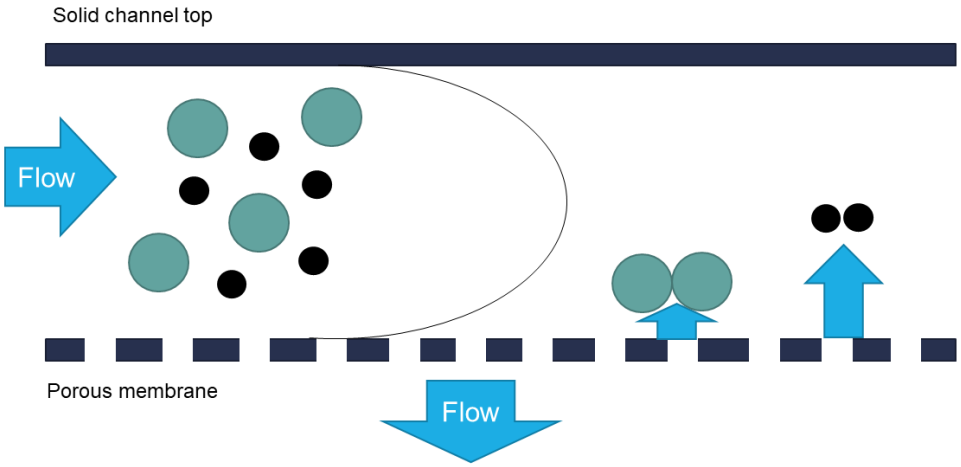


**Figure 2.2** The principles of Asymmetric Flow Field Flow Fractionation (AF4).

Schematic representation of events taking place inside the channel column during asymmetric flow field flow fractionation for sample analysis.

### 2.4.2 Preparing Amyloid-beta aggregates

#### *Oligomeric Amyloid-beta preparations*

Protocol optimisation was carried out prior to carrying out experiments using $A\beta_{1-42}$ oligomeric preparations. Oligomeric $A\beta_{1-42}$ was prepared using the following protocols:

1) Initially, oligomeric $A\beta_{1-42}$ preparation followed the protocol described by Stine *et al.* (2011), and Cerf *et al.* (2009). Briefly, the prepared 1 mg/mL monomeric $A\beta_{1-42}$ was dissolved in TBS buffer (20 mM Tris/HCl, 100 mM NaCl, pH 7.4) to a final concentration of 100 µM, and incubated at 4$^{o}$C for 24 hrs.
2) Later, a refined protocol was developed to account for the high pH level of the 1 mg/mL monomeric $A\beta_{1-42}$. The monomeric $A\beta_{1-42}$ preparation was dissolved in 2xTBS buffer (40 mM Tris base; 155 mM NaCl adjusted to pH 7.4; then add 45 mM HCl), pre-adjusted to a correct pH with 45 mM HCl, to a final concentration of 100 µM. The $A\beta_{1-42}$ peptide preparation was incubated at 4$^{o}$C for 24 hrs, 72 hrs and 2 weeks.

#### *Fibrillary Amyloid-beta preparations*

Protocol optimisation was carried out prior to carrying out experiments using $A\beta_{1-42}$ fibrillary preparations. Fibrillary $A\beta_{1-42}$ was prepared using the following protocols:

1) Initially, fibrillary $A\beta_{1-42}$ preparation followed the protocol described by Stine *et al.* (2011). Briefly, 1 mg/mL monomeric $A\beta_{1-42}$ was dissolved in 10 mM HCl (pH 3.01), to a final concentration of 100 µM, and incubated at 37$^{o}$C for 24 hrs.
2) Later, to account for the high pH levels obtained due to the 50 mM NaOH present in the monomeric $A\beta_{1-42}$, a refined protocol was developed. 1 mg/mL monomeric $A\beta_{1-42}$ was dissolved in 2xTBS buffer (pH 7.4), pre-adjusted to a correct pH with 45 mM HCl, to a final concentration of 100 µM. The preparation was incubated at 37$^{o}$C for 24 hrs.

### 2.4.3 Characterisation of the Amyloid-beta aggregates

#### *Size Exclusion Chromatography and Size Exclusion Chromatography with Multi-Angle Light Scattering*

Size exclusion chromatography (SEC), and size exclusion chromatography with multi-angle light scattering (SEC-MALS) were carried out to analyse oligomeric $A\beta_{1-42}$ preparations. SEC is a robust method, which separates molecules according to their size. The molecules have different retention times, which are dependent on the time spent diffusing in and out of the pores present in the SEC column during the stationary phase. Therefore, the molecules can elute out of the SEC column at different times. Reference molecules and proteins are used to help construct a calibration curve, based on which the molecular weight of the analyte can be derived (Some *et al.*, 2019).

SEC can be coupled with MALS and differential refractive index (dRI) detectors. A MALS detector measures the proportion of light scattered by the molecules of interest into multiple angles. A dRI detector determines the concentration of the analyte based on the change in solution refractive index. In SEC-MALS, the retention times has no significance on the analysis, and is used only for separation of molecules so that they enter the concentration detector individually. Hence, the reference standards are not needed (Some *et al.*, 2019).

Initially a Superdex75 10/300 GL column (GE Healthcare Life Sciences) was used for analysis of Aβ oligomers. However, due to difficulties in detecting oligomers due to their potential size range, a Superdex200 10/300 GL (GE Healthcare Life Sciences) was subsequently used to increase detection range. The eluted samples were analysed on the AF2000 analysis software (Postnova, Postnova Analytics GmbH, Germany), where distinct peaks of interest were observed. For SEC analysis, the peaks were compared to known protein standards. For SEC-MALS, the software was able to determine the MW and distribution of the molecules within the sample.

#### *Electron Microscopy*

$A\beta_{1-42}$ preparations were qualitatively analysed using transmission electron microscopy (TEM). Carbon-coated grids were glow-discharged for a minimum of 30 seconds prior to loading 5 µL of 100 µM prepared $A\beta_{1-42}$. Protein samples were left to adsorb for 1 minute on the carbon-coated grids. The grid was washed twice in $ddH_2O$, followed by a wash in 0.75% Uranyl Formate, and then negatively stained with 0.75% Uranyl Formate for 20 seconds. Remaining moisture was removed by blotting with Whatmann filter paper and aspiration using a small vacuum pump. Negatively stained grids were stored in darkness until further analysis. Carbon-coated grids were imaged using TEM (Philips/FEI CM 100).

### *Sodium Dodecyl Sulphate – Polyacrylamide Gel Electrophoresis and immunoblotting*

Sodium Dodecyl Sulphate – Polyacrylamide Gel Electrophoresis (SDS-PAGE) and immunoblotting were carried out to optimise methods for routine analysis of $A\beta_{1-42}$ preparations.

Varying concentrations (100 ng, 10 ng and 1 ng) of $A\beta_{1-42}$ oligomers and fibrils were loaded on Novex™ 4-20% Tris-Glycine gradient gels for detection by immunoblotting with the 6e10 antibody (Biolegend, SIG-39320), which is known to specifically recognise amino acid residues 1-16 of Aβ, but it also has been reported that the 6e10 antibody maps to residues 4-10 of Aβ (Baghallab *et al.*, 2018). The sample boiling step was omitted, to avoid changing the conformation of the oligomers/ fibrils. The gel was run at 120 V until the dye-front has reached the bottom of the gel (XCell SureLock™ Mini-Cell and XCell II™ Blot Module, Invitrogen™). The gel was transferred using a wet transfer system, for 1 hour at constant 0.33 A onto a 0.2 µm nitrocellulose membrane. The membrane was incubated with the 6e10 primary antibody at 4°C overnight on a roller.

Following incubation in primary antibody, membranes were washed 3 times in PBS-T (10 minutes/ wash), and incubated with a species-specific Horseradish Peroxidase (HRP)-conjugated secondary antibody (Table 2.2) for 1 hour at ambient temperature, and washed a further three times in PBS-T, on a roller. Signal was detected using enhanced chemiluminescence (ECL). Membrane was imaged using the G:BOX (Syngene).

### *Dot blot and immunoblotting*

Dot blots were used to detect oligomeric $A\beta_{1-42}$ to confirm their presence. 0.2 µm nitrocellulose membrane (GE Healthcare) was soaked in 1x transfer buffer and assembled onto the 96-well Bio-Dot® apparatus (Bio-Rad, 1706545). 1 µM of oligomeric $A\beta_{1-42}$ diluted in 1x PBS was dotted onto nitrocellulose membrane for analysis. Empty wells were filled with 200 µL of 1x PBS. Dot blot was left to dry using a vacuum for 20 minutes. Afterwards, the nitrocellulose membrane was removed, and wells of interests marked. The membrane was left to air-dry at room temperature for 1 hour.

Membrane was then placed in a blocking solution (5% milk (Marvel)/ TBST) for 1 hour at room temperature to block non-specific binding of primary antibodies. Membrane was incubated in primary antibodies (table.2.1) overnight, on a roller, at 4°C. A11 antibody was used to detect oligomeric $A\beta_{1-42}$. 6e10 antibody was used to detect all conformations of $A\beta_{1-42}$. Following incubation in primary antibody, membrane was washed three times (10 minutes/ wash) with TBST and incubated with species-specific HRP-conjugated secondary antibody (table.2.2) for 1 hour, at room temperature. Membrane was further washed three times (10 minutes/ wash) with TBST. Signal was detected using ECL, and membrane was imaged using the G:BOX system (Syngene).

Densitometric signal quantification of the chemiluminescent images was performed using the GeneTools software (Syngene). Specific bands were selected manually, and background readings were subtracted automatically.

#### *Thioflavin T assay*

Thioflavin T (ThT) assay was carried out to detect fibril formation and investigate the progression of Aβ aggregation. The parameters measured the fluorescence of Aβ fibrils, scrambled peptide, PBS, vehicle control and ThT only.

Aβ fibrils, or scrambled peptide, were detected at 100 µM with added 20µM of ThT. The samples were allowed to aggregate overnight in a PHERAstar Microplate Reader, at 37$^{o}$C, with hourly fluorescence readouts.

## 2.5 Results

### 2.5.1 Monomeric Amyloid-beta preparation

Monomeric $A\beta_{1\text{-}42}$ was analysed using AF4. Monomeric $A\beta_{1\text{-}42}$ was injected onto AF2000 MultiFlow Universal Separator (Postnova). A plot of detector signal versus retention time was obtained. Of the sample injected, 95% was recovered and eluted from the column. In the initial analysis both column and buffer noise were present (fig.2.3.). This could be due to the left-over material not being removed from the column during the wash-step, or small amounts of contamination in the buffer. However, the region of interest limits were narrowed down to exclude this from the final analysis (fig.2.3). The regions of interest were always adjusted to the peak signals of the UV detector. The light scattering detector alongside the UV detector are used to measure the molecular weight and concentration of the sample.

The majority of the monomeric $A\beta_{1\text{-}42}$ was eluted from the column after 5 minutes. This corresponded with a peptide size of 4072 Da, suggesting the sample was largely monomeric, as the molecular weight of $A\beta_{1\text{-}42}$ is ~4514.1 Da. The monomeric sample fully eluted out of the AF4 column after 10 minutes (fig.2.3).

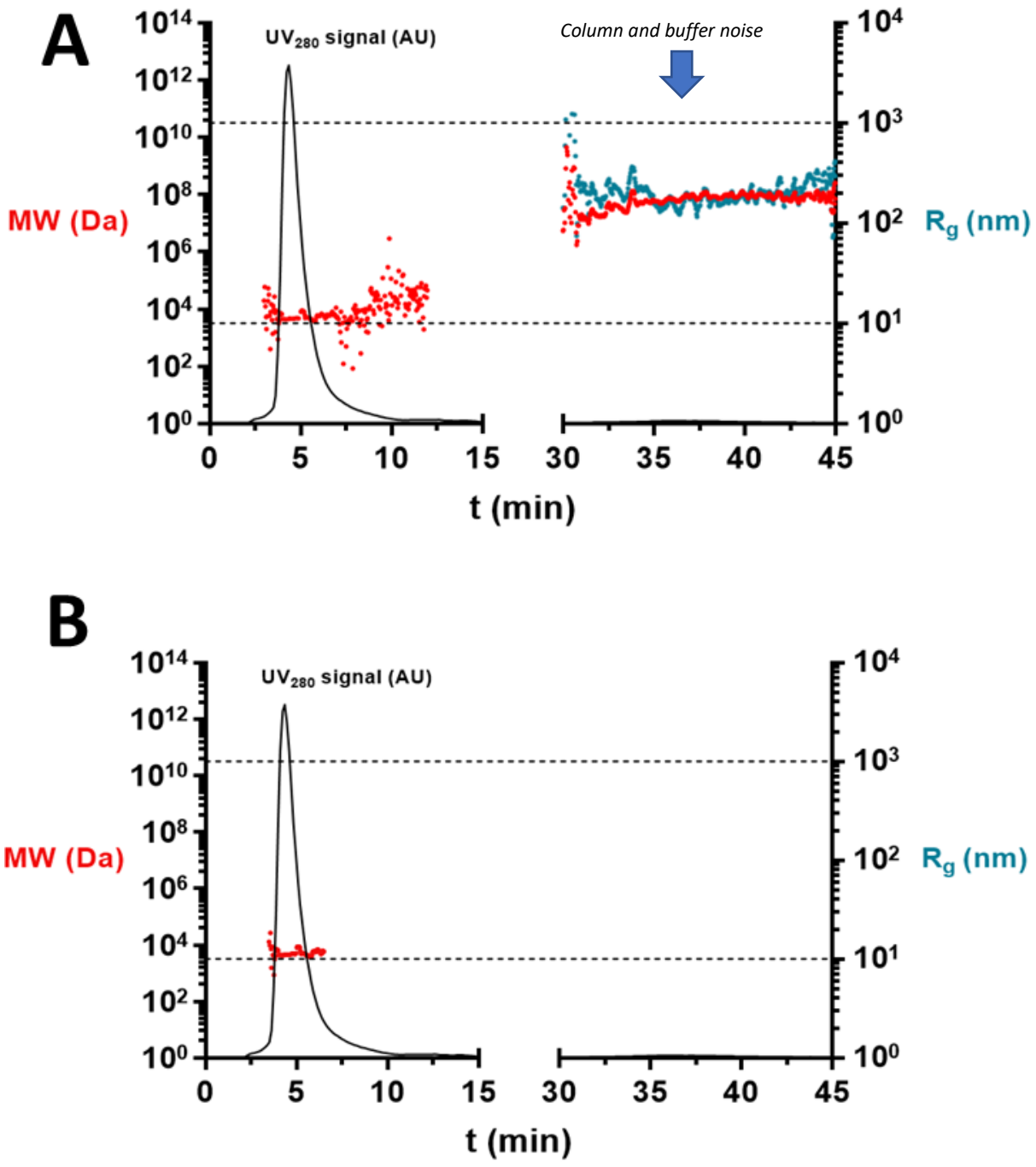


**Figure 2.3.** AF4 analysis of prepared monomeric $A\beta_{1-42}$

Elugram showing sample elution time, the corresponding molecular weight (Mw) and radius of gyration (Rg) for monomeric $A\beta_{1-42}$. **(A)** The elugram shows the column and buffer noise data (annotated), before trimming. **(B)** Elugram shows final, trimmed data, which corresponds to the monomeric $A\beta_{1-42}$ signal (representative graph of n=3).

AF4 analysis can separate soluble and colloidal components over a wide size range, as well as sensitive and "sticky" samples, since there is no stationary phase. AF4 coupled with multi light scattering (MALS) detectors allowed for the detection of specific regions of interest, based on the light scattering and UV signals. Using the equipment PostNova software, the peptide mass at each time point of elution was calculated, based on the specific regions of interest selected.

The light scattering and UV detectors provided the refractive index measurement, which was used to determine concentration of the protein (fig.2.4.). Masses across the protein peak were averaged. The ratio between number average molecular weight (Mn) and the weight average molecular weight (Mw) provided the information about the dispersity of the sample. The polydispersity index (PDI) calculated by the software was ~2.475, indicating the sample was polydisperse. The Zimm plot is a graphical representation of the sample data plotted linearly. The plotted data corresponds to the Rayleigh Ratio, from which molar mass and radius of gyration can be derived. Rayleigh Ratio characterises the intensity of scattered light at a specific scattering angle (in this case $90^{o}$ light scattering), which determines the mass-average molecular weight of the sample. Meanwhile, radius of gyration measures the distance of the centre of mass and the size of an object or surface, at multiple points, revealing the compactness of the sample. This means that Aβ monomers would have a radius of gyration closer to 1, as they are more compact than the aggregated forms.

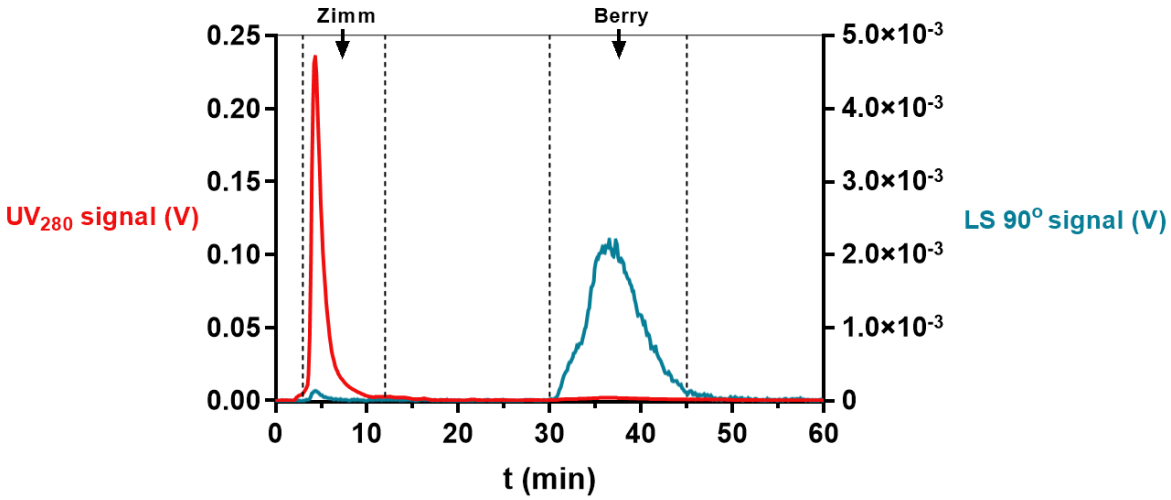


**Figure 2.4.** UV and Light Scattering signal of monomeric $A\beta_{1-42}$.

A graph showing the UV signal and Light Scattering signal at 90° for the monomeric $A\beta_{1-42}$ preparation, against the sample elution time. The values from these plots can be used for concentration and mass calculations. Zimm plot = inverse intensity plot. Berry plot = variation of Zimm, where intercept yields the reciprocal of $Mw^2$ (representative graph of n=3).

AF4 with MALS analysis estimated the molecular weight of the peptide to be ~4574 Da (fig.2.5). This analysis also showed that the sample was largely monomeric; however, there may also be small amounts of dimer present in the preparation. The small amounts of $A\beta_{1-42}$ dimer should not affect the stability of the monomer, due to the high pH provided by NaOH, as well as low storage temperature of -80°C. Further analysis showing the cumulative proportion of monomers and dimers in the sample confirmed this observation. There were no trimers and other large protein conformations present in the sample.

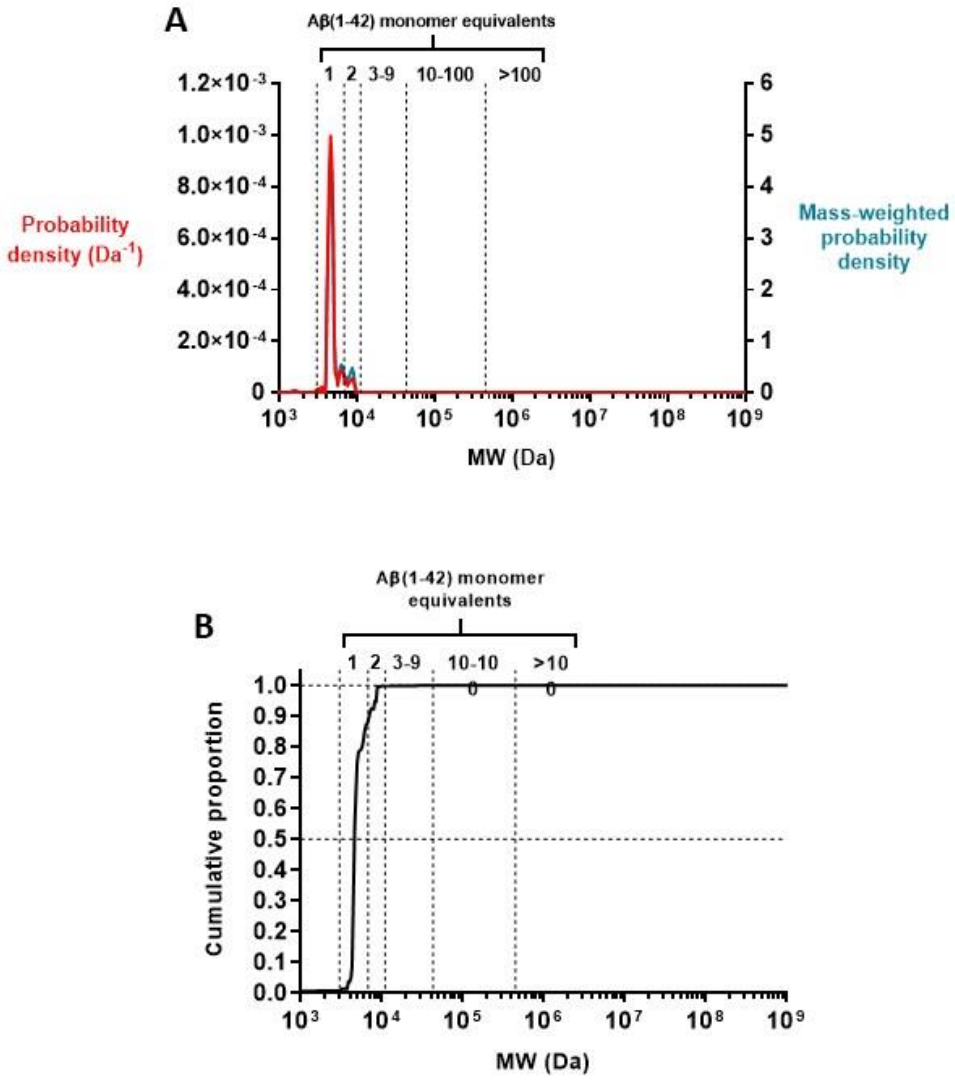


**Figure 2.5** AF4 analysis of monomeric $A\beta_{1-42}$ preparation.

**(A)** Observed probability density and the calculated mass-weighted probability density of the prepared $A\beta_{1-42}$ peptide eluted from the AF4 column. **(B)** Cumulative proportion of $A\beta_{1-42}$ monomer present in the elution sample. MW; molecular weight. Both were calculated based on the light scattering and UV detectors, enabling predition of the molecular weight and peptide shape, (representative graphs of n=3).

Overall, the final sample prepared by the addition of 50 mM NaOH, is a monomeric form of $A\beta_{1-42}$, at a final concentration of 1 mg/ml. The molecular weight distribution shows that the sample corresponds to the correct MW for $A\beta_{1-42}$, which is around 4574 Da. There was no signal detected, which would suggest that larger Aβ aggregates have formed, indicating a high purity of the monomeric material.

### 2.5.2 Initial protocol for preparing oligomeric and fibrillary amyloid-beta

Protocols described by Stine et al. (2011), Cerf et al. (2009) were initially used to derive oligomeric, and fibrillar $A\beta_{1-42}$. The methods for deriving $A\beta_{1-42}$ aggregates are described in detail in section 2.4.2 of the thesis. Preparations were analysed by immunoblotting, EM and SEC-MALS, the methods corresponding to the characterisation and analysis of these preparations are described in section 2.4.3 of the thesis.

#### *Immunoblotting analysis*

Firstly, immunoblotting analysis was carried out to characterise the prepared aggregated $A\beta_{1-42}$. For the analysis, 1 ng, 10 ng and 100 ng of monomer, oligomer and fibril preparations were diluted in 6X Laemmli sample buffer, without boiling, and loaded onto 4-20% gradient gels. Immunoblotting with the 6e10 antibody against amino acid residues 1-16 of human Aβ revealed the presence of a band at approximately 17 kDa for all Aβ aggregation species, where 100 ng was loaded onto the gel (fig.5). No signal was detected when 1 ng or 10 ng of Aβ was loaded, indicating that immunoblotting detection limits were reached.

The oligomeric Aβ preparation resulted in the strongest band at ~17 kDa, suggesting that this preparation contained the most oligomers. Presence of the ~17 kDa band in the monomeric Aβ sample was also detected, however at a much lower intensity than the oligomer preparation, which indicated that Aβ aggregation into larger species might have taken place. Lower molecular weight species were not retained on the gel, and therefore it was not possible to confirm whether any monomers were present in the sample. Fibrillary Aβ had a similar band profile to monomeric Aβ, which may be due to high molecular weight aggregates not entering the gel, but also could be due to the insufficient aggregation taking place. It may also be due to the fact, that the gels were run under reducing conditions, which denatures proteins. Furthermore, it was not possible to quantify the bands, therefore the analysis remained qualitative. Due to these technical difficulties, future experiments utilised dot blots to characterise Aβ preparations.

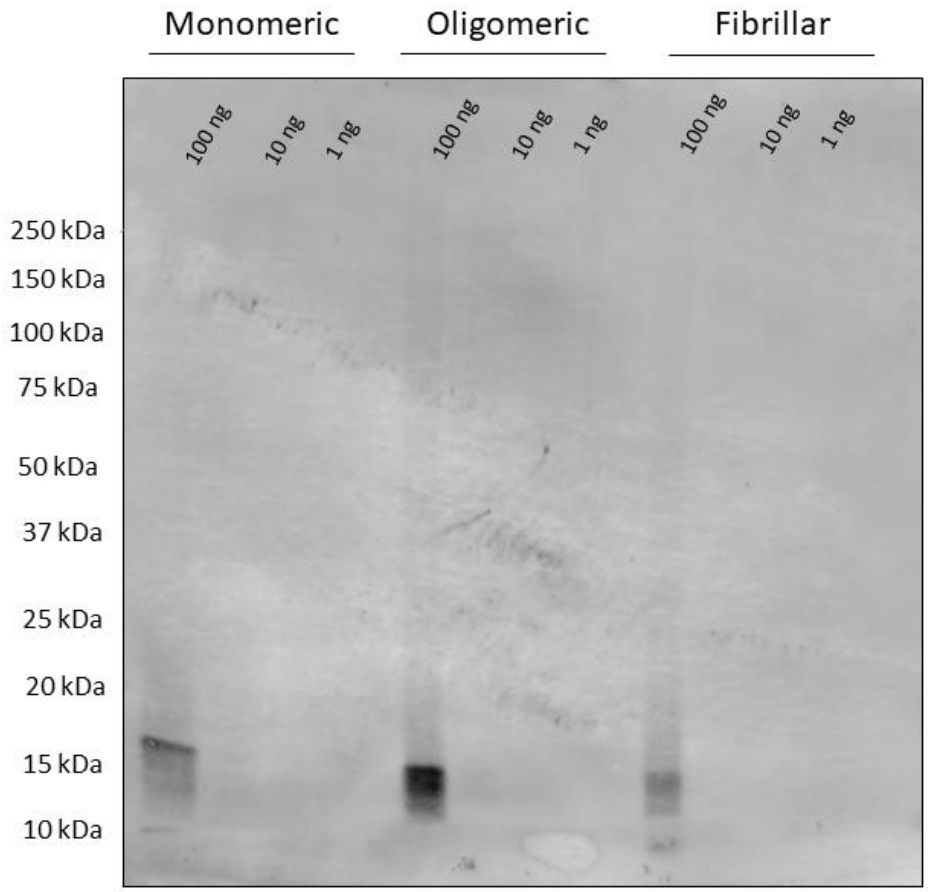


**Figure 2.6.** Comparison of monomeric, oligomeric and fibrillar $A\beta_{1-42}$ preparations

Immunoblotting comparison of monomeric, oligomeric and fibrillar preparations of $A\beta_{1-42}$, at different concentrations of the protein. 6e10 anti-amyloid antibody was used at a concentration of 1:1000; samples were loaded on the Novex 4-20% Tris-Glycine Mini Gel (gradient gel), (n=1).

*Transmission electron microscopy*

To determine the morphology of Aβ aggregates, the 'oligomeric' and 'fibrillary' $A\beta_{1-42}$ preparations were analysed by transmission electron microscopy (TEM). Protein samples were negatively stained with 0.75% uranyl formate (fig.2.7). Qualitative analysis of the preparations revealed a low yield of aggregation. Oligomers were mostly localised around long Aβ fibrils (fig.2.7.a), suggesting the aggregation process was inefficient. TEM micrographs of fibrillar $A\beta_{1-42}$ preparation also indicated an inefficient aggregation process. The fibrils formed were sparse, long and not associated with other fibrils in obvious aggregates (fig.2.7.b).

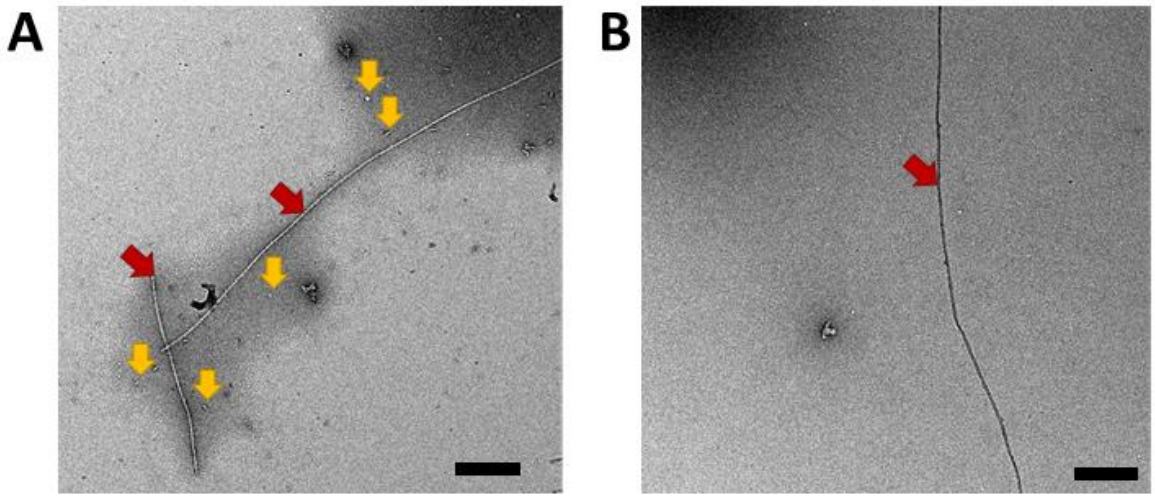


**Figure 2.7.** Representative transmission electron microscopy micrographs for $A\beta_{1-42}$ preparations

Electron microscopy micrographs showing $A\beta_{1-42}$ aggregates prepared prior to protocol re-optimisation. **A**. $A\beta_{1-42}$ oligomers (yellow arrows) surrounding long $A\beta_{1-42}$ fibrils (red arrows). Oligomers prepared by dissolving monomeric $A\beta_{1-42}$ in TBS buffer (20 mM Tris/HCl, 100 mM NaCl, pH 7.4) to a final concentration of 100 µM and incubating at 4°C for 24 hrs. **B.** Sparse and long $A\beta_{1-42}$ fibril (red arrow), not forming obvious aggregates. Fibrils prepared by dissolving monomeric $A\beta_{1-42}$ in 10 mM HCl (pH 3.01), to a final concentration of 100 µM, and incubating at 37°C for 24 hrs. Scale bars= 0.2 µm (representative images of n=3).

*SEC-MALS analysis*

$A\beta_{1-42}$ 'oligomer' preparations were further analysed by SEC-MALS to determine the molecular weight of peptides. SEC columns Superdex75 (3 kDa - 70 kDa detection range), as well as Superdex200 (10 kDa - 600 kDa detection range) were used to detect varying molecular weight ranges of $A\beta_{1-42}$ oligomers. SEC-MALS analysis on $A\beta_{1-42}$ 'fibril' preparations was not performed, because the cut-off points of the available columns would not detect such high molecular weight particles, which would correspond to the fibrillary $A\beta_{1-42}$.

Initial analysis revealed that the 'oligomeric' $A\beta_{1-42}$ preparation did not differ from the starting peptide material of monomeric $A\beta_{1-42}$, suggesting that the sample remained largely monomeric, and that aggregation did not take place (fig.2.8). The 'oligomeric' $A\beta_{1-42}$ sample was compared to known sizes of other standard proteins. Blue dextran is a column marker used to determine the void volume of the column. Insulin monomer has a molecular weight of 5.8 kDa, biophosphoglycerate mutase (bPGM) monomer has a molecular weight of 30 kDa, whilst BSA monomer has a molecular weight of 66.5 kDa. Smaller particles need more elution time, as they pass into the porous membrane inside the column. The elution time is a good estimate of the size of particles passing the column. Oligomeric Aβ ranges from less than 10 kDa to more than 100 kDa (Sakono and Zako, 2010), therefore oligomeric Aβ would be expected to elute at around the same time as BSA or bPGM, however, this was not the case. The 'oligomeric' sample eluted at the same time as monomeric $A\beta_{1-42}$, and at a similar time to insulin, further suggesting that the prepared sample was largely monomeric.

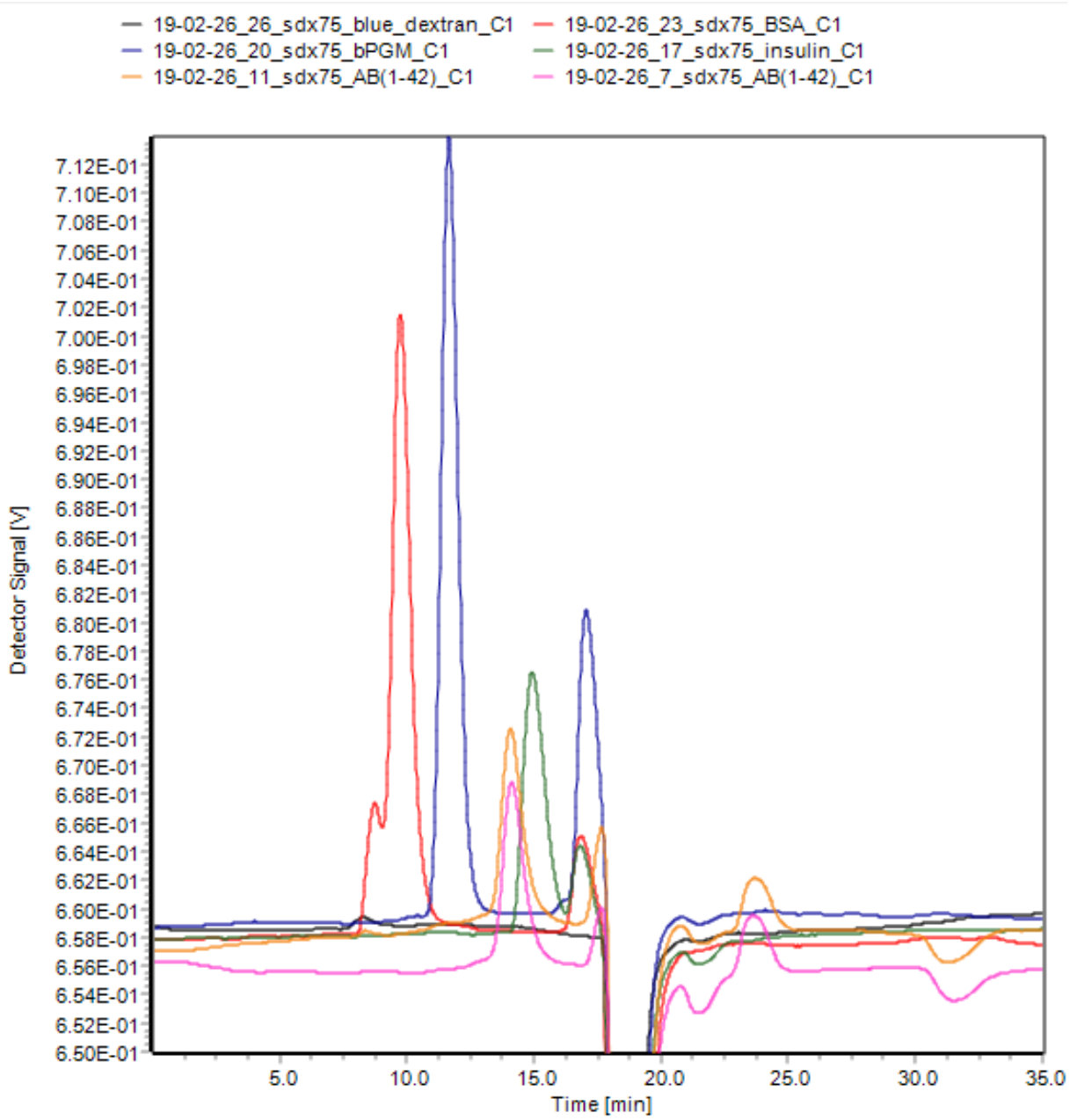


**Figure 2.8.** Size exclusion chromatography comparison of standards and oligomeric $A\beta_{1-42}$

A representative graph showing the UV detector signal and the elution time for the prepared 'oligomeric' Aβ sample (magenta), compared to other known protein standards, as well as monomeric Aβ (orange). The graph was produced using the AF2000 Postnova software and reveals that the prepared 'oligomeric' sample is monomeric. Protein standards are listed above the graph. **A**) An enlarged copy of the image of the relevant peaks for clarity (n=3).

'Oligomeric' $A\beta_{1-42}$ samples were initially passed through the Superdex75 column three times, and analysis was carried out using AF2000 software (Postnova). One region of interest was identified for all three runs (n=3). The regions of interest were chosen based on 90° light scattering, and 280 nm UV readout from the concentration detector, as well as Zimm plot, calculated by the software.

All regions of interest corresponded to a monomeric peak (fig.2.9). The analysis showed that the molecular mass of the peptide was ~4,262 Da, and this corresponded to 100% of the relative amount of peptide detected and analysed. The PDI measures the ratio of sample molecular weight and sample molecular mass. The PDI values for the samples were ~1.1, indicating a homogeneous peak, where the range of size distribution of peptides is not high. This further showed that the protocol resulted in a preparation that has not aggregated and remained as a stable monomer. The aggregation process was not efficient. However, the Superdex75 column may not be suitable for detecting higher molecular weight peptides. To investigate this possibility, a larger capacity column, Superdex200, was subsequently used.

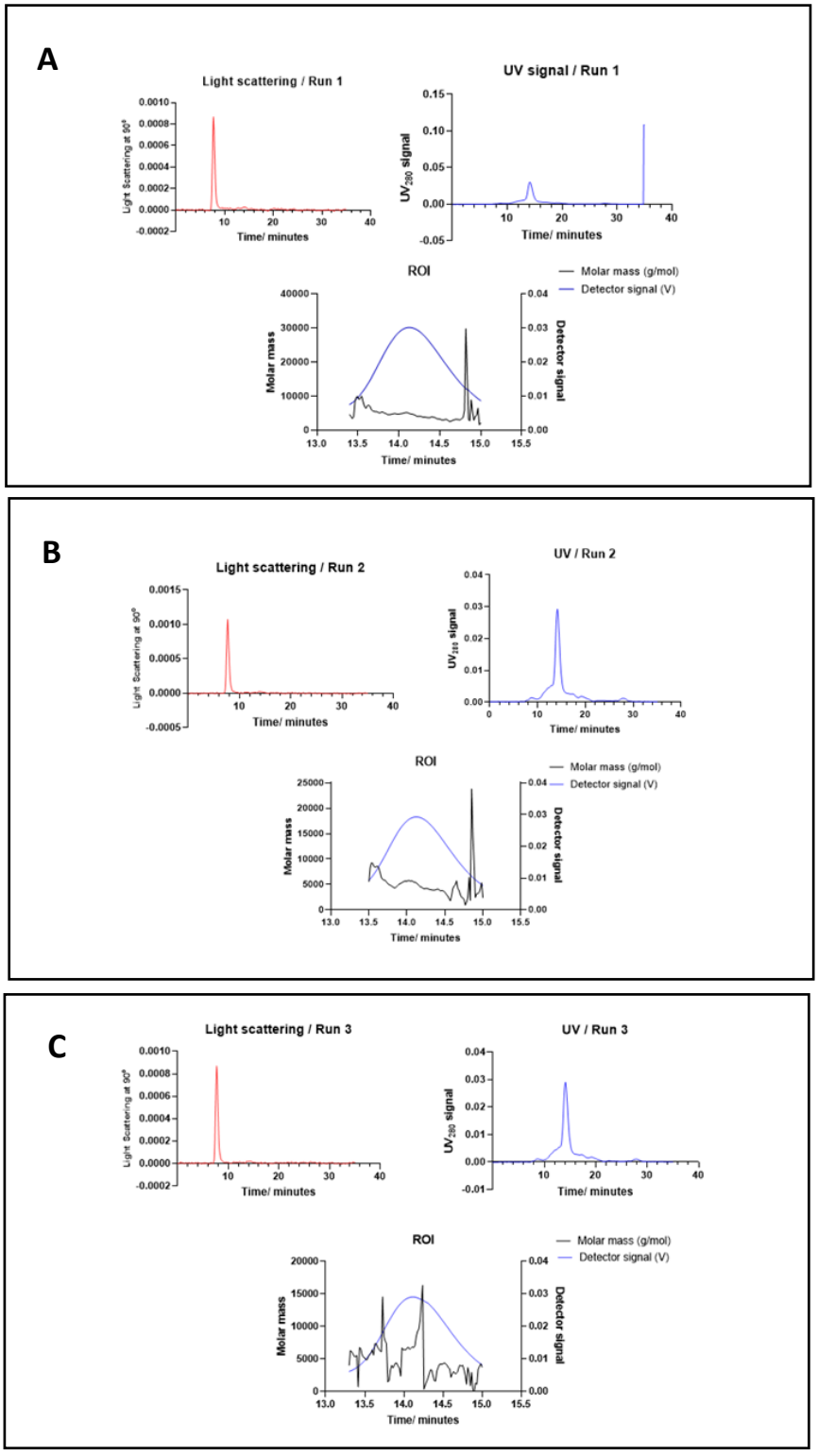


**Figure 2.9.** Size-exclusion chromatography elugrams for oligomeric $A\beta_{1-42}$ preparations, using the Superdex75 column.

Data corresponds to three separate runs (A-C) of 'oligomeric' sample. Light scattering and UV elugrams peaks correspond to the time of peptide elution and detection signal, which shows the calculated molar mass of eluted peptide. The region of interest (ROI) corresponds to the peptide signal at a time point where the sample data most closely resembled the calculated Zimm plot, from which the molar mass is further confirmed. N=3

The Superdex 200 column, which is capable of detecting larger proteins in the range of 10 kDa to 600 kDa, indicated that the sample was largely monomeric (fig.2.10). The results indicated that there could be smaller oligomers present in the sample. However, the relative amount of the 'oligomeric' sample recovered was less than that of monomers. Furthermore, the results had a high PDI value, indicating that the sample could be heterogenous, or approaching the detection limits for lower-molecular weight peptides. High PDI values make it difficult to determine the identity of the Aβ species present in the preparation. The results prompted revision of the original protocol, and further optimisation.

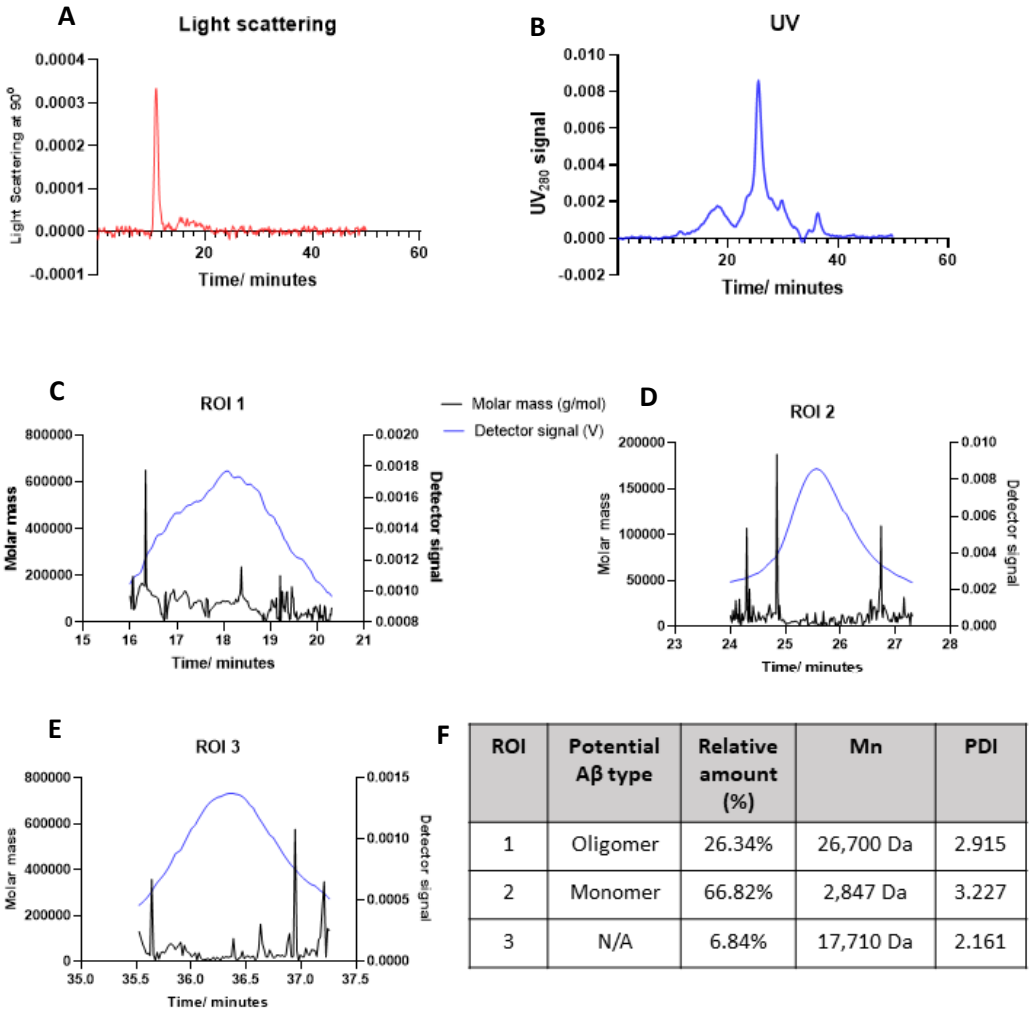


F

| ROI | Potential Aβ type | Relative amount (%) | Mn | PDI |
|---|---|---|---|---|
| 1 | Oligomer | 26.34% | 26,700 Da | 2.915 |
| 2 | Monomer | 66.82% | 2,847 Da | 3.227 |
| 3 | N/A | 6.84% | 17,710 Da | 2.161 |

**Figure 2.10.** Size-exclusion chromatography elugrams for oligomeric $A\beta_{1-42}$ preparations, using the Superdex200 column.

Elugrams showing $A\beta_{1-42}$ sample elution times from the Superdex200 column. Light scattering elugram (A) indicates that there is heterogeneity in the sample. UV signal detected three significant regions of interest (ROI) based on the UV detection signal (B). The three regions of interest are characterised (C-E). The three regions of interest correspond to different $A\beta_{1-42}$ aggregates, with differing molecular weights calculated based on the UV and light scattering detection signals (F). All data is reported at time points where the sample data most closely resembled the Zimm plot calculated by the AF2000 software (n=3).

### 2.5.3 Revised protocol for preparing oligomeric and fibrillary amyloid-beta

The initial preparation method generated predominantly monomeric $A\beta_{1-42}$, as aggregation of the peptide was inefficient, resulting in low aggregation yields, and insufficient aggregated Aβ morphology. Therefore, the protocol was revised. This is due to the suspicion that the highly alkaline conditions, in which the monomeric $A\beta_{1-42}$ was prepared, most likely inhibited the aggregation process. As mentioned previously, Aβ aggregation can be affected by pH levels (Stine Jr. *et al.*, 2003). Therefore, the preparation was amended to account for the initial high pH and to allow a more efficient Aβ aggregation process to take place. The full methods for the optimisation steps are described in section 2.4.2. $A\beta_{1-42}$ oligomers were incubated at 4°C for 24 hours, 72 hours and 2 weeks; whilst $A\beta_{1-42}$ fibrils were incubated for 24 hours at 37°C.

#### *Transmission electron microscopy*

EM was used to analyse $A\beta_{1-42}$ oligomers and fibrils, prepared using the amended protocol. EM analysis, using negative staining with 0.75% uranyl formate of the $A\beta_{1-42}$ oligomers incubated for 2 weeks, revealed a high yield of oligomeric $A\beta_{1-42}$ (fig.2.11). Large oligomers were visible (Fig.2.11, yellow box); it is also possible that these aggregates represented small protofibrils.

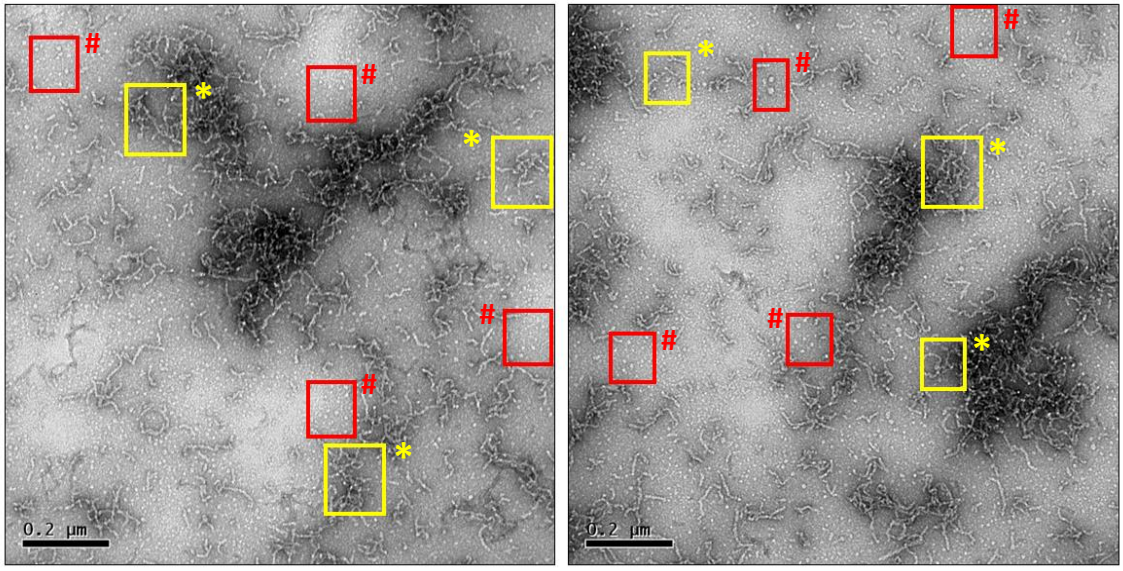


**Figure 2.11.** Electron microscopy images of $A\beta_{1-42}$ oligomers.

Aβ preparations incubated for 2 weeks at 4 °C were negative stained with 0.75% uranyl formate and imaged**.** Representative electron microscopy micrographs showing $A\beta_{1-42}$ oligomers. The micrographs show aggregates corresponding to small oligomers (red boxes, labelled #), as well as aggregates corresponding to larger oligomers (yellow boxes, labelled *). Scale bars= 0.2 µm.

EM analysis also showed that the revised protocol generated an improved yield of fibrillar $A\beta_{1-42}$ (fig.2.12). The $A\beta_{1-42}$ was largely aggregated into fibrils. No $A\beta_{1-42}$ oligomers were observed on the EM micrographs (fig.2.12), suggesting that the fibrillar $A\beta_{1-42}$ preparation was predominantly fibrillary.

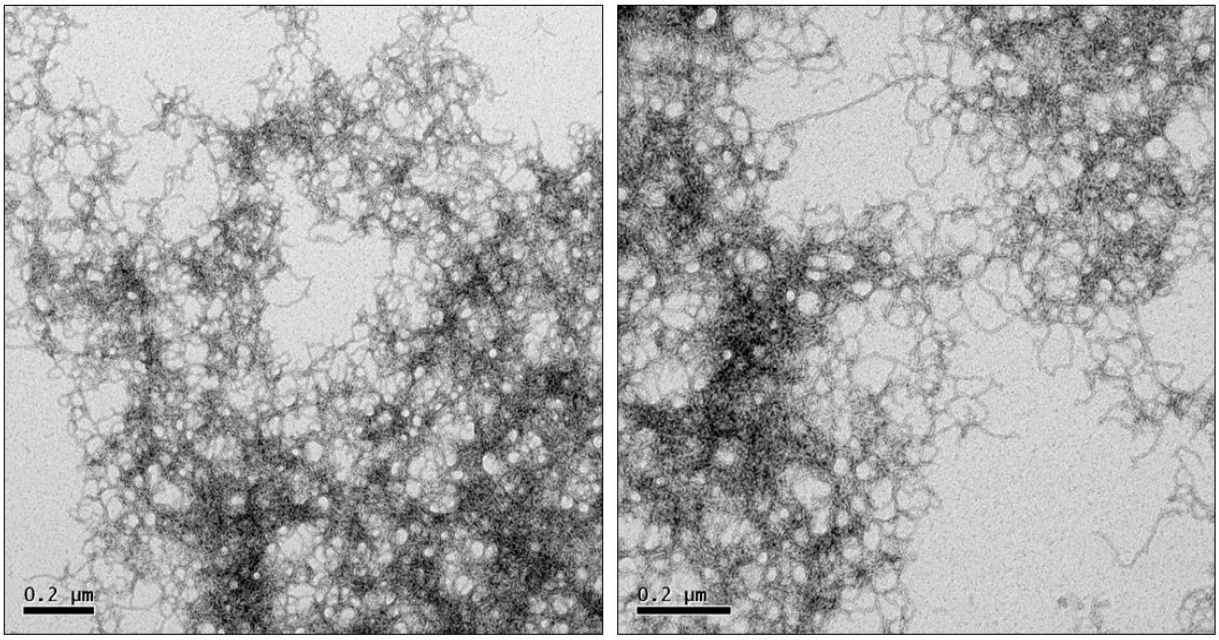


**Figure 2.12** Electron microscopy images of fibrillary $A\beta_{1-42}$

Representative electron microscopy micrographs of $A\beta_{1-42}$ fibrils prepared by dissolving monomeric $A\beta_{1-42}$ in 2xTBS, accounting for high pH of monomeric $A\beta_{1-42}$ used as starting material. Micrographs show aggregated $A\beta_{1-42}$ fibrils. Micrographs were negatively stained with 0.75% Uranyl Formate Stain. Scale bars= 0.2 µm. Representative images of n=3.

### *SEC-MALS analysis*

SEC-MALS can provide a quantitative estimation of the amount of oligomeric Aβ present, given as a percentage; therefore, this method of analysis was utilised for the analysis of oligomers prepared using the amended preparation method. Samples were incubated for 24 hours, 72 hours and 2 weeks, and analysed using SEC-MALS with a Superdex200 column.

24-hour incubation of Aβ resulted in three significant regions of interest (fig.2.13). 69.29% of the sample eluted corresponded to a monomeric peak, however the PDI value was high. This indicated a degree of heterogeneity within the sample, and therefore the reported molecular mass of the peptide may not be the true value. 25.61% of the sample corresponded to an oligomer of 151,000 Da, with a PDI value of 1.17. This suggested that the oligomer was largely homogeneous. The third peak could correspond to a dimer or small peptide fragments, which were retained in the column. It was not possible to distinguish these, as the PDI value was high for this peak.

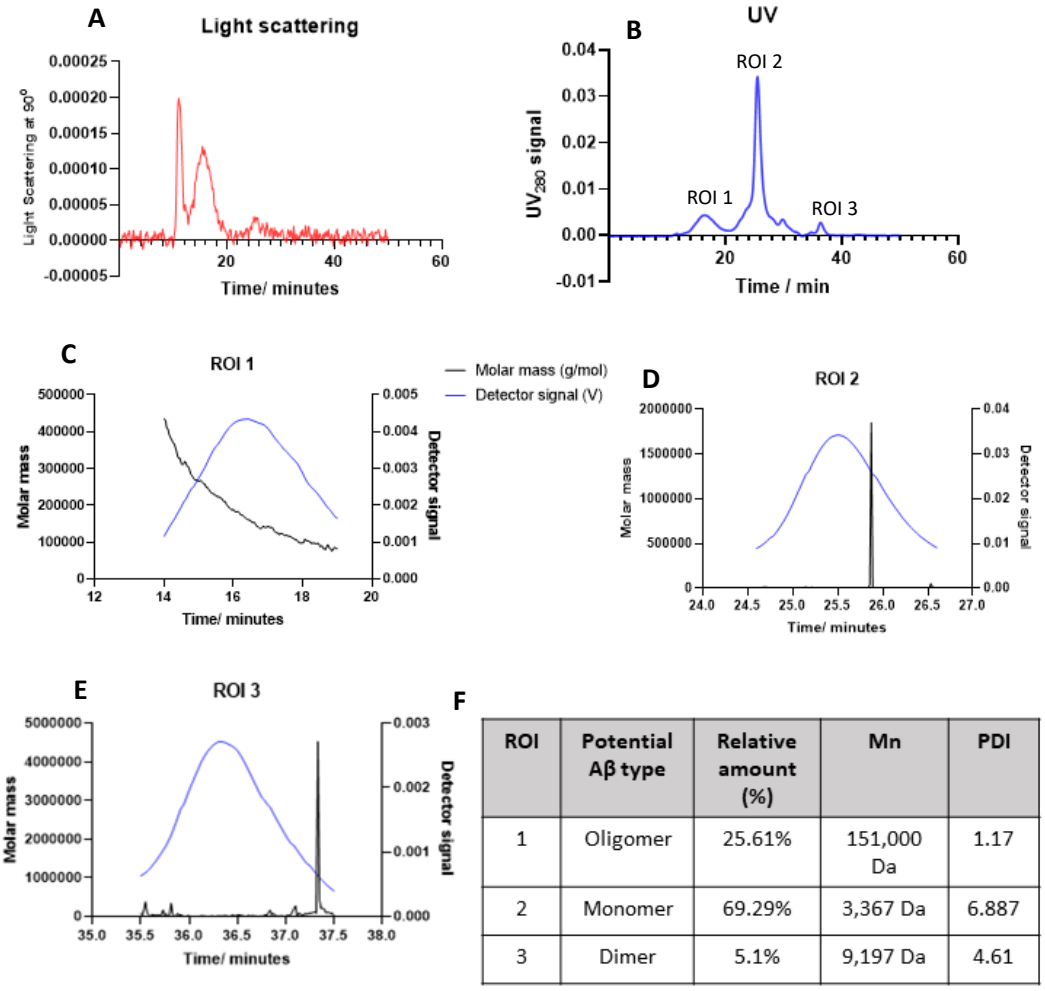


| ROI | Potential Aβ type | Relative amount (%) | Mn | PDI |
|---|---|---|---|---|
| 1 | Oligomer | 25.61% | 151,000 Da | 1.17 |
| 2 | Monomer | 69.29% | 3,367 Da | 6.887 |
| 3 | Dimer | 5.1% | 9,197 Da | 4.61 |

**Figure 2.13.** Size exclusion chromatography elugrams for oligomeric $A\beta_{1-42}$, prepared by dissolving monomeric $A\beta_{1-42}$ in 2xTBS, incubated at 4°C for 24 hours.

Elugrams showing $A\beta_{1-42}$ sample elution times from the Superdex200 column. Light scattering elugram (A) indicates that there is heterogeneity in the sample. UV signal detected three significant regions of interest (ROI) based on the UV detection signal (B). The three regions of interest are characterised (C-E). The three regions of interest correspond to different $A\beta_{1-42}$ aggregates, with differing molecular weights calculated based on the UV and light scattering detection signals (F). All data is reported at time points where the sample data most closely resembled the Zimm plot calculated by the AF2000 software (n=3).

Incubating $A\beta_{1-42}$ for 72 hours resulted in two significant regions of interest (fig.2.14). The oligomer content present in the samples increased with the longer incubation time. The size of the oligomer also increased and was detected at 208,800 Da with a PDI of 1.128 indicating homogeneity of the peptide. The monomeric peak corresponded to 58.42% of the eluted sample. However, the monomeric peak did not correspond to the correct molar mass of monomeric Aβ cited in the literature (~4.5 kDa). The low molecular mass for the monomeric peak could be attributed to the detection range of the Superdex200 column, and future analysis will also utilise AF4 analysis to overcome this. The results suggested that the new protocol produced a higher yield of oligomers, which increased with extended incubation time. The revised protocol results in a preparation enriched with oligomers.

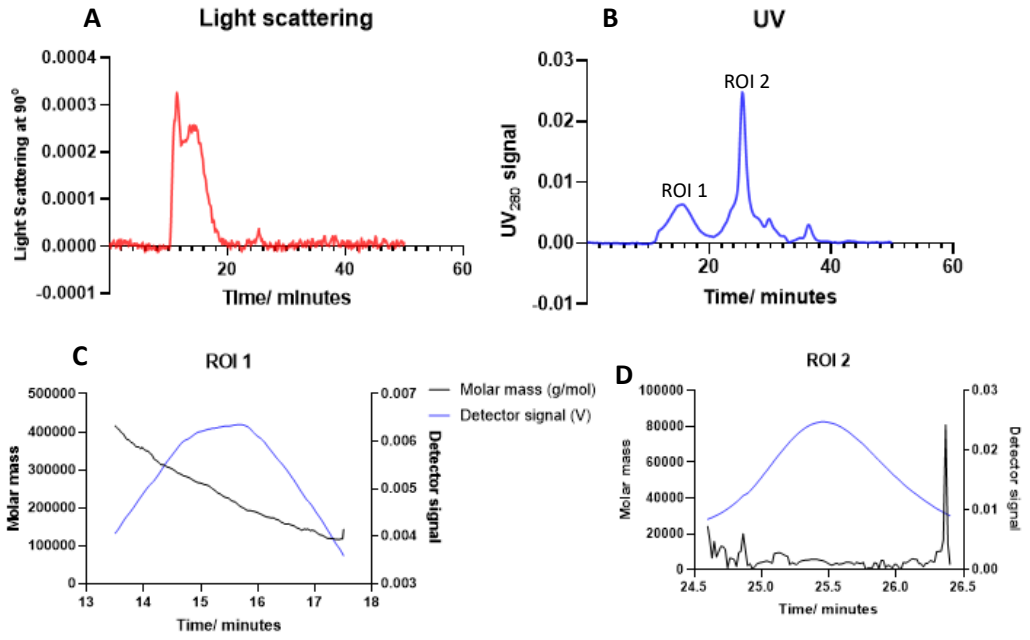


**E**

| ROI | Potential Aβ type | Relative amount (%) | Mn | PDI |
|---|---|---|---|---|
| 1 | Oligomer | 41.58% | 208,800 Da | 1.128 |
| 2 | Monomer | 58.42% | 2,736 Da | 1.936 |

**Figure 2.14.** Size exclusion chromatography elugrams for oligomeric $A\beta_{1-42}$, prepared by dissolving monomeric $A\beta_{1-42}$ in 2x TBS, and incubating at 4°C for 72 hours.

Elugrams showing $A\beta_{1-42}$ sample elution times from the Superdex200 column. Light scattering elugram (A) indicates that there is heterogeneity in the sample. UV signal detected three significant regions of interest (ROI) based on the UV detection signal (B). The three regions of interest are characterised (C-D). The three regions of interest correspond to different $A\beta_{1-42}$ aggregates, with differing molecular weights calculated based on the UV and light scattering detection signals (E). All data is reported at time points where the sample data most closely resembled the Zimm plot calculated by the AF2000 software (n=3).

Extending the incubation period to 2 weeks resulted in a decreased amount of monomer (45.07%), and an increase in high molecular weight oligomers (46%), as well as separation of lower molecular weight oligomers, such as trimers (8.94%) (fig.2.15). The PDI values for all three regions of interests were low, and therefore indicated low mass variability and more reliable results. The molar mass of the monomeric sample eluted also corresponded to the correct molecular weight of monomeric Aβ described in the literature. 2-week incubation protocol was therefore used in all further experiments utilising Aβ oligomers.

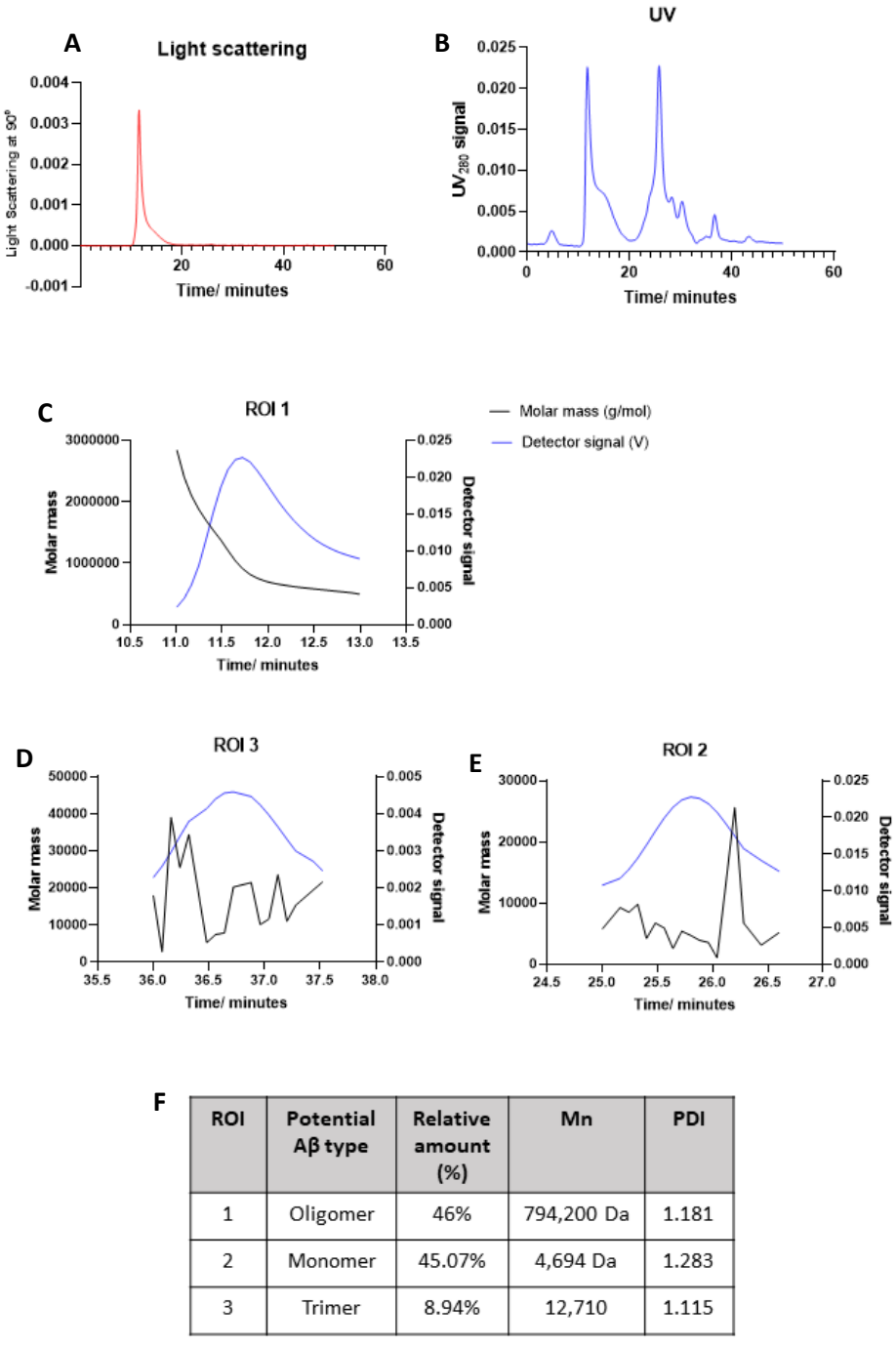


F

| ROI | Potential Aβ type | Relative amount (%) | Mn | PDI |
|---|---|---|---|---|
| 1 | Oligomer | 46% | 794,200 Da | 1.181 |
| 2 | Monomer | 45.07% | 4,694 Da | 1.283 |
| 3 | Trimer | 8.94% | 12,710 | 1.115 |

**Figure 2.15.** Size exclusion chromatography elugrams for oligomeric $A\beta_{1-42}$, prepared by dissolving monomeric $A\beta_{1-42}$ in 2x TBS, and incubating at 4°C for 2 weeks.

Elugrams showing $A\beta_{1-42}$ sample elution times from the Superdex200 column. Light scattering elugram (A) indicates that there is heterogeneity in the sample. UV signal detected three significant regions of interest (ROI) based on the UV detection signal (B). The three regions of interest are characterised (C-E). The three regions of interest correspond to different $A\beta_{1-42}$ aggregates, with differing molecular weights calculated based on the UV and light scattering detection signals (F). All data is reported at time points where the sample data most closely resembled the Zimm plot calculated by the AF2000 software (n=3).

*Dot blots*

To further characterise and detect $A\beta_{1-42}$ oligomers specifically, a dot blot and immunoblotting was carried out using the conformation-specific A11 antibody, which detects Aβ oligomers. The qualitative immunoblotting dot blot analysis with the A11 antibody revealed that the $A\beta_{1-42}$ oligomers are detectable when formed using the revised aggregation protocol (dissolving monomers in 2x TBS) (fig.2.16.). The intellichemi signal was quantified and compared between the conditions using an unpaired t-test statistical analysis. The signal for the oligomers was significantly higher ($p= 0.04$) than the signal for the PBS blank controls, indicating that the signal detected was reliable and did not show background noise. The analysis was qualitative to show that the correct conformation and morphology of the Aβ preparation was achieved.

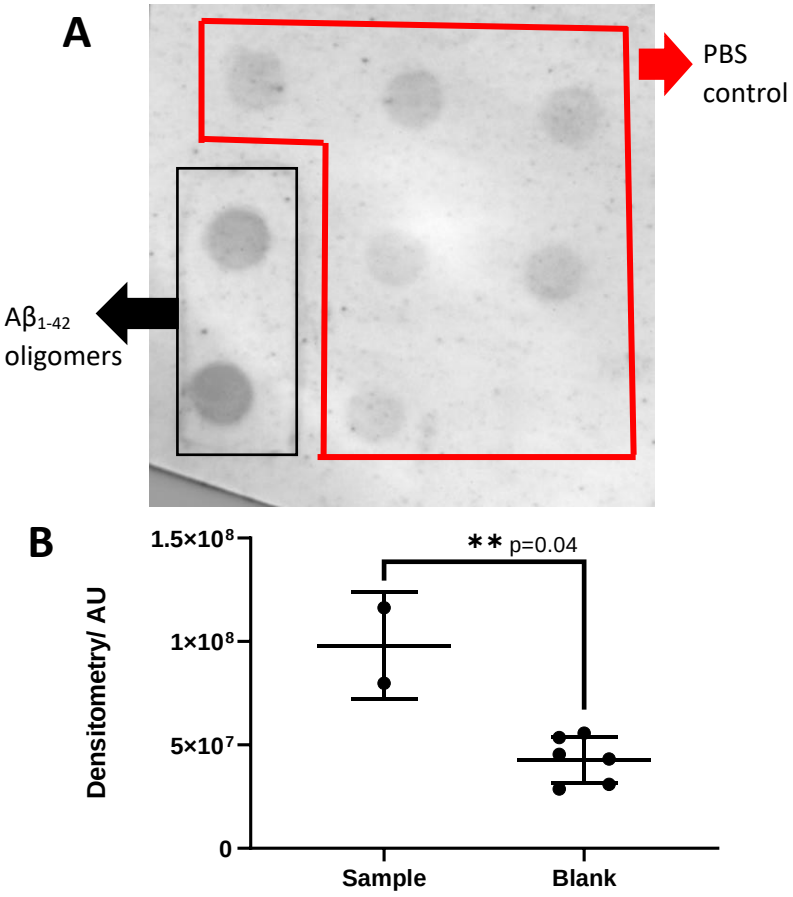


**Figure 2.16.** The detection of $A\beta_{1-42}$ oligomers using conformation specific A11 antibody and dot blots.

**A)** Dot blot immunoblots of 100 µM $A\beta_{1-42}$ oligomers (black box) and PBS blank controls (red box). 100 µL of sample were loaded into each well. Blots were probed with conformation specific A11 antibody which detects Aβ oligomers. **B)** The intellichemi signal was quantified and compared between the conditions. The graph shows that there is a detectable, significant signal for $A\beta_{1-42}$ oligomers (arbitrary units). Unpaired t-test, error bars show mean +- SD, p= 0.04

*Thioflavin T Assay*

To detect the progression and formation of $A\beta_{1-42}$ fibrils, a ThT assay was carried out (for details, see the methods section 2.4.3). 20 µM of ThT was incubated with 100 µM of $A\beta_{1-42}$, 100 µM of scrambled peptide, PBS, vehicle control or thioflavin only control. This resulted in an Aβ aggregation time-course curve, showing the kinetics of the aggregation process for all conditions (fig.2.17). The overnight incubation at 37°C of $A\beta_{1-42}$ fibrils resulted in a rapid aggregation growth phase, which has lasted ~4 hours, as indicated by the curve reaching a plateau after that time. An unpaired t-test was carried out to analyse the difference in signal between Aβ fibrils and the scrambled peptide control. The Aβ fibril signal was significantly increased compared to the scrambled peptide ($p<0.001$***). The results indicated that $A\beta_{1-42}$ fibrils form rapidly when prepared according to the new aggregation protocol.

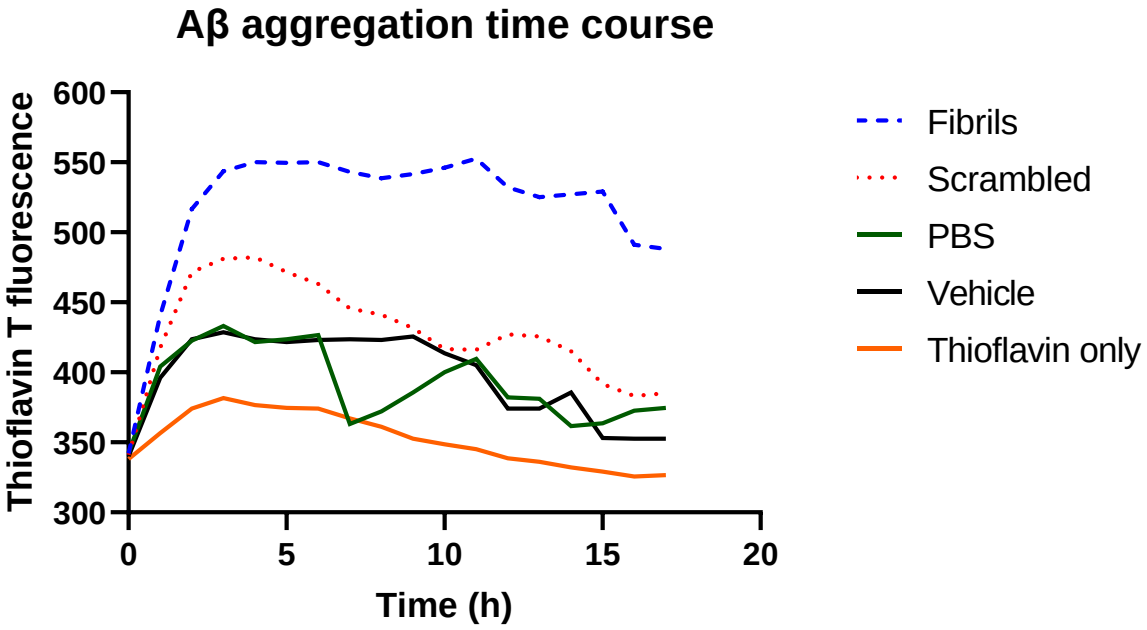


**Figure 2.17.** Thioflavin T assay to detect $A\beta_{1-42}$ fibril aggregation.

Aggregation kinetics of $A\beta_{1-42}$ fibrils (blue), scrambled peptide (red), PBS (green), vehicle control (black) and thioflavin control (orange). The aggregation kinetics is based on Thioflavin T fluorescence signal (arbitratu units). Aggregation was performed at 37°C overnight without agitation.

## 2.6 Discussion

### 2.6.1 Preparation of monomeric amyloid-beta

A protocol developed by Dr Staniforth's group (Molecular Biology and Biotechnology, The University of Sheffield) was used to prepare stable monomeric $A\beta_{1-42}$ (unpublished). Dissolving the recombinant $A\beta_{1-42}$ in a highly alkaline buffer (50 mM NaOH), combined with appropriate storage conditions (in low bind Eppendorfs®, at -80°C), self-aggregation and assembly of monomeric Aβ into oligomers and fibrils was inhibited.

AF4 analysis revealed that the sample prepared by dissolving the recombinant peptide in 50 mM NaOH was largely monomeric. AF4 analysis allowed for calculation of various protein characteristics. The retention time, as well as the multi-angle light scattering detection associated with a concentration detector (in this case UV detector) enabled determination of the concentration and molecular weight of the peptide, which predominantly corresponded to the correct peptide parameters for $A\beta_{1-42}$ monomers. AF4 is a widely used proteomics technique, which enables the separation and characterisation of macromolecules, including proteins. It can be used as an alternative method to SEC, especially for the purpose of quantifying protein aggregates in the sample. AF4, coupled with MALS, is able to resolve and characterise low molecular weight proteins, that can range from ~2 kDa to 5 kDa in size. Moreover, AF4 coupled with MALS can effectively provide accurate extinction coefficients, and calculate accurate masses of the peptide in question (Manning *et al.*, 2021).

The probability density, calculated from the AF4 analysis, determined that the sample was largely monomeric, with a possibility of the presence of a small amount of dimer. It may not be entirely possible to prevent dimer formation, due to the high propensity of Aβ to aggregate (Cohen *et al.*, 2013). However, it is also possible that the detected 'dimer' signal was column or buffer noise, although the analysis is not sensitive enough to check such small quantities of the 'dimer' to confirm this. Furthermore, it has been shown that different carrier buffers can change the stability and aggregation of peptides inside the AF4 column. Even syringe injection to introduce the samples into AF4 columns can have an impact on the shear stress, and subsequently can induce aggregation of peptides (Bria and Williams, 2016). Thus, the presence of a detectable dimer in the column may not necessarily mean that there are dimers present in the stock monomeric preparations, but rather that the aggregation process was induced through the process of AF4 analysis. It would be interesting, and more reliable, to test the peptide preparation with a technique of a higher resolution and/or a technique that would not allow for the Aβ aggregation to start. This is however a limitation in the current field. Such techniques of higher reliability and resolution are not yet widely available.

As the prepared monomeric Aβ peptide is pure and stable, the resulting monomeric $A\beta_{1-42}$ preparation was used in subsequent experiments.

### 2.6.2 Preparation of oligomeric and fibrillary amyloid-beta

#### *Initial protocol for deriving Amyloid-beta aggregates and their characterisation*

There is a general consensus that oligomeric Aβ is the more toxic Aβ species (Sengupta, Nilson and Kayed, 2016), and the reasons for this may relate to the structural arrangement of oligomers compared to fibrils (Verma, Vats and Taneja, 2015). Three major Aβ assemblies can be distinguished: monomers, oligomers and fibrils. In AD, soluble oligomeric Aβ can be organised into structures of varying sizes, ranging from dimers to decamers, as well as larger Aβ-derived diffusible ligands and dodecamers (Sengupta, Nilson and Kayed, 2016).

Small oligomers in particular can have a larger propensity for binding to phospholipids, and may elicit increased neurotoxicity (Cizas *et al.*, 2010). This could be due to their smaller size, which could enable oligomers to diffuse into cells more easily than fibrils (Verma, Vats and Taneja, 2015). Oligomers may also be hidden within Aβ plaques, and, after reaching a certain physical limit, they may diffuse out and become sequestered within cell surfaces. This could trigger neuronal and synaptic loss (Hong *et al.*, 2014). Moreover, oligomers are highly unstable, disordered structures, whereas fibrils are stable and organised (Verma, Vats and Taneja, 2015). By nature, Aβ oligomers are also heterogeneous. This not only means that they range in size from dimers to dodecamers, but also, especially in the human brain, there may be a high variability in the oligomeric structures and isoforms. Furthermore, Aβ in the brain can be very heterogenous, and often multiple Aβ forms can be found in the brain, ranging from smaller oligomers to larger fibrils in plaques. This heterogeneity can lead to varying rates of aggregation, as well as varying morphology and structures of Aβ. It may also mean that the varying Aβ structures could have differential effects on neurotoxicity, as well as downstream effects influencing the events described by the amyloid hypothesis.

The unstable and heterogeneous nature of Aβ is also what makes generation and characterisation of Aβ oligomers difficult. There are number of methods available, which allow for stabilisation of the prepared Aβ oligomers *in vitro*. Due to the non-crystalline and heterogenous nature of Aβ peptides, standard protein characterisation techniques such as X-ray diffraction or liquid state nuclear magnetic resonance (NMR) spectroscopy are often not suitable (Lührs *et al.*, 2005; Colvin *et al.*, 2016). To characterise aggregated Aβ in terms of size and mass, we used SEC analysis methods, coupled with MALS method.

Microscopy analysis of Aβ preparations is essential for confirming and analysing the morphology of Aβ peptides prepared *in vitro*. This includes TEM, which can help to distinguish Aβ forms, as well as to evaluate Aβ aggregation, as multiple aggregate types can be grown from monomeric Aβ (Anderson and Webb, 2011).

Microscopy analysis has been useful in revealing morphological and structural differences between Aβ species. For example, microscopy techniques have revealed that *ex vivo* and *in vitro* Aβ may vary, with *ex vivo* Aβ adopting a right-hand twist structure, and *in vitro* Aβ adopting a left-hand twist structure (Sachse *et al.*, 2006; Schmidt *et al.*, 2015; Kollmer *et al.*, 2019). The twisting structural variations of Aβ could be due to the varying experimental protocols and conditions in which the peptides are allowed to aggregate, and most importantly, these structures may be the cause of clinical and pathological heterogeneity of AD between patients (Qiang *et al.*, 2017b; Periole *et al.*, 2018). Hence, in the current study, we decided to utilise TEM imaging to visualise the morphology of the Aβ preparations. TEM micrographs revealed morphological differences between Aβ aggregates prepared using different protocols. The results suggested that the samples prepared using the initial aggregation protocols described by Cerf *et al.* (2009) and Stine *et al.* (2011) were monomeric in both cases ('oligomeric' and 'fibrillary'), and suggested that ineffective aggregation has taken place. In the case of those preparations, long and singular fibrils were formed, without obvious aggregated networks of fibrils. Moreover, the oligomers were associated around the fibrillary structures of the peptides, suggesting slow and inefficient aggregation. This is because during the aggregation process, the fibril structure can act as a catalyst structure for oligomers to associate together (Cohen *et al.*, 2013). This could potentially be observed here, suggesting slow aggregation kinetics.

As mentioned previously, the high-resolution microscopy techniques are usually supplemented by other, proteomics-based techniques, which are capable of characterising the peptides more quantitatively, calculating their mass and size. Therefore, the Aβ preparations using the initial protocols (Cerf *et al.*, 2009; Stine *et al.*, 2011) were also analysed by methods, which allow for the estimation of the peptide's mass and size. These included analysis via SDS-PAGE and immunoblotting, as well as SEC-MALS.

SEC-MALS enables separation of sample according to its size and mass. EM has long been used alongside SEC-MALS for the analysis of Aβ peptides, allowing for the characterisation of the structural and biophysical differences between oligomers and protofibrils (Walsh *et al.*, 1997; Nichols *et al.*, 2015). SEC can be successfully used to separate high and low molecular weight oligomers, as well as separating oligomers from fibrils, allowing for the investigation of the peptide size and weight distributions (Yang *et al.*, 2017; Shea *et al.*, 2019). The SEC-MALS analysis of the Aβ 'oligomers'

prepared using the initial protocols (Cerf *et al.*, 2009; Stine *et al.*, 2011) indicated that the peptides did not enter sufficient aggregation kinetics, and that the samples remained no different from the monomeric $A\beta_{1-42}$ prepared initially. Even after switching to a larger cut-off column (from SuperDex75 to SuperDex200), there were no oligomers detected via the SEC-MALS analysis, suggesting no low molecular weight or high molecular weight oligomers were formed. Again, this could be due to insufficient aggregation, caused by the peptide environment not being correct for Aβ aggregation.

Different Aβ species can be separated using gel electrophoresis and detected with Aβ antibodies, such as 6e10, which detects amino acid residues 1-16 of Aβ. It can be seen on the immunoblots, that for all three preparations (monomeric, oligomeric and fibrillary), visible bands can be observed. The bands corresponded to the correct size of small molecular weight oligomers (~17 kDa) in all three preparations. The findings contradicted the TEM and SEC-MALS findings. Reports indicate that SDS-PAGE analysis may not be entirely appropriate for the detection of different aggregation states of Aβ, as SDS can affect the aggregation of Aβ, providing false representation of the species present in the sample (Pujol-Pina *et al.*, 2015). As temperature can affect aggregation kinetics of Aβ (Klement *et al.*, 2007), it is also possible that the increase in temperature during electrophoresis will affect aggregation. Moreover, even though gradient gels were used, it might have been more beneficial to use native gels instead, to prevent any denaturing of the protein. As Aβ is notoriously unstable *in vitro*, it might be that the conditions for SDS-PAGE were enough to start the aggregation process in this case. This would explain why the band profile looks very similar in all three cases, as the rate of aggregation would most likely be comparable across all three samples. To avoid this, a method called cross-linking would have been beneficial to use. Covalent crosslinking has been previously used to stabilise Aβ aggregates (Levine, 1995). The method called photo-induced cross-linking of unmodified proteins (PICUP) can stabilise Aβ aggregates, which can then be analysed using SDS-PAGE, enabling quantitative analysis of the aggregated peptides (Rahimi, Maiti and Bitan, 2009; Banerjee *et al.*, 2017). By using PICUP-based methods, the SDS-PAGE could have been more reliable in this case.

### *Amended protocol for deriving Amyloid-beta aggregates and their characterisation*

As the initial analysis of the preparations revealed that the aggregation process of Aβ was inefficient, an amended protocol was developed. The revised protocol accounts for the highly alkaline conditions of the stock $A\beta_{1-42}$ monomer, which may have prevented aggregation from taking place. Self-nucleation of monomeric Aβ, in the absence of an initial 'seed', is a kinetically unfavourable reaction (Cohen *et al.*, 2013). The presence of HCL in the TBS buffer lowers the pH levels of the stock enough to equalise the effects of NaOH on the final pH level of the peptide solution. The results suggest that the long incubation time of $A\beta_{1-42}$ oligomers may be suggestive of the high purity of monomeric $A\beta_{1-42}$ stock, as initial long process of Aβ self-nucleation could have been delaying the aggregation process.

SEC-MALS analysis revealed that small amounts of oligomers were present initially, and that this yield could be increased by extending the incubation time from 24 hours to 72 hours. We have therefore, optimised the protocol further, allowing Aβ to aggregate into fully formed oligomers after 2 weeks. The revised protocol results in the formation of a mixture of higher and lower molecular weight oligomers, which could represent a more physiological environment, as heterogeneity of Aβ species is observed in the brain (M Kollmer *et al.*, 2019). The morphology analysis of the oligomeric preparation using TEM confirmed this, as there were visible populations of small and globular oligomeric species, as well as larger and elongated oligomeric species. This indicated the presence of low molecular weight and high molecular weight oligomers respectively. The SEC-MALS and TEM analyses of oligomers were also supplemented using dot blots and immunoblotting, which revealed that the oligomeric preparations were detected via the conformation-specific A11 antibody. The A11 antibody can recognise the Aβ oligomers, as the antibody utilises the fact that all soluble oligomers can display a common conformation-dependent structure, unique to the oligomers. This structure is adopted by all oligomers, regardless of their peptide sequence, and they are very uniquely distinct from Aβ fibrillary structures (Kayed *et al.*, 2003). The A11 has therefore been routinely used to confirm the oligomeric state of Aβ (Vandersteen *et al.*, 2012b; Periole *et al.*, 2018)

The aggregation of Aβ into fibrils was rapid. The ThT assay results showed that the aggregates start to form at around 3 hrs post-incubation. The speed of fibrillation is to be expected, as $A\beta_{1\text{-}42}$ has been shown to have a higher propensity to aggregate than other Aβ isoforms. For example, $A\beta_{42}$ aggregation into fibrils can take around 1 hr, with a half time of 0.81 +- 0.12 h. $A\beta_{40}$ aggregation is much longer, taking around 25 hrs with a half time of 21.75 +- 1.36 h. (Wang, Eom and Kwon, 2021). While the ThT spectra is a good indicator of Aβ fibrillation process, it should be noted that it provides limited information about the aggregation of these peptides. Notably, it cannot provide any information of the structure of fibrils, or the mechanism of aggregation (Wang, Eom and Kwon, 2021). Therefore, visualisation of such aggregates using microscopy was an important step to further characterise Aβ fibril formation. The TEM analysis of the prepared Aβ fibrils showed that the improved aggregation protocols resulted in a typical fibril morphology, of large peptide aggregated into fibril networks. These fibrils were much larger in size than the prepared high molecular weight oligomers, and therefore we are confident that the fibrillary preparations were reliable.

It is unknown whether the processes behind aggregation of Aβ differ *in vitro* and *in vivo* on a structural and molecular level. However, the conditions in which the peptide is allowed to aggregate differ *in vitro* and *in vivo*. Since the environment of the peptide is important, it is likely that the Aβ used in many studies is not physiological, and each manipulation of its delicate environment may change protein morphology and kinetics, potentially skewing the results. Furthermore, Aβ found *in vivo* has

been shown to adopt different conformations, which may be difficult to reproduce *in vitro* (Liu *et al.*, 2021). Moreover, it is very difficult to mimic the delicate nature of the *in vivo* brain environment, as there may be multiple other factors involved, which may impact the aggregation process of Aβ. Controlling for all of these variables is not possible and is therefore a limitation of the current study. However, the development of robust protocols, together with extensive analysis of the resulting Aβ preparations will ensure that reliable and reproducible data is generated.

## 2.7 Conclusions

The current field of Aβ preparation is limited by the number of variables that can influence Aβ aggregation, as well as the technology available to analyse Aβ. The complex biochemistry of Aβ species can make experimental design difficult, and a great emphasis should be put on studying the characteristics, aggregation, and the role of different Aβ species in the context of disease. A thorough characterisation of the peptide kinetics and chemistry, as well as peptide conformation and standardisation of the aggregate preparation methods is crucial. It is also important to utilise current state-of-the-art analytical approaches, as novel technologies and methods for the reliable characterisation of Aβ are being developed.

A variety of techniques can be used to study Aβ, from looking at morphology to analysing the molecular structure of the peptides. However, the mechanisms behind Aβ aggregation and self-assembly are not yet fully understood, thus making it difficult to replicate the environment in which Aβ aggregates. The current study focused on deriving well-characterised, reliable preparations for monomeric, oligomeric and fibrillar $Aβ_{1-42}$. Through careful manipulation of the peptide environment, a stable and pure monomeric $Aβ_{1-42}$ was prepared. The monomeric starting material was used to derive well-characterised and optimised oligomeric and fibrillary Aβ. A careful and thorough characterisation of these preparations raised the reliability and confidence of the results generated and allowed for a characterisation of the morphology and profile of the aggregates. The generated preparations will be used to determine whether astrocytes elicit differing responses to oligomeric and fibrillary $Aβ_{1-42}$ (described in chapters 3 and 4).

The optimisation steps for preparing reliable Aβ preparations for different aggregation stages revealed that even minimal changes to the peptide environment will have detrimental effects on the overall aggregation kinetics and the morphology of prepared peptides.

The rigorous approach to the generation and analysis of Aβ described in this chapter will enable us to design a reproducible and reliable study, enabling evaluation of the effects of different Aβ aggregate

species *in vitro*. In addition, deriving the structure-toxicity relationship of Aβ is essential for improving drug discovery efforts focused on targeting Aβ.

# Chapter 3 – The effect of disease-relevant stressors on human astrocytes *in vitro*

## 3.1 Introduction

### 3.1.1 Oxidative stress and neurodegeneration

The brain composes only 2% of the body weight, yet it receives 15% of the cardiac output, and, remarkably, consumes 20% of the total body oxygen (Jain, Langham and Wehrli, 2010). Furthermore, it is estimated that neurons consume approximately 75- 80% of the energy produced in the brain (Watts *et al.*, 2018). Therefore, the brain has a high rate of oxidative metabolic activity due to its high energy requirements (Lee, Cha and Lee, 2021). Due to its high energy and oxygen consumption, the CNS is highly susceptible to oxidative stress.

Astrocytes are the most abundant glial cells in the CNS. Astrocytes not only facilitate neuronal communication via tripartite synapses, but they also maintain the integrity of the blood brain barrier, regulate nutrition and metabolite processing to facilitate neuronal survival, and play a crucial role in regulating events relating to oxidative stress (Garwood *et al.*, 2017). However, regulation of processes relating to oxidative stress may disrupt normal astrocyte roles, especially in terms of CNS maintenance. The function of astrocytes may become dysregulated during periods of stress and/ or disease, when oxidative stress is involved (Chen *et al.*, 2020). Oxidative stress has been implicated in many neurodegenerative processes. Furthermore, dysfunctions in antioxidant enzymes have been linked to neurodegenerative diseases, such as Amyotrophic lateral sclerosis (ALS), Alzheimer's disease, Huntington's disease and Parkinson's disease (Matés, 2000).

In the CNS, astrocytes are thought to be more resistant to oxidative stress than other cell types (Matés, 2000). There is evidence that astrocytes play a supportive role during the times of oxidative stress, in that they facilitate antioxidant activity, clear reactive oxygen species (ROS) produced in the CNS and promote the decomposition of ROS. However, certain pathological conditions may disrupt these processes, and instead astrocytes can act as one of the main sources of ROS. This in turn promotes the activation of other glial cells such as microglia and facilitates inflammation causing damage to the CNS and neurons (Chen *et al.*, 2020). Hence, astrocytes can become both protective and damaging as a response to disease stressors, including oxidative stress.

Astrocytes and oxidative stress have been shown to be a major contributor to disease, including neurodegenerative diseases such as Alzheimer's disease (Phatnani and Maniatis, 2015). Astrocytes can contribute to neurodegeneration via astrocytic DNA damage caused directly or indirectly by oxidative stress.

### 3.1.2 Oxidative stress and DNA damage

DNA damage occurs commonly in cells, and each cell can experience $10^4$- $10^5$ DNA lesions per day (Kok *et al.*, 2021). DNA damage can be caused by several factors, including UV light, ionizing radiation,

errors in DNA replication, as well as oxidative stress. To cope with these stresses and damage, the cells are equipped with a DNA damage response (DDR) system. The DDR can detect and repair damage, but also can coordinate repair with other cellular processes such as cell cycle progression and apoptosis. Depending on the type of DNA damage that occurs, the cell can elicit different, tailored DDR. DNA damage usually takes place as single strand breaks, or double strand breaks which tend to be more lethal to cells (Madabhushi, Pan and Tsai, 2014; Pilié *et al.*, 2018; Martins *et al.*, 2021). Double stranded DNA breaks are most lethal as they occur in both strands of the DNA double helix, which means that there is no intact strand left to be used as a template. This means that the effective DNA repair cannot take place (Thadathil *et al.*, 2019). Exposure of DNA to ROS can cause a modification of guanine into 8-oxoguanine, allowing it to pair with cytosine and adenine leading to DNA mutations, can also cause double stranded DNA breaks (DSBs), and lead to genome instability.

DSBs can trigger the DDR to halt the cell cycle and repair the damage via either non-homologous end joining or homologous recombination. The occurrence of DSBs and DNA damage in the brain can be causative of neurodegeneration independently of other factors. Extensive DNA damage can cause cell senescence and cell death. In particular, neural cells are highly susceptible to the profound adverse effects of DSBs, as their DNA repair is greatly reduced compared to cells which are able to proliferate (Merlo *et al.*, 2016). Postmitotic cells are long lived, unable to divide, and often irreplaceable, and therefore the accumulation of DNA damage in such cells can have detrimental effects on overall brain health (Shanbhag *et al.*, 2019). Indeed, an accumulation of DNA damage can contribute to neuronal dysfunction and cognitive impairment, independently of Alzheimer's disease pathology (Simpson *et al.*, 2015). It is suggested that DNA damage and DSBs accumulate with cognitive decline in Alzheimer's disease. The source of DSBs in Alzheimer's disease is yet to be uncovered; however, it has been suggested that oxidative stress (a contributor to DSB formation) can be one of the driving events in the development of Alzheimer's disease (Tönnies and Trushina, 2017). Regardless of the source of such damage, defects in DNA damage repair or insufficient DNA damage repair, may be responsible for the formation and subsequent accumulation of DSBs in the brain. This could cause astrocytes, as well as neurons, to become defective and lose their healthy functions, leading to neurodegeneration and Alzheimer's disease pathology (Lin *et al.*, 2020).

DNA damage and oxidative stress may be linked to the Aβ peptide; however, it is still unclear to what extent amyloid beta is involved in oxidative stress during Alzheimer's disease. Tissue from Alzheimer's disease patients has been shown to display increased levels of DNA damage associated with oxidative stress. Furthermore, Aβ can cause formation of ROS, which can contribute to neuronal loss in disease. On the other hand, reports also suggest that oxidative stress can increase secretion of Aβ, which could contribute to early Alzheimer's disease pathology (Misonou, Morishima-Kawashima and Ihara, 2000;

Welty, Thathiah and Levine, 2022). Aβ has also been found to promote DNA damage, which includes upregulation and phosphorylation of γH2AX. These mechanisms can contribute to neuronal loss, and can cause neuronal cell senescence (Mao and Reddy, 2011; Y. Li *et al.*, 2022). However, interestingly, reports have also suggested that DNA damage may precede Aβ production in neurons, and the processes relating to cellular DNA damage could upregulate enzymatic activity of BACE1, leading to an increased production of Aβ (Das *et al.*, 2021).

Studies investigating the impact of oxidative stress and Aβ in Alzheimer's disease have mostly focused on the neuronal cellular damage, oxidative stress, and DNA damage. However, not a lot is known about how oxidative stress, DNA damage and Aβ impact astrocytes and their functions; and whether astrocytes contribute to Alzheimer's disease through those mechanisms. Furthermore, even though there are studies investigating the impact of Aβ oligomers on oxidative stress and DNA damage, these mostly address how oligomers impact those processes in neuronal cells (Butterfield, Swomley and Sultana, 2013b).

### 3.1.3 Astrocytes in Alzheimer's disease

In Alzheimer's disease, the current research adopted a very neuro-centric view of the disease, however studies also implicate astrocytes in disease pathology. In neurodegenerative diseases, astrocytes can display a toxic gain-of function, or a toxic loss-of-function. Astrocyte pathology could manifest itself as a loss of neuronal support, loss of BBB support, decrease in glucose metabolism, dysfunctions in neurotransmitter signalling, as well as increased oxidative stress, and increase in the release of pro-inflammatory factors (Li *et al.*, 2019). Such astrocyte pathology could contribute to neuronal loss, and disease progression. However, the exact mechanisms behind astrocyte pathology in Alzheimer's disease, and the impact of the different Aβ species on astrocytes, remain poorly understood.

As mentioned in Chapter 1, astrocytes can become progressively reactive in Alzheimer's disease (Kamphuis *et al.*, 2014). However, astrocyte responses to pathological conditions and stimuli can be very heterogenic. It has been reported, that acute and chronic injury of the CNS can lead to different astrocyte responses, as seen by the differences in transcriptomics (Das *et al.*, 2020). It has also been reported that external stimuli can elicit differential responses in astrocytes, contributing to a change in their physiological functions, for example inducing a more neurotoxic or neuroprotective astrocytic phenotype (Liddelow *et al.*, 2017).

An interplay between disease stressors could take place in astrocytes, and evidence suggests that Aβ can strongly influence astrocyte responses in disease. For example, astrocytes can cause a production of ROS as a response to Aβ-mediated stimuli. Furthermore, Aβ exposure can trigger pro-inflammatory

pathways in astrocytes (Singh *et al.*, 2020). Astrocytes may also be a key site of Aβ production in disease, as they have been reported to be involved in duplicating and spreading Aβ oligomers, facilitating neurotoxicity and neuronal dysfunction (Wang *et al.*, 2019). Interestingly, Aβ peptide has been reported to elicit varying responses based on the peptide aggregation states. Oligomeric Aβ has been reported to induce apoptosis, neuronal loss, inhibition of long-term potentiation and oxidative stress (Cline *et al.*, 2018; Parodi-Rullán *et al.*, 2020). Meanwhile, fibrillary Aβ can increase BBB permeability, activation of glial cells, and can mediate neuritic pathology (Meyer-Luehmann *et al.*, 2008; Parodi-Rullán *et al.*, 2020). However, the full impact of Aβ oligomers and Aβ fibrils on astrocyte functions and pathological changes remains to be characterised.

### 3.1.4 Available models of Alzheimer's disease

As described previously, AD is characterised by the formation Aβ plaques and intracellular neurofibrillary tau tangles. It is now clear, that the contribution of both pathologies is essential to disease progression, and as a result, they have been at the forefront of intense AD research. However, the difficulty in generating reliable models of the two pathologies has been a limiting factor in the progression of research efforts in this area.

The *in vivo* models available currently include transgenic rodents, which mostly express genetic mutations of fAD, particularly those involved with impaired Aβ processing. These mutations can be present in the models alone (for example the Tg2576 mouse model carrying *APP* gene), or in a combination with others (for example the 5xFAD mouse model carrying *APP* and *PSEN1* mutations). To fully examine the pathology of AD, other models of the disease have been developed where both Aβ and tau misprocessing are represented (for example the 3xTg mouse model carrying *APP, PSEN1* and *MAPT* mutations). As described, the mouse models of AD include models of familial AD, with APP and/or PSEN mouse models. As such models can mimic the AD pathology (Aβ plaques) *in vivo*, they can be a great source of information about the disease mechanisms. From the perspective of astrocytes, animal models can give an important insight into the functionality of astrocytes in healthy vs AD systems. For example, the astrocyte functions in AD can be assessed *in vivo* by measuring the electrophysiology, gap junctions, glutamate uptake, release of inflammatory cytokines, and Aβ uptake and clearance (Spanos and Liddelow, 2020). Although, pre-clinical models of AD may not be entirely representative of disease process and changes to astrocytes during AD pathology in humans. This is mainly due to human astrocytes having different morphology, gene expression, and functions when compared to the mouse model astrocytes. As the current work aimed to investigate the astrocyte responses to Aβ specifically, the *in vitro* model seemed to be a more appropriate choice.

Whilst animal models are very useful in studying AD pathologies, they may not give a full overview of the disease. Even though AD pathology can be replicated, most of the AD mouse models do not develop neurodegeneration. Furthermore, these models are largely utilising familial AD mutations which, in humans, can translate to early-onset AD. Therefore, the sporadic and late onset AD may not be fully modelled *in vivo*. The overexpression of genes needed for the onset of typical AD pathology in these mouse models can also cause behavioural deficits and symptoms which do not occur in humans, creating issues with replicating human physiology and translatability of results (Vitek *et al.*, 2020). Physiologically relevant models are therefore needed to enhance the research and understanding of the disease aetiology. Thus, the use of physiologically relevant *in vitro* models would be highly advantageous.

To fully replicate the human astrocyte pathology in AD, *post-mortem* astrocytes could also be used. They are an invaluable resource to study true disease-specific astrocytes. However, these astrocytes have their own limitations due to their availability, and the fact that they are only representative of the end-stage AD. Whilst still incredibly useful, research efforts should also focus on the earlier events that would lead to AD, as this poses a great treatment development opportunity.

One of the popular choices of modelling AD *in vitro* is the use of induced pluripotent stem cells (iPSCs). iPSCs can be derived from reprogramming donor fibroblasts, and subsequent differentiation into many cell types, including neurons and astrocytes. The use of iPSCs allows researchers to utilise cells directly reprogrammed from AD patients, creating a physiologically relevant model. This *in vitro* model can be utilised for mechanistic studies, as well as pre-clinical treatment development and discovery (Arber, Lovejoy and Wray, 2017). For example, iPSCs derived from fibroblasts of patients carrying the *PSEN1* and *PSEN2* mutations have been differentiated into neurons in the past, where such neurons have been shown to secrete higher levels of $A\beta_{42}$ compared to healthy controls (Yagi *et al.*, 2011). Furthermore, CRISPR/Cas9 knock-in neurons have been generated from AD iPSCs, however these do not fully reproduce all aspects of the disease pathology, and therefore their use may be more limited (Slanzi *et al.*, 2020).

The iPSCs have been a great resource in the field of AD research. Unlike animal models, the iPSC lines derived from AD patients do not need to exhibit overexpressed AD-related genes, which is a great advantage of using the iPSC models of disease. Even in the early stages of differentiation, neurons derived from AD iPSCs show disease-relevant phenotypes and early cell changes. Such changes are often overlooked and/or difficult to study using other means, therefore iPSC models may be an advantageous option for studying early and pre-symptomatic stages of AD (Penney, Ralvenius and Li-Huei, 2020). Moreover, iPSC lines have been utilised in the development of organoids, which aim to

model whole tissues by combining multiple cell types together. These organoids can be a useful tool when studying various disease processes, such as protein aggregation, selective vulnerability of cells and excitotoxicity, dysfunction in cell networks, and neuroinflammation (Venkataraman *et al.*, 2022). However, even though they are a useful tool for studying AD *in vitro,* such organoids do have disadvantages, as they cannot fully replicate the living brain. This is due to the lack of ageing phenotype, and lack of brain vasculature, as well as a formation of an immature brain network. Therefore, such organoid-based models should be implemented by validation experiments to draw more reliable conclusions of what disease processes occur in AD.

Age is one of the risk factors of AD, as well as many other neurodegenerative diseases. For example, in AD, Aβ and tau accumulation can take place in an age-dependent manner. The process of differentiation of human primary cells into embryonic-like cells includes the expression of transcription factors OCT4, KLF4, SOX2, and C-MYC and culturing cells under embryonic stem cell medium conditions. This process causes the ageing features of the cells to reset, and these features include for example telomere shortening or mitochondrial function (Studer, Vera and Cornacchia, 2015). However, the age-dependent changes could also extend to DNA damage response and changes characteristic to senescent cells. The loss of such features of ageing and disease could be detrimental in modelling AD appropriately. To circumvent this, the use of tripotent induced neural progenitor cells (iNPCs) may be a good way to model AD. These iNPCs can be directly converted from donor fibroblasts. The iNPCs can be directly converted from donor fibroblasts using retroviral vectors OCT3, Sox2, KLF4, and C-MYC. Rather than the embryonic stem cell medium, the cells are maintained in the NPC medium containing FGF2 and EGF. Once the iNPC culture is established, these tripotent cells are maintained in DMEM/F12 medium supplemented by 1%N2, 1%B27, and FGF only (without the use of FBS). These iNPCs can then be differentiated to oligodendrocytes, neurons, and astrocytes (Meyer *et al.*, 2014)

The conversion of fibroblasts to iNPCs, and their subsequent differentiation into astrocytes, oligodendrocytes, or neurons does not re-set the ageing phenotype of the cells. Moreover, it does not involve any clonal expansion of the cells, which can also reduce variability in the methodology, and can lead to more reliable results when studying the roles of cells in AD (Meyer *et al.*, 2014; Gatto *et al.*, 2021). Gatto *et al.* (2021) sought to compare the iNPC-derived astrocytes other astrocyte *in vitro* models, with the aim to characterise the ageing phenotype of these astrocytes at functional and transcriptional level. They have revealed that the iNPC-derived astrocytes retain the ageing phenotype of donors, i.e., the young astrocytes were not dissimilar to commercially available fetal astrocytes. Meanwhile astrocytes from older donors were not dissimilar to astrocytes obtained *post mortem* (Gatto *et al.*, 2021).

Due to their efficiency and their ability to preserve the ageing phenotype of the donors, induced astrocytes (iAstrocytes) from these directly converted iNPCs have been chosen as the *in vitro* model in the current work. To characterise the DNA damage response, and for optimisation of Aβ treatment protocols *in vitro*, commercially available fetal astrocytes have been chosen. These astrocytes were chosen due to their relatively low cost, efficiency, and robustness.

## 3.2 Aims and objectives

Astrocytes are involved in the progression and pathology of neurodegenerative diseases, including Alzheimer's disease. Astrocytes can change early in the disease, leading to profound downstream effects contributing to neuronal loss and dementia.

Two distinctive astrocyte models were used to characterise the astrocyte responses to disease-related stressors. Firstly, fetal astrocytes were used for the initial characterisation of astrocyte responses to Aβ and oxidative stress. The fetal astrocytes are well-characterised, robust, easy to maintain, and commercially available, making them an advantageous model. However, fetal astrocytes may not entirely represent the ageing phenotype and ageing changes that can occur in older individuals. For this reason, a second astrocyte model was utilised. The model relies on reprogramming skin fibroblasts from donors into induced neural progenitor cells (iNPCs). These can then be differentiated further to induced astrocytes (iAstrocytes), which retain the ageing phenotypes of the donors (Meyer *et al.*, 2014; Gatto *et al.*, 2021). This makes the iAstrocytes an attractive model for diseases, where ageing could play a factor in disease pathology and onset, and this includes Alzheimer's disease.

This chapter focuses on characterisation of the astrocyte responses to different types of stressors that are relevant mechanisms of disease. We hypothesise that astrocytes will show heterogenic responses to various disease-related stressors, namely different types of $A\beta_{1-42}$ aggregation species (oligomers vs fibrils), and oxidative stress.

Firstly, astrocytes may be susceptible to oxidative stress. We hypothesise that oxidative stress can elicit DNA damage, which could have profound effects on the astrocyte function and viability. Oxidative stress-related DNA damage of astrocytes could be one of the mechanisms behind the astrocyte changes in Alzheimer's disease, and therefore human fetal astrocytes as well as adult induced astrocytes were characterised in terms of their responses to oxidative stress. Secondly, astrocytes may be susceptible to Aβ-mediated morphological and molecular changes, which could be disease-relevant. These changes could depend on the type of Aβ aggregation species the astrocytes are exposed to, and this could reveal an important mechanism for the astrocyte-mediated Alzheimer's disease onset and/or pathology. The main aim of the current chapter is therefore to characterise the responses of astrocytes to oligomeric $A\beta_{1-42}$ and fibrillary $A\beta_{1-42}$. Such responses can be compared to the oxidative stress responses, to evaluate how different disease stressors modulate astrocyte function.

The aims of the current chapter are going to be fulfilled by the following objectives:

i. To characterise the DNA damage response of human fetal astrocytes to oxidative stress using immunoblotting and immunocytochemistry for DNA damage markers.
ii. To characterise the responses of human fetal astrocytes to oxidative stress in the context of cell death, using lactase dehydrogenase assay.
iii. To characterise the DNA damage response of human fetal astrocytes, as well as induced Astrocytes (iAstrocytes) to oligomeric and fibrillary $A\beta_{1-42}$ using immunoblotting, immunocytochemistry, and cell death assay (lactate dehydrogenase assay)
iv. To compare the astrocyte responses to oxidative stress to the astrocyte responses to various types of $A\beta_{1-42}$, which could indicate a common mechanism of astrocyte dysfunction in Alzheimer's disease.

## 3.3 Materials

Where required, equipment was bought pre-sterilised, or sterilised by autoclaving for 15 minutes at 121 °C, 15 psi. All solutions and buffers were prepared using Milli-Q pure water. Unless otherwise stated, all reagents were purchased from Sigma-Aldrich.

### 3.3.1 Cell culture materials

#### Human fetal astrocytes

| | |
|---|---|
| 1 x Phosphate Buffered Saline (PBS) | *137 mM NaCl; 2.7 mM KCl; 10 mM Na2HPO4; KH2PO4; pH 7.4* |
| 10x Trypsin / Ethylenediaminetetraacetic acid (EDTA) | Lonza, BE02-007E;<br>*Includes 5 g/L trypsin 1:250 and 2g/L Versene® (EDTA)* |
| Cell Culture 10 $cm^2$ dishes | Nunclon™ Delta Surface, Thermo Scientific, 150350 |
| Cell culture 12-well plates | CELLSTAR® Greiner Bio-ONE, 665180 |
| Cell culture 24-well plates | CELLSTAR® Greiner Bio-ONE, 662160 |
| Cell culture 25 $cm^2$ (T25) flasks | CELLSTAR® Greiner Bio-ONE, 690170 |
| Cell culture 75 $cm^2$ (T75) flasks | CELLSTAR® Greiner Bio-ONE, 658170 |
| Cell culture 96-well microplate | Cellstar, Greiner Bio-One, 655090 |
| Complete Astrocyte medium - *Phenol-red free* | ScienCell®, 1801-prf |
| Complete Astrocyte medium – W*ith phenol-red* | ScienCell®, 1801 |
| Penicillin/Streptomycin | ScienCell®, 0503 |
| Fetal Bovine Serum (FBS) | ScienCell®, 00100 |
| Astrocyte Growth Supplement | ScienCell®, 1852 |
| Human fetal primary astrocytes | ScienCell®, 1800 |
| Ministart 0.2 µm syringe filters | Sartorius, 17597-K |
| Trypan Blue solution, 0.4% | Sigma-Aldrich, T8154 |

**Table 3.1.** Fetal astrocyte cell lines used in the experiments

| Cell line | Description | Source |
|---|---|---|
| **17704** | Human primary fetal astrocytes | ScienCell® (1800) |
| **25417** | Human primary fetal astrocytes | ScienCell® (1800) |
| **25893** | Human primary fetal astrocytes | ScienCell® (1800) |

Fetal astrocyte lines used in the experiments throughout. Cell line name, description and source are stated.

## Induced Astrocytes

| | |
|---|---|
| 1 x Phosphate Buffered Saline (PBS) | *137 mM NaCl; 2.7 mM KCl; 10 mM Na2HPO4; KH2PO4; pH 7.4* |
| Accutase | Sigma, A6964 |
| Cell Culture 10 $cm^2$ dishes | Nunclon™ Delta Surface, Thermo Scientific, 150350 |
| DMEM – *phenol red free* | Gibco**™,** 31053028 |
| DMEM, high glucose – *with phenol red* | Gibco™, 41965039 |
| Fetal Bovine Serum | Biosera, FB-1001 |
| Fibronectin | Merck, FC010 |
| L-glutamine | Gibco™ 25030081 |
| N2 supplement | Gibco, 17502001 |
| Penicillin/Streptomycin | Lonza, DE17-603E |

**Table 3.2.** Cell lines of iAstrocytes used in the experiments.

| Cell line | Type | M/F | Age at biopsy collection |
|---|---|---|---|
| 155v2 | Control line | M | 40 |
| 161 | Control line | M | 31 |
| CS-14 | Control line | F | 52 |

**Cell lines of iAstrocytes used in the experiments throughout.** Cell line name, type, gender, and age of the donors at biopsy are reported.

### 3.3.2 Cell treatments

| | |
|---|---|
| Hydrogen peroxide (30% w/w), with stabilisers | Sigma-Aldrich, H1009 |
| Oligomeric $A\beta_{1-42}$; prepared from the monomeric $A\beta_{1-42}$ | rPeptide, A-1163-1; A1163-2<br>*Monomeric Aβ diluted in 2xTBS buffer (pH 7.4), pre-adjusted to a correct final pH with 45 mM HCl, to a final concentration of 100 µM and incubated for 2 weeks at 4°C.* |
| Fibrillary $A\beta_{1-42}$; prepared from the monomeric $A\beta_{1-42}$ | rPeptide, A-1163-1; A1163-2<br>*Monomeric Aβ diluted in 2xTBS buffer (pH 7.4), pre-adjusted to a correct final pH with 45 mM HCl, to a final concentration of 100 µM and incubated for 24 hrs at 37°C.* |
| $A\beta_{(1-42)}$; scrambled (1.0 mg) | rPeptide, A-1004-2 |

### 3.3.3. Biochemicals

#### Sample preparation

| | |
|---|---|
| Extra Strong Lysis Buffer (XSLB) | *100 mM TrisHCl; 75 mM NaCl; 0.5% w/v SDS; 20 mM sodium deoxycholate; 1% v/v Triton X-100; 2 mM sodium orthovanadate; 1.25 mM sodium fluoride; 1 mM sodium pyrophosphate; 10 mM EDTA* |
| Halt™ Protease and Phosphatase Inhibitor Cocktail (100X) | ThermoFisher Scientific, 78440 |

### Bicinchoninic acid (BCA) protein assay

All measurements were carried out on the Pherastar plate reader (BMG Labtech).

| | |
|---|---|
| Pierce™ BCA Protein Assay<br>Reagent A | ThermoFisher Scientific, 23223 |
| Pierce™ BCA Protein Assay<br>Reagent B | ThermoFisher Scientific, 23224 |
| Pierce™ Bovine Serum Albumin<br>Standard, 2 mg/ml | ThermoFisher Scientific, 23210 |
| 96-well EIA/RIA plates,<br>high binding | Costar, 3590 |

### Sodium Dodecyl Sulphate-Polyacrylamide Gel Electrophoresis (SDS-PAGE) reagents

| | |
|---|---|
| 10 % (w/v) Ammonium Persulphate (APS) | Sigma, A3678-100G *in* $ddH_2O$ |
| 10x Running Buffer | *144 g glycine; 30.2 g Tris Base; 10 g SDS; 0.9 L* $H_2O$ |
| 10x Transfer Buffer | *144 g glycine; 30.2 g Tris Base; 0.9 L* $H_2O$ |
| 1x PBS | *137 mM NaCl; 2.7 mM KCl; 10 mM* $Na_2HPO_4$*;* $KH_2PO_4$*; pH 7.4* |
| 1x PBS-T | *1x PBS; 0.05% Tween-20* |
| 4x Resolving Buffer | *1.5 M Tris HCl, pH 8.8; 0.4% SDS* |
| 4x Stacking Buffer | *0.5 M Tris HCl, pH 6.8; 0.4% SDS* |

| | |
|---|---|
| 6x Laemmli Sample Buffer | *2.4 g SDS; 9.4 mL glycerol; 2.4 mL Tris 0.5M - pH 6.8; 4.2 mL dd$H_2O$; 24 mg bromophenol blue; 1.86 DTT* |
| Bovine Serum Albumin (BSA) | Sigma, 05482-100G |
| Novex™ 4-20% Tris-Glycine Mini Gels, WedgeWell™ format, (Gradient gels) | ThermoFisher Scientific, Invitrogen™, XP04202BOX |
| Ponceau stain | *0.1% (w/w) Ponceau S dye; 1% v/v acetic acid; in 500 mL dd$H_2O$* |
| ProtoGel<br>(30% w/v Acrylamide) | Geneflow, A2-0072 |
| N,N,N',N'-Tetramethylethylenediamine (TEMED) | Melford, T3100 |

### Protein molecular weight marker

Unless stated otherwise, Precision Plus Protein™ Standards Dual Colour protein ladder (Bio-Rad, 161-0374) was used for immunoblotting with SDS-PAGE gels (table 3.3). The protein markers range from 10 kDa to 250 kDa.

Precision Plus Protein™ Dual Xtra Prestained Protein Standards protein ladder (Bio-Rad, 1610377) was used when immunoblotting for low molecular weight proteins, and Aβ detection. The protein markers range from 2 kDa to 250 kDa.

## Gel compositions for SDS-PAGE

**Table 3.3.** Gel compositions for SDS-PAGE gels used.

| Reagent | 6% Stacking Gel | 10% Resolving Gel | 12% Resolving Gel |
|---|---|---|---|
| $dH_2O$ | 4.1 mL | 7.9 mL | 6.6 mL |
| 30% Acrylamide | 1 mL | 6.7 mL | 8 mL |
| 4x Resolving buffer | - | 5 mL | 5 mL |
| 4x Stacking Buffer | 750 µL | - | - |
| 10% APS | 60 µL | 200 µL | 200 µL |
| TEMED | 6 µL | 8 µL | 8 µL |

Table showing the compositions for making 6 mL of 6% stacking gel, and 20 mL of 10% and 12% resolving gels.

### Immunoblotting antibodies

**Table 3.4.** Primary antibodies used for western blotting.

| Antibody | Specificity | Species / type | Dilution | Source and catalogue number |
|---|---|---|---|---|
| Anti-p21 | Human p21 | Mouse / monoclonal | 1:500 | BD Pharmingen™, 556431 |
| GFAP | Endogenous levels of total GFAP protein | Rabbit / Monoclonal | 1:1000 | Cell Signalling Technology, 12389 |
| γH2A.X | Endogenous levels of γH2A.X only when phosphorylated at serine 139 | Rabbit / Monoclonal | 1:1000 | Cell Signalling Technology, 9718 |
| Phospho-Chk2 (pChk2) | Endogenous levels of Chk2 only when phosphorylated at Thr68 | Rabbit / Monoclonal | 1:1000 | Cell Signalling Technology, 2197 |
| Phospho-cdc2 (Tyr15) | Endogenous levels of cdc2 protein only when phosphorylated at tyrosine 15 | Rabbit / Monoclonal | 1:1000 | Cell Signalling Technology, 4539 |

Primary antibodies used for western blotting. Antibody name, specificity, species, dilution used, and source are shown.

**Table 3.5.** Secondary antibodies used for western blotting.

| Antibody | Raised species | Dilution | Source and catalogue number |
|---|---|---|---|
| Anti-rabbit IgG, HRP- linked antibody | Goat | 1:2000 | Cell Signalling Technology, 7074 |
| Anti-mouse IgG, HRP- linked antibody | Horse | 1:2000 / 1:5000 | Cell Signalling Technology, 7076 |

Secondary antibodies used for western blotting. Antibody name, species the antibody was raised in, dilution used, and source are shown.

### Immunocytochemistry reagents

| | |
|---|---|
| 4% Paraformaldehyde in 1xPBS | Sigma-Aldrich, |
| Permeabilising solution | *0.3% Triton X-100-1xPBS* |
| Blocking buffer | *3% BSA – 0.01% Tween-20 – 1xPBS* |
| H3342 10 mg/ml | *Used at 1:2000 dilution in 1xPBS* |
| 1x PBS | *137 mM NaCl; 2.7 mM KCl; 10 mM $Na_2HPO_4$; $KH_2PO_4$; pH 7.4* |
| Storage solution | *1x PBS – 0.01% Sodium Azide* |

### Immunocytochemistry antibodies

**Table 3.6.** Primary antibodies used for immunocytochemistry.

| Antibody | Specificity | Species/ Type | Dilution | Source and catalogue number |
|---|---|---|---|---|
| Rabbit IgG | Purified total rabbit IgG to use as an isotype control | Rabbit | Antibody-dependent | BioVision, 1268 |
| γH2A.X | Endogenous levels of H2A.X only when phopshorylated at serine 139 | Rabbit / Monoclonal | 1:150 | Cell Signalling Technology, 9718 |
| Vimentin | Recognises vimentin | Chicken / Polyclonal | 1:1000 | Merck, AB5733 |

Table showing a list of primary antibodies used for immunocytochemistry. Antibody name, specificity, species, type, dilution, and source are shown.

**Table 3.7.** Secondary antibodies for immunocytochemistry.

| Fluorophore | Dilution | Source |
|---|---|---|
| Goat anti-rabbit AlexaFluor 568 | 1:1000 | Invitrogen, A11011 |
| Goat Anti-Chicken AlexaFluor 488 | 1:1000 | Invitrogen, A11039 |

Details of secondary antibodies used for immunocytochemistry. Fluorophore used, dilution, and source are shown.

### 3.3.4 Lactate Dehydrogenase assay reagents

| | |
|---|---|
| Cytotox 96® Non-Radioactive<br>cytotoxicity assay | Promega, G1780 |
| Positive control | 1 µL LDH positive control in<br>10 mL 1% BSA-1xPBS |

## 3.4 Methods

### 3.4.1 Culture of fetal human primary astrocytes

Fetal astrocytes (table 3.1) were cultured in complete astrocyte medium with all supplements at 37°C in 5 % $CO_2$ and 95 % air, in 75 $cm^2$ cell culture flasks. Cells were passaged when approaching ~85% confluency. To passage, cell medium was removed, and flasks were washed with sterile PBS (140 mM NaCL, 10 mM phosphate buffer, 3 mM KCl, pH 7.4; sterilised by autoclaving). Astrocytes were incubated in trypsinising solution (1x trypsin (trypsin/EDTA 0.025%/PBS) for approximately 5 minutes at 37°C to detach cells from the culture vessel and pelleted by centrifugation at 550 rcf for 5 minutes.

When required, cells were plated at a specific cell density, appropriate to the cell line and/or size of the cell culture dish. For 96 well plates, cells were plated at 10,000 cells/ well; for 12-well plates, cells were plated at 60,000 cells/ well; for 10 cm dishes, cells were plated according to their growth rate and confluency. The confluency of the cells was dependent on the passage number and cell line. Cell seeding densities were adjusted to reach 80% confluency. Cells were diluted in Trypan-blue, so that cell viability could be assessed qualitatively, and viable cells were counted using haemocytometer. The dilution factor was estimated depending on the cell line and confluency.

Astrocytes were plated at appropriate densities and cultured for at least 24 hours prior to commencing cell treatments. For LDH assays, astrocytes were cultured in phenol red-free cell media, to avoid the phenol red from giving false absorbance readouts.

### 3.4.2 Differentiation and culture of human induced astrocytes

Human induced astrocytes (iAstrocytes) were also used as a model of an aged brain, and for comparison of the effects of treatments between human fetal astrocytes and human iAstrocytes (table 3.2). iAstrocytes were differentiated from induced neural progenitor cells (iNPCs), as described by the methods of Meyer *et al.*, 2014. Briefly, the iNPCs were cultured and maintained by Professor Ferraiuolo's research team and switched to astrocyte differentiation medium on day 1 of iAstrocyte differentiation. To differentiate iNPCs into mature iAstrocytes, the cells were cultured in astrocyte differentiation medium for 7 days. The medium was composed of 500 ml Dulbecco's Modified Eagle Medium (DMEM), supplemented with 1% Pencilin/ Streptomycin 100X, 0.2% N2 Supplement 100X, and 10% of fetal bovine serum. For amyloid beta treatments, iAstrocytes were cultured in phenol red-free iAstrocyte differentiation medium to minimise the interactions of amyloid beta with the phenol red, composed of 500 ml DMEM supplemented with 1% Pencilin/ Streptomycin 100X (10,000 U/mL), 0.2% N2 Supplement 100X, 10% of fetal bovine serum, and 100X l-glutamine (200 mM). Prior to

seeding, cell culture dishes and plates were coated with 1:400 human fibronectin (1 mg/ml) in PBS to ensure cell adherence. When necessary, iAstrocytes were replated on day 3 or 4 of differentiation and were cultured for at least 24 hours prior to cell treatments. To passage, cell medium was removed, and dishes were washed with PBS. Astrocytes were incubated in accutase for 5 minutes at 37$^{o}$C to detach cells from the culture vessel and pelleted by centrifugation at 550 rcf for 5 minutes. The cells were counted using haemocytometer and diluted in appropriate media to a desired cell density. The iAstrocytes used in the experiments originated from a single corresponding donor, where iNPCs were maintained and expanded. The iAstrocytes were used at passages 16-20. Unless otherwise stated, three separate control lines of iAstrocytes were used as three biological repeats. Unless otherwise state, three technical repeats were performed for each cell line and experiment.

### 3.4.3 Treatment protocols

#### Hydrogen Peroxide treatments

Oxidative stress was induced with 100 µM $H_2O_2$ (30% w/v stock diluted in PBS to 100 mM working stock) in fetal astrocyte lines, for either 1 hour, 6 hours or 24 hours.

The effects of $H_2O_2$ treatments were analysed through ICC, SDS-PAGE and immunoblotting, and LDH assays (see section 3.4.2).

Furthermore, oxidative stress in iAstrocytes was induced with 100 µM $H_2O_2$ (30% w/v stock diluted in PBS to 100 mM working stock) for 1 hour, and the effect of this treatment was analysed through ICC for detection of γH2AX-positive DNA foci.

#### Amyloid beta treatments

$A\beta_{1-42}$ oligomers and fibrils were prepared as previously described in the methods of Chapter 2. Scrambled amyloid peptide was also included as a vehicle control for the treatments and was prepared in the same manner as $A\beta_{1-42}$ oligomers and fibrils.

Human fetal astrocytes, and iAstrocytes were treated with 1 µM $A\beta_{1-42}$ oligomers and fibrils, as well as 1 µM scrambled peptide as vehicle control, for a time course treatment. To assess the cell viability of human fetal astrocytes, the cells were treated for 24 hours and 48 hours. To assess the DNA damage response, and changes in cell morphology, human fetal astrocytes were treated for 1 hour, 24 hours and 48 hours. To assess the cell viability of iAstrocytes, as well as DNA damage and cell morphology changes, the cells were treated for 1 hour, 2 hours, 24 hours and 48 hours.

The effects of amyloid beta treatments on human fetal astrocytes and iAstrocytes were analysed through LDH assays and ICC (see section 3.4.2).

### 3.4.2 Protein analysis

#### Lactate Dehydrogenase assay

Lactate Dehydrogenase (LDH) assays were carried out to determine astrocyte viability as a response to oxidative stress. LDH assay measures the amount of LDH released by damaged cells. When the cell plasma membrane is damaged, LDH enzyme is released into the cell culture media (Kumar, Nagarajan and Uchil, 2018). This output can be measured using absorbance measurements. The results for the LDH release were used to estimate the percentage cell death.

Astrocyte viability was determined using the CytoTox96 cytotoxicity assay (Promega), according to the manufacturer's instructions. The absorbance was read using the Pherastar plate reader at 490 nm wavelength. The absorbance was used to calculate percent cytotoxicity, after accounting for media volume corrections.

#### Immunocytochemistry

Cells were washed in pre-warmed PBS and fixed using 4% PFA for 10 minutes. Following fixation, cells were washed three times with cold PBS, and permeabilised in 0.3% triton - X100 for 3 minutes at ambient temperature, followed by washing in PBS. Cells were blocked for 30 minutes in ICC blocking buffer at ambient temperature. Cells were incubated in primary antibody diluted in blocking solution overnight at 4$^{o}$C with gentle rocking. Following three washes in PBS, cells were incubated with the appropriate species of secondary antibody, diluted in blocking buffer, for 1 hour at ambient temperature. To prevent bleaching of flurophores, the secondary antibody incubation and all subsequent steps were performed in darkness. Cells were washed again three times in PBS and incubated with Hoescht H33342 for 10 minutes. Subsequently, cells were washed three times and wither imaged immediately after or stored in darkness at 4$^{o}$C in PBS until imaged using the Opera Phenix® High Content Imaging System (PerkinElmer). Immunocytochemical staining following cell treatments was quantified using Harmony High Content Imaging and Analysis Software (PerkinElmer) (see table 3.6 for the list of antibodies used).

### Preparation of cell lysates

Media was aspirated from astrocytes, cells were washed with ice-cold PBS and detached from plates by vigorous scarping in ice-cold PBS and collected in Eppendorfs. Cells were pelleted by centrifugation at 400 rcf for 4 minutes, at 4°C. The supernatant was discarded. Pellets were snap-frozen in liquid Nitrogen and stored at -80°C. To complete cell lysis, pellets were resuspended in ice-cold extra strong lysis buffer (XSLB, 50 mM Tris HCl pH 7.4, 50 mM NaCL, 2 mM EDTA, 0.1% SDS, protease inhibitor cocktail) and incubated on ice for a minimum of 15 minutes. Samples were sonicated at 70% amplitude for 5 seconds, using a Soniprep 150 Ultrasonic Disintegrator. Samples were then centrifuged at 13,000 rcf for 30 minutes at 4°C and stored at -20 °C until further analysis.

### BCA protein quantification

The Pierce BCA assay (ThermoFisher Scientific) was carried out to determine the protein concentration of the cell lysates. The BCA assay was carried out on high-binding 96-well plates (Greiner) according to the manufacturer's instructions. BCA protein standards, ranging from 0 mg/ml to 2 mg/ml (diluted in PBS) were plated out in duplicate, to calculate a standard curve for determining protein concentrations.

Protein samples were diluted 1:10 with PBS and plated out in duplicate in 96-well plates (EIA/RIA plates, high binding). BCA working reagent was prepared at a ratio of 50:1 of reagent A:B and 200 µL of the working reagent was added to each well. The plate was incubated at 37°C for 30 minutes in darkness. Absorbance at 562 nm wavelength was determined using the Pherastar plate reader.

The calculated standard curve was used to calculate protein concentration for each sample. Prior to western blotting, the samples were diluted to a final concentration of 2 mg/ml using XSLB.

### SDS-PAGE

Prior to electrophoresis, cell lysates were mixed with 6x Laemmli Buffer, boiled at 100°C for 5 minutes to ensure protein denaturing, and centrifuged briefly. Molecular weight standards and protein samples were loaded onto either 12% or 4-12% Tris-Glycine gradient polyacrylamide gels (Invitrogen). Gels were electrophoresed in 1x Running buffer at 130 V until the dye front reached the bottom of the gel.

### Immunoblotting

Gels were placed onto 0.2 µm nitrocellulose membranes (GE Healthcare) sandwiched between Grade 1A Whatmann Filter paper and sponges, in a XCell SureLock™ Mini-Cell Electrophoresis System (ThermoFisher Scientific), immersed in 1x transfer buffer. Proteins were transferred onto nitrocellulose membrane at 0.3 A for 1 hour, membranes were stained with Ponceau stain to ensure

successful protein transfer. Non-specific binding of primary antibodies was blocked by incubating membranes in 5% BSA/PBS-T for 30 minutes, followed by overnight incubation with the appropriate primary antibodies, diluted in 5% BSA/PBS-T, at 4°C.

Following incubation in primary antibody, membranes were washed 3 times in PBS-T (10 minutes/ wash), and incubated with a species-specific HRP-conjugated secondary antibody for 1 hour at ambient temperature, and washed a further three times in PBS-T. Signal was detected using ECL, and membranes were imaged using the G:BOX (Syngene).

Semi-quantitative densitometric analysis of the chemiluminescent images was performed using the GeneTools software (Syngene). Specific bands were selected manually, and background readings were subtracted automatically. All antibody bands detected were normalised to an appropriate loading control.

### Statistical analysis

For each experiment, three replicates (n=3) for technical and biological repeats were achieved, unless stated otherwise. The three biological repeats corresponded to the three cell lines used for fetal astrocytes and iAstrocytes. The technical repeats for each cell line were averaged, and these corresponded to a single biological repeat. All statistical analysis was carried out using GraphPad Prism statistical software. All error bars are reported as standard deviation.

## 3.5 Results

### 3.5.1 Oxidative stress response in astrocytes

To induce oxidative stress in fetal astrocytes, the cells were treated with 100 µM $H_2O_2$ for 1 hr, 6 hrs and 24 hrs. The timeframe of the treatments was selected based on previously generated data in the group (unpublished). 100 µM of $H_2O_2$ is a sublethal dose in astrocytes. The treated astrocytes were compared to control (untreated) astrocytes. The impact of oxidative stress on cell viability was investigated by cytotoxicity assays (LDH assays). The impact of $H_2O_2$ treatment on the DDR was analysed using immunoblotting (SDS-PAGE and western blotting) and immunocytochemistry (ICC).

#### Oxidative stress induces significant cytotoxicity and cell death in fetal astrocytes

Cytotoxicity assays (LDH assays) were performed to measure astrocyte viability after $H_2O_2$ treatments (fig.3.1), expressed as percentage cell death. LDH assay results showed that in fetal astrocytes, there was no change in cell viability after 1 and 6 hrs of treatment. However, there was a significant increase in cell death after 24 hrs of treatment ($p<0.0001$****).

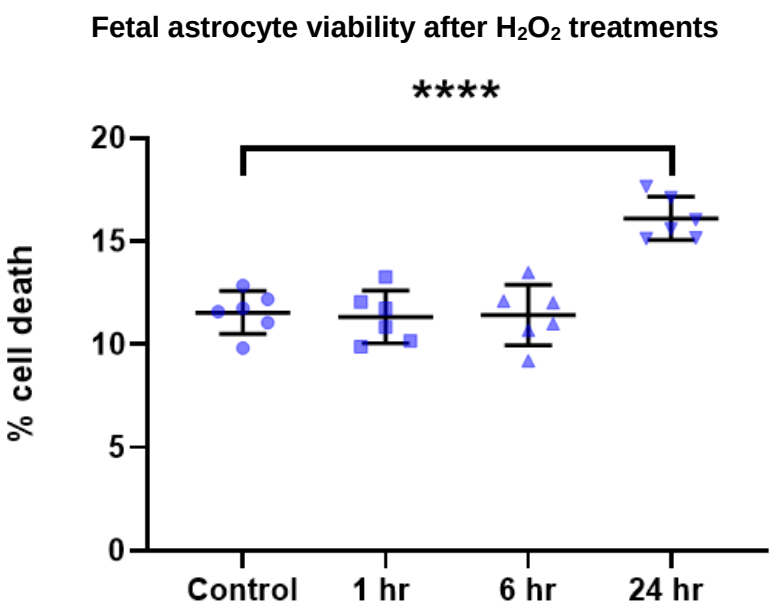


**Figure 3.1** Fetal astrocyte viability after H2O2 treatments.

LDH release from cells was measured in primary astrocytes exposed to 100 µM $H_2O_2$ for 1 hour, 6 hours and 24 hours. The graph illustrates percentage cell death relative to the percentage of LDH released into the cell media compared to LDH retain within cells. Values represent mean±SD experiment. One-way ANOVA: $p<0.0001$**** with post-hoc Dunnett's test for multiple comparisons (n=3).

### Oxidative stress induces a rapid DNA damage response in human fetal astrocytes

Treatment of fetal astrocytes with $H_2O_2$ induced a rapid DNA damage response (fig.3.2), detectable after 1 hour of treatment. Immunoblotting for a panel of DNA damage response and senescence markers was carried out.

There was a significant increase in the expression of phosphorylated checkpoint kinase 2 (pChk2) after 1 hr of treatment ($p<0.001$***) (fig.3.2). The expression of pChk2 decreased after 6 hrs of $H_2O_2$ treatment, returning to control levels. There was a significant increase in the expression of phosphorylated gamma-H2A histone family member X (γH2AX) after 1 hr ($p<0.01$**), which is persistent at 6 hrs and 24 hrs of treatment. p21, a marker for cell senescence, was not significantly upregulated at any time point, compared to untreated controls. Cyclin-dependent kinase 2 (cdc2) phosphorylation was significantly upregulated after 6 hrs of $H_2O_2$ treatment ($p<0.05$); its expression returned to control levels after 24 hrs. Overall, the results indicate that there is a rapid DNA damage response to oxidative stress in human fetal astrocytes, which may be subsequently repaired before cells can progress through the cell cycle.

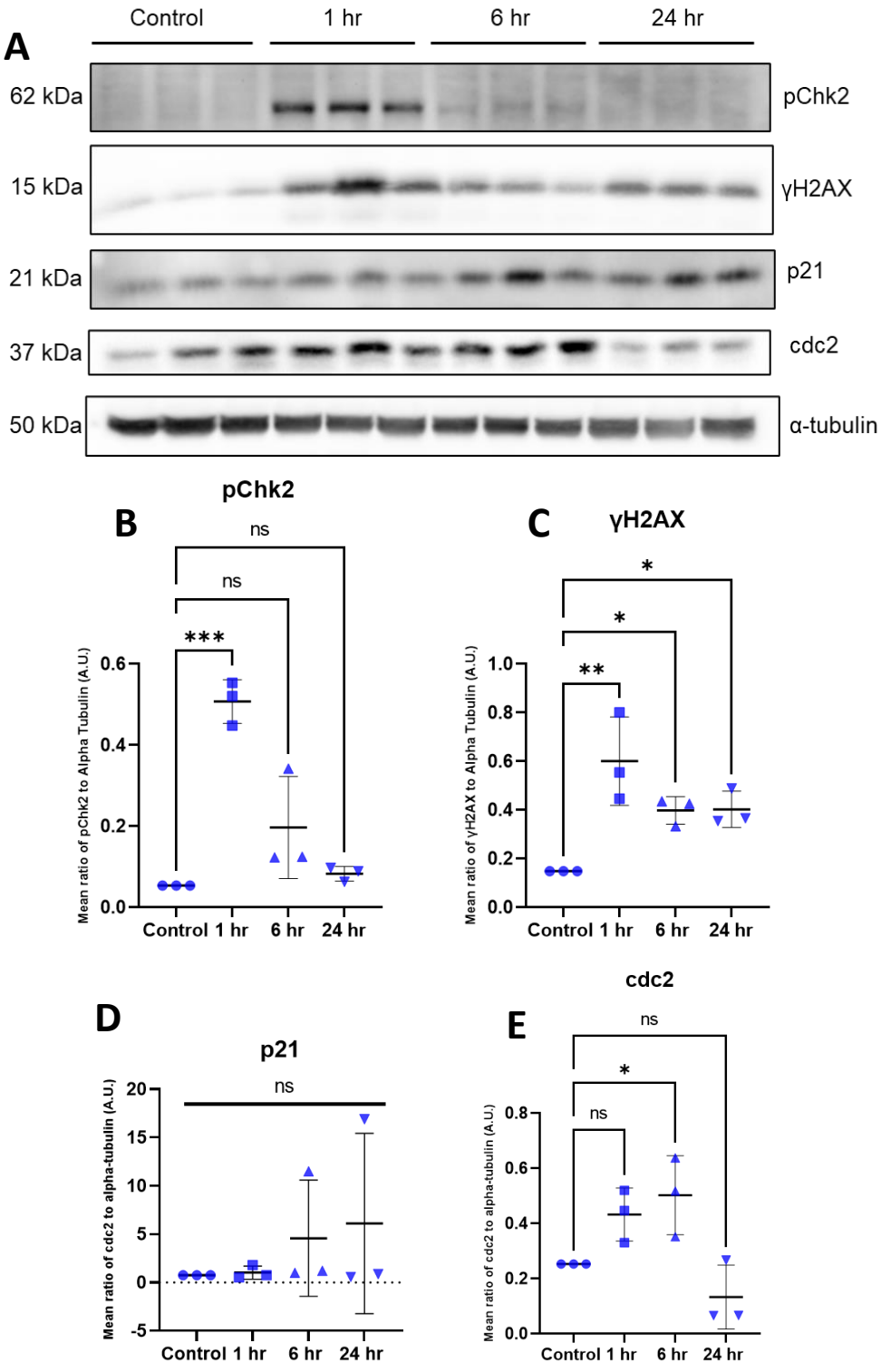


**Figure 3.2** DNA damage response of human fetal astrocytes to oxidative stress induced by H2O2 treatment.

**(A)** Representative immunoblots of cell lysates from human primary astrocytes treated with $H_2O_2$ for 1 hours, 6 hours and 24 hours. Blots were probed with antibodies against γH2AX, pChk2, p21, and cdc2. α-tubulin was used as a loading control. Molecular weight markers are indicated. Graphs showing amounts of (**B**) γH2AX, (**C**) pChk2, (**D**) p21, and (**E**) cdc2 as proportion of α-tubulin. Values represent mean±SD. One-way ANOVA: p<0.05*, p<0.01**, p<0.001*** with post-hoc Dunnett's test for multiple comparisons. n=3

### Oxidative stress induces the formation of γH2AX-positive DNA foci in fetal astrocytes

A feature of DNA damage in cells is the presence of γH2AX-positive DNA foci inside cell nuclei (Podhorecka, Skladanowski and Bozko, 2010). The effect of $H_2O_2$ on the formation of γH2AX-positive DNA foci was assessed using the Opera Phenix High Content Imaging System and subsequent analysis on the Harmony 4.9 software (PerkinElmer). ICC results indicated that the γH2AX-positive DNA foci inside the astrocyte nuclei are detectable after 1 hr of $H_2O_2$ treatment, and that there were significantly more positive nuclei containing DNA foci in the treated astrocytes compared with the control ($p<0.001$***) (fig.3.3). This further shows that the DNA damage response is rapidly upregulated during periods of acute DNA damage to cells, particularly during oxidative stress. The results also indicate that acute oxidative stress facilitates double stranded DNA breaks, which indicates more profound and detrimental cellular damage.

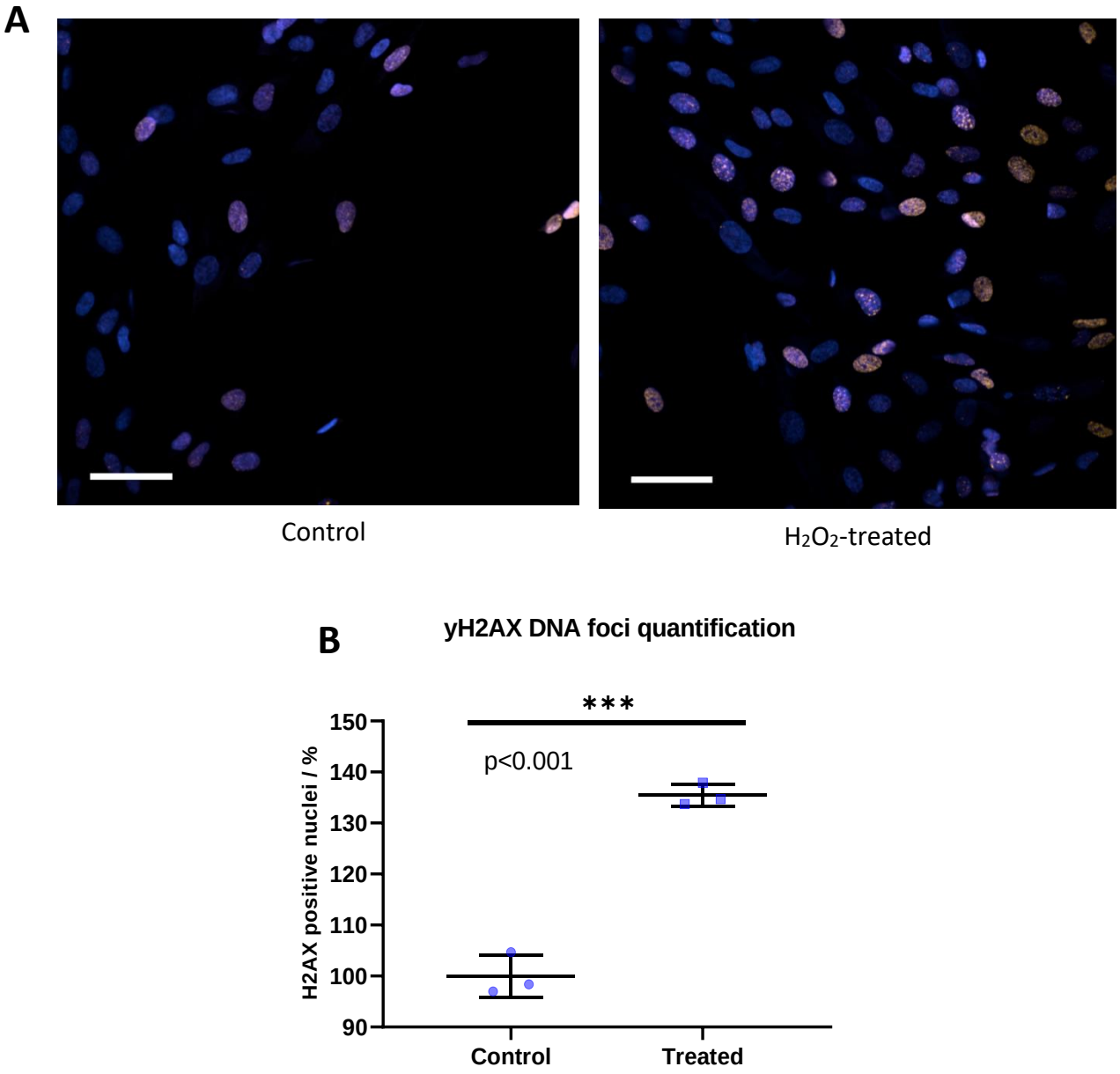


**Figure 3.3** Immunocytochemistry results showing the amount of γH2AX- positive DNA foci in human fetal primary astrocytes.

**(A)** (left) Control (untreated) human fetal astrocytes stained with γH2AX antibody (red) and Hoescht H33342 (blue), and (right) human fetal astrocytes treated with 100 µM $H_2O_2$ for 1 hour, stained with γH2AX antibody (red) and Hoescht H3342 (blue). **(B)** Graph showing the number of γH2AX-positive nuclei in control and treated astrocytes. Data is presented as a percentage value of positive nuclei to all nuclei present, as detected by the Harmony software (PerkinElmer). Values represent mean±SD. Unpaired t-test, p<0.001***. Scale bars = 50 µm.

### Oxidative stress does not induce human fetal astrocyte reactivity

The expression of GFAP in fetal astrocytes treated with $H_2O_2$ was investigated, to characterise whether acute oxidative stress is a triggering factor in the induction of astrocyte reactivity.

Treatment of human fetal astrocytes with 100 µM of $H_2O_2$ for 1 hour, 6 hours and 24 hours did not significantly upregulate the expression of GFAP at any time point compared to the untreated control group (fig.3.4). However, the impact of oxidative stress on GFAP upregulation is difficult to assess, as the data is representative of n=2. Therefore, further repeats are needed to make a more meaningful conclusion.

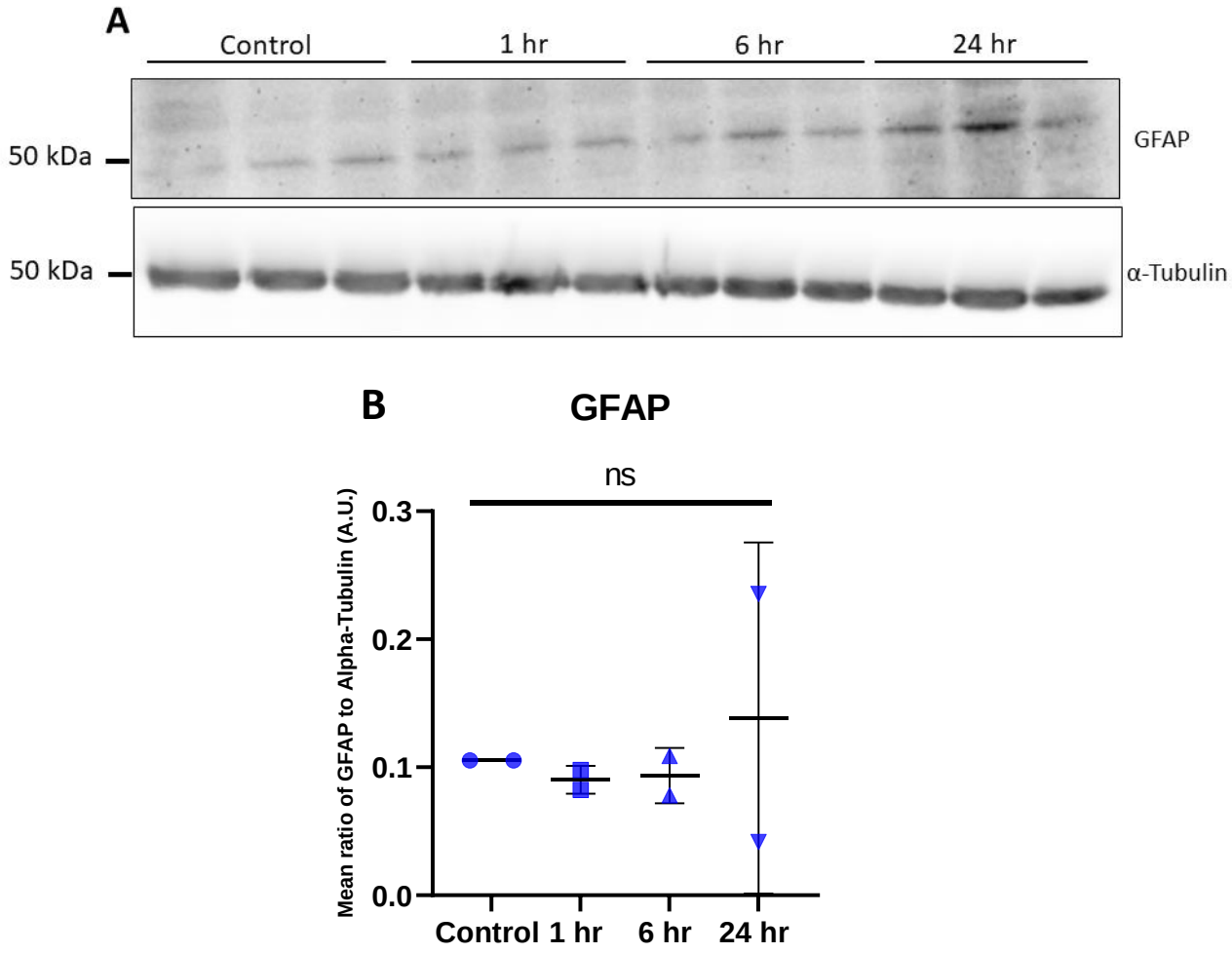


**Figure 3.4.** The impact of H2O2 on reactivity of human primary fetal astrocytes.

**(A)** Representative immunoblots of cell lysates from human primary astrocytes treated with $H_2O_2$ for 1 hours, 6 hours and 24 hours. Blots were probed with an antibody against GFAP. α-tubulin was used as a loading control. Molecular weight markers are indicated. **(B)** A graph showing relative amounts of GFAP expression, as proportion of α-tubulin. Values represent mean±SD. One- way ANOVA: p<0.05*, p<0.01**, p<0.001***, p<0.0001****. n=2 (two cell lines; three technical repeats per cell line).

### Oxidative stress response in human induced astrocytes

To induce oxidative stress in iAstrocytes, the cells were treated with 100 µM $H_2O_2$ for 1 hr to measure the formation of γH2AX DNA foci. The treated astrocytes were compared to control (untreated) astrocytes. The impact of $H_2O_2$ treatment on the DDR was analysed using ICC.

ICC results indicated that the γH2AX-positive DNA foci inside the astrocyte nuclei were detectable after 1 hour of 100 µM $H_2O_2$ treatment in all three iAstrocyte cell lines (fig.3.5). Throughout experimental investigation, we used three separate cell lines, originating from three separate donors (healthy controls), as biological repeats (there were three technical repeats per cell line for each experiment conducted). When the results for all three cell lines were collated, there was no significant difference between the treated and control groups (fig.3.5.b). Interestingly, when the results were separated by each cell line, there is significantly more DNA foci present in the treated astrocytes compared to the control (fig.3.5.c); higher DNA foci formation was seen in iAstrocytes from older donors (for example CS-14), and lower DNA foci formation was seen in iAstrocytes from younger donors (for example 161). This suggests that the DNA damage response was rapidly upregulated during periods of acute DNA damage to cells, particularly during oxidative stress in iAstrocytes, and that this response could be differential based on the individual. The results also indicate that acute oxidative stress caused double stranded DNA breaks, as γH2AX detects the more detrimental double stranded DNA breaks.

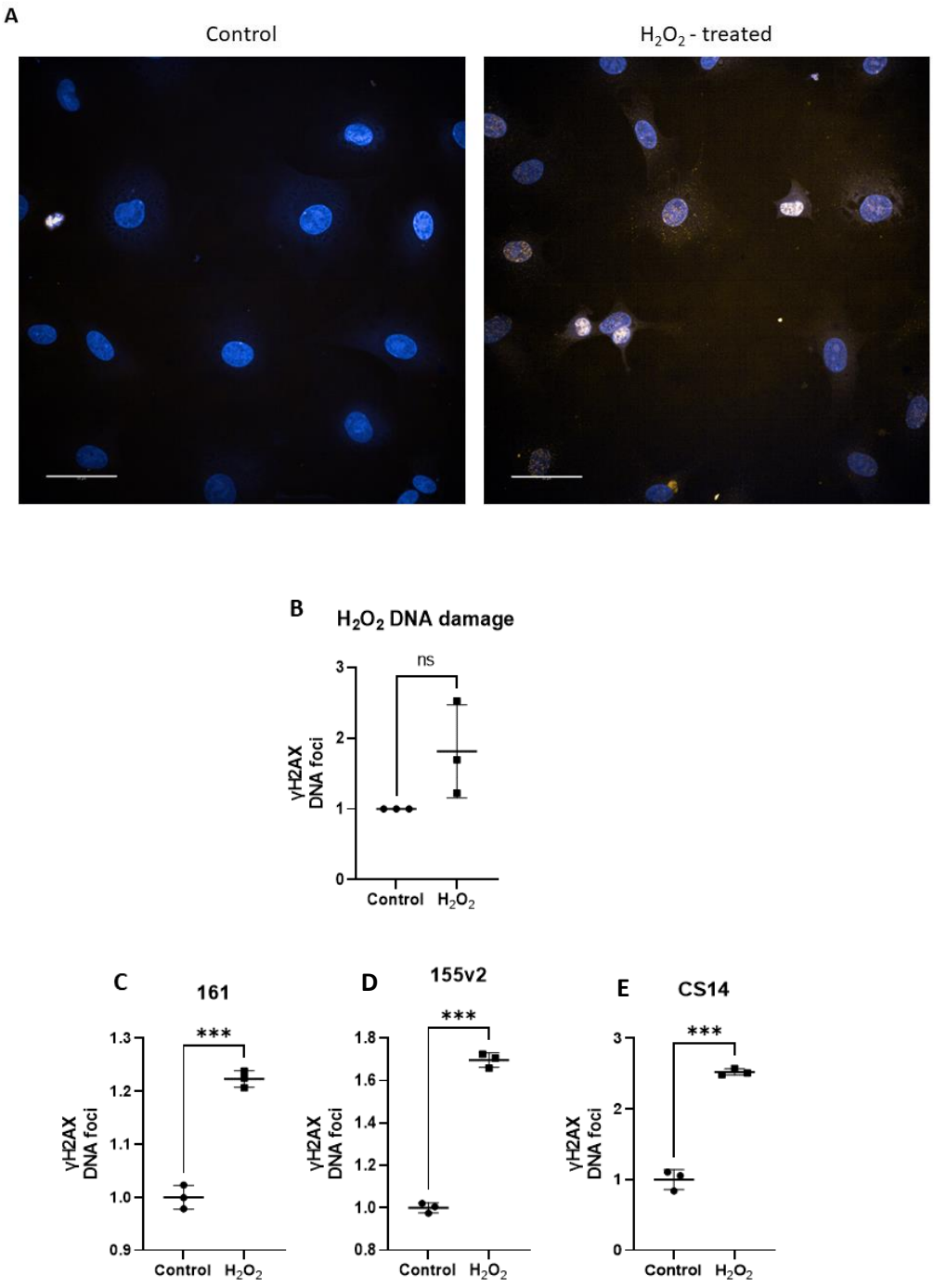


**Figure 3.5.** Immunocytochemistry results showing the amount of γH2AX- positive DNA foci in human iAstrocytes.

**(A)** (left) Control (untreated) iAstrocytes stained with γH2AX antibody (red) and Hoescht H33342 (blue), and (right) iAstrocytes treated with 100 µM $H_2O_2$ for 1 hour, stained with γH2AX antibody (red) and Hoescht H3342 (blue). **(B)** Graph showing the amount of γH2AX-positive nuclei in control and treated astrocytes (all cell lines). **(C-E)** Graphs showing the amount of γH2AX-positive nuclei in control and treated astrocytes in individual cell lines. **(C)** cell line 161 (31 year old healthy donor); **(D)** 155v2 (40 year old healthy donor); **(E)** CS-14 (50 year old healthy donor). Data is presented as a fold change value of positive nuclei to all nuclei present (number of positive nuclei/ number of all nuclei). Values represent mean±SD. Unpaired t-test, $p<0.001$***. Scale bars = 50 µm. n=3

### 3.5.2 Response of fetal astrocytes to amyloid-beta treatments

To compare the effects of oxidative stress with another Alzheimer's disease relevant stress, fetal astrocytes were subjected to treatments with oligomeric and fibrillary $A\beta_{1-42}$. Scrambled peptide treatments were used as vehicle control. This allowed for an initial characterisation of the mechanisms and heterogeneity behind astrocyte responses during Alzheimer's disease-associated injury.

#### Amyloid-beta does not cause changes in human fetal astrocyte cell viability

Astrocytes were treated with 1 µM $A\beta_{1-42}$ oligomers or fibrils for 24 hours or 48 hours (see section 3.4.3 for methods). The time points of 24 and 48 hours were chosen, as oxidative stress did not cause any significant changes in astrocyte viability at earlier time points. The fetal astrocyte viability as a response to $A\beta_{1-42}$ was investigated using LDH cytotoxicity assays.

Treatment of fetal astrocytes with 1 µM $A\beta_{1-42}$ oligomers for 24 hours and 48 hours did not cause any significant change to the astrocyte viability when compared to the control group (untreated) (fig.3.6). Likewise, treatment of fetal astrocytes with 1 µM $A\beta_{1-42}$ fibrils for the same length of time also did not cause any significant change to the astrocyte viability compared to the control group (untreated) (fig.3.6). This suggests that neither $A\beta_{1-42}$ oligomers or $A\beta_{1-42}$ fibrils are toxic to fetal astrocytes *in vitro* at this concentration.

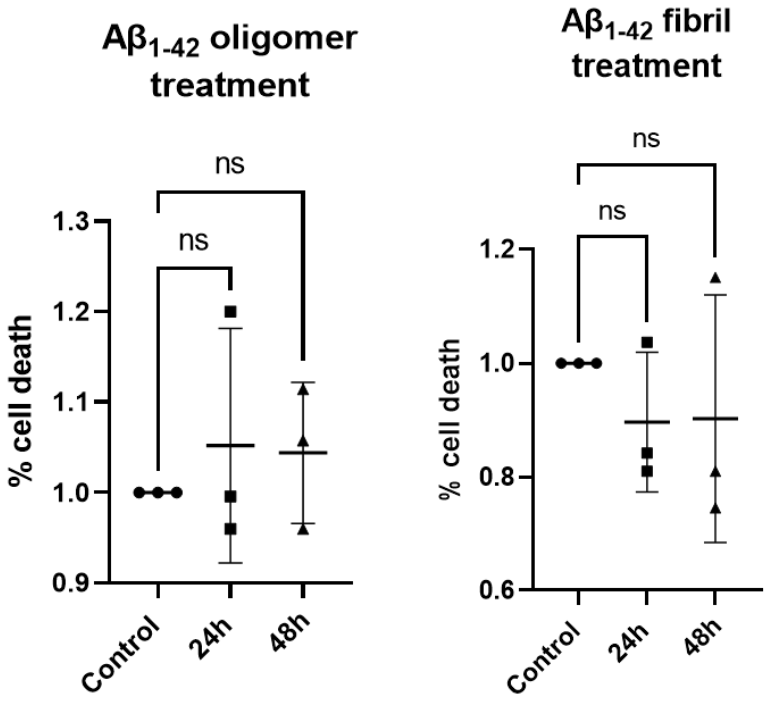


**Figure 3.6.** The viability of human fetal astrocytes after treatment with oligomeric and fibrillary $A\beta_{1-42}$.

The viability of human fetal astrocytes as measured by the LDH release, normalise to the control values. Astrocytes were treated with 1 µM $A\beta_{1-42}$ oligomers and fibril for 24 hours and 48 hours, compared to control (untreated). The graph illustrates LDH release from cells into the medium, expressed as a fold change of percentage cell death. Values represent mean±SD experiment. One-way ANOVA with post-hoc Dunnett's test for multiple comparisons, n=3.

## Investigation of the effects of amyloid-beta oligomers on human fetal astrocytes

Firstly, the impact of $A\beta_{1-42}$ oligomers on human fetal astrocytes *in vitro* was investigated. As described in the introduction chapter (chapter 1), Aβ oligomers may be the main aggregation species promoting adverse effects leading to cellular dysfunction and neuronal loss in Alzheimer's disease. Human fetal astrocytes were treated with 1 µM of $A\beta_{1-42}$ for a time course to detect DNA damage response, as well as cell morphology changes.

## Amyloid beta oligomers do not cause DNA damage in human fetal astrocytes

To detect DNA damage in human fetal astrocytes, ICC was performed to detect γH2AX-positive DNA foci (fig.3.7). The time course for this was 1 hour, to match the time course of the acute oxidative stress induced DNA damage response in these astrocytes. Additional time points at 24 and 48 hours were also included, as there was no detectable cell viability changes or cell morphology changes at those points. The DNA damage response would naturally precede such events, and therefore the additional points were added.

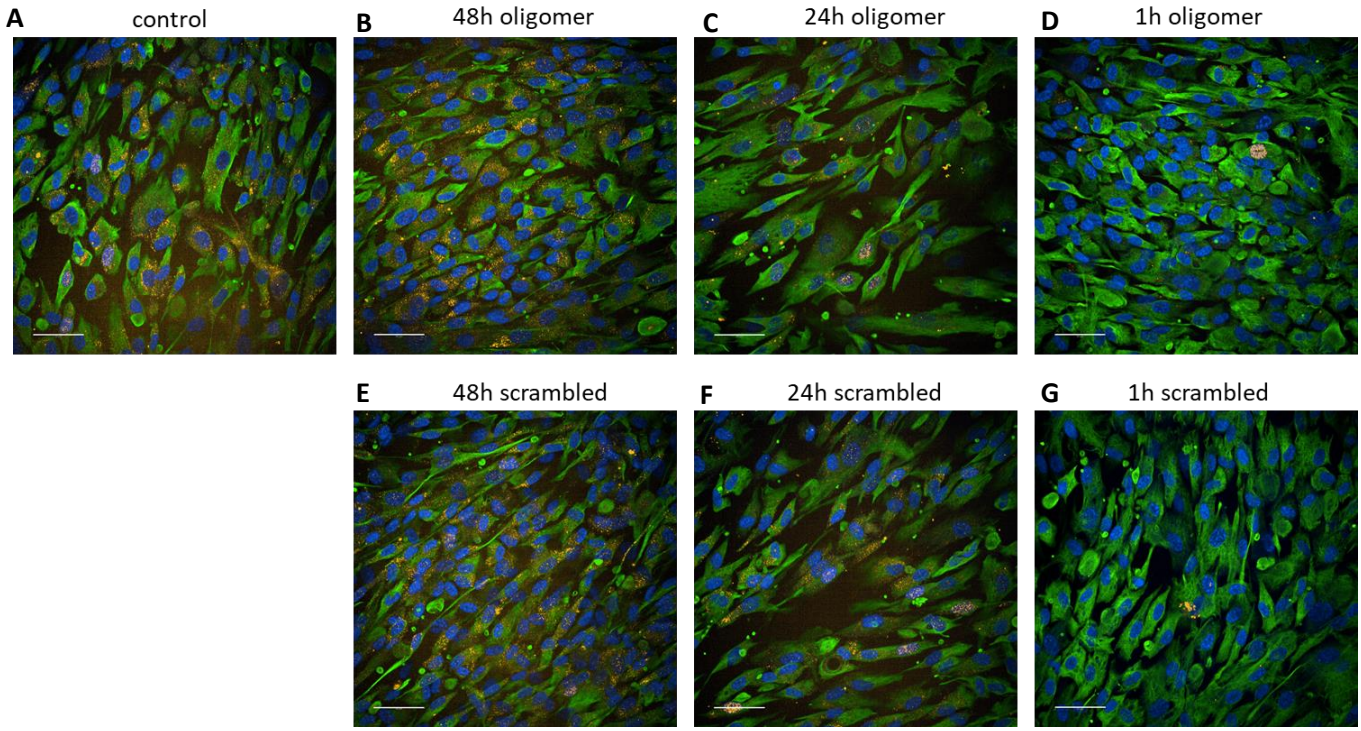


**Figure 3.7.** Representative immunocytochemistry images of fetal astrocyte morphology and formation of DNA damage γH2AX foci, as a response to amyloid beta oligomers.

Immunocytochemistry images detecting astrocyte morphology with astrocyte marker vimentin (green), and γH2AX-positive DNA foci detected with γH2AX antibody (red). The nuclei are stained with Hoescht (blue). **(A)** untreated (control) fetal astrocytes; fetal astrocytes treated with with 1 µM oligomeric $A\beta_{1\text{-}42}$ for **(B)** 48 hours, **(C)** 24 hours, **(D)** 1 hour; as well as fetal astrocytes treated with 1 µM scrambled Aβ peptide as vehicle control for **(E)** 48 hours, **(F)** 24 hours, and **(G)** 1 hour. Representative images of n=3. Imaged on the Opera Phenix High Content Imaging System (PerkinElmer). Scale bars = 50 µm.

The formation of γH2AX foci was investigated, as well as low and high damage. Positive γH2AX nuclei refer to any nuclei which contain more than, or equal to, three γH2AX DNA foci. Low damage counts the γH2AX-positive foci when there are between 3 to 10 foci per nucleus. High damage represents the foci count of more than 10 per nucleus. The all-damage parameter encompasses all potential damage combined (both low and high damage parameters).

The astrocyte responses were compared statistically using one-way ANOVA. The post-hoc analysis was also performed for multiple comparisons, using Bonferroni's test. This test aimed to determine whether there is a significant difference in the amount of γH2AX positive DNA foci in pre-selected treatment groups. The comparisons were made for control versus all treatment groups at all time-points. Additionally, the comparisons were made for the scrambled control group versus the time-matched amyloid-treated group (fig.3.8). There was no significant difference in the number of γH2AX-positive DNA foci between control (untreated) group and the treated groups at any time point (fig.3.8). Additionally, there was no significant difference in the number of γH2AX-positive DNA foci between all remaining treatment groups, suggesting that the Aβ oligomers do not induce a DNA damage response in these astrocytes within 48 hours of treatment. For details regarding the results of one-way ANOVA and Bonferrroni's multiple comparisons test see Appendix 3.1.

Interestingly, compared to the ICC results in fig.3.3, there was a higher detectable, non-specific background for the γH2AX marker. This was evident, as there was staining that was not localised to the nucleus specifically. The analysis parameters of the software were set to exclude the values for background staining. However, the presence of this non-specific staining may further suggest that the signal is not being detected as there is no upregulation of γH2AX inside the nuclei.

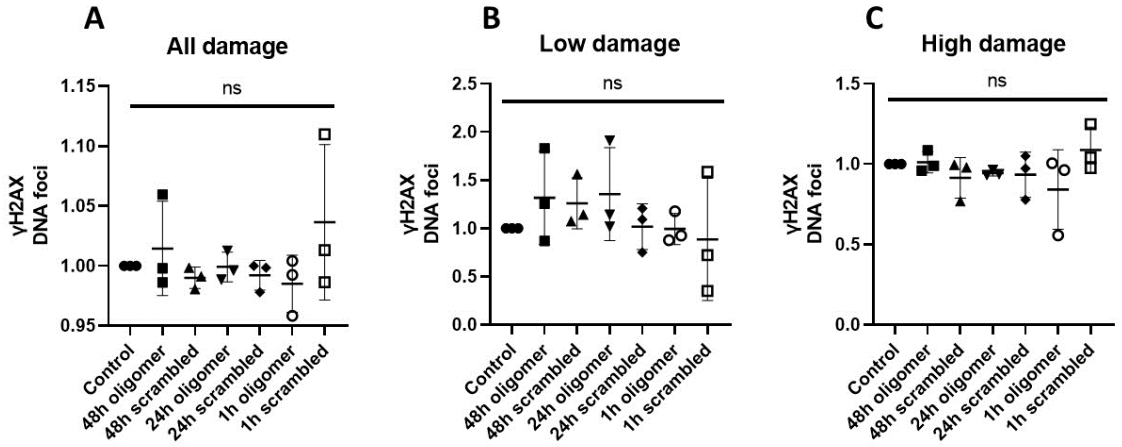


**Figure 3.8** The quantification of DNA damage based on the number of γH2AX- positive DNA foci in human fetal primary astrocytes, as a response to $A\beta_{1-42}$ oligomer treatment.

The quantification of DNA damage based on the number of γH2AX positive DNA foci in human fetal primary astrocytes, as a response to $A\beta_{1-42}$ oligomer treatment. Fetal astrocytes treated with oligomers for 48 h, 24 h, and 1 h. All analysis was carried out using the Harmony Analysis Software (PerkinElmer). Graphs showing: **(A)** All damage detected; **(B)** Low damage detected (between 3-10 foci/ nucleus); **(C)** High damage detected (>10 foci/ nucleus). Data is presented as a fold change value of foci-positive nuclei to all nuclei detected. Standard error bars represent mean±SD. One-way ANOVA with Bonferroni's post-hoc test for multiple comparisons of pre-selected groups. Groups for statistical analysis: Control vs all treatment groups; and scrambled control group vs time-matched $A\beta_{1-42}$-treated group. Significant differences indicated.

### Amyloid beta oligomers do not cause changes in the morphology of human fetal astrocytes

Changes in astrocyte morphology were investigated by measuring mean cell area, cytoplasm region, cell roundness, cell width and cell length. The astrocyte morphology was investigated using a cytoplasm astrocyte specific marker, vimentin, imaged on the Opera Phenix High Content Imaging System (PerkinElmer) (fig.3.7). The vimentin intensity was analysed and quantified using the Harmony Software (PerkinElmer).

The statistical differences in morphology for the different parameters were tested using one-way ANOVA with Bonferroni's post-hoc test for multiple comparisons of pre-selected treatment groups. The results showed that there was no significant change in the mean cell area, cytoplasm region, cell roundness, cell width or cell length after 1, 24 and 48 hours of treatment when compared to the control (untreated) group (fig.3.9). Moreover, the results showed that there was no significant difference between any of the treatment groups. For detailed results of the one-way ANOVA and the Bonferroni's post-hoc analysis, see Appendix 3.2. This could suggest that the astrocytes do not become reactive, and/or do not become stressed *in vitro* as a response to amyloid beta treatments. As these astrocytes have been characterised prior (see section 3.5.1), there is a degree of confidence that the astrocytes were not stressed and not reactive at baseline (untreated control).

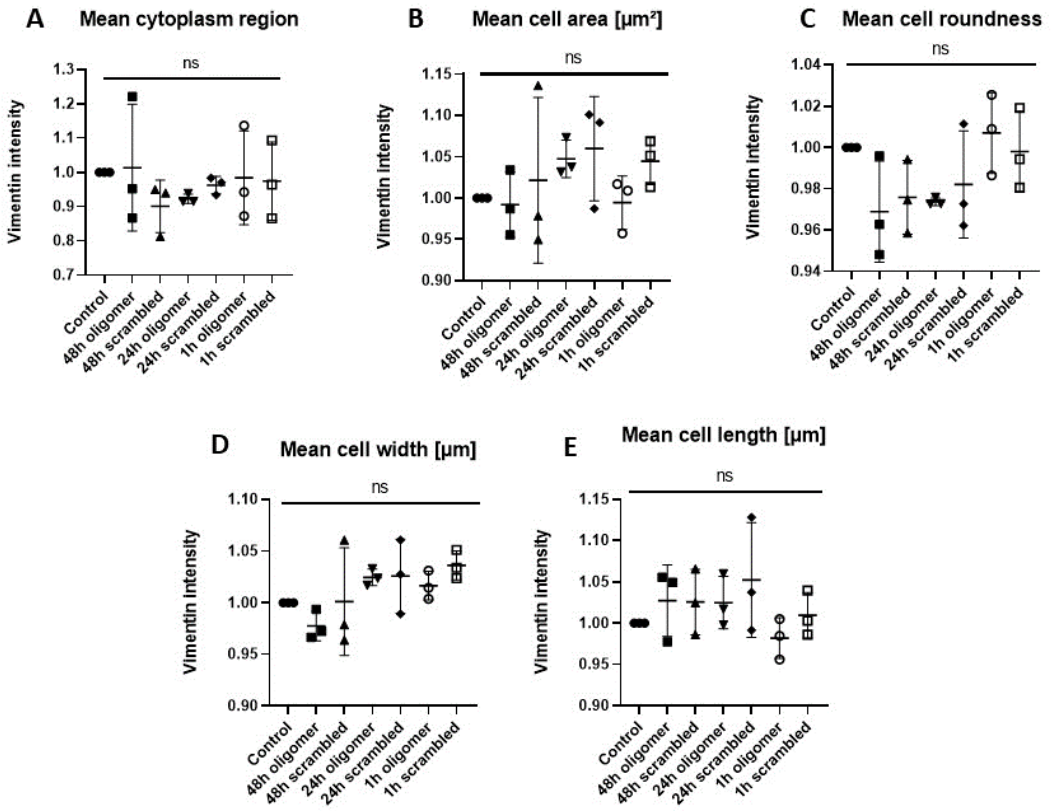


**Figure 3.9.** The effect of $A\beta_{1-42}$ oligomers on fetal astrocyte morphology observed by vimentin immunocytochemistry analysis.

Fetal astrocytes were treated with 1 µM $A\beta_{1-42}$ oligomers for 48, 24, 1 hour as well 1 µM of scrambled Aβ peptide as a vehicle control, and untreated control. All analysis of vimentin intensity was carried out using the Harmony Analysis Software (PerkinElmer). The graphs represent changes in vimentin intensity for morphological parameters of: (**A**) mean cytoplasm region, (**B**) mean cell area, (**C**) mean cell roundness, (**D**) mean cell width, (**E**) mean cell length. The values have been normalised to untreated control group. Values are represented as percentage fold change of vimentin intensity (arbitrary units). Error bars represent mean±SD. One way ANOVA with Bonferroni's post-hoc analysis for multiple comparisons, n=3.

### Investigation of the effect of amyloid-beta fibrils on human fetal astrocytes

Amyloid beta fibrils are the main component of amyloid plaques associated with the development of Alzheimer's disease. According to the original amyloid cascade hypothesis (Hardy and Higgins, 1992), the amyloid plaques drive further progression of Alzheimer's disease, which includes events such as reactive astrogliosis. Hence, it is entirely possible that in these astrocytes, it would be the amyloid beta fibrils that have a more detrimental effect on their morphology and function. Therefore, the effects of $A\beta_{1-42}$ fibrils were investigated next in human fetal astrocytes.

Human fetal astrocytes were treated with amyloid beta fibrils, to investigate whether the aggregated peptide elicits a different effect on astrocytes than oligomeric amyloid beta. The astrocytes were treated with 1 µM of amyloid beta fibrils, to represent the highest physiological concentration of amyloid beta to see the maximum potential effects of Aβ on astrocytes. The morphology of astrocytes was investigated using an astrocyte-specific marker, vimentin. Meanwhile, the DNA damage response, using a DNA damage detection marker γH2AX, was also investigated. This specifically focused on the detection of γH2AX-positive DNA foci (fig.3.10).

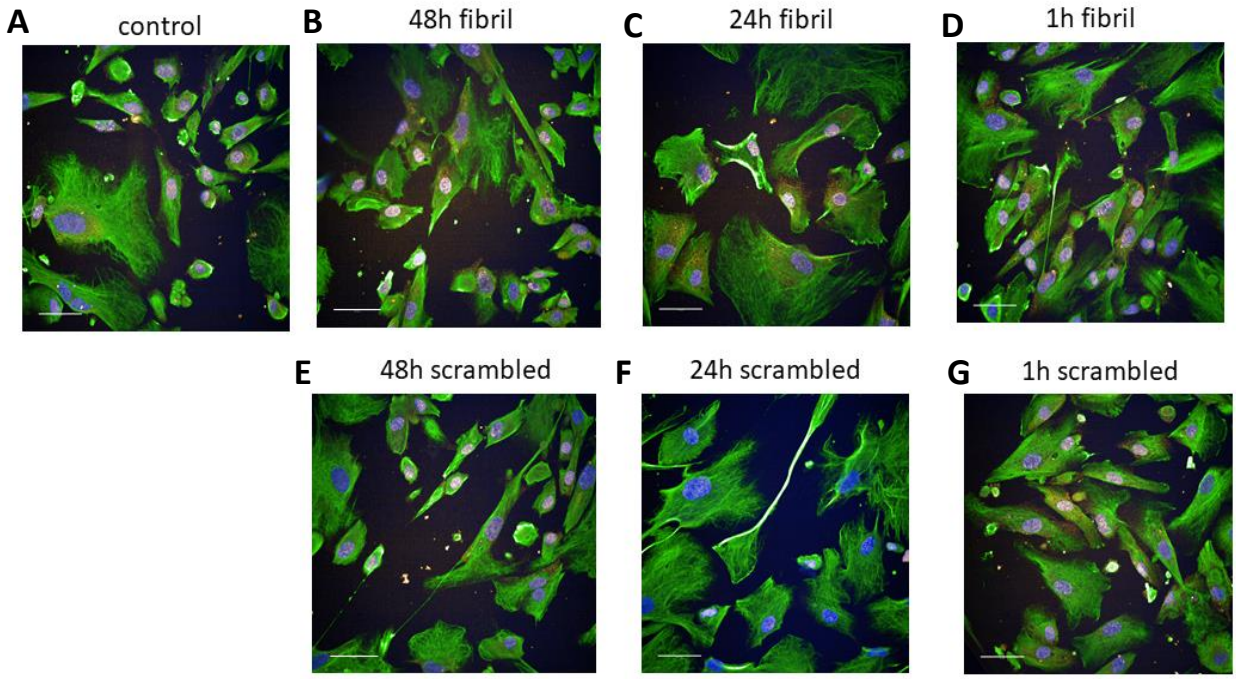


**Figure 3.10.** Representative immunocytochemistry images detecting changes to fetal astrocyte morphology and formation of DNA damage γH2AX foci as a response to amyloid beta fibrils.

Immunocytochemistry images detecting astrocyte morphology with astrocyte marker vimentin (green), and γH2AX-positive DNA foci detected with γH2AX antibody (red). The nuclei are stained with Hoescht (blue). **(A)** untreated (control) fetal astrocytes; fetal astrocytes treated with with 1 µM fibrillary $A\beta_{1-42}$ for **(B)** 48 hours, **(C)** 24 hours, **(D)** 1 hour; as well as fetal astrocytes treated with 1 µM scrambled Aβ peptide as vehicle control for **(E)** 48 hours, **(F)** 24 hours, and **(G)** 1 hour. Representative images of n=3. Imaged on the Opera Phenix High Content Imaging System (PerkinElmer). Scale bars = 50 µm.

### Amyloid beta fibrils do not cause DNA damage in human fetal astrocytes

The DNA damage response was investigated in human fetal astrocytes, in response to the amyloid beta fibril treatments.

Treatment of human fetal astrocytes with 1 µM of $A\beta_{1-42}$ fibrils did not cause any significant changes to the upregulation of DNA damage response marker, γH2AX. This was specifically examined in the context of the formation of γH2AX-positive DNA foci, which are a hallmark of the onset of cellular DNA damage. The statistical analysis used was one-way ANOVA with post-hoc Bonferroni's test for multiple comparisons. No increase in DNA damage or DNA foci, were detected as a response to amyloid beta fibril treatments, when compared to the untreated control group (fig.3.11). Further post-hoc analyses (Bonferroni's post-hoc analysis for multiple comparisons), which compared the mean of pre-selected treatment groups as described in the oligomer analysis section, revealed that there was no significant difference in the amount of DNA damage detected by γH2AX staining in any of the treatment groups. The details on the results of one-way ANOVA and Bonferroni's post-hoc test can be found in Appendix 4.1.

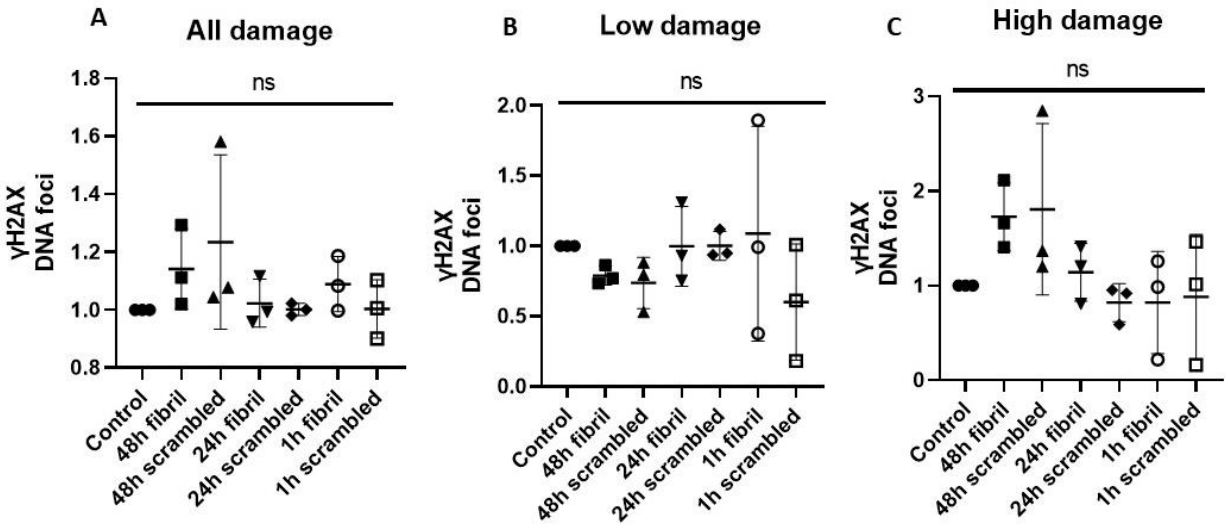


**Figure 3.11**. The quantification of DNA damage based on the number of γH2AX- positive DNA foci in human fetal primary astrocytes, as a response to $A\beta_{1-42}$ fibril treatment.

The quantification of DNA damage based on the number of γH2AX positive DNA foci in human fetal primary astrocytes, as a response to $A\beta_{1-42}$ fibril treatment. Fetal astrocytes treated with fibrils for 48 h, 24 h, and 1 h. All analysis was carried out using the Harmony Analysis Software (PerkinElmer). Graphs showing: **(A)** All damage detected; **(B)** Low damage detected (between 3-10 foci/ nucleus); **(C)** High damage detected (>10 foci/ nucleus). Data is presented as a fold change value of foci-positive nuclei to all nuclei detected. Standard error bars represent mean±SD. One-way ANOVA with Bonfrroni's post-hoc test for multiple comparisons of pre-selected groups. Groups for statistical analysis: Control vs all treatment groups; and scrambled control group vs time-matched $A\beta_{1-42}$-treated group. Significant differences indicated.

### Amyloid beta fibrils do not cause changes in morphology of human fetal astrocytes

Vimentin was used again to investigate the changes in astrocyte morphology following time-course treatments with amyloid beta fibrils. The time-course treatments of astrocytes with amyloid beta fibrils matched the time course treatments with amyloid beta oligomers, and these were: 1 hour, 24 hours and 48 hours at 1 µM.

Changes in astrocyte morphology were investigated by measuring mean cell area, cytoplasm region, cell roundness, cell width and cell length. The astrocyte morphology was investigated using a cytoplasm astrocyte specific marker, vimentin, imaged on the Opera Phenix High Content Imaging System (PerkinElmer) (fig.3.10). The vimentin intensity was analysed and quantified using Harmony Software (PerkinElmer).

The statistical differences in morphology for the different parameters were tested using one-way ANOVA with Bonferroni's post-hoc test for multiple comparisons of pre-selected treatment groups. The results showed that there was no significant change in the mean cell area, cytoplasm region, cell roundness, cell width or cell length after 1, 24 and 48 hours of treatment when compared to the control (untreated) group (fig.3.12). Moreover, the results showed that there was no significant difference between any of the treatment groups. For detailed results of the one-way ANOVA and the Bonferroni's post-hoc analysis, see Appendix 4.2. This could suggest that the astrocytes do not become reactive, and/or do not become stressed *in vitro* as a response to amyloid beta fibril treatments.

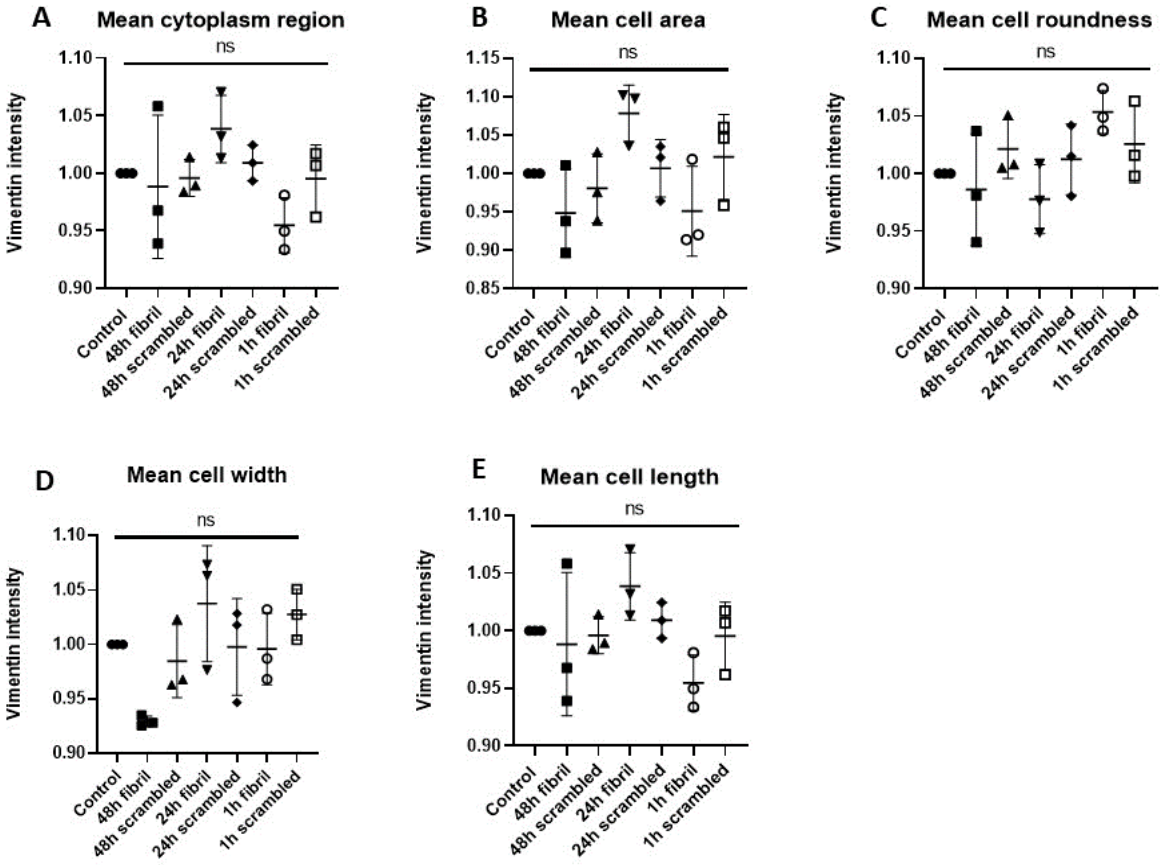


**Figure 3.12.** The effect of $A\beta_{1-42}$ fibrils on fetal astrocyte morphology observed by vimentin immunocytochemistry analysis.

Fetal astrocytes were treated with 1 µM $A\beta_{1-42}$ fibrils for 48, 24, 1 hour as well 1 µM of scrambled Aβ peptide as a vehicle control, and untreated control. All analysis of vimentin intensity was carried out using the Harmony Analysis Software (PerkinElmer). The graphs represent changes in vimentin intensity for morphological parameters of: (**A**) mean cytoplasm region, (**B**) mean cell area, (**C**) mean cell roundness, (**D**) mean cell width, (**E**) mean cell length. The values have been normalised to untreated control group. Values are represented as percentage fold change of vimentin intensity (arbitrary units). Error bars represent mean±SD. One way ANOVA with Bonferroni's post-hoc analysis for multiple comparisons, n=3.

### 3.5.3 Response of induced Astrocytes to amyloid beta

#### Amyloid beta does not cause changes in the cell viability of induced Astrocytes

iAstrocytes were treated with 1 µM $A\beta_{1-42}$ oligomers or fibrils for 1 hour, 2 hours, 24 hours or 48 hours. For comparison, both untreated control group and scrambled peptide as vehicle control group were added. The latter controls for the effect of an irrelevant peptide on astrocytes. The time points of 24 hours and 48 hours were chosen to match the Aβ treatments for fetal astrocytes. Additional 1 hour and 2-hour time points were also chosen, to investigate the potential of Aβ being more toxic to a model of aged astrocytes (iAstrocytes). The iAstrocyte viability as a response to $A\beta_{1-42}$ was investigated using LDH cytotoxicity assays.

One-way ANOVA with Bonferroni's post-hoc analysis for multiple comparisons was carried out as the statistical test. All treatment groups were compared to the untreated control group. Additionally, scrambled peptide controls were compared to their timed amyloid-treated counterpart treatments.

When all three cell lines were collated, the treatment of iAstrocytes with 1 µM $A\beta_{1-42}$ oligomers for, 1 hour, 2 hours, 24 hours and 48 hours did not cause any significant change to the overall astrocyte viability when compared to the control group (untreated), and scrambled vehicle group (fig.3.13). Furthermore, when treatment groups were compared to scrambled peptide controls, there were no significant differences between any of the treatment groups. This suggests that $A\beta_{1-42}$ oligomers do not cause a reduction in cell viability of iAstrocytes within 48 hours of treatment (fig.3.13). For further details on the statistical analysis results, see Appendix 5.1.

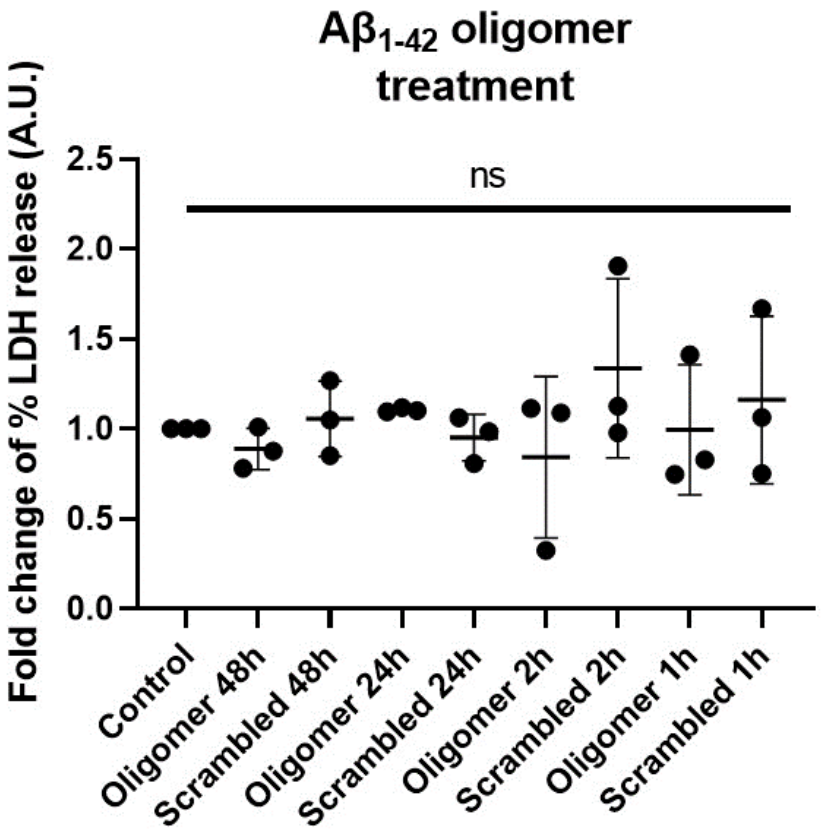


A graph showing cell death measurements of iAstrocytes, as measured by the % LDH release normalised to the control values. Astrocytes were treated with 1 µM $A\beta_{1-42}$ oligomers and scrambled peptide for 1 hour, 2 hours, 24 hours, and 48 hours, compared to control (untreated). The graph illustrates LDH release from cells into the medium, expressed as a fold change of percentage cell death. Error bars represent mean±SD. One-way ANOVA with Bonferroni's post-hoc analysis. n=3

Interestingly, separating the results by cell line revealed that there were no significant differences in the treatment groups of CS14 and 161 cell lines when compared to the untreated control group, as well as when applying the post-hoc test for comparison of all the remaining treatment groups (Bonferroni's post-hoc test) (fig.3.14.a, fig.13.4.b). Meanwhile, the 155v2 cell line showed significant differences when the untreated control group was compared to scrambled 2h group. Interestingly, there was also a significant decrease in the % LDH release in the oligomer 2h treatment group when compared to the 2h scrambled group (fig.3.14.c). This could indicate a potential issue with the response of 155v2 iAstrocytes to the vehicle control. For further details on the statistical analysis results, see Appendix 5.1.

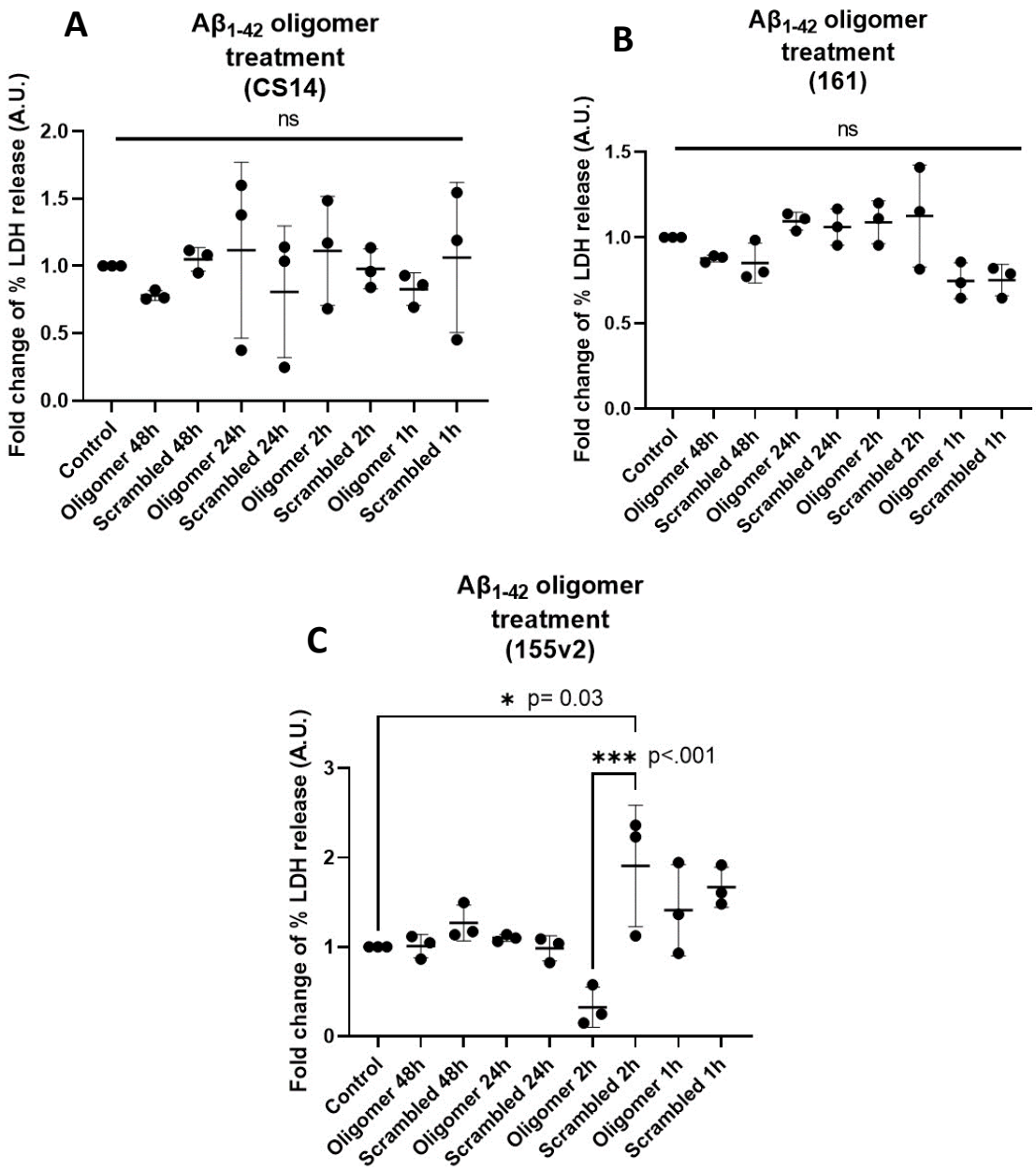


**Figure 3.14.** The cell death of all three iAstrocyte cell lines separately, represented as fold change of % LDH release, after treatment with oligomeric Aβ1-42.

Graphs showing cell death measurements of iAstrocytes, as measured by the % LDH release normalised to the control values. Astrocytes were treated with 1 µM $A\beta_{1-42}$ oligomers and scrambled peptide for 1 hour, 2 hours, 24 hours, and 48 hours, compared to control (untreated). The graph illustrates LDH release from cells into the medium, expressed as a fold change of percentage cell death. Graphs represent results for: **(A)** CS-14 iAstrocytes; **(B)** 161 iAstrocytes; **(C)** 155v2 iAstrocytes. Error bars represent mean±SD. One-way ANOVA with Bonferroni's post-hoc analysis. The relevant significance is shown. n=3

Likewise, treatment of iAstrocytes with 1 µM $A\beta_{1-42}$ fibrils for the same length of time (1 hour, 2 hours, 24 hours, and 48 hours) did not cause any significant change to the astrocyte viability compared to the control (untreated) group (fig.3.15). When all iAstrocyte data was collated, the post-hoc pairwise analysis showed that there were no significant differences in LDH release between any of the treatment groups (fig.3.15). For further details on the statistical analysis results, see Appendix 5.1.

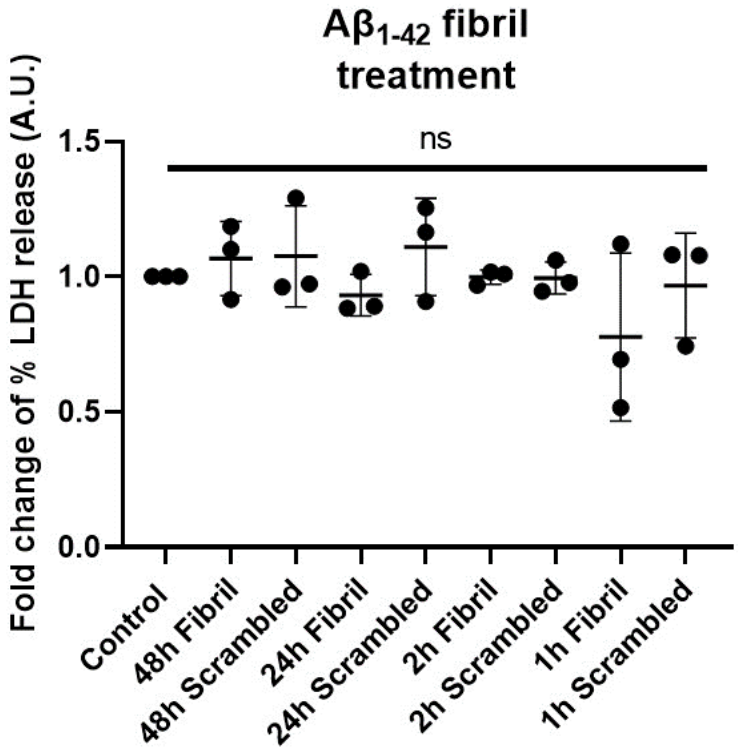


**Figure 3.15.** The cell death of all three iAstrocyte cell lines collated, represented as fold change of % LDH release, after treatment with fibrillary Aβ1-42.

A graph showing cell death measurements of iAstrocytes, as measured by the % LDH release normalised to the control values. Astrocytes were treated with 1 µM $A\beta_{1-42}$ fibrils and scrambled peptide for 1 hour, 2 hours, 24 hours, and 48 hours, compared to control (untreated). The graph illustrates LDH release from cells into the medium, expressed as a fold change of percentage cell death. Error bars represent mean±SD. One-way ANOVA with Bonferroni's post-hoc analysis. n=3

Similar to the results above for iAstrocytes treated with oligomeric $A\beta_{1-42}$, separating the results by cell line revealed that there were no significant differences in the treatment groups of CS14 (fig.3.16.a) cell line, when compared to the untreated control group, as well as when applying the post-hoc Bonferroni's test for multiple comparisons. For the 161 cell line, when compared to the untreated control group, the 48h scrambled peptide group showed a significant increase in the LDH release (fig.3.16.b). Meanwhile, the 155v2 cell line showed significant differences in some of the treatment groups (fig.3.16.c). Interestingly, for 155v2 control iAstrocytes, treatment of astrocytes with fibrillary Aβ for 1h significantly reduced the LDH release when compared to the untreated control group. Furthermore, the 24h fibril treatment showed a reduction in LDH release as well, when compared to the 24h scrambled vehicle control. For further details on the statistical analysis results, see Appendix 5.1.

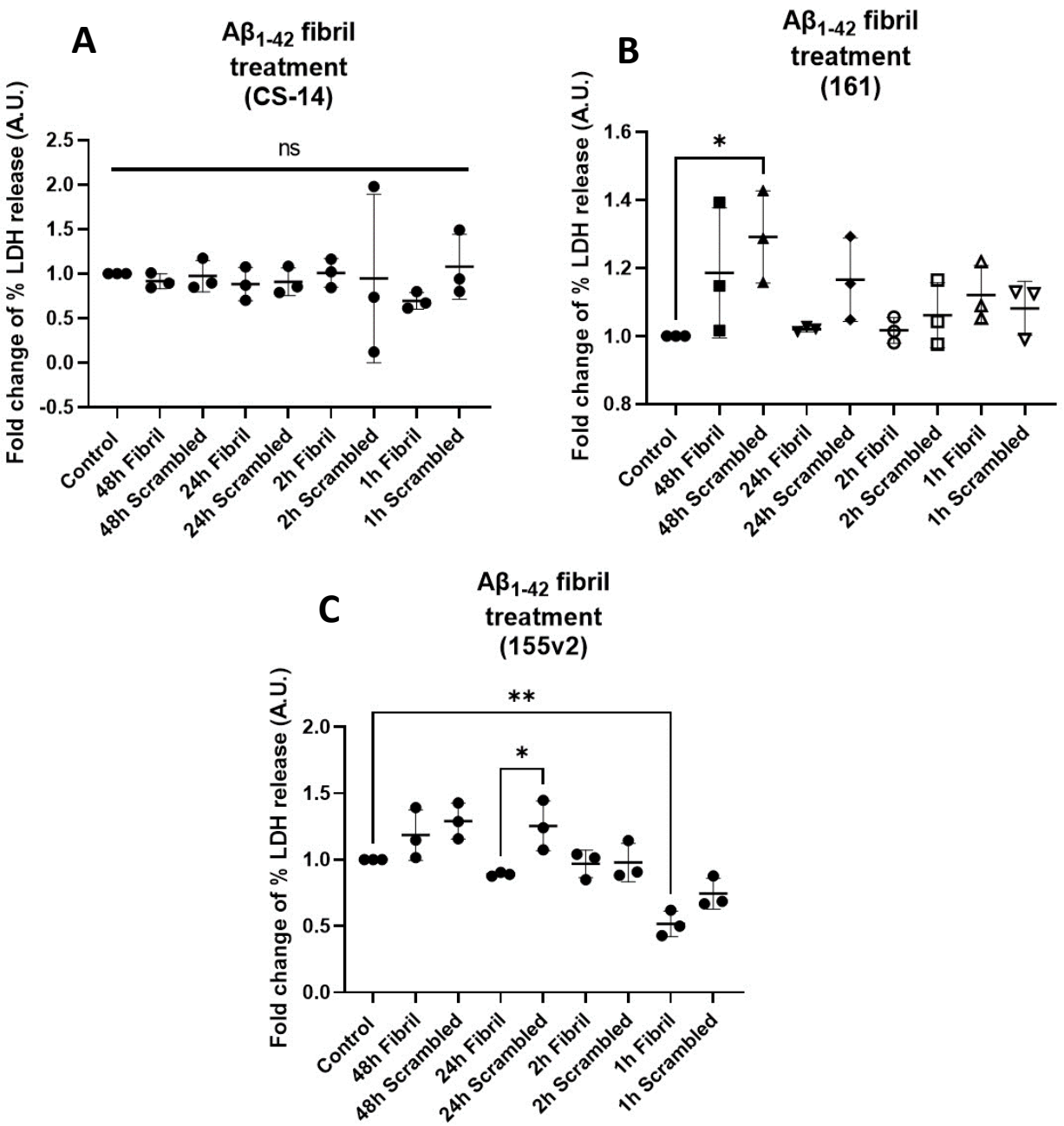


**Figure 3.16.** The cell death of all three iAstrocyte cell lines separately, represented as fold change of % LDH release, after treatment with fibrillary Aβ1-42.

Graphs showing cell death measurements of iAstrocytes, as measured by the % LDH release normalised to the control values. Astrocytes were treated with 1 µM $A\beta_{1-42}$ fibrils and scrambled peptide for 1 hour, 2 hours, 24 hours, and 48 hours, compared to control (untreated). The graph illustrates LDH release from cells into the medium, expressed as a fold change of percentage cell death. Graphs show results for **(A)** CS-14 iAstrocytes; **(B)** 161 iAstrocytes; **(C)** 155v2 iAstrocytes. Error bars represent mean±SD. One-way ANOVA with Bonferroni's post-hoc analysis. Relevant significance is indicated. n=3

### Investigation of amyloid beta oligomers on induced Astrocytes

iAstrocytes were treated with 1 µM of $A\beta_{1-42}$ oligomers, as well as scrambled peptide (vehicle control), and untreated control group. Immunocytochemistry was performed to investigate the DNA damage response, as detected by the formation of γH2AX-positive DNA foci; and the cell morphology changes of iAstrocytes, as detected by the vimentin marker.

### Amyloid beta oligomers do not cause changes in DNA damage response or cell morphology of induced Astrocytes

The iAstrocytes were treated with oligomers for 1 hour, 2 hours, 24 hours, and 48 hours, as well as scrambled peptide as vehicle control. Further treatment was also added to assess the impact of repeated $A\beta_{1\text{-}42}$ stress on iAstrocytes. This treatment, referred to as 'repeated stress', consisted of repeated dosing of iAstrocytes with 1 µM of $A\beta_{1\text{-}42}$ oligomers at 1 hour, 2 hours, 24 hours and 48 hours of iAstrocyte cell culture. This meant that for repeated stress, iAstrocytes were dosed four times with 1 µM of $A\beta_{1\text{-}42}$ oligomers over a course of 48 hours.

For all time points, the cytoplasmic astrocyte-specific marker, vimentin, was used to investigate the changes in astrocyte morphology by measuring changes in the mean cell area, cytoplasm region, cell roundness, cell width, and cell length of iAstrocytes after oligomer treatments. To detect DNA damage in iAstrocytes, ICC was performed to detect γH2AX-positive DNA foci, which are indicative of the induction of the DNA damage response. The statistical analysis used for each read-out was a one-way ANOVA with a Bonferroni's post-hoc test to look for differences between pre-selected groups. For all time points, both amyloid-treated and scrambled (vehicle)-treated groups were compared to the untreated control. Within the same analysis, the amyloid-treated group was also compared to the scrambled (vehicle) control. Furthermore, different set of analyses were performed. At first, all cell lines were pooled together and normalised to the untreated control groups to achieve three biological repeats for each time point treatment. Then, to look for individual differences in cell lines at the different time points, every iAstrocyte cell line was separated. The results were analysed again using one-way ANOVA with Bonferroni's post-hoc test as described above. For details of the statistical analysis results for all time points see appendix 5.2.

However, for some of the treatment groups there is an absence of three replicates. This is due to a persistent mycoplasma infection in the cell line 161, which made it difficult to complete all experiments to full replicate numbers. As mycoplasma infection could interfere with the results, the respective cell line results were not used in some of the experimental data and subsequent analysis. The lines were tested every week for mycoplasma infection; due to time constraints of the project it

was not possible to thaw and expand early vials for iAstrocyte differentiation for the purpose of repeating the ICC analysis for that cell line.

The differences in cell morphology (vimentin) and DNA damage (γH2AX) were investigated in pooled iAstrocyte cell lines treated with $A\beta_{1-42}$ for 1 hour (fig.3.17).

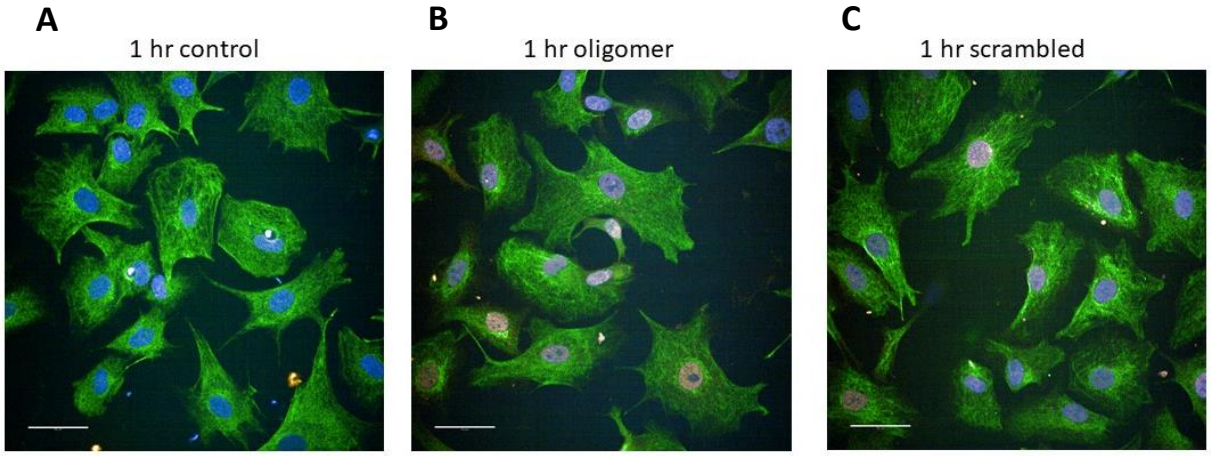


**Figure 3.17.** Representative immunocytochemistry images detecting changes to induced astrocyte (iAstrocyte) morphology and formation of DNA damage γH2AX foci as a response to amyloid beta oligomers.

Immunocytochemistry images detecting induced Astrocyte (iAstrocyte) morphology with astrocyte marker vimentin (green), and γH2AX-positive DNA foci detected with γH2AX antibody (red). The nuclei are stained with Hoescht (blue). iAstrocytes treated for 1 hour with **(A)** untreated (control); **(B)** 1 µM oligomeric Aβ1-42; **(C)** 1 µM scrambled Aβ peptide as vehicle control. Representative images of n=3. Imaged on the Opera Phenix High Content Imaging System (PerkinElmer). Scale bars = 50 µm.

There was no significant difference in the amount of γH2AX-positive DNA foci present in any of the treatment groups (fig.3.18).

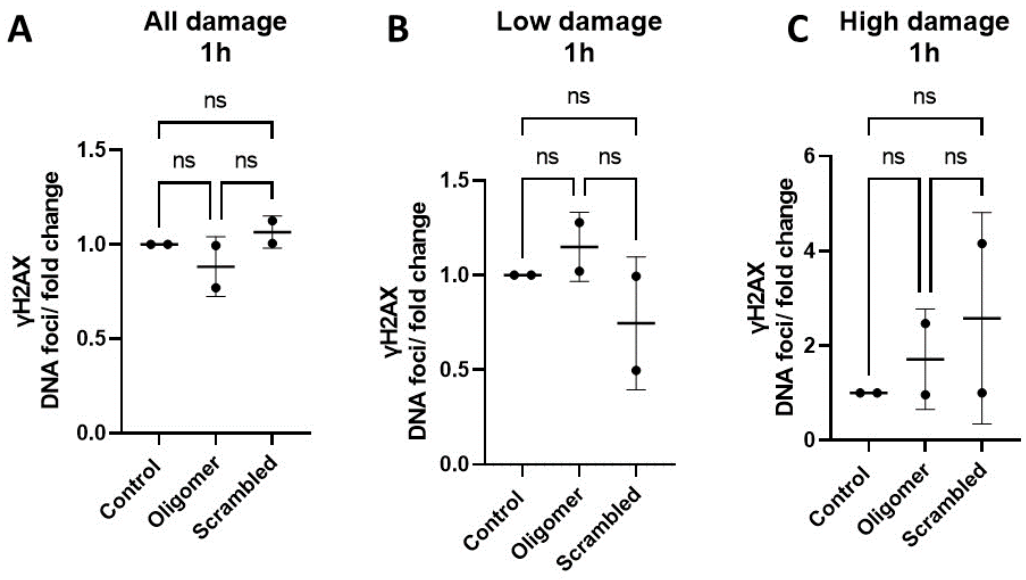


**Figure 3.18.** Formation of DNA damage indicative γH2AX-positive foci in iAstrocytes as a response to 1 hour $A\beta_{1-42}$ oligomer treatment.

The quantification of DNA damage based on the number of γH2AX positive DNA foci in human induced astrocytes (iAstrocytes), as a response to $A\beta_{1-42}$ oligomer treatment for 1 hour. Analysis was carried out using the Harmony Analysis Software (PerkinElmer). Graphs showing: **(A)** All damage detected; **(B)** Low damage detected (between 3-10 foci/ nucleus); **(C)** High damage detected (>10 foci/ nucleus). Data is presented as a fold change value of foci-positive nuclei to all nuclei detected. Standard error bars represent mean±SD. One-way ANOVA with Bonferroni's post-hoc test for multiple comparisons of pre-selected groups. Groups for statistical analysis: Control vs all treatment groups; and scrambled control group vs time-matched $A\beta_{1-42}$-treated group. N=2 (two separate iAstrocyte cell lines as biological repeats)

Additionally, the results were separated by individual cell lines. This was for the purpose of looking for potential differences in DNA damage responses that could have been influenced by the individual donors' responses to $A\beta_{1-42}$. There was no significant difference in the DNA damage detected in CS14 iAstrocytes as a response to $A\beta_{1-42}$ oligomers after 1 hour (fig.3.19).

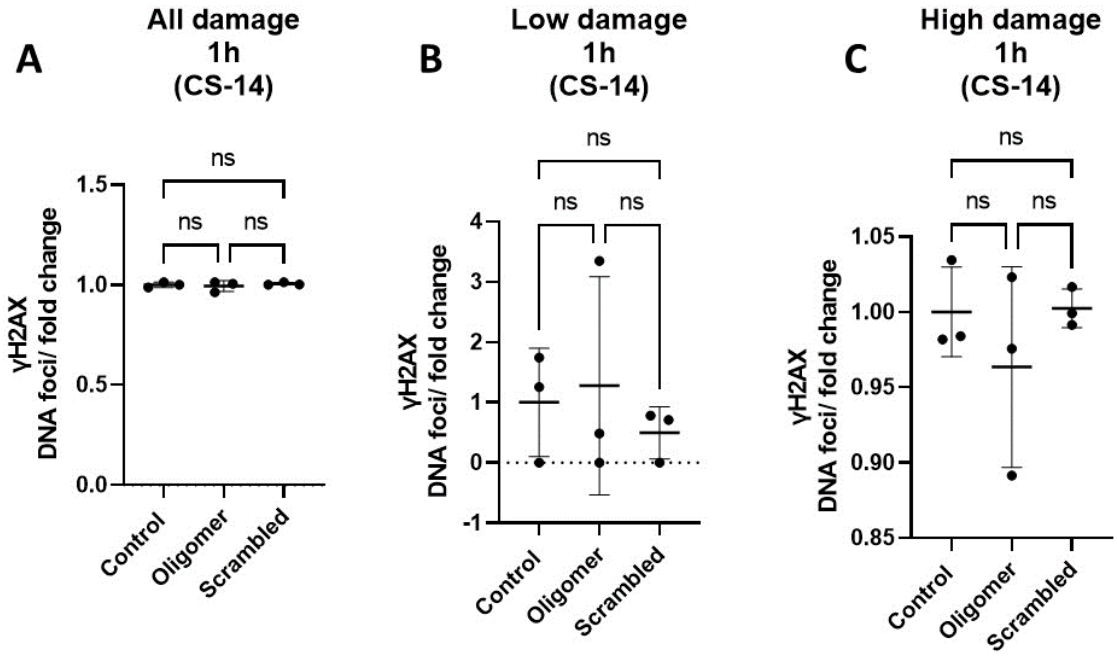


**Figure 3.19.** Formation of DNA damage indicative γH2AX-positive foci in CS14 iAstrocytes as a response to 1 hour $A\beta_{1-42}$ oligomer treatment.

The quantification of DNA damage based on the number of γH2AX positive DNA foci in human CS14 induced astrocytes (iAstrocytes), as a response to $A\beta_{1-42}$ oligomer treatment for 1 hour. Analysis was carried out using the Harmony Analysis Software (PerkinElmer). Graphs showing: **(A)** All damage detected; **(B)** Low damage detected (between 3-10 foci/ nucleus); **(C)** High damage detected (>10 foci/ nucleus). Data is presented as a fold change value of foci-positive nuclei to all nuclei detected. Standard error bars represent mean±SD. One-way ANOVA with Bonferroni's post-hoc test for multiple comparisons of pre-selected groups. Groups for statistical analysis: Control vs all treatment groups; and scrambled control group vs time-matched $A\beta_{1-42}$-treated group. N=3 (CS-14 iAstrocytes).

Furthermore, there was no significant difference overall in the DNA damage detected in 155v2 iAstrocytes as a response to $A\beta_{1-42}$ oligomers after 1 hour (fig.3.20). However, there was a significantly higher amount of DNA damage (all damage detected) in the scrambled peptide-treated group compared to the oligomer-treated group. However, as the scrambled peptide-treated group was not significantly different to the untreated control, this result could be an artifact.

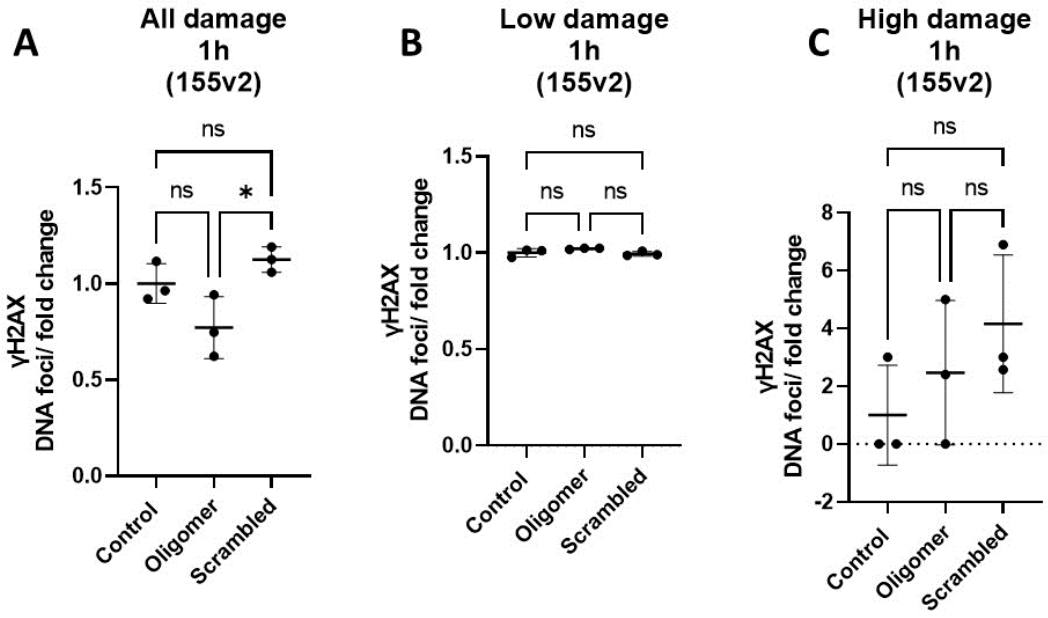


**Figure 3.20.** Formation of DNA damage indicative γH2AX-positive foci in 155v2 iAstrocytes as a response to 1 hour $A\beta_{1-42}$ oligomer treatment.

The quantification of DNA damage based on the number of γH2AX positive DNA foci in human 155v2 induced astrocytes (iAstrocytes), as a response to $A\beta_{1-42}$ oligomer treatment for 1 hour. Analysis was carried out using the Harmony Analysis Software (PerkinElmer). Graphs showing: **(A)** All damage detected; **(B)** Low damage detected (between 3-10 foci/ nucleus); **(C)** High damage detected (>10 foci/ nucleus). Data is presented as a fold change value of foci-positive nuclei to all nuclei detected. Standard error bars represent mean±SD. One-way ANOVA with Bonferroni's post-hoc test for multiple comparisons of pre-selected groups. Groups for statistical analysis: Control vs all treatment groups; and scrambled control group vs time-matched $A\beta_{1-42}$-treated group. N=3 (155v2 iAstrocytes).

Furthermore, the morphology analysis revealed that there was no significant change in morphological parameters (mean cytoplasm region, mean cell area, mean cell roundness, mean cell width, mean cell length) in iAstrocytes after 1 hour treatment with $A\beta_{1-42}$ oligomers (fig.3.21).

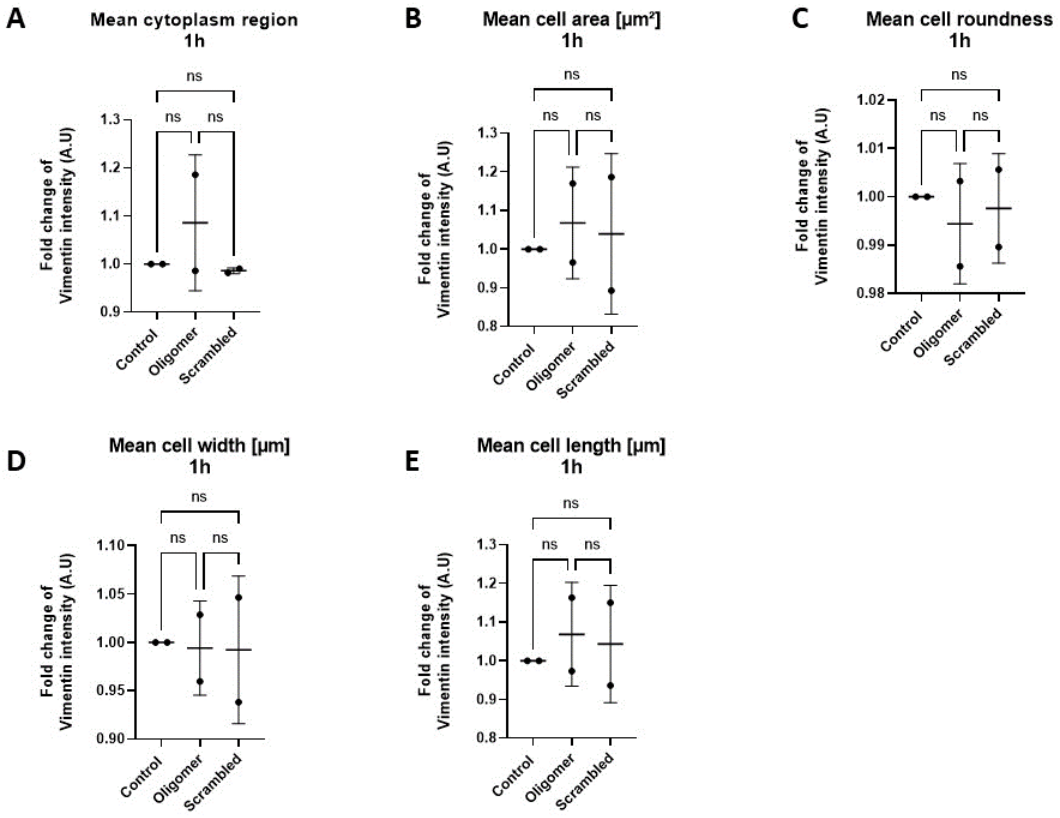


**Figure 3.21.** Cell morphology changes in iAstrocytes as a response to 1 hour $A\beta_{1-42}$ oligomer treatment.

The quantification of vimentin intensity in human induced astrocytes (iAstrocytes), indicative of cell morphology changes, as a response to $A\beta_{1-42}$ oligomer treatment for 1 hour. Analysis was carried out using the Harmony Analysis Software (PerkinElmer). Graphs showing changes in **(A)** mean cytoplasm region; **(B)** mean cell area; **(C)** mean cell roundness; **(D)** mean cell width; **(E)** mean cell length. Data is presented as a fold change value vimentin intensity, normalised to untreated control. Standard error bars represent mean±SD. One-way ANOVA with Bonferroni's post-hoc test for multiple comparisons of pre-selected groups. Groups for statistical analysis: Control vs all treatment groups; and scrambled control group vs time-matched $A\beta_{1-42}$-treated group. N=2 (two separate iAstrocyte cell lines as biological repeats).

When separated by cell line, the results showed there was no significant change in any of the tested morphological parameters in CS14 (fig.3.22) and 155v2 iAstrocytes (fig.3.23).

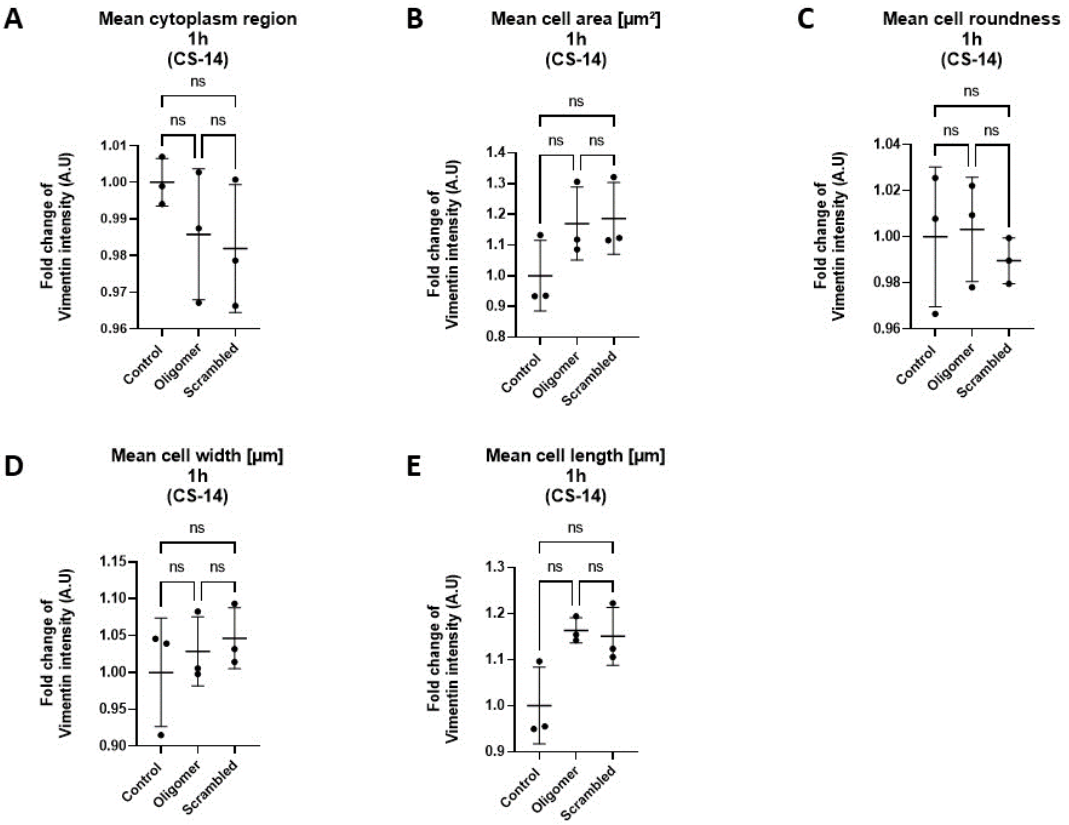


**Figure 3.22.** Cell morphology changes in CS14 iAstrocytes as a response to 1 hour $A\beta_{1-42}$ oligomer treatment.

The quantification of vimentin intensity in CS14 human induced astrocytes (iAstrocytes), indicative of cell morphology changes, as a response to $A\beta_{1-42}$ oligomer treatment for 1 hour. Analysis was carried out using the Harmony Analysis Software (PerkinElmer). Graphs showing changes in **(A)** mean cytoplasm region; **(B)** mean cell area; **(C)** mean cell roundness; **(D)** mean cell width; **(E)** mean cell length. Data is presented as a fold change value vimentin intensity, normalised to untreated control. Standard error bars represent mean±SD. One-way ANOVA with Bonferroni's post-hoc test for multiple comparisons of pre-selected groups. Groups for statistical analysis: Control vs all treatment groups; and scrambled control group vs time-matched $A\beta_{1-42}$-treated group. N=3 (CS-14 iAstrocytes)

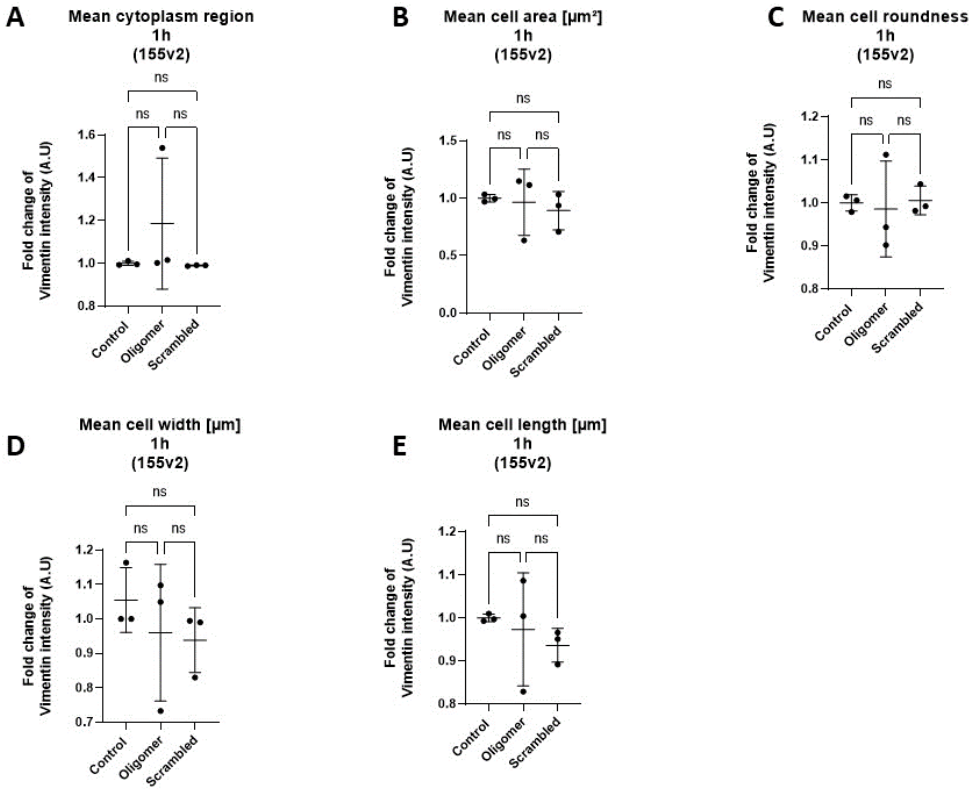


**Figure 3.23.** Cell morphology changes in 155v2 iAstrocytes as a response to 1 hour $A\beta_{1-42}$ oligomer treatment.

The quantification of vimentin intensity in 155v2 human induced astrocytes (iAstrocytes), indicative of cell morphology changes, as a response to $A\beta_{1-42}$ oligomer treatment for 1 hour. Analysis was carried out using the Harmony Analysis Software (PerkinElmer). Graphs showing changes in **(A)** mean cytoplasm region; **(B)** mean cell area; **(C)** mean cell roundness; **(D)** mean cell width; **(E)** mean cell length. Data is presented as a fold change value vimentin intensity, normalised to untreated control. Standard error bars represent mean±SD. One-way ANOVA with Bonferroni's post-hoc test for multiple comparisons of pre-selected groups. Groups for statistical analysis: Control vs all treatment groups; and scrambled control group vs time-matched $A\beta_{1-42}$-treated group. N=3 (155v2 iAstrocytes)

The differences in cell morphology (vimentin) and DNA damage (γH2AX) were investigated in pooled iAstrocyte cell lines treated with $A\beta_{1-42}$ for 2 hours (fig.3.23).

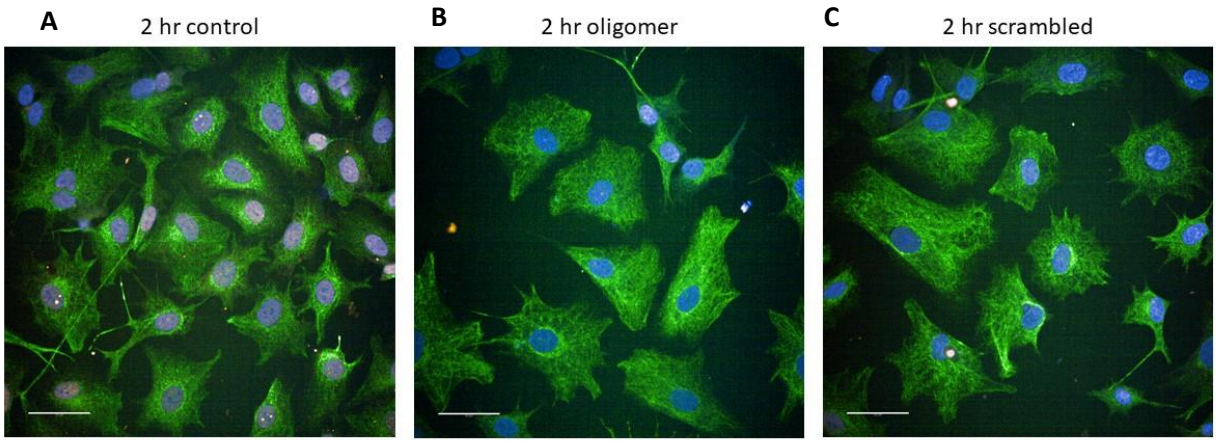


**Figure 3.23.** Representative immunocytochemistry images detecting changes to induced astrocyte (iAstrocyte) morphology and formation of DNA damage γH2AX foci as a response to 2 hour treatment with amyloid beta oligomers.

Immunocytochemistry images detecting induced Astrocyte (iAstrocyte) morphology with astrocyte marker vimentin (green), and γH2AX-positive DNA foci detected with γH2AX antibody (red). The nuclei are stained with Hoescht (blue). iAstrocytes treated for 2 hours with **(A)** untreated (control); **(B)** 1 µM oligomeric Aβ1-42; **(C)** 1 µM scrambled Aβ peptide as vehicle control. Representative images of n=2. Imaged on the Opera Phenix High Content Imaging System (PerkinElmer). Scale bars = 50 µm.

When all cell lines were pooled together, there were no significant differences in DNA damage between the groups after a 2h treatment with $A\beta_{1-42}$ oligomers (fig.3.24). Similarly, there were no differences in DNA damage between groups, when the cell lines were separated and analysed individually for CS14 (fig.3.25) and 155v2 (fig.3.26), suggesting that there was no change in DNA damage detected in iAstrocytes after 2 hours of oligomer treatments.

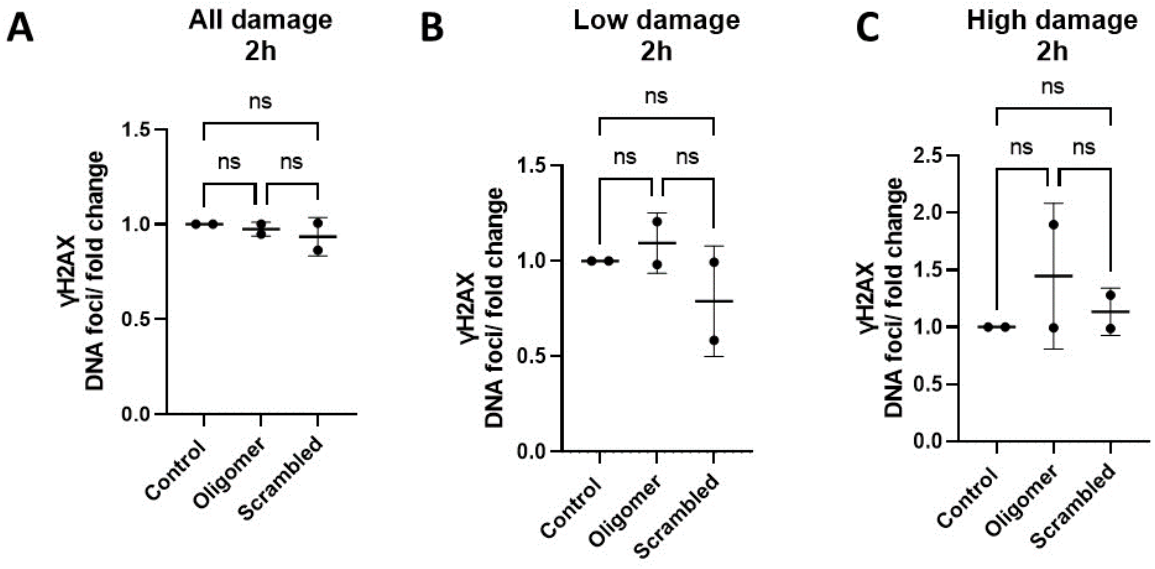


**Figure 3.24.** Formation of DNA damage indicative γH2AX-positive foci in iAstrocytes as a response to 2 hour $A\beta_{1-42}$ oligomer treatment.

The quantification of DNA damage based on the number of γH2AX positive DNA foci in human induced astrocytes (iAstrocytes), as a response to $A\beta_{1-42}$ oligomer treatment for 2 hours. Analysis was carried out using the Harmony Analysis Software (PerkinElmer). Graphs showing: **(A)** All damage detected; **(B)** Low damage detected (between 3-10 foci/ nucleus); **(C)** High damage detected (>10 foci/ nucleus). Data is presented as a fold change value of foci-positive nuclei to all nuclei detected. Standard error bars represent mean±SD. One-way ANOVA with Bonferroni's post-hoc test for multiple comparisons of pre-selected groups. Groups for statistical analysis: Control vs all treatment groups; and scrambled control group vs time-matched $A\beta_{1-42}$-treated group. N=2 (iAstrocyte cell lines pooled)

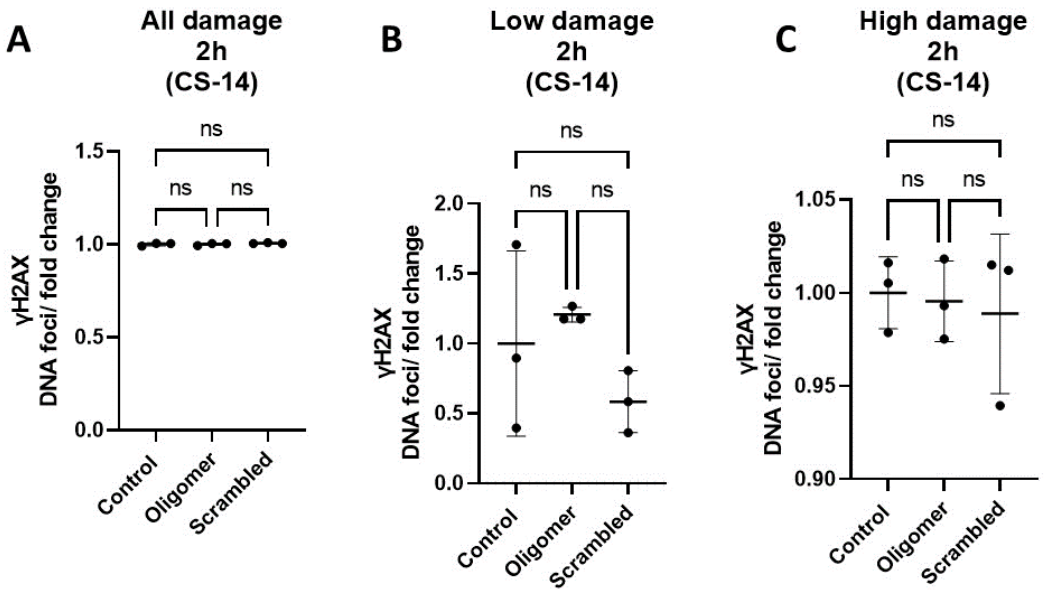


**Figure 3.25.** Formation of DNA damage indicative γH2AX-positive foci in CS14 iAstrocytes as a response to 2 hour $A\beta_{1-42}$ oligomer treatment.

The quantification of DNA damage based on the number of γH2AX positive DNA foci in human CS14 induced astrocytes (iAstrocytes), as a response to $A\beta_{1-42}$ oligomer treatment for 2 hour. Analysis was carried out using the Harmony Analysis Software (PerkinElmer). Graphs showing: **(A)** All damage detected; **(B)** Low damage detected (between 3-10 foci/ nucleus); **(C)** High damage detected (>10 foci/ nucleus). Data is presented as a fold change value of foci-positive nuclei to all nuclei detected. Standard error bars represent mean±SD. One-way ANOVA with Bonferroni's post-hoc test for multiple comparisons of pre-selected groups. Groups for statistical analysis: Control vs all treatment groups; and scrambled control group vs time-matched $A\beta_{1-42}$-treated group. N=3 (CS14 iAstrocytes).

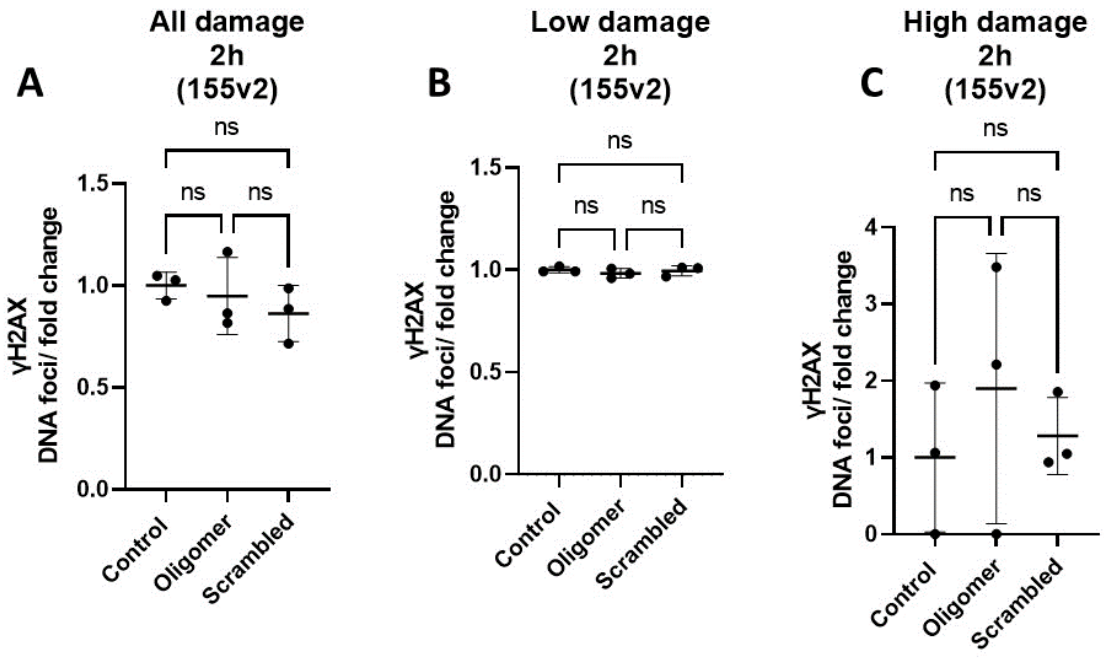


**Figure 3.26.** Formation of DNA damage indicative γH2AX-positive foci in 155v2 iAstrocytes as a response to 2 hour $A\beta_{1-42}$ oligomer treatment.

The quantification of DNA damage based on the number of γH2AX positive DNA foci in human 155v2 induced astrocytes (iAstrocytes), as a response to $A\beta_{1-42}$ oligomer treatment for 2 hour. Analysis was carried out using the Harmony Analysis Software (PerkinElmer). Graphs showing: **(A)** All damage detected; **(B)** Low damage detected (between 3-10 foci/ nucleus); **(C)** High damage detected (>10 foci/ nucleus). Data is presented as a fold change value of foci-positive nuclei to all nuclei detected. Standard error bars represent mean±SD. One-way ANOVA with Bonferroni's post-hoc test for multiple comparisons of pre-selected groups. Groups for statistical analysis: Control vs all treatment groups; and scrambled control group vs time-matched $A\beta_{1-42}$-treated group. N=3 (155v2 iAstrocytes).

Furthermore, cell morphology changes (with vimentin) were also investigated. When all iAstrocyte cell lines were pooled and analysed, there were no significant differences in any of the parameters investigated (mean cytoplasm region, mean cell area, mean cell roundness, mean cell width, mean cell length) (fig.3.27). When results were separated by each cell line there were no significant differences in any of the parameters in the iAstrocyte cell line CS14 (fig.3.28) and 155v2 (fig.3.29).

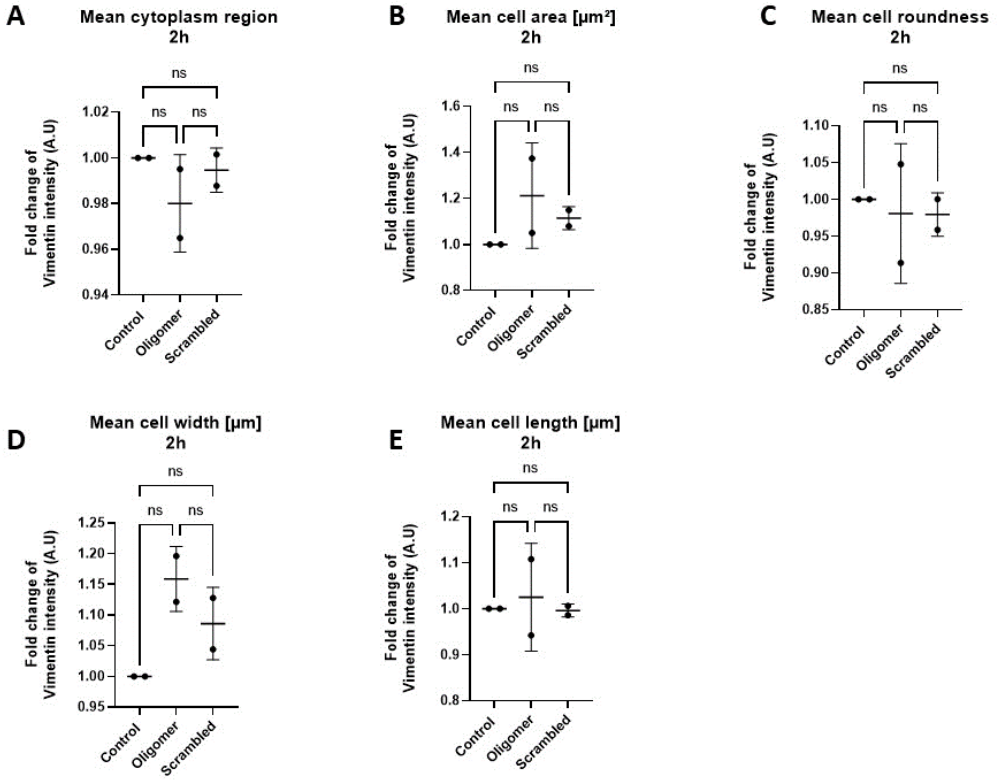


**Figure 3.27.** Cell morphology changes in iAstrocytes as a response to 2 hour $A\beta_{1-42}$ oligomer treatment.

The quantification of vimentin intensity in human induced astrocytes (iAstrocytes), indicative of cell morphology changes, as a response to $A\beta_{1-42}$ oligomer treatment for 2 hour. Analysis was carried out using the Harmony Analysis Software (PerkinElmer). Graphs showing changes in **(A)** mean cytoplasm region; **(B)** mean cell area; **(C)** mean cell roundness; **(D)** mean cell width; **(E)** mean cell length. Data is presented as a fold change value vimentin intensity, normalised to untreated control. Standard error bars represent mean±SD. One-way ANOVA with Bonferroni's post-hoc test for multiple comparisons of pre-selected groups. Groups for statistical analysis: Control vs all treatment groups; and scrambled control group vs time-matched $A\beta_{1-42}$-treated group. N=2 (iAstrocyte cell lines pooled).

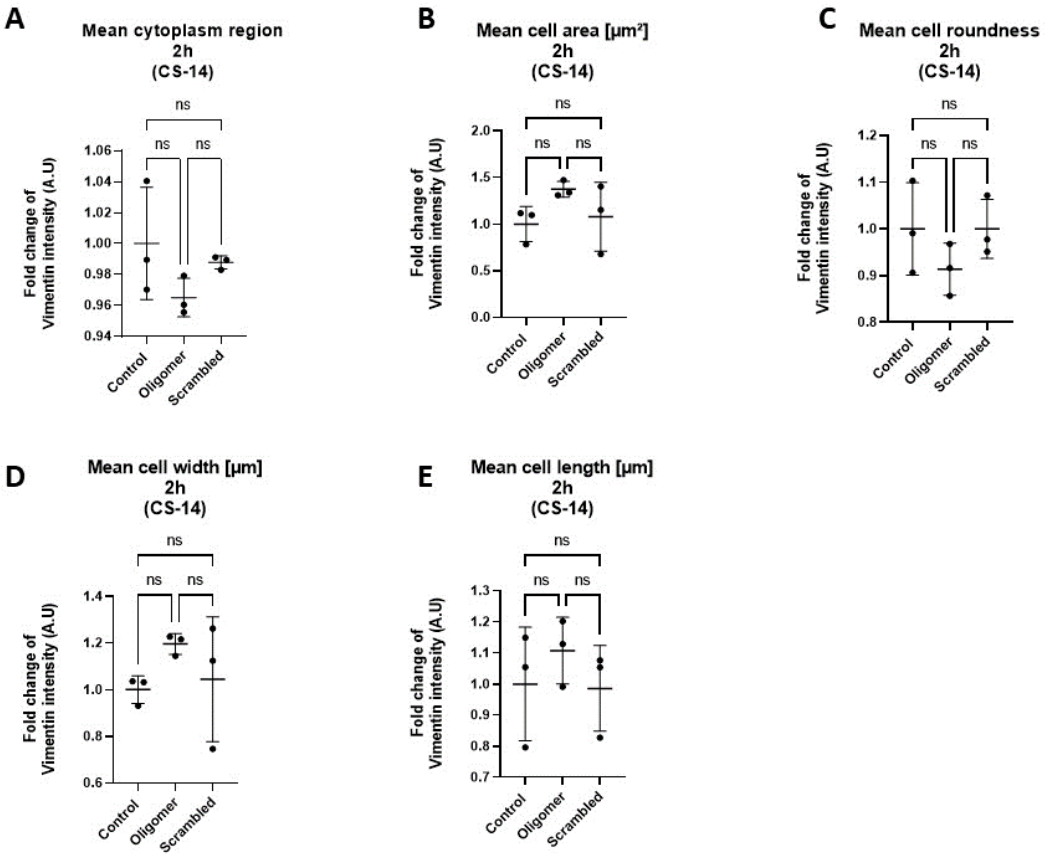


**Figure 3.28.** Cell morphology changes in CS14 iAstrocytes as a response to 2 hour $A\beta_{1-42}$ oligomer treatment.

The quantification of vimentin intensity in CS14 human induced astrocytes (iAstrocytes), indicative of cell morphology changes, as a response to $A\beta_{1-42}$ oligomer treatment for 2 hour. Analysis was carried out using the Harmony Analysis Software (PerkinElmer). Graphs showing changes in **(A)** mean cytoplasm region; **(B)** mean cell area; **(C)** mean cell roundness; **(D)** mean cell width; **(E)** mean cell length. Data is presented as a fold change value vimentin intensity, normalised to untreated control. Standard error bars represent mean±SD. One-way ANOVA with Bonferroni's post-hoc test for multiple comparisons of pre-selected groups. Groups for statistical analysis: Control vs all treatment groups; and scrambled control group vs time-matched $A\beta_{1-42}$-treated group. N=3 (CS14 iAstrocytes)

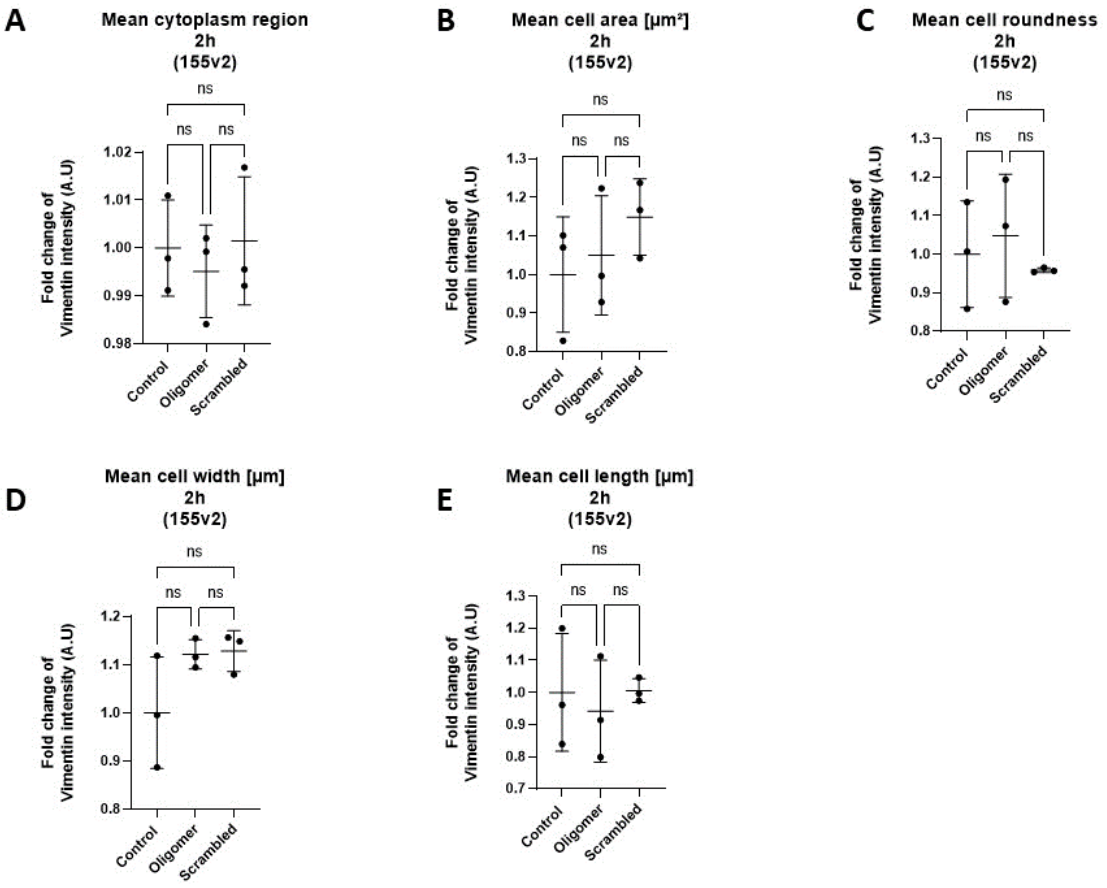


**Figure 3.29.** Cell morphology changes in 155v2 iAstrocytes as a response to 2 hour $A\beta_{1-42}$ oligomer treatment.

The quantification of vimentin intensity in 155v2 human induced astrocytes (iAstrocytes), indicative of cell morphology changes, as a response to $A\beta_{1-42}$ oligomer treatment for 2 hour. Analysis was carried out using the Harmony Analysis Software (PerkinElmer). Graphs showing changes in **(A)** mean cytoplasm region; **(B)** mean cell area; **(C)** mean cell roundness; **(D)** mean cell width; **(E)** mean cell length. Data is presented as a fold change value vimentin intensity, normalised to untreated control. Standard error bars represent mean±SD. One-way ANOVA with Bonferroni's post-hoc test for multiple comparisons of pre-selected groups. Groups for statistical analysis: Control vs all treatment groups; and scrambled control group vs time-matched $A\beta_{1-42}$-treated group. N=3 (155v2 iAstrocytes)

The iAstrocytes were also treated with $A\beta_{1-42}$ oligomers for 24 hours and investigated for the detection of DNA damage and cell morphology changes (fig.3.30).

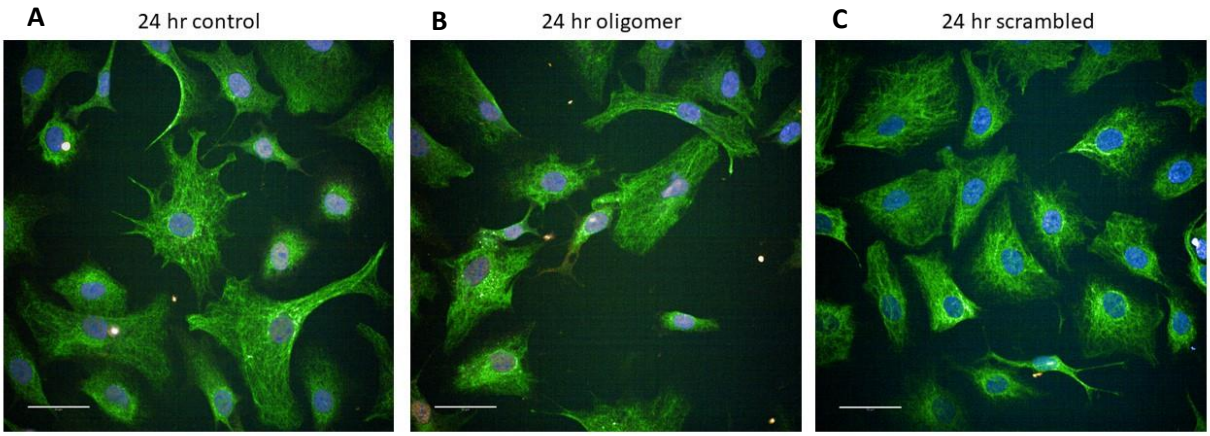


**Figure 3.30.** Representative immunocytochemistry images detecting changes to induced astrocyte (iAstrocyte) morphology and formation of DNA damage γH2AX foci as a response to 24 hour treatment with amyloid beta oligomers.

Immunocytochemistry images detecting induced Astrocyte (iAstrocyte) morphology with astrocyte marker vimentin (green), and γH2AX-positive DNA foci detected with γH2AX antibody (red). The nuclei are stained with Hoescht (blue). iAstrocytes treated for 24 hours with **(A)** untreated (control); **(B)** 1 µM oligomeric Aβ1-42; **(C)** 1 µM scrambled Aβ peptide as vehicle control. Representative images of n=2. Imaged on the Opera Phenix High Content Imaging System (PerkinElmer). Scale bars = 50 µm.

When all iAstrocyte cell lines were pooled together, there was no significant difference in the DNA damage between any of the treatment groups (fig.3.31). When the iAstrocyte cell lines were separated for analysis, there were no differences between any of the treatment groups for CS14 iAstrocytes (fig.3.32). However, for 155v2 iAstrocytes, there was a significant decrease in 'all damage' when comparing oligomer-treated group to the untreated control. Interestingly, for 'low damage' parameter, there was a significantly higher amount of DNA damage in the oligomer-treated group compared to both untreated and vehicle controls (fig.3.33). This could suggest that amyloid oligomers could induce a low-grade of DNA damage in some individuals after 24 hours.

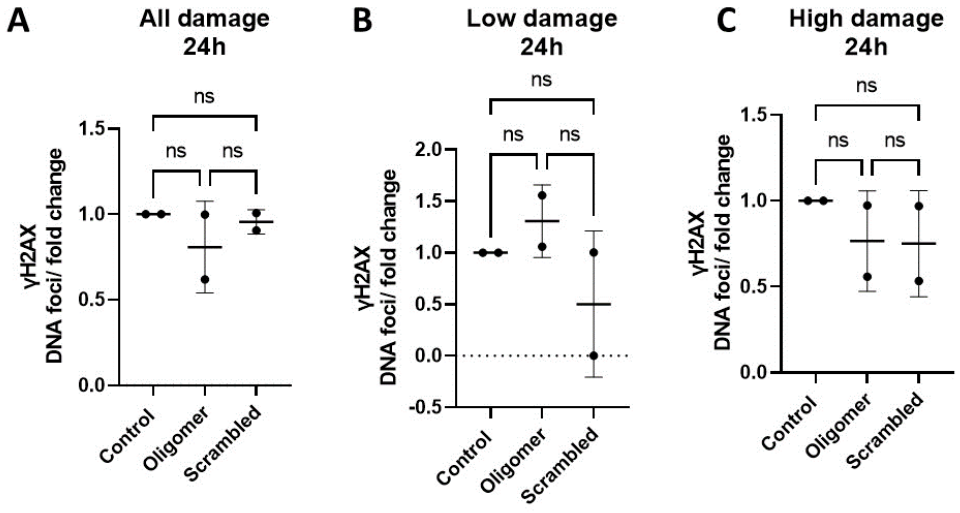


**Figure 3.31.** Formation of DNA damage indicative γH2AX-positive foci in iAstrocytes as a response to 24 hour $A\beta_{1-42}$ oligomer treatment.

The quantification of DNA damage based on the number of γH2AX positive DNA foci in human induced astrocytes (iAstrocytes), as a response to $A\beta_{1-42}$ oligomer treatment for 24 hour. Analysis was carried out using the Harmony Analysis Software (PerkinElmer). Graphs showing: **(A)** All damage detected; **(B)** Low damage detected (between 3-10 foci/ nucleus); **(C)** High damage detected (>10 foci/ nucleus). Data is presented as a fold change value of foci-positive nuclei to all nuclei detected. Standard error bars represent mean±SD. One-way ANOVA with Bonferroni's post-hoc test for multiple comparisons of pre-selected groups. Groups for statistical analysis: Control vs all treatment groups; and scrambled control group vs time-matched $A\beta_{1-42}$-treated group. N=2 (iAstrocytes pooled).

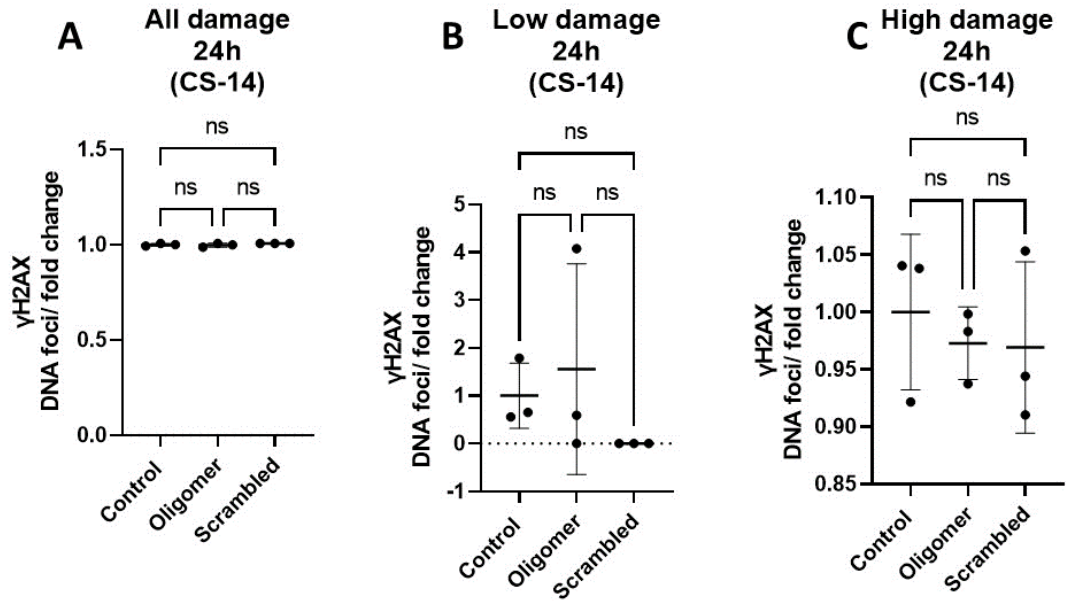


**Figure 3.32.** Formation of DNA damage indicative γH2AX-positive foci in CS-14 iAstrocytes as a response to 24 hour $A\beta_{1-42}$ oligomer treatment.

The quantification of DNA damage based on the number of γH2AX positive DNA foci in human CS14 induced astrocytes (iAstrocytes), as a response to $A\beta_{1-42}$ oligomer treatment for 24 hour. Analysis was carried out using the Harmony Analysis Software (PerkinElmer). Graphs showing: **(A)** All damage detected; **(B)** Low damage detected (between 3-10 foci/ nucleus); **(C)** High damage detected (>10 foci/ nucleus). Data is presented as a fold change value of foci-positive nuclei to all nuclei detected. Standard error bars represent mean±SD. One-way ANOVA with Bonferroni's post-hoc test for multiple comparisons of pre-selected groups. Groups for statistical analysis: Control vs all treatment groups; and scrambled control group vs time-matched $A\beta_{1-42}$-treated group. N=3 (CS14 iAstrocytes).

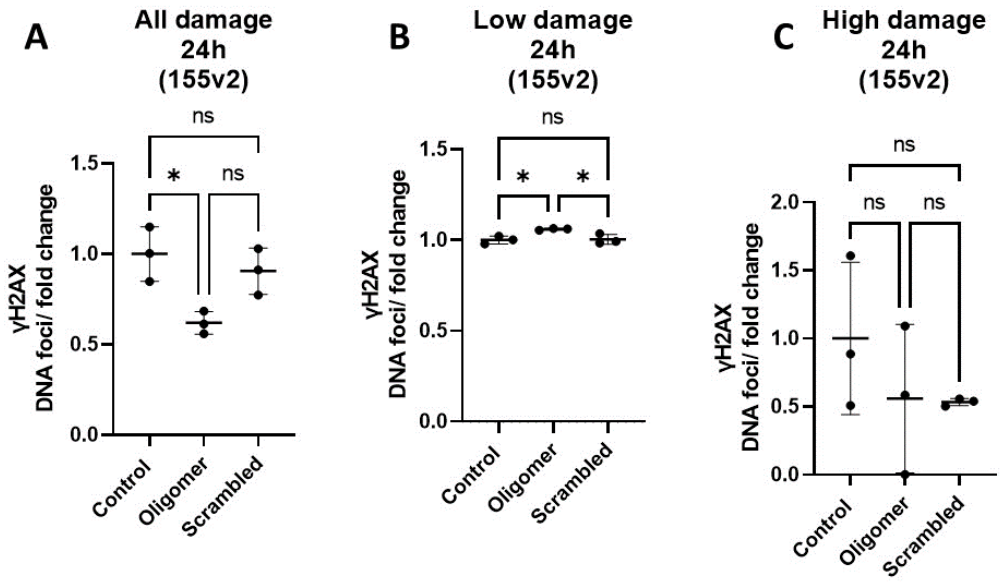


**Figure 3.33.** Formation of DNA damage indicative γH2AX-positive foci in 155v2 iAstrocytes as a response to 24 hour $A\beta_{1-42}$ oligomer treatment.

The quantification of DNA damage based on the number of γH2AX positive DNA foci in human 155v2 induced astrocytes (iAstrocytes), as a response to $A\beta_{1-42}$ oligomer treatment for 24 hour. Analysis was carried out using the Harmony Analysis Software (PerkinElmer). Graphs showing: **(A)** All damage detected; **(B)** Low damage detected (between 3-10 foci/ nucleus); **(C)** High damage detected (>10 foci/ nucleus). Data is presented as a fold change value of foci-positive nuclei to all nuclei detected. Standard error bars represent mean±SD. One-way ANOVA with Bonferroni's post-hoc test for multiple comparisons of pre-selected groups. Groups for statistical analysis: Control vs all treatment groups; and scrambled control group vs time-matched $A\beta_{1-42}$-treated group. N=3 (155v2 iAstrocytes).

Furthermore, cell morphology changes (with vimentin) were also investigated. When all iAstrocyte cell lines were pooled and analysed. Overall, there were no significant differences in any of the parameters investigated (mean cytoplasm region, mean cell area, mean cell roundness, mean cell width, mean cell length) (fig.3.34). The only parameter significantly different was a decrease in the mean cell length of scrambled treatment group compared to untreated control (fig.3.34.e). When results were separated by each cell line there were no significant differences in any of the parameters in the iAstrocyte cell line CS14 (fig.3.35) and 155v2 (fig.3.36).

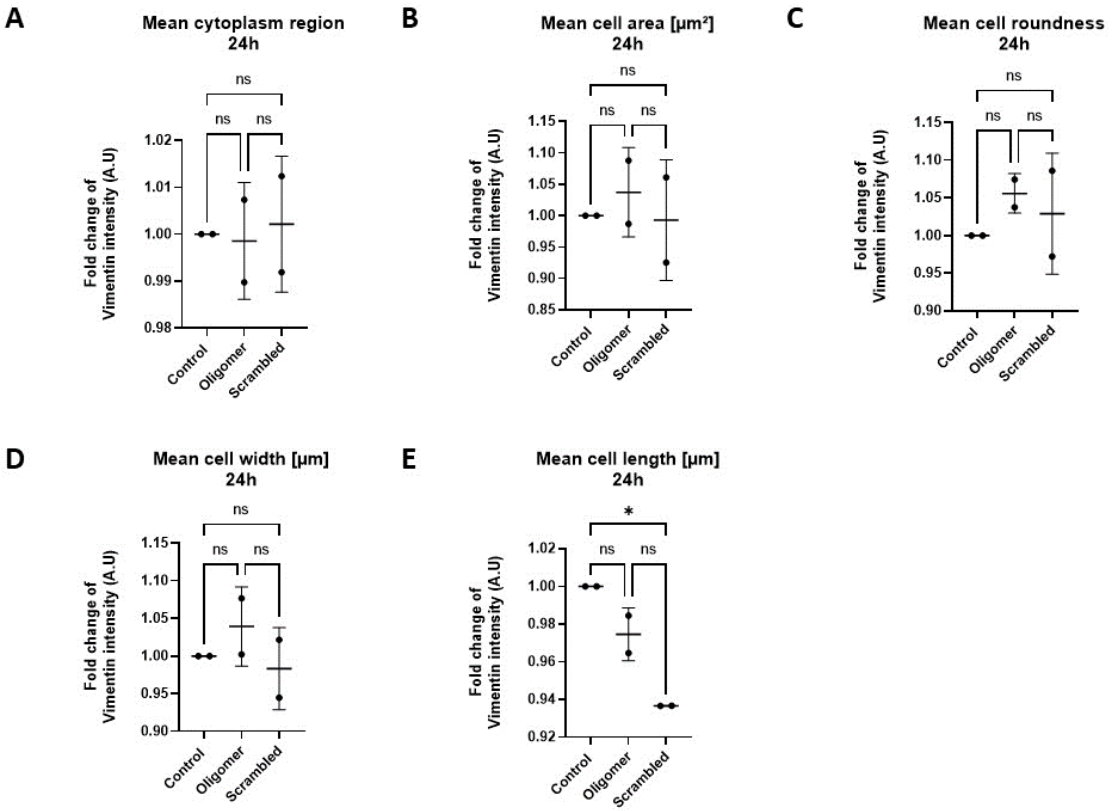


**Figure 3.34.** Cell morphology changes in iAstrocytes as a response to 24 hour $A\beta_{1-42}$ oligomer treatment.

The quantification of vimentin intensity in human induced astrocytes (iAstrocytes), indicative of cell morphology changes, as a response to $A\beta_{1-42}$ oligomer treatment for 24 hour. Analysis was carried out using the Harmony Analysis Software (PerkinElmer). Graphs showing changes in **(A)** mean cytoplasm region; **(B)** mean cell area; **(C)** mean cell roundness; **(D)** mean cell width; **(E)** mean cell length. Data is presented as a fold change value vimentin intensity, normalised to untreated control. Standard error bars represent mean±SD. One-way ANOVA with Bonferroni's post-hoc test for multiple comparisons of pre-selected groups. Groups for statistical analysis: Control vs all treatment groups; and scrambled control group vs time-matched $A\beta_{1-42}$-treated group. N=2 (iAstrocyte cell lines pooled).

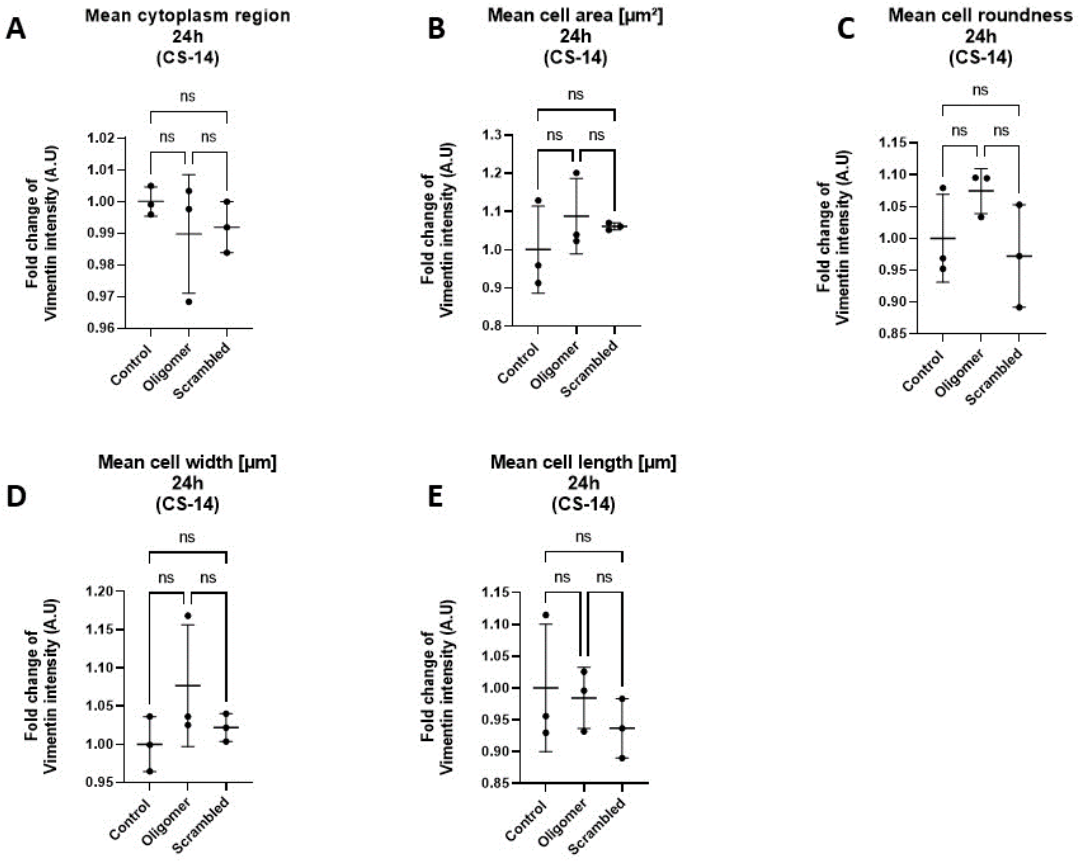


**Figure 3.35.** Cell morphology changes in CS14 iAstrocytes as a response to 24 hour $A\beta_{1-42}$ oligomer treatment.

The quantification of vimentin intensity in CS14 human induced astrocytes (iAstrocytes), indicative of cell morphology changes, as a response to $A\beta_{1-42}$ oligomer treatment for 24 hour. Analysis was carried out using the Harmony Analysis Software (PerkinElmer). Graphs showing changes in **(A)** mean cytoplasm region; **(B)** mean cell area; **(C)** mean cell roundness; **(D)** mean cell width; **(E)** mean cell length. Data is presented as a fold change value vimentin intensity, normalised to untreated control. Standard error bars represent mean±SD. One-way ANOVA with Bonferroni's post-hoc test for multiple comparisons of pre-selected groups. Groups for statistical analysis: Control vs all treatment groups; and scrambled control group vs time-matched $A\beta_{1-42}$-treated group. N=3 (CS14 iAstrocytes)

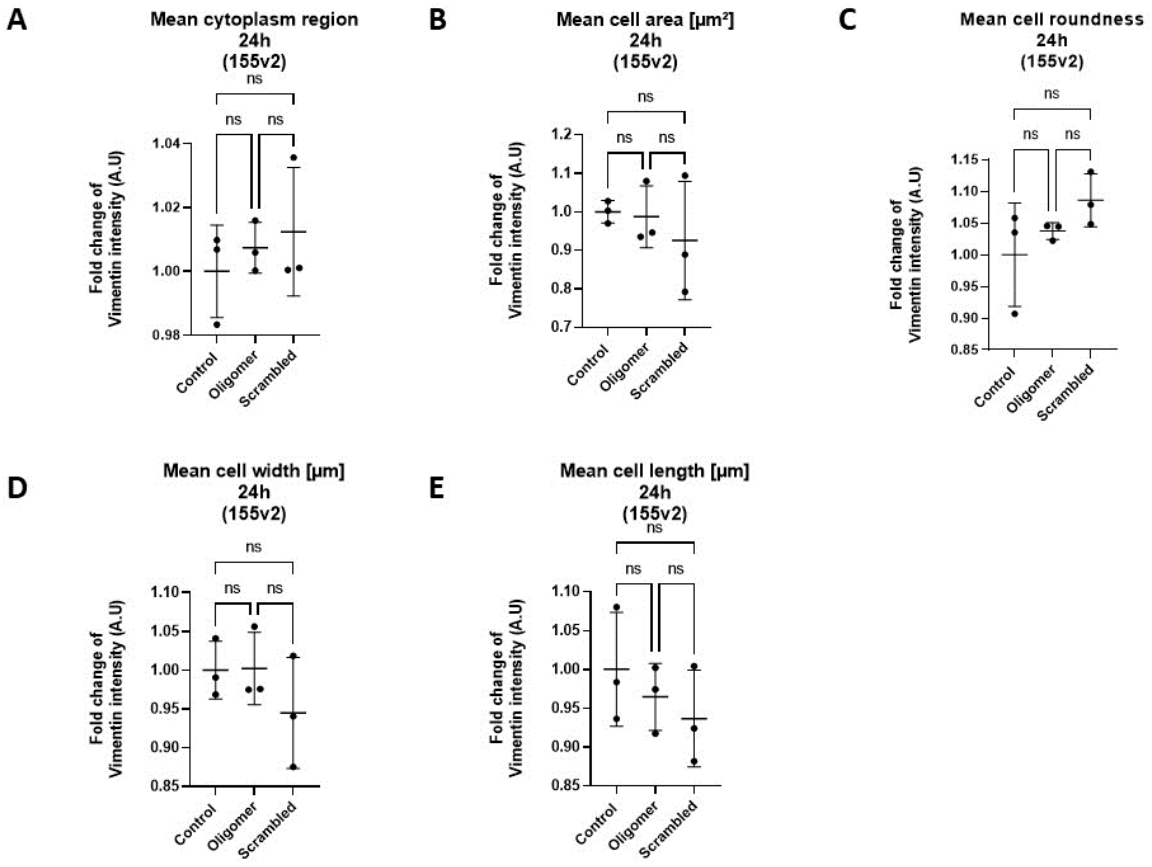


**Figure 3.36.** Cell morphology changes in 155v2 iAstrocytes as a response to 24 hour $A\beta_{1-42}$ oligomer treatment.

The quantification of vimentin intensity in 155v2 human induced astrocytes (iAstrocytes), indicative of cell morphology changes, as a response to $A\beta_{1-42}$ oligomer treatment for 24 hour. Analysis was carried out using the Harmony Analysis Software (PerkinElmer). Graphs showing changes in **(A)** mean cytoplasm region; **(B)** mean cell area; **(C)** mean cell roundness; **(D)** mean cell width; **(E)** mean cell length. Data is presented as a fold change value vimentin intensity, normalised to untreated control. Standard error bars represent mean±SD. One-way ANOVA with Bonferroni's post-hoc test for multiple comparisons of pre-selected groups. Groups for statistical analysis: Control vs all treatment groups; and scrambled control group vs time-matched $A\beta_{1-42}$-treated group. N=3 (155v2 iAstrocytes)

The iAstrocytes were also investigated for DNA damage changes and cell morphology changes after 48 hours of oligomer treatments (fig.3.37).

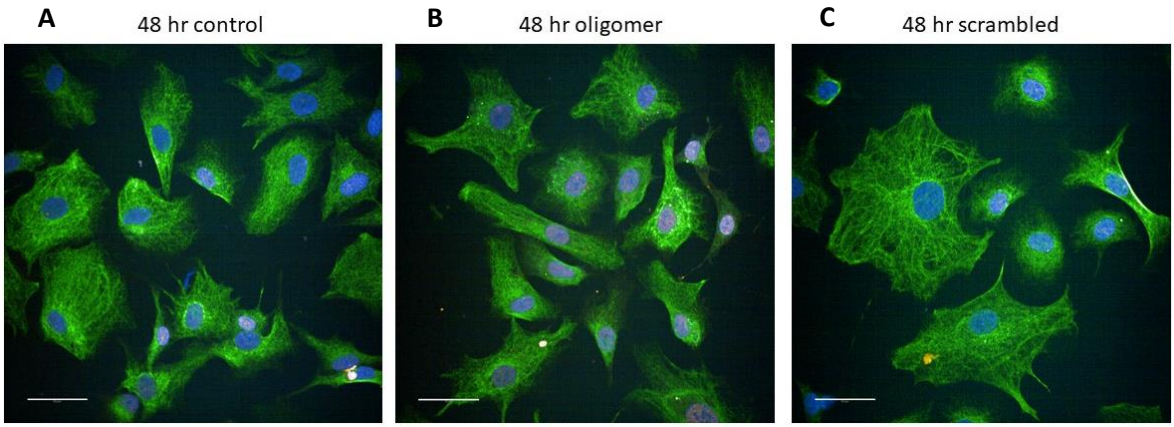


**Figure 3.37.** Representative immunocytochemistry images detecting changes to induced astrocyte (iAstrocyte) morphology and formation of DNA damage γH2AX foci as a response to 48 hour treatment with amyloid beta oligomers.

Immunocytochemistry images detecting induced Astrocyte (iAstrocyte) morphology with astrocyte marker vimentin (green), and γH2AX-positive DNA foci detected with γH2AX antibody (red). The nuclei are stained with Hoescht (blue). iAstrocytes treated for 24 hours with **(A)** untreated (control); **(B)** 1 µM oligomeric Aβ1-42; **(C)** 1 µM scrambled Aβ peptide as vehicle control. Representative images of n=2. Imaged on the Opera Phenix High Content Imaging System (PerkinElmer). Scale bars = 50 µm.

When iAstrocyte cell lines were pooled and investigated for changes in DNA damage, the results showed that there was no change in DNA damage between any of the treatment groups (fig.3.38). When the iAstrocyte cell lines were investigated separately, the results showed that for CS14 iAstrocytes there were no significant changed in DNA damage at any of the treatment groups (fig.3.39). Meanwhile, for 155v2 iAstrocytes, there was a significant decrease in the 'all damage' parameter of oligomer-treated iAstrocytes when compared to both untreated control and vehicle control treatment groups. There was no significant difference between any of the treatment groups in the 'high damage' parameter, however interestingly, for 'low damage', there was a significant increase in the DNA damage detected for oligomer-treated iAstrocytes when compared to untreated and vehicle control groups. This suggests that after 48 hours, there may be a low-grade increase in DNA damage of iAstrocytes as a response to $A\beta_{1-42}$ oligomers (fig.3.40). This further suggests that there may be individually different responses to oligomers.

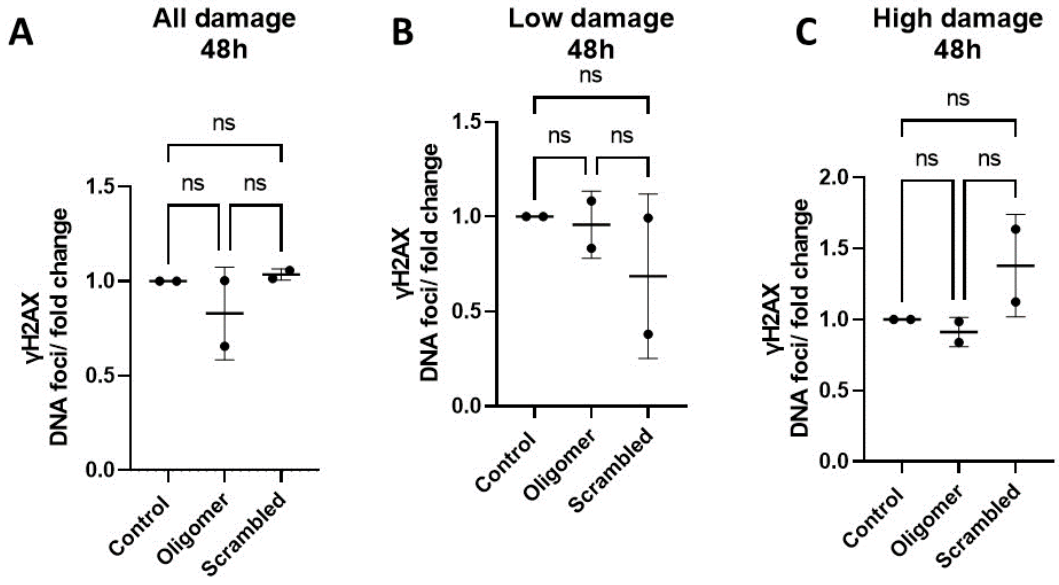


**Figure 3.38.** Formation of DNA damage indicative γH2AX-positive foci in iAstrocytes as a response to 48 hour $A\beta_{1-42}$ oligomer treatment.

The quantification of DNA damage based on the number of γH2AX positive DNA foci in human induced astrocytes (iAstrocytes), as a response to $A\beta_{1-42}$ oligomer treatment for 48 hour. Analysis was carried out using the Harmony Analysis Software (PerkinElmer). Graphs showing: **(A)** All damage detected; **(B)** Low damage detected (between 3-10 foci/ nucleus); **(C)** High damage detected (>10 foci/ nucleus). Data is presented as a fold change value of foci-positive nuclei to all nuclei detected. Standard error bars represent mean±SD. One-way ANOVA with Bonferroni's post-hoc test for multiple comparisons of pre-selected groups. Groups for statistical analysis: Control vs all treatment groups; and scrambled control group vs time-matched $A\beta_{1-42}$-treated group. N=2 (iAstrocyte cell lines pooled).

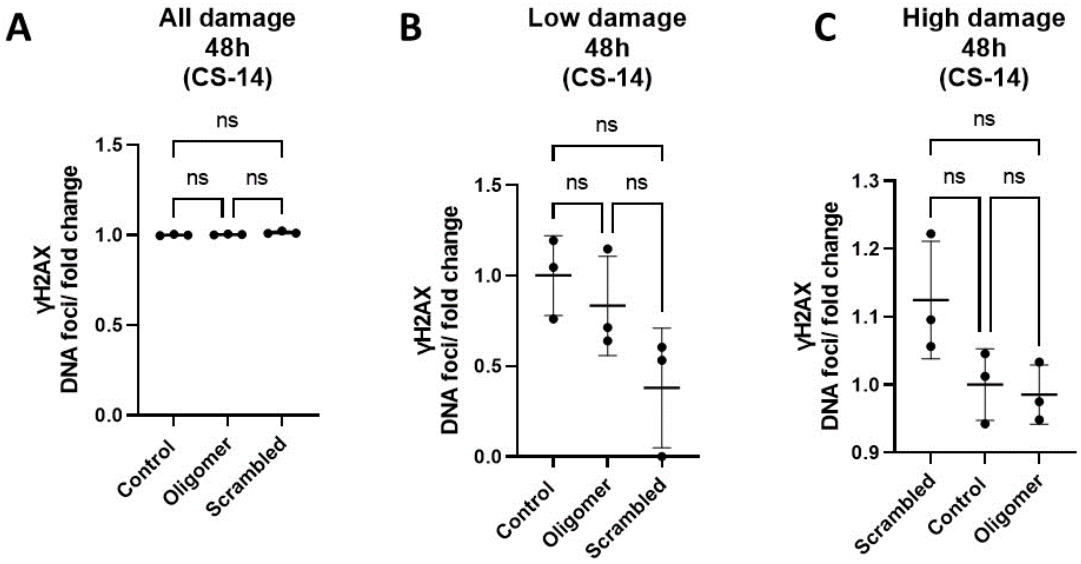


**Figure 3.39.** Formation of DNA damage indicative γH2AX-positive foci in CS14 iAstrocytes as a response to 48 hour $A\beta_{1-42}$ oligomer treatment.

The quantification of DNA damage based on the number of γH2AX positive DNA foci in human CS14 induced astrocytes (iAstrocytes), as a response to $A\beta_{1-42}$ oligomer treatment for 48 hour. Analysis was carried out using the Harmony Analysis Software (PerkinElmer). Graphs showing: **(A)** All damage detected; **(B)** Low damage detected (between 3-10 foci/ nucleus); **(C)** High damage detected (>10 foci/ nucleus). Data is presented as a fold change value of foci-positive nuclei to all nuclei detected. Standard error bars represent mean±SD. One-way ANOVA with Bonferroni's post-hoc test for multiple comparisons of pre-selected groups. Groups for statistical analysis: Control vs all treatment groups; and scrambled control group vs time-matched $A\beta_{1-42}$-treated group. N=3 (CS14 iAstrocytes).

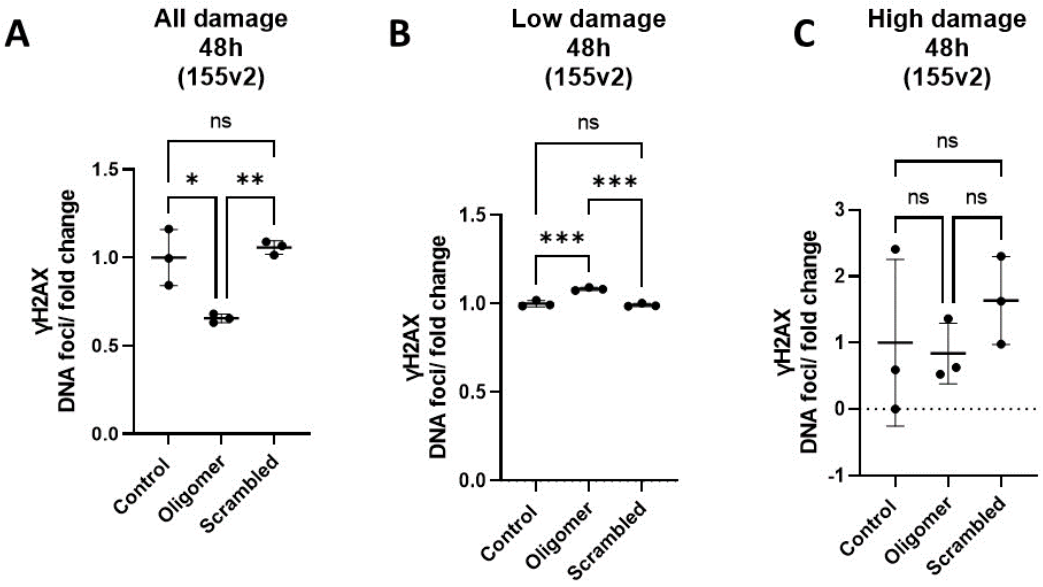


**Figure 3.40.** Formation of DNA damage indicative γH2AX-positive foci in 155v2 iAstrocytes as a response to 48 hour $A\beta_{1-42}$ oligomer treatment.

The quantification of DNA damage based on the number of γH2AX positive DNA foci in human 155v2 induced astrocytes (iAstrocytes), as a response to $A\beta_{1-42}$ oligomer treatment for 48 hour. Analysis was carried out using the Harmony Analysis Software (PerkinElmer). Graphs showing: **(A)** All damage detected; **(B)** Low damage detected (between 3-10 foci/ nucleus); **(C)** High damage detected (>10 foci/ nucleus). Data is presented as a fold change value of foci-positive nuclei to all nuclei detected. Standard error bars represent mean±SD. One-way ANOVA with Bonferroni's post-hoc test for multiple comparisons of pre-selected groups. Groups for statistical analysis: Control vs all treatment groups; and scrambled control group vs time-matched $A\beta_{1-42}$-treated group. N=3 (155v2 iAstrocytes).

The iAstrocytes were also investigated for any potential changes to morphology (vimentin) after 48 hours of oligomer treatments. When iAstrocyte cell lines were pooled together, the $A\beta_{1-42}$ oligomers did not cause any significant changes in cell morphology when looking at the parameters analysed (mean cytoplasm region, mean cell area, mean cell roundness, mean cell width, mean cell length). However, the scrambled vehicle control peptide had caused a decrease in mean cell area and mean cell width at 48 hours post-treatment, when compared to the untreated control (fig.3.41).

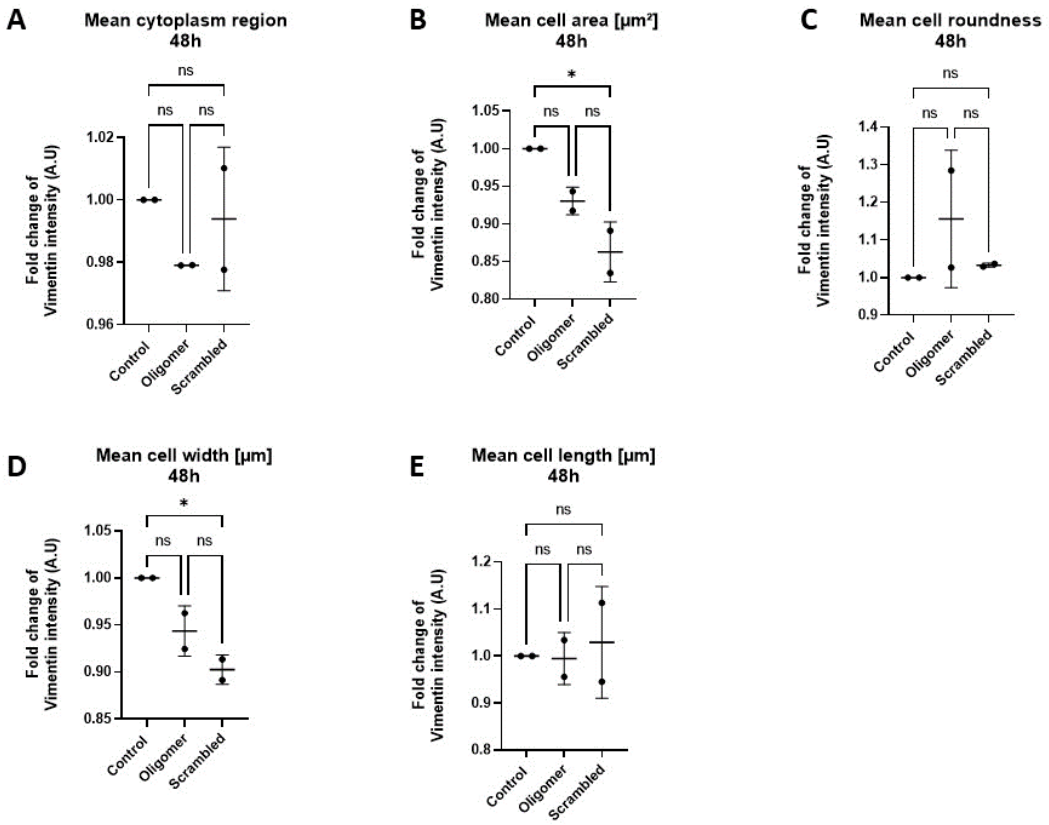


**Figure 3.41.** Cell morphology changes in iAstrocytes as a response to 48 hour $A\beta_{1-42}$ oligomer treatment.

The quantification of vimentin intensity in human induced astrocytes (iAstrocytes), indicative of cell morphology changes, as a response to $A\beta_{1-42}$ oligomer treatment for 48 hour. Analysis was carried out using the Harmony Analysis Software (PerkinElmer). Graphs showing changes in **(A)** mean cytoplasm region; **(B)** mean cell area; **(C)** mean cell roundness; **(D)** mean cell width; **(E)** mean cell length. Data is presented as a fold change value vimentin intensity, normalised to untreated control. Standard error bars represent mean±SD. One-way ANOVA with Bonferroni's post-hoc test for multiple comparisons of pre-selected groups. Groups for statistical analysis: Control vs all treatment groups; and scrambled control group vs time-matched $A\beta_{1-42}$-treated group. N=2 (iAstrocyte cell lines pooled)

When iAstrocyte cell lines were separated for individual analysis, there was no significant difference in the cell morphology parameters (mean cytoplasm region, mean cell area, mean cell roundness, mean cell width, mean cell length) for CS14 iAstrocytes (fig.3.42). Moreover, there were no significant differences in the 155v2 iAstrocytes, except a decrease in mean cell area in the scrambled vehicle control compared to the untreated control (fig.3.43).

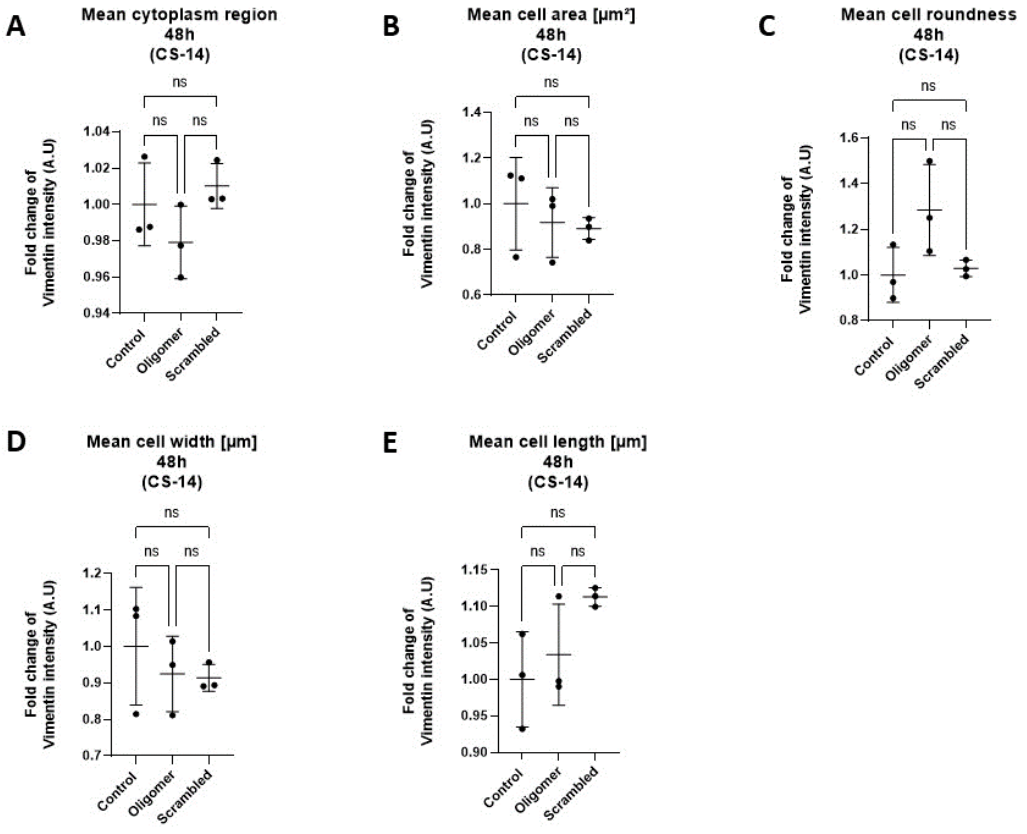


**Figure 3.42.** Cell morphology changes in CS14 iAstrocytes as a response to 48 hour $A\beta_{1-42}$ oligomer treatment.

The quantification of vimentin intensity in CS14 human induced astrocytes (iAstrocytes), indicative of cell morphology changes, as a response to $A\beta_{1-42}$ oligomer treatment for 48 hour. Analysis was carried out using the Harmony Analysis Software (PerkinElmer). Graphs showing changes in **(A)** mean cytoplasm region; **(B)** mean cell area; **(C)** mean cell roundness; **(D)** mean cell width; **(E)** mean cell length. Data is presented as a fold change value vimentin intensity, normalised to untreated control. Standard error bars represent mean±SD. One-way ANOVA with Bonferroni's post-hoc test for multiple comparisons of pre-selected groups. Groups for statistical analysis: Control vs all treatment groups; and scrambled control group vs time-matched $A\beta_{1-42}$-treated group. N=3 (CS14 iAstrocytes)

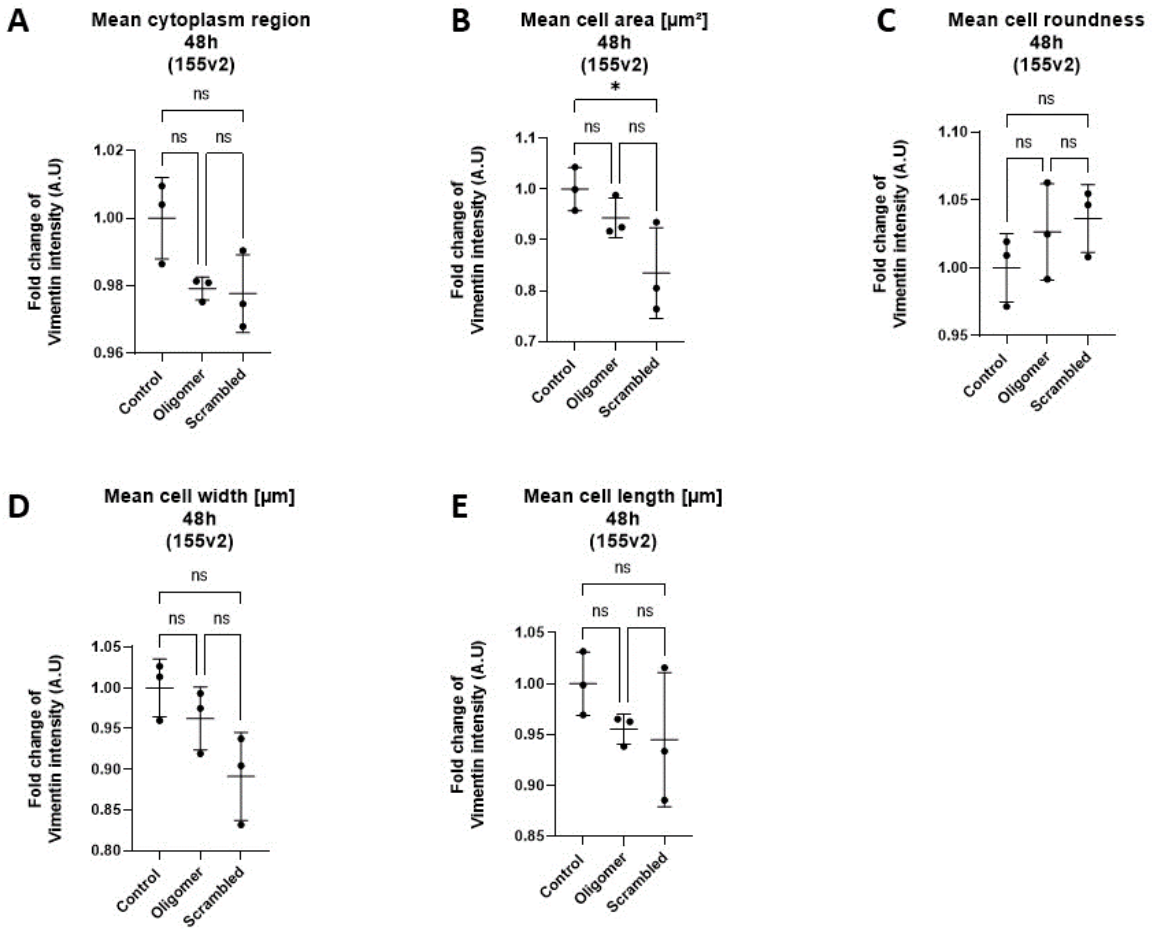


**Figure 3.43.** Cell morphology changes in 155v2 iAstrocytes as a response to 48 hour $A\beta_{1-42}$ oligomer treatment.

The quantification of vimentin intensity in 155v2 human induced astrocytes (iAstrocytes), indicative of cell morphology changes, as a response to $A\beta_{1-42}$ oligomer treatment for 48 hour. Analysis was carried out using the Harmony Analysis Software (PerkinElmer). Graphs showing changes in **(A)** mean cytoplasm region; **(B)** mean cell area; **(C)** mean cell roundness; **(D)** mean cell width; **(E)** mean cell length. Data is presented as a fold change value vimentin intensity, normalised to untreated control. Standard error bars represent mean±SD. One-way ANOVA with Bonferroni's post-hoc test for multiple comparisons of pre-selected groups. Groups for statistical analysis: Control vs all treatment groups; and scrambled control group vs time-matched $A\beta_{1-42}$-treated group. N=3 (155v2 iAstrocytes)

Lastly, the iAstrocytes were treated repeatedly over a period of 48 hours (at 1h, 2h, 24h, 48h) to investigate how repeated exposure or stress with $A\beta_{1-42}$ oligomers may affect the changes in DNA damage and cell morphology of iAstrocytes (fig.3.44).

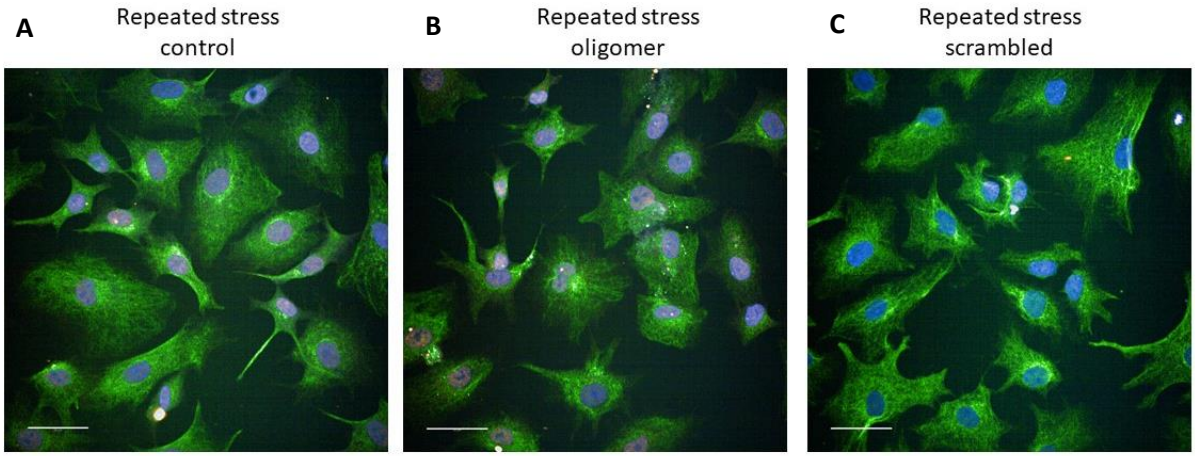


**Figure 3.44.** Representative immunocytochemistry images detecting changes to induced astrocyte (iAstrocyte) morphology and formation of DNA damage γH2AX foci as a response to a repeated stress treatment with amyloid beta oligomers.

Immunocytochemistry images detecting induced Astrocyte (iAstrocyte) morphology with astrocyte marker vimentin (green), and γH2AX-positive DNA foci detected with γH2AX antibody (red). The nuclei are stained with Hoescht (blue). iAstrocytes treated for a repeated stress with **(A)** untreated (control); **(B)** 1 µM oligomeric Aβ1-42; **(C)** 1 µM scrambled Aβ peptide as vehicle control. Representative images of n=2. Imaged on the Opera Phenix High Content Imaging System (PerkinElmer). Scale bars = 50 µm.

Firstly, the changes in DNA damage were investigated as a response to repeated stress exposure with $A\beta_{1-42}$ oligomers. Overall, the repeated stress exposure did not cause any significant differences in the changes to DNA damage when iAstrocytes were pooled for analysis (fig.3.45). When separated by cell line, there were no DNA damage changes in CS14 iAstrocytes, except an increase in DNA damage (high damage) for oligomer and scrambled peptide-treated iAstrocytes when compared to the untreated control group. However, as there were no significant differences between the scrambled vehicle control and oligomer-treated group, this could be an artifact result (fig.3.46). When 155v2 iAstrocytes were analysed, there were no significant differences in DNA damage response for any treatment group (fig.3.47).

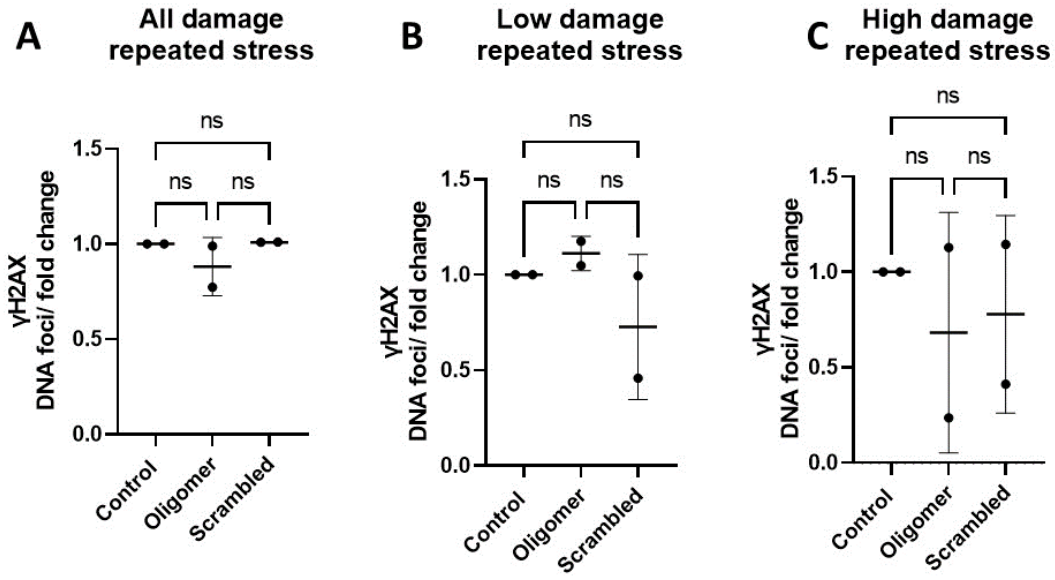


**Figure 3.45.** Formation of DNA damage indicative γH2AX-positive foci in iAstrocytes as a response to a repeated stress $A\beta_{1-42}$ oligomer treatment.

The quantification of DNA damage based on the number of γH2AX positive DNA foci in human 155v2 induced astrocytes (iAstrocytes), as a response to $A\beta_{1-42}$ oligomer treatment for repeated stress. Analysis was carried out using the Harmony Analysis Software (PerkinElmer). Graphs showing: **(A)** All damage detected; **(B)** Low damage detected (between 3-10 foci/ nucleus); **(C)** High damage detected (>10 foci/ nucleus). Data is presented as a fold change value of foci-positive nuclei to all nuclei detected. Standard error bars represent mean±SD. One-way ANOVA with Bonferroni's post-hoc test for multiple comparisons of pre-selected groups. Groups for statistical analysis: Control vs all treatment groups; and scrambled control group vs time-matched $A\beta_{1-42}$-treated group. N=2 (iAstrocytes pooled).

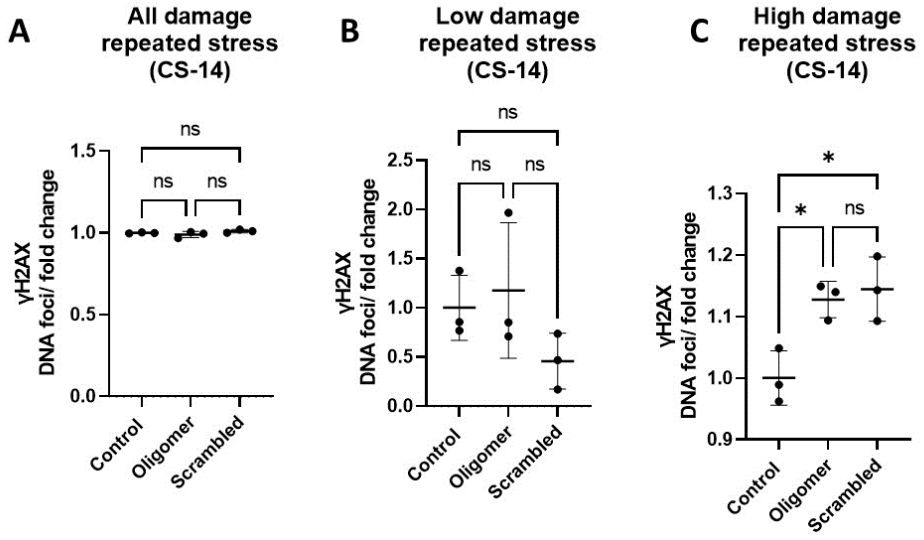


**Figure 3.46.** Formation of DNA damage indicative γH2AX-positive foci in CS14 iAstrocytes as a response to a repeated stress $A\beta_{1-42}$ oligomer treatment.

The quantification of DNA damage based on the number of γH2AX positive DNA foci in human CS14 induced astrocytes (iAstrocytes), as a response to $A\beta_{1-42}$ oligomer treatment for repeated stress. Analysis was carried out using the Harmony Analysis Software (PerkinElmer). Graphs showing: **(A)** All damage detected; **(B)** Low damage detected (between 3-10 foci/ nucleus); **(C)** High damage detected (>10 foci/ nucleus). Data is presented as a fold change value of foci-positive nuclei to all nuclei detected. Standard error bars represent mean±SD. One-way ANOVA with Bonferroni's post-hoc test for multiple comparisons of pre-selected groups. Groups for statistical analysis: Control vs all treatment groups; and scrambled control group vs time-matched $A\beta_{1-42}$-treated group. N=3 (CS14 iAstrocytes).

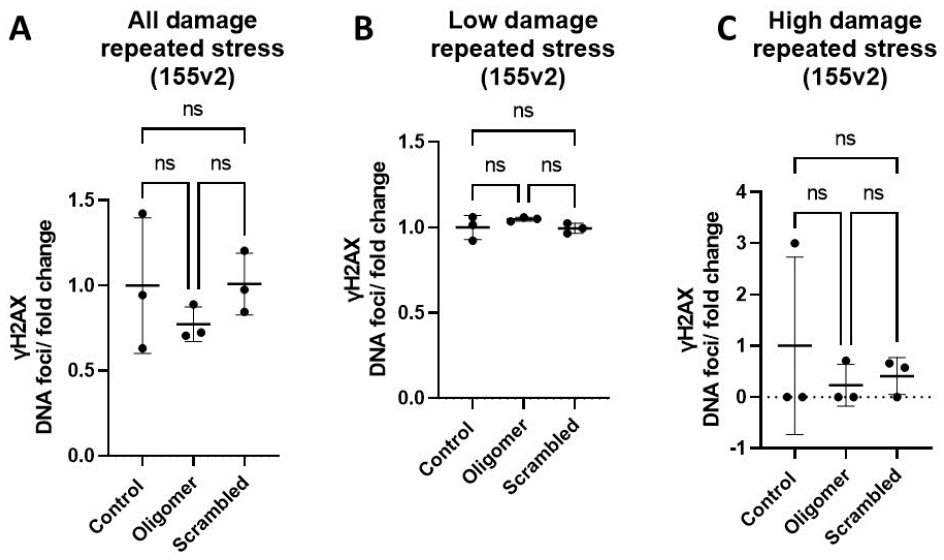


**Figure 3.47.** Formation of DNA damage indicative γH2AX-positive foci in 155v2 iAstrocytes as a response to repeated stress $A\beta_{1-42}$ oligomer treatment.

The quantification of DNA damage based on the number of γH2AX positive DNA foci in human 155v2 induced astrocytes (iAstrocytes), as a response to $A\beta_{1-42}$ oligomer treatment for repeated stress. Analysis was carried out using the Harmony Analysis Software (PerkinElmer). Graphs showing: **(A)** All damage detected; **(B)** Low damage detected (between 3-10 foci/ nucleus); **(C)** High damage detected (>10 foci/ nucleus). Data is presented as a fold change value of foci-positive nuclei to all nuclei detected. Standard error bars represent mean±SD. One-way ANOVA with Bonferroni's post-hoc test for multiple comparisons of pre-selected groups. Groups for statistical analysis: Control vs all treatment groups; and scrambled control group vs time-matched $A\beta_{1-42}$-treated group. N=3 (155v2 iAstrocytes).

Next, iAstrocytes were analysed to look for any morphology changes as a response to the repeated stress oligomer treatment (mean cytoplasm region, mean cell area, mean cell roundness, mean cell width, mean cell length). The analysis showed that there were no significant differences in the cell morphology of iAstrocytes when cell lines were pooled together, for any treatment group (fig.3.48). When cell lines were separated for analysis, there were no significant differences in the cell morphology in CS14 iAstrocytes (fig.3.49) and 155v2 iAstrocytes, for any treatment group (fig.3.50).

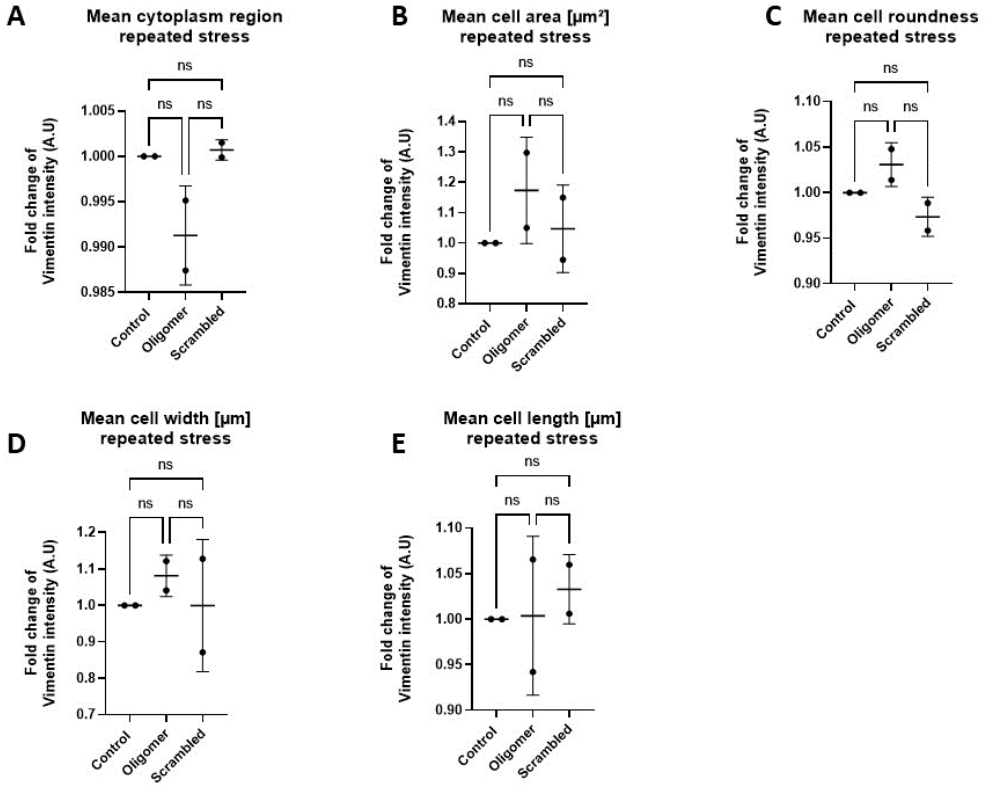


**Figure 3.48.** Cell morphology changes in iAstrocytes as a response to repeated stress $A\beta_{1-42}$ oligomer treatment.

The quantification of vimentin intensity in human induced astrocytes (iAstrocytes), indicative of cell morphology changes, as a response to $A\beta_{1-42}$ oligomer treatment for repeated stress. Analysis was carried out using the Harmony Analysis Software (PerkinElmer). Graphs showing changes in **(A)** mean cytoplasm region; **(B)** mean cell area; **(C)** mean cell roundness; **(D)** mean cell width; **(E)** mean cell length. Data is presented as a fold change value vimentin intensity, normalised to untreated control. Standard error bars represent mean±SD. One-way ANOVA with Bonferroni's post-hoc test for multiple comparisons of pre-selected groups. Groups for statistical analysis: Control vs all treatment groups; and scrambled control group vs time-matched $A\beta_{1-42}$-treated group. N=2 (iAstrocytes pooled)

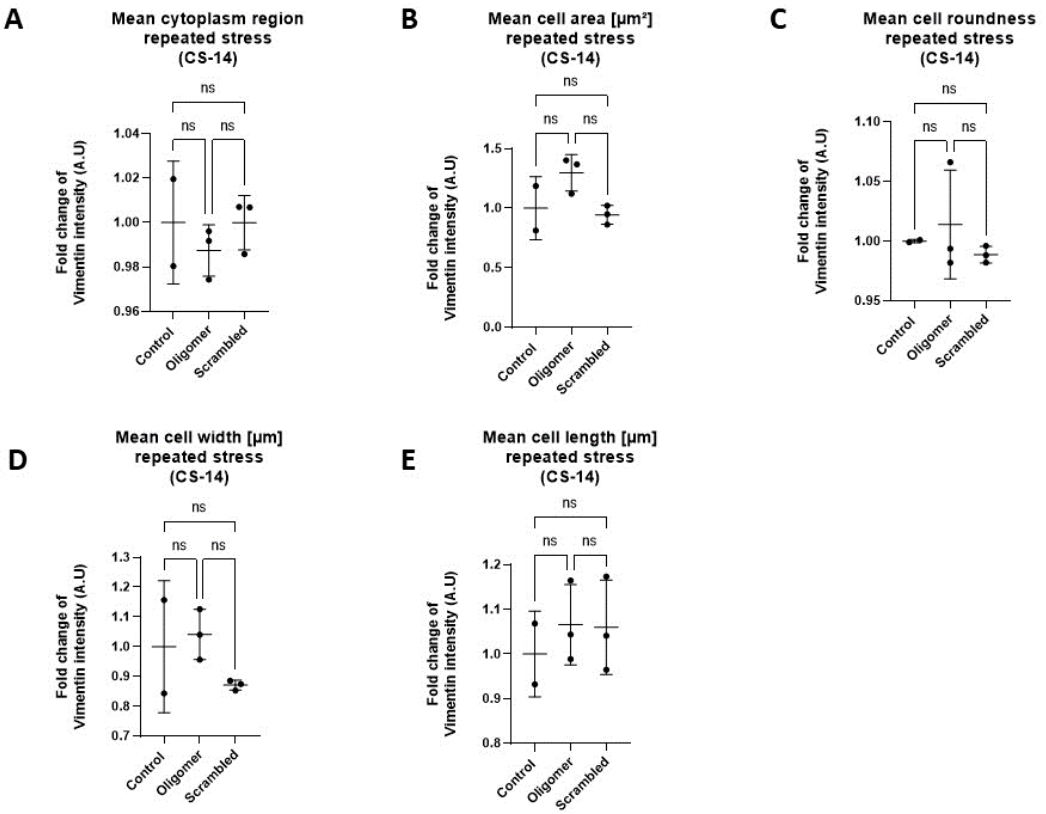


**Figure 3.49.** Cell morphology changes in CS14 iAstrocytes as a response to repeated stress $A\beta_{1-42}$ oligomer treatment.

The quantification of vimentin intensity in CS14 human induced astrocytes (iAstrocytes), indicative of cell morphology changes, as a response to $A\beta_{1-42}$ oligomer treatment for repeated stress. Analysis was carried out using the Harmony Analysis Software (PerkinElmer). Graphs showing changes in **(A)** mean cytoplasm region; **(B)** mean cell area; **(C)** mean cell roundness; **(D)** mean cell width; **(E)** mean cell length. Data is presented as a fold change value vimentin intensity, normalised to untreated control. Standard error bars represent mean±SD. One-way ANOVA with Bonferroni's post-hoc test for multiple comparisons of pre-selected groups. Groups for statistical analysis: Control vs all treatment groups; and scrambled control group vs time-matched $A\beta_{1-42}$-treated group. N=3 (CS14 iAstrocytes)

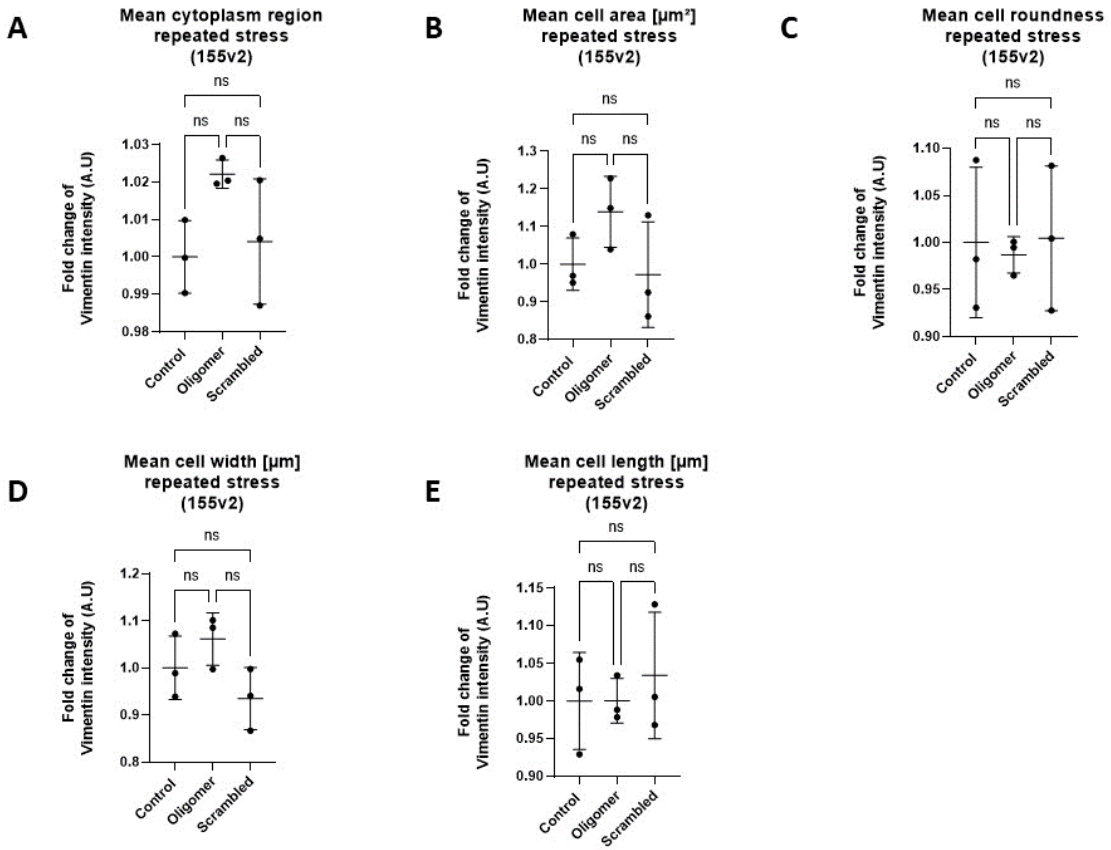


**Figure 3.50.** Cell morphology changes in 155v2 iAstrocytes as a response to repeated stress $A\beta_{1-42}$ oligomer treatment.

The quantification of vimentin intensity in 155v2 human induced astrocytes (iAstrocytes), indicative of cell morphology changes, as a response to $A\beta_{1-42}$ oligomer treatment for repeated stress. Analysis was carried out using the Harmony Analysis Software (PerkinElmer). Graphs showing changes in **(A)** mean cytoplasm region; **(B)** mean cell area; **(C)** mean cell roundness; **(D)** mean cell width; **(E)** mean cell length. Data is presented as a fold change value vimentin intensity, normalised to untreated control. Standard error bars represent mean±SD. One-way ANOVA with Bonferroni's post-hoc test for multiple comparisons of pre-selected groups. Groups for statistical analysis: Control vs all treatment groups; and scrambled control group vs time-matched $A\beta_{1-42}$-treated group. N=3 (155v2 iAstrocytes)

### Amyloid fibrils do not cause changes in DNA damage response or cell morphology of induced Astrocytes

To further investigate the impact of different aggregation species of amyloid beta on iAstrocytes, the cells were treated with 1 µM of $A\beta_{1-42}$ fibrils for 1 hour, 2 hours, 24 hours and 48 hours, as well as repeated stress treatment as described above. The fibril treatments of iAstrocytes matched the treatments with oligomers described above.

As described above, for all time points, the cytoplasmic astrocyte-specific marker, vimentin, was used to investigate the changes in astrocyte morphology by measuring changes in the mean cell area, cytoplasm region, cell roundness, cell width, and cell length of iAstrocytes after $A\beta_{1-42}$ fibril treatments. To detect DNA damage in iAstrocytes, ICC was performed to detect γH2AX-positive DNA foci, which are indicative of the induction of the DNA damage response. The statistical analysis used for each read-out was a one-way ANOVA with a Bonferroni's post-hoc test to look for differences between pre-selected groups. For all time points, both amyloid-treated and scrambled (vehicle)-treated groups were compared to the untreated control. Within the same analysis, the amyloid-treated group was also compared to the scrambled (vehicle) control. Furthermore, different set of analyses were performed. At first, all cell lines were pooled together and normalised to the untreated control groups to achieve three biological repeats for each time point treatment. Then, to look for individual differences in cell lines at the different time points, every iAstrocyte cell line was separated. The results were analysed again using one-way ANOVA with Bonferroni's post-hoc test as described above. For details of the statistical analysis results for all time points see appendix 5.3.

It is worth noting that some parameters did not reach full technical repeats again (as described above), as the cell line 161 experienced multiple mycoplasma infections at the time, and due to time constraints, it was not possible to repeat some experiments. This would also contribute to higher variability between groups and may not be fully representative in terms of statistical analysis.

Firstly, the iAstrocytes were treated with $A\beta_{1-42}$ fibrils for 1 hour. ICC was performed to analyse the iAstrocyte changes in DNA damage (γH2AX) and cell morphology changes (vimentin) (fig.3.51).

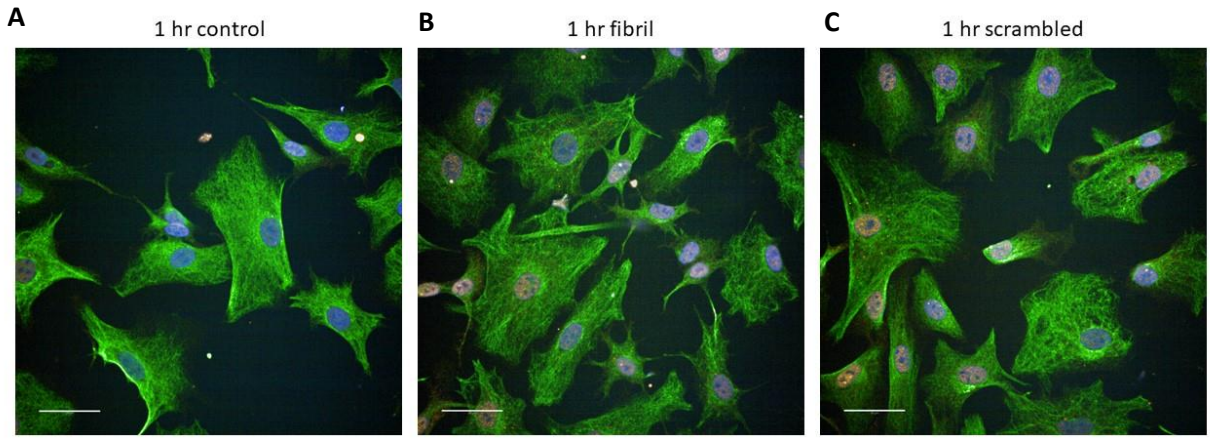


**Figure 3.51.** Representative immunocytochemistry images detecting changes to induced astrocyte (iAstrocyte) morphology and formation of DNA damage γH2AX foci as a response to 1 hour treatment with amyloid beta fibrils.

Immunocytochemistry images detecting induced Astrocyte (iAstrocyte) morphology with astrocyte marker vimentin (green), and γH2AX-positive DNA foci detected with γH2AX antibody (red). The nuclei are stained with Hoescht (blue). iAstrocytes treated for 1h with **(A)** untreated (control); **(B)** 1 µM fibrillary Aβ1-42; **(C)** 1 µM scrambled Aβ peptide as vehicle control. Representative images of n=3. Imaged on the Opera Phenix High Content Imaging System (PerkinElmer). Scale bars = 50 µm.

When all iAstrocyte cell lines were pooled, there was no significant change in the DNA damage level after 1h of $A\beta_{1-42}$ treatment (fig.3.52). When cell lines were split for analysis, the CS14 iAstrocytes revealed that there was significantly higher DNA damage at 1h fibril treatment when compared to the untreated control (fig.3.53). Meanwhile, in the 161 iAstrocytes, there were no significant differences in any of the treatment groups for DNA damage. Likewise, the 155v2 iAstrocytes revealed no significant differences in DNA damage between fibril treated group and the untreated control group (fig.3.54).

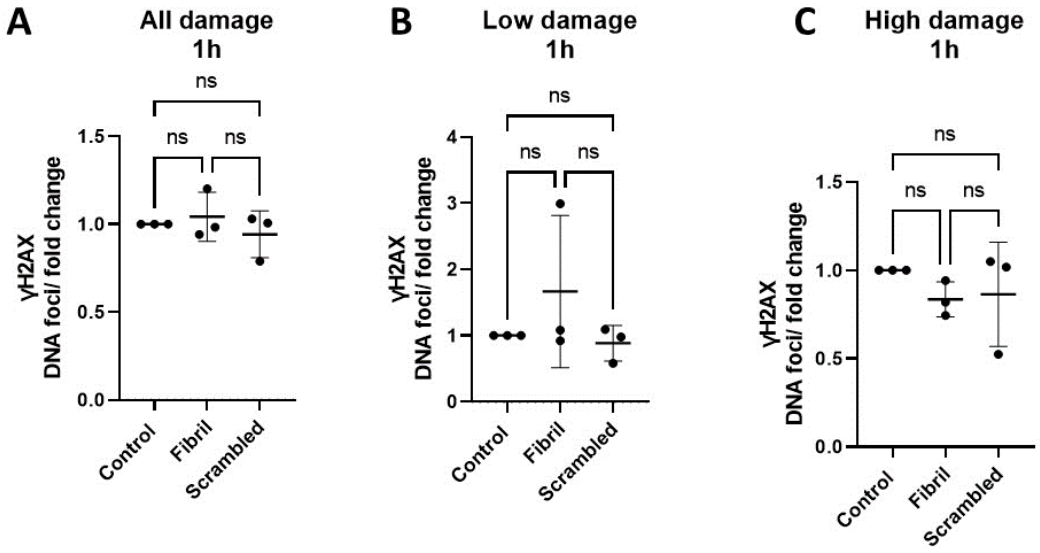


**Figure 3.52.** Formation of DNA damage indicative γH2AX-positive foci in iAstrocytes as a response to 1 hour $A\beta_{1-42}$ fibril treatment.

The quantification of DNA damage based on the number of γH2AX positive DNA foci in human induced astrocytes (iAstrocytes), as a response to $A\beta_{1-42}$ fibril treatment for 1 h. Analysis was carried out using the Harmony Analysis Software (PerkinElmer). Graphs showing: **(A)** All damage detected; **(B)** Low damage detected (between 3-10 foci/ nucleus); **(C)** High damage detected (>10 foci/ nucleus). Data is presented as a fold change value of foci-positive nuclei to all nuclei detected. Standard error bars represent mean±SD. One-way ANOVA with Bonferroni's post-hoc test for multiple comparisons of pre-selected groups. Groups for statistical analysis: Control vs all treatment groups; and scrambled control group vs time-matched $A\beta_{1-42}$-treated group. N=3 (iAstrocytes pooled).

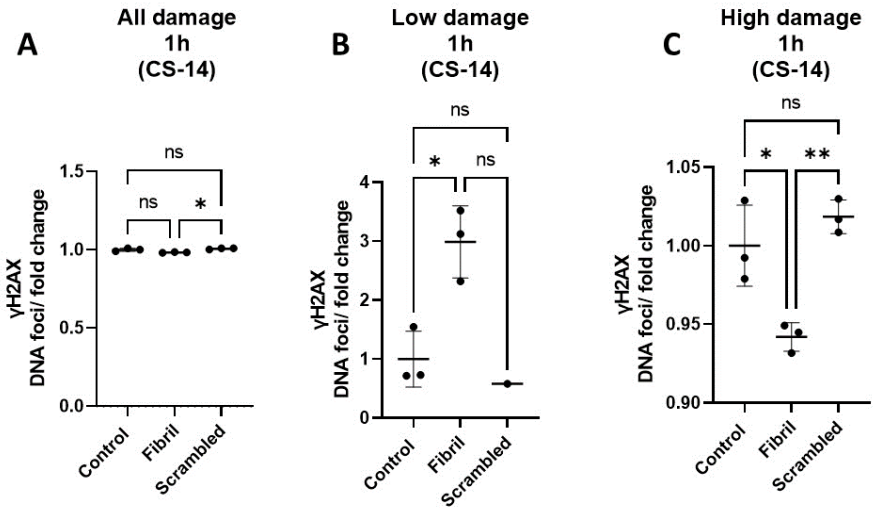


**Figure 3.53.** Formation of DNA damage indicative γH2AX-positive foci in CS14 iAstrocytes as a response to 1 hour $A\beta_{1-42}$ fibril treatment.

The quantification of DNA damage based on the number of γH2AX positive DNA foci in CS14 human induced astrocytes (iAstrocytes), as a response to $A\beta_{1-42}$ fibril treatment for 1 h. Analysis was carried out using the Harmony Analysis Software (PerkinElmer). Graphs showing: **(A)** All damage detected; **(B)** Low damage detected (between 3-10 foci/ nucleus); **(C)** High damage detected (>10 foci/ nucleus). Data is presented as a fold change value of foci-positive nuclei to all nuclei detected. Standard error bars represent mean±SD. One-way ANOVA with Bonferroni's post-hoc test for multiple comparisons of pre-selected groups. Groups for statistical analysis: Control vs all treatment groups; and scrambled control group vs time-matched $A\beta_{1-42}$-treated group. N=3 (CS14 iAstrocytes).

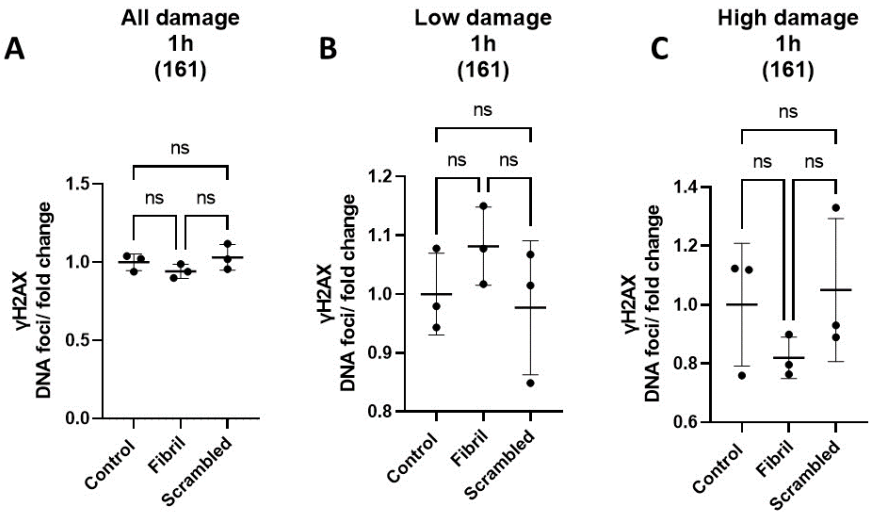


**Figure 3.54.** Formation of DNA damage indicative γH2AX-positive foci in 161 iAstrocytes as a response to 1 hour $A\beta_{1-42}$ fibril treatment.

The quantification of DNA damage based on the number of γH2AX positive DNA foci in 161 human induced astrocytes (iAstrocytes), as a response to $A\beta_{1-42}$ fibril treatment for 1 h. Analysis was carried out using the Harmony Analysis Software (PerkinElmer). Graphs showing: **(A)** All damage detected; **(B)** Low damage detected (between 3-10 foci/ nucleus); **(C)** High damage detected (>10 foci/ nucleus). Data is presented as a fold change value of foci-positive nuclei to all nuclei detected. Standard error bars represent mean±SD. One-way ANOVA with Bonferroni's post-hoc test for multiple comparisons of pre-selected groups. Groups for statistical analysis: Control vs all treatment groups; and scrambled control group vs time-matched $A\beta_{1-42}$-treated group. N=3 (161 iAstrocytes).

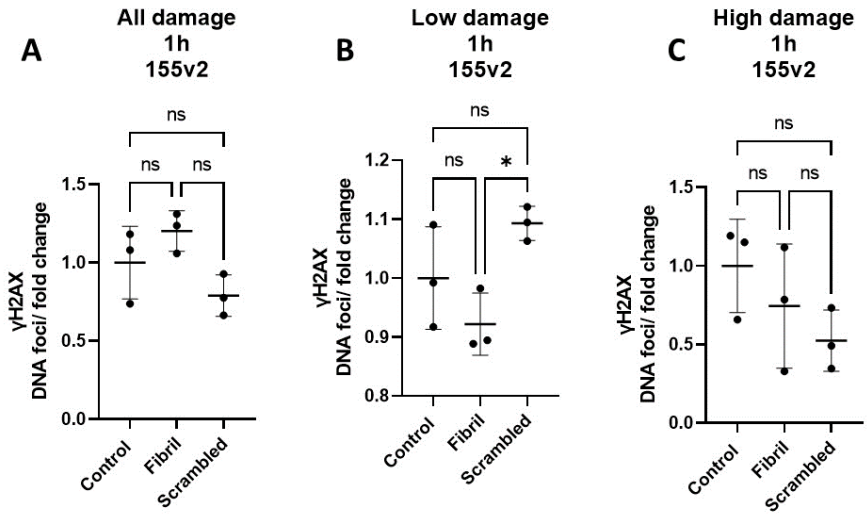


**Figure 3.55.** Formation of DNA damage indicative γH2AX-positive foci in 155v2 iAstrocytes as a response to 1 hour $A\beta_{1-42}$ fibril treatment.

The quantification of DNA damage based on the number of γH2AX positive DNA foci in 155v2 human induced astrocytes (iAstrocytes), as a response to $A\beta_{1-42}$ fibril treatment for 1 h. Analysis was carried out using the Harmony Analysis Software (PerkinElmer). Graphs showing: **(A)** All damage detected; **(B)** Low damage detected (between 3-10 foci/ nucleus); **(C)** High damage detected (>10 foci/ nucleus). Data is presented as a fold change value of foci-positive nuclei to all nuclei detected. Standard error bars represent mean±SD. One-way ANOVA with Bonferroni's post-hoc test for multiple comparisons of pre-selected groups. Groups for statistical analysis: Control vs all treatment groups; and scrambled control group vs time-matched $A\beta_{1-42}$-treated group. N=3 (155v2 iAstrocytes).

Next, the iAstrocyte morphology was investigated as a response to 1h treatment with $A\beta_{1-42}$ fibrils. When all iAstrocyte cell lines were pooled, there was no change in iAstrocyte morphology when looking at mean cytoplasm region, mean cell area, mean cell roundness, mean cell width, and mean cell length (fig.3.56). When iAstrocyte cell lines were separated for analysis, there were no significant differences in any of the cell morphology parameters in both CS14 (fig.3.57) and 155v2 (fig.3.58) iAstrocytes.

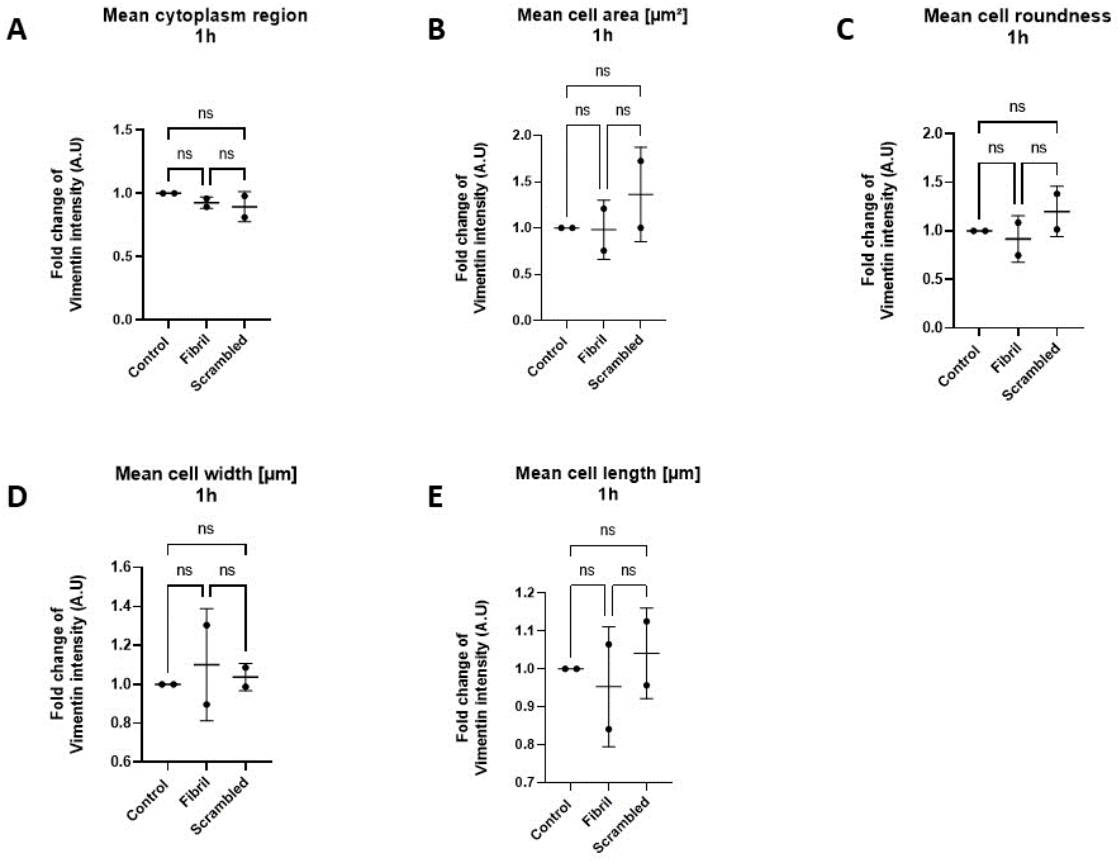


**Figure 3.56.** Cell morphology changes in iAstrocytes as a response to 1 hour $A\beta_{1-42}$ fibril treatment.

The quantification of vimentin intensity in human induced astrocytes (iAstrocytes), indicative of cell morphology changes, as a response to $A\beta_{1-42}$ fibril treatment for 1 hour. Analysis was carried out using the Harmony Analysis Software (PerkinElmer). Graphs showing changes in **(A)** mean cytoplasm region; **(B)** mean cell area; **(C)** mean cell roundness; **(D)** mean cell width; **(E)** mean cell length. Data is presented as a fold change value vimentin intensity, normalised to untreated control. Standard error bars represent mean±SD. One-way ANOVA with Bonferroni's post-hoc test for multiple comparisons of pre-selected groups. Groups for statistical analysis: Control vs all treatment groups; and scrambled control group vs time-matched $A\beta_{1-42}$-treated group. N=2 (iAstrocytes pooled)

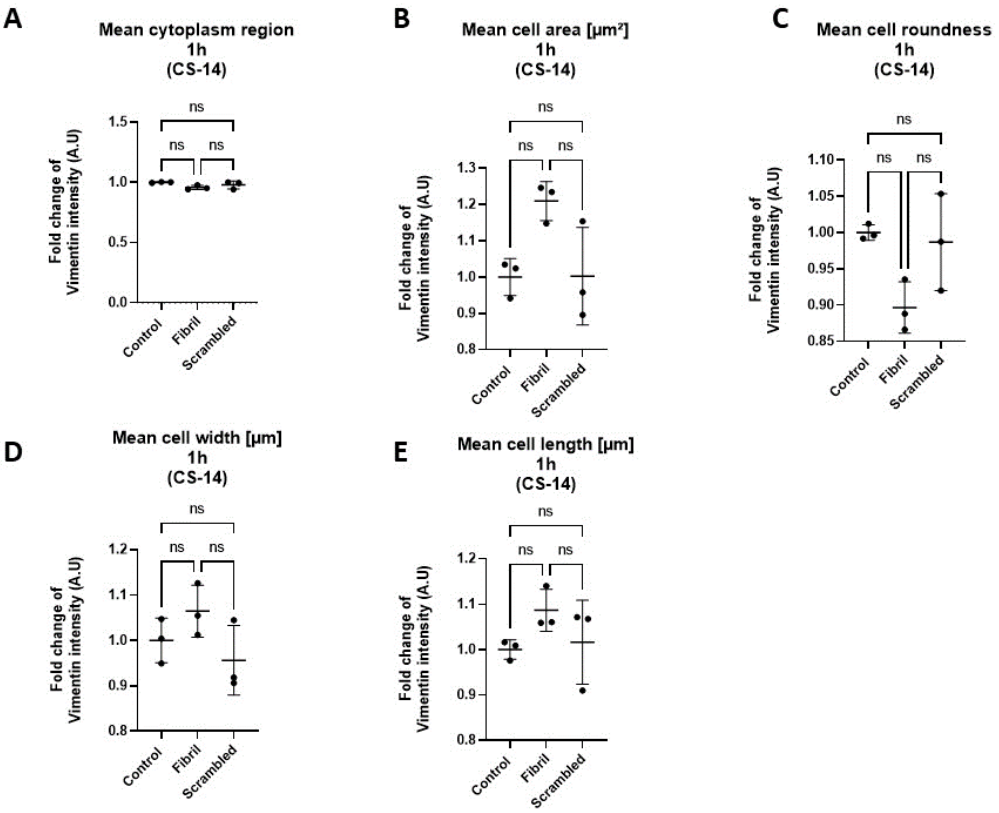


**Figure 3.57.** Cell morphology changes in CS14 iAstrocytes as a response to 1 hour $A\beta_{1-42}$ fibril treatment.

The quantification of vimentin intensity in CS14 human induced astrocytes (iAstrocytes), indicative of cell morphology changes, as a response to $A\beta_{1-42}$ fibril treatment for 1 hour. Analysis was carried out using the Harmony Analysis Software (PerkinElmer). Graphs showing changes in **(A)** mean cytoplasm region; **(B)** mean cell area; **(C)** mean cell roundness; **(D)** mean cell width; **(E)** mean cell length. Data is presented as a fold change value vimentin intensity, normalised to untreated control. Standard error bars represent mean±SD. One-way ANOVA with Bonferroni's post-hoc test for multiple comparisons of pre-selected groups. Groups for statistical analysis: Control vs all treatment groups; and scrambled control group vs time-matched $A\beta_{1-42}$-treated group. N=3 (CS14 iAstrocytes)

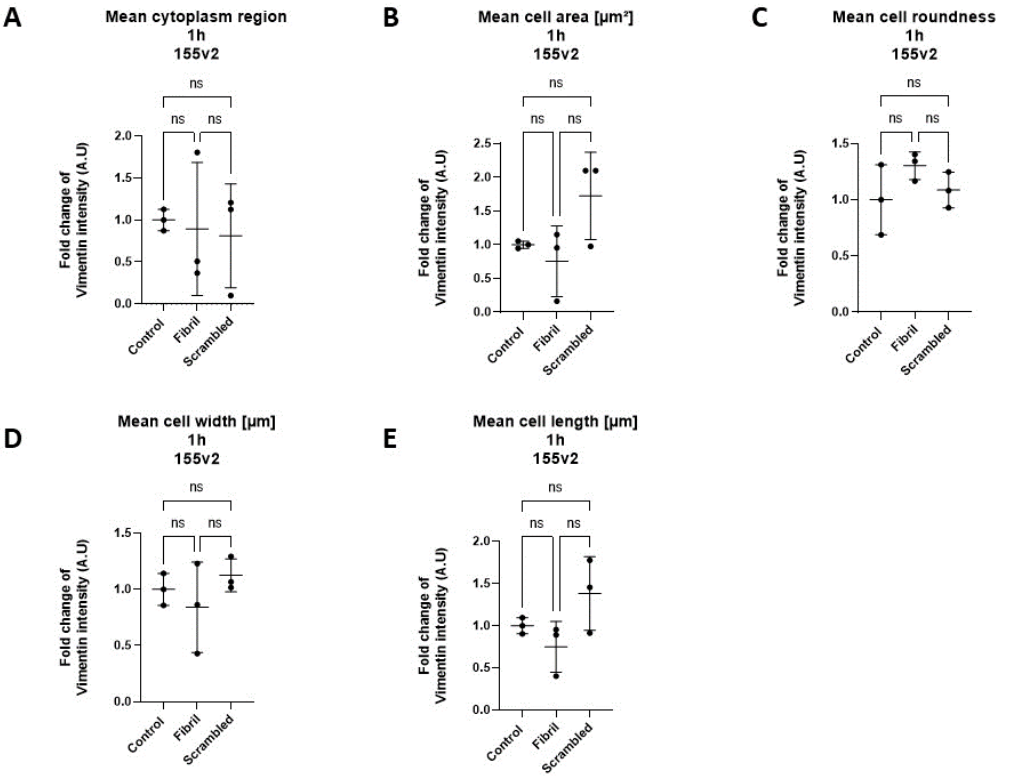


**Figure 3.58.** Cell morphology changes in 155v2 iAstrocytes as a response to 1 hour $A\beta_{1-42}$ fibril treatment.

The quantification of vimentin intensity in 155v2 human induced astrocytes (iAstrocytes), indicative of cell morphology changes, as a response to $A\beta_{1-42}$ fibril treatment for 1 hour. Analysis was carried out using the Harmony Analysis Software (PerkinElmer). Graphs showing changes in **(A)** mean cytoplasm region; **(B)** mean cell area; **(C)** mean cell roundness; **(D)** mean cell width; **(E)** mean cell length. Data is presented as a fold change value vimentin intensity, normalised to untreated control. Standard error bars represent mean±SD. One-way ANOVA with Bonferroni's post-hoc test for multiple comparisons of pre-selected groups. Groups for statistical analysis: Control vs all treatment groups; and scrambled control group vs time-matched $A\beta_{1-42}$-treated group. N=3 (155v2 iAstrocytes)

Next, the DNA damage (γH2AX) and cell morphology of iAstrocytes was investigated after a 2 hour treatment with $A\beta_{1-42}$ fibrils (fig.3.59).

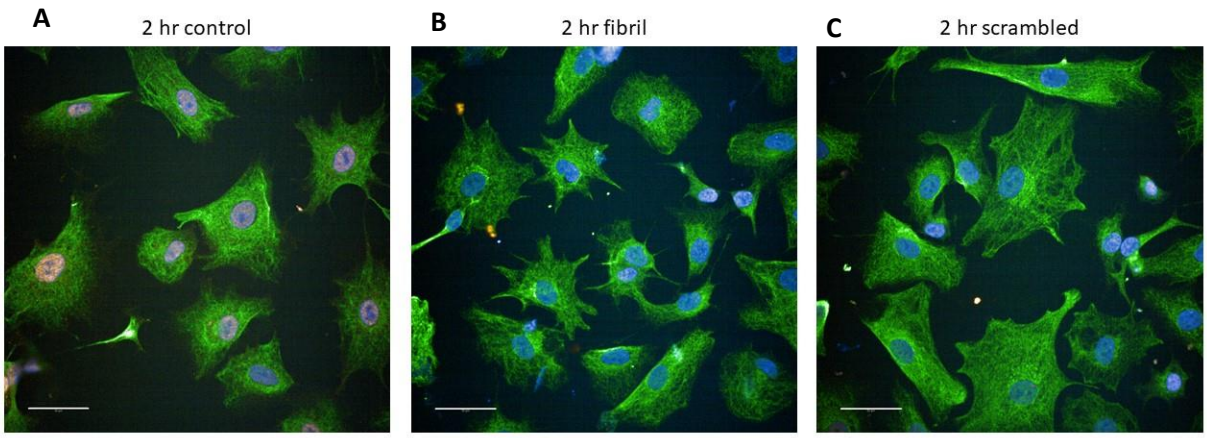


**Figure 3.59.** Representative immunocytochemistry images detecting changes to induced astrocyte (iAstrocyte) morphology and formation of DNA damage γH2AX foci as a response to 2 hour treatment with amyloid beta fibrils.

Immunocytochemistry images detecting induced Astrocyte (iAstrocyte) morphology with astrocyte marker vimentin (green), and γH2AX-positive DNA foci detected with γH2AX antibody (red). The nuclei are stained with Hoescht (blue). iAstrocytes treated for 2h with **(A)** untreated (control); **(B)** 1 µM fibrillary Aβ1-42; **(C)** 1 µM scrambled Aβ peptide as vehicle control. Representative images of n=3. Imaged on the Opera Phenix High Content Imaging System (PerkinElmer). Scale bars = 50 µm.

When all iAstrocyte cell lines were pooled, there was no significant change in the DNA damage level after 2h of $A\beta_{1-42}$ treatment for all damage and low damage parameters. There was however a significant decrease in the formation of DNA foci (high damage) in the fibril-treated group when compared to the untreated and vehicle controls (fig.3.60).

When cell lines were split for analysis, the CS14 iAstrocytes revealed that there was a higher amount of DNA damage (low damage) when compared to the untreated and vehicle controls. At the same time, for CS14 iAstrocytes, there was a lower amount of DNA damage (high damage) when compared to both control groups. This could indicate that CS14 iAstrocytes develop a low-grade DNA damage after the 2h amyloid fibril treatment (fig.3.61). Interestingly, there were no significant differences in any of the DNA damage parameters for 155v2 iAstrocytes (fig.3.62), and 161 iAstrocytes (fig.3.63).

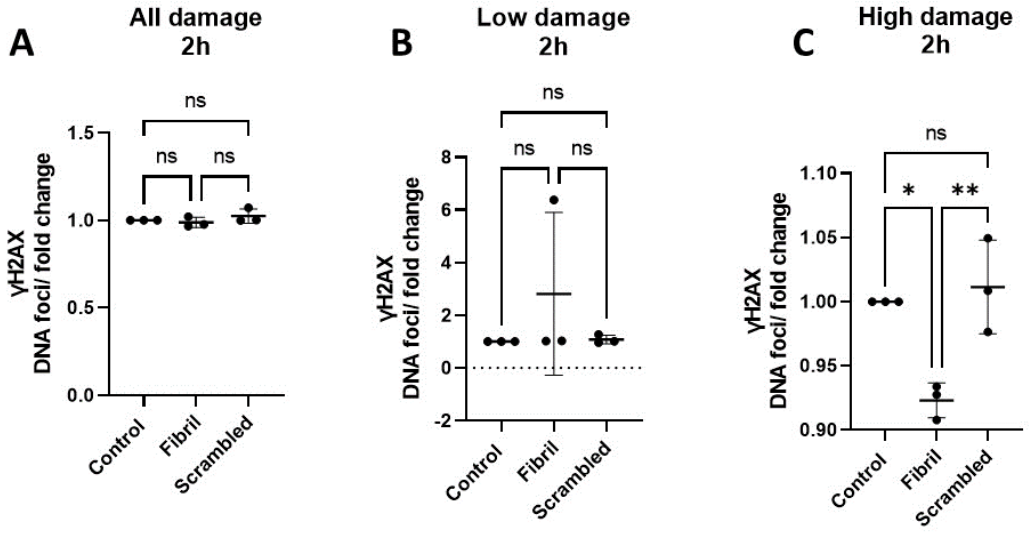


**Figure 3.60.** Formation of DNA damage indicative γH2AX-positive foci in iAstrocytes as a response to 2 hour $A\beta_{1-42}$ fibril treatment.

The quantification of DNA damage based on the number of γH2AX positive DNA foci in human induced astrocytes (iAstrocytes), as a response to $A\beta_{1-42}$ fibril treatment for 2 h. Analysis was carried out using the Harmony Analysis Software (PerkinElmer). Graphs showing: **(A)** All damage detected; **(B)** Low damage detected (between 3-10 foci/ nucleus); **(C)** High damage detected (>10 foci/ nucleus). Data is presented as a fold change value of foci-positive nuclei to all nuclei detected. Standard error bars represent mean±SD. One-way ANOVA with Bonferroni's post-hoc test for multiple comparisons of pre-selected groups. Groups for statistical analysis: Control vs all treatment groups; and scrambled control group vs time-matched $A\beta_{1-42}$-treated group. N=3 (iAstrocytes pooled).

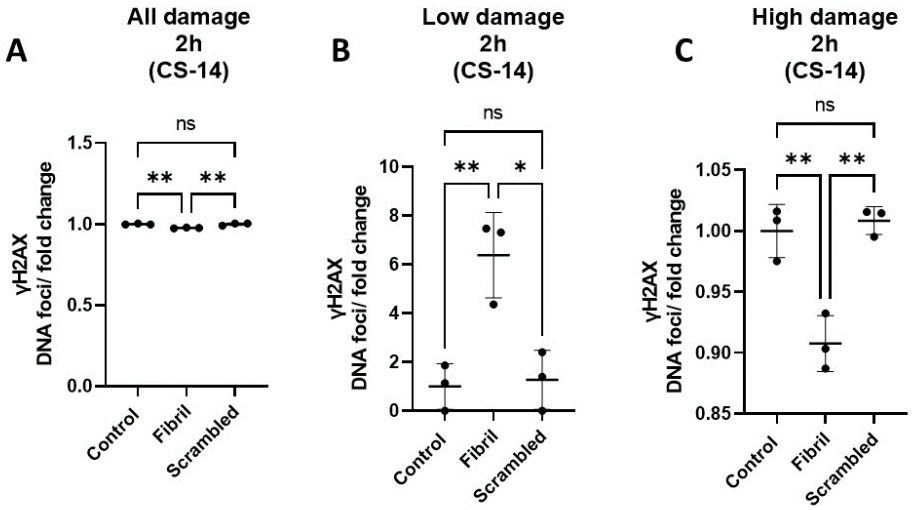


**Figure 3.61.** Formation of DNA damage indicative γH2AX-positive foci in CS14 iAstrocytes as a response to 2 hour $A\beta_{1-42}$ fibril treatment.

The quantification of DNA damage based on the number of γH2AX positive DNA foci in CS14 human induced astrocytes (iAstrocytes), as a response to $A\beta_{1-42}$ fibril treatment for 2 h. Analysis was carried out using the Harmony Analysis Software (PerkinElmer). Graphs showing: **(A)** All damage detected; **(B)** Low damage detected (between 3-10 foci/ nucleus); **(C)** High damage detected (>10 foci/ nucleus). Data is presented as a fold change value of foci-positive nuclei to all nuclei detected. Standard error bars represent mean±SD. One-way ANOVA with Bonferroni's post-hoc test for multiple comparisons of pre-selected groups. Groups for statistical analysis: Control vs all treatment groups; and scrambled control group vs time-matched $A\beta_{1-42}$-treated group. N=3 (CS14 iAstrocytes).

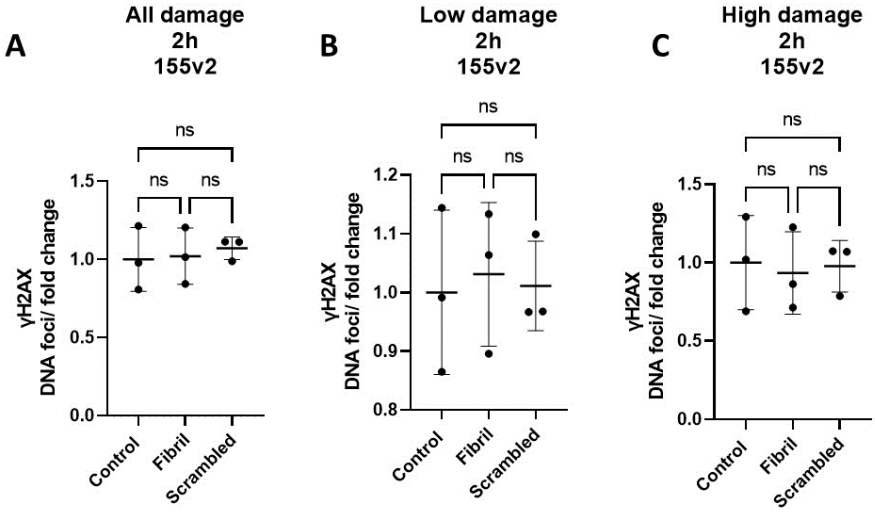


**Figure 3.62.** Formation of DNA damage indicative γH2AX-positive foci in 155v2 iAstrocytes as a response to 2 hour $A\beta_{1-42}$ fibril treatment.

The quantification of DNA damage based on the number of γH2AX positive DNA foci in 155v2 human induced astrocytes (iAstrocytes), as a response to $A\beta_{1-42}$ fibril treatment for 2 h. Analysis was carried out using the Harmony Analysis Software (PerkinElmer). Graphs showing: **(A)** All damage detected; **(B)** Low damage detected (between 3-10 foci/ nucleus); **(C)** High damage detected (>10 foci/ nucleus). Data is presented as a fold change value of foci-positive nuclei to all nuclei detected. Standard error bars represent mean±SD. One-way ANOVA with Bonferroni's post-hoc test for multiple comparisons of pre-selected groups. Groups for statistical analysis: Control vs all treatment groups; and scrambled control group vs time-matched $A\beta_{1-42}$-treated group. N=3 (155v2 iAstrocytes).

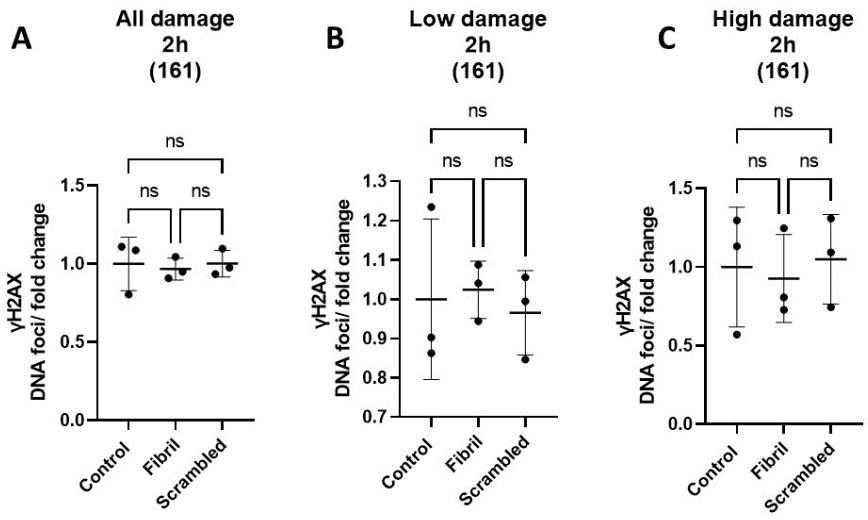


**Figure 3.63.** Formation of DNA damage indicative γH2AX-positive foci in 161 iAstrocytes as a response to 2 hour $A\beta_{1-42}$ fibril treatment.

The quantification of DNA damage based on the number of γH2AX positive DNA foci in 161 human induced astrocytes (iAstrocytes), as a response to $A\beta_{1-42}$ fibril treatment for 2 h. Analysis was carried out using the Harmony Analysis Software (PerkinElmer). Graphs showing: **(A)** All damage detected; **(B)** Low damage detected (between 3-10 foci/ nucleus); **(C)** High damage detected (>10 foci/ nucleus). Data is presented as a fold change value of foci-positive nuclei to all nuclei detected. Standard error bars represent mean±SD. One-way ANOVA with Bonferroni's post-hoc test for multiple comparisons of pre-selected groups. Groups for statistical analysis: Control vs all treatment groups; and scrambled control group vs time-matched $A\beta_{1-42}$-treated group. N=3 (161 iAstrocytes).

Next, the cell morphology changes (mean cytoplasm region, mean cell area, mean cell roundness, mean cell width, mean cell length) were investigated in the iAstrocytes as a response to 2h fibril treatment. When all iAstrocytes were pooled together there were no significant changes in any of the morphology parameters (fig.3.64). Likewise, when cell lines were separated for analysis, the CS14 iAstrocytes also showed no significant changes in cell morphology (fig.3.65). This was also the result for 155v2 iAstrocytes, with no differences in the cell morphology changes for all parameters (fig.3.66).

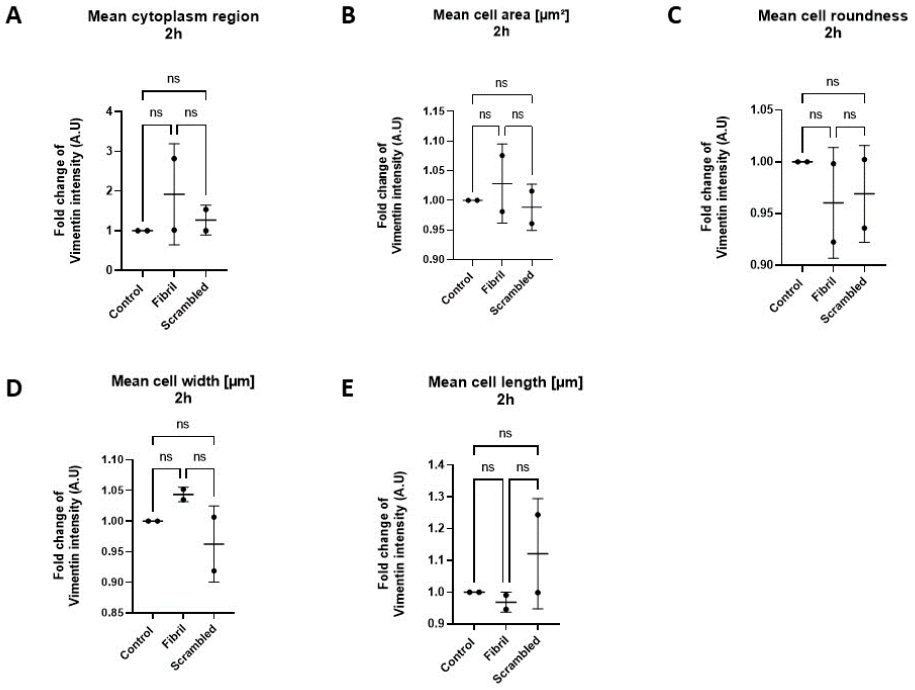


**Figure 3.64.** Cell morphology changes in iAstrocytes as a response to 2 hour $A\beta_{1-42}$ fibril treatment.

The quantification of vimentin intensity in human induced astrocytes (iAstrocytes), indicative of cell morphology changes, as a response to $A\beta_{1-42}$ fibril treatment for 2 hour. Analysis was carried out using the Harmony Analysis Software (PerkinElmer). Graphs showing changes in **(A)** mean cytoplasm region; **(B)** mean cell area; **(C)** mean cell roundness; **(D)** mean cell width; **(E)** mean cell length. Data is presented as a fold change value vimentin intensity, normalised to untreated control. Standard error bars represent mean±SD. One-way ANOVA with Bonferroni's post-hoc test for multiple comparisons of pre-selected groups. Groups for statistical analysis: Control vs all treatment groups; and scrambled control group vs time-matched $A\beta_{1-42}$-treated group. N=2 (iAstrocytes pooled)

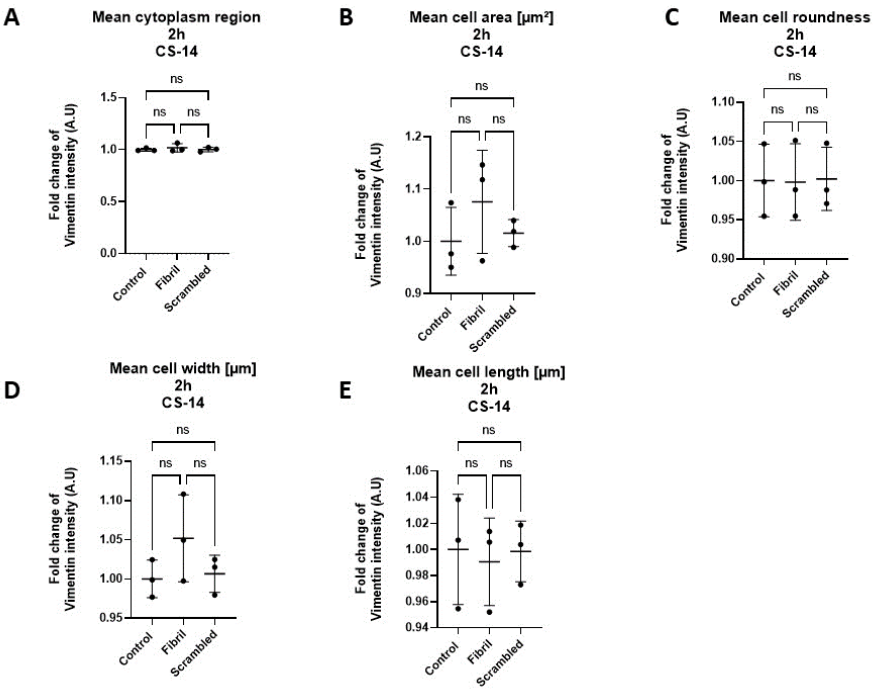


**Figure 3.65.** Cell morphology changes in CS14 iAstrocytes as a response to 2 hour $A\beta_{1-42}$ fibril treatment.

The quantification of vimentin intensity in CS14 human induced astrocytes (iAstrocytes), indicative of cell morphology changes, as a response to $A\beta_{1-42}$ fibril treatment for 2 hour. Analysis was carried out using the Harmony Analysis Software (PerkinElmer). Graphs showing changes in **(A)** mean cytoplasm region; **(B)** mean cell area; **(C)** mean cell roundness; **(D)** mean cell width; **(E)** mean cell length. Data is presented as a fold change value vimentin intensity, normalised to untreated control. Standard error bars represent mean±SD. One-way ANOVA with Bonferroni's post-hoc test for multiple comparisons of pre-selected groups. Groups for statistical analysis: Control vs all treatment groups; and scrambled control group vs time-matched $A\beta_{1-42}$-treated group. N=3 (CS14 iAstrocytes)

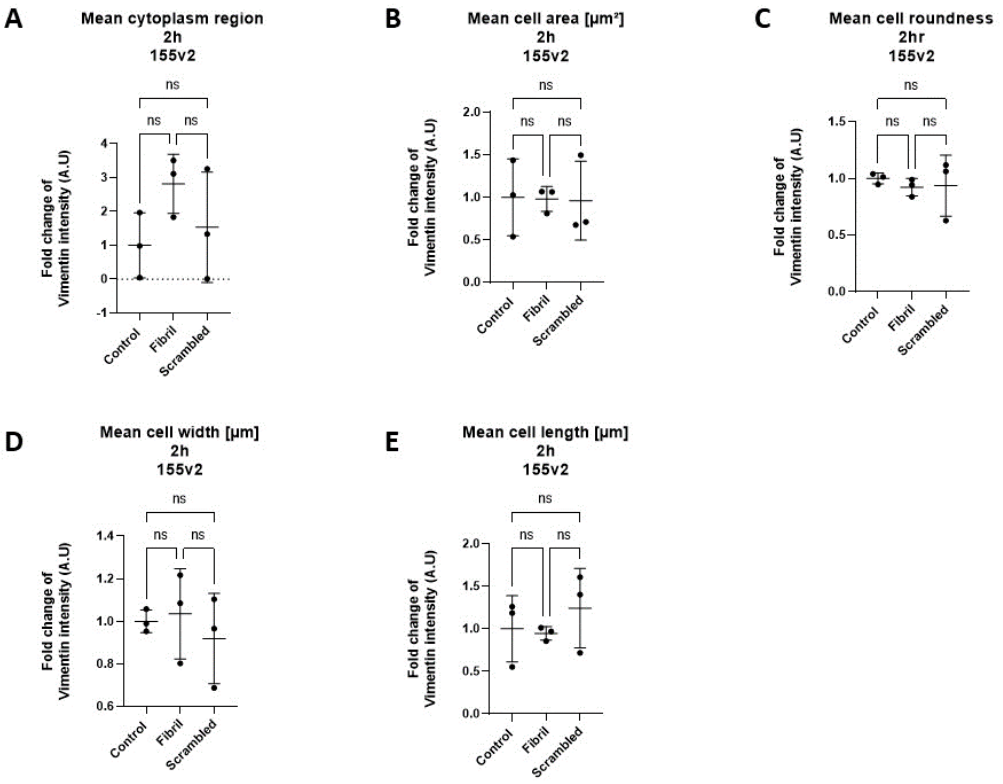


**Figure 3.66.** Cell morphology changes in 155v2 iAstrocytes as a response to 2 hour $A\beta_{1-42}$ fibril treatment.

The quantification of vimentin intensity in 155v2 human induced astrocytes (iAstrocytes), indicative of cell morphology changes, as a response to $A\beta_{1-42}$ fibril treatment for 2 hour. Analysis was carried out using the Harmony Analysis Software (PerkinElmer). Graphs showing changes in **(A)** mean cytoplasm region; **(B)** mean cell area; **(C)** mean cell roundness; **(D)** mean cell width; **(E)** mean cell length. Data is presented as a fold change value vimentin intensity, normalised to untreated control. Standard error bars represent mean±SD. One-way ANOVA with Bonferroni's post-hoc test for multiple comparisons of pre-selected groups. Groups for statistical analysis: Control vs all treatment groups; and scrambled control group vs time-matched $A\beta_{1-42}$-treated group. N=3 (155v2 iAstrocytes)

Next, the DNA damage changes and cell morphology changes in iAstrocytes were investigated as a response to amyloid fibrils after 24 hours of treatment (fig.3.67).

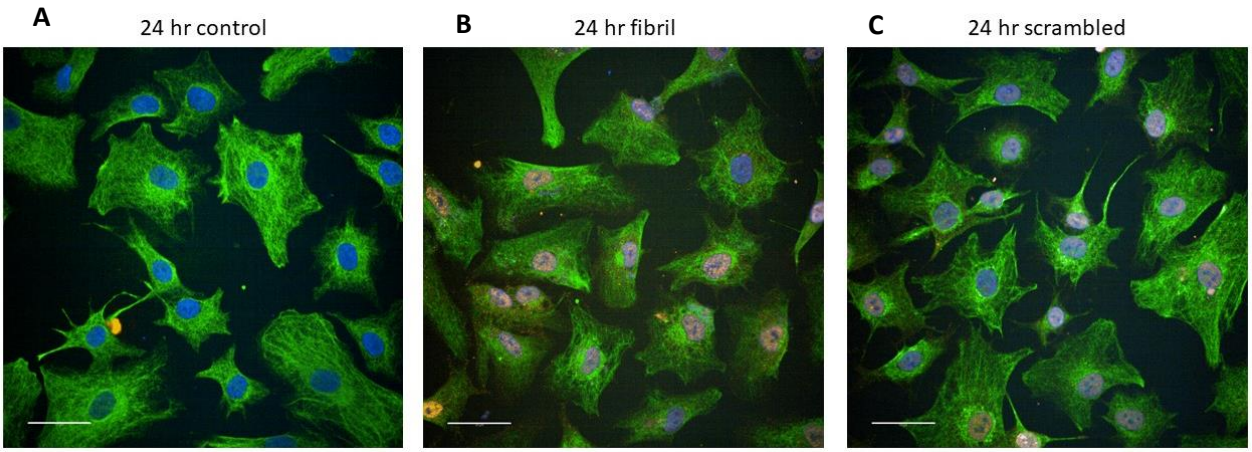


**Figure 3.67.** Representative immunocytochemistry images detecting changes to induced astrocyte (iAstrocyte) morphology and formation of DNA damage γH2AX foci as a response to 24 hour treatment with amyloid beta fibrils.

Immunocytochemistry images detecting induced Astrocyte (iAstrocyte) morphology with astrocyte marker vimentin (green), and γH2AX-positive DNA foci detected with γH2AX antibody (red). The nuclei are stained with Hoescht (blue). iAstrocytes treated for 24h with **(A)** untreated (control); **(B)** 1 µM fibrillary Aβ1-42; **(C)** 1 µM scrambled Aβ peptide as vehicle control. Representative images of n=3. Imaged on the Opera Phenix High Content Imaging System (PerkinElmer). Scale bars = 50 µm.

Firstly, γH2AX-positive DNA foci, indicative of DNA damage were investigated. When iAstrocytes were pooled together for analysis, there was no significant change in the resulting DNA damage (fig.3.68). When cell lines were separated for analysis, the CS14 iAstrocytes revealed a significant increase in the DNA damage (low damage), compared to both untreated and vehicle controls (fig.3.69). This suggests that the CS14 iAstrocytes could respond with a low level of DNA damage after amyloid beta fibril treatments. There was no significant change in the DNA damage for 155v2 (fig.3.70) and 161 iAstrocytes (fig.3.71).

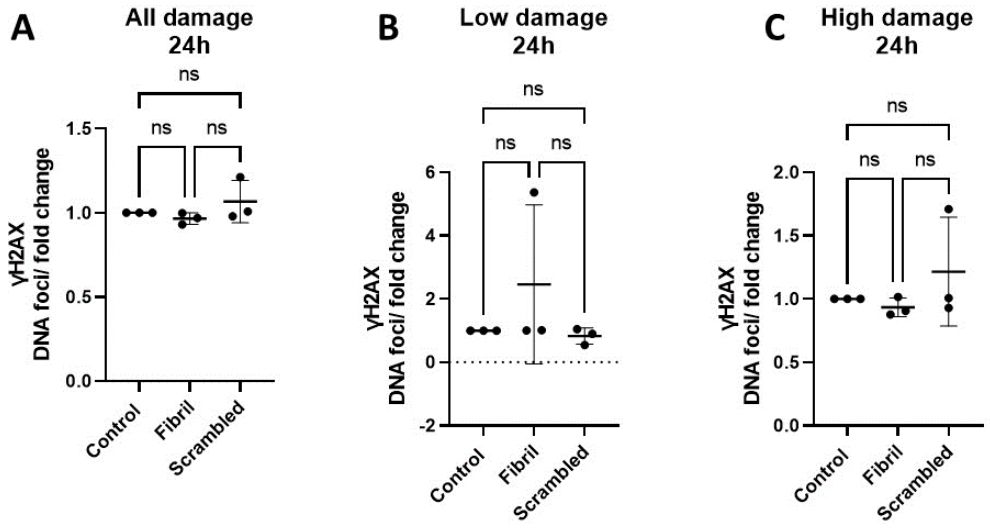


**Figure 3.68.** Formation of DNA damage indicative γH2AX-positive foci in iAstrocytes as a response to 24 hour $A\beta_{1-42}$ fibril treatment.

The quantification of DNA damage based on the number of γH2AX positive DNA foci in human induced astrocytes (iAstrocytes), as a response to $A\beta_{1-42}$ fibril treatment for 24 h. Analysis was carried out using the Harmony Analysis Software (PerkinElmer). Graphs showing: **(A)** All damage detected; **(B)** Low damage detected (between 3-10 foci/ nucleus); **(C)** High damage detected (>10 foci/ nucleus). Data is presented as a fold change value of foci-positive nuclei to all nuclei detected. Standard error bars represent mean±SD. One-way ANOVA with Bonferroni's post-hoc test for multiple comparisons of pre-selected groups. Groups for statistical analysis: Control vs all treatment groups; and scrambled control group vs time-matched $A\beta_{1-42}$-treated group. N=3 (iAstrocytes pooled).

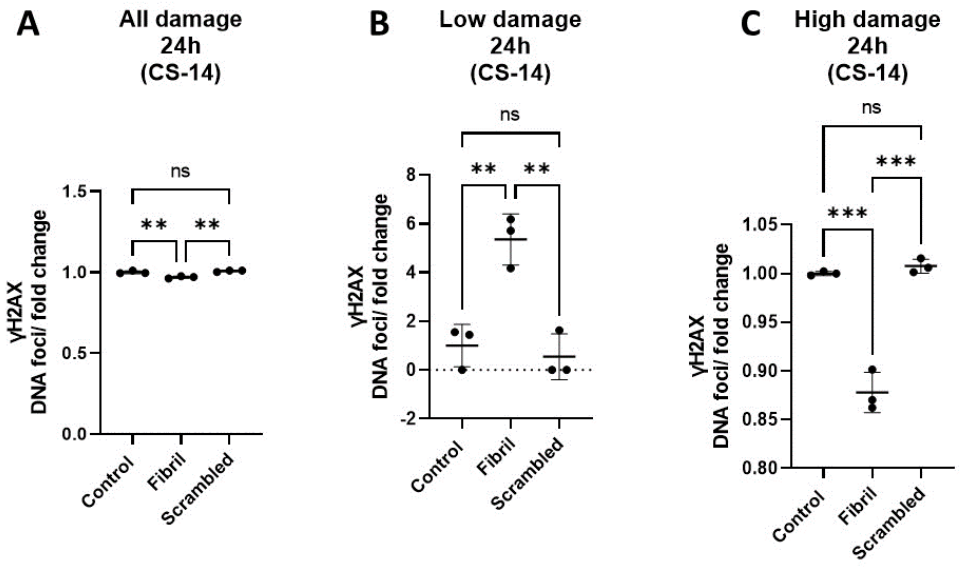


**Figure 3.69.** Formation of DNA damage indicative γH2AX-positive foci in CS14 iAstrocytes as a response to 24 hour $A\beta_{1-42}$ fibril treatment.

The quantification of DNA damage based on the number of γH2AX positive DNA foci in CS14 human induced astrocytes (iAstrocytes), as a response to $A\beta_{1-42}$ fibril treatment for 24 h. Analysis was carried out using the Harmony Analysis Software (PerkinElmer). Graphs showing: **(A)** All damage detected; **(B)** Low damage detected (between 3-10 foci/ nucleus); **(C)** High damage detected (>10 foci/ nucleus). Data is presented as a fold change value of foci-positive nuclei to all nuclei detected. Standard error bars represent mean±SD. One-way ANOVA with Bonferroni's post-hoc test for multiple comparisons of pre-selected groups. Groups for statistical analysis: Control vs all treatment groups; and scrambled control group vs time-matched $A\beta_{1-42}$-treated group. N=3 (CS14 iAstrocytes).

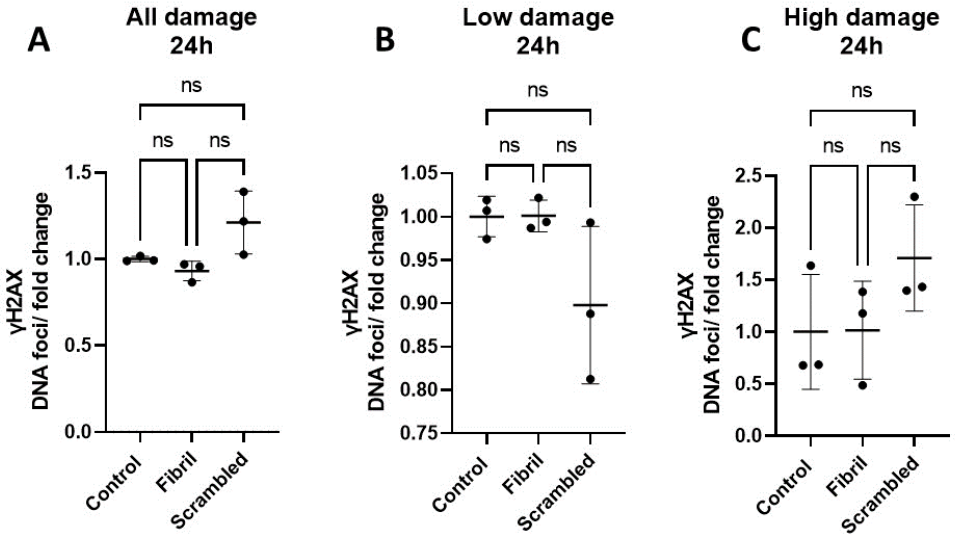


**Figure 3.70.** Formation of DNA damage indicative γH2AX-positive foci in 155v2 iAstrocytes as a response to 24 hour $A\beta_{1-42}$ fibril treatment.

The quantification of DNA damage based on the number of γH2AX positive DNA foci in 155v2 human induced astrocytes (iAstrocytes), as a response to $A\beta_{1-42}$ fibril treatment for 24h. Analysis was carried out using the Harmony Analysis Software (PerkinElmer). Graphs showing: **(A)** All damage detected; **(B)** Low damage detected (between 3-10 foci/ nucleus); **(C)** High damage detected (>10 foci/ nucleus). Data is presented as a fold change value of foci-positive nuclei to all nuclei detected. Standard error bars represent mean±SD. One-way ANOVA with Bonferroni's post-hoc test for multiple comparisons of pre-selected groups. Groups for statistical analysis: Control vs all treatment groups; and scrambled control group vs time-matched $A\beta_{1-42}$-treated group. N=3 (155v2 iAstrocytes).

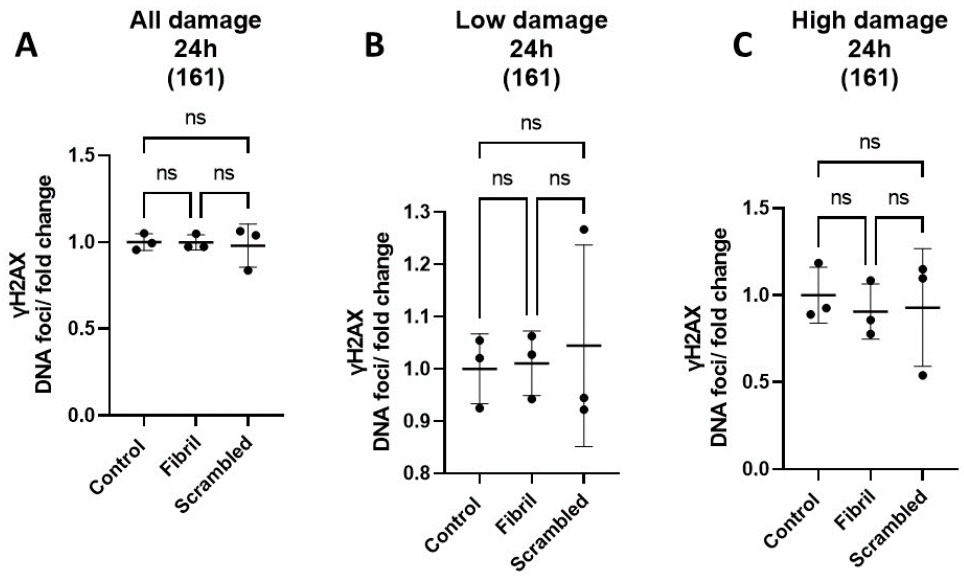


**Figure 3.71.** Formation of DNA damage indicative γH2AX-positive foci in 161 iAstrocytes as a response to 24 hour $A\beta_{1-42}$ fibril treatment.

The quantification of DNA damage based on the number of γH2AX positive DNA foci in 161 human induced astrocytes (iAstrocytes), as a response to $A\beta_{1-42}$ fibril treatment for 24h. Analysis was carried out using the Harmony Analysis Software (PerkinElmer). Graphs showing: **(A)** All damage detected; **(B)** Low damage detected (between 3-10 foci/ nucleus); **(C)** High damage detected (>10 foci/ nucleus). Data is presented as a fold change value of foci-positive nuclei to all nuclei detected. Standard error bars represent mean±SD. One-way ANOVA with Bonferroni's post-hoc test for multiple comparisons of pre-selected groups. Groups for statistical analysis: Control vs all treatment groups; and scrambled control group vs time-matched $A\beta_{1-42}$-treated group. N=3 (161 iAstrocytes).

Next, cell morphology changes were investigated in iAstrocytes (mean cytoplasm region, mean cell area, mean cell roundness, mean cell width, mean cell length). There were no changes to the cell morphology when iAstrocytes were pooled together (fig.3.72). Likewise, there were no changes to morphology of CS14 iAstrocytes (fig.3.73) and 155v2 iAstrocytes (fig.3.74).

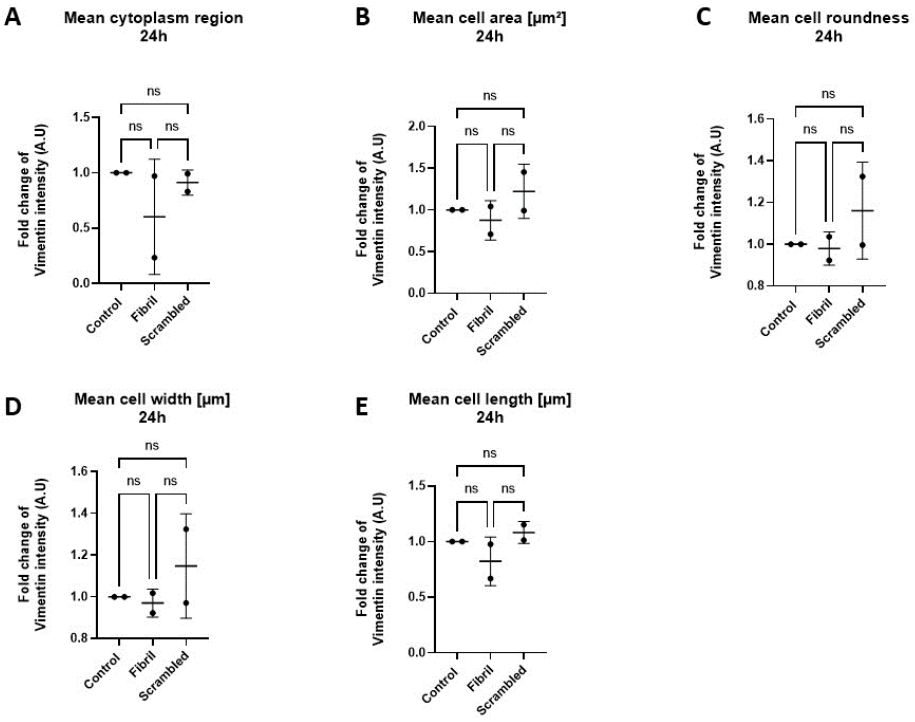


**Figure 3.72.** Cell morphology changes in iAstrocytes as a response to 24 hour $A\beta_{1-42}$ fibril treatment.

The quantification of vimentin intensity in human induced astrocytes (iAstrocytes), indicative of cell morphology changes, as a response to $A\beta_{1-42}$ fibril treatment for 24 hour. Analysis was carried out using the Harmony Analysis Software (PerkinElmer). Graphs showing changes in **(A)** mean cytoplasm region; **(B)** mean cell area; **(C)** mean cell roundness; **(D)** mean cell width; **(E)** mean cell length. Data is presented as a fold change value vimentin intensity, normalised to untreated control. Standard error bars represent mean±SD. One-way ANOVA with Bonferroni's post-hoc test for multiple comparisons of pre-selected groups. Groups for statistical analysis: Control vs all treatment groups; and scrambled control group vs time-matched $A\beta_{1-42}$-treated group. N=2 (iAstrocytes pooled)

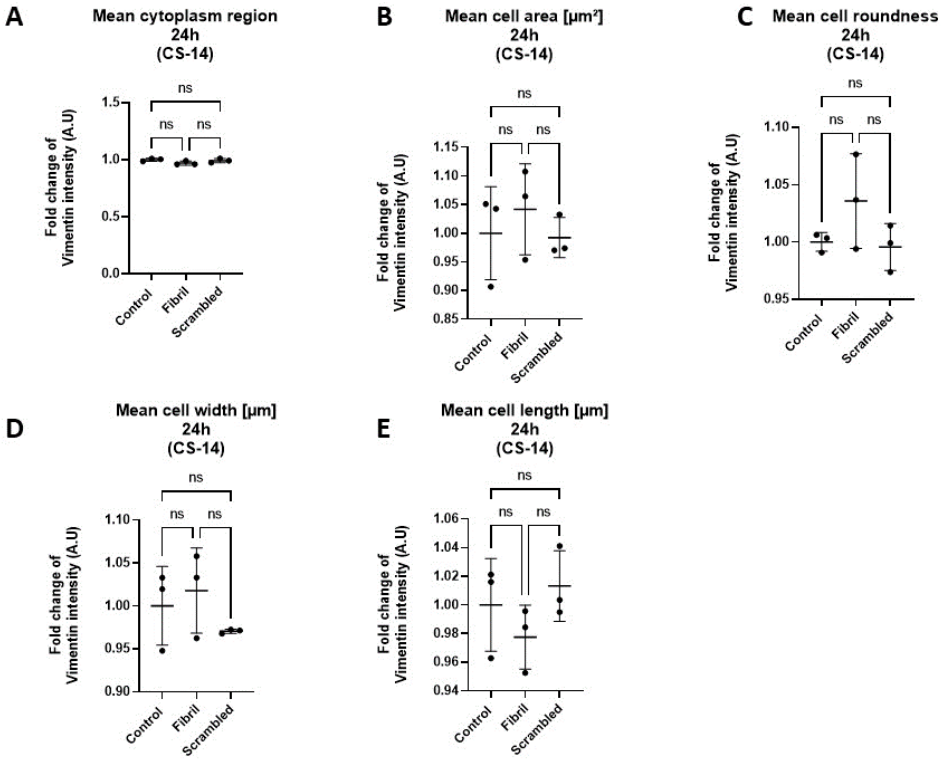


**Figure 3.73.** Cell morphology changes in CS14 iAstrocytes as a response to 24 hour $A\beta_{1-42}$ fibril treatment.

The quantification of vimentin intensity in CS14 human induced astrocytes (iAstrocytes), indicative of cell morphology changes, as a response to $A\beta_{1-42}$ fibril treatment for 24 hour. Analysis was carried out using the Harmony Analysis Software (PerkinElmer). Graphs showing changes in **(A)** mean cytoplasm region; **(B)** mean cell area; **(C)** mean cell roundness; **(D)** mean cell width; **(E)** mean cell length. Data is presented as a fold change value vimentin intensity, normalised to untreated control. Standard error bars represent mean±SD. One-way ANOVA with Bonferroni's post-hoc test for multiple comparisons of pre-selected groups. Groups for statistical analysis: Control vs all treatment groups; and scrambled control group vs time-matched $A\beta_{1-42}$-treated group. N=3 (CS14 iAstrocytes)

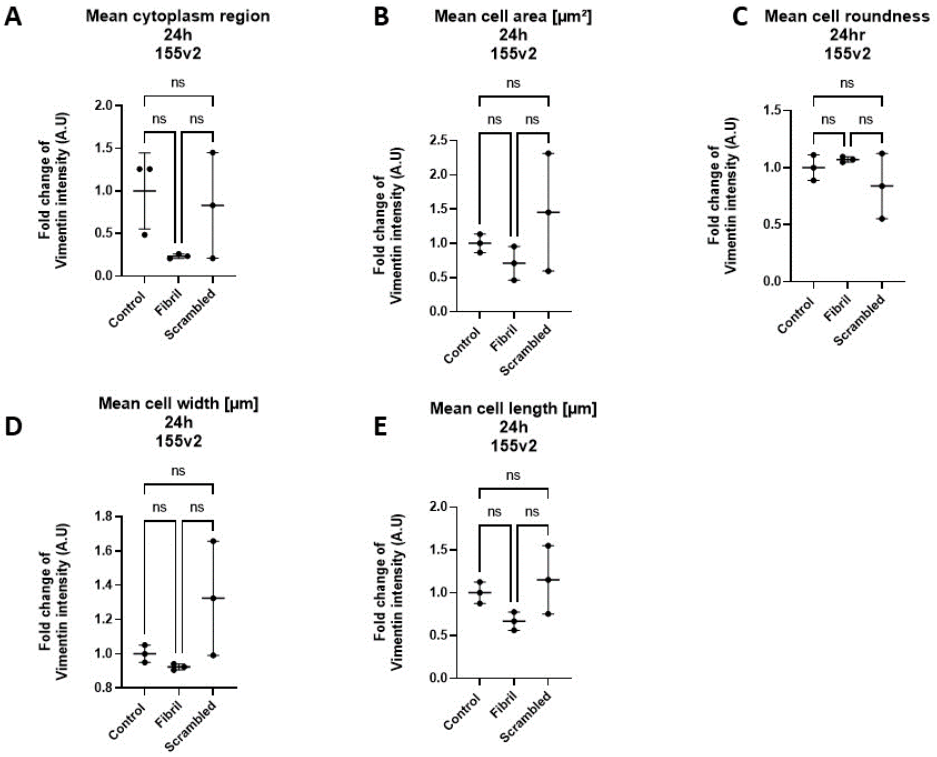


**Figure 3.74.** Cell morphology changes in 155v2 iAstrocytes as a response to 24 hour $A\beta_{1-42}$ fibril treatment.

The quantification of vimentin intensity in 155v2 human induced astrocytes (iAstrocytes), indicative of cell morphology changes, as a response to $A\beta_{1-42}$ fibril treatment for 24 hour. Analysis was carried out using the Harmony Analysis Software (PerkinElmer). Graphs showing changes in **(A)** mean cytoplasm region; **(B)** mean cell area; **(C)** mean cell roundness; **(D)** mean cell width; **(E)** mean cell length. Data is presented as a fold change value vimentin intensity, normalised to untreated control. Standard error bars represent mean±SD. One-way ANOVA with Bonferroni's post-hoc test for multiple comparisons of pre-selected groups. Groups for statistical analysis: Control vs all treatment groups; and scrambled control group vs time-matched $A\beta_{1-42}$-treated group. N=3 (155v2 iAstrocytes)

Next, DNA damage changes and cell morphology changes were investigated in iAstrocytes treated with amyloid beta fibrils for 48 hours (fig. 3.75).

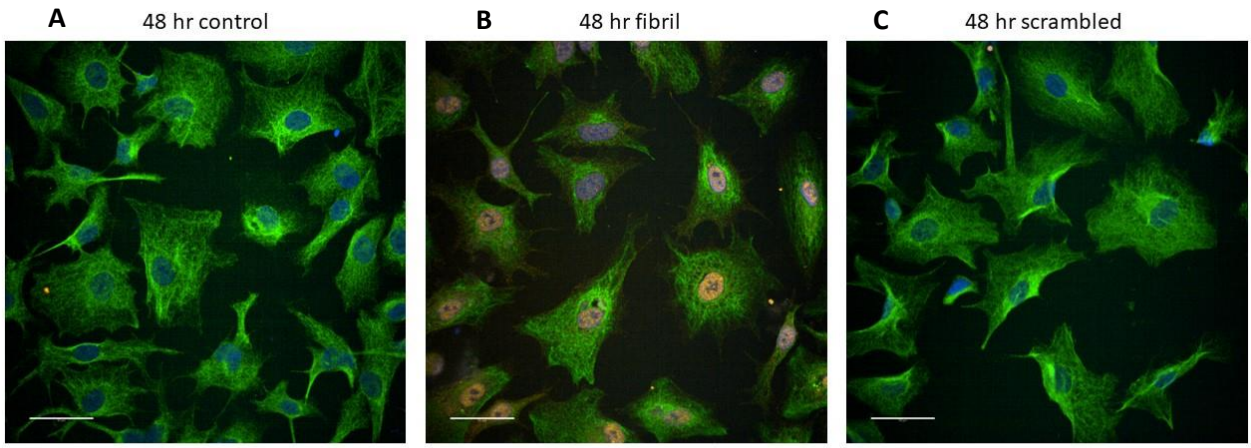


**Figure 3.75.** Representative immunocytochemistry images detecting changes to induced astrocyte (iAstrocyte) morphology and formation of DNA damage γH2AX foci as a response to 48 hour treatment with amyloid beta fibrils.

Immunocytochemistry images detecting induced Astrocyte (iAstrocyte) morphology with astrocyte marker vimentin (green), and γH2AX-positive DNA foci detected with γH2AX antibody (red). The nuclei are stained with Hoescht (blue). iAstrocytes treated for 48h with **(A)** untreated (control); **(B)** 1 µM fibrillary Aβ1-42; **(C)** 1 µM scrambled Aβ peptide as vehicle control. Representative images of n=3. Imaged on the Opera Phenix High Content Imaging System (PerkinElmer). Scale bars = 50 µm.

When all iAstrocyte cell lines were pooled, there were overall no significant difference in DNA damage (all damage detected), as well as low damage parameter. However, for the high damage parameter, there was a significant increase in the DNA damage detected in the fibril-treated group. There was also a significant decrease in DNA damage detected for the scrambled peptide control (high damage detected), which could indicate a technical issue or an issue with the vehicle control (fig.3.76).

When the cell lines were separated for analysis, there was no significant difference in the DNA damage changes for CS14 iAstrocytes (fig.3.77), 155v2 iAstrocytes (fig.3.78), and 161 iAstrocytes (fig.3.79).

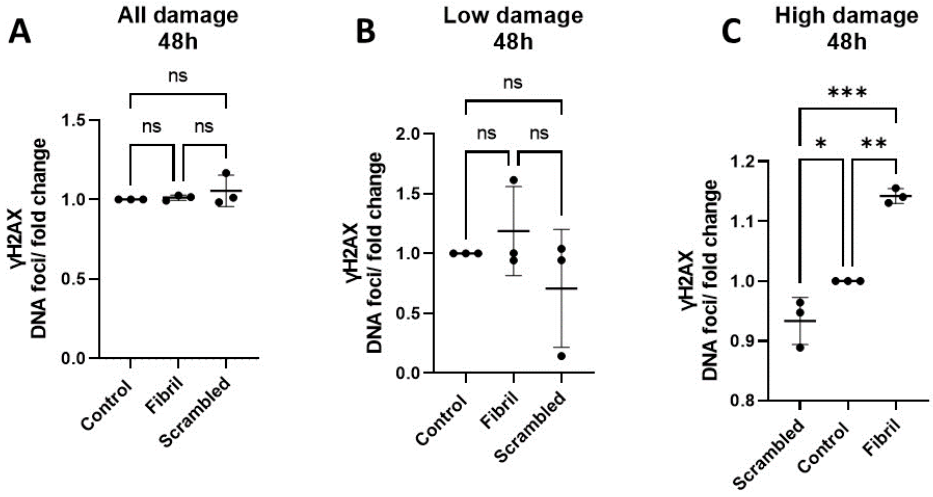


**Figure 3.76.** Formation of DNA damage indicative γH2AX-positive foci in iAstrocytes as a response to 48 hour $A\beta_{1-42}$ fibril treatment.

The quantification of DNA damage based on the number of γH2AX positive DNA foci in human induced astrocytes (iAstrocytes), as a response to $A\beta_{1-42}$ fibril treatment for 48 h. Analysis was carried out using the Harmony Analysis Software (PerkinElmer). Graphs showing: **(A)** All damage detected; **(B)** Low damage detected (between 3-10 foci/ nucleus); **(C)** High damage detected (>10 foci/ nucleus). Data is presented as a fold change value of foci-positive nuclei to all nuclei detected. Standard error bars represent mean±SD. One-way ANOVA with Bonferroni's post-hoc test for multiple comparisons of pre-selected groups. Groups for statistical analysis: Control vs all treatment groups; and scrambled control group vs time-matched $A\beta_{1-42}$-treated group. N=3 (iAstrocytes pooled).

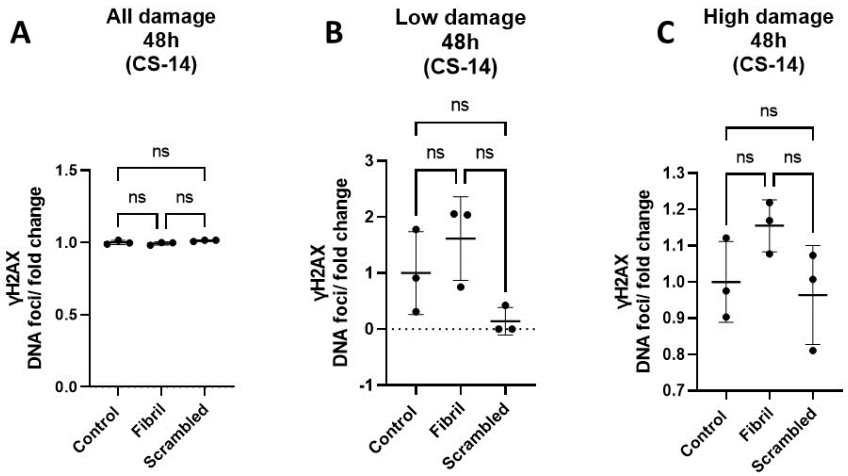


**Figure 3.77.** Formation of DNA damage indicative γH2AX-positive foci in CS14 iAstrocytes as a response to 48 hour $A\beta_{1-42}$ fibril treatment.

The quantification of DNA damage based on the number of γH2AX positive DNA foci in CS14 human induced astrocytes (iAstrocytes), as a response to $A\beta_{1-42}$ fibril treatment for 48 h. Analysis was carried out using the Harmony Analysis Software (PerkinElmer). Graphs showing: **(A)** All damage detected; **(B)** Low damage detected (between 3-10 foci/ nucleus); **(C)** High damage detected (>10 foci/ nucleus). Data is presented as a fold change value of foci-positive nuclei to all nuclei detected. Standard error bars represent mean±SD. One-way ANOVA with Bonferroni's post-hoc test for multiple comparisons of pre-selected groups. Groups for statistical analysis: Control vs all treatment groups; and scrambled control group vs time-matched $A\beta_{1-42}$-treated group. N=3 (CS14 iAstrocytes).

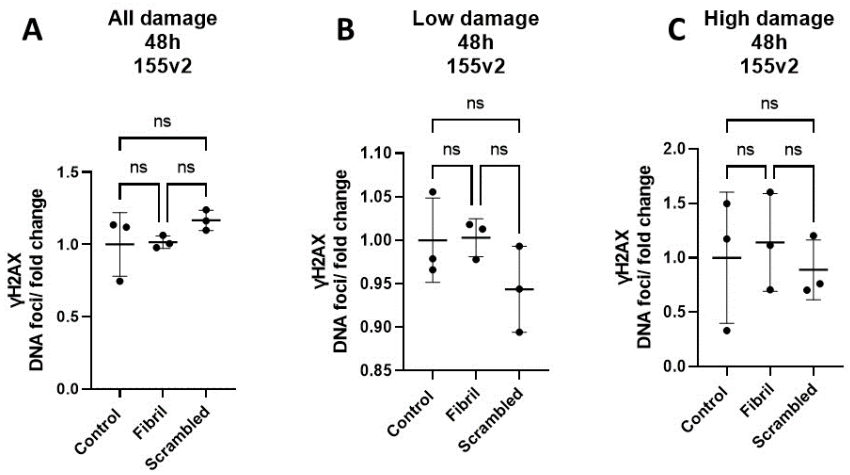


**Figure 3.78.** Formation of DNA damage indicative γH2AX-positive foci in 155v2 iAstrocytes as a response to 48 hour $A\beta_{1-42}$ fibril treatment.

The quantification of DNA damage based on the number of γH2AX positive DNA foci in 155v2 human induced astrocytes (iAstrocytes), as a response to $A\beta_{1-42}$ fibril treatment for 48 h. Analysis was carried out using the Harmony Analysis Software (PerkinElmer). Graphs showing: **(A)** All damage detected; **(B)** Low damage detected (between 3-10 foci/ nucleus); **(C)** High damage detected (>10 foci/ nucleus). Data is presented as a fold change value of foci-positive nuclei to all nuclei detected. Standard error bars represent mean±SD. One-way ANOVA with Bonferroni's post-hoc test for multiple comparisons of pre-selected groups. Groups for statistical analysis: Control vs all treatment groups; and scrambled control group vs time-matched $A\beta_{1-42}$-treated group. N=3 (155v2 iAstrocytes).

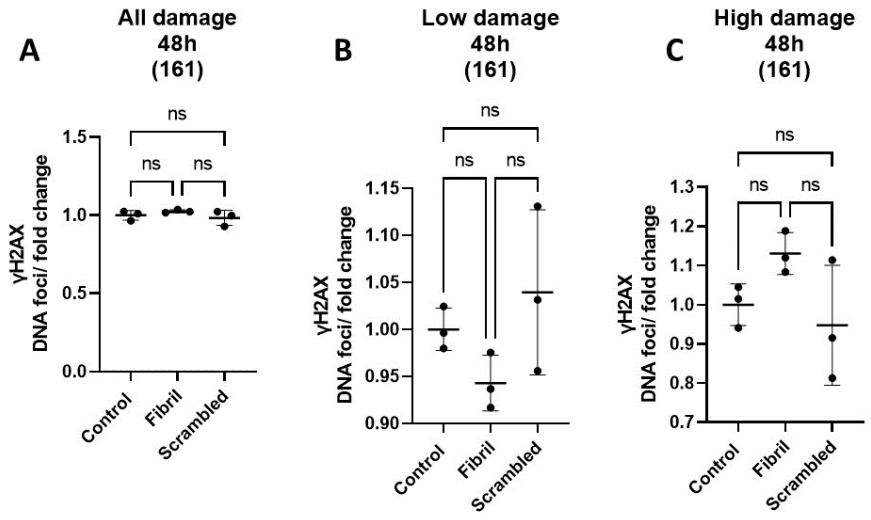


**Figure 3.79.** Formation of DNA damage indicative γH2AX-positive foci in 161 iAstrocytes as a response to 48 hour $A\beta_{1-42}$ fibril treatment.

The quantification of DNA damage based on the number of γH2AX positive DNA foci in 161 human induced astrocytes (iAstrocytes), as a response to $A\beta_{1-42}$ fibril treatment for 48h. Analysis was carried out using the Harmony Analysis Software (PerkinElmer). Graphs showing: **(A)** All damage detected; **(B)** Low damage detected (between 3-10 foci/ nucleus); **(C)** High damage detected (>10 foci/ nucleus). Data is presented as a fold change value of foci-positive nuclei to all nuclei detected. Standard error bars represent mean±SD. One-way ANOVA with Bonferroni's post-hoc test for multiple comparisons of pre-selected groups. Groups for statistical analysis: Control vs all treatment groups; and scrambled control group vs time-matched $A\beta_{1-42}$-treated group. N=3 (161 iAstrocytes).

Next, cell morphology changes (mean cytoplasm region, mean cell area, mean cell roundness, mean cell width, mean cell length) were investigated in iAstrocytes as a response to 48h fibril treatment. When all cell lines were pooled, there were no significant changes in cell morphology parameters (fig.3.80). When cell lines were separated for analysis, there were no significant differences in cell morphology parameters of mean cytoplasm region, mean cell area, mean cell width, and mean cell length for CS14 iAstrocytes. However, for CS14 iAstrocytes, there was a significant increase in the mean cell roundness for the fibril-treated group (fig.3.81). Meanwhile, for 155v2 iAstrocytes, there were no significant differences in the cell morphology parameters (fig.3.82).

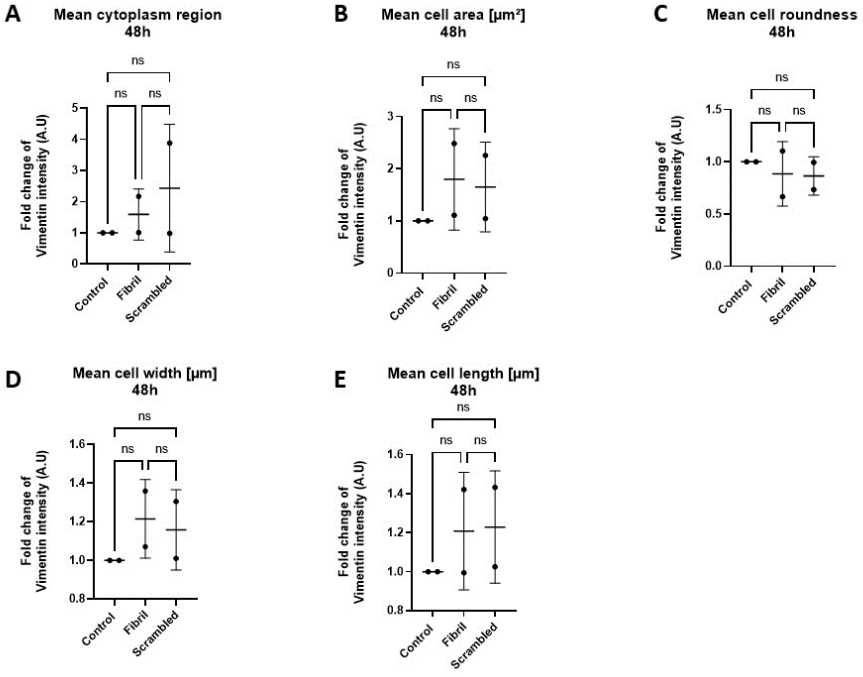


**Figure 3.80.** Cell morphology changes in iAstrocytes as a response to 48 hour $A\beta_{1-42}$ fibril treatment.

The quantification of vimentin intensity in human induced astrocytes (iAstrocytes), indicative of cell morphology changes, as a respons e to $A\beta_{1-42}$ fibril treatment for 48 hour. Analysis was carried out using the Harmony Analysis Software (PerkinElmer). Graphs showing changes in **(A)** mean cytoplasm region; **(B)** mean cell area; **(C)** mean cell roundness; **(D)** mean cell width; **(E)** mean cell length. Data is presented as a fold change value vimentin intensity, normalised to untreated control. Standard error bars represent mean±SD. One-way ANOVA with Bonferroni's post-hoc test for multiple comparisons of pre-selected groups. Groups for statistical analysis: Control vs all treatment groups; and scrambled control group vs time-matched $A\beta_{1-42}$-treated group. N=2 (iAstrocytes pooled)

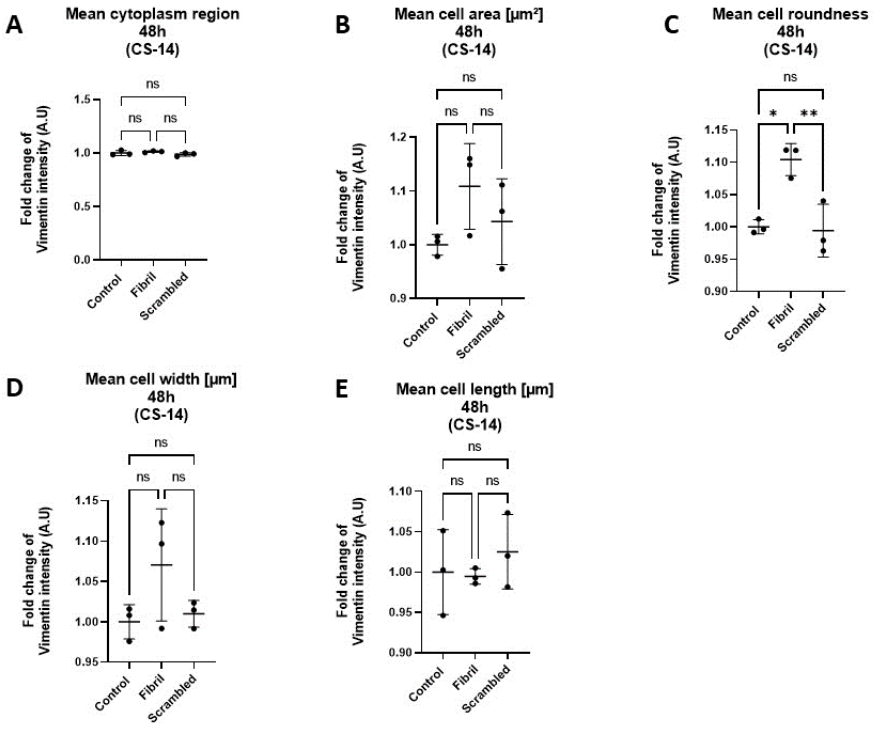


**Figure 3.81.** Cell morphology changes in CS14 iAstrocytes as a response to 48 hour $A\beta_{1-42}$ fibril treatment.

The quantification of vimentin intensity in CS14 human induced astrocytes (iAstrocytes), indicative of cell morphology changes, as a response to $A\beta_{1-42}$ fibril treatment for 48 hour. Analysis was carried out using the Harmony Analysis Software (PerkinElmer). Graphs showing changes in **(A)** mean cytoplasm region; **(B)** mean cell area; **(C)** mean cell roundness; **(D)** mean cell width; **(E)** mean cell length. Data is presented as a fold change value vimentin intensity, normalised to untreated control. Standard error bars represent mean±SD. One-way ANOVA with Bonferroni's post-hoc test for multiple comparisons of pre-selected groups. Groups for statistical analysis: Control vs all treatment groups; and scrambled control group vs time-matched $A\beta_{1-42}$-treated group. N=3 (CS14 iAstrocytes)

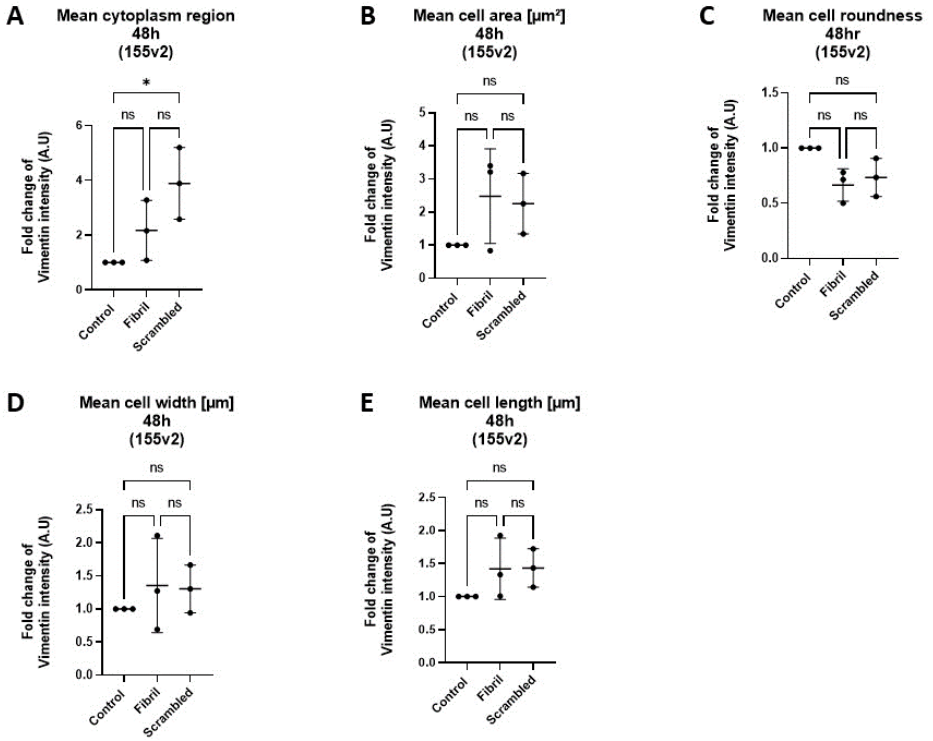


**Figure 3.82.** Cell morphology changes in 155v2 iAstrocytes as a response to 48 hour $A\beta_{1-42}$ fibril treatment.

The quantification of vimentin intensity in 155v2 human induced astrocytes (iAstrocytes), indicative of cell morphology changes, as a response to $A\beta_{1-42}$ fibril treatment for 48 hour. Analysis was carried out using the Harmony Analysis Software (PerkinElmer). Graphs showing changes in **(A)** mean cytoplasm region; **(B)** mean cell area; **(C)** mean cell roundness; **(D)** mean cell width; **(E)** mean cell length. Data is presented as a fold change value vimentin intensity, normalised to untreated control. Standard error bars represent mean±SD. One-way ANOVA with Bonferroni's post-hoc test for multiple comparisons of pre-selected groups. Groups for statistical analysis: Control vs all treatment groups; and scrambled control group vs time-matched $A\beta_{1-42}$-treated group. N=3 (155v2 iAstrocytes)

Lastly, the DNA damage changes, and cell morphology changes were investigated in iAstrocytes as a response to a repeated stress (fig.3.83). As described above in the oligomer treatment, the repeated stress treatment refers to treating iAstrocytes repeatedly over the period of 48 hours.

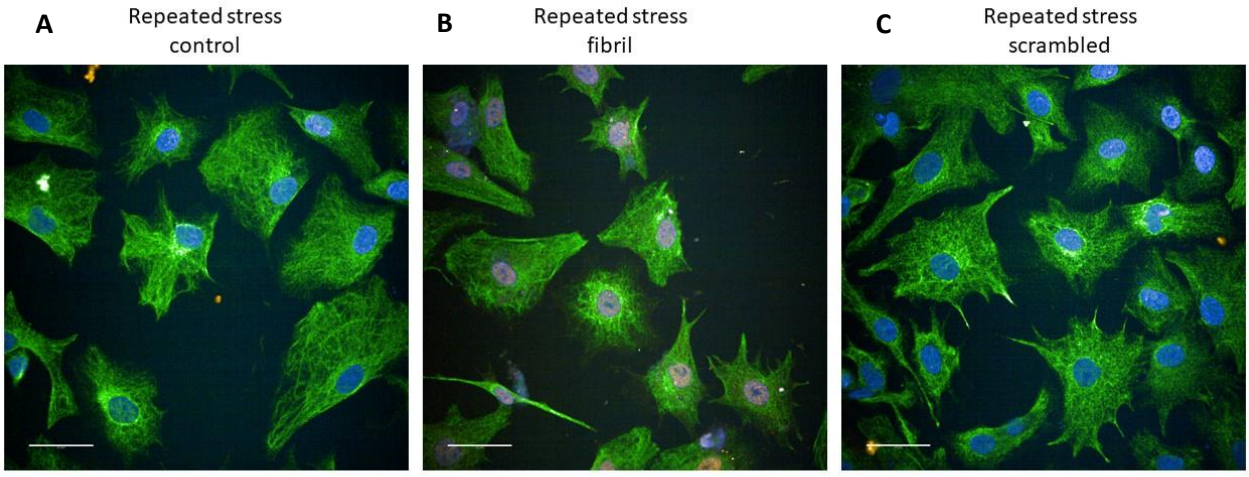


**Figure 3.83.** Representative immunocytochemistry images detecting changes to induced astrocyte (iAstrocyte) morphology and formation of DNA damage γH2AX foci as a response to repeated stress treatment with amyloid beta fibrils.

Immunocytochemistry images detecting induced Astrocyte (iAstrocyte) morphology with astrocyte marker vimentin (green), and γH2AX-positive DNA foci detected with γH2AX antibody (red). The nuclei are stained with Hoescht (blue). iAstrocytes treated for repeated stress with **(A)** untreated (control); **(B)** 1 µM fibrillary Aβ1-42; **(C)** 1 µM scrambled Aβ peptide as vehicle control. Representative images of n=3. Imaged on the Opera Phenix High Content Imaging System (PerkinElmer). Scale bars = 50 µm.

When looking at the DNA damage, the results showed that there was no change when iAstrocyte cell lines were pooled together (fig.3.84). When iAstrocyte cell lines were separated for analysis, interestingly, there was a significant decrease in DNA damage for fibril-treated CS14 iAstrocytes (fig.3.85). For 161 iAstrocytes, there was no significant difference in DNA damage changes (fig.3.86). Likewise, there was no significant difference in DNA damage changes for 155v2 iAstrocytes (fig.3.87).

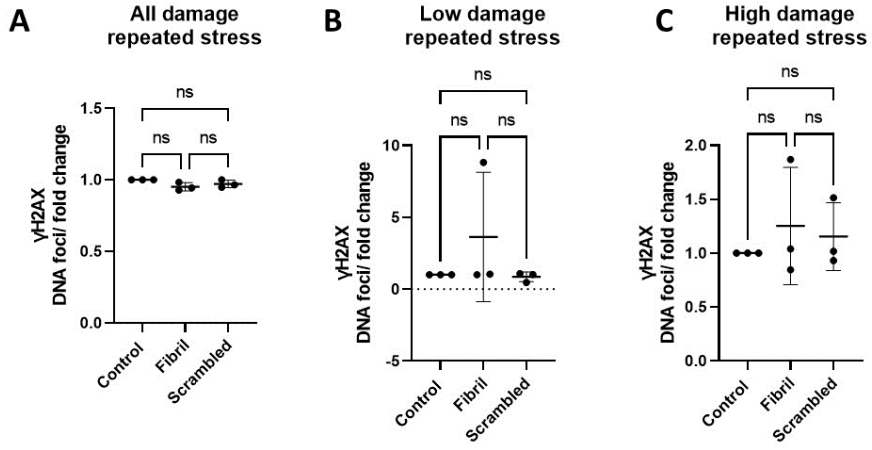


**Figure 3.84.** Formation of DNA damage indicative γH2AX-positive foci in iAstrocytes as a response to repeated stress $A\beta_{1-42}$ fibril treatment.

The quantification of DNA damage based on the number of γH2AX positive DNA foci in human induced astrocytes (iAstrocytes), as a response to $A\beta_{1-42}$ fibril treatment for repeated stress. Analysis was carried out using the Harmony Analysis Software (PerkinElmer). Graphs showing: **(A)** All damage detected; **(B)** Low damage detected (between 3-10 foci/ nucleus); **(C)** High damage detected (>10 foci/ nucleus). Data is presented as a fold change value of foci-positive nuclei to all nuclei detected. Standard error bars represent mean±SD. One-way ANOVA with Bonferroni's post-hoc test for multiple comparisons of pre-selected groups. Groups for statistical analysis: Control vs all treatment groups; and scrambled control group vs time-matched $A\beta_{1-42}$-treated group. N=3 (iAstrocytes pooled).

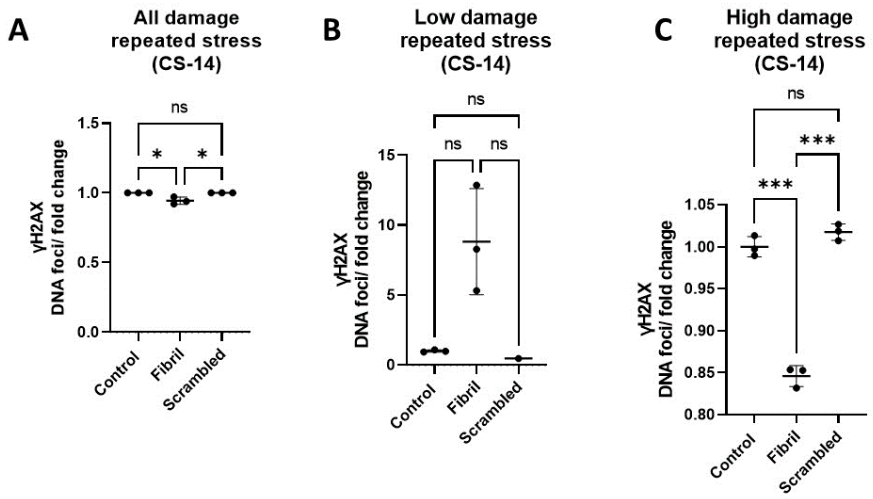


**Figure 3.85.** Formation of DNA damage indicative γH2AX-positive foci in CS14 iAstrocytes as a response to repeated stress $A\beta_{1-42}$ fibril treatment.

The quantification of DNA damage based on the number of γH2AX positive DNA foci in CS14 human induced astrocytes (iAstrocytes), as a response to $A\beta_{1-42}$ fibril treatment for repeated stress. Analysis was carried out using the Harmony Analysis Software (PerkinElmer). Graphs showing: **(A)** All damage detected; **(B)** Low damage detected (between 3-10 foci/ nucleus); **(C)** High damage detected (>10 foci/ nucleus). Data is presented as a fold change value of foci-positive nuclei to all nuclei detected. Standard error bars represent mean±SD. One-way ANOVA with Bonferroni's post-hoc test for multiple comparisons of pre-selected groups. Groups for statistical analysis: Control vs all treatment groups; and scrambled control group vs time-matched $A\beta_{1-42}$-treated group. N=3 (CS14 iAstrocytes).

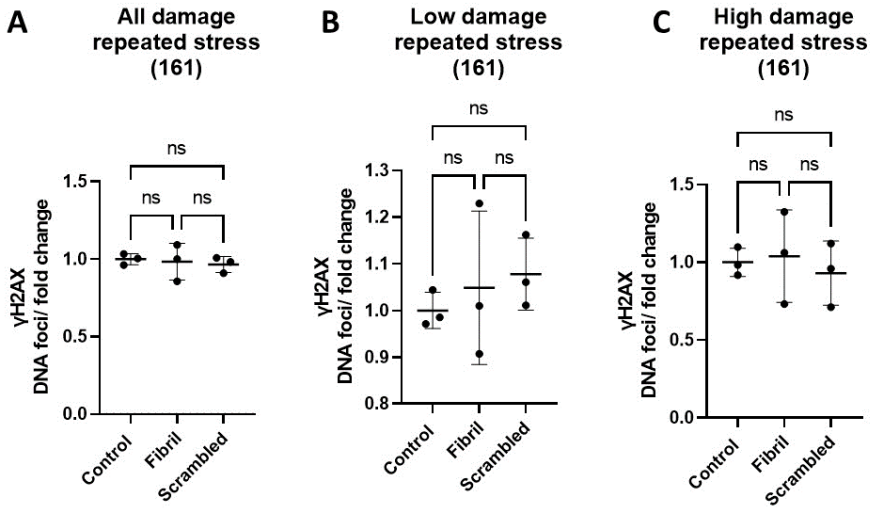


**Figure 3.86.** Formation of DNA damage indicative γH2AX-positive foci in 161 iAstrocytes as a response to repeated stress $A\beta_{1-42}$ fibril treatment.

The quantification of DNA damage based on the number of γH2AX positive DNA foci in 161 human induced astrocytes (iAstrocytes), as a response to $A\beta_{1-42}$ fibril treatment for repeated stress. Analysis was carried out using the Harmony Analysis Software (PerkinElmer). Graphs showing: **(A)** All damage detected; **(B)** Low damage detected (between 3-10 foci/ nucleus); **(C)** High damage detected (>10 foci/ nucleus). Data is presented as a fold change value of foci-positive nuclei to all nuclei detected. Standard error bars represent mean±SD. One-way ANOVA with Bonferroni's post-hoc test for multiple comparisons of pre-selected groups. Groups for statistical analysis: Control vs all treatment groups; and scrambled control group vs time-matched $A\beta_{1-42}$-treated group. N=3 (161 iAstrocytes).

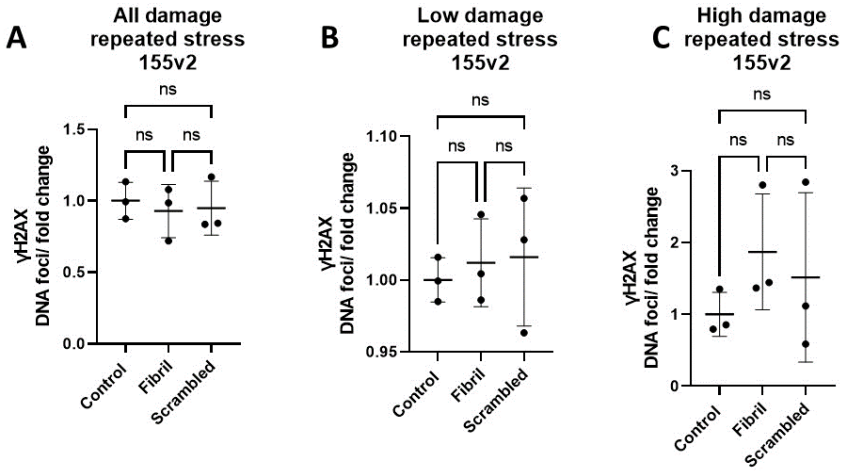


**Figure 3.87.** Formation of DNA damage indicative γH2AX-positive foci in 155v2 iAstrocytes as a response to repeated stress $A\beta_{1-42}$ fibril treatment.

The quantification of DNA damage based on the number of γH2AX positive DNA foci in 155v2 human induced astrocytes (iAstrocytes), as a response to $A\beta_{1-42}$ fibril treatment for repeated stress. Analysis was carried out using the Harmony Analysis Software (PerkinElmer). Graphs showing: **(A)** All damage detected; **(B)** Low damage detected (between 3-10 foci/ nucleus); **(C)** High damage detected (>10 foci/ nucleus). Data is presented as a fold change value of foci-positive nuclei to all nuclei detected. Standard error bars represent mean±SD. One-way ANOVA with Bonferroni's post-hoc test for multiple comparisons of pre-selected groups. Groups for statistical analysis: Control vs all treatment groups; and scrambled control group vs time-matched $A\beta_{1-42}$-treated group. N=3 (155v2 iAstrocytes).

Lastly, the cell morphology changes (mean cytoplasm region, mean cell area, mean cell roundness, mean cell width, mean cell length) in iAstrocytes were investigated, as a response to repeated stress. When iAstrocyte cell lines were pooled together for analysis, there were no significant differences in the cell morphology parameters (fig.3.88). When iAstrocyte cell lines were separated by cell line, the CS14 iAstrocytes showed no changes in cell morphology after repeated stress (fig.3.89). For 155v2 iAstrocytes, there were no significant changes in cell morphology for any parameters except cell width. In 155v2 iAstrocytes, the mean cell width increased in fibril-treated group when compared to both untreated and vehicle controls (fig.3.90).

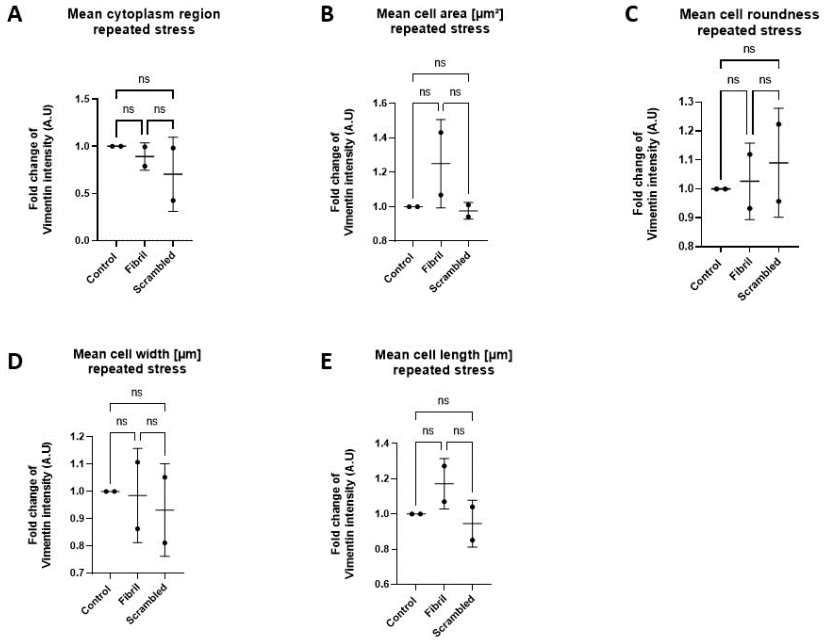


**Figure 3.88.** Cell morphology changes in iAstrocytes as a response to repeated stress $A\beta_{1-42}$ fibril treatment.

The quantification of vimentin intensity in human induced astrocytes (iAstrocytes), indicative of cell morphology changes, as a response to $A\beta_{1-42}$ fibril treatment for repeated stress. Analysis was carried out using the Harmony Analysis Software (PerkinElmer). Graphs showing changes in **(A)** mean cytoplasm region; **(B)** mean cell area; **(C)** mean cell roundness; **(D)** mean cell width; **(E)** mean cell length. Data is presented as a fold change value vimentin intensity, normalised to untreated control. Standard error bars represent mean±SD. One-way ANOVA with Bonferroni's post-hoc test for multiple comparisons of pre-selected groups. Groups for statistical analysis: Control vs all treatment groups; and scrambled control group vs time-matched $A\beta_{1-42}$-treated group. N=2 (iAstrocytes pooled)

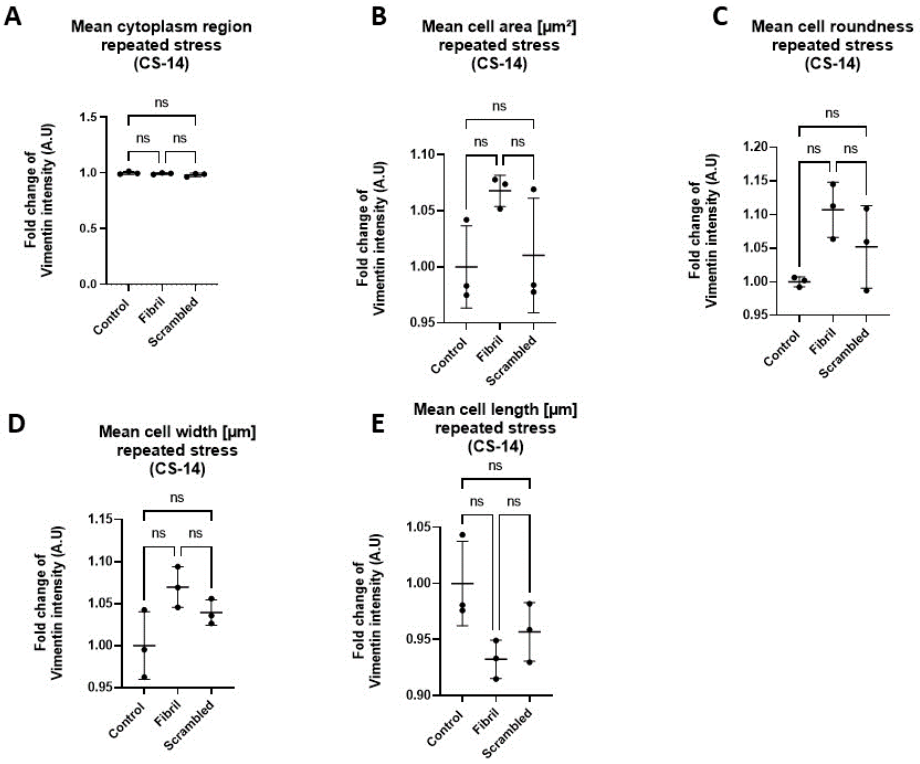


**Figure 3.89.** Cell morphology changes in CS14 iAstrocytes as a response to repeated stress $A\beta_{1-42}$ fibril treatment.

The quantification of vimentin intensity in CS14 human induced astrocytes (iAstrocytes), indicative of cell morphology changes, as a response to $A\beta_{1-42}$ fibril treatment for repeated stress. Analysis was carried out using the Harmony Analysis Software (PerkinElmer). Graphs showing changes in **(A)** mean cytoplasm region; **(B)** mean cell area; **(C)** mean cell roundness; **(D)** mean cell width; **(E)** mean cell length. Data is presented as a fold change value vimentin intensity, normalised to untreated control. Standard error bars represent mean±SD. One-way ANOVA with Bonferroni's post-hoc test for multiple comparisons of pre-selected groups. Groups for statistical analysis: Control vs all treatment groups; and scrambled control group vs time-matched $A\beta_{1-42}$-treated group. N=3 (CS14 iAstrocytes)

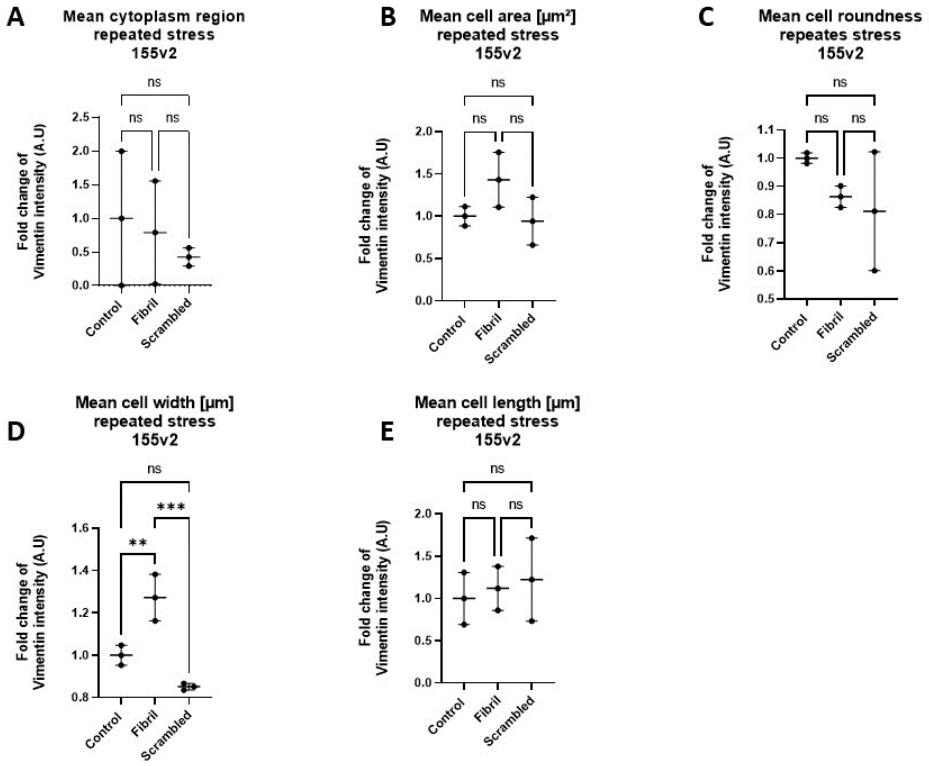


**Figure 3.90.** Cell morphology changes in 155v2 iAstrocytes as a response to repeated stress $A\beta_{1-42}$ fibril treatment.

The quantification of vimentin intensity in 155v2 human induced astrocytes (iAstrocytes), indicative of cell morphology changes, as a response to $A\beta_{1-42}$ fibril treatment for repeated stress. Analysis was carried out using the Harmony Analysis Software (PerkinElmer). Graphs showing changes in **(A)** mean cytoplasm region; **(B)** mean cell area; **(C)** mean cell roundness; **(D)** mean cell width; **(E)** mean cell length. Data is presented as a fold change value vimentin intensity, normalised to untreated control. Standard error bars represent mean±SD. One-way ANOVA with Bonferroni's post-hoc test for multiple comparisons of pre-selected groups. Groups for statistical analysis: Control vs all treatment groups; and scrambled control group vs time-matched $A\beta_{1-42}$-treated group. N=3 (155v2 iAstrocytes)

## 3.6 Discussion

The results showed that oxidative stress induced significant increase in cell death of human fetal astrocytes after 24 hours of treatment. Oxidative stress induced a rapid DNA damage response in human fetal astrocytes (1 hr). This damage was detectable using DNA damage response markers specific to double stranded DNA breaks, which are the more harmful type of DNA damage in cells. Furthermore, this DNA damage response can be characterised by the formation and detection of γH2AX-positive DNA foci, and this was detected in human fetal astrocytes 1 hour post-treatment with 100 µM $H_2O_2$. Acute oxidative stress did not induce the formation of γH2AX-positive DNA foci in iAstrocytes after 1 hour of $H_2O_2$ treatment. However, when results were separated based on specific cell lines, there was an increase in the number of γH2AX-positive DNA foci. As iAstrocytes are reprogrammed from individual donors, these results could suggest that there may be a heterogenic response of astrocytes to oxidative stress between different individuals. This heterogeneity of astrocytic responses could be an interesting avenue to explore from the point of personalised medicine and patient stratification approaches.

In comparison, the highest physiological concentration of $A\beta_{1-42}$ oligomers or fibrils did not cause any significant DNA damage response (detected by the formation of γH2AX-positive DNA foci) in fetal astrocytes or in iAstrocytes (cell lines pooled together). However, when separated by the cell line, it was clear that iAstrocytes could react in a varying way to $A\beta_{1-42}$ oligomers or fibrils. For example, one cell line could be more susceptible to damage from oligomers, whereas other cell line could be more susceptible to the damage of fibrils. This speculative idea is an interesting avenue to explore in the future. Furthermore, there were no detectable changes in cell morphology in fetal astrocytes or iAstrocytes when treated with either species of Aβ aggregates. The results suggest that astrocytes can elicit a differential response to different disease stressors, further confirming the idea of astrocyte heterogeneity.

### Effects of oxidative stress on astrocytes

Oxidative stress is the result of excess ROS, deficiency in antioxidants, or both. The imbalance between ROS and antioxidants in favour of ROS production can lead to an increase in oxidative stress (Ray, Huang and Tsuji, 2012). ROS, also called free radicals, have been reported to be involved in the processes of ageing, as well as in age-related diseases such as Alzheimer's disease (Ray, Huang and Tsuji, 2012; Ionescu-Tucker and Cotman, 2021). Due to its high energy demands, the brain is highly susceptible to the effects of oxidative stress. This is especially prominent in neurons, as these are non-dividing cells that cannot be replaced. If neurons encounter significant oxidative stress damage, this could lead to significant adverse effects later on (Ionescu-Tucker and Cotman, 2021).

Hydrogen peroxide ($H_2O_2$) is a potent inducer of oxidative stress and could be implicated in Alzheimer's disease. Aβ peptide could induce damage via oxidative stress due to the production of $H_2O_2$. Indeed, Aβ has been found to generate $H_2O_2$ early during the aggregation stages, whilst mature fibrils do not generate $H_2O_2$. Hence, $H_2O_2$ may be an important mediator in Alzheimer's disease progression (Tabner *et al.*, 2005). Furthermore, it has been shown *in vivo* that reactive astrocytes can activate autophagy pathways which mediate the production of $H_2O_2$, leading to downstream effects such as transcription changes, microglial activation and tauopathy. Such adverse effects can be prevented by potent $H_2O_2$ inhibitors (Chun *et al.*, 2020). $H_2O_2$ also has a potent neurotoxic effect, where neurons undergo cell death 24 hours after $H_2O_2$ exposure. However, co-culturing neurons with astrocytes reveals their protective roles against $H_2O_2$ mediated neurotoxicity (Desagher, Glowinski and Premont, 1996). This further shows that the interplay between astrocytes and $H_2O_2$ may play a crucial role in neurodegeneration and Alzheimer's disease pathology.

### *Fetal astrocyte viability as a response to oxidative stress*

The impact of oxidative stress on astrocyte viability and reactivity is not well defined, especially in human astrocytes, and in the wider contexts of neurodegenerative diseases (Oberheim *et al.*, 2009). Oxidative stress is proposed as a player contributing to the onset and progression of neurodegenerative diseases. Moreover, it is also a contributing factor relating to the processes of normal ageing. Indeed, oxidative damage might be one of the early events relating to Alzheimer's disease onset and pathology (Cheignon *et al.*, 2018).

LDH is amongst one of the assays available for the measurement of cell cytotoxicity. Other assays include trypan blue exclusion and 3-(4,5-dimethylthiazol-2-yl)-2,5-diphenyltetrazolium bromide (MTT) reduction assays (Kim *et al.*, 2009). It has previously been determined by our research group that significant toxicity is observed after 24 hours, at concentrations > 100µM (unpublished data). This previous work utilised MTT assays to measure cellular toxicity. Both trypan blue and LDH assays can effectively be used for measuring the damage to cell membranes, meanwhile an MTT assay is appropriate to measure mitochondrial-related damage activity in the cells. Both trypan blue exclusion and LDH assays are comparable measures, meanwhile MTT is quite different. The MTT assay is a sensitive and appropriate way of measuring changes in mitochondrial functional activity, however, may not be appropriate for measuring cytotoxicity directly. Therefore, an appropriate assay should be utilised based on the damage that is being investigated, as well as the cytotoxicity stimulus and target (Kim *et al.*, 2009). Hence, the LDH assay has been used to investigate the effects of oxidative stress on fetal astrocyte viability.

Astrocyte viability has been previously shown to decrease after treatment with 0.5 mM of $H_2O_2$ and this effect can be reduced via a treatment which aims to promote the activity of antioxidant enzymes (Bi *et al.*, 2008). Moreover, organotypic hippocampal slice cultures of astrocytes have been shown to be more vulnerable to oxidative stress than neurons, and that astrocytes exhibit oxidative stress damage first, and this could take place before a downstream onset of any neuronal damage. This toxicity can be attenuated by pre-treatment with antioxidants (Feeney *et al.*, 2008). Here, fetal astrocytes exhibit increased cell death 24 hours after treatment with $H_2O_2$ as measured by the LDH assay.

As a response to peroxides, astrocyte cell death can be mediated by Janus kinase (JAK) 2/ Signal transducer and activator of transcription 1 (STAT1) pathway. This pathway can also be activated via cytokines, such as interferon (INF)-γ and interleukin (IL)-6, suggesting mutual pathways being activated when cell damage occurs from inflammation and oxidative stress (Gorina *et al.*, 2005). The JAK/STAT pathway has been implicated in neuroinflammation and could play an important role in Alzheimer's disease progression. JAK/STAT pathway is suggested to be an important factor mediating the induction of astrocyte reactivity (Jain *et al.*, 2021). Moreover, disruptions in the JAK/STAT pathway can lead to disrupted glial and neuronal survival and have been implicated in Alzheimer's disease (Nicolas *et al.*, 2013). It would therefore be interesting to investigate the JAK/STAT pathway further in the context of oxidative stress and Alzheimer's disease. This could be carried out by investigating the expression of related proteins upon treatment with $H_2O_2$ for example by immunoblotting or immunocytochemistry. It would also be interesting to investigate whether such pathway is also activated in Alzheimer's disease. For example, by treating the astrocytes with amyloid beta peptide, or investigating the expression of the relevant proteins in post-mortem tissue for validation. These experiments would allow us to further characterise the mechanisms relating to astrocyte cell death and astrocyte DNA damage during periods of oxidative stress and in disease.

### *Oxidative stress induced DNA damage in astrocytes*

It has been previously reported that low, non-lethal doses of $H_2O_2$ (0.1-0.5 mmol/L) can cause single stranded DNA breaks, as well as double stranded DNA breaks (Driessens *et al.*, 2009; Ye *et al.*, 2016). However, these DNA breaks have been investigated in various cell types such as hepatocytes and thyroid cells (Olson, 1988; Driessens *et al.*, 2009). It is not known whether a similar effect of low $H_2O_2$ would be observed in astrocytes *in vitro*.

Here, supra-physiological (defined as >100 nM) (Sies, 2017) concentrations of $H_2O_2$ were used to induce oxidative stress in human fetal astrocytes. These astrocytes are commercially available and have been previously well-characterised for astrocyte-specific astrocyte markers (Ratcliffe *et al.*, 2018).

Treatment of human fetal astrocytes with 100 µM of $H_2O_2$ elicited a rapid DNA damage response, which was detected mainly by the upregulation of the serine 139-phosphorylated version of H2A histone family member X (γH2AX). γH2AX is a histone protein, which has been implicated in the DNA damage repair response, alongside DNA-dependent protein kinase (DNA-PK), ataxia telangiectasia mutated (ATM) and ATM-Rad3-related (ATR) proteins (Kuo and Yang, 2008). γH2AX has been shown to accumulate at the site of damage where double-stranded DNA breaks (DSBs) occur (Martinez *et al.*, 2016; Ye *et al.*, 2016). This is typically seen as a formation of nuclear DNA foci, which form quickly after the onset of DSBs (Kuo and Yang, 2008; Ye *et al.*, 2016). γH2AX is a 14 kDa protein, which is a part of nucleosome. Phosphorylation of γH2AX at Ser139 is known to be an important event in DNA damage response to double stranded DNA breaks and may have a role in cell signalling as well as precede apoptosis.

Here, a significant increase in γH2AX expression was observed 1 hr, 6 hrs and 24 hrs after treatment with $H_2O_2$, with the signal seeing a decrease after 6 hours of treatment. There was also an increase in the formation of γH2AX-positive DNA foci in human fetal astrocytes as a response to 1 hour treatment with $H_2O_2$. This indicated that $H_2O_2$ induces DSBs and DNA damage in astrocytes. It also indicated a rapid DNA damage response in fetal astrocytes, where the damage can be detected just after 1 hr post-stress. In contrast, iAstrocytes did not show any significant difference in the formation of γH2AX-positive DNA foci 1 hour post treatment with hydrogen peroxide. Interestingly, when the results for iAstrocytes were separated by cell line, there was a significant difference between the untreated and treated groups. iAstrocytes are derived by reprogramming and differentiating human skin fibroblasts into neural progenitor cells, and then later into iAstrocytes (Meyer *et al.*, 2014). They retain the ageing properties of their donors and can be a good direct representation of an ageing brain (Meyer *et al.*, 2014). They retain all the epigenetics and phenotype of ageing, and can express varying phenotypes, morphology, and responses to external stimuli. This is very comparable to what occurs in the brain of individual people and can model interindividual variation. Indeed, in this case, when the results were separated by cell line, there was a significant increase in the formation of γH2AX-positive DNA foci in iAstrocytes compared to untreated control groups, albeit at different amounts, potentially suggesting inter-individual variation in responses to oxidative stress. However, this would require more cell lines to verify, and the differential responses of iAstrocytes to external stimuli is beyond the scope of the current work.

To determine the subsequent downstream DDR events in human fetal astrocytes, the DSB DNA damage pathway was investigated. ATM is a part of the DNA damage response cell machinery and coordinates various responses in the cell life cycle (Bensimon, Aebersold and Shiloh, 2011). For example, ATM (as well as ATR signalling) can re-direct the cells into various events. Using different

signal transducers, the cell can be redirected into cell cycle checkpoints, DNA repair, or cell death. The ATM signalling pathway is activated via the phosphorylation of γH2AX, which detects the DNA damage, and the activation of this pathway also involved a cell cycle checkpoint protein and a transducer kinase known as Chk2 (Zannini, Delia and Buscemi, 2014). Upon damage, checkpoint kinase 2 (Chk2) is phosphorylated and activated by ATM. Phosphorylated Chk2 (pChk2) directs the cell further into either DNA repair, cell cycle arrest or apoptosis based on the cell cycle checkpoints (Zannini, Delia and Buscemi, 2014). This takes place when double stranded DNA breaks are detected. In the case of single stranded DNA breaks, ATR pathway and ATR is activated instead. This in turn phosphorylates checkpoint kinase 1 (Chk1), which again forces the cell to undergo cell cycle checkpoints (Smith *et al.*, 2010). In fetal astrocytes, the treatment with 100 µM of $H_2O_2$ increased the expression of pChk2 after 1 hour of treatment, whereas no change in pChk1 was detected (not shown). This further indicates that oxidative stress in fetal astrocytes causes DSBs rather than SSBs, and that this damage can be quickly recognised and dealt with by astrocytes.

Cellular senescence is associated with cell cycle arrest (Yosef *et al.*, 2017), and can be triggered by DNA damage. One of the universal markers of cell senescence and cell cycle arrest is expression of p21. Treatment of fetal astrocytes with $H_2O_2$ did not result in a significant increase in p21 at any time point. This suggests that the cells do not become senescent as a response to oxidative stress damage. This could potentially be due to the ability of younger astrocytes to cope with DNA damage effectively. p21 is a primary marker of cell senescence, specifically targeting cell cycle arrest and it is associated with the p53 pathway. Since neither p53 nor p21 were upregulated here, other traits and pathways could be investigated instead. For example, looking at cell cycle arrest more closely, with an upregulation of p16 or lack of Ki-67, as well as upregulation of SA-β-gal, SASP, and looking at morphology changes to the cells (González-Gualda *et al.*, 2021).

Cyclin dependent kinase 1 (CDK1), also related cdc2, is a key regulator of the cell cycle. Phosphorylation and dephosphorylation of cdc2 at Tyrosine 15 residue is a highly conserved mechanism in human cells. It plays a major role in controlling the cell cycle, particularly in cell cycle progression through the G2/M phase (Welburn *et al.*, 2007). Early studies of the cell cycle showed that dephosphorylation of the tyrosine 15 residue is a key step for cell progression into mitosis (Gould and Nurse, 1989; Atherton-Fessler *et al.*, 1994). The phosphorylation mechanism is controlled by the Wee1 and Mik1 proteins (Den Haese *et al.*, 1995). Mitotic checkpoint, cdc2, is phosphorylated when cell progression into mitosis is inhibited (Welburn *et al.*, 2007); here, $H_2O_2$ induced a significant increase in phosphorylated cdc2 at 1 and 6 hours, indicating cell cycle inhibition, and that the cell cycle progression is halted immediately after acute DNA damage response. However, after 24 hours, the levels of phosphorylated cdc2 decreased, and there was no significant difference between the level of

cdc2 expression at 24 hours and control (untreated). This could suggest that the cell cycle progression to mitosis was restored. This could potentially indicate that DNA damage was repaired after 24 hours, allowing astrocytes to progress into mitosis. Furthermore, this would support the notion that fetal (younger) astrocytes are well equipped to deal with DNA damage.

Overall, human fetal astrocytes respond rapidly to hydrogen peroxide-mediated oxidative stress. The DNA damage response indicates that the damage might be resolved quickly and that this process does not lead to cell senescence.

### *Oxidative stress and astrocyte reactivity*

The concept of astrocyte reactivity has been a topic of debate amongst researchers. The typical notion in the literature states that reactive astrocytes are a feature of injury and disease in the CNS. Elevated expression of GFAP has been used as an indicator of astrocyte reactivity (Liddelow and Barres, 2017). Here, the results showed no change in GFAP expression in hydrogen peroxide-treated fetal astrocytes compared with untreated control group. Therefore, this indicates that acute oxidative stress is not sufficient to induce the reactive phenotype in human fetal astrocytes. Since these fetal astrocytes showed a DNA damage response as well as a reduction of cell viability as a response to oxidative stress, it could mean that DNA damage and astrocyte reactivity may not necessarily go together, and factors other than oxidative stress may be the culprit behind the induction of reactive astrocytes.

## The impact of amyloid beta on astrocytes

The treatment of astrocytes with 1 µM of $A\beta_{1-42}$ oligomers and fibrils did not cause any significant DNA damage response or cell morphology changes in fetal astrocytes. Aged model of human astrocytes was also used to characterise their responses to Aβ. The analysis for iAstrocytes was carried out for all cell lines pooled together, as well as separating each cell line due to the cell lines being derived from individual donors. When iAstrocyte cell lines were pooled together, the treatment of astrocytes with 1 µM of $A\beta_{1-42}$ oligomers did not cause any significant DNA damage response or cell morphology changes. However, when the cell lines were separated for individual analyses, the DNA damage results changed slightly. For 155v2 iAstrocytes, there was detectable low amount of DNA damage, as measured by the amount of γH2AX-positive DNA foci (between 3-10 detectable foci in the nucleus), at 24 and 48 hours post treatment with $A\beta_{1-42}$ oligomers. Although there were no detectable differences for the repeated stress treatment. Furthermore, for 155v2 iAstrocytes, there were no profound changes to the cell morphology.

Similarly, the treatment of astrocytes with 1 µM of $A\beta_{1-42}$ fibrils did not cause any significant DNA damage response or cell morphology changes, when iAstrocyte cell lines were pooled together. However, as previously, separating the cell lines for analysis revealed that CS14 iAstrocytes were

susceptible to the fibril treatment. In this case, the CS14 iAstrocytes showed an increase in the low damage output of DNA damage at 1, 2, and 24 hours. This was not observable in other cell lines, nor it was observable when CS14 iAstrocytes were treated with oligomeric amyloid beta. This suggests that there may be a differential mechanism of action yielded my both oligomers and fibrils, in terms of inducing DNA damage. Furthermore, this suggests that various individuals could respond to different $A\beta_{1-42}$ aggregate species in a unique manner. For example, in one individual the plaques could have a more detrimental effect than in another individual. This, however, is only a speculation and further work should be carried out to fully understand the individual responses of people with AD to $A\beta_{1-42}$. Indeed, it is a well-known phenomenon that the Aβ load in human brains can be distributed differently across AD patients and cognitively healthy individuals. Therefore, it would be an interesting avenue to explore potential risk factors of the disease, and how these could influence the correlations between Aβ burden, cognition, and astrocyte dysfunction specifically.

Both human fetal astrocytes and iAstrocytes were included in the experimental design. Human fetal astrocytes are young astrocytes that may not be entirely representative of the ageing phenotype of astrocytes found in the brain of older individuals. Ageing brain is more susceptible to oxidative stress, DNA damage and may be more susceptible to amyloid beta-mediated toxicity than a younger brain. Therefore, the impact of $A\beta_{1-42}$ fibrils and oligomers was also investigated in aged astrocytes.

The aged astrocytes were derived by reprogramming human fibroblasts from donors into induced neural progenitor cells (iNPCs), which are precursors of astrocytes. iNPCs were then differentiated further to generate induced astrocytes (iAstrocytes), which retain the ageing phenotype of their donors. The methods for differentiating and culturing iAstrocytes are described in section 3.4.2. The methods are based on the methods described by Meyer *et al.*, 2014. The generated iAstrocytes were previously characterised in previous works via immunocytochemistry with astrocyte-specific markers (Meyer *et al.*, 2014). This has removed any concern of iAstrocytes not being truly astrocytic and increased the confidence in the results presented in this chapter. However, other astrocyte *in vitro* models could have been used in the present work. AD pathology can be modelled using iPSC models. For example, astrocytes from PSEN1 patients showed an increased Aβ production, increase in production of ROS, as well as impaired release of cytokines (Oksanen *et al.*, 2017).

Amyloid beta oligomers have been suggested to be the more neurotoxic species, contributing more to Alzheimer's disease than amyloid beta fibrils. On the other hand, amyloid beta fibrils are the main component of amyloid plaques present in Alzheimer's disease, which have long been thought to contribute to disease pathology (Hardy and Higgins, 1992; Sengupta, Nilson and Kayed, 2016). As the

different Aβ species could elicit differential astrocytic responses, these were investigated in the current chapter.

The cell morphology changes were investigated, as it has been found that, in Alzheimer's disease, morphological changes to astrocytes and astrocytic cytoskeleton can be detected. Namely, in transgenic AD mouse models, there is a significant cytoskeletal atrophy present in astrocytes (Kulijewicz-Nawrot *et al.*, 2012). Furthermore, iPSC cell lines derived from AD patients show cell atrophy and altered astrocyte morphology (Lin *et al.*, 2018). Transplanting patient-derived iPSC astrocytes into mouse brains can respond to amyloid plaques and undergo morphological changes as a result (Preman *et al.*, 2021)

As the Aβ treatment did not cause any profound effects on astrocytes, it could indicate that astrocytes, both young (fetal astrocytes) and aged (iAstrocytes), may be resistant to damage and stress caused by amyloid beta. On the other hand, it could also indicate that the treatment with 1 μM of $A\beta_{1-42}$ oligomers and fibrils may not be enough to cause significant stress to astrocytes, and therefore a higher dosage would be needed to investigate this. However, increasing the dosage and concentration of amyloid beta may cause a few issues in the experimental design. Firstly, amyloid beta is present at small concentrations *in vivo* (30.13 pg/ml for $A\beta_{42}$ in human plasma) (Ovod *et al.*, 2017). Therefore, increasing the concentration of amyloid beta may not be directly comparable to the events occurring in the Alzheimer's disease brain. This could then skew the results, and not represent the disease events well. Additionally, increasing the concentration of amyloid beta could in theory cause a higher rate of amyloid beta aggregation. This could mean that the amyloid beta oligomers may not be entirely in their oligomeric state, and instead they might have progressed into mature fibrils, gain further skewing the results. Lastly, high concentrations of amyloid beta could disturb the pH levels of the cell environment *in vitro*, due to the buffers and diluents used for the preparation of the recombinant peptides, which is the reason why a treatment of 1 μM of $A\beta_{1-42}$ oligomers and fibrils was used. It has been shown that in 3x Tg AD mouse models, the astrocytes experience significant cytoskeletal atrophy compared to control animals. This has been investigated by looking at the expression of GFAP specifically. However, this atrophy has not been linked to amyloid beta aggregates, suggesting this atrophy may not linked to amyloid beta toxicity (Kulijewicz-Nawrot *et al.*, 2012). This response has also been observed in the current study, as neither oligomeric or fibrillary amyloid beta caused any significant differences in the cytoskeletal morphology of fetal and adult astrocytes. This was investigated by looking at vimentin expression.

Vimentin is one of the major cytoskeleton proteins of astrocytes, (Chiu, Norton and Fields, 1981). An upregulation of vimentin can be correlated with astrocyte reactivity in CNS injury (Das *et al.*, 2020).

Hence, vimentin was used to characterise any changes in astrocyte morphology, specifically changes in the cytoskeleton, as a response to amyloid beta treatments. However, treatment of fetal astrocytes and iAstrocytes with 1 µM of $A\beta_{1-42}$ oligomers and fibrils did not cause any significant changes in the cell morphology within 48 hours of treatment. To further evaluate these responses, repeated stress treatment was carried out on the iAstrocytes, however no significant changes in cell morphology were detected. This suggested that no cell atrophy or hypertrophy was taking place as a response to amyloid beta.

It is possible to obtain iAstrocytes derived from Alzheimer's disease patients. It would therefore be interesting to compare the control iAstrocytes and disease iAstrocytes with each other, especially if amyloid beta is not the main contributing factor relating to initial disease onset. It could be that disease iAstrocytes cannot cope as well with amyloid beta fibrils and/or oligomers, and this could lead to profound effects manifesting in increased oxidative stress, DNA damage and changes to astrocyte reactivity and astrocyte morphology. It could also be possible that amyloid beta is cleared away by healthy astrocytes in a much more efficient manner than patient astrocytes. It would be interesting to further investigate these mechanisms by tagging the amyloid beta and tracking the clearance of the peptides in both patient and healthy astrocytes using high throughput live imaging systems. However, as the aim of the current work was to determine whether astrocytes change as a response to different disease stressors, it was therefore important to firstly use control healthy astrocytes. The majority of current field focuses on disease, AD-derived astrocytes to study the astrocytic dysfunction. However, the current work was aiming to provide an insight into whether Aβ could change healthy astrocytes *in vitro* to reveal a more disease-like astrocyte morphology and function. The field of astrocyte functions in AD is currently lacking the knowledge about the early stages of the disease, which is what the current work was trying to investigate.

Using the same techniques, it could also be possible to derive iNeurons from healthy individuals or patients with Alzheimer's disease. This could be beneficial, as amyloid beta could be investigated in the context of neuronal survival, and neuronal DNA damage. Furthermore, iNeurons could be co-cultured with iAstrocytes. The pre-treatment of iAstrocytes with amyloid beta fibrils or oligomers, and subsequent culture of such astrocytes with neurons, could help to investigate whether astrocytes treated with amyloid beta retain their normal roles and functions, which includes whether they are supportive to neurons in co-culture.

## 3.7 Conclusions

Astrocyte heterogeneity (resulting from different stimuli) has been implicated as an important factor mediating astrocyte injury response (Liddelow *et al.*, 2017). Furthermore, Aβ oligomers and fibrils could have differential impact on neurons in Alzheimer's disease. The relationship between the different Aβ aggregation species and astrocyte heterogeneity is unclear, and characterisation of astrocyte responses to different disease-related stressors was the main aim of the current chapter. The results show that fetal astrocytes show a rapid DNA damage response and cell viability reduction as a response to oxidative stress *in vitro*. Aged iAstrocytes show DNA damage response that is differential to each individual cell line. In comparison, neither fetal astrocytes or iAstrocytes show changes to cell viability, DNA damage, or cell morphology after treatment with Aβ oligomers or fibrils. However, iAstrocytes separated by cell lines could indicate potential individual differences in responses to the different aggregation species amyloid proteins. The results indicate that astrocyte responses are heterogenous to varying disease-related stressors. Astrocytes can display differences in cellular responses to stressors and could show selective sensitivity as well. This further confirms that astrocyte responses in injury and disease may be complex and investigating the mechanisms behind these differences could be beneficial towards our understanding of astrocyte-mediated disease pathology. As the changes presented in the current chapter have not been profound and indicative of a disease mechanism, further work was set out to determine what astrocytic changes could be implicated in AD. These changes could be on molecular, and gene expression levels, and therefore a more precise approach to determining these changes was undertaken using RNAseq analysis.

# Chapter 4 – Defining astrocyte changes as a response to Amyloid Beta

## 4.1 Introduction

As described in Chapter 1, Alzheimer's disease is characterised by the aggregation of Aβ. The Aβ protein has long been at the forefront of the amyloid cascade hypothesis, and later the oligomer hypothesis. The hypothesis states that Aβ, or more toxic Aβ oligomers, contribute to the adverse molecular effects in the CNS, ultimately leading to neuronal degeneration. Clinically, this manifests as an onset of cognitive impairment and dementia (Breijyeh and Karaman, 2020). Astrocytes have been proposed to contribute to Alzheimer's disease pathology. It is unclear whether astrocytes contribute to Alzheimer's disease via a toxic gain of function, or a toxic loss of function, or perhaps a combination of both. This means that in disease, astrocytes could change their molecular profiles which can contribute to the loss of neuroprotection, but they could also gain more neurotoxic functions (Siracusa, Fusco and Cuzzocrea, 2019).

In recent years, astrocytes have been proposed to become reactive in various disease and injury states. A classification of astrocytes into A1 (reactive, neurotoxic) and A2 (neuroprotective) subtypes has been proposed. A1 neurotoxic astrocytes have been shown to cause synaptic dysfunction and can promote neuronal cell death; A2 astrocytes have been shown to promote neuronal survival and tissue repair (Liddelow and Barres, 2017; Liddelow *et al.*, 2017) . However, the characterisation of such astrocytes is difficult, and may not manifest itself in an all-or-nothing response, so there is likely to be greater heterogeneity of astrocyte responses.

As described by the results in the previous chapter, astrocytes treated with various conformations of Aβ (oligomers and fibrils) do not show any changes to astrocyte viability and morphology. Additionally, in Aβ-treated astrocytes there was no evidence of DNA damage. This however is not representative of the complex changes to astrocytes that may take place at the gene expression level, reflecting functional alterations. For this reason, it is important to investigate the gene expression changes to astrocytes treated with different forms of amyloid beta, which is the focus of the current chapter.

The choice of Aβ is a crucial step in experimental design. The use of recombinant Aβ can be an easy, widely available, reproducible, and cheap option for studying the effects of Aβ in disease models (LeVatte *et al.*, 2019). However, the recombinant Aβ may not be entirely reliable. There could be variability in peptide preparations due to the presence of intrinsic impurities in synthetic/ recombinant Aβ peptides. Chemically prepared Aβ can vary depending on the source, preparation methods, batch variations, and storage. Most importantly, the Aβ derived from recombinant or synthetic sources may differ in the shape, aggregation rates, seeding capabilities, and final morphology based on the protocols used to prepare the peptides (Finder *et al.*, 2010; Matuszyk *et al.*, 2022). Furthermore, the results presented in chapter 3 suggested that the recombinant $A\beta_{1\text{-}42}$ may not be toxic to astrocytes

and may not induce profound changes to astrocytes *in vitro*. Hence, other sources of Aβ could be beneficial to investigate in the context of disease and could allow us to draw more reliable conclusions. To fully characterise the roles of Aβ on astrocyte changes in AD, and to supplement the results presented in chapter 3, other sources of Aβ may need to be considered. For example, a good option would be to use cell derived Aβ. The use of modified Chinese hamster ovary cell line expressing a human amyloid precursor protein has been shown to be a useful tool in deriving disease-relevant Aβ *in vitro*. Such Aβ can produce dendritic spinal loss, synaptic vesicle loss, and synaptotoxicity (Welzel *et al.*, 2014; Matuszyk *et al.*, 2022). It is also true, that iPSCs and primary cultures of cells modelling AD could also be used in modelling the interactions of Aβ with astrocytes. However, the use of conditioned media from cells derived from AD patients may not be the most reliable choice for the aims of the current work. This is because there may be other factors, and various proteins and cues in the cell secretome that may also be disease-relevant, whereas the aim of the current work is to characterise the astrocyte responses to different types of Aβ alone. Therefore, isolating specific Aβ isoforms from cell conditioned media may be difficult.

Additionally, one of the ways of modelling the disease *in vitro* would be to obtain Aβ from human brains. This method could model the heterogeneity of Aβ in disease better. Furthermore, the brain-derived Aβ can exhibit disease-relevant seeding patterns which may not be present in recombinant Aβ, suggesting that brain-specific conditions may be essential for Aβ aggregation and pathological effects (Meyer-Luehmann *et al.*, 2006). Also, the structure and β-sheet twisting patterns of brain-derived Aβ can differ from recombinant or synthetic Aβ (Paravastu *et al.*, 2008; Lu *et al.*, 2013; Qiang *et al.*, 2017a; Marius Kollmer *et al.*, 2019). One caveat of using the brain-derived Aβ is the fact that often the preparations contain post-translational modifications, as well as a mixture of various Aβ isoforms (Marius Kollmer *et al.*, 2019). Therefore, isolating the disease-relevant form of Aβ may be a difficult task. To fully characterise the astrocyte responses to different forms of Aβ, it would be beneficial to compare the different sources of Aβ, and how these affect astrocytic function and roles in AD. However, the characterisation of astrocyte responses of cell-derived Aβ would be beyond the scope of the current work. Therefore, the focus of this chapter was to specifically isolate and extract human $A\beta_{1\text{-}42}$ from Alzheimer's disease brains, as it is thought to be the most disease relevant isoform. The extracted human $A\beta_{1\text{-}42}$ would then be used to compare whether amyloid beta extracts cause a differential astrocyte response to recombinant amyloid beta.

## 4.2 Aims and objectives

The aim of this chapter is to investigate whether astrocytes show differential responses to different forms of Aβ. We hypothesise that different $A\beta_{1-42}$ types, namely fibrils, oligomers, and extracts isolated from human AD brain samples, cause a varying response in iAstrocytes at a gene expression level, which may reflect differences in functional alterations. Therefore, the current chapter focuses on characterising the differing responses of astrocytes to the varying types of $A\beta_{1-42}$, on a level of gene expression.

This aim is going to be fulfilled by the following objectives:

i. To extract and isolate human $A\beta_{1-42}$ from Alzheimer's disease brains for the use in iAstrocyte treatments by immunoprecipitation;
ii. To treat iAstrocytes with extracted human $A\beta_{1-42}$; as well as recombinant $A\beta_{1-42}$ fibrils and $A\beta_{1-42}$ oligomers *in vitro* prior to extraction of RNA for transcriptomic analysis;
iii. To compare the transcriptomic profile of iAstrocytes treated with various types of $A\beta_{1-42}$ through RNAseq analysis;
iv. To identify potential gene targets that could be responsible for the amyloid beta-mediated effects responsible for Alzheimer's disease pathology.

## 4.3 Materials

Where required, equipment was bought pre-sterilised, or sterilised by autoclaving for 15 minutes at 121 $^{o}$C, 15 psi. All solutions and buffers were prepared using Milli-Q pure water. Unless otherwise stated, all reagents were purchased from Sigma-Aldrich.

### 4.3.1 Amyloid beta brain extracts

| | |
|---|---|
| Artificial cerebrospinal fluid buffer (aCSFb) | *124 mM NaCl, 2.8 mM KCl, 1.25 mM $NaH_2PO_4$, 26 mM $NaHCO_3$, pH 7.4* |
| Ethylenediaminetetraacetic acid (EDTA) | Sigma-Aldrich, E6511 |
| Ethylene glycol-bis (β-aminoethyl ether)-N,N,N',N'-tetraacetic acid (EGTA) | Sigma-Aldrich, E9884 |
| Aprotinin Protease Inhibitor | ThermoFisher Scientific, 78432 |
| Pepstatin A Protease Inhibitor | ThermoFisher Scientific, 78436 |
| Pefabloc® SC (4-(2-Aminoethyl) benzolsulfonylfluorid-hydrochloride) | Merck, 124839 |
| Sodium Fluoride (NaF) | Scientific Laboratory Supplies, S6776-100G |
| Slide-A-Lyzer™ G2 Dialysis Cassettes | 2k molecular weight cut off, 0.5 mL ThermoFisher Scientific, 87717 |
| Protein A and Protein G Magnetic Sepharose™ beads | Cytiva, 28-9513-79 |
| 6e10, Purified anti-β-Amyloid, 1-16 antibody | Mouse monoclonal, Biolegend, SIG-39320 |
| Mouse serum | Merck, M5905 |
| Amyloid beta 42 Human ELISA Kit | ThermoFisher Scientific, KHB3441 |

**Table 4.1.** The Alzheimer's disease cases chosen for amyloid beta extractions

| Case number | Block number | Area | Diagnosis | Age | Sex | Weight of tissue used/ g |
|---|---|---|---|---|---|---|
| 045/2013 | 6 | CL16 | Alzheimer's disease | 65 | F | 0.8 |
| 031/2013 | 8 | CL16-18 | Alzheimer's disease | 92 | F | 0.4 |
| 003/2007 | 5 | CL-16 | Alzheimer's disease | 79 | F | 0.7 |

### 4.3.2 Cell culture materials

| | |
|---|---|
| 1 x Phosphate Buffered Saline (PBS) | *137 mM NaCl; 2.7 mM KCl; 10 mM Na2HPO4; KH2PO4; pH 7.4* |
| Accutase | Sigma, A6964 |
| Cell Culture 10 $cm^2$ dishes | Nunclon™ Delta Surface, Thermo Scientific, 150350 |
| DMEM – *phenol red free* | Gibco™, 31053028 |
| DMEM, high glucose – *with phenol red* | Gibco™, 41965039 |
| Fetal Bovine Serum | Biosera, FB-1001 |
| Fibronectin | Merck, FC010 |
| L-glutamine | Gibco™ 25030081 |
| N2 supplement | Gibco, 17502001 |
| Penicillin/Streptomycin | Lonza, DE17-603E |

### 4.3.3 Cell treatments

| | |
|---|---|
| Oligomeric $A\beta_{1-42}$; prepared from the monomeric $A\beta_{1-42}$ | rPeptide, A-1163-1; A1163-2<br>*Monomeric Aβ diluted in 2xTBS buffer (pH 7.4), pre-adjusted to a correct final pH with 45 mM HCl, to a final concentration of 100 µM and incubated for 2 weeks at 4°C.* |
| Fibrillary $A\beta_{1-42}$; prepared from the monomeric $A\beta_{1-42}$ | rPeptide, A-1163-1; A1163-2<br>*Monomeric Aβ diluted in 2xTBS buffer (pH 7.4), pre-adjusted to a correct final pH with 45 mM HCl, to a final concentration of 100 µM and incubated for 24 hrs at 37°C.* |
| $A\beta_{1-42}$; scrambled (1.0 mg) | rPeptide, A-1004-2<br>*Used as a vehicle control* |
| Human $A\beta_{1-42}$ extracts | *Extracted from human Alzheimer's disease brains. (Ethical permission granted from the Management Board of The Sheffield Brain Tissue Bank, see appendix for details)* |

### 4.3.4 RNA extraction

| | |
|---|---|
| DNase/ RNase-free water | Zymo Research; W1001-10 |
| TRIzol Reagent | Invitrogen, 15596018 |
| Ice cold 1xPBS | *137 mM NaCl; 2.7 mM KCl; 10 mM Na2HPO4; KH2PO4; pH 7.4* |
| Ethanol | |
| Isopropanol | |
| Chloroform | |

## 4.4 Methods

### 4.4.1 Extraction of $A\beta_{1-42}$ from human Alzheimer's disease brains

Three lateral temporal cortex samples (BA21/22) from Alzheimer's disease brains were sub-dissected from coronal slices (table 4.1). The brain tissue was obtained from the Sheffield Brain Tissue Bank, which granted ethical permission for the use of the tissue (see appendix) These slices had been flash-frozen in liquid nitrogen at autopsy and were stored at -80°C. The slices were brought to -20°C for sub-dissection. The resulting brain samples were weighed and taken forward for Aβ extractions.

The Aβ extraction was performed using a modification of the protocol described in Wang *et al.*, (2017). Briefly, all three samples were prepared by homogenising the tissue in an artificial CSF base buffer (aCSF-B) containing 5 mM EDTA, 1 mM EGTA, 5 µg/ml aprotinin, 2 µg/ml pepstatin, 120 µg/ml pefabloc, and 5 mM NaF. Homogenates were pooled and centrifuged at 198,000 x g for 110 min, at 4°C in a SW 41-Ti rotor (Beckman Coulter). The upper 90% of supernatant was dialysed at 4°C using Slide-A-Lyzer G2 Dialysis Cassettes with a 2 kDa molecular weight cut-off. Dialysis was performed against at least a 100-fold excess of aCSF-B, with the buffer changes 3 times over a 72-hour period, according to manufacturer's instructions. Afterwards, the extracts were divided into two portions. One portion of the extracts was immunodepleted of Aβ by 3 rounds of 12 h incubations with the anti-Aβ 6e10 antibody plus Protein G Magnetic Sepharose beads at 4°C according to the manufacturer's instructions, to remove Aβ from the homogenate mixture. The second portion of the extracts was treated in an identical manner, except the immunodepletion was carried out with a mouse IgG control, which acted as a negative control. Samples were cleared of beads, and aliquots were flash frozen in liquid nitrogen, and stored at -80°C until further use. Samples were thawed only once before use. An ELISA, to specifically quantify $A\beta_{1-42}$ was performed according to the manufacturer's instructions (ThermoFisher Scientific), to quantify the amount of $A\beta_{1-42}$ extracted, and this was calculated from a standard curve.

### 4.4.2 Cell culture and treatment of iAstrocytes

The details of cell culture of iAstrocytes were described in the Methods section of Chapter 3 and are based on the methods described by Meyer *et al.* (2014). Briefly, iAstrocytes were differentiated from iNPCs. iAstrocytes were cultured on fibronectin-coated 10 $cm^2$ tissue culture dishes, in iAstrocyte cell medium for 7 days. iAstrocytes were media changed on day 3 for cell maintenance. On day 6, the cells were treated with 1 µM of oligomeric or fibrillary $A\beta_{1-42}$, as well as 1 µM of scrambled peptide as vehicle control, for 24 hours. The cells were also treated with 73.436 pg/ml of $A\beta_{1-42}$ (the extracts were diluted at 1:100) extracted from human Alzheimer's disease brains on day 6, for 24 hours. iAstrocytes were harvested for RNA isolation and extraction on day 7, at a point when iAstrocyte differentiation was fully completed.

### 4.4.3 RNA isolation and extraction

The iAstrocytes were harvested on day 7 of differentiation (24 hours post-treatment). Firstly, the iAstrocytes were washed with 2 mL of ice-cold PBS once to remove any previous treatment, and/or cell media. The cells were harvested in 1 mL of TRIzol reagent and scraped vigorously using a cell scraper. Furthermore, the cell lysates were passed through a pipette several times to ensure sufficient cell lysis. The collected cell lysates were transferred into 1.5 mL Eppendorf tubes and kept on ice.

For phase separation, 0.2 mL of chloroform per 1 mL of TRIzol reagent was added. The tubes were vortexed vigorously for 15 seconds and incubated at room temperature for 3 minutes. The samples were centrifuged at 12,000 x g for 15 minutes at 4$^{o}$C. Following centrifugation, the mixture separated into visible layers. The upper aqueous phase was carefully transferred into a fresh tube.

RNA was precipitated from the aqueous phase by mixing with 0.5 mL of 100% isopropanol per 1 mL of TRIzol reagent. The samples were incubated at room temperature for 10 minutes and centrifuged at 12,000 x g for 10 minutes at 4$^{o}$C.

The supernatant was removed from the tube, to leave RNA pellet only. The pellet was washed with 1 mL of 75% ethanol. The samples were mixed by vortexing and centrifuged at 7,500 x g for 5 minutes at 4$^{o}$C. The wash was discarded, and the pellets were air dried for 10 minutes. The RNA pellets were subsequently resuspended in RNase-free water (50 µL) and stored at -80$^{o}$C before RNAseq analysis. The RNA concentration was measured using the Nanodrop (table 4.2).

### 4.4.4 RNAseq analysis

Human mRNA sequencing of the samples, and subsequent RNAseq data analysis was carried out commercially by Novogene. The Novogene cDNA libraries were sequenced using Illumina NovaSeq PE150 platform. The analysis included RNA sample quality control prior to further RNAseq analysis, mRNA library preparation, sequencing, and data analysis.

The bioinformatics analysis included data quality control and data filtering; mapping to the reference genome; gene expression quantification and correlation analysis; differential expression analysis; enrichment analysis and GSEA enrichment analysis.

## 4.5 Results

### 4.5.1 Amyloid beta brain extracts from human brain tissue

#### $A\beta_{1-42}$ ELISA

$A\beta_{1-42}$ was extracted from three human AD brain tissue samples, and an ELISA kit specific for human $A\beta_{1-42}$ detection was used to quantify the resulting $A\beta_{1-42}$ extracts (fig.4.1.). The ELISA results for IgG control and for Aβ extracts were calculated from a standard curve, which was derived per manufacturer's instructions. The ELISA showed that the total content of $A\beta_{1-42}$ in the pooled Aβ extracts was 73.436 pg/ml., whilst the content of $A\beta_{1-42}$ in the IgG control was 58.11 pg/ml. The concentration of extracted $A\beta_{1-42}$ was significantly higher than the IgG control. This confirmed that the extractions were successful, and that there is $A\beta_{1-42}$ present in the samples.

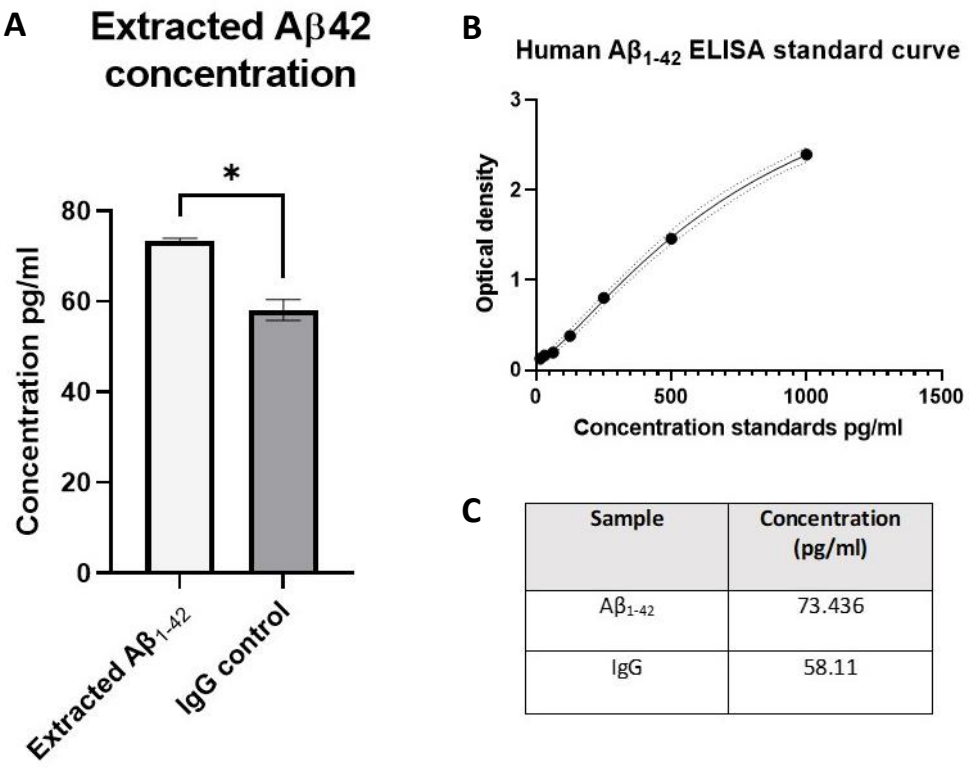


C

| Sample | Concentration (pg/ml) |
|---|---|
| $A\beta_{1-42}$ | 73.436 |
| IgG | 58.11 |

**Figure 4.1** ELISA results for the Aβ brain extracts and IgG control.

**A)** A graph showing the difference between the concentration of $A\beta_{1-42}$ extracted from human brain tissue, and the IgG control. **B)** Standard curve from which the concentrations of $A\beta_{1-42}$ extracted from human brain tissue, as well as of the respective IgG control was calculated. **C)** The calculated concentrations of $A\beta_{1-42}$ and the IgG control. Unpaired t-test, error bars show mean±SD.

### 4.5.2 Quality control of RNA isolation and preparation prior to RNAseq analysis

Prior to sending the collected and isolated RNA samples (n=3; three cell lines used for each treatment group) for RNAseq commercial analysis (Novogene), the RNA samples were analysed for sample quantitation using Nanodrop (table 4.2). The RNA quality and quantity was also confirmed using RNA Electrophoresis (Agilent) prior to sending samples for commercial analysis.

**Table 4.2.** Nanodrop results showing the sample, the corresponding concentration, and the sample volume

| Sample number | Sample | Concentration (ng/µL) | Volume (µL) |
|---|---|---|---|
| 1 | 155v2 control | 439.7 | 4 |
| 2 | 155v2 extracts | 389.9 | 4 |
| 3 | 155v2 oligomers | 438.0 | 4 |
| 4 | 155v2 fibrils | 1049.6 | 4 |
| 5 | 155v2 scrambled | 442.7 | 4 |
| 6 | 161 control | 737.6 | 4 |
| 7 | 161 extracts | 1385.6 | 4 |
| 8 | 161 oligomers | 780.0 | 4 |
| 9 | 161 fibrils | 726.1 | 4 |
| 10 | 161 scrambled | 822.8 | 4 |
| 11 | CS14 control | 416.2 | 4 |
| 12 | CS14 extracts | 1695.3 | 4 |
| 13 | CS14 oligomers | 1000.0 | 4 |
| 14 | CS14 fibrils | 751.8 | 4 |
| 15 | CS14 scrambled | 446.7 | 4 |

Subsequently, the RNA samples were sent to Novogene for full RNAseq analysis. The company has also carried out an in-house quality control analysis of the samples, which included sample quantitation analysis, sample integrity analysis, as well as sample purity analysis (table 4.3). The quality control analysis revealed that all samples, apart from iAstrocyte cell line 161 for fibril treatment, achieved a RIN number higher than 9. All samples passed the quality control checks.

**Table 4.3.** Novogene quality control results showing the sample ID, the corresponding concentration, the sample volume, total RNA amount, and RIN number for each sample

| No. | Sample Name | Nucleic Acid ID | Concentration(ng/ul) | Volume(ul) | Total amount(ng) | RIN | Sample QC Results |
|---|---|---|---|---|---|---|---|
| 1 | ctrl_155 | EKRN220027252-1A | 228.00 | 43 | 9.80400 | 10.0 | Pass |
| 2 | ext_155 | EKRN220027253-1A | 333.00 | 38 | 12.65400 | 9.6 | Pass |
| 3 | olig_155 | EKRN220027254-1A | 369.00 | 36 | 13.28400 | 9.7 | Pass |
| 4 | fib_155 | EKRN220027255-1A | 265.00 | 43 | 11.39500 | 9.1 | Pass |
| 5 | scr_155 | EKRN220027256-1A | 290.00 | 43 | 12.47000 | 10.0 | Pass |
| 6 | ctrl_161 | EKRN220027257-1A | 2622.00 | 43 | 112.74600 | 9.7 | Pass |
| 7 | ext_161 | EKRN220027258-1A | 1554.00 | 47 | 73.03800 | 9.6 | Pass |
| 8 | olig_161 | EKRN220027259-1A | 972.00 | 35 | 34.02000 | 9.9 | Pass |
| 9 | fib_161 | EKRN220027260-1A | 529.00 | 39 | 20.63100 | 7.3 | Pass |
| 10 | scr_161 | EKRN220027261-1A | 1046.00 | 44 | 46.02400 | 9.8 | Pass |
| 11 | ctrl_CS14 | EKRN220027262-1A | 137.00 | 43 | 5.89100 | 10.0 | Pass |
| 12 | ext_CS14 | EKRN220027263-1A | 172.00 | 44 | 7.56800 | 9.7 | Pass |
| 13 | olig_CS14 | EKRN220027264-1A | 314.00 | 42 | 13.18800 | 9.8 | Pass |
| 14 | fib_CS14 | EKRN220027265-1A | 242.00 | 44 | 10.64800 | 9.6 | Pass |
| 15 | scr_CS14 | EKRN220027266-1A | 351.00 | 41 | 14.39100 | 9.7 | Pass |

### 4.5.3 RNAseq data analysis quality control

As part of the commercial RNAseq and the gene expression data analysis, the data was firstly analysed to ensure quality control and data filtering of the results.

For each cell line and associated treatment, the error rate distribution analysis was carried out, which gives an overview of the quality of the data and of the sequencing quality. The error scores indicate the probability of correct sequencing and are based on Phred quality scores, which allows for measurement of the reliability of sequencing (Li *et al.*, 2015). Smaller percentage error values indicate that the values are close to the true value. For all three cell lines, and all cell treatments, the percentage error rate along the position of the read was less than 1%, according indicating accurate results (fig.4.2).

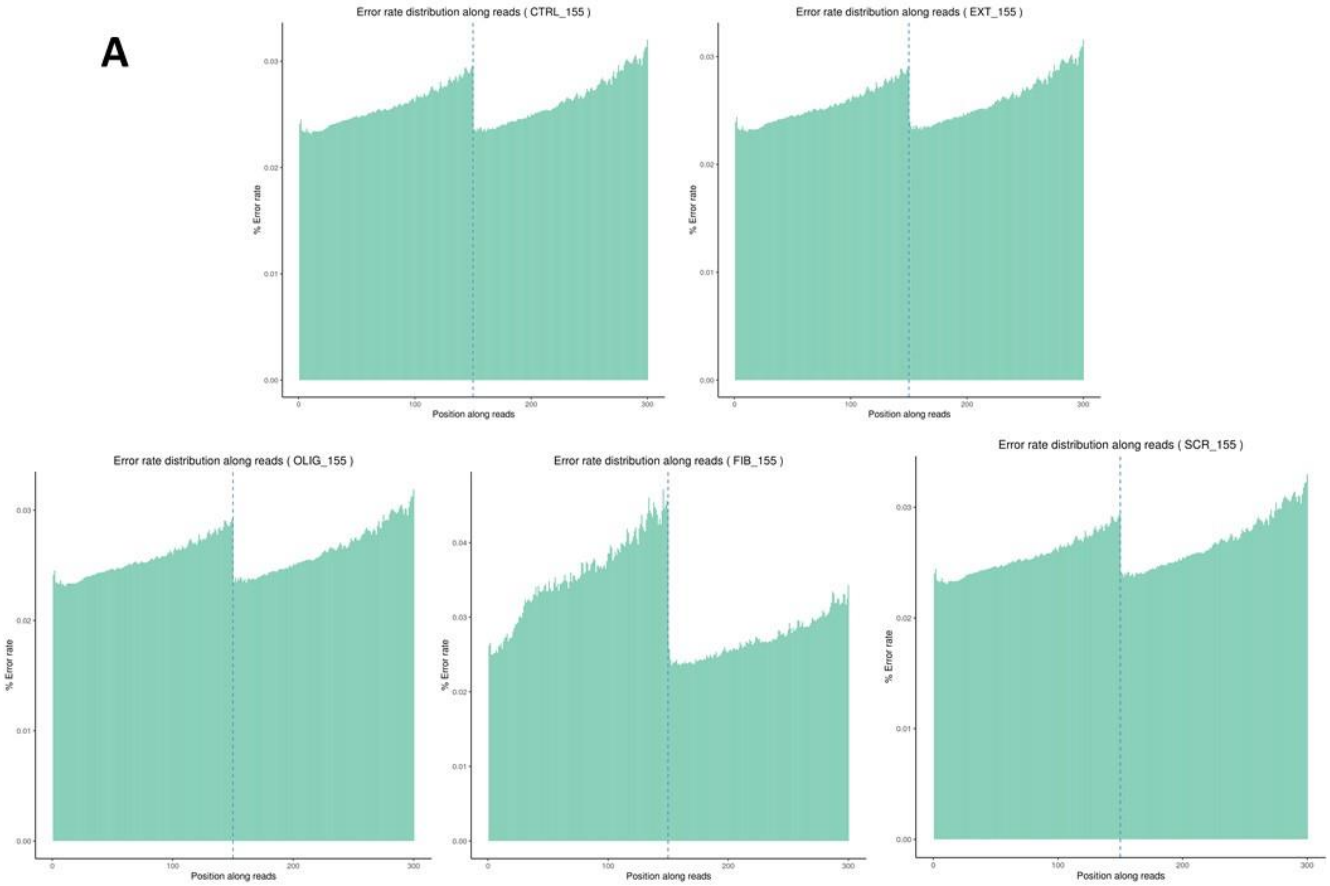
A
Error rate distribution along reads ( CTRL_155 )
Error rate distribution along reads ( EXT_155 )
Error rate distribution along reads ( OLIG_155 )
Error rate distribution along reads ( FIB_155 )
Error rate distribution along reads ( SCR_155 )
% Error rate
Position along reads

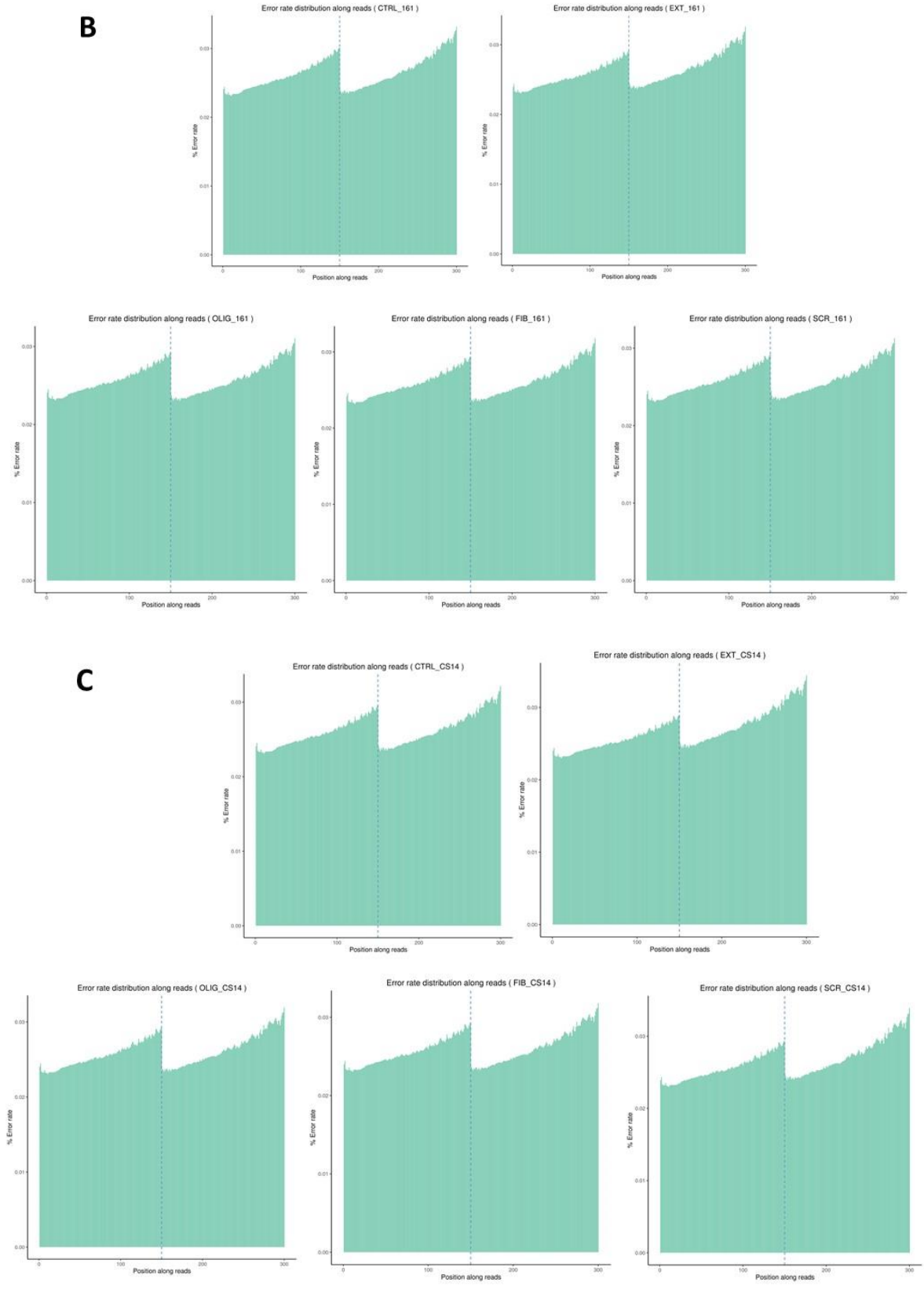


**Figure 4.2.** The percentage error scores for all three iAstrocyte cell lines.

Histograms showing the distribution of **(A)** the percentage error rate scores for iAstrocyte line 155v2; **(B)** the percentage error rate scores for iAstrocyte line 161; **(C)** the percentage error rate scores for iAstrocyte line CS14. Figure provided by Novogene.

The next part of quality control analysis involved investigating the GC (guanine-cytosine) distribution, or GC content. The AT (adenine-thymine) and GC contents should be equal and constant through each sequencing cycle. However, due to primer amplification bias, the first few nucleotides (around 6-7 nucleotides) can fluctuate, which is a normal result. The GC content is favoured for RNAseq quality control, as it is more stable and has more biological meaning. In general, exons have a higher GC content, and the read coverage can be dependent on the GC content of the reference genome. In an average GC content plot, a 'clean' read with stable distribution across the 'position along reads' is expected. When there are issues with nucleotide distribution, the GC plot will appear largely unstable with large variations. GC content is an important quality control step, which helps to evaluate GC content bias, transcript detection and nucleotide base quantification. Here, the GC distribution graphs for each cell line and cell treatment shows a normal and expected fluctuation within the first nucleotide reads, and no obvious fluctuations at later reads. This indicates there were no abnormal AT and GC fluctuations within the dataset (fig.4.3).

**A**

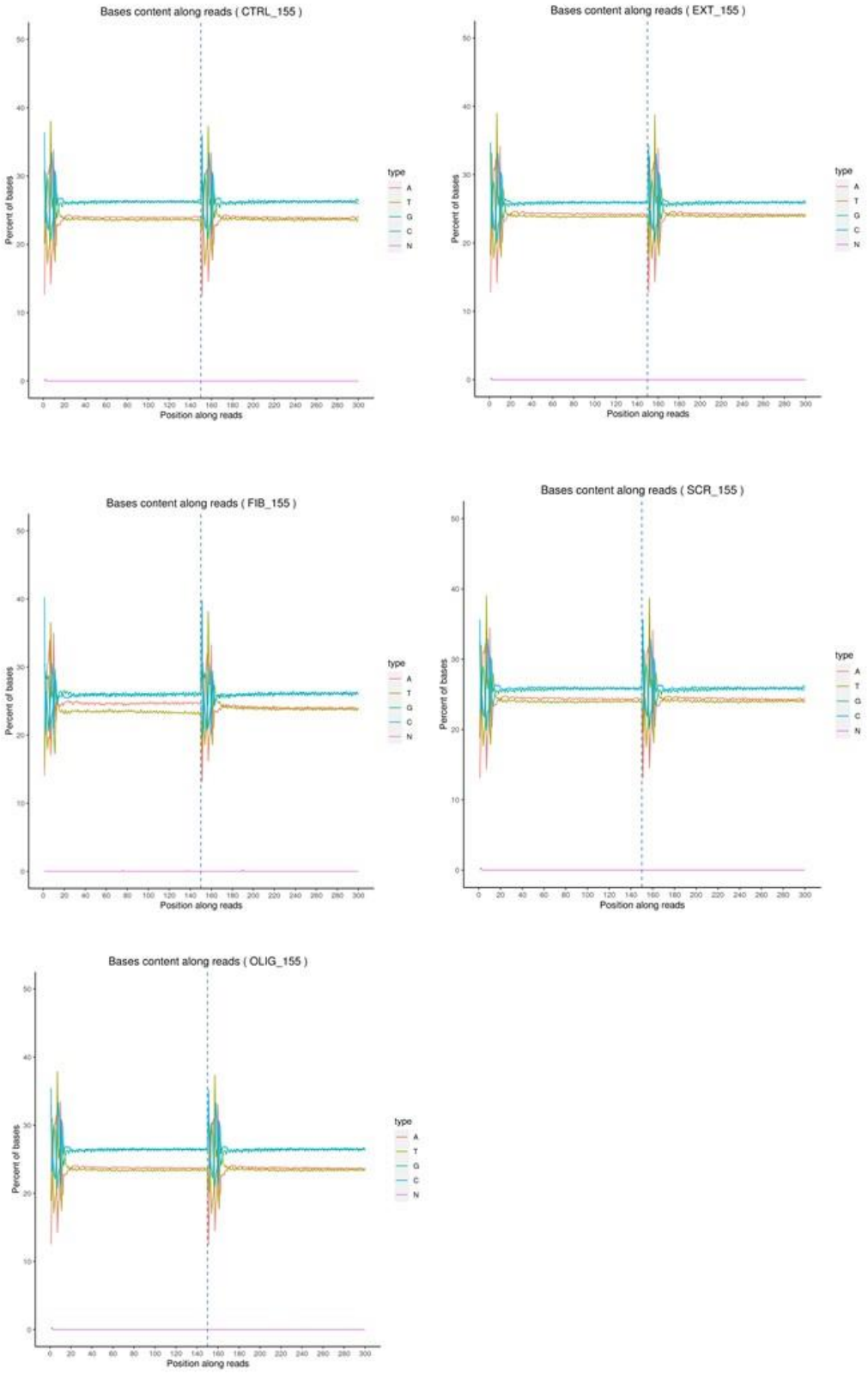
Bases content along reads ( CTRL_155 )
Bases content along reads ( EXT_155 )
Bases content along reads ( FIB_155 )
Bases content along reads ( SCR_155 )
Bases content along reads ( OLIG_155 )
Percent of bases
Position along reads
type
A
T
G
C
N

**B**

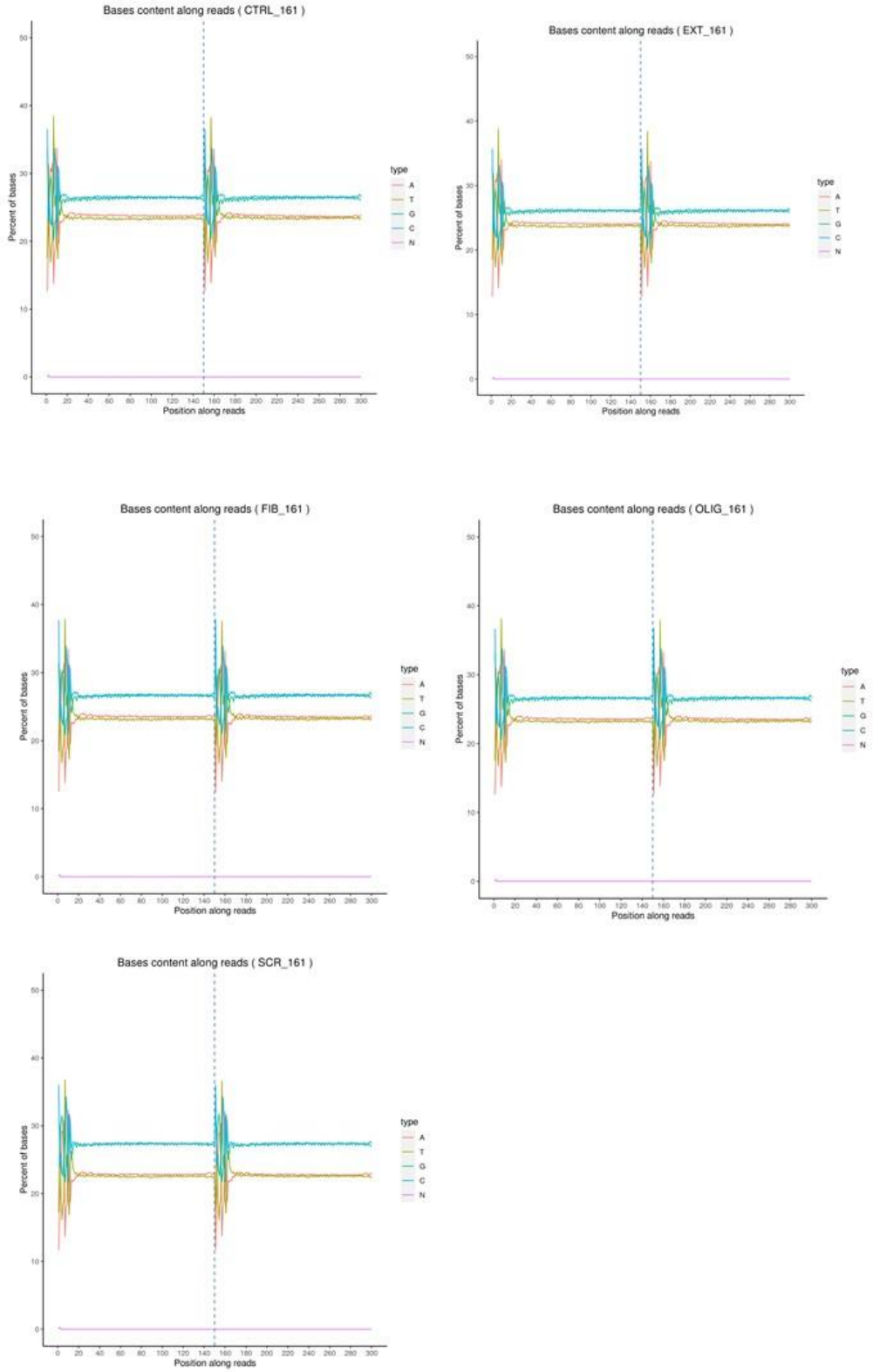
Bases content along reads ( CTRL_161 )
Bases content along reads ( EXT_161 )
Bases content along reads ( FIB_161 )
Bases content along reads ( OLIG_161 )
Bases content along reads ( SCR_161 )
Percent of bases
Position along reads
type
A
T
G
C
N

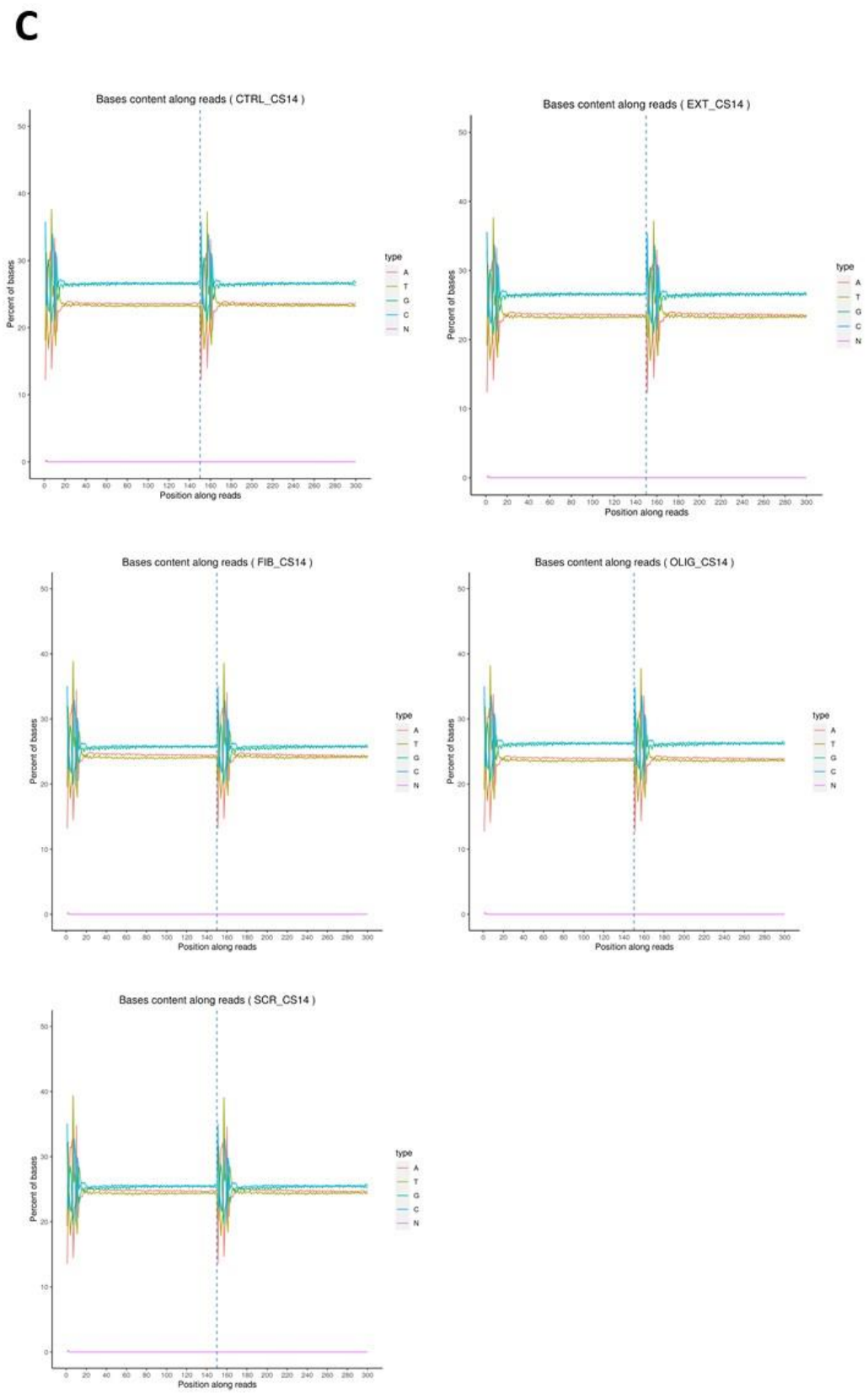


**Figure 4.3** GC distribution plots for all iAstrocyte cell lines and treatments, for quality control purposes. **(A)** GC distribution plot for iAstrocyte line 155v2; **(B)** GC distribution plot for iAstrocyte line 161; **(C)** GC distribution plot for iAstrocyte line CS14. Figure provided by Novogene.

As part of the quality control process for the RNAseq data, data filtering was carried out. This data filtering step ensures that only clean data is used for subsequent analyses (fig.4.4). The distribution of raw reads within the data for each cell line and cell treatments is shown. Genes attributed to low quality data were filtered out. The category 'containing N' shows any uncertainties within the data and these were also filtered out. The percentage of adapter reads is shown, and this data was filtered out as well. The adapter reads are artificial pieces of DNA which are introduced prior to sequencing to ensure that the DNA fragment that is being sequenced can attach to the sequencing flow cells. These adapters are part of the sequencing workflow but are ultimately filtered out from the dataset at quality control.

**A**

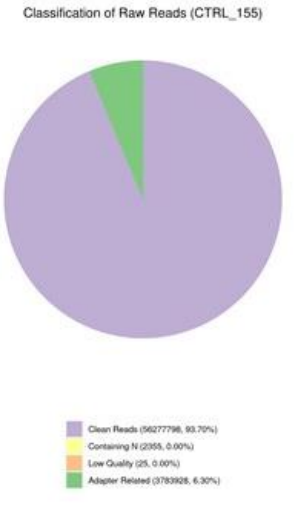
Classification of Raw Reads (CTRL_155)
Clean Reads (56277796, 93.70%)
Containing N (2355, 0.00%)
Low Quality (25, 0.00%)
Adapter Related (3783928, 6.30%)

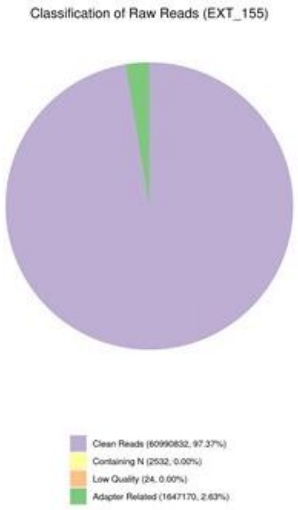
Classification of Raw Reads (EXT_155)
Clean Reads (60990832, 97.37%)
Containing N (2532, 0.00%)
Low Quality (24, 0.00%)
Adapter Related (1647170, 2.63%)

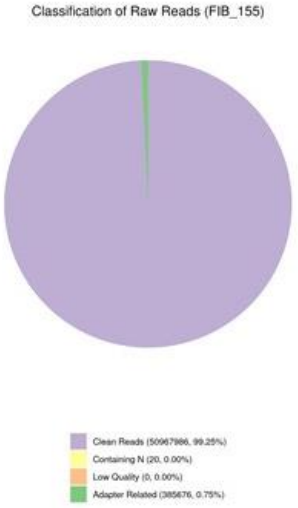
Classification of Raw Reads (FIB_155)
Clean Reads (50967986, 99.25%)
Containing N (20, 0.00%)
Low Quality (0, 0.00%)
Adapter Related (385676, 0.75%)

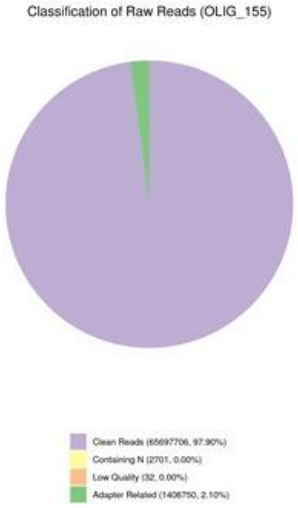
Classification of Raw Reads (OLIG_155)
Clean Reads (65697706, 97.90%)
Containing N (2701, 0.00%)
Low Quality (32, 0.00%)
Adapter Related (1406750, 2.10%)

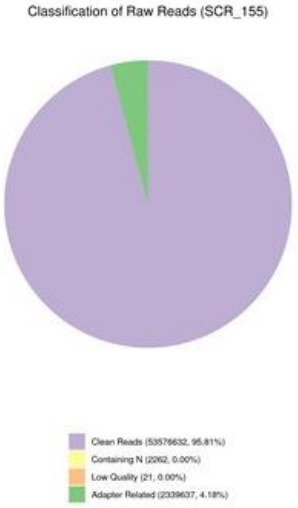
Classification of Raw Reads (SCR_155)
Clean Reads (53578632, 95.81%)
Containing N (2262, 0.00%)
Low Quality (21, 0.00%)
Adapter Related (2339637, 4.18%)

**B**

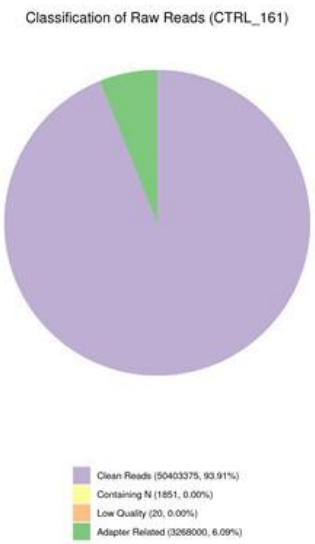
Classification of Raw Reads (CTRL_161)
Clean Reads (50403375, 93.91%)
Containing N (1851, 0.00%)
Low Quality (20, 0.00%)
Adapter Related (3268000, 6.09%)

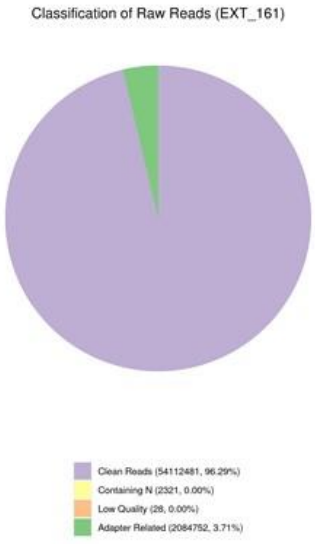
Classification of Raw Reads (EXT_161)
Clean Reads (54112481, 96.29%)
Containing N (2321, 0.00%)
Low Quality (28, 0.00%)
Adapter Related (2084752, 3.71%)

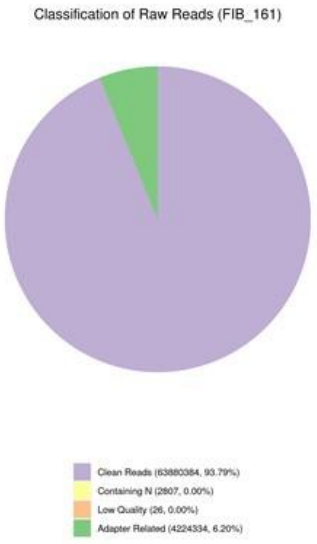
Classification of Raw Reads (FIB_161)
Clean Reads (63880384, 93.79%)
Containing N (2807, 0.00%)
Low Quality (26, 0.00%)
Adapter Related (4224334, 6.20%)


Classification of Raw Reads (OLIG_161)
Clean Reads (64118338, 93.51%)
Containing N (2728, 0.00%)
Low Quality (19, 0.00%)
Adapter Related (4448465, 6.49%)


Classification of Raw Reads (SCR_161)
Clean Reads (59149095, 92.29%)
Containing N (2635, 0.00%)
Low Quality (32, 0.00%)
Adapter Related (4935600, 7.70%)


**Figure 4.4.** Data filtering pie charts for all iAstrocyte lines, representing the distribution of clean data and artifact data that was filtered out from the final data analysis.

**(A)** data filtering charts for iAstrocyte line 155v2; **(B)** data filtering charts for iAstrocyte line 161; **(C)** data filtering charts for iAstrocyte line CS14. Figure provided by Novogene.

Lastly, the reads distribution was examined. This evaluates the proportion of detected exons, introns, and intergenic regions within the sequenced samples mapped to the reference genome. This is an important quality control step because it investigates the presence of mapping artefacts, presence of sample contaminations, pre-mRNAs and reads bias, which could be due to RNA degradation. Here, the samples passed quality control analysis, as within all of the samples the majority of reads were found to be within the exons (fig.4.5).

**A**

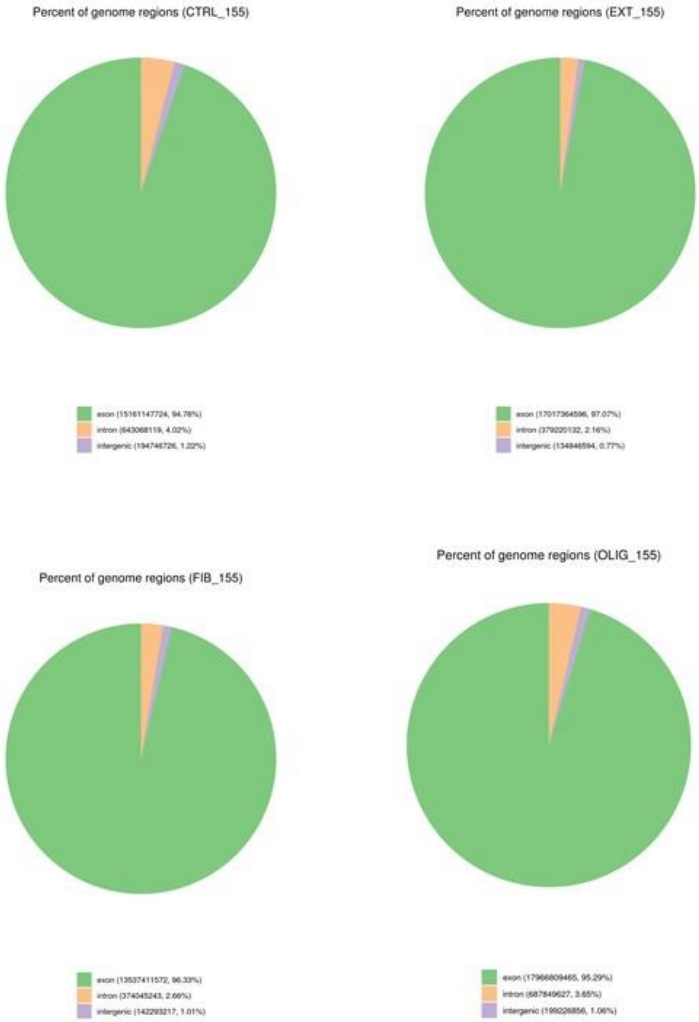
Percent of genome regions (CTRL_155)
exon (15161147724, 94.76%)
intron (643068119, 4.02%)
intergenic (194746726, 1.22%)
Percent of genome regions (EXT_155)
exon (17017364596, 97.07%)
intron (378220132, 2.16%)
intergenic (134846594, 0.77%)
Percent of genome regions (FIB_155)
exon (13537411572, 96.33%)
intron (374045243, 2.66%)
intergenic (142293217, 1.01%)
Percent of genome regions (OLIG_155)
exon (17966809465, 95.29%)
intron (687849627, 3.65%)
intergenic (199226856, 1.06%)
Percent of genome regions (SCR_155)
exon (14766322623, 96.62%)
intron (389430861, 2.55%)
intergenic (127739146, 0.84%)

**B**

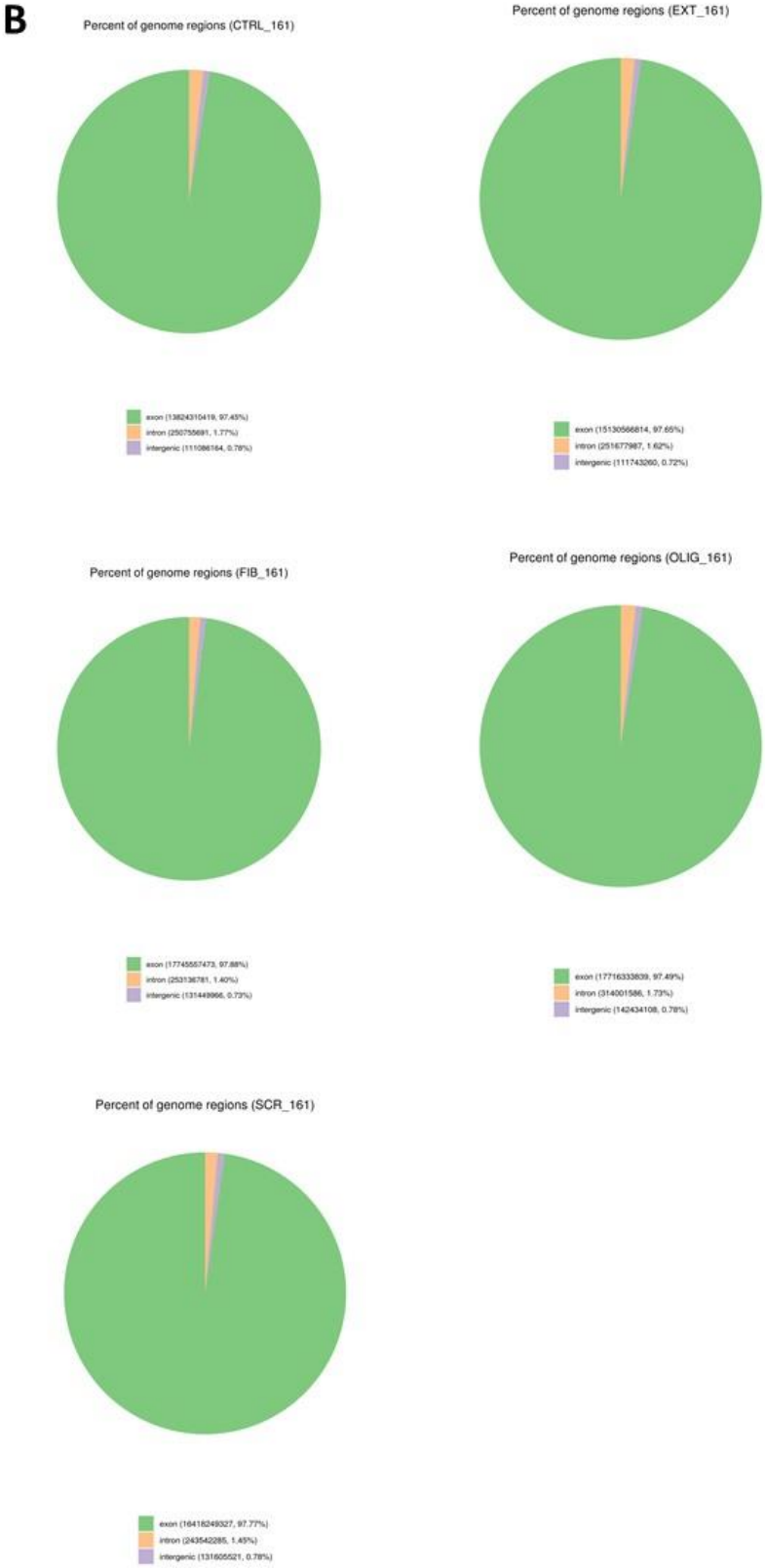
Percent of genome regions (CTRL_161)
exon (13824310419, 97.45%)
intron (250755691, 1.77%)
intergenic (111086164, 0.78%)
Percent of genome regions (EXT_161)
exon (15130566814, 97.65%)
intron (251677987, 1.62%)
intergenic (111743260, 0.72%)
Percent of genome regions (FIB_161)
exon (17745557473, 97.88%)
intron (253136781, 1.40%)
intergenic (131449966, 0.73%)
Percent of genome regions (OLIG_161)
exon (17716333839, 97.49%)
intron (314001586, 1.73%)
intergenic (142434108, 0.78%)
Percent of genome regions (SCR_161)
exon (16418249327, 97.77%)
intron (243542285, 1.45%)
intergenic (131605521, 0.78%)

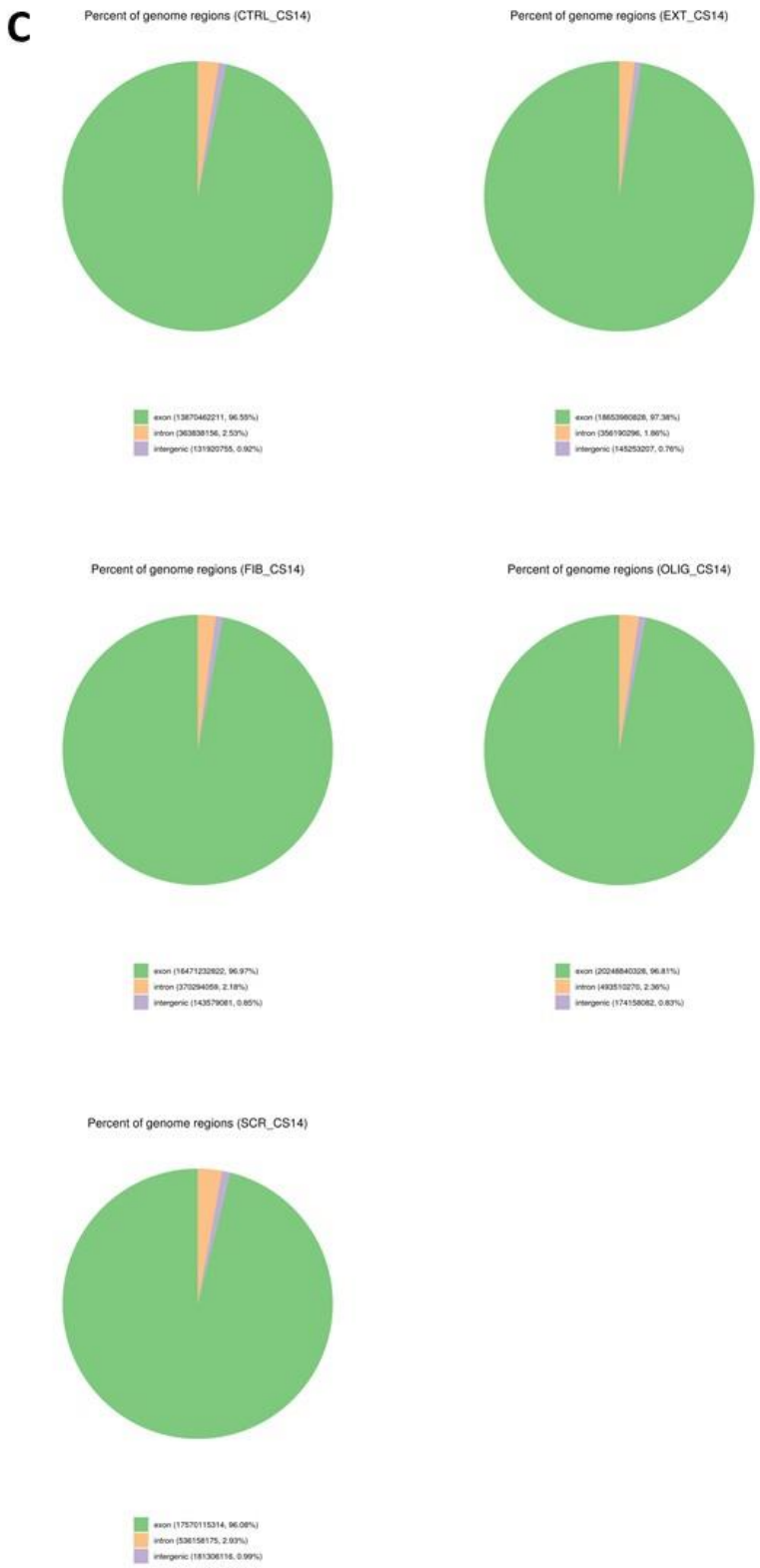


**Figure 4.5.** Percentage genome regions for RNAseq data for all iAstrocyte cell lines and treatments.

**(A)** Genome regions for iAstrocyte cell line 155v2; **(B)** Genome regions for iAstrocyte cell line 161; **(C)** Genome regions for iAstrocyte cell line CS14. Figure provided by Novogene.

### 4.5.4 Principal components analysis

To evaluate the differences in gene expression between the different treatment groups and iAstrocyte cell lines, a principal components analysis (PCA) was carried out. PCA was used to investigate the variation and patterns within the dataset. On the PCA plot, the axes represent principal components, with PC1 and PC2 axes representing data variation between different treatment groups. The variation between the groups can therefore be represented on the PCA plot, where treatment groups in the vicinity of each other do not have much variation in gene expression.

Interestingly, the treatment groups were not the main cause of variation in the gene expression. Instead, the iAstrocyte cell lines were separated, with specific cell lines grouped closely together, displaying a varying gene expression pattern. This meant that the 155v2 cell line was different to 161 cell line and CS14 cell line, and vice versa (fig.4.6). However, PC2 axis revealed that CS14 and 161 cell lines are more closely grouped together, meanwhile 155v2 cell line shows larger variation in comparison to Cs14 and 161 iAstrocytes. The PCA plot also showed that there is not a large intragroup variation for each cell line between the different treatment groups. Hence, the PCA showed that cell line differences may be more important to gene expression changes than amyloid beta treatments, further suggesting that individual cell lines could be affected by amyloid beta in different and unique ways.

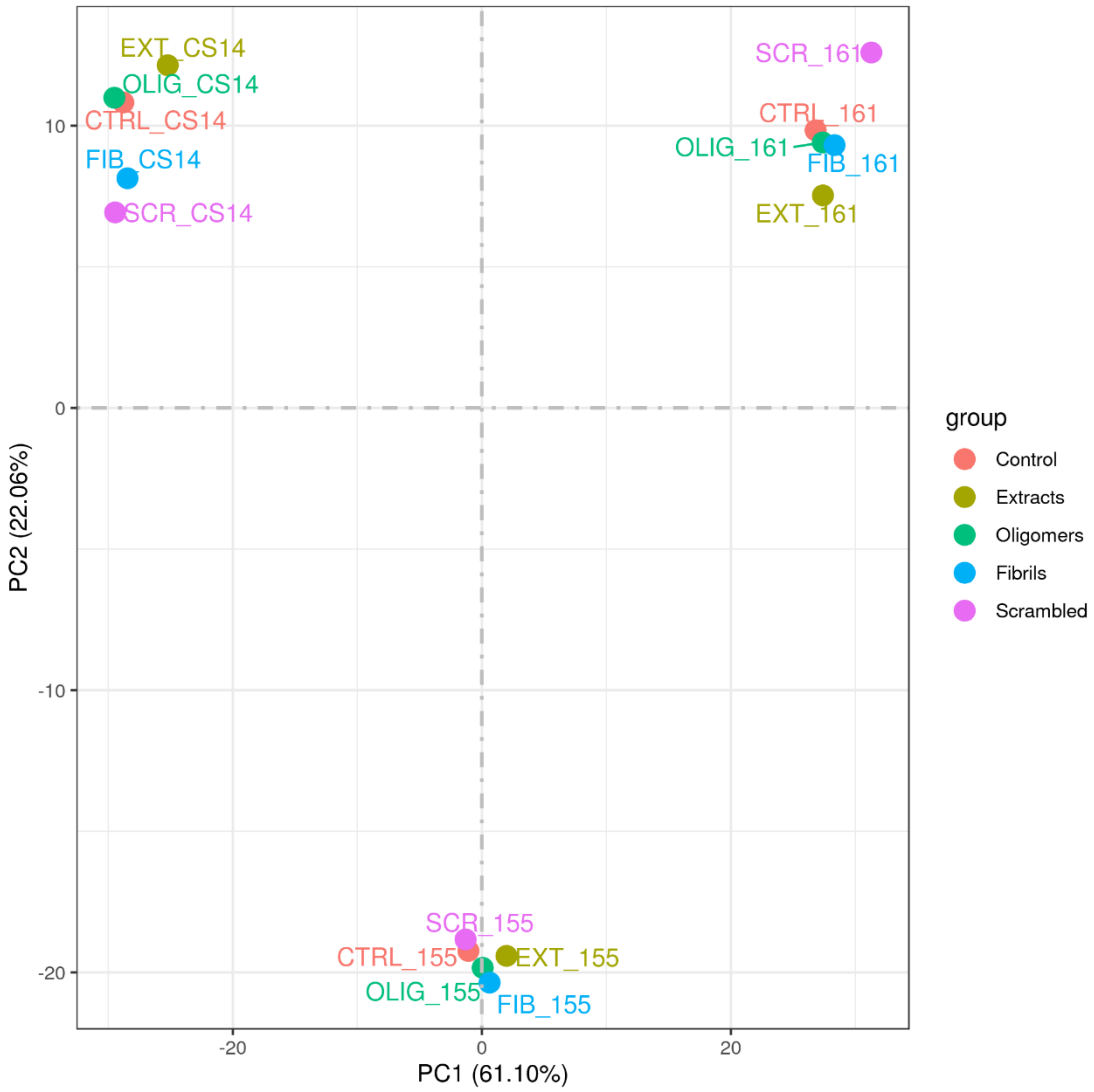


**Figure 4.6**. Principal components analysis for the iAstrocyte cell lines and corresponding cell treatments.

The principal components analysis lot of control lines of iAstrocytes: 155v2, CS14, and 161, and their corresponding cell treatments: untreated control, scrambled vehicle control, extract-treated, oligomer-treated, and fibril-treated. Figure provided by Novogene.

### 4.5.5 Differential expression, pathway enrichment, and gene set enrichment analysis of RNAseq data

For all treatments, a set of gene and pathway enrichment analyses was carried out. The purpose of enrichment analyses was to investigate differentially expressed genes between the treatment groups, and to investigate their associated biological functions or pathways. In order to find the common biological functions of the differentially expressed genes, the genes were gathered based on various pathway databases. Gene Ontology (GO) helps to identify genes relating to similar biological processes, molecular functions, and cellular components (http://geneontology.org/). Kyoto Encyclopedia of Genes and Genomes (KEGG) is a pathway analysis (https://www.genome.jp/kegg/). Meanwhile, Gene Set Enrichment Analysis (GSEA) can help to determine whether a set of genes is statistically significant when investigating the differences between two treatment groups (https://www.gsea-msigdb.org/gsea/index.jsp). Lastly, The Human Disease Ontology (DO, http://www.disease-ontology.org) is a public and community-driven standardized ontology for human diseases.

Differential expression analysis and gene set enrichment analyses were performed on the treated iAstrocytes for each cell line. The purpose of this investigation was to identify genes that were differentially expressed between the different experimental conditions. The experimental comparisons were extracts vs control (untreated); fibrils vs scrambled (vehicle control), oligomers vs scrambled (vehicle control), as well as fibrils vs control (untreated), and oligomers vs control (untreated). However, the oligomer vs scrambled treatment parameter did not result in good quality pathway enrichment analysis and therefore KEGG pathway analysis and GSEA were omitted from the results. The results were split between the different experimental conditions and were interpreted based on the current literature available.

The enrichment pathway analyses are described in detail in this chapter. The upregulation and downregulation of relevant pathways and genes is described in the context of whether the genes are up-, or down- regulated in the amyloid-treated group, in comparison to the untreated control or vehicle control group. All of the results are described as n=3 (biological repeats, n= one cell line), and GSEA results are described for individual cell lines.

## Gene ontology for all iAstrocyte cell treatments

Firstly, a gene ontology analysis was carried out for all of the genes differentially expressed in iAstrocytes. Gene ontology analysis gives a list of genes that were found to be differentially expressed in treated vs control iAstrocytes. A total of 29,960 genes were annotated to the gene ontology (GO) database. Three main ontologies were identified, and these corresponded to biological process, cellular component, and molecular function.

Within the biological process category, the most abundant subcategories of genes were 'biological regulation', 'cellular process', 'metabolic process', 'regulation of biological process', 'response to stimulus', and 'single-organism process', with more than 10,000 genes being associated with those subcategories.

Within the cellular component category, the most abundant subcategories were 'cell', 'cell part', 'membrane', 'organelle', and 'organelle part', with more than 10,000 genes being associated.

Within the molecular function category, the most abundant subcategory was 'binding', with more than 10,000 genes being associated, and this was also the subcategory with the largest number of genes associated (fig. 4.7). Further enrichment pathway analyses were carried out for all iAstrocyte treatment and comparison groups, and the results are discussed in this chapter.

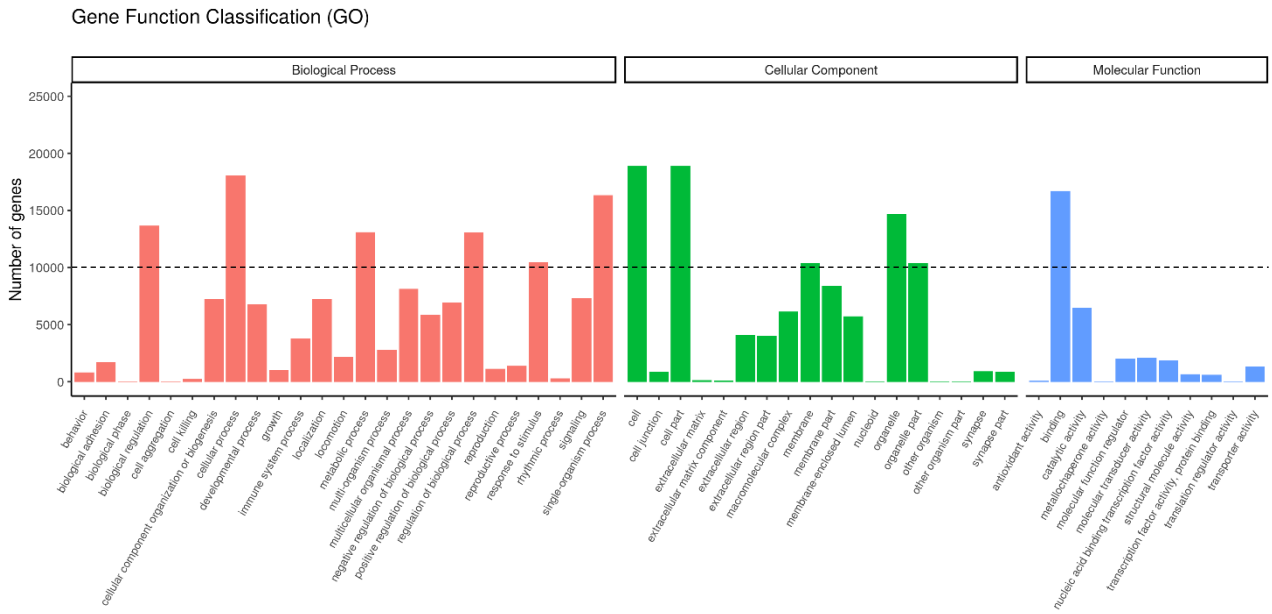


**Figure 4.7** Gene ontology (GO) classification for all iAstrocyte treatments.

A bar chart representing categories of gene transcripts annotated from the RNAseq data of human iAstrocytes. The results are summarised into three categories: biological process, cellular component, and molecular function. Figure provided by Novogene.

### Differentially expressed genes for all iAstrocyte treatment groups

The analysis of differentially expressed genes per each comparison of treatment groups was carried out. The genes are deemed as differentially expressed when a difference observed in read counts between two conditions (in this case treatment groups) is significantly different by the measure of the number of differentially expressed genes. The gene expression analysis included normalisation of read counts, estimation of p-value, and estimation of false rate discovery value. The analysis showed gene counts for statistically significant differentially expressed genes for all iAstrocyte treatment and comparison groups (fig. 4.8). The analysis showed that in the extracts vs control group, there were 173 differentially expressed genes, where 159 were downregulated and 14 were upregulated. In the fibrils vs control group, there were 117 genes differentially expressed, of which 93 were downregulated and 24 were upregulated. In the fibrils vs scrambled group, only 44 genes were differentially expressed, with 26 being downregulated and 18 being upregulated. In the oligomers vs control group, 80 genes were differentially expressed, with 49 being downregulated and 31 being upregulated; and lastly, 76 genes were differentially expressed in the oligomers vs scrambled group, where 27 were downregulated and 51 were upregulated.

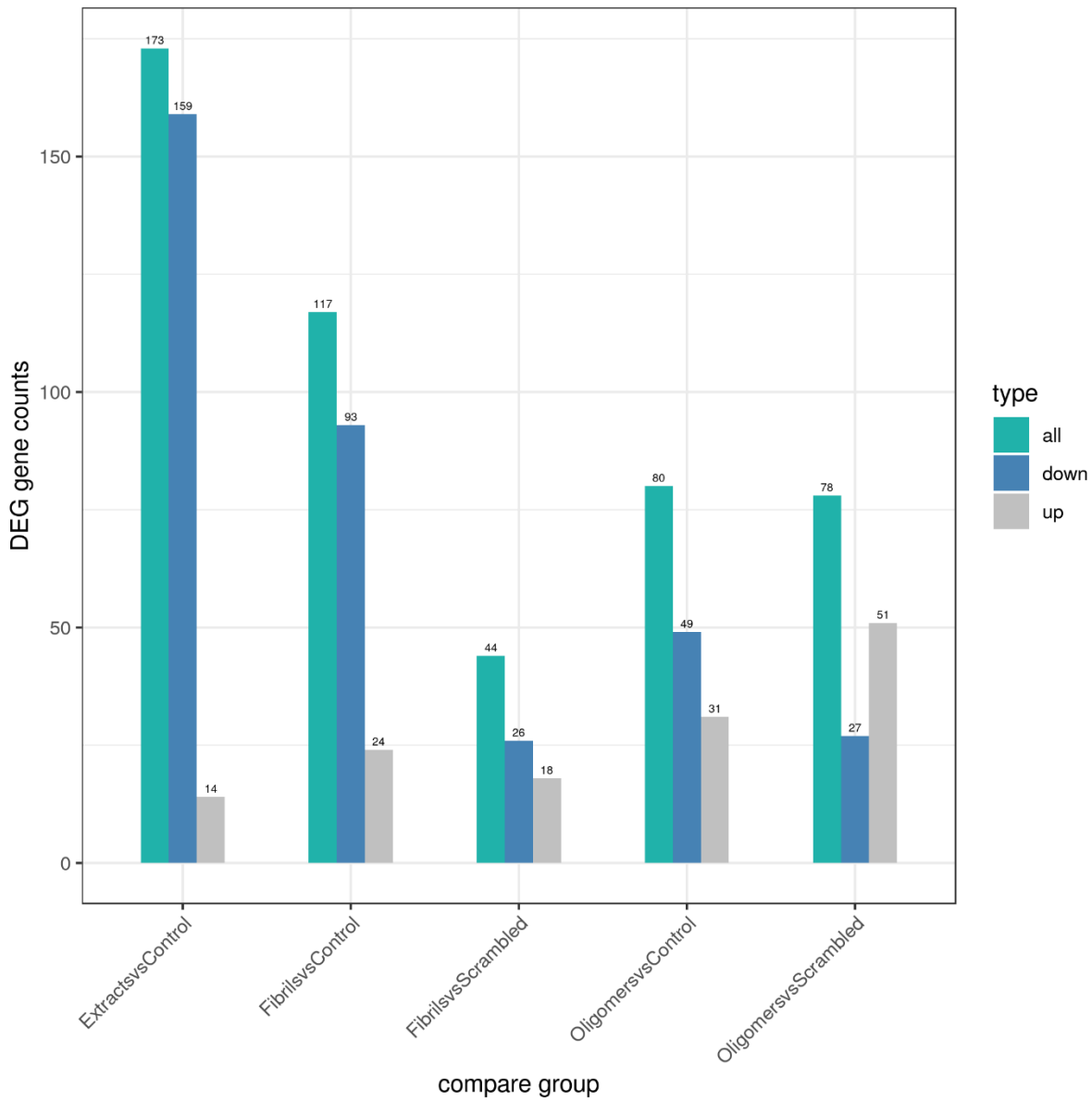


**Figure 4.8** Gene counts for differentially expressed genes (DEG) in all iAstrocyte treatment and comparison groups.

The DEG gene counts are shown for all differentially expressed genes, as well as down- and up-regulated genes per group. The DEG analysis aimed to investigate the number of genes expressed, and the changes, for each treatment group of iAstrocytes. The groups analysed are extracts vs control, fibrils vs control, fibrils vs scrambled, oligomers vs control, oligomers vs scrambled. iAstrocytes were poled together for the analysis, with cell lines 161, Cs14, and 155v2 used. iAstrocytes treated with oligomeric or fibrillary $A\beta_{1-42}$, human-brain extracted Aβ, scrambled vehicle control, or untreated control, for 24 hours. Figure provided by Novogene.

### Extracts vs Control

Gene ontology analysis was carried out to assess which genes are differentially expressed in the iAstrocyte treatment group (Aβ extracts) vs control. The gene ontology analysis revealed that there were no significant GO pathways, and corresponding genes which were differentially expressed between extracts and control groups, after p-value adjustments. However, there was a plethora of significant differentially expressed genes prior to p-value adjustments. These results were classified into three separate gene ontology categories: biological processes, cellular components, and molecular function. The top 10 gene ontology pathways for each gene ontology category, and the corresponding genes were identified (fig.4.9).

Within the biological processes gene ontology category, the only upregulated gene was *SHISA7.* Common, downregulated genes across all pathways were *EPHB2, TBC1D3E, TBC1D3D,* and *SGSM1* (table 4.4).

Within the cellular components gene ontology category, *SHISA7* was again the only upregulated gene, which was also common to two gene ontology pathways (ionotropic glutamate receptor complex and neurotransmitter receptor complex). The highest number of downregulated genes was within the cell-cell junction gene ontology pathway, with 6 genes being downregulated. The other pathways with a high number of downregulated genes were bicellular tight junction, occluding unction, and apical junction complex pathways. Inn all the pathways that had the highest number of downregulated genes, the common genes included *CLDN2, CGN, MARVELD3,* and *CLDN18* (table 4.4).

Within the molecular function gene ontology category, there were no upregulated genes. The downregulated genes included *EPHB2, EPHB6, CDH17, TOMM7, RAB27B,* and *RAB25* (table 4.4).

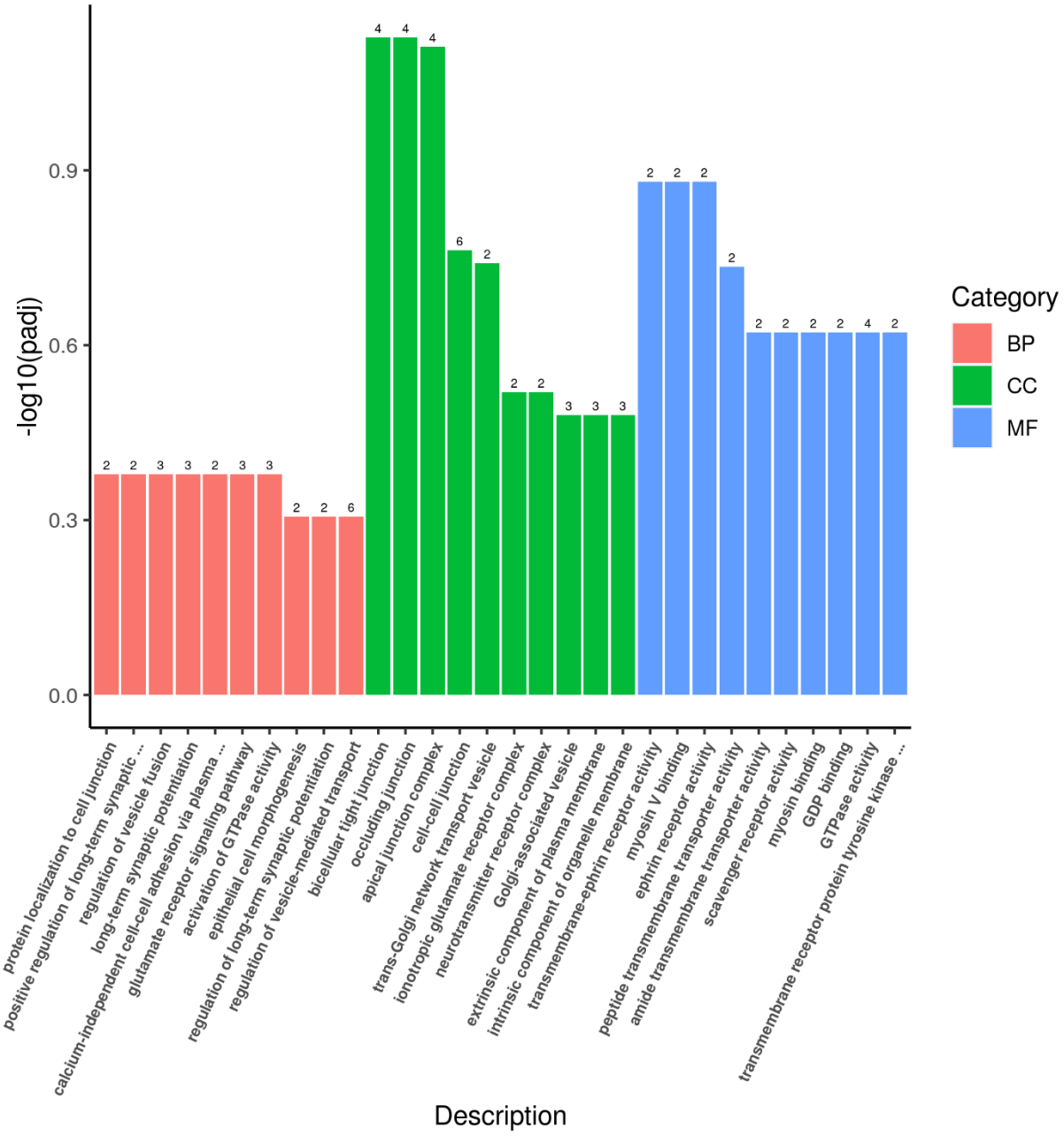


**Figure 4.9** Gene ontology (GO) classification for extracts vs control iAstrocyte treatments.

A bar chart representing Gene ontology subcategories of gene transcripts annotated from the RNAseq data of human iAstrocytes. The results show top 10 significant differently expressed gene ontology pathways, per category, prior to p-value adjustments (BP- biological process; CC- cellular function; MF- molecular function). iAstrocytes were poled together for the analysis, with cell lines 161, Cs14, and 155v2 used. iAstrocytes treated with oligomeric or fibrillary $A\beta_{1-42}$, human-brain extracted Aβ, scrambled vehicle control, or untreated control, for 24 hours. The y-axis shows log value of adjusted p-value. Figure provided by Novogene.

**Table 4.4.** Gene ontology (GO) classification for extracts vs control iAstrocyte treatments.

| Category | Gene ontology ID | Subcategory description | P-value | Adjusted P-value | Upregulated | Gene name | Downregulated | Gene name |
|---|---|---|---|---|---|---|---|---|
| BP | GO:1902414 | protein localization to cell junction | 0.000557373 | 0.418826852 | 0 | | 2 | *DSP/MARVELD3* |
| BP | GO:1900273 | positive regulation of long-term synaptic potentiation | 0.001465967 | 0.418826852 | 1 | *SHISA7* | 1 | *EPHB2* |
| BP | GO:0031338 | regulation of vesicle fusion | 0.001485884 | 0.418826852 | 0 | | 3 | *TBC1D3E/TBC1D3D/SGSM1* |
| BP | GO:0060291 | long-term synaptic potentiation | 0.001774475 | 0.418826852 | 1 | *SHISA7* | 2 | *EPHB2/GRIN2C* |
| BP | GO:0016338 | calcium-independent cell-cell adhesion via plasma membrane cell-adhesion molecules | 0.002299896 | 0.418826852 | 0 | | 2 | *CLDN2/CLDN18* |
| BP | GO:0007215 | glutamate receptor signaling pathway | 0.002841894 | 0.418826852 | 1 | *SHISA7* | 2 | *EPHB2/GRIN2C* |
| BP | GO:0090630 | activation of GTPase activity | 0.003050768 | 0.418826852 | 0 | | 3 | *TBC1D3E/TBC1D3D/SGSM1* |
| BP | GO:0003382 | epithelial cell morphogenesis | 0.005146234 | 0.493828164 | 0 | | 2 | *ST14/RAB25* |
| BP | GO:1900271 | regulation of long-term synaptic potentiation | 0.005146234 | 0.493828164 | 1 | *SHISA7* | 1 | *EPHB2* |
| BP | GO:0060627 | regulation of vesicle-mediated transport | 0.005340394 | 0.493828164 | 0 | | 6 | *TBC1D3E/TBC1D3D/RAB25/RAB27B/SGSM1/TRPV6* |
| CC | GO:0005923 | bicellular tight junction | 0.000878866 | 0.074497952 | 0 | | 4 | *CLDN2/CGN/MARVELD3/CLDN18* |
| CC | GO:0070160 | occluding junction | 0.000967506 | 0.074497952 | 0 | | 4 | *CLDN2/CGN/MARVELD3/CLDN18* |
| CC | GO:0043296 | apical junction complex | 0.001507006 | 0.077359663 | 0 | | 4 | *CLDN2/CGN/MARVELD3/CLDN18* |
| CC | GO:0005911 | cell-cell junction | 0.004487713 | 0.172776951 | 0 | | 6 | *DSP/CLDN2/CD53/CGN/MARVELD3/CLDN18* |
| CC | GO:0030140 | trans-Golgi network transport vesicle | 0.005905509 | 0.181889682 | 0 | | 2 | *STEAP2/RAB27B* |
| CC | GO:0008328 | ionotropic glutamate receptor complex | 0.012684006 | 0.30268256 | 1 | *SHISA7* | 1 | *GRIN2C* |
| CC | GO:0098878 | neurotransmitter receptor complex | 0.013758298 | 0.30268256 | 1 | *SHISA7* | 1 | *GRIN2C* |
| CC | GO:0005798 | Golgi-associated vesicle | 0.021711613 | 0.331274985 | 0 | | 3 | *STEAP2/RAB27B/GNRH1* |
| CC | GO:0019897 | extrinsic component of plasma membrane | 0.022424601 | 0.331274985 | 0 | | 3 | *ST14/NLRP10/PRSS22* |
| CC | GO:0031300 | intrinsic component of organelle membrane | 0.032850137 | 0.331274985 | 0 | | 3 | *STEAP2/RAB27B/TOMM7* |
| MF | GO:0005005 | transmembrane-ephrin receptor activity | 0.001772028 | 0.131571393 | 0 | | 2 | *EPHB2/EPHB6* |
| MF | GO:0031489 | myosin V binding | 0.001772028 | 0.131571393 | 0 | | 2 | *RAB25/RAB27B* |
| MF | GO:0005003 | ephrin receptor activity | 0.002217495 | 0.131571393 | 0 | | 2 | *EPHB2/EPHB6* |
| MF | GO:1904680 | peptide transmembrane transporter activity | 0.004145057 | 0.184455016 | 0 | | 2 | *CDH17/TOMM7* |
| MF | GO:0042887 | amide transmembrane transporter activity | 0.009164145 | 0.239128903 | 0 | | 2 | *CDH17/TOMM7* |
| MF | GO:0005044 | scavenger receptor activity | 0.015903359 | 0.239128903 | 0 | | 2 | *SCART1/SBSPON* |
| MF | GO:0017022 | myosin binding | 0.019547083 | 0.239128903 | 0 | | 2 | *RAB25/RAB27B* |
| MF | GO:0019003 | GDP binding | 0.019547083 | 0.239128903 | 0 | | 2 | *RAB27B/RASEF* |
| MF | GO:0003924 | GTPase activity | 0.020216573 | 0.239128903 | 0 | | 4 | *NLRP10/RAB25/RAB27B/RASEF* |
| MF | GO:0004714 | transmembrane receptor protein tyrosine kinase activity | 0.024892577 | 0.239128903 | 0 | | 2 | *EPHB2/EPHB6* |

A table showing the category, subcategory description, corresponding gene ontology ID, p-value, adjusted p-value, gene count, number of upregulated and downregulated genes, and associated gene names.

The GSEA was performed on all differentially expressed genes in the iAstrocyte extracts vs control treatments. The GSEA produced a heatmap, which shows the clustered genes and their expression values as represented by colours (red = high expression value; blue = low expression value).

The GSEA heatmap showed a differential expression of many genes (fig.4.10). Within those, based on the literature search carried out, there were 5 genes of interest which were upregulated in iAstrocytes treated with amyloid beta extracts. These were *SHISA7, STX11,* and *MIRLET7I.* There were also 3 genes of interest which were downregulated in iAstrocytes treated with amyloid beta extracts. These were *CASP12, IL17C, CXCL17.*

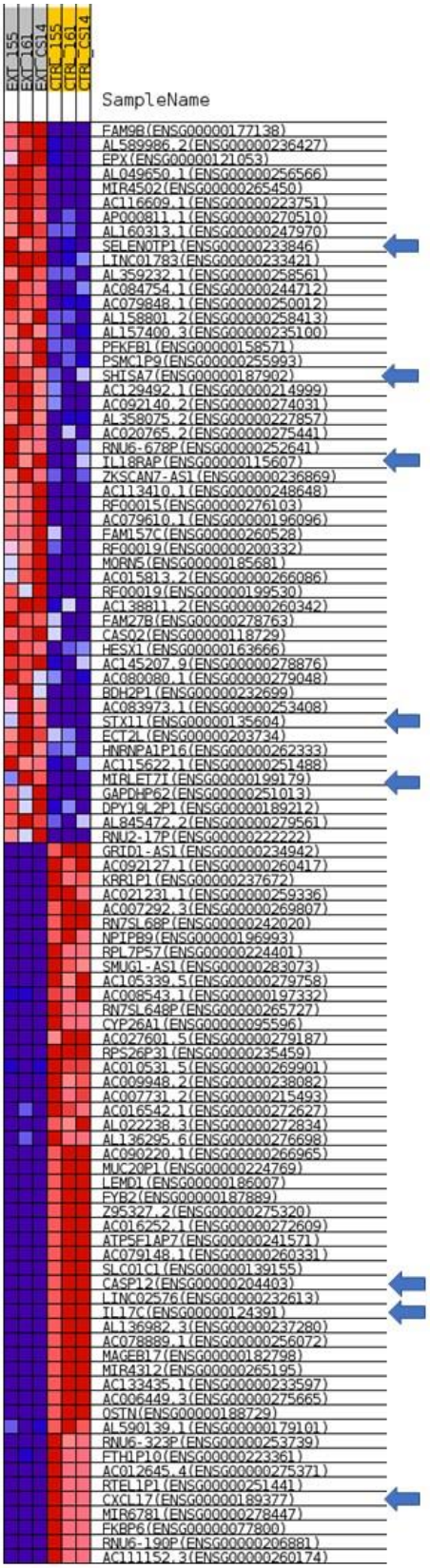


**Figure 4.10** Gene set enrichment analysis (GSEA) heatmap representing differentially expressed genes in iAstrocyte extracts vs control treatment group.

The GSEA represents the top differentially expressed genes identified. The analysis was separated to look at each cell line individually. The genes of interest are marked with arrows. Red= upregulated; blue= downregulated. Figure provided by Novogene, annotated for clarity.

Next, the KEGG pathway analysis was performed. No significantly expressed genes and pathways were found for the extracts vs control treatment group, when the p-value was adjusted. However, when investigating the p-values prior to adjustments, there were significantly expressed genes and pathways. The top 20 significant pathways (non-adjusted p-value) are shown (fig.4.11). Within those, a few genes of interest were identified (table 4.5).

The KEGG pathway analysis revealed no upregulated genes within the top 20 pathways. However, there were a few downregulated genes in each pathway. The pathway with the highest number of downregulated genes was 'tight junction', which showed a downregulation of 4 genes- *CLDN2, CGN, MARVELD3*, and *CLDN18. CLDN2* and *CLDN18* are genes which were often repeated in various differentially expressed pathways. Other pathways of interest and the corresponding genes could be 'amyotrophic lateral sclerosis', as well as 'calcium signalling' with a downregulation of *GRIN2C*.

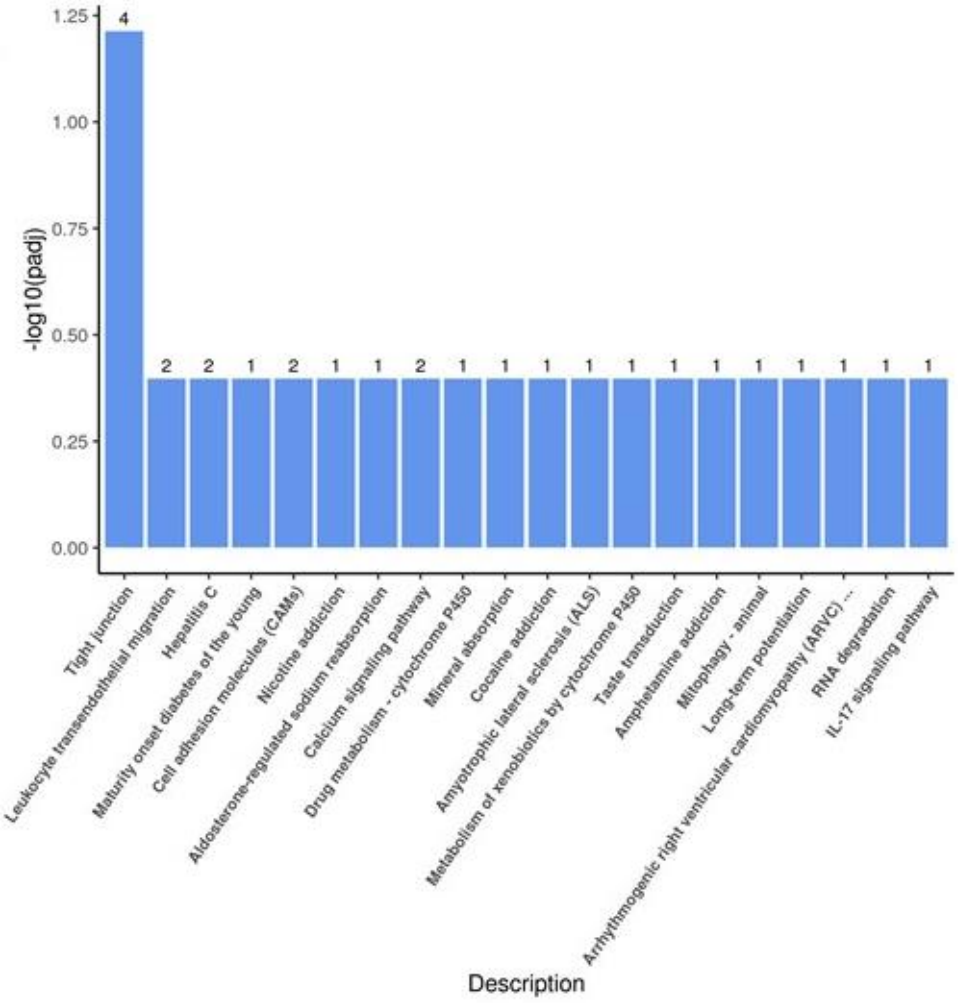


**Figure 4.11** KEGG pathway analysis for extracts vs control iAstrocyte treatments.

A bar chart representing categories of top 20 significant differentially expressed pathways, prior to p-value adjustments. Figure provided by Novogene.

**Table 4.5.** KEGG pathway analysis for extracts vs control iAstrocyte treatments

| KEGGID | Description | P-value | Adjusted P-value | Upregulated | Gene name | Downregulated | Gene name |
|---|---|---|---|---|---|---|---|
| hsa04530 | Tight junction | 0.00152976 | 0.061190468 | 0 | | 4 | *CLDN2/CGN/MARVELD3/CLDN18* |
| hsa04670 | Leukocyte transendothelial migration | 0.0480217 | 0.400450399 | 0 | | 2 | *CLDN2/CLDN18* |
| hsa05160 | Hepatitis C | 0.05138741 | 0.400450399 | 0 | | 2 | *CLDN2/CLDN18* |
| hsa04950 | Maturity onset diabetes of the young | 0.05316859 | 0.400450399 | 0 | | 1 | *HNF4A* |
| hsa04514 | Cell adhesion molecules (CAMs) | 0.05659267 | 0.400450399 | 0 | | 2 | *CLDN2/CLDN18* |
| hsa05033 | Nicotine addiction | 0.10363804 | 0.400450399 | 0 | | 1 | *GRIN2C* |
| hsa04960 | Aldosterone-regulated sodium reabsorption | 0.1097635 | 0.400450399 | 0 | | 1 | *SCNN1B* |
| hsa04020 | Calcium signaling pathway | 0.11276126 | 0.400450399 | 0 | | 2 | *PHKG1/GRIN2C* |
| hsa00982 | Drug metabolism - cytochrome P450 | 0.13979754 | 0.400450399 | 0 | | 1 | *CYP2D6* |
| hsa04978 | Mineral absorption | 0.14274728 | 0.400450399 | 0 | | 1 | *STEAP2* |
| hsa05030 | Cocaine addiction | 0.14274728 | 0.400450399 | 0 | | 1 | *GRIN2C* |
| hsa05014 | Amyotrophic lateral sclerosis (ALS) | 0.15153883 | 0.400450399 | 0 | | 1 | *GRIN2C* |
| hsa00980 | Metabolism of xenobiotics by cytochrome P450 | 0.15735209 | 0.400450399 | 0 | | 1 | *CYP2D6* |
| hsa04742 | Taste transduction | 0.1660009 | 0.400450399 | 0 | | 1 | *SCNN1B* |
| hsa05031 | Amphetamine addiction | 0.19144297 | 0.400450399 | 0 | | 1 | *GRIN2C* |
| hsa04137 | Mitophagy - animal | 0.1969955 | 0.400450399 | 0 | | 1 | *TOMM7* |
| hsa04720 | Long-term potentiation | 0.1969955 | 0.400450399 | 0 | | 1 | *GRIN2C* |
| hsa05412 | Arrhythmogenic right ventricular cardiomyopathy (ARVC) | 0.21343604 | 0.400450399 | 0 | | 1 | *DSP* |
| hsa03018 | RNA degradation | 0.22153561 | 0.400450399 | 0 | | 1 | *PABPC1L* |
| hsa04657 | IL-17 signaling pathway | 0.22421777 | 0.400450399 | 0 | | 1 | *MUC5AC* |

A table showing the KEGG pathway ID, pathway description, p-value, adjusted p-value, upregulated and downregulated genes, and the corresponding gene names.

Lastly, the Human Disease Ontology (DO) analysis was carried out on the differentially expressed genes for iAstrocyte extracts vs control treatment group. The analysis revealed that when the adjusted p-value was applied, there were no significant genes which were differentially expressed. However, prior to p-value adjustment, there were significant differentially expressed genes present. The top 20 genes are shown (fig.4.12). The top 20 pathways included a lot of cancer-associated pathways, however there were some which were relating to inflammation or neurodegeneration, such as pathways relating to infections and disease, as well as a pathway relating to Lewy body dementia (table 4.6).

Within the top 20 pathways, several genes of interest were identified. Namely, *EPX* gene and *U2AF1* gene were repeatedly upregulated across the different DO pathways. For the downregulated genes, the common genes across all pathways were *MUC5AC, CDH17, EPHB2,* and *CYP2D6.*

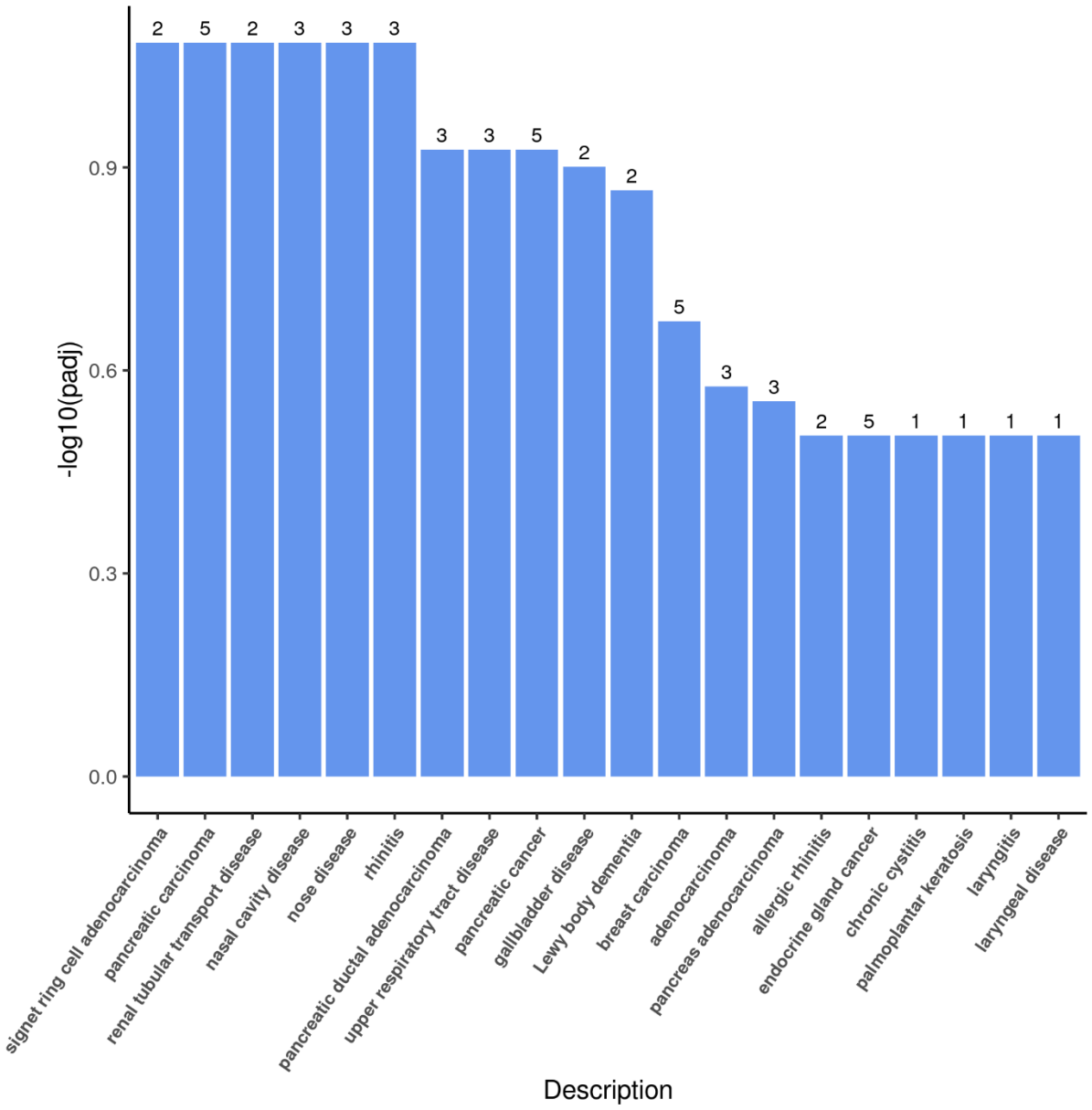


**Figure 4.12** The human disease ontology (DO) analysis for extracts vs control iAstrocyte treatments.

A bar chart representing categories of top 20 significant differentially expressed pathways, prior to p-value adjustments. Figure provided by Novogene.

**Table 4.6.** The human disease ontology (DO) analysis for extracts vs control iAstrocyte treatments.

| DOID | Description | P-value | Adjusted P-value | Upregulated | Gene name | Downregulated | Gene name |
|---|---|---|---|---|---|---|---|
| DOID:3493 | signet ring cell adenocarcinoma | 0.00071721 | 0.082367923 | 0 | | 2 | *MUC5AC/CLDN18* |
| DOID:4905 | pancreatic carcinoma | 0.00171919 | 0.082367923 | 1 | *U2AF1* | 4 | *ST14/CDH17/MUC5AC/EPHB2* |
| DOID:447 | renal tubular transport disease | 0.00238945 | 0.082367923 | 0 | | 2 | *SLC5A2/SCNN1B* |
| DOID:2163 | nasal cavity disease | 0.00294171 | 0.082367923 | 1 | *EPX* | 2 | *MUC5AC/CYP2D6* |
| DOID:2825 | nose disease | 0.00294171 | 0.082367923 | 1 | *EPX* | 2 | *MUC5AC/CYP2D6* |
| DOID:4483 | rhinitis | 0.00294171 | 0.082367923 | 1 | *EPX* | 2 | *MUC5AC/CYP2D6* |
| DOID:3498 | pancreatic ductal adenocarcinoma | 0.00610218 | 0.118420679 | 0 | | 3 | *ST14/CDH17/MUC5AC* |
| DOID:974 | upper respiratory tract disease | 0.00628836 | 0.118420679 | 1 | *EPX* | 2 | *MUC5AC/CYP2D6* |
| DOID:1793 | pancreatic cancer | 0.00634396 | 0.118420679 | 1 | *U2AF1* | 4 | *ST14/CDH17/MUC5AC/EPHB2* |
| DOID:0060262 | gallbladder disease | 0.00747619 | 0.12559993 | 0 | | 2 | *CLDN2/MUC5AC* |
| DOID:12217 | Lewy body dementia | 0.00890061 | 0.135936621 | 0 | | 2 | *CHAT/CYP2D6* |
| DOID:3459 | breast carcinoma | 0.01517102 | 0.212394293 | 0 | | 5 | *CLDN2/MUC5AC/EPHB6/CYP2D6/TRPV6* |
| DOID:299 | adenocarcinoma | 0.02054654 | 0.265524478 | 0 | | 3 | *CLDN2/MUC5AC/CLDN18* |
| DOID:4074 | pancreas adenocarcinoma | 0.02326636 | 0.279196263 | 0 | | 3 | *ST14/CDH17/MUC5AC* |
| DOID:4481 | allergic rhinitis | 0.03221336 | 0.313807484 | 1 | *EPX* | 1 | *MUC5AC* |
| DOID:170 | endocrine gland cancer | 0.03851353 | 0.313807484 | 1 | *U2AF1* | 4 | *ST14/CDH17/MUC5AC/EPHB2* |
| DOID:1680 | chronic cystitis | 0.04034321 | 0.313807484 | 0 | | 1 | *MUC5AC* |
| DOID:3390 | palmoplantar keratosis | 0.04034321 | 0.313807484 | 0 | | 1 | *DSP* |
| DOID:3437 | laryngitis | 0.04034321 | 0.313807484 | 0 | | 1 | *MUC5AC* |
| DOID:786 | laryngeal disease | 0.04034321 | 0.313807484 | 0 | | 1 | *MUC5AC* |

A table showing the DO ID, pathway description, p-value, adjusted p-value, upregulated and downregulated genes, and the corresponding gene names.

### Fibrils vs Control

As previously, gene ontology analysis was performed first. When the adjusted p-value was considered, there were no significant differentially expressed pathways in the iAstrocyte treatment group fibrils vs control. However, when looking at the p-value prior to adjustment, significant differentially expressed pathways and genes were found. The top 10 pathways for each gene ontology category are shown (fig.4.13).

Within the biological processes gene ontology category, there was a repeated upregulation of the gene *PI3.* Meanwhile, most genes within this category were downregulated. The most common downregulated genes were *DSP, MARVELD3, ST14, GRHL3.*

Within the cellular components gene ontology category, there were three upregulated genes, which were *PI3, GIMAP2*, and *CDCD4A*. Within the downregulated genes of the cellular components category, repeated downregulated genes were found. These were *MARVELD3, CLDN2, CLDN18,* and *RAB27B. RAB27B* was a gene associated with the synaptic vesicle, and exocytic vesicle pathways.

Within the molecular function gene ontology category, the most common upregulated genes were *MMP1* and *MMP13.* The most common downregulated genes were *PRSS22* and *ST14.* The pathways of interest within the molecular function category were neurotransmitter receptor activity, metal ion transmembrane transporter activity, and glutamate binding pathways. The genes associated with those pathways were *CHRM5, GRIN2C, SLC1A3,* and *SLC39A5* (all downregulated) respectively; as well as *CACNA1S* (upregulated) in the metal ion transmembrane transporter activity pathway.

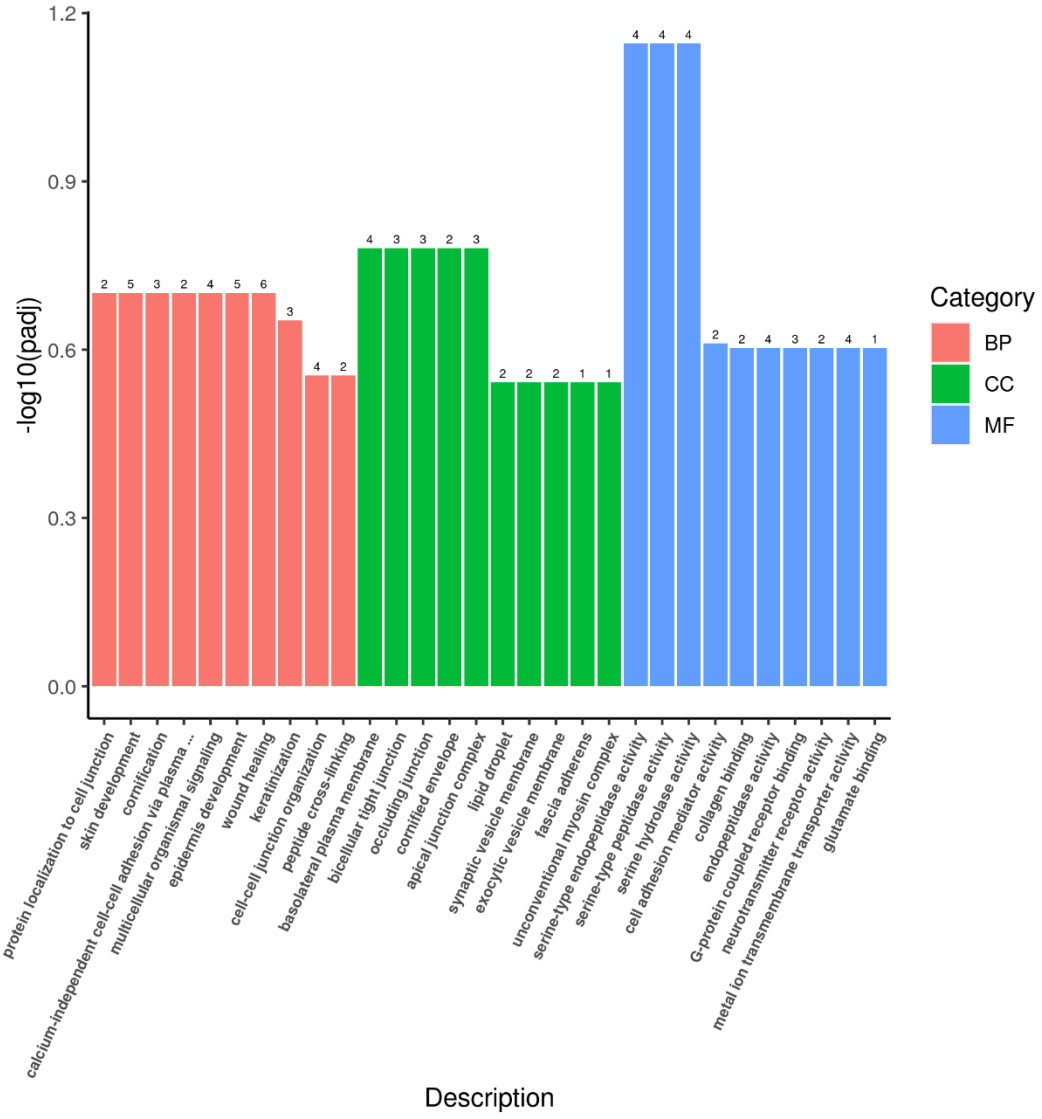


**Figure 4.13.** Gene ontology (GO) classification for fibrils vs control iAstrocyte treatments

A bar chart representing subcategories of gene transcripts annotated from the RNAseq data of human iAstrocytes. The results show top 10 significant differently expressed gene ontology pathways, per category, prior to p-value adjustments (BP- biological process; CC- cellular function; MF- molecular function). Figure provided by Novogene.

**Table 4.7.** Gene ontology (GO) classification for fibrils vs control iAstrocyte treatments.

| Category | Gene ontology ID | Subcategory description | P-value | Adjusted P-value | Upregulated | Gene name | Downregulated | Gene name |
|---|---|---|---|---|---|---|---|---|
| BP | GO:1902414 | protein localization to cell junction | 0.000287987 | 0.199194545 | 0 | | 2 | *DSP/MARVELD3* |
| BP | GO:0043588 | skin development | 0.00064465 | 0.199194545 | 1 | *PI3* | 4 | *DSP/ST14/GRHL3/LGR5* |
| BP | GO:0070268 | cornification | 0.000836865 | 0.199194545 | 1 | *PI3* | 2 | *DSP/ST14* |
| BP | GO:0016338 | calcium-independent cell-cell adhesion via plasma membrane cell-adhesion molecules | 0.001078413 | 0.199194545 | 0 | | 2 | *CLDN2/CLDN18* |
| BP | GO:0035637 | multicellular organismal signaling | 0.00120248 | 0.199194545 | 1 | *CACNA1S* | 3 | *DSP/CHRM5/NPPA* |
| BP | GO:0008544 | epidermis development | 0.001207426 | 0.199194545 | 1 | *PI3* | 4 | *DSP/ST14/GRHL3/LGR5* |
| BP | GO:0042060 | wound healing | 0.001372403 | 0.199194545 | 1 | *SAA1* | 5 | *DSP/GRHL3/ODAM/HNF4A/TSPAN8* |
| BP | GO:0031424 | keratinization | 0.001754135 | 0.22277513 | 1 | *PI3* | 2 | *DSP/ST14* |
| BP | GO:0045216 | cell-cell junction organization | 0.002826734 | 0.27909938 | 0 | | 4 | *DSP/CDH17/INAVA/MARVELD3* |
| BP | GO:0018149 | peptide cross-linking | 0.003254844 | 0.27909938 | 1 | *PI3* | 1 | *DSP* |
| CC | GO:0016323 | basolateral plasma membrane | 0.002211953 | 0.165726274 | 0 | | 4 | *DSP/CDH17/ST14/SLC39A* |
| CC | GO:0005923 | bicellular tight junction | 0.004341668 | 0.165726274 | 0 | | 3 | *MARVELD3/CLDN2/CLDN18* |
| CC | GO:0070160 | occluding junction | 0.004668536 | 0.165726274 | 0 | | 3 | *MARVELD3/CLDN2/CLDN18* |
| CC | GO:0001533 | cornified envelope | 0.005376269 | 0.165726274 | 1 | *PI3* | 1 | *DSP* |
| CC | GO:0043296 | apical junction complex | 0.006524656 | 0.165726274 | 0 | | 3 | *MARVELD3/CLDN2/CLDN18* |
| CC | GO:0005811 | lipid droplet | 0.018370198 | 0.287128126 | 1 | *GIMAP2* | 1 | *PLIN4* |
| CC | GO:0030672 | synaptic vesicle membrane | 0.02672351 | 0.287128126 | 1 | *C2CD4A* | 1 | *RAB27B* |
| CC | GO:0099501 | exocytic vesicle membrane | 0.02672351 | 0.287128126 | 1 | *C2CD4A* | 1 | *RAB27B* |
| CC | GO:0005916 | fascia adherens | 0.028534921 | 0.287128126 | 0 | | 1 | *DSP* |
| CC | GO:0016461 | unconventional myosin complex | 0.028534921 | 0.287128126 | 0 | | 1 | *MYO18B* |
| MF | GO:0004252 | serine-type endopeptidase activity | 0.000562173 | 0.071491766 | 2 | *MMP1/MMP13* | 2 | *ST14/PRSS22* |
| MF | GO:0008236 | serine-type peptidase activity | 0.001096485 | 0.071491766 | 2 | *MMP1/MMP13* | 2 | *ST14/PRSS22* |
| MF | GO:0017171 | serine hydrolase activity | 0.001198186 | 0.071491766 | 2 | *MMP1/MMP13* | 2 | *ST14/PRSS22* |
| MF | GO:0098631 | cell adhesion mediator activity | 0.005465449 | 0.244578827 | 0 | | 2 | *DSP/ITGA10* |
| MF | GO:0005518 | collagen binding | 0.012361203 | 0.249593705 | 1 | *MMP13* | 1 | *ITGA10* |
| MF | GO:0004175 | endopeptidase activity | 0.015224029 | 0.249593705 | 2 | *MMP1/MMP13* | 2 | *ST14/PRSS22* |
| MF | GO:0001664 | G-protein coupled receptor binding | 0.019727325 | 0.249593705 | 2 | *SAA1/CXCL8* | 1 | *NPPA* |
| MF | GO:0030594 | neurotransmitter receptor activity | 0.023128924 | 0.249593705 | 0 | | 2 | *CHRM5/GRIN2C* |
| MF | GO:0046873 | metal ion transmembrane transporter activity | 0.027305122 | 0.249593705 | 1 | *CACNA1S* | 3 | *GRIN2C/SLC1A3/SLC39A* |
| MF | GO:0016595 | glutamate binding | 0.027364307 | 0.249593705 | 0 | | 1 | *SLC1A3* |

A table showing the category, subcategory description, corresponding gene ontology ID, p-value, adjusted p-value, gene count, number of upregulated and downregulated genes, and associated gene names.

Next, a GSEA was carried out on all differentially expressed genes in the iAstrocyte fibrils vs control treatments. As previously, the GSEA produced a heatmap, showing the clustered genes and their expression values as represented by different colours. There were no significantly differential genes between the two treatment groups, based on the adjusted p-value. However, multiple genes of significance were found prior to p-value adjustment.

The GSEA heatmap has shown a differential expression of many genes, the top differentially expressed genes are shown (fig.4.14). Based on the literature search, 5 genes of interest were identified. These genes were upregulated in the fibril-treated group and downregulated in the untreated control group. The genes of interest were *CLTRN, GUCY1B1, GIMAP2, RAB41.*

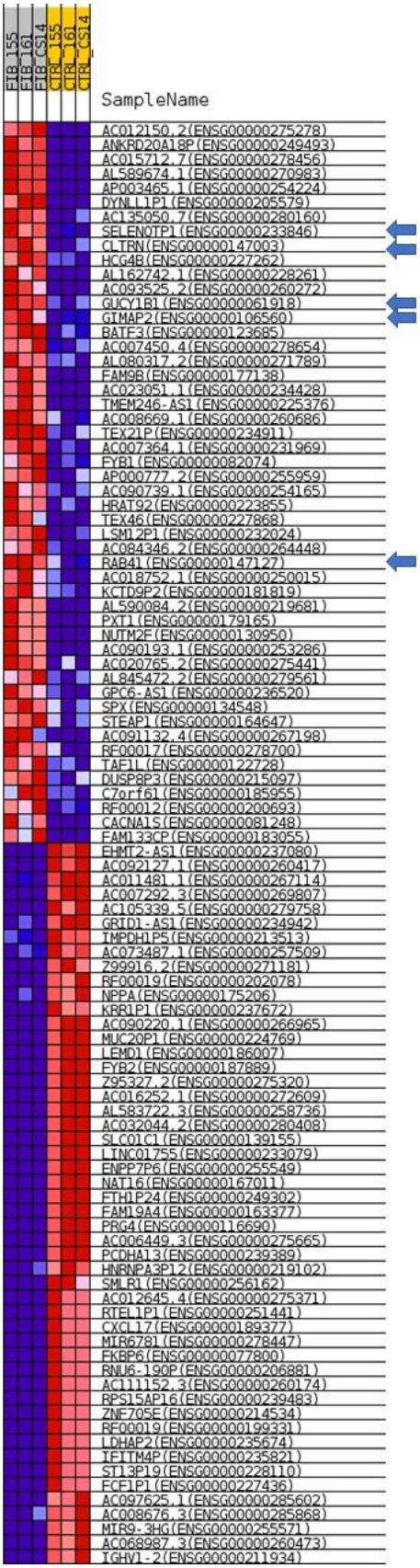


**Figure 4.14.** Gene set enrichment analysis (GSEA) heatmap representing differentially expressed genes in iAstrocyte fibrils vs control treatment group.

The GSEA represents the top differentially expressed genes identified. The analysis was separated to look at each cell line individually. The genes of interest are marked with arrows. Red= upregulated; blue= downregulated. Figure provided by Novogene.

KEGG pathway analysis was also performed on the iAstrocyte treatment group fibrils vs controls. The analysis showed one pathway which was significant when considering adjusted p-value as well as considering the p-value prior to adjustment. This was the IL-17 signalling pathway (P-value= 0.00013; adjusted P-value= 0.010665). This pathway was included when selecting the top 20 pathways that were differentially expressed (fig.4.15).

The KEGG pathway analysis showed differentially expressed genes across the different pathways (table 4.8). The IL-17 signalling pathway showed three significantly upregulated genes (*MMP1, CXCL8,* and *MMP13*); as well as one significantly downregulated gene (*MUC5AC*). The *MMP1* and *CXCL8* genes were also found to be upregulated across the different pathways. Other genes of interest were included in the Alzheimer's disease pathway, and these included an upregulation of the *CACNA1S* gene, as well as a downregulation of *GRIN2C* gene. The *GRIN2C* gene was also downregulated across different pathways. Moreover, *CACNA1S* gene was upregulated across the different pathways. Previously identified genes of interest, *CLDN2, CLDN18,* and *MARVELD3* were also downregulated in the iAstrocyte fibril vs control treatment group.

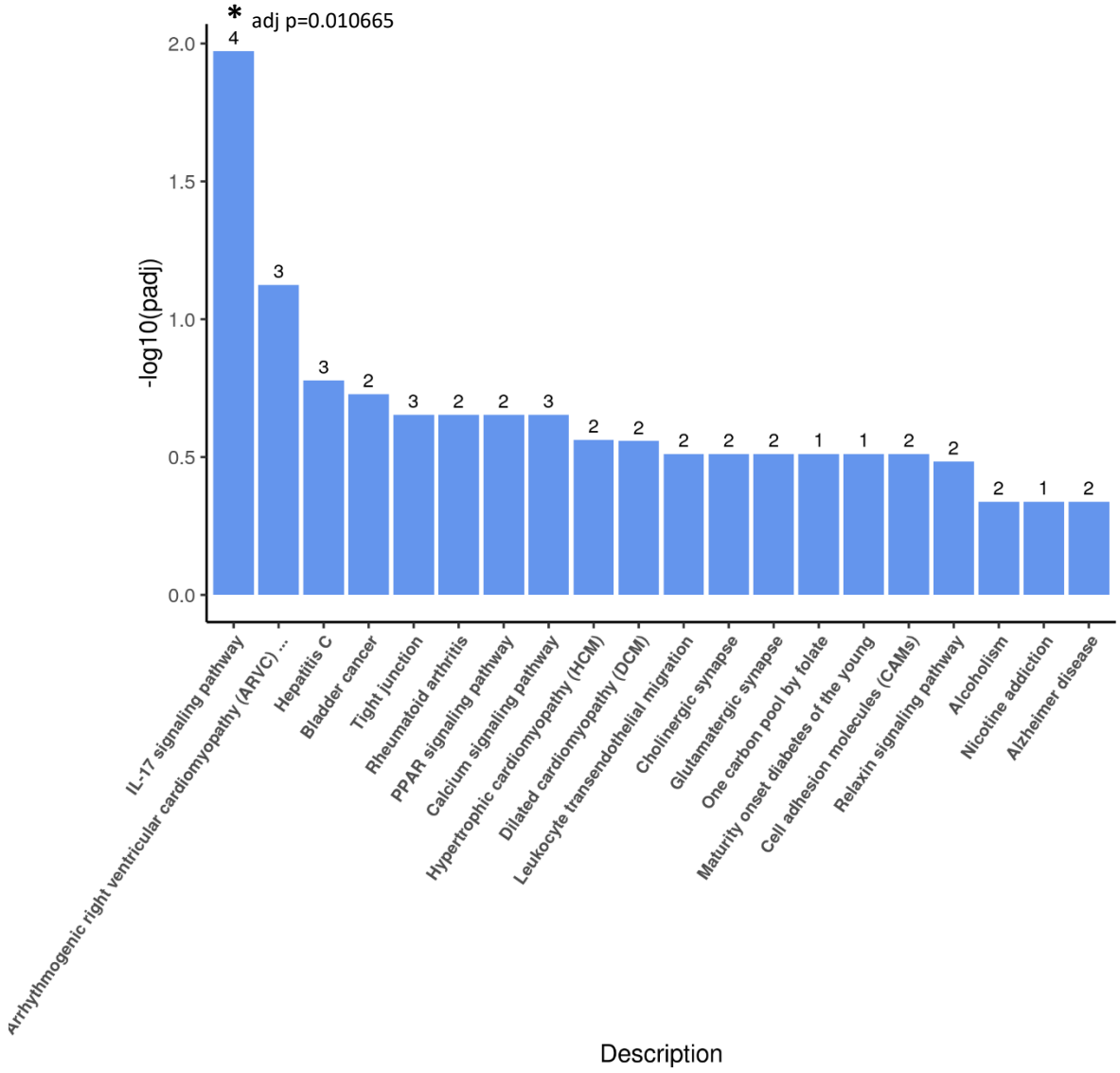


**Figure 4.15.** KEGG pathway analysis for fibrils vs control iAstrocyte treatments.

A bar chart representing categories of top 20 differentially expressed pathways. Figure provided by Novogene. Annotations made separately.

**Table 4.8.** KEGG pathway analysis for fibrils vs control iAstrocyte treatments.

| KEGGID | Description | P-value | Adjusted P-value | Upregulated | Gene name | Downregulated | Gene name |
|---|---|---|---|---|---|---|---|
| hsa04657 | IL-17 signaling pathway | 0.00013006 | 0.010664889 | 3 | *MMP1/CXCL8/MMP13* | 1 | *MUC5AC* |
| hsa05412 | Arrhythmogenic right ventricular cardiomyopathy (ARVC) | 0.001830967 | 0.075069652 | 1 | *CACNA1S* | 2 | *DSP/ITGA10* |
| hsa05160 | Hepatitis C | 0.006097199 | 0.166656783 | 1 | *CXCL8* | 2 | *CLDN2/CLDN18* |
| hsa05219 | Bladder cancer | 0.009101625 | 0.186583319 | 2 | *MMP1/CXCL8* | 0 | |
| hsa04530 | Tight junction | 0.01617614 | 0.222581363 | 0 | | 3 | *MARVELD3/CLDN 2/CLDN18* |
| hsa05323 | Rheumatoid arthritis | 0.020066149 | 0.222581363 | 2 | *MMP1/CXCL8* | 0 | |
| hsa03320 | PPAR signaling pathway | 0.020679798 | 0.222581363 | 1 | *MMP1* | 1 | *PLIN4* |
| hsa04020 | Calcium signaling pathway | 0.021715255 | 0.222581363 | 1 | *CACNA1S* | 2 | *CHRM5/GRIN2C* |
| hsa05410 | Hypertrophic cardiomyopathy (HCM) | 0.030070193 | 0.27397287 | 1 | *CACNA1S* | 1 | *ITGA10* |
| hsa05414 | Dilated cardiomyopathy (DCM) | 0.033767717 | 0.276895278 | 1 | *CACNA1S* | 1 | *ITGA10* |
| hsa04670 | Leukocyte transendothelial migration | 0.051078901 | 0.308732333 | 0 | | 2 | *CLDN2/CLDN18* |
| hsa04725 | Cholinergic synapse | 0.051078901 | 0.308732333 | 1 | *CACNA1S* | 1 | *CHRM5* |
| hsa04724 | Glutamatergic synapse | 0.054677277 | 0.308732333 | 0 | | 2 | *GRIN2C/SLC1A3* |
| hsa00670 | One carbon pool by folate | 0.0588339 | 0.308732333 | 0 | | 1 | *ALDH1L1* |
| hsa04950 | Maturity onset diabetes of the young | 0.0588339 | 0.308732333 | 0 | | 1 | *HNF4A* |
| hsa04514 | Cell adhesion molecules (CAMs) | 0.060240455 | 0.308732333 | 0 | | 2 | *CLDN2/CLDN18* |
| hsa04926 | Relaxin signaling pathway | 0.067951707 | 0.327767057 | 2 | *MMP1/MMP13* | 0 | |
| hsa05034 | Alcoholism | 0.114261999 | 0.458928333 | 1 | *H4C15* | 1 | *GRIN2C* |
| hsa05033 | Nicotine addiction | 0.114354805 | 0.458928333 | 0 | | 1 | *GRIN2C* |
| hsa05010 | Alzheimer disease | 0.117749924 | 0.458928333 | 1 | *CACNA1S* | 1 | *GRIN2C* |

A table showing the KEGG pathway ID, pathway description, p-value, adjusted p-value, upregulated and downregulated genes, and the corresponding gene names.

Lastly, the human disease ontology analysis was performed for the iAstrocyte treatment group of fibrils vs control. This time, there were no significant differentially expressed pathways when considering the adjusted P-value. The top 20 differentially expressed pathways prior to P-value adjustment are shown (fig.4.16). The majority of the pathways shown corresponded to cancer and infection pathways, suggesting that pathways which relate to inflammation are differentially expressed in the fibrils vs control group.

There was a number of upregulated and downregulated genes (table 4.9). The most common upregulated genes were *MMP1, MMP13, PI3, CXCL8.* Meanwhile, the most common downregulated genes were *MUC5AC,* and *NPPA.*

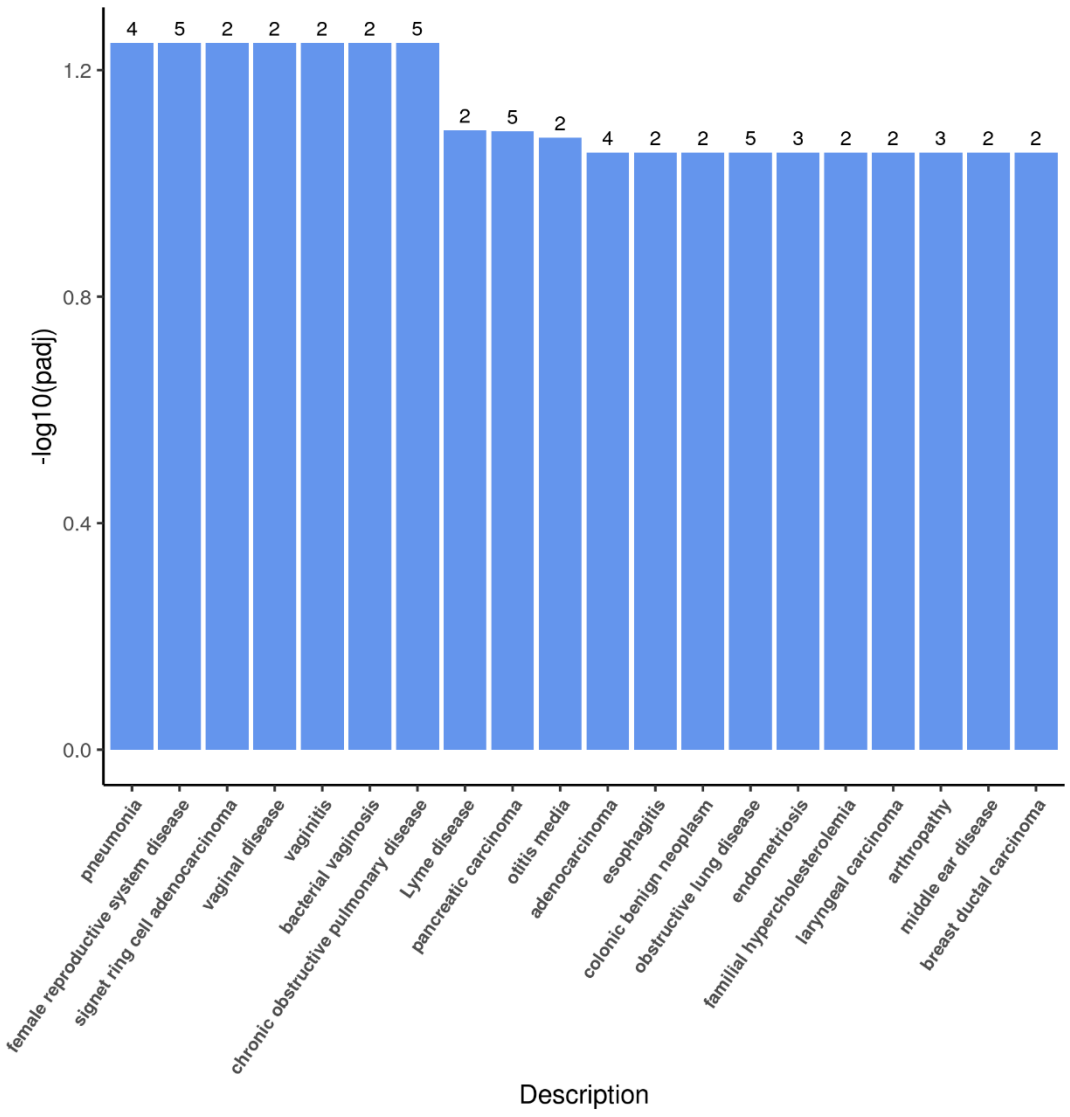


**Figure 4.16.** KEGG pathway analysis for fibrils vs control iAstrocyte treatments.

KEGG pathway analysis for fibrils vs control iAstrocyte treatments. A bar chart representing categories of top 20 significant differentially expressed pathways, prior to p-value adjustments. Figure provided by Novogene.

**Table 4.9.** The human disease ontology (DO) analysis for fibrils vs control iAstrocyte treatments.

| DOID | Description | P-value | Adjusted P-value | Upregulated | Gene name | Downregulated | Gene name |
|---|---|---|---|---|---|---|---|
| DOID:552 | pneumonia | 0.00043434 | 0.056460729 | 2 | *MMP1/CXCL8* | 2 | *MUC5AC/NPPA* |
| DOID:229 | female reproductive system disease | 0.00049456 | 0.056460729 | 4 | *PI3/MMP1/CXCL8/MMP13* | 1 | *NPPA* |
| DOID:3493 | signet ring cell adenocarcinoma | 0.00076395 | 0.056460729 | 0 | | 2 | *MUC5AC/CLDN18* |
| DOID:121 | vaginal disease | 0.00093127 | 0.056460729 | 2 | *PI3/CXCL8* | 0 | |
| DOID:2170 | vaginitis | 0.00093127 | 0.056460729 | 2 | *PI3/CXCL8* | 0 | |
| DOID:3385 | bacterial vaginosis | 0.00093127 | 0.056460729 | 2 | *PI3/CXCL8* | 0 | |
| DOID:3083 | chronic obstructive pulmonary disease | 0.00107985 | 0.056460729 | 4 | *PI3/MMP1/CXCL8/MMP13* | 1 | *MUC5AC* |
| DOID:11729 | Lyme disease | 0.00175928 | 0.080487233 | 2 | *MMP1/MMP13* | 0 | |
| DOID:4905 | pancreatic carcinoma | 0.0019907 | 0.080955231 | 2 | *CXCL8/U2AF1* | 3 | *CDH17/MUC5AC/ST14* |
| DOID:10754 | otitis media | 0.00226675 | 0.082963175 | 1 | *CXCL8* | 1 | *MUC5AC* |
| DOID:299 | adenocarcinoma | 0.00296528 | 0.088153183 | 1 | *MMP1* | 3 | *MUC5AC/CLDN2/CLDN18* |
| DOID:11963 | esophagitis | 0.00314195 | 0.088153183 | 1 | *CXCL8* | 1 | *MUC5AC* |
| DOID:235 | colonic benign neoplasm | 0.00314195 | 0.088153183 | 1 | *SAA1* | 1 | *MUC5AC* |
| DOID:2320 | obstructive lung disease | 0.00374011 | 0.088153183 | 4 | *PI3/MMP1/CXCL8/MMP13* | 1 | *MUC5AC* |
| DOID:289 | endometriosis | 0.00405434 | 0.088153183 | 3 | *MMP1/CXCL8/MMP13* | 0 | |
| DOID:13810 | familial hypercholesterolemia | 0.00415096 | 0.088153183 | 1 | *CXCL8* | 1 | *NPPA* |
| DOID:2600 | laryngeal carcinoma | 0.00489635 | 0.088153183 | 2 | *MMP1/CXCL8* | 0 | |
| DOID:381 | arthropathy | 0.00500656 | 0.088153183 | 3 | *MMP1/SAA1/CXCL8* | 0 | |
| DOID:5100 | middle ear disease | 0.00529049 | 0.088153183 | 1 | *CXCL8* | 1 | *MUC5AC* |
| DOID:3007 | breast ductal carcinoma | 0.00569878 | 0.088153183 | 1 | *CXCL8* | 1 | *MUC5AC* |

A table showing the DO ID, pathway description, p-value, adjusted p-value, upregulated and downregulated genes, and the corresponding gene names.

### Fibrils vs Scrambled

After investigating the differences between the fibril-treated iAstrocytes vs control (untreated); the investigation shifted towards looking at the differentially expressed genes and pathways in the fibrils vs scrambled (vehicle control) treatment groups.

Firstly, gene ontology pathway analysis was carried out (fig.4.17). The pathways were investigated by separating the results by their gene ontology categories, which were: biological processes, cellular components, and molecular function. The top 10 significant pathways (prior to p-value adjustment) per gene ontology category are shown. Only the top two pathways of the 'biological processes' category were significant post p-value adjustment.

Within the biological processes category, the top two pathways were statistically significant after p-value adjustment (p=0.000074 with adjusted p-value=0.01726; and p=0.000306 with adjusted p-value 0.035488 respectively). These pathways corresponded to the upregulation of *PI3* and *KLK14* genes. These genes were widely upregulated across the pathways in the biological processes category.

Within the cellular components category, the most common upregulated genes were *PI3, MMP1, DGCR6, SAA1.* The majority of the genes in the pathways corresponding to the 'cellular components' pathway were upregulated. Only two genes, *SNORA74A,* and *CD37* were downregulated.

Lastly, within the molecular function category, the *MMP1, KLK14*, and *SAA1* genes were commonly upregulated across all pathways. This is similar to the biological processes category, where *MMP1* and *KLK14* genes were also upregulated. The common downregulated genes across the pathways withing the molecular function category were *QRFP,* and *ANKRD36C.*

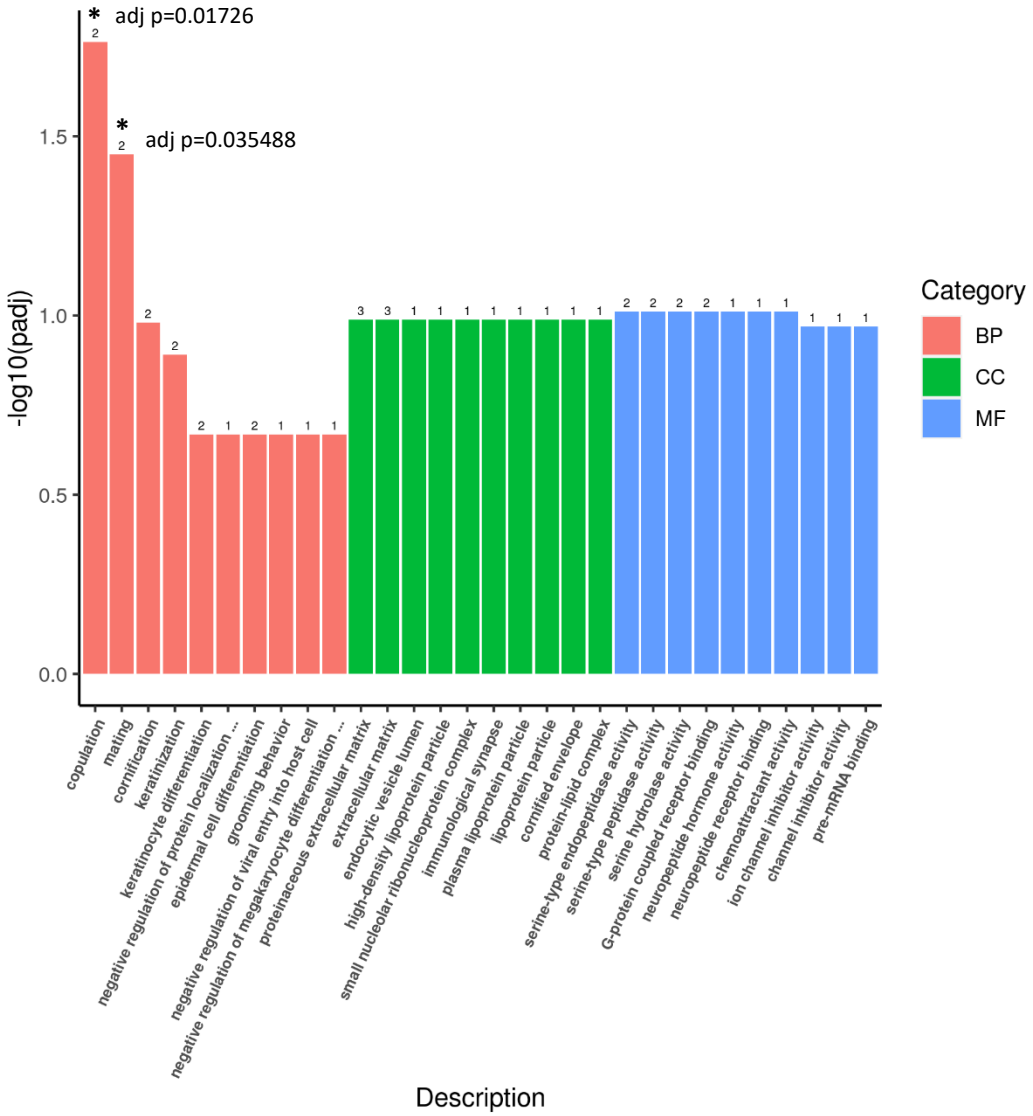


**Figure 4.17.** Gene ontology (GO) classification for fibrils vs scrambled iAstrocyte treatments.

A bar chart representing subcategories of gene transcripts annotated from the RNAseq data of human iAstrocytes. The results show top 10 significant differently expressed gene ontology pathways, per category, prior to p-value adjustments (BP- biological process; CC- cellular function; MF- molecular function). The significant gene pathways post p-value adjustments are marked with corresponding -values. Figure provided by Novogene, annotations made separately.

**Table 4.10.** Gene ontology (GO) classification for fibrils vs scrambled iAstrocyte treatments.

| Category | Gene ontology ID | Subcategory description | P-value | Adjusted P-value | Upregulated | Gene name | Downregulated | Gene name |
|---|---|---|---|---|---|---|---|---|
| BP | GO:0007620 | copulation | 7.44E-05 | 0.017259814 | 2 | *PI3/KLK14* | 0 | |
| BP | GO:0007618 | mating | 0.000305927 | 0.035487527 | 2 | *PI3/KLK14* | 0 | |
| BP | GO:0070268 | cornification | 0.00135122 | 0.104494341 | 2 | *PI3/KLK14* | 0 | |
| BP | GO:0031424 | keratinization | 0.002221748 | 0.128861362 | 2 | *PI3/KLK14* | 0 | |
| BP | GO:0030216 | keratinocyte differentiation | 0.007501197 | 0.214382366 | 2 | *PI3/KLK14* | 0 | |
| BP | GO:2000009 | negative regulation of protein localization to cell surface | 0.011370396 | 0.214382366 | 1 | *TAX1BP3* | 0 | |
| BP | GO:0009913 | epidermal cell differentiation | 0.012865118 | 0.214382366 | 2 | *PI3/KLK14* | 0 | |
| BP | GO:0007625 | grooming behavior | 0.013977328 | 0.214382366 | 0 | | 1 | *QRFP* |
| BP | GO:0046597 | negative regulation of viral entry into host cell | 0.013977328 | 0.214382366 | 1 | *TRIM10* | 0 | |
| BP | GO:0045653 | negative regulation of megakaryocyte differentiation | 0.014844895 | 0.214382366 | 1 | *HIST2H4B* | 0 | |
| CC | GO:0005578 | proteinaceous extracellular matrix | 0.005499066 | 0.102856059 | 3 | *PI3/MMP1/DGCR6* | 0 | |
| CC | GO:0031012 | extracellular matrix | 0.010129735 | 0.102856059 | 3 | *PI3/MMP1/DGCR6* | 0 | |
| CC | GO:0071682 | endocytic vesicle lumen | 0.017334343 | 0.102856059 | 1 | *SAA1* | 0 | |
| CC | GO:0034364 | high-density lipoprotein particle | 0.020552885 | 0.102856059 | 1 | *SAA1* | 0 | |
| CC | GO:0005732 | small nucleolar ribonucleoprotein complex | 0.024828842 | 0.102856059 | 0 | | 1 | *SNORA74A* |
| CC | GO:0001772 | immunological synapse | 0.03226952 | 0.102856059 | 0 | | 1 | *CD37* |
| CC | GO:0034358 | plasma lipoprotein particle | 0.033328101 | 0.102856059 | 1 | *SAA1* | 0 | |
| CC | GO:1990777 | lipoprotein particle | 0.033328101 | 0.102856059 | 1 | *SAA1* | 0 | |
| CC | GO:0001533 | cornified envelope | 0.034385593 | 0.102856059 | 1 | *PI3* | 0 | |
| CC | GO:0032994 | protein-lipid complex | 0.035441996 | 0.102856059 | 1 | *SAA1* | 0 | |
| MF | GO:0004252 | serine-type endopeptidase activity | 0.007631048 | 0.097431119 | 2 | *MMP1/KLK14* | 0 | |
| MF | GO:0008236 | serine-type peptidase activity | 0.01091368 | 0.097431119 | 2 | *MMP1/KLK14* | 0 | |
| MF | GO:0017171 | serine hydrolase activity | 0.011444831 | 0.097431119 | 2 | *MMP1/KLK14* | 0 | |
| MF | GO:0001664 | G-protein coupled receptor binding | 0.01656544 | 0.097431119 | 1 | *SAA1* | 1 | *QRFP* |
| MF | GO:0005184 | neuropeptide hormone activity | 0.018034378 | 0.097431119 | 0 | | 1 | *QRFP* |
| MF | GO:0071855 | neuropeptide receptor binding | 0.020019349 | 0.097431119 | 0 | | 1 | *QRFP* |
| MF | GO:0042056 | chemoattractant activity | 0.022000575 | 0.097431119 | 1 | *SAA1* | 0 | |
| MF | GO:0008200 | ion channel inhibitor activity | 0.033809643 | 0.107500435 | 0 | | 1 | *ANKRD36C* |
| MF | GO:0016248 | channel inhibitor activity | 0.0347877 | 0.107500435 | 0 | | 1 | *ANKRD36C* |
| MF | GO:0036002 | pre-mRNA binding | 0.035764834 | 0.107500435 | 1 | *U2AF1* | 0 | |

A table showing the category, subcategory description, corresponding gene ontology ID, p-value, adjusted p-value, gene count, number of upregulated and downregulated genes, and associated gene names.

Next, GSEA analysis was carried out to find clustered genes and their expression values between the groups (fibrils vs scrambled), for each cell line. The differentially expressed genes are shown (fig.4.18), and their expression values were represented by colours (red= high expression; blue= low expression). Within the upregulated genes (in fibril-treated iAstrocytes), there were 7 genes of interest. These corresponded to *CHRND, TRIM10, DUOXA1, ITGAM, TMEM246-AS1, HIST1H1T,* and *AMT.* Meanwhile, within the downregulated genes, there were 4 genes of interest. These corresponded to *TNFAIP8L2, GJB7, LPA, and POU2AF1.*

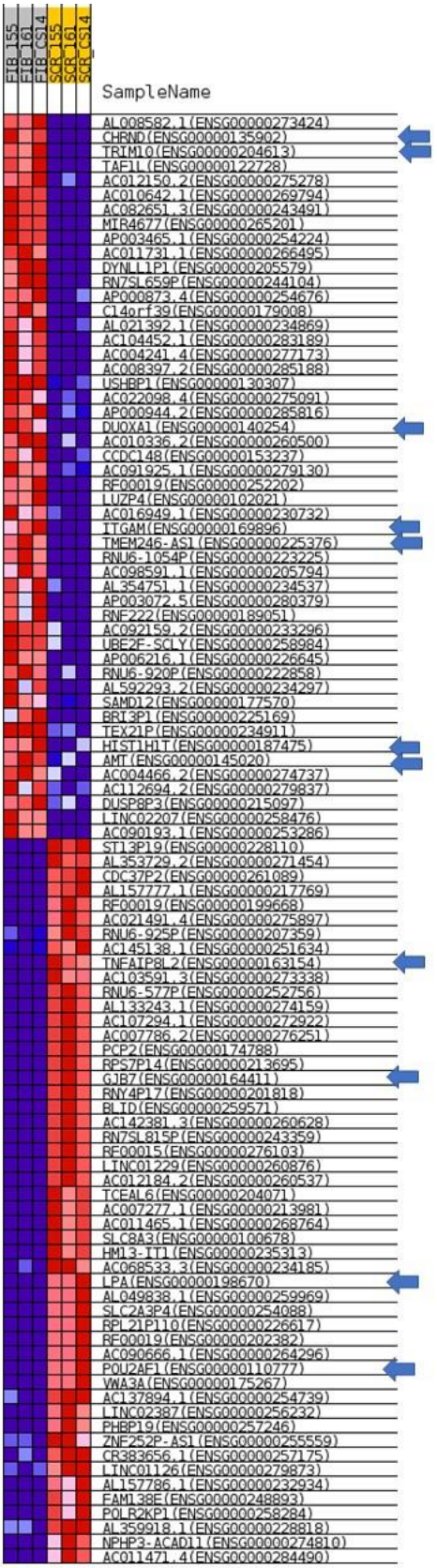


**Figure 4.18.** Gene set enrichment analysis (GSEA) heatmap representing differentially expressed genes in iAstrocyte fibrils vs scrambled treatment group.

The GSEA represents the top differentially expressed genes identified. The analysis was separated to look at each cell line individually. The genes of interest are marked with arrows. Red= upregulated; blue= downregulated.

KEGG pathway analysis was also carried out for the fibrils vs scrambled treatment group. The analysis showed 9 pathways of interest. Only 7 were significant before p-value adjustment, and none were significant after p-value adjustment. The resulting 9 pathways are shown (fig.4.19). Within those, no genes were significantly downregulated, and all 9 pathways showed genes which were upregulated. Two genes were commonly upregulated across all 9 pathways, and these were *MMP1,* and *HIST2H4B* (table 4.11).

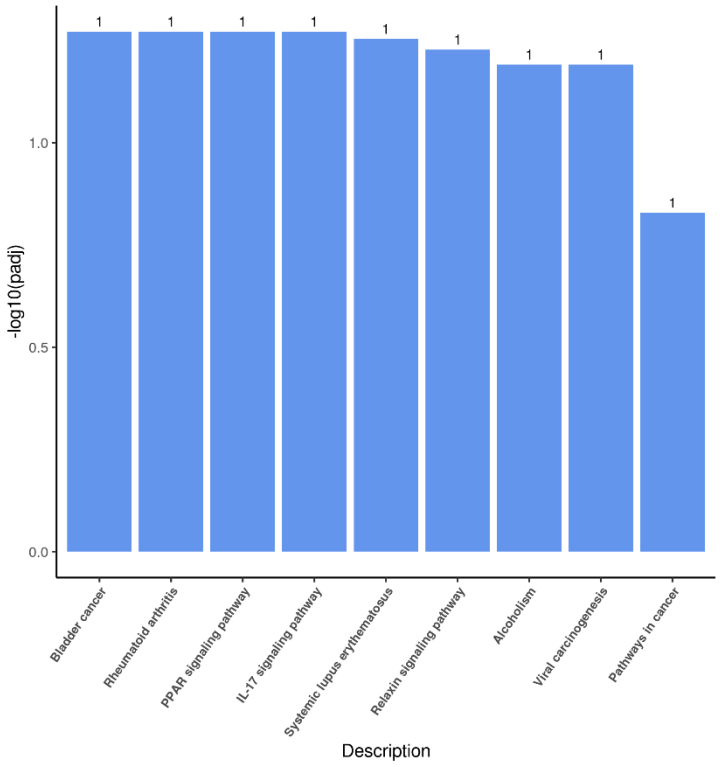


**Figure 4.19.** KEGG pathway analysis for fibrils vs scrambled iAstrocyte treatments.

A bar chart representing categories of the available 9 differentially expressed pathways. Figure provided by Novogene.

**Table 4.11.** KEGG pathway analysis for fibrils vs scrambled iAstrocyte treatments.

| KEGGID | Description | P-value | Adjusted P-value | Upregulated | Gene name | Downregulated | Gene name |
|---|---|---|---|---|---|---|---|
| hsa05219 | Bladder cancer | 0.013569262 | 0.053476673 | 1 | *MMP1* | 0 | |
| hsa05323 | Rheumatoid arthritis | 0.018839439 | 0.053476673 | 1 | *MMP1* | 0 | |
| hsa03320 | PPAR signaling pathway | 0.020154778 | 0.053476673 | 1 | *MMP1* | 0 | |
| hsa04657 | IL-17 signaling pathway | 0.02376741 | 0.053476673 | 1 | *MMP1* | 0 | |
| hsa05322 | Systemic lupus erythematosus | 0.030972659 | 0.055750786 | 1 | *HIST2H4B* | 0 | |
| hsa04926 | Relaxin signaling pathway | 0.039453544 | 0.059180316 | 1 | *MMP1* | 0 | |
| hsa05034 | Alcoholism | 0.053397821 | 0.064429932 | 1 | *HIST2H4B* | 0 | |
| hsa05203 | Viral carcinogenesis | 0.057271051 | 0.064429932 | 1 | *HIST2H4B* | 0 | |
| hsa05200 | Pathways in cancer | 0.148459467 | 0.148459467 | 1 | *MMP1* | 0 | |

A table showing the KEGG pathway ID, pathway description, p-value, adjusted p-value, upregulated and downregulated genes, and the corresponding gene names.

Lastly, human disease ontology analysis was carried out for fibrils vs scrambled treatment group. The top 20 differentially expressed disease ontology pathways are shown (fig.4.20). None of the pathways reached significance after p-value adjustment. However, all top 20 pathways were significant prior to p-value adjustment. None of the top 20 pathways displayed any downregulated genes, and all genes within those differentially expressed disease ontology pathways were upregulated (table 4.12). Amongst the genes, the most common upregulated genes were *MMP9, H19* and *SAA1* across the top 20 disease ontology pathways.

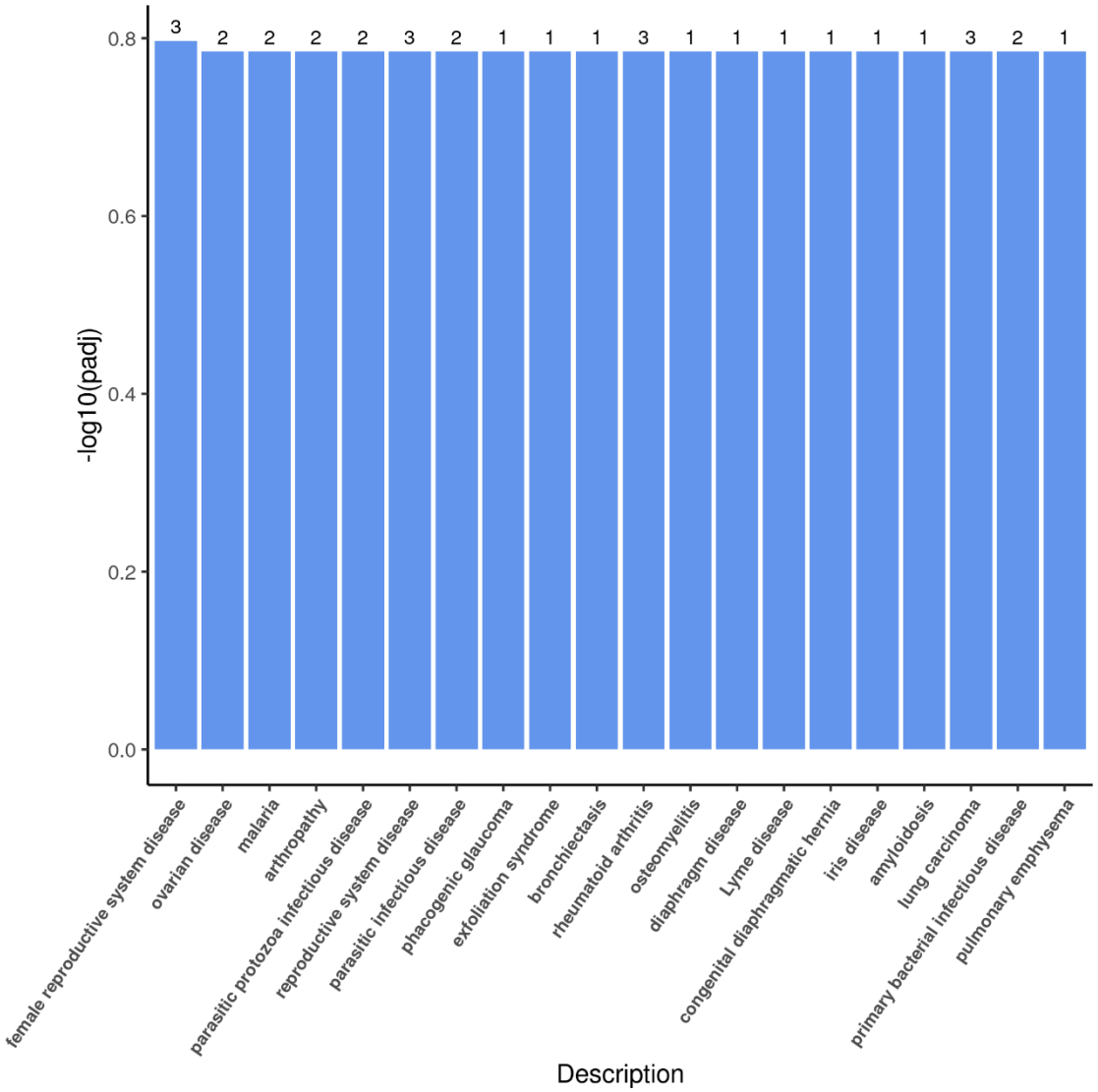


**Figure 4.20** The human disease ontology (DO) analysis for fibrils vs scrambled iAstrocyte treatments. A bar chart representing categories of top 20 significant differentially expressed pathways, prior to p-value adjustments. Figure provided by Novogene.

**Table 4.12.** The human disease ontology (DO) analysis for fibrils vs scrambled iAstrocyte treatments.

| DOID | Description | P-value | Adjusted P-value | Upregulated | Gene name | Downregulated | Gene name |
|---|---|---|---|---|---|---|---|
| DOID:229 | female reproductive system disease | 0.00091147 | 0.159506847 | 3 | *PI3/MMP1/H19* | 0 | |
| DOID:1100 | ovarian disease | 0.00214586 | 0.164140142 | 2 | *MMP1/H19* | 0 | |
| DOID:12365 | malaria | 0.00403549 | 0.164140142 | 2 | *SAA1/MMP1* | 0 | |
| DOID:381 | arthropathy | 0.0043672 | 0.164140142 | 2 | *SAA1/MMP1* | 0 | |
| DOID:2789 | parasitic protozoa infectious disease | 0.0062094 | 0.164140142 | 2 | *SAA1/MMP1* | 0 | |
| DOID:15 | reproductive system disease | 0.00662588 | 0.164140142 | 3 | *PI3/MMP1/H19* | 0 | |
| DOID:1398 | parasitic infectious disease | 0.00865767 | 0.164140142 | 2 | *SAA1/MMP1* | 0 | |
| DOID:12571 | phacogenic glaucoma | 0.01473188 | 0.164140142 | 1 | *MMP1* | 0 | |
| DOID:13641 | exfoliation syndrome | 0.01473188 | 0.164140142 | 1 | *MMP1* | 0 | |
| DOID:9563 | bronchiectasis | 0.01606153 | 0.164140142 | 1 | *MMP1* | 0 | |
| DOID:7148 | rheumatoid arthritis | 0.01725046 | 0.164140142 | 3 | *SAA1/MMP1/H19* | 0 | |
| DOID:1019 | osteomyelitis | 0.01738958 | 0.164140142 | 1 | *MMP1* | 0 | |
| DOID:10481 | diaphragm disease | 0.01738958 | 0.164140142 | 1 | *MMP1* | 0 | |
| DOID:11729 | Lyme disease | 0.01738958 | 0.164140142 | 1 | *MMP1* | 0 | |
| DOID:3827 | congenital diaphragmatic hernia | 0.01738958 | 0.164140142 | 1 | *MMP1* | 0 | |
| DOID:240 | iris disease | 0.01871604 | 0.164140142 | 1 | *MMP1* | 0 | |
| DOID:9120 | amyloidosis | 0.01871604 | 0.164140142 | 1 | *SAA1* | 0 | |
| DOID:3905 | lung carcinoma | 0.02039899 | 0.164140142 | 3 | *SAA1/MMP1/KLK14* | 0 | |
| DOID:0050338 | primary bacterial infectious disease | 0.02129966 | 0.164140142 | 2 | *SAA1/MMP1* | 0 | |
| DOID:9675 | pulmonary emphysema | 0.02136418 | 0.164140142 | 1 | *MMP1* | 0 | |

A table showing the DO ID, pathway description, p-value, adjusted p-value, upregulated and downregulated genes, and the corresponding gene names.

### Oligomers vs Control

For the oligomers vs control treatment group, the first enrichment analysis that was carried out was gene ontology analysis (fig.4.21). The gene ontology analysis separates the results into three gene ontology categories, which are: biological processes, cellular components, and molecular function. The top 10 pathways within each category were investigated (table 4.13).

The first gene ontology category that was investigated was 'biological processes'. Within this category, one pathway reached significance after adjustment of the p-value. The remaining pathways were not significant after p-value adjustment; however, all remaining pathways within the top 10 pathways were significant prior to p-value adjustment. The significant (for both pre, and post p-value adjustment) differentially expressed pathway corresponded to 'extracellular matrix disassembly' gene ontology pathway (p-value= 0.0000487; adjusted p-value= 0.044585483). Within this pathway, 3 genes were upregulated, and these were *MMP1*, *MMP13*, and *MMP9*. Two genes were downregulated across the pathways, and these were the *A2M* gene (most common), and *NANOS3* gene. Within the remaining top 10 pathways, most genes were upregulated overall. The most common upregulated genes were: *MMP1, MMP13, MMP9, ICAM1,* and *IL1A*.

The next gene ontology category which was investigated was 'cellular components'. Only one pathway reached significance after adjustment of p-value (p-value= 0.000452363; adjusted p-value= 0.046140985), and this corresponded to the 'extracellular matrix' pathway. Within this pathway, 5 genes were upregulated. These genes included: *MMP1, PI3, MMP13, MMP9*, and *ICAM1.* Meanwhile, one gene was downregulated, and this gene was *MMP25.* Within the remaining pathways, the most common upregulated genes were *MMP1, PI3, MMP13, MMP9*, *GABRA1.* Meanwhile downregulated genes within the remaining gene ontology pathways included *MMP25, DSP.*

The gene ontology category termed 'molecular function', contained 6 significant differentially expressed gene ontology pathways. This was the highest number of significant differentially expressed gene ontology pathways amongst all gene ontology categories. These pathways were significant before and after p-value adjustments. The remaining 4 gene ontology pathways were significant prior to p-value adjustments, however, they did not reach significance with adjusted p-values. The top 6 significant differentially expressed gene ontology pathways corresponded to: metalloendopeptidase activity (p-value= 3.24E-06; adjusted p-value= 0.000415205), with 3 upregulated genes (*MMP1, MMP13, MMP9*), and 2 downregulated genes (*MMEL1, MMP25)*; metallopeptidase activity (p-value= 3.88E-05; adjusted p-value= 0.002485438), with 3 upregulated genes (*MMP1, MMP13, MMP9*), and 2 downregulated genes (*MMEL1, MMP25*); endopeptidase activity (p-value= 0.000121729; adjusted p-value= 0.005193752), with 3 upregulated genes (*MMP1, MMP13, MMP9)*, and 3 downregulated genes

(*MMEL1, PRS22, MMP25*); serine-type endopeptidase activity (p-value= 0.00029247m adjusted p-value= 0.009359045), with 3 upregulated genes (*MMP1, MMP13, MMP9*), and 1 downregulated gene (*PRS22*); serine-type peptidase activity (p-value= 0.00055636, adjusted p-value= 0.012934632), with 3 upregulated genes (*MMP1, MMP13, MMP9*), and 1 downregulated gene (*PRS22*); and serine hydrolase activity (p-value= 0.000606311, adjusted p-value= 0.012934632), with 3 upregulated genes (*MMP1, MMP13, MMP9*), and 1 downregulated gene (*PRS22*).

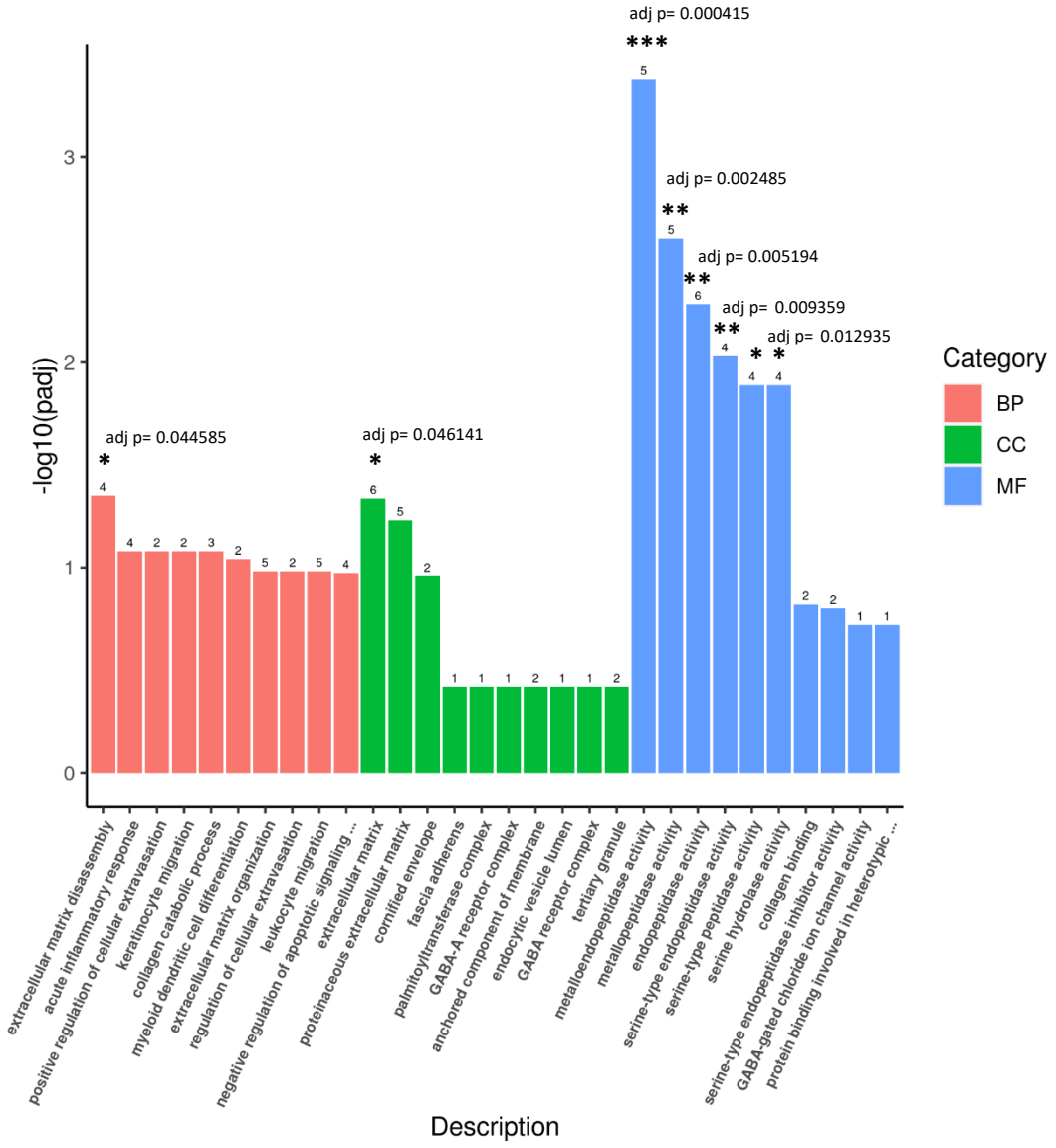


**Figure 4.21.** Gene ontology (GO) classification for oligomers vs control iAstrocyte treatments

A bar chart representing subcategories of gene transcripts annotated from the RNAseq data of human iAstrocytes. The results show top 10 significant differently expressed gene ontology pathways, per category, prior to p-value adjustments (BP- biological process; CC- cellular function; MF- molecular function). The significant gene pathways post p-value adjustments are marked with corresponding -values. Figure provided by Novogene, annotations added separately.

**Table 4.13**. Gene ontology (GO) classification for oligomers vs control iAstrocyte treatments

| Category | Gene ontology ID | Subcategory description | P-value | Adjusted P-value | Upregulated | Gene name | Downregulated | Gene name |
|---|---|---|---|---|---|---|---|---|
| BP | GO:0022617 | extracellular matrix disassembly | 4.87E-05 | 0.044585483 | 3 | *MMP1/MMP13/MMP9* | 1 | *A2M* |
| BP | GO:0002526 | acute inflammatory response | 0.000193937 | 0.083104724 | 3 | *SAA1/IL1A/ICAM1* | 1 | *A2M* |
| BP | GO:0002693 | positive regulation of cellular extravasation | 0.0002758 | 0.083104724 | 2 | *IL1A/ICAM1* | 0 | |
| BP | GO:0051546 | keratinocyte migration | 0.000390013 | 0.083104724 | 2 | *MMP9/LTB4R2* | 0 | |
| BP | GO:0030574 | collagen catabolic process | 0.000454124 | 0.083104724 | 3 | *MMP1/MMP13/MMP9* | 0 | |
| BP | GO:0043011 | myeloid dendritic cell differentiation | 0.00059744 | 0.091109532 | 2 | *RELB/BATF3* | 0 | |
| BP | GO:0030198 | extracellular matrix organization | 0.000862307 | 0.104230976 | 4 | *MMP1/MMP13/MMP9/ICAM1* | 1 | *A2M* |
| BP | GO:0002691 | regulation of cellular extravasation | 0.000940529 | 0.104230976 | 2 | *IL1A/ICAM1* | 0 | |
| BP | GO:0050900 | leukocyte migration | 0.001025223 | 0.104230976 | 5 | *MMP1/SAA1/IL1A/MMP9/ICAM1* | 0 | |
| BP | GO:2001234 | negative regulation of apoptotic signaling pathway | 0.001160726 | 0.10620645 | 3 | *IL1A/MMP9/ICAM1* | 1 | *NANOS3* |
| CC | GO:0031012 | extracellular matrix | 0.000452363 | 0.046140985 | 5 | *MMP1/PI3/MMP13/MMP9/ICAM1* | 1 | *MMP25* |
| CC | GO:0005578 | proteinaceous extracellular matrix | 0.001153024 | 0.058804218 | 4 | *MMP1/PI3/MMP13/MMP9* | 1 | *MMP25* |
| CC | GO:0001533 | cornified envelope | 0.003243716 | 0.110286339 | 1 | *PI3* | 1 | *DSP* |
| CC | GO:0005916 | fascia adherens | 0.022716527 | 0.383398176 | 0 | | 1 | *DSP* |
| CC | GO:0002178 | palmitoyltransferase complex | 0.024960368 | 0.383398176 | 0 | | 1 | *SPTLC3* |
| CC | GO:1902711 | GABA-A receptor complex | 0.038318519 | 0.383398176 | 1 | *GABRA1* | 0 | |
| CC | GO:0031225 | anchored component of membrane | 0.03932233 | 0.383398176 | 0 | | 2 | *PRSS22/MMP25* |
| CC | GO:0071682 | endocytic vesicle lumen | 0.040527497 | 0.383398176 | 1 | *SAA1* | 0 | |
| CC | GO:1902710 | GABA receptor complex | 0.040527497 | 0.383398176 | 1 | *GABRA1* | 0 | |
| CC | GO:0070820 | tertiary granule | 0.044656415 | 0.383398176 | 1 | *MMP9* | 1 | *DSP* |
| MF | GO:0004222 | metalloendopeptidase activity | MMP1/MMP13/MMEL1/MMP9/MMP25 | MMP1/MMP13/MMEL1/MMP9/MMP25 | 3 | *MMP1/MMP13/MMP9* | 2 | *MMEL1/MMP25* |
| MF | GO:0008237 | metallopeptidase activity | MMP1/MMP13/MMEL1/MMP9/MMP25 | MMP1/MMP13/MMEL1/MMP9/MMP25 | 3 | *MMP1/MMP13/MMP9* | 2 | *MMEL1/MMP25* |
| MF | GO:0004175 | endopeptidase activity | MMP1/MMP13/MMEL1/MMP9/PRSS22/MMP25 | MMP1/MMP13/MMEL1/MMP9/PRSS22/MMP25 | 3 | *MMP1/MMP13/MMP9* | 3 | *MMEL1/PRSS22/MMP25* |
| MF | GO:0004252 | serine-type endopeptidase activity | MMP1/MMP13/MMP9/PRSS22 | MMP1/MMP13/MMP9/PRSS22 | 3 | *MMP1/MMP13/MMP9* | 1 | *PRSS22* |
| MF | GO:0008236 | serine-type peptidase activity | MMP1/MMP13/MMP9/PRSS22 | MMP1/MMP13/MMP9/PRSS22 | 3 | *MMP1/MMP13/MMP9* | 1 | *PRSS22* |
| MF | GO:0017171 | serine hydrolase activity | MMP1/MMP13/MMP9/PRSS22 | MMP1/MMP13/MMP9/PRSS22 | 3 | *MMP1/MMP13/MMP9* | 1 | *PRSS22* |
| MF | GO:0005518 | collagen binding | MMP13/MMP9 | MMP13/MMP9 | 2 | *MMP13/MMP9* | 0 | |
| MF | GO:0004867 | serine-type endopeptidase inhibitor activity | PI3/A2M | PI3/A2M | 1 | *PI3* | 1 | *A2M* |
| MF | GO:0022851 | GABA-gated chloride ion channel activity | GABRA1 | GABRA1 | 1 | *GABRA1* | 0 | |
| MF | GO:0086080 | protein binding involved in heterotypic cell-cell adhesion | DSP | DSP | 0 | | 1 | *DSP* |

A table showing the category, subcategory description, corresponding gene ontology ID, p-value, adjusted p-value, gene count, number of upregulated and downregulated genes, and associated gene names.

Next, GSEA was performed for oligomers vs control treatment group, to show the differentially expressed genes between the two treatment groups (fig.4.22). The expression of the genes was identified on the heatmap by the colours (red= high expression, blue= low expression). Four genes of interest which were upregulated in the oligomer-treated iAstrocytes were identified, and these corresponded to: *NKAIN4*, *MIRLET7I*, and *IL1A*. Meanwhile, two genes which were downregulated in the oligomer-treated iAstrocytes were identified, and these corresponded to: *STARD6,* and *MMEL1.*

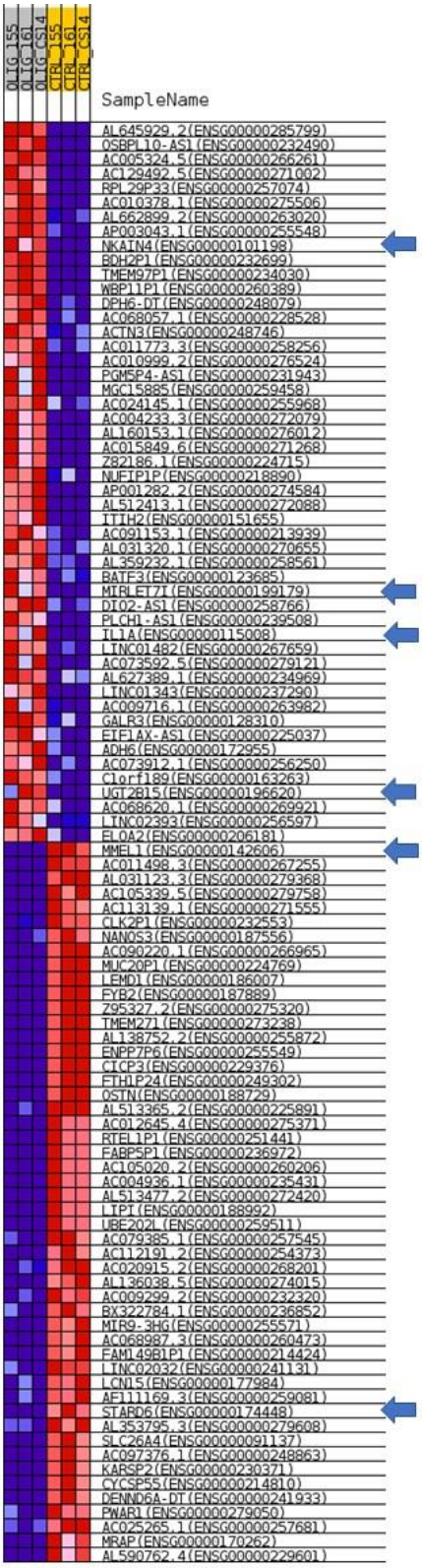


**Figure 4.22.** Gene set enrichment analysis (GSEA) heatmap representing differentially expressed genes in iAstrocyte oligomers vs control treatment group.

The GSEA represents the top differentially expressed genes identified. The analysis was separated to look at each cell line individually. The genes of interest are marked with arrows. Red= upregulated; blue= downregulated. Figure provided by Novogene.

Interestingly, the analysis showed two additional heat maps which corresponded to the following gene ontology pathways: 'positive regulation of nuclear transcribed mRNA catabolic deadenylation dependent decay', and 'regulation of cysteine type endopeptidase activity involved in apoptotic signalling pathway' (fig.4.23). These two GSEA heatmaps clustered genes together which were significant to the specific gene ontology pathways. There is cell line variation in the gene expression of the relevant genes within those pathways, as represented by the colours (red= high expression; blue= low expression).

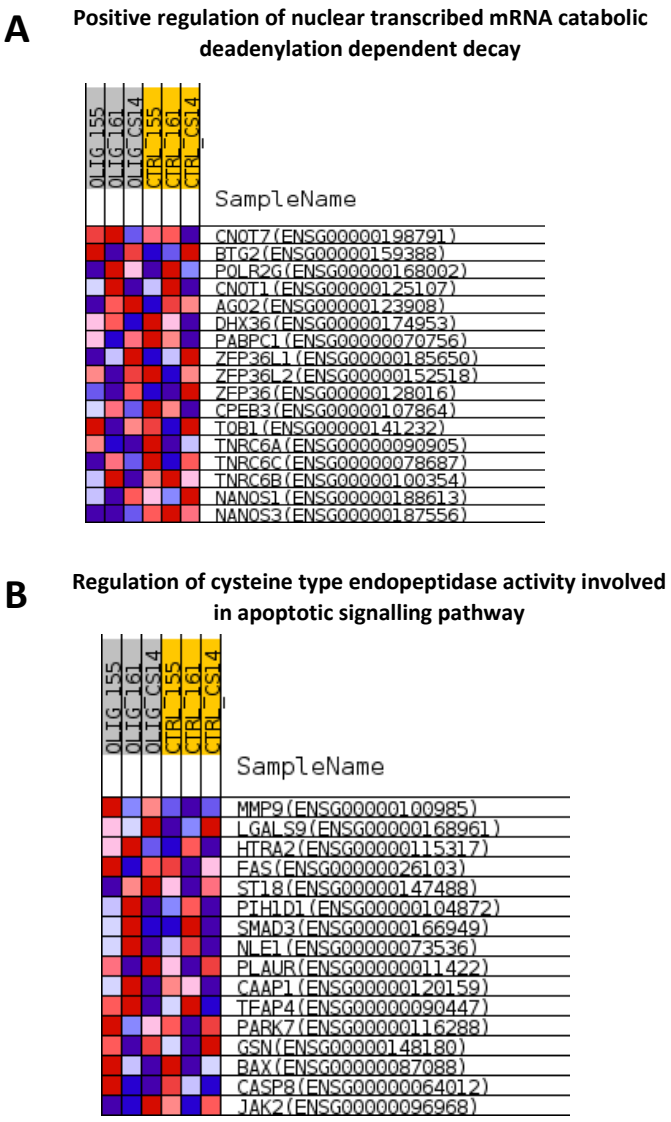


**Figure 4.23.** Gene set enrichment analysis (GSEA) heatmap representing differentially expressed genes in iAstrocyte oligomer vs control treatment group.

**(A)** The GSEA represents the differentially expressed genes identified in the positive regulation of nuclear transcribed mRNA catabolic deadenylation dependent pathway. **(B)** the GSEA represents the differentially expressed genes identified in the regulation of cysteine type endopeptidase activity involved in apoptotic signalling pathway. The analysis was separated to look at each cell line individually. The genes of interest are marked with arrows. Red= upregulated; blue= downregulated. Figure provided by Novogene.

The KEGG pathway analysis showed that within the oligomer vs control treatment group, there were significantly upregulated pathways, and no downregulated pathways of significance. The top 20 upregulated differentially expressed pathways are shown (fig.4.24). Within those pathways, 5 pathways reached significance both prior to p-value adjustment, and after p-value adjustment (table 4.14). These pathways corresponded to 'Rheumatoid arthritis' (p-value= 0.000265, adjusted p-value= 0.018994), with 3 genes being significantly upregulated (*MMP1, IL1A, ICAM1*); 'IL-17 signalling pathway' (p-value= 0.000493, adjusted p-value= 0.018994), with 3 genes being significantly upregulated (*MMP1, MMP13, MMP9*); 'Relaxin signaling pathway' (p-value= 0.001709, adjusted p-value= 0.037805), with 3 genes being significantly upregulated (*MMP1, MMP13, MMP9*); 'Fluid shear stress and atherosclerosis' (p-value= 0.001964, adjusted p-value= 0.037805), with 3 genes being significantly upregulated (*IL1A, MMP9, ICAM1*); and 'Bladder cancer' (p-value= 0.002924, adjusted p-value= 0.045022), with 2 genes being significantly upregulated (*MMP1, MMP9).*

The remaining pathways did not reach significance when p-values were adjusted, however they were significant prior to p-value adjustments. Within the top 20 remaining pathways, common upregulated genes included *CACNA1S, ICAM1,* and *RELB.*

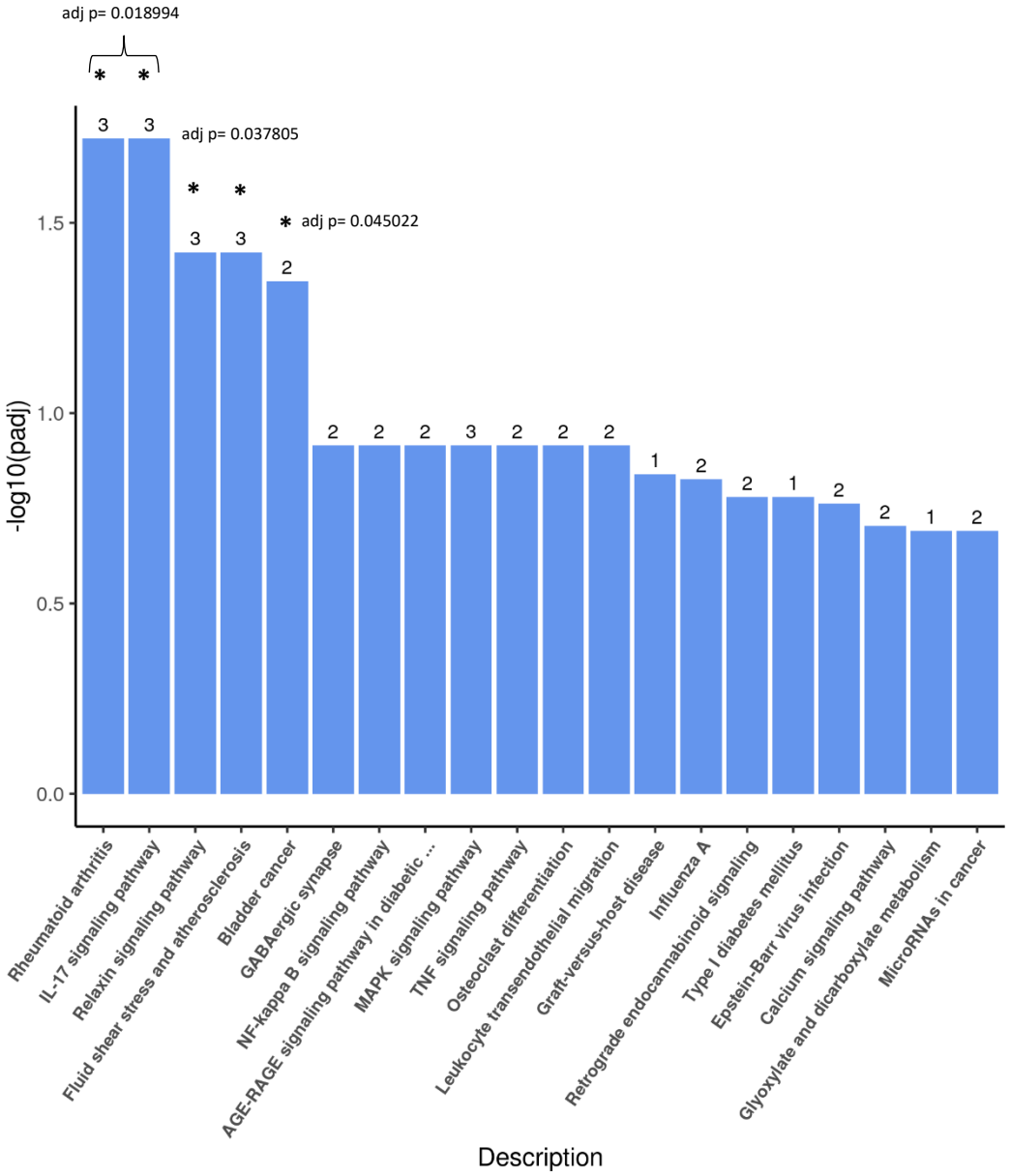


**Figure 4.24.** KEGG pathway analysis for oligomers vs control iAstrocyte treatments.

A bar chart representing categories of top 20 differentially expressed pathways. Figure provided by Novogene, annotations added separately.

**Table 4.14.** KEGG pathway analysis for oligomers vs control iAstrocyte treatments

| KEGGID | Description | P-value | Adjusted P-value | Upregulated | Gene name | Downregulated | Gene name |
|---|---|---|---|---|---|---|---|
| hsa05323 | Rheumatoid arthritis | 0.000264624 | 0.018993972 | 3 | *MMP1/IL1A/ICAM1* | 0 | |
| hsa04657 | IL-17 signaling pathway | 0.00049335 | 0.018993972 | 3 | *MMP1/MMP13/MMP9* | 0 | |
| hsa04926 | Relaxin signaling pathway | 0.00170868 | 0.037804658 | 3 | *MMP1/MMP13/MMP9* | 0 | |
| hsa05418 | Fluid shear stress and atherosclerosis | 0.001963878 | 0.037804658 | 3 | *IL1A/MMP9/ICAM1* | 0 | |
| hsa05219 | Bladder cancer | 0.002923531 | 0.045022375 | 2 | *MMP1/MMP9* | 0 | |
| hsa04727 | GABAergic synapse | 0.01130655 | 0.121773395 | 2 | *CACNA1S/GABRA1* | 0 | |
| hsa04064 | NF-kappa B signaling pathway | 0.011579348 | 0.121773395 | 2 | *RELB/ICAM1* | 0 | |
| hsa04933 | AGE-RAGE signaling pathway in diabetic complications | 0.015387588 | 0.121773395 | 2 | *IL1A/ICAM1* | 0 | |
| hsa04010 | MAPK signaling pathway | 0.016746141 | 0.121773395 | 3 | *CACNA1S/RELB/IL1A* | 0 | |
| hsa04668 | TNF signaling pathway | 0.016978637 | 0.121773395 | 2 | *MMP9/ICAM1* | 0 | |
| hsa04380 | Osteoclast differentiation | 0.017966041 | 0.121773395 | 2 | *RELB/IL1A* | 0 | |
| hsa04670 | Leukocyte transendothelial migration | 0.018977672 | 0.121773395 | 2 | *MMP9/ICAM1* | 0 | |
| hsa05332 | Graft-versus-host disease | 0.024461694 | 0.144888498 | 1 | *IL1A* | 0 | |
| hsa05164 | Influenza A | 0.027109548 | 0.149102513 | 2 | *IL1A/ICAM1* | 0 | |
| hsa04723 | Retrograde endocannabinoid signaling | 0.032904397 | 0.165983489 | 2 | *CACNA1S/GABRA1* | 0 | |
| hsa04940 | Type I diabetes mellitus | 0.034490076 | 0.165983489 | 1 | *IL1A* | 0 | |
| hsa05169 | Epstein-Barr virus infection | 0.038230462 | 0.173161503 | 2 | *RELB/ICAM1* | 0 | |
| hsa04020 | Calcium signaling pathway | 0.046309434 | 0.198101467 | 2 | *CACNA1S/LTB4R2* | 0 | |
| hsa00630 | Glyoxylate and dicarboxylate metabolism | 0.054261961 | 0.203599228 | 1 | *HAO2* | 0 | |
| hsa05206 | MicroRNAs in cancer | 0.054973555 | 0.203599228 | 2 | *MMP9/MIRLET7I* | 0 | |

A table showing the KEGG pathway ID, pathway description, p-value, adjusted p-value, upregulated and downregulated genes, and the corresponding gene names.

Lastly, human disease ontology pathway analysis was performed for oligomer vs control group. A total of 114 differentially expressed DO pathways were significant prior to p-value adjustment, as well as post p-value adjustment (appendix). The top 20 differentially expressed significant DO pathways are shown. All of the p-values, and adjusted p-values are also reported for each pathway (fig.4.25).

Most genes across the DO pathways were upregulated (table 4.15). Amongst these, the most common upregulated genes across the pathways were: *MMP1, PI3, MMP13, IL1A, MMP9, ICAM1, IL32.* These were present across all of the top 20 significant differentially expressed disease ontology pathways.

The downregulated genes across the DO pathways included: *NANOS3, DSP*, and *GATA6.*

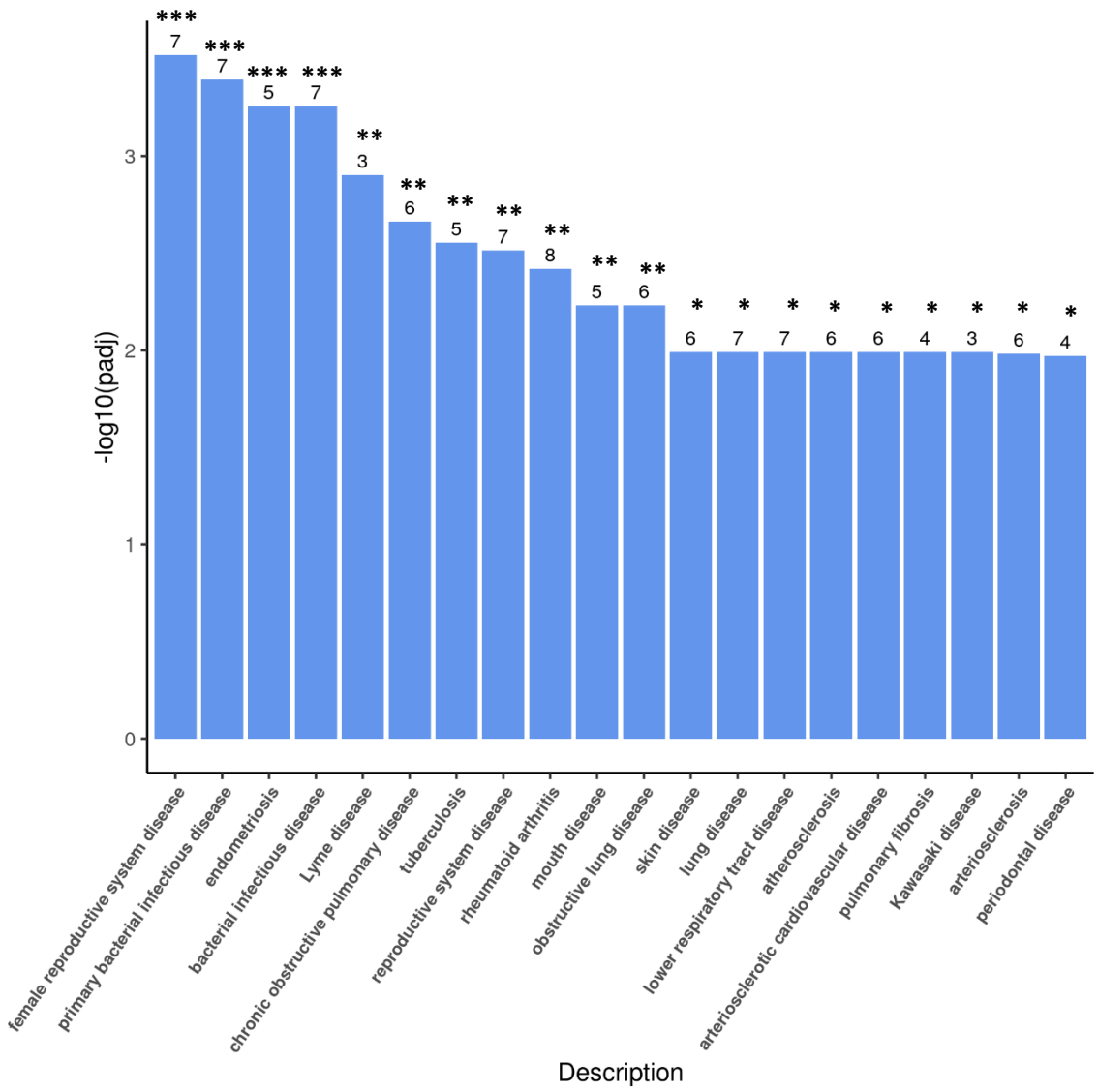


**Figure 4.25** The human disease ontology (DO) analysis for oligomers vs control iAstrocyte treatments.

A bar chart representing categories of top 20 significant differentially expressed pathways, adjusted p-values. Figure provided by Novogene, annotations added separately.

**Table 4.15.** The human disease ontology (DO) analysis for oligomers vs control iAstrocyte treatments.

| DOID | Description | P-value | Adjusted P-value | Upregulated | Gene name | Downregulated | Gene name |
|---|---|---|---|---|---|---|---|
| DOID:229 | female reproductive system disease | 6.80E-07 | 0.000301211 | 6 | *MMP1/PI3/MMP13/IL1A/MMP9/ICAM1* | 1 | *NANOS3* |
| DOID:0050338 | primary bacterial infectious disease | 1.83E-06 | 0.000404728 | 7 | *MMP1/SAA1/MMP13/IL1A/MMP9/ICAM1/IL32* | 0 | |
| DOID:289 | endometriosis | 4.56E-06 | 0.000552591 | 5 | *MMP1/MMP13/IL1A/MMP9/ICAM1* | 0 | |
| DOID:104 | bacterial infectious disease | 4.99E-06 | 0.000552591 | 7 | *MMP1/SAA1/MMP13/IL1A/MMP9/ICAM1/IL32* | 0 | |
| DOID:11729 | Lyme disease | 1.42E-05 | 0.001255145 | 3 | *MMP1/MMP13/MMP9* | 0 | |
| DOID:3083 | chronic obstructive pulmonary disease | 2.94E-05 | 0.002168276 | 6 | *MMP1/PI3/MMP13/IL1A/MMP9/ICAM1* | 0 | |
| DOID:399 | tuberculosis | 4.40E-05 | 0.002784352 | 5 | *MMP1/IL1A/MMP9/ICAM1/IL32* | 0 | |
| DOID:15 | reproductive system disease | 5.53E-05 | 0.003062438 | 6 | *MMP1/PI3/MMP13/IL1A/MMP9/ICAM1* | 1 | *NANOS3* |
| DOID:7148 | rheumatoid arthritis | 7.73E-05 | 0.003804278 | 8 | *MMP1/SAA1/MMP13/IL1A/MMP9/ICAM1/LTB4R2/IL32* | 0 | |
| DOID:403 | mouth disease | 0.00014386 | 0.005862467 | 5 | *MMP1/MMP13/IL1A/MMP9/IL32* | 0 | |
| DOID:2320 | obstructive lung disease | 0.00014557 | 0.005862467 | 6 | *MMP1/PI3/MMP13/IL1A/MMP9/ICAM1* | 0 | |
| DOID:37 | skin disease | 0.0002818 | 0.01018915 | 5 | *MMP1/IL1A/MMP9/ICAM1/IL32* | 1 | *DSP* |
| DOID:850 | lung disease | 0.00029969 | 0.01018915 | 6 | *MMP1/PI3/MMP13/IL1A/MMP9/ICAM1* | 1 | *GATA6* |
| DOID:0050161 | lower respiratory tract disease | 0.00034147 | 0.01018915 | 6 | *MMP1/PI3/MMP13/IL1A/MMP9/ICAM1* | 1 | *GATA6* |
| DOID:1936 | atherosclerosis | 0.00037019 | 0.01018915 | 6 | *MMP1/SAA1/IL1A/MMP9/ICAM1/IL32* | 0 | |
| DOID:2348 | arteriosclerotic cardiovascular disease | 0.00037678 | 0.01018915 | 6 | *MMP1/SAA1/IL1A/MMP9/ICAM1/IL32* | 0 | |
| DOID:3770 | pulmonary fibrosis | 0.00040746 | 0.01018915 | 3 | *MMP1/IL1A/MMP9* | 1 | *GATA6* |
| DOID:13378 | Kawasaki disease | 0.00041401 | 0.01018915 | 3 | *MMP1/MMP13/MMP9* | 0 | |
| DOID:2349 | arteriosclerosis | 0.00044791 | 0.010443357 | 6 | *MMP1/SAA1/IL1A/MMP9/ICAM1/IL32* | 0 | |
| DOID:3388 | periodontal disease | 0.00049969 | 0.010703988 | 4 | *MMP1/MMP13/IL1A/MMP9* | 0 | |

A table showing the DO ID, pathway description, p-value, adjusted p-value, upregulated and downregulated genes, and the corresponding gene names.

### Oligomers vs Scrambled

Lastly, the oligomers vs scrambled iAstrocyte treatment group was analysed and evaluated. However, the pathway enrichment analysis did not include the KEGG pathway analysis and GSEA, and these were omitted from the results. There were no downregulated genes or pathways that reached statistical significance; hence all of the results are described in the context of upregulated genes and pathways in the oligomer-treated iAstrocytes when compared to scrambled treatments (vehicle control).

Gene ontology analysis was carried out (fig.4.26). The results were separated based on the three gene ontology categories: 'biological processes', 'cellular components', 'molecular function'. The top 10 significant (prior to p-value adjustment) gene pathways are shown for each category, and the significant post p-value adjustment pathways are labelled (table 4.16).

Within the 'biological process' category, 5 pathways reached statistical significance post p-value adjustment. These statistically significant differentially expressed gene ontology pathways were: 'regulation of humoral immune response' (p-value= 0.0000704; adjusted p-value= 0.026604), where 3 genes were upregulated (*HPX, ZP4, CFB*); 'humoral immune response' (p-value= 0.000086; adjusted p-value= 0.026604), where 4 genes were significantly upregulated (*HPX, PI3, ZP4, CFB*); 'positive regulation of humoral immune response' (p-value= 0.000133; adjusted p-value= 0.026604), where two genes were significantly upregulated (*HPX, ZP4*); 'regulation of acrosome reaction' (p-value= 0.000159; adjusted p-value= 0.026604), where 2 genes were significantly upregulated (*ZP4*, *PLB1*); and 'interferon-gamma-mediated signalling pathway' (p-value= 0.00028; adjusted p-value= 0.037408), where 3 genes were significantly upregulated (*HPX, ICAM1, TXK*).

Within the 'cellular components' category, 2 pathways reached statistical significance post p-value adjustment. These statistically significant differentially expressed gene ontology pathways were: 'endocytic vesicle lumen' (p-value= 0.000419; adjusted p-value= 0.026967), where 2 genes were significantly upregulated (*SAA1*, and *HPX*); and 'extracellular matrix' (p-value= 0.000749; adjusted p-value= 0.026967), where 5 genes were significantly upregulated (*MMP1, PI3, DGCR6, ZP4, ICAM1*).

Within the 'molecular function' category, none of the gene ontology pathways reached significance post p-value adjustment, however all 10 genes within the top 10 pathways were significant prior to p-value adjustment. Within this category, there were various pathways and genes that were upregulated. The pathways of interest included 'GABA receptor binding' gene ontology pathway, with an upregulation of *GABARAP* gene, and 'complement binding' gene ontology pathway, with an upregulation of *CFB* gene.

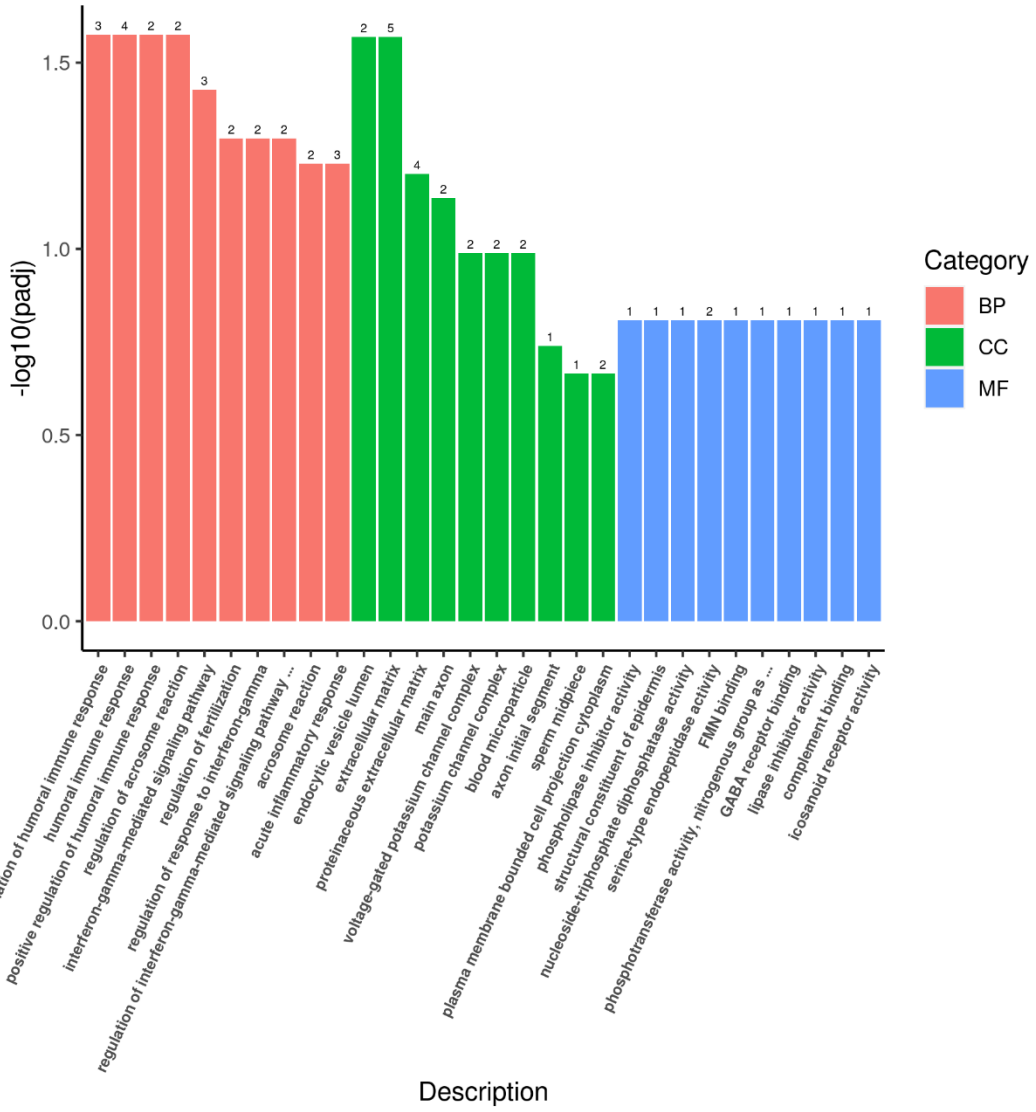


**Figure 4.26.** Gene ontology (GO) classification for oligomers vs scrambled iAstrocyte treatments.

A bar chart representing subcategories of gene transcripts annotated from the RNAseq data of human iAstrocytes. The results show top 10 significant differently expressed gene ontology pathways, per category, prior to p-value adjustments (BP- biological process; CC- cellular function; MF- molecular function). Figure provided by Novogene.

**Table 4.16.** Gene ontology (GO) classification for oligomers vs scrambled iAstrocyte treatments

| Category | Gene ontology ID | Subcategory description | P-value | Adjusted P-value | Upregulated | Gene name | Downregulated | Gene name |
|---|---|---|---|---|---|---|---|---|
| BP | GO:0002920 | regulation of humoral immune response | 7.04E-05 | 0.026603567 | 3 | HPX/ZP4/CFB | 0 | |
| BP | GO:0006959 | humoral immune response | 8.60E-05 | 0.026603567 | 4 | HPX/PI3/ZP4/CFB | 0 | |
| BP | GO:0002922 | positive regulation of humoral immune response | 0.000132683 | 0.026603567 | 2 | HPX/ZP4 | 0 | |
| BP | GO:0060046 | regulation of acrosome reaction | 0.000159065 | 0.026603567 | 2 | ZP4/PLB1 | 0 | |
| BP | GO:0060333 | interferon-gamma-mediated signaling pathway | 0.000279583 | 0.037408246 | 3 | HPX/ICAM1/TXK | 0 | |
| BP | GO:0080154 | regulation of fertilization | 0.000454361 | 0.050447132 | 2 | ZP4/PLB1 | 0 | |
| BP | GO:0060330 | regulation of response to interferon-gamma | 0.000603254 | 0.050447132 | 2 | HPX/TXK | 0 | |
| BP | GO:0060334 | regulation of interferon-gamma-mediated signaling pathway | 0.000603254 | 0.050447132 | 2 | HPX/TXK | 0 | |
| BP | GO:0007340 | acrosome reaction | 0.000833675 | 0.059108713 | 2 | ZP4/PLB1 | 0 | |
| BP | GO:0002526 | acute inflammatory response | 0.000883538 | 0.059108713 | 3 | SAA1/CFB/ICAM1 | 0 | |
| CC | GO:0071682 | endocytic vesicle lumen | 0.000419377 | 0.026967344 | 2 | SAA1/HPX | 0 | |
| CC | GO:0031012 | extracellular matrix | 0.000749093 | 0.026967344 | 5 | MMP1/PI3/DGCR6/ZP4/ICAM1 | 0 | |
| CC | GO:0005578 | proteinaceous extracellular matrix | 0.00262106 | 0.06290543 | 4 | MMP1/PI3/DGCR6/ZP4 | 0 | |
| CC | GO:0044304 | main axon | 0.004056409 | 0.07301536 | 2 | TRIM46/CNTNAP1 | 0 | |
| CC | GO:0008076 | voltage-gated potassium channel complex | 0.008314209 | 0.10250096 | 2 | KCNH4/CNTNAP1 | 0 | |
| CC | GO:0034705 | potassium channel complex | 0.009539916 | 0.10250096 | 2 | KCNH4/CNTNAP1 | 0 | |
| CC | GO:0072562 | blood microparticle | 0.009965371 | 0.10250096 | 2 | HPX/CFB | 0 | |
| CC | GO:0043194 | axon initial segment | 0.020232869 | 0.182095818 | 1 | TRIM46 | 0 | |
| CC | GO:0097225 | sperm midpiece | 0.02854637 | 0.216329458 | 1 | GABARAP | 0 | |
| CC | GO:0032838 | plasma membrane bounded cell projection cytoplasm | 0.035064027 | 0.216329458 | 2 | TRIM46/GABARAP | 0 | |
| MF | GO:0004859 | phospholipase inhibitor activity | 0.015117368 | 0.155634335 | 1 | SNCB | 0 | |
| MF | GO:0030280 | structural constituent of epidermis | 0.015117368 | 0.155634335 | 1 | PI3 | 0 | |
| MF | GO:0047429 | nucleoside-triphosphate diphosphatase activity | 0.015117368 | 0.155634335 | 1 | ENPP3 | 0 | |
| MF | GO:0004252 | serine-type endopeptidase activity | 0.019230775 | 0.155634335 | 2 | MMP1/CFB | 0 | |
| MF | GO:0010181 | FMN binding | 0.019609785 | 0.155634335 | 1 | HAO2 | 0 | |
| MF | GO:0016775 | phosphotransferase activity, nitrogenous group as acceptor | 0.019609785 | 0.155634335 | 1 | KCNH4 | 0 | |
| MF | GO:0050811 | GABA receptor binding | 0.021102897 | 0.155634335 | 1 | GABARAP | 0 | |
| MF | GO:0055102 | lipase inhibitor activity | 0.021102897 | 0.155634335 | 1 | SNCB | 0 | |
| MF | GO:0001848 | complement binding | 0.022593834 | 0.155634335 | 1 | CFB | 0 | |
| MF | GO:0004953 | icosanoid receptor activity | 0.022593834 | 0.155634335 | 1 | LTB4R2 | 0 | |

A table showing the category, subcategory description, corresponding gene ontology ID, p-value, adjusted p-value, gene count, number of upregulated and downregulated genes, and associated gene names.

For the human disease ontology pathway analysis, the results showed that none of the enriched pathways reached statistical significance post p-value adjustment. The top 20 disease ontology pathways and corresponding upregulated genes are shown (fig.4.27, table 4.17). All of the genes within the top 20 disease ontology pathways were statistically significant prior to p-value adjustments.

Within the top 20 disease ontology pathways, there were no genes that were downregulated. The most common upregulated genes across all the disease ontology pathways were: *MMP1, ICAM1, SAA1,* and *IL32.*

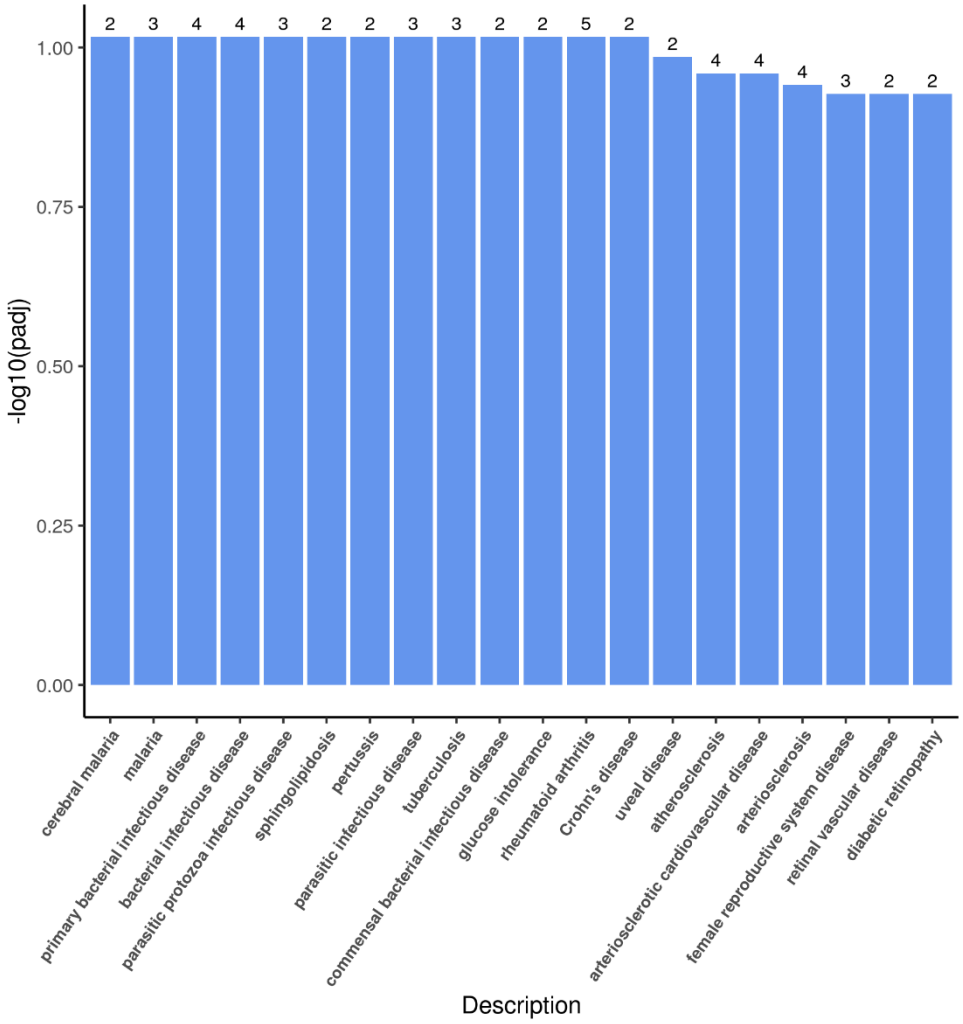


**Figure 4.27.** The human disease ontology (DO) analysis for oligomers vs scrambled iAstrocyte treatments.

A bar chart representing categories of top 20 significant differentially expressed pathways, prior to p-value adjustments. Figure provided by Novogene.

**Table 4.17.** The human disease ontology (DO) analysis for oligomers vs scrambled iAstrocyte treatments.

| DOID | Description | P-value | Adjusted P-value | Upregulated | Gene name | Downregulated | Gene name |
|---|---|---|---|---|---|---|---|
| DOID:14069 | cerebral malaria | 0.00097862 | 0.096299205 | 2 | MMP1/ICAM1 | 0 | |
| DOID:12365 | malaria | 0.00101354 | 0.096299205 | 3 | MMP1/SAA1/ICAM1 | 0 | |
| DOID:0050338 | primary bacterial infectious disease | 0.0010511 | 0.096299205 | 4 | MMP1/SAA1/IL32/ICAM1 | 0 | |
| DOID:104 | bacterial infectious disease | 0.00181161 | 0.096299205 | 4 | MMP1/SAA1/IL32/ICAM1 | 0 | |
| DOID:2789 | parasitic protozoa infectious disease | 0.00185206 | 0.096299205 | 3 | MMP1/SAA1/ICAM1 | 0 | |
| DOID:1927 | sphingolipidosis | 0.0024496 | 0.096299205 | 2 | SNCB/ICAM1 | 0 | |
| DOID:1116 | pertussis | 0.00278493 | 0.096299205 | 2 | SAA1/ICAM1 | 0 | |
| DOID:1398 | parasitic infectious disease | 0.00303078 | 0.096299205 | 3 | MMP1/SAA1/ICAM1 | 0 | |
| DOID:399 | tuberculosis | 0.00332618 | 0.096299205 | 3 | MMP1/IL32/ICAM1 | 0 | |
| DOID:0050339 | commensal bacterial infectious disease | 0.00351662 | 0.096299205 | 2 | SAA1/ICAM1 | 0 | |
| DOID:10603 | glucose intolerance | 0.00391261 | 0.096299205 | 2 | CFB/ICAM1 | 0 | |
| DOID:7148 | rheumatoid arthritis | 0.00407715 | 0.096299205 | 5 | MMP1/SAA1/IL32/LTB4R2/ICAM1 | 0 | |
| DOID:8778 | Crohn's disease | 0.00411806 | 0.096299205 | 2 | MMP1/ICAM1 | 0 | |
| DOID:3480 | uveal disease | 0.00476395 | 0.103445848 | 2 | MMP1/ICAM1 | 0 | |
| DOID:1936 | atherosclerosis | 0.00570718 | 0.109716534 | 4 | MMP1/SAA1/IL32/ICAM1 | 0 | |
| DOID:2348 | arteriosclerotic cardiovascular disease | 0.00577455 | 0.109716534 | 4 | MMP1/SAA1/IL32/ICAM1 | 0 | |
| DOID:2349 | arteriosclerosis | 0.00640533 | 0.114542329 | 4 | MMP1/SAA1/IL32/ICAM1 | 0 | |
| DOID:229 | female reproductive system disease | 0.00727693 | 0.118253103 | 3 | MMP1/PI3/ICAM1 | 0 | |
| DOID:2462 | retinal vascular disease | 0.00777981 | 0.118253103 | 2 | MMP1/ICAM1 | 0 | |
| DOID:8947 | diabetic retinopathy | 0.00777981 | 0.118253103 | 2 | MMP1/ICAM1 | 0 | |

A table showing the DO ID, pathway description, p-value, adjusted p-value, upregulated and downregulated genes, and the corresponding gene names.

### 4.5.6. Summary of the pathway analysis findings

To summarise, the pathway analyses for each iAstrocyte treatment group (extracts, fibrils, oligomers) displayed a differential response of gene expression changes, and gene pathway changes, in astrocytes. The potentially disease-relevant gene expression pathways encompassed a variety of disease-related processes, such as apoptosis, BBB integrity, extracellular matrix, inflammation, neurotransmitter dysfunction, and oxidative stress. Although some gene expression pathways, as well as individual genes have overlapped between different treatment groups (notably IL-17 signalling pathway), we can conclude that astrocytes can respond with a varying molecular profile to different types and aggregation species of Aβ. A summary of the disease-relevant pathways can be found in table 4.18.

**Table 4.18.** Differentially expressed pathways relating to Alzheimer's disease

| Pathway | Disease process | Extracts | Fibrils | Oligomers |
|---|---|---|---|---|
| Apoptotic signalling pathway | Apoptosis | No | No | Yes |
| Tight junction | BBB integrity | Yes | Yes | No |
| Extracellular matrix | Extracellular matrix | No | Yes | Yes |
| Metallopeptidase activity | Extracellular matrix | No | No | Yes |
| Extracellular matrix disassembly | Extracellular matrix | No | No | Yes |
| IL-17 signalling | Inflammation | Yes | Yes | Yes |
| INγ-mediated signalling | Inflammation | No | No | Yes |
| NFκB | Inflammation | No | No | Yes |
| TNF signalling | Inflammation | No | No | Yes |
| Acute inflammatory response | Inflammation | No | No | Yes |
| MAPK signalling pathway | Inflammation/ apoptosis | No | No | Yes |
| GABA receptor binding | Neurotransmitter dysfunction | No | No | Yes |
| GABA receptor complex | Neurotransmitter dysfunction | No | No | Yes |
| GABA-A receptor complex | Neurotransmitter dysfunction | No | No | Yes |
| GABAergic synapse | Neurotransmitter dysfunction | No | No | Yes |
| Glutamate binding | Neurotransmitter dysfunction | No | Yes | No |
| Glutamergic synapse | Neurotransmitter dysfunction | No | Yes | No |
| Glutamate receptor binding | Neurotransmitter dysfunction | Yes | No | No |
| Ionotropic glutamate receptor complex | Neurotransmitter dysfunction | Yes | No | No |
| AGE-RAGE signalling | Oxidative stress | No | No | Yes |

Table reporting pathways relating to Alzheimer's disease; the specific disease process; and whether they were differentially expressed in specific Aβ treatment groups.

## 4.6 Discussion

### 4.6.1 Variation between experimental groups and cell lines

The principal components analysis shows the association between samples and allows for investigation of groups with similar expression profiles. Therefore, the principal components analysis can capture the differences and the variation between the different groups. Here, the principal components analysis revealed that the different iAstrocyte cell lines cluster together based on the cell line more than the treatment applied. The iAstrocytes used in this study originate from reprogramming skin fibroblasts of donors into iNPCs, from which iAstrocytes can be differentiated (Meyer *et al.*, 2014). The principal components analysis showed that the different iAstrocyte cell lines display varying gene expression profiles regardless of the cell treatment. The cell treatments grouped closely within each cell line. The iAstrocyte model used in the current study closely retains the ageing phenotype of the donors (Meyer *et al.*, 2014; Gatto *et al.*, 2021). This is interesting, as it may mean that different individuals may respond differently to amyloid beta in disease. In Chapter 3, there was an indication that oxidative stress may elicit differential responses in different cell lines in terms of DNA damage and formation of γH2AX-positive DNA foci. Furthermore, in Chapter 3, there was a particular LDH release response of 155v2 iAstrocytes, as there were more significant differences between amyloid treatment groups in this cell line. Meanwhile, the CS-14 and 161 iAstrocytes showed no significant differences in LDH percentage release in any of the treatment groups. The mechanisms behind these differential responses are unknown; however, this would be an interesting avenue to explore. Another interesting avenue to explore would be to compare the gene expression and PCA of iAstrocytes presented in the current study to other models of astrocytes, such as iPSC lines. However, due to iPSC lines not retaining the ageing phenotypes of the donor, they may elicit a similar response to fetal astrocytes. The gene expression of fetal astrocytes has been shown to vary significantly from adult iAstrocytes, although they do not vary from young iAstrocytes (Gatto *et al.*, 2021). Therefore, there is a certain degree of confidence that the iAstrocyte model chosen in the current work closely resembles the human astrocytes found *in vivo*.

As mentioned previously, Alzheimer's disease is a multifactorial disease, which can display various genetic risk factors. Furthermore, there may be varying environmental and multimorbidity factors involved, which could modulate the risk of developing Alzheimer's disease in individuals. For this reason, the development of a single therapy which would benefit all patients may be difficult. As every individual is different and unique, precision medicine (or personalised medicine) could be a more appropriate option for diseases such as Alzheimer's disease (Forloni, 2020; Di Meco and Vassar, 2021). The implications of this variation for future experimental design would be that each cell line may need to be further characterised individually. It would be interesting to differentiate Alzheimer's disease

patient-derived iAstrocytes to identify potential disease biomarkers, and to further elucidate the relationship between amyloid beta and astrocytes. Characterisation of variation of responses in different cell lines and individuals may shine a light on the reasons behind why many clinical trials for Alzheimer's disease therapeutics have failed, especially when looking at anti-amyloid treatments. Patient stratification approaches could be implemented using different cell lines, which could allow investigators to differentiate between responders and non-responders to anti-amyloid treatments. This would allow for a more tailored and streamlined therapeutics approach for Alzheimer's disease patients.

### 4.6.2 Differential expression and gene set enrichment analysis of RNAseq data

The gene ontology analysis identified a total of 29,960 genes that were differentially expressed in the treated vs control iAstrocytes. Gene ontology analysis answers a question of which biological processes, cellular components and molecular functions are implicated in iAstrocytes treated with amyloid beta. Arbitrary cut-off point (10,000 genes) was set for the subcategories. Within the biological processes category, the most abundant pathways related to 'biological regulation', 'cellular process', 'metabolic process', 'regulation of biological process', 'response to stimulus', and 'single-organism process'. Within the cellular component category, the most abundant pathways related to 'cell', 'cell part', 'membrane', 'organelle', and 'organelle part'. Within the molecular function category, the most abundant pathway was 'binding'. These pathways therefore represent the biological processes, cellular components and molecular functions which have been impacted in iAstrocytes following amyloid beta treatment.

Furthermore, the analysis showed that there is a wide variety of up- and down-regulated genes within each group, and that the response to the amyloid beta treatments is very heterogenous in iAstrocytes. This is unsurprising, as varying responses to different amyloid beta aggregates has been reported before. For example, infusion of Aβ oligomers into the rat brain can cause a more profound neurodegeneration, as well as impairment in cognitive function, when compared to Aβ fibrils (He *et al.*, 2012). Moreover, Aβ oligomers are reported to be more neurotoxic species of Aβ, as they have been found to reduce neuronal viability at a much higher rate than Aβ fibrils (Dahlgren *et al.*, 2002). Aβ oligomers and fibrils have also been found to differentially stimulate microglia to elicit very unique signalling responses, suggesting that the conformation of Aβ may be an important factor contributing to the heterogeneity of cellular responses (Cindy M. Sondag, Dhawan and Combs, 2009). The mechanisms behind the differential toxicity of Aβ oligomers and fibrils remains unclear. However, it is known that Aβ oligomers and fibrils vary structurally, and this variation could contribute to their differential roles in Alzheimer's disease pathology. For example, Aβ oligomers are much smaller in size, and this could mean they could diffuse more easily inside tissues when compared to Aβ fibrils.

Additionally, Aβ oligomers are more soluble, unstable and disorganised than Aβ fibrils (Verma, Vats and Taneja, 2015). The results presented show that Aβ oligomers, Aβ fibrils, as well as Aβ extracted from human Alzheimer's disease brains can cause a differential response in iAstrocytes, which was manifested by the differential gene expression profile of each treatment group.

For each treatment and comparison group (extracts vs control, fibrils vs control, fibrils vs scrambled, oligomers vs control, oligomers vs scrambled), pathway enrichment analyses were carried out. These included gene ontology pathway analysis, KEGG pathway analysis, GSEA, and human disease ontology pathway analysis. The pathway analyses further highlighted the heterogenous responses of iAstrocytes to different Aβ species and conformations. There were a number of significant genes and corresponding pathways that were differentially expressed in the treatment groups. Furthermore, there were a number of potentially disease-relevant gene expression pathways. Not all pathways or genes reached significance post p-value adjustments; however, the top 10 or 20 gene expression pathways, alongside the corresponding genes, in each analysis were investigated further. Even though there was a large heterogeneity in terms of iAstrocyte responses to Aβ, there were also some similarities in the gene expression profiles across the different treatment groups. These pathways, alongside uniquely expressed genes, are discussed further in the current chapter. Due to the large number of genes that were differentially expressed, it is not possible to characterise and describe all in detail, as this is beyond the scope of the study. All effort was made to characterise and describe the gene expression results for genes and pathways which may be of interest in Alzheimer's disease. However, it is possible that other genes and pathways may have novel disease-related roles in Alzheimer's disease, and as such should not be completely disregarded in the future.

The main aims of the current chapter were to establish whether different types of Aβ elicit differential astrocyte responses; and whether these responses could be Alzheimer's disease relevant. Furthermore, the aims of the chapter were to investigate and characterise the differential responses to varying Aβ species in iAstrocytes by investigating the specific gene expression pathways and genes which may be disease relevant. Indeed, the results showed that Aβ brain extracts, $A\beta_{1\text{-}42}$ fibrils, and $A\beta_{1\text{-}42}$ oligomers could cause astrocytes to react differently, showing an upregulation and downregulation of various genes, as well as a differential expression of gene pathways. However, the response in astrocytes was very heterogenous, where some pathways were differentially expressed across all treatment groups, and some pathways were uniquely differentially expressed in individual treatment groups. This would indicate that astrocyte responses in disease and neurodegeneration may not be as simple as once thought, and any small changes to the astrocyte environment (for example, elicited by the different Aβ aggregation species) may be detrimental to the overall astrocyte health and function. Future work could include the addition of Aβ human brain extracts to the

morphological, DNA damage, and cell toxicity assays described in Chapter 3. This investigation could reveal whether the astrocytes change in response to a mixture of Aβ isoforms, which would more closely resemble the astrocyte responses to Aβ *in vivo*, during disease.

### Apoptosis

Apoptotic signalling pathway was among the top pathways that were uniquely identified as differentially expressed in iAstrocytes treated with oligomeric $A\beta_{1-42}$. Interestingly, the apoptotic signalling pathway was not differentially expressed in iAstrocytes treated with Aβ extracts, nor in iAstrocytes treated with $A\beta_{1-42}$ fibrils. This suggests that oligomeric $A\beta_{1-42}$ may be a key player contributing to apoptosis pathways in astrocytes during Alzheimer's disease.

Apoptosis refers to a programmed cell death, where a cell will progress into cell death upon detecting a specific stimulus. Apoptosis can occur in normal processes during development and ageing, as well as a defence mechanism against cell damage and inflammation (Elmore, 2007). Early research investigating apoptosis in Alzheimer's disease showed that apoptosis may be one of the key mechanisms of neuronal cell death in disease (Su *et al.*, 1994). Cultured rat cortical neurons exposed to Aβ has been shown to induce neuronal apoptosis (Copani *et al.*, 2002). Furthermore, Aβ oligomers specifically could be the key initiators of neuronal apoptosis via caspase activation, mitochondrial dysfunction, and pro-inflammatory pathways; and this could subsequently result in cognitive dysfunction (Florent *et al.*, 2006; Youssef *et al.*, 2008; Yang, Hsu and Kuo, 2009).

In astrocytes, the pathogenic role of apoptosis is unclear, however in an astrocyte-neuron co-culture system, Aβ can impact astrocyte lysosomal function and lead to Aβ spread as well as Aβ-mediated neuronal apoptosis (Söllvander *et al.*, 2016). The full roles of Aβ on astrocyte apoptosis remain to be elucidated. The majority of research available focuses on astrocyte-mediated neuronal apoptosis, however the impact of Aβ, and Aβ oligomers, on astrocyte apoptosis is a current gap in knowledge. The astrocyte programmed cell death would be an interesting avenue to explore in Alzheimer's disease. In Parkinson's disease, an amyloid protein α-synuclein, can trigger an endoplasmic reticulum stress, astrocyte apoptosis, and this can result in a decreased neuronal support from astrocytes preventing neurite outgrowth (Liu *et al.*, 2018). Therefore, amyloid proteins could directly affect apoptosis pathways in astrocytes, which could encompass early astrocytic changes in disease, leading to more profound effects on neuronal survival downstream.

### Blood brain barrier integrity

The blood brain barrier (BBB) is an essential component of the brain vasculature. The function of the BBB is to regulate the movement of ions and molecules between the blood and CNS, which helps in

maintaining the ion homeostasis, as well as transport of nutrients and hormones to the brain. Therefore, the BBB is an integral component in regulating the brain's delicate microenvironment (Cabezas *et al.*, 2014). Astrocytes are involved in maintaining the BBB via their connections to the brain vasculature through astrocytic end-feet. It has been reported that a loss of GFAP-positive astrocytes can be accompanied by the loss of tight junction proteins, modulating the BBB integrity (reviewed in Garwood *et al.*, 2017).

BBB dysfunction has been reported in Alzheimer's disease. MRI investigations have shown that mild cognitive impairment correlates with BBB breakdown, which can start in the hippocampus (Montagne *et al.*, 2015). Additionally, BBB dysfunction has been reported in a variety of Alzheimer's disease transgenic models, which further confirms the involvement of BBB in disease (Montagne, Zhao and Zlokovic, 2017).

### *Tight junctions*

Tight junctions are protein complexes forming an intercellular barrier between epithelial cells. Tight junctions localised at the BBB can overlap, forming occlusions between the brain endothelial cells, and therefore they function to control the molecules entering the CNS. Claudins are a family of proteins that are located at the tight junctions. In fact, claudins are thought to be the main component of tight junctions, and therefore can be essential in the maintenance of the BBB (Tsukita, Tanaka and Tamura, 2019; Lochhead *et al.*, 2020).

As tight junctions are involved in BBB integrity, it is important to note that BBB breakdown is an event that is related to Alzheimer's disease pathology. The BBB contains many components, including the association of astrocytes. Amyloid beta has recently been shown to adversely affect tight junctions (Yamazaki *et al.*, 2019), but amyloid beta can also be associated with the damage to blood vessels, further exacerbating the BBB breakdown (Sweeney, Sagare and Zlokovic, 2018).

The results presented in section 4.5.5 showed that tight junction gene expression pathway was differentially expressed in iAstrocytes treated with Aβ extracts and Aβ fibrils, suggesting a tight junction dysfunction. Additionally, there was an observed downregulation of the *CLDN2* and *CLDN18* genes in iAstrocytes treated with Aβ extracts and Aβ fibrils. *CLDN2* and *CLDN18* code for claudin-2 and claudin-18 proteins respectively. Furthermore, the RNAseq analysis has shown a downregulation of the *MARVELD3*, encoding the protein of the same name. MARVELD3 proteins are proteins which are also associated with the integrity of the tight junctions. The differential expression of tight-junction related genes and pathways was not observed in oligomer treatments of iAstrocytes, which could suggest that Aβ fibrils (and amyloid plaques) may be the specific Aβ species causing BBB disruptions

rather than oligomers. This could further suggest that, as more Aβ fibrils are present at later disease stages, the BBB dysfunction can be an event taking place at later stages of Alzheimer's disease.

Previous studies have shown that another claudin protein, claudin-5, can affect BBB permeability. Claudin-5-deficient mice have been reported to exhibit a more permeable BBB (Nitta *et al.*, 2003), suggesting that a loss of claudin-5 can adversely affect the integrity of the BBB. Furthermore, in Alzheimer's disease, it has been shown that there is a decrease in claudin-5, which can correlate with the loss of tight junctions (Yamazaki *et al.*, 2019). Amyloid beta can also activate proinflammatory molecules, which can further disrupt tight junctions (Jo *et al.*, 2020). However, ageing-related inflammation has also been shown to disrupt tight junctions, and, as a result can contribute to the BBB breakdown (Elahy *et al.*, 2015).

The exact function and role of claudin-2, claudin-18, and MARVELD3 has not been extensively researched in Alzheimer's disease. Based on the research conducted on the claudin and occludin protein families, it can be proposed that amyloid beta can modulate astrocytic responses to promote BBB breakdown. This could occur due to the loss of claudin proteins, and proteins associated with tight junctions. The BBB breakdown can then lead to neuronal loss, and disruptions in the CNS homeostasis. This could be one of the mechanisms behind the onset and progression of Alzheimer's disease.

### Extracellular matrix

In the CNS, the extracellular matrix is a structural network of molecules (such as collagen, elastin, fibronectin). The extracellular matrix can function to modulate learning and memory, as well as synaptogenesis, synaptic plasticity, and can act as a physical barrier within the CNS (Melrose, Hayes and Bix, 2021). In Alzheimer's disease the extracellular matrix can be involved in the formation and degradation of Aβ plaques, reduction of oxidative stress, and regulating inflammation. The integrity of extracellular matrix is therefore an important protective component against Alzheimer's disease-related injury (Sun *et al.*, 2021).

#### *Matrix metalloproteinases*

MMPs are proteins of an important protease family, which play various roles in the CNS. For example, they are involved in the regulation of signalling cascade during synaptic dysfunction, as well as can be involved in the processes regarding the disruption of the blood brain barrier (BBB), neuroinflammation and neurodegeneration (Behl *et al.*, 2021). Importantly, MMPs are a family of proteins which function to cleave the extracellular matrix, causing its remodelling (Stamenkovic, 2003). The iAstrocytes treated with $A\beta_{1\text{-}42}$ oligomers and fibrils show a differential expression of gene pathways and specific genes relating to the extracellular matrix. Here, an upregulation of matrix metalloproteinases, (MMPs)

namely MMP1, MMP9, and MMP13 can be seen in iAstrocytes treated with oligomers and fibrils. This suggests that astrocytes treated with Aβ fibrils and oligomers can be involved in extracellular matrix disassembly, which could then lead to a loss of protective effects of the extracellular matrix in disease.

MMPs have been reported to be elevated in Alzheimer's disease (Duits *et al.*, 2015). MMP9 has been previously shown to be upregulated in the Alzheimer's disease brains, namely in neurons, senile plaques and NFTs; but also in the plasma, hippocampus, and cerebral cortex (Bruno *et al.*, 2009). Previous studies have also reported that Aβ can induce an increase in expression of MMPs, especially MMP12 and MMP13 in microglia (Ito *et al.*, 2007). MMP13 can impact microglial morphology and signalling in Parkinson's disease, where MMP13 can activate proinflammatory cytokines, as well as it can activate MMP9, leading to further adverse downstream events (Sánchez and Maguire-Zeiss, 2020).

A common Alzheimer's disease allele, APOE4, has been shown to cause a BBB breakdown through the activation of cyclophilin A/MMP9 pathway (Behl *et al.*, 2021). Furthermore, the levels of MMP1 are elevated in Alzheimer's disease, where it could be linked to the dysfunction and breakdown of BBB (Leake, Morris and Whateley, 2000). Reduced expression of MMP9 in astrocytes can also have a positive effect on BBB. Toll-like receptor 2 is a receptor protein which can stimulate inflammatory responses. Toll-like receptor 2 has been implicated in injury response, by activating microglia and astrocytes, which further contributes to inflammation. Toll-like receptor 2 can contribute to BBB damage and breakdown and can also stimulate activation of MMP9 in astrocytes. This can be attenuated by diminishing toll-like receptor 2 and its consequent signalling, which suggests that astrocyte-related toll-like receptor 2 signalling, MMP9 activation, and subsequent inflammation, can contribute to the BBB damage and breakdown in Alzheimer's disease (Min *et al.*, 2015).

MMP9 has also been linked to inflammation, as MMP9 can activate proinflammatory cytokines, affecting tight junctions at the neurovascular unit, further contributing to inflammation, release of free radicals, brain hypoxia, and increased permeability of the BBB (Vafadari, Salamian and Kaczmarek, 2016). In astrocytes, reactive oxygen species can stimulate the activation and upregulation of MMP9 (Yang *et al.*, 2015). Furthermore, it has been reported that blocking MMP9 expression in microglia could have a positive effect on alleviating oxidative stress-induced neuroinflammation (Dwir *et al.*, 2019). This further highlights the importance of MMP9 upregulation in disease.

Aβ has previously been shown to cause an increase in the expression of MMP9, which in turn can cause cognitive impairment and neuronal loss (Mizoguchi *et al.*, 2009). Meanwhile, MMP13 can directly affect BACE1 activity. Inhibition of MMP13 can lead to a decrease of BACE1 in neurons, which can in turn decrease the levels of Aβ (Zhu *et al.*, 2019). This suggests that there may be an interplay

between MMPs and Aβ, with decreasing the levels of MMPs being a potential therapeutic target for Alzheimer's disease.

The present study found an upregulation of MMP1, MMP9, and MMP13 in iAstrocytes following Aβ oligomer and fibril treatment. Not much is known about the role of MMP1 in Alzheimer's disease and neurodegeneration, however the roles of MMPs in Alzheimer's disease have been previously reported. Aβ-mediated upregulation and induction of MMPs signalling could therefore be a contributing factor to the activation of glial cells, induction of neuroinflammation, and breakdown of BBB. This would reveal a potential mechanism, by which amyloid beta can modulate astrocytes to contribute to neurodegeneration in Alzheimer's disease.

### Inflammation

Inflammation has long been reported and described as one of the major events contributing to neurodegeneration, including Alzheimer's disease pathology. Neuroinflammation can be defined as an inflammatory response in the brain and/or spinal cord. Neuroinflammation can be mediated by the production of reactive oxygen species, secondary molecular mediators, and cytokines and chemokines. These cytokines and chemokines can be produced by glial cells of the CNS, including astrocytes (DiSabato, Quan and Godbout, 2016). Indeed, the results reported a variety of immune responses of astrocytes after treatment with different types of Aβ. Interestingly, all three treatment groups (extracts, fibrils, oligomers) displayed a differential expression of gene pathway relating to IL-17 signalling, suggesting that this is a common inflammatory pathway in astrocytes as a response to an Aβ stimulus. However, further inflammatory pathways have all related specifically to the Aβ oligomer treatment in iAstrocytes. Interferon-γ pathway, TNF signalling pathway, NFκB pathway, MAPK signalling pathway, and acute inflammatory response pathway were all uniquely differentially expressed in oligomer-treated iAstrocytes. These were not differentially expressed in iAstrocytes treated with Aβ extracts or Aβ fibrils, suggesting that astrocyte-mediated inflammation may be an early event in disease pathology, induced specifically by Aβ oligomers.

#### *Interleukins*

The KEGG pathway analysis revealed that the IL-17 signalling pathway was commonly differentially expressed across all treatment groups. The differential expression was significant before p-value adjustment in all treatment conditions; and it was also significant post p-value adjustment in oligomers vs control and fibrils vs control treatment groups. IL-17 is a proinflammatory cytokine which has been implicated in many inflammatory and autoimmune diseases. Cytokines are small signalling proteins, which function to regulate inflammation, as well as regulate cellular activities, which include cell growth, cell survival and cell differentiation. Chemokines are a group of secreted proteins within

the cytokine family, which can function to induce cell migration, and can be involved in homeostasis and inflammation (Ramesh, Maclean and Philipp, 2013).

IL-17 has been reported to activate common proinflammatory pathways, which include NF-κB, mitogen-mediated protein kinases, and phosphoionositide 3-kinase (PI3K) (Qian *et al.*, 2010). In neurodegeneration, IL-17 has been associated with cognitive impairments and synaptic dysfunction in Alzheimer's disease (Brigas *et al.*, 2021). Additionally, in astrocytes, IL-17 can downregulate the expression of glutamate transporters, as well as glutamate release, which can contribute to glutamate excitotoxicity (Kostic *et al.*, 2017). This would indicate that IL-17 signalling pathway could promote neurodegeneration and neuroinflammation as a response to Aβ. Indeed, neutralising IL-17 in CD1 mice injected with $A\beta_{1-42}$ has been reported to improve cognition and reduce neurodegeneration as well as reduce the levels of other proinflammatory cytokines (Cristiano *et al.*, 2019). It would therefore be interesting to investigate and characterise the impact of IL-17 signalling on astrocytes in Alzheimer's disease.

Regarding specific gene expression changes, three cytokines and chemokines were upregulated in oligomer- and fibril-treated iAstrocytes. These were interleukin 32 (IL-32), encoded by *IL32;* interleukin-1 alpha (IL-1A), encoded by *IL1A;* and interleukin-8 (IL-8), encoded by *CXCL8.* This suggests a neuroinflammatory response of astrocytes to amyloid beta. IL-32 and IL-1A were specifically upregulated in oligomer treatments only, while IL-8 was specifically upregulated in fibril treatments only, which suggests that both Aβ species may play a role in interleukin-mediated inflammation in astrocytes, although potentially via different mechanisms and mediators.

IL-32 has been described as a pluripotent immunoregulator, which has been implicated in mediating proinflammatory responses. IL-32 can function to mediate the production of other proinflammatory cytokines and chemokines, including IL-1β, IL-6, and TNFα (Gong *et al.*, 2020). However, IL-32 has not been extensively characterised in terms of neuroinflammation and neurodegeneration. In terms of Alzheimer's disease, it has been shown that overexpression of IL-32β in mice could result in memory impairment, activation of glial cells, and neuroinflammation (Yun *et al.*, 2015). IL-32 has also been shown to increase the production of reactive oxygen species and nitric oxide in astrocytes. Furthermore, IL-32 can also induce the expression of MMP9 (which has previously been described as a potential player in astrocyte-mediated BBB breakdown) (Cho *et al.*, 2010). In fact, the relationship between MMPs, BBB breakdown, and neuroinflammation, could be one of the mechanisms behind amyloid beta-induced neurodegeneration (Xie, Hoecke and Vandenbroucke, 2022).

IL-1A is a potent inflammatory cytokine, and alongside IL-1B, can function to activate inflammatory processes as a response to cell stress and injury. Extensive research has been carried out looking into

the processes governing IL-1B, however not much is known about IL-1A (Di Paolo and Shayakhmetov, 2016). Both IL-1A and IL-1B belong to the interleukin 1 family of proteins. IL-1, especially IL-1A polymorphisms have previously been associated with early onset Alzheimer's disease (Grimaldi *et al.*, 2000).

Previous studies showed that treatment of microglia with $A\beta_{1-42}$ can induce an upregulation of IL-8 (Franciosi *et al.*, 2005). Administration of Aβ has also been shown to upregulate IL-8 in monocytes (Meda, Bonaiuto, *et al.*, 1995). Furthermore, there has been reports of an expression of IL-8 receptor in Alzheimer's disease neurons, and it was suggested that IL-8 could be a potential mediator between glial-neuron interactions (Xia *et al.*, 1997). The IL-8 receptor has also been reported to be upregulated in microglia, following the administration of Aβ (Ryu *et al.*, 2015). The effects of IL-8 upregulation have not been extensively studied in Alzheimer's disease; however, the chemokine could be a potential player contributing to the disease pathology. In other neurodegenerative diseases, IL-8 has also been reported to be upregulated. These included Huntington's disease, ALS, and Parkinson's disease (Mclarnon, 2016). It is therefore clear that IL-8 upregulation could be contributing to neurodegeneration, and this could be taking place by modulating neuroinflammation.

Neither IL-32, IL-1A, nor IL-8 have been extensively studied in terms of Aβ or Alzheimer's disease. However, there are reports suggesting that all three described cytokines could be implicated in disease. Further validation and investigation into the mechanisms of action, and their impact on astrocyte-mediated neuroinflammation is needed to fully understand their roles in disease.

### Interferon-γ

Interferon (IFN)-γ is an inflammatory cytokine produced mainly by T-cells and natural killer cells; and can be an inducer of reactive astrocytes (Hashioka *et al.*, 2009). Here, the results showed that IFNγ-mediated signalling pathway is differentially expressed in iAstrocytes treated with $A\beta_{1-42}$ oligomers. Early studies showed that IFN-γ may be a key cytokine mediating inflammation and Alzheimer's disease pathology. For example, in primary human astrocytes, a stimulus of IFNγ combined with TNFα or IL-1β can trigger the production of Aβ (Blasko *et al.*, 2000). This has been confirmed *in vivo* using transgenic APP mice, where IFNγ has been reported to increase Aβ production in astrocytes and neurons; and IFNγ can also disrupt Aβ clearance from the brain (Yamamoto *et al.*, 2007). Furthermore, IFNγ and Aβ together can activate microglia, producing toxic reactive nitrogen species, which in turn can lead to neuronal loss (Meda, Cassatella, *et al.*, 1995). *In vivo* studies in transgenic APP mice showed an increase in IFNγ expression in reactive microglia and reactive astrocytes which surround amyloid deposits in the cortical regions of the brain (Abbas *et al.*, 2002). IFNγ can also sensitise neurones to the toxic effects of $A\beta_{1-42}$ significantly decreasing neuronal survival

in cell culture (Bate *et al.*, 2006). There is evidence in literature of the interplay of IFNγ and Aβ, and their neurotoxic effects. It would therefore be interesting to explore this relationship further, especially in the context of astrocytes and oligomeric species especially, to evaluate the intricate mechanisms behind astrocyte-mediated neurotoxicity in Alzheimer's disease.

### NFkB and TNF

Nuclear factor kappa B (NFκB) is a transcription factor with a function in immune response. Astrocytic NFκB has been reported to have a role in induction of pro-inflammatory factors in disease (Dresselhaus and Meffert, 2019). The tumour necrosis factor (TNF) family of cytokines can trigger and activate the NF-κB pathway (Hayden and Ghosh, 2014). Here, NFκB and TNF signalling pathways are uniquely differentially expressed in Aβ oligomer-treated iAstrocytes and not in iAstrocytes treated with Aβ fibrils or extracts, again suggesting a proinflammatory responses in astrocytes mediated by Aβ oligomers. NFκB signalling could be an important player in Alzheimer's disease. There is an increased NFκB activation in reactive astrocytes. Inhibition of NFκB in astrocytes can protect from microglia activation, demyelination and loss of axonal integrity (Saggu *et al.*, 2016). Additionally, an increase in levels of NFκB can be seen in Alzheimer's disease brains, and it has been suggested that NFκB can increase Aβ production (Chen *et al.*, 2012). NFκB can promote the transcription of cytokines, which in turn can induce not only Aβ accumulation but also increase tau hyperphosphorylation further contributing to Alzheimer's disease pathology (Sun *et al.*, 2022). With regards to the TNF signalling, the Aβ induced TNF-alpha cytokine has been shown to induce the expression of toxic nitric oxide, can promote excitotoxicity, stimulate the induction of reactive astrocytes and cause synaptic loss (Zeng *et al.*, 2005; Decourt, Lahiri and Sabbagh, 2017). This further suggests the involvement of astrocytes in neuroinflammation, and related adverse effects in the CNS. It also suggests that $A\beta_{1\text{-}42}$ oligomers could be strong inducers of pro-inflammatory reactive astrocytes, which can be a feature of the early disease changes as this response was not detected in astrocytes treated with Aβ extracts or fibrils. However, the full mechanism of oligomer-mediated astrocyte reactivity and inflammation, as well as their role in Alzheimer's disease pathology, should be confirmed by additional validation work.

#### *MicroRNA Let-7i*

The gene *MIRLET7I* was found to be upregulated in both extract-treated and oligomer-treated iAstrocytes when compared to untreated controls. *MIRLET7i* encodes miRNA, named MicroRNA Let-7i (or Hsa-Let-7i).

MicroRNAs (miRNAs) are non-coding RNAs, which play an important role in the regulation of gene expression. MiRNAs can also activate and regulate transcription and translation, and can act as

messengers facilitating cell to cell communications (O'Brien *et al.*, 2018). Previous studies suggested that abnormal regulation of miRNA-dependent gene expression could be associated with neurodegeneration, as well as increased Aβ production, and formation of NFTs. Furthermore, expression of many Alzheimer's disease proteins could be regulated directly or indirectly by the action of miRNAs. These proteins include APP processing, presenilin, and tau (Maciotta *et al.*, 2013). Dysregulation of miRNAs could therefore be one of the mechanisms behind many neurodegenerative diseases, including Alzheimer's disease.

The let-7 family of miRNAs is the most studied family of miRNAs, which have been found to be involved in various biological processes such as development, stem cell biology, ageing, and metabolism (Su *et al.*, 2012). The let-7 family of miRNAs can be found abundantly expressed in the brain. It has been shown that different miRNAs belonging to the let-7 family of miRNAs can be found elevated in the cerebrospinal fluid of Alzheimer's disease patients (Derkow *et al.*, 2018). Let-7 upregulation can impair glucose homeostasis, and this can lead to neuronal loss (Kumar, Haque and Nazir, 2016). Indeed, miRNA Let-7 have been found to activate Toll-like receptor 7, in turn causing neurodegeneration in mice (Lehmann *et al.*, 2012). Activation of toll-like receptor 7 through miRNA Let-7 can also induce the release of pro-inflammatory cytokines via microglial activation (Buonfiglioli *et al.*, 2019). Overexpression of MIRLET7A can induce the M2 phenotype in microglia, promoting neuroinflammation, as well as making them more vulnerable to cell death (Cho *et al.*, 2015). Meanwhile, the overexpression of MIRLET7I itself has recently been shown as a potential biomarker for post-stroke cognitive impairment (Wang *et al.*, 2020).

This suggests that the miRNA let-7 family may be an important factor contributing to the widespread inflammation and neurodegeneration in Alzheimer's disease. As iAstrocytes treated with amyloid beta extracts and oligomers show a significant upregulation in the let-7i variant, which has also been linked to cognitive impairment, this could indicate the potential mechanism of astrocyte-mediated cognitive impairment in Alzheimer's disease. Moreover, this potential impairment could be linked specifically to the oligomers, as *MIRLET7I* has not been upregulated in the fibril-treated iAstrocytes.

### *Serum Amyloid A1*

Serum Amyloid A1 (SAA1) protein is encoded by the *SAA1* gene, which has been found to be upregulated in both oligomer- and fibril-treated iAstrocytes. SAA1 has been linked to inflammation, as its expression is usually modulated by proinflammatory cytokines, such as IL-1B, IL-6, and tumour necrosis factor-α (TNFα) (Abouelasrar Salama *et al.*, 2020). An increased expression of SAA1 can be detected in Alzheimer's disease brains (Liang *et al.*, 1997). An upregulation of SAA proteins in the mouse brains can lead to an increase in amyloid A deposition, and an increase in release of cytokines,

suggesting that SAA proteins can be involved in inflammation (Guo *et al.*, 2002). Particularly, SAA proteins have been shown to increase the levels of TNF-α, IL-1B, and IL-8 in neutrophils (Furlaneto and Campa, 2000). SAA proteins can also activate NLRP3 inflammasome (Niemi *et al.*, 2011), which has been shown to be an important component in astrocyte-mediated neuroinflammation. Inhibition of NLRP3 inflammasome can improve cognitive deficits in mouse models (Hou *et al.*, 2020). Additionally, SAA1 upregulation can be associated with the increased levels of Aβ in the brain, as well as cytokine-mediated microglial activation (Jang *et al.*, 2017). Also, SAA1 can exacerbate Aβ aggregation and glial activation in Alzheimer's disease transgenic mice, further suggesting its role in Alzheimer's disease pathology (Jang *et al.*, 2019). Interestingly, SAA1 has also been shown to induce the expression of MMPs (Vallon *et al.*, 2001), which were discussed before in the context of astrocyte-mediated BBB breakdown.

Therefore, the upregulation of SAA1 in oligomer- and fibril-treated iAstrocytes could indicate that the astrocytes are involved in inducing neuroinflammation as a response to amyloid beta. The widespread and persistent inflammation can be one of the factors leading to Alzheimer's disease onset and progression. One of the potential mechanisms could be that amyloid beta mediated SAA1 upregulation could induce the production and release of proinflammatory cytokines and chemokines, which in turn can lead to further adverse downstream effects resulting in neuronal loss. The mechanism and pathway of SAA1 and its interplay with cytokines and chemokines should be investigated further.

## Neurotransmitter dysfunction

### *GABAergic dysfunction in Alzheimer's disease*

γ-aminobutryic acid (GABA) is the main inhibitory neurotransmitter in the CNS. GABA can be released from the presynaptic vesicles into the synaptic cleft when an action potential causes membrane depolarisation. The released GABA binds to the GABA receptors on the postsynaptic membrane, and this can inhibit the activity of the postsynaptic neurons. Studies show that GABAergic transmission could be a potential mechanism behind Alzheimer's disease pathology, where an imbalance of excitatory and inhibitory neuronal network activity could be one of the disease contributing factors (Li *et al.*, 2016). A loss of GABA currents, as well as a desensitisation of GABA receptors in Alzheimer's disease brains have been reported (Limon, Reyes-Ruiz and Miledi, 2012). The loss of GABAergic transmission in neurons, as well as deficient synaptic function have been reported in Alzheimer's disease (Li *et al.*, 2016). Aβ has been found to weaken the synaptic inhibition by downregulating the expression of GABA-a receptors (Ulrich, 2015). Additionally, Aβ has been found to decrease the inhibitory synaptic transmission, which can lead to hyperexcitability and neuronal loss (Ren *et al.*, 2018).

Here, a treatment of iAstrocytes with Aβ oligomers and Aβ extracted from Alzheimer's disease brains, have resulted in an upregulation of *GABRA1, GABARAP, SHISA7*, all encoding GABA-a receptors. Furthermore, GABAergic dysfunction was implicated specifically in Aβ oligomer-treated astrocytes, as the relating gene pathways have been uniquely differentially expressed in that treatment group. This could further suggest that Aβ oligomers and fibrils can elicit specific effects on different neurotransmitter receptors, modulating disease pathology. In the healthy CNS, GABA uptake is mostly carried out by neurons and their transporter, however, astrocytes also play a role in GABA uptake. Astrocytes have been reported to remove around 20% of GABA in the CNS (Garaschuk and Verkhratsky, 2019).

Interestingly, an upregulation of GABA receptors has been reported to promote long term potentiation, and this can also be a protective mechanism against the accumulation of free radicals in the hippocampus (Tu *et al.*, 2019). Therefore, this could indicate a potential neuroprotective effect of astrocytes as a response to amyloid beta oligomers and extracts. As astrocytes are the main glial cells of the CNS, functioning to maintain brain homeostasis, it is possible that the upregulation of GABA receptors by astrocytes post-Aβ treatment might be an attempt to restore balance and provide neuroprotective effects. By upregulating GABA receptors and enhancing GABA trafficking, astrocytes might therefore attempt to prevent hyperexcitability-induced neuronal loss. It is true, that amyloid beta oligomers can cause synaptic dysregulation and neuronal hyperexcitability, subsequently causing neuronal loss in Alzheimer's disease (Fernandez-Perez *et al.*, 2021). As the GABAa receptors are

upregulated due to amyloid beta oligomer treatments, it may be that astrocytes can detect and anticipate the potential damage that may occur. This could mean that the upregulation of GABA receptors may be a compensatory mechanism, which would aim to counter the potential synaptotoxic effects of Aβ. However, there's been reports that an upregulation of neurotransmitters and their receptors may indicate an impairment in synaptic plasticity. Indeed, transgenic models of Alzheimer's disease, which display amyloid pathology, also display an upregulation of glutamatergic, GABAergic and cholinergic transmissions. This phenomenon is present at the early stages of the disease, but then this upregulation declines as disease progresses (Bell *et al.*, 2003; Bell, Bennett and Cuello, 2007). As oligomers are the early aggregate species of amyloid beta, it is plausible that a treatment with oligomers could represent the events that take place in early disease. It would be interesting to investigate whether GABAergic transmissions diminish when amyloid fibrils are applied to iAstrocytes.

Therefore, the intricate mechanisms behind how astrocytes may become neuroprotective in disease should be investigated further. Also, the mechanisms behind neurotransmitter impairments and the involvement of astrocytes in these processes could reveal potential disease mechanisms.

### *Glutamate dysfunction in Alzheimer's disease*

In the CNS, glutamatergic neurons are involved in learning, memory, and synaptic plasticity. Glutamate is the primary excitatory neurotransmitter in the CNS. In disease, increased amounts of glutamate can lead to excitotoxicity and subsequently a loss of neurons (Willard and Koochekpour, 2013). Glutamatergic transmission is mediated by glutamatergic receptors, which include NMDA receptors. NMDA receptors can play an important role in synaptic plasticity, where blocking NMDA receptors has been found to induce neuronal apoptosis and neurodegeneration. Meanwhile, activation of NMDA receptors can promote cell survival (Wang and Reddy, 2017).

*GRIN2C* is a gene encoding an NMDA receptor protein, called glutamate ionotropic receptor NMDA subunit 2C (GRIN2C, or GluN2C). *GRIN2C* is downregulated in amyloid-beta treated iAstrocytes. Furthermore, *EPHB2* and *EPHB6* genes encoding EPH Receptor B2 (EPHB2), and EPH Receptor B6 (EPHB6) respectively, are downregulated in amyloid-beta treated iAstrocytes.

It is therefore interesting that an NMDA receptor GRIN2C (or GluN2C) is downregulated in amyloid-treated iAstrocytes. This could suggest that amyloid beta-mediated blockage of NMDA receptor could cause astrocytes to become less supportive towards neurons, by changing their signalling and functions in the context of neurotransmitters. Indeed, application of Aβ has been found to promote endocytosis of NMDA receptors, can decrease the expression of NMDA receptors, and can reduce NMDA signalling (Snyder *et al.*, 2005). Furthermore, it has been postulated that a loss of NMDA receptors in Alzheimer's disease could take place in the early stages of the disease, making neurons

more vulnerable to further pathological changes occurring in Alzheimer's disease (Mishizen-Eberz *et al.*, 2004). Aβ has also been suggested as a mediator involved in inhibition of glutamate uptake by glial cells, contributing to synaptic dysfunction. Interestingly, Aβ has been proposed as a molecule causing overstimulation of NMDA receptors, which in turn can cause synaptotoxicity (Tu *et al.*, 2014).

It is therefore clear that changes in the normal expression of NMDA receptors can adversely affect neuronal survival. Here, we have shown that in amyloid beta-treated astrocytes, there may be a downregulation of at least one NMDA receptor directly. The exact mechanism and role of downregulated NMDA receptors in astrocytes should be investigated further in the context of neurodegeneration.

EPHB2 and EPHB6 are receptor proteins that belong to the Ephrin B (EphB) family of proteins. Both receptors were found to be downregulated in amyloid beta-treated iAstrocytes. EphB receptors are found to be localised at the synapses in hippocampal neurons, where they may be involved in synaptic functions (Dalva *et al.*, 2000). EphB receptors can cluster at the excitatory synapses and can associate with NMDA receptors. The EphB receptor binding can stimulate the EphB protein, which consequently can cause NMDA receptor activation (Dalva *et al.*, 2000; Takasu *et al.*, 2002). Thus, the downregulation of the EphB receptors could have a detrimental effect on synaptic function and neuronal survival. As shown here, this effect could be mediated by astrocytes and amyloid beta in Alzheimer's disease, further suggesting the importance of astrocytes in amyloid beta-mediated toxicity. Indeed, amyloid beta has been shown to degrade EphB receptors in Alzheimer's disease, where depletion of EphB causes impairments in long-term potentiation. In mouse models, increasing the expression of EphB can cause activation of NMDA receptors, and reverse memory impairments (Cissé *et al.*, 2011; Hu *et al.*, 2017). Hence, one of the proposed mechanisms of action here could be that amyloid beta can act on astrocytes, decreasing the expression of EphB receptors. These in turn can no longer interact with NMDA receptors. These events can mediate loss of synaptic plasticity, and can cause synaptic impairments, resulting in neuronal loss and cognitive deficits. This mechanism of action has not been extensively researched in the context of neurodegeneration and Alzheimer's disease and would be very interesting to investigate further.

Furthermore, the expression of *SLC1A3*, and *SLC39A5* have been found to be downregulated in the fibrils treatment group compared to the untreated controls. These genes encode proteins involved with glutamate transport, and zinc transport respectively. SLC1A3 protein, also known as GLAST, is a glutamate aspartate transporter, which alongside the glutamate transporter (GLT-1), is responsible for 90% of glutamate uptake by astrocytes in the brain (Monterey *et al.*, 2021). Furthermore, SLC39A5 protein is a zinc transporter protein. Zinc transport is an important component of glutamate uptake,

and astrocytes incubated with zinc *in vitro* have been shown to decrease in ATP levels and decrease in glutamate uptake (Sang *et al.*, 2007). Therefore, decreasing those proteins could suggest a decrease in glutamate uptake and/ or transport in fibril-treated iAstrocytes.

Glutamate dysfunction has been previously reported in AD. The presented results have further indicated that glutamate dysfunction could be a mechanism by which astrocytes become toxic to neurons during AD. As multiple different genes were found to be differentially expressed as a response to amyloid treatments, glutamate dysfunction during disease could therefore be mediated through various mechanisms. It has been previously reported, that Aβ protein can bind to glutamate receptors, causing their overactivation, and subsequently an abnormal glutamate accumulation (Yeung *et al.*, 2020). Therefore, it would be interesting to further investigate astrocytic changes in glutamate transport as a response to amyloid beta treatments. This could reveal potential mechanisms by which astrocytes may change in AD, and mechanisms by which astrocytes could mediate neuronal toxicity in AD.

### 4.6.3 Technical discussion

#### ELISA for quantification and detection of $A\beta_{1-42}$ extracted from human AD brain tissue

An ELISA kit was used to detect and quantify the extracted $A\beta_{1-42}$ from human AD brain tissue. The results showed that there is detectable $A\beta_{1-42}$ present in the sample, and that the concentration of this Aβ was 73.436 pg/ml. This is a much lower concentration when comparing to the concentration of $A\beta_{1-42}$ obtained when preparing the aggregates *in vitro* (described in chapter 2). However, it is important to note that the concentrations of Aβ *in vitro* may not be comparable to the concentrations of Aβ *in vivo*. The concentration of Aβ isoforms in human plasma have been reported as 23.81 pg/ml ($A\beta_{38}$), 272.4 pg/ml ($A\beta_{40}$) and 30.13 pg/ml ($A\beta_{42}$) (Ovod *et al.*, 2017). Meanwhile, the soluble levels of $A\beta_{1-42}$ in AD CSF have been reported as 617.46 pg/ml. It is therefore difficult to establish whether the Aβ content extracted from the human AD brain was enough to elicit substantial iAstrocyte response *in vitro*.

One possible explanation for the low concentration of the Aβ extracts would be that the Aβ was obtained from a small amount of brain tissue. Naturally, one could assume that the concentration of Aβ would have increased if the entire brain tissue was used and sampled for this purpose. However, this is neither possible or feasible. Furthermore, a human ELISA kit that is specific for $A\beta_{1-42}$ was used. This means that other Aβ isoforms would have not been detected with the kit, and therefore the final Aβ concentration of the extracts could be higher. This, however, is favourable to the current study. The Aβ present *in vivo* is very heterogenous, and there is a wide range of Aβ polymorphisms present in the Alzheimer's disease brains. These can subsequently cause a varying AD phenotype in patients (Matuszyk *et al.*, 2022). There is a high possibility that the extracted Aβ contained isoforms other than $A\beta_{1-42}$, and therefore this could be more toxic and/or more representative of the disease mechanisms than $A\beta_{1-42}$ prepared *in vitro*. To carry out full characterisation and analysis of Aβ brain extracts, a combination of microscopy, chromatography-based methods, and mass spectrometry would be needed. The full characterisation and quantification of Aβ brain extracts was beyond the scope of the current investigation. Furthermore, the Aβ extract may have been contaminated with the 6e10 antibody during immunoprecipitation. In the future, to avoid this issue, a good idea would be to covalently cross-link the antibody prior to bead extraction, which could ensure that the antibody is retained and only the protein is eluted at the end.

To immunoprecipitate the Aβ peptides from the brain homogenates, the 6e10 antibody was used, which recognises the 1-16 amino acids of the peptide structure (Baghallab *et al.*, 2018). Therefore, the N-truncated Aβ species would not have been isolated. In AD, the plaques can consist entirely of $A\beta_{1-42}$, but some plaques can also consist of N-terminally truncated Aβ, and, in some cases, a mixture of

both, as well as other Aβ isoforms (Näslund *et al.*, 1994; Saido *et al.*, 1995). Moreover, the amount of N-terminally truncated Aβ species increases, as the AD pathology progresses in the brain, and therefore it may be an important component in AD pathology (Meral and Urbanc, 2013). N-terminally truncated Aβ peptides have previously been isolated from the brains of sporadic and familial AD cases (Russo *et al.*, 2000). N-terminally truncated Aβ have been found to cause dose-dependent neurotoxicity *in vitro*, as well as neuronal loss and hypertoxicity (Nussbaum *et al.*, 2012; Bouter *et al.*, 2013). Therefore, in future experiments, it would be interesting to isolate the N-truncated Aβ from AD brain tissue and investigate their roles *in vitro*.

### Quality control of RNA isolation and preparation prior to RNAseq analysis

Good RNA yield and quality prior to RNAseq analysis is essential to reliably obtain the data necessary for investigating the question or hypothesis of interest (Conesa *et al.*, 2016). The RNA integrity number (RIN) measures the integrity of the total RNA samples. Typically, the method of choice for analysing RNA samples utilises the Agilent bioanalyzer technology. This is an automated bio-analytical device which performs electrophoretic separations and fluorescence detection of the sample material. The RIN can be classified into RNA integrity categories from 1 (completely degraded) to 10 (intact) (Schroeder *et al.*, 2006). The RIN is widely used by researchers as a method of standardisation of RNA integrity measurements, which can facilitate reliable and reproducible gene expression results (Lightfoot, Salowsky and Buhlmann, 2005). It is generally accepted that high-quality RNA would display a RIN of at least 8, whilst any RNA samples with RIN below 5 would be too degraded for further analysis. In the current study, the isolated RNA was of high-quality RNA, as indicated by the RIN higher than 9. In one case (iAstrocyte cell line 161, fibril-treated), the RIN was 7.3, indicating that the RNA was partially fragmented. In the future, to help with the RNA fragmentation and degradation, the RNA integrity can be improved at the preparation stage. This could involve simple protocol alterations, such as using RNA purification columns, cleaning the work surfaces to remove RNase, using RNA extraction kits available commercially to ensure minimal RNase contamination, and snap-freezing the extracted samples to ensure that the samples remain intact. However, most samples have reached a high-quality RNA and remained intact prior to RNAseq analysis. All samples have passed quality control checks and were able to be used successfully for the subsequent RNAseq analysis.

### RNAseq data analysis quality control

RNAseq is a high-throughput sequencing technology allowing the investigation of the quantity and sequences of RNA in a sample. To achieve this, RNAseq technique uses next-generation sequencing. The RNAseq results can be a powerful tool helping researchers to investigate the differentially expressed genes by looking at the transcriptome. During RNAseq, the RNA extracted from cellular material is used to create a complementary DNA (cDNA). This is then sequenced, which produces

reads that can be mapped to a reference genome. The read counts indicate and measure the gene expression level (D. Li *et al.*, 2022). RNAseq provides a higher resolution and coverage of the transcriptome, making it a favourable choice compared to microarray- or Sanger-based methods (Kukurba and Montgomery, 2015).

Often, due to the multi-step nature of RNAseq analysis, the technique is described as complicated. The steps that are required for successful RNAseq analysis can introduce errors into the data, making it biased or unusable. For this reason, before the RNAseq data is acquired for subsequent analysis, necessary specific checks need to be performed to ensure the good quality of the data. Investigating the raw reads data, GC content and error rates aids in the detection of adapters, duplicate reads, sequencing errors, and contaminations (Li *et al.*, 2015; Conesa *et al.*, 2016). Here, the quality control checks for the data revealed good error rates, GC content and genome reads that were mostly mapped to exons. The data filtering analysis showed that the majority of data was 'clean', and any remaining confounding factors were removed. This ensured a good and unbiased foundation for subsequent data analysis, allowing for a reliable investigation of gene expression data.

## 4.7 Conclusions and future work

The aim of the current chapter was to investigate the varying responses of astrocytes to different types of Aβ aggregates in Alzheimer's disease.

First and foremost, it is important to highlight the results from the principal components analysis. The analysis showed that each individual cell line reacts differently to external stimuli, in this case amyloid beta. This is an interesting result, as it could mean that different individuals may display different tolerances and/ or susceptibility to Aβ-mediated astrocyte changes. For this reason, future work should focus on separating the cell lines to further investigate the individual differences to gene expression following a disease stressor. It would therefore be important to isolate specific biomarkers, characterising the astrocyte responses to different stimuli, which would aid in further understanding of how Aβ modulates astrocytic response in injury and disease. Additionally, it would allow to identify common mechanisms and pathways, shared by various individuals, which could be a potential therapeutic option in disease. It could also provide an insight to why some therapeutic options have not been as successful at clinical trials, as it would allow researchers to understand how Aβ modulates disease pathology in more depth. Therefore, this would give researchers a better chance to finding a more fitting therapeutic option for non-responding individuals or develop a more tailored blanket therapeutic option which would be effective in the majority of individuals with Alzheimer's disease.

The RNAseq analysis of iAstrocytes treated with Aβ extracts, oligomers and fibrils revealed a number of differentially expressed pathways and genes, which could have an impact on astrocyte-mediated AD pathology. Interestingly, the astrocytes show a heterogenic response to different types of Aβ. As heterogenic Aβ species exist in AD, the results presented in the current chapter indicate a large complexity of disease mechanisms. Astrocyte responses to Aβ, and astrocyte-related mechanisms of neurotoxicity and disease pathology are not extensively studied in AD. Most of the research focuses mainly on the roles of neurons. However, it is clear that other cell types, such as astrocytes described here, could be important players and mediators of AD and deserve to be investigated further. In order to fully understand the roles of these differentially expressed genes, further work should be carried out. All the genes of interest could be validated using immunohistochemistry staining for the relevant proteins in AD brains. This would ensure that the proteins expressed *in vitro* are also expressed *in vivo*, and therefore are relevant to disease pathology. The disease-relevant differentially expressed pathways could also be investigated further, in order to characterise the different mechanisms by which specific Aβ aggregates could contribute to disease pathology. The results from RNAseq analysis provide information about iAstrocyte changes at genome level. Quantitative real-time PCR (qPCR) could be an approach to measure the expression of a selected genes of interest to validate the results obtained from RNAseq. To supplement these results further, it would be beneficial to confirm protein expression levels in iAstrocytes treated with Aβ via western blot analysis of proteins of interest. Such approaches would add more confidence in the results presented and permit early stages of discovery of potentially novel mechanisms of disease.

The results indicate that although all Aβ species could cause inflammation via IL-17 signalling pathway, it is Aβ oligomers which seem to elicit the biggest inflammatory response in astrocytes. As Aβ oligomers represent the early aggregation species, it is possible that astrocyte reactivity and inflammation takes place early in the disease processes, which could initiate further downstream events. Investigating the mechanisms of oligomer-mediated inflammation as an early disease event would be an interesting avenue to explore. It is especially interesting as Aβ has been linked to inflammation in the literature with Aβ protofibrils accumulating in astrocytes, including activated astrocytes (Hampel *et al.*, 2021).

Results described in this chapter also revealed a potential role of novel chemokines and cytokines, which have been upregulated in astrocytes treated with Aβ. It has also been suggested in literature that Aβ alongside chemokines and cytokines could act as an activator of neurotoxic, reactive astrocytes (LaRocca *et al.*, 2021). This further indicates that Aβ may be an important factor in mediating pro-inflammatory astrocyte responses in AD. Treatment of neuronal cultures with the identified cytokines would be one of the potential experiments to fully characterise the role of these

cytokines on neuronal survival. Consequently, neuronal viability using LDH cytotoxicity assays could be investigated. The role of microglia in neuroinflammation would also be an interesting avenue to explore, where the effects of Aβ oligomers on microglial cytokine expression could reveal more information about how neuroinflammation might take place in disease (Ji *et al.*, 2019).

The breakdown of BBB mediated by fibril-treated astrocytes could also be investigated further, such as the roles of tight junction proteins. It was revealed that although oligomers induced differential expression of gene pathways relating to extracellular matrix remodelling, it was Aβ fibrils (as well as extracted Aβ) which induced differential expression of pathways relating to BBB breakdown.

*Post-mortem* investigations could be carried out. For example, investigating the correlation of the protein expression (i.e. the upregulation of MMPs, or downregulation of tight junction-associated proteins) and the capillary leakage, which could be measured by investigating the expression of blood-derived proteins via immunohistochemistry and/or immunoblotting, could also be an interesting avenue for future work. Furthermore, the mechanisms modulating potential BBB breakdown could be investigated by looking at the expression of MMPs, and claudin proteins directly in iNPC-derived iAstrocytes. For this reason, healthy vs Alzheimer's disease astrocytes could be compared. The levels of the protein of interest would be higher in Alzheimer's disease iAstrocytes compared to the healthy cells. This would indicate that astrocytes might be involved in BBB breakdown via the release of MMPs, and/or downregulation of tight junction proteins.

Lastly, the effect of astrocytes on neurotransmitters and synaptic plasticity could be investigated further. The results indicated that Aβ oligomers and Aβ fibrils could affect neurotransmitter receptors and signalling differentially. Namely, oligomers could specifically act on GABA pathways, whilst fibrils could act on glutamate pathways in astrocytes. Therefore, the full impact of Aβ aggregates on specific neurotransmitters could be characterised. For this reason, the relevant neurotransmitter receptor dysfunction could be investigated over a time course where Aβ is allowed to aggregate in both *in vivo* and *in vitro* studies. Additionally, healthy astrocytes pre-treated with amyloid beta could be co-cultured with healthy neurons. The levels of NMDA receptor activity, as well as GABA and glutamate levels could be measured against the control (untreated) astrocytes. The hyperexcitability, as well as synaptic plasticity and impairment could also be investigated. The investigation would reveal whether astrocyte-mediated neurotransmitter dysregulation has an impact on neuronal survival in disease.

To conclude, the RNAseq analysis revealed that different Aβ species (fibrils, oligomers, extracts) can elicit varying responses in astrocytes. Aβ oligomers could represent early disease events, modulating inflammation, GABA-specific neurotransmitter dysfunctions, and extracellular matrix remodelling in astrocytes. Such events could change, or lead to, later stage events represented by the action of Aβ

fibrils (and/ or plaques). This could include astrocyte-mediated glutamate neurotransmitter dysfunction and BBB breakdown. Overall, the results revealed the varying astrocyte responses to $A\beta_{1-42}$ oligomers and fibrils in Alzheimer's disease.

# Chapter 5 – Conclusions and Future Work

Alzheimer's disease is a neurodegenerative disease and the most common cause of dementia. At the centre of Alzheimer's disease pathogenesis is the amyloid cascade hypothesis. This posits that an abnormal accumulation and aggregation of the Aβ protein is central to the onset of Alzheimer's disease, leading to a cascade of downstream events contributing to neuronal loss and dementia. One of the potential downstream effects of Aβ accumulation is the activation of glial cells, including astrocytes.

Astrocytes are the most common glial cells in the CNS. They function to provide essential metabolic and trophic support to neurons. In disease, there has been a notion that astrocytes may undergo a molecular 'switch', leading to astrocytic heterogeneity. This means that during disease, including Alzheimer's disease, astrocytes could display a more neurotoxic or a more neuroprotective phenotype. The factors contributing to these astrocytic changes are unknown.

In Alzheimer's disease, $A\beta_{1-42}$ is thought to be the most neurotoxic species of Aβ. Additionally, Aβ can exist as fibrils or oligomers, where fibrils are the main components of senile plaques in disease. Meanwhile oligomers are smaller and more soluble and are thought to be more neurotoxic than fibrils. However, the mechanism behind amyloid beta toxicity of both fibrils and oligomers remains to be characterised. Furthermore, Aβ in Alzheimer's disease can be found to be very heterogenic, where populations of high- and low molecular weight Aβ aggregates can exist in one sample at the same time. This makes the characterisation of Aβ extremely important, in order to reliably investigate their roles in Alzheimer's disease.

Astrocytes can respond to amyloid plaques and can correlate with tangle burden in Alzheimer's disease. Furthermore, astrocyte pathology can be observed in the ageing brain, contributing to synaptic impairment, astrocyte reactivity, neuroinflammation, and hyperexcitability. Therefore, it is possible that astrocyte heterogeneity as a response to amyloid beta could be one of the mechanisms contributing to the onset and progression of Alzheimer's disease.

For this reason, the project aimed to investigate whether different types of $A\beta_{1-42}$, namely oligomers and fibrils, affect astrocytes and produce different responses. For comparison, and to act as a positive control, the astrocytic responses to oxidative stress were also characterised. The astrocyte responses were investigated by assessing DNA damage response, changes to morphology, changes to cell viability, and transcriptomic expression using RNAseq analysis.

The first objective of the project was to prepare and characterise $A\beta_{1-42}$ aggregates. This was an important step, as characterisation of Aβ is not routinely carried out in the literature. The optimisation steps of the project showed that aggregating Aβ *in vitro* is a difficult task, as Aβ aggregation can be

dependent on various environmental conditions. These include, but are not limited to, the composition, pH levels and temperature of the buffers the peptide is diluted in.

First steps of Aβ preparation included developing a protocol for the preparation and characterisation of stable monomeric $A\beta_{1-42}$ of high purity (work described in chapter 2). The peptide was characterised using transmission electron microscopy for qualitative analysis, and asymmetric flow field flow fractionation for quantitative analysis. These revealed that high pH, achieved by dissolving the recombinant peptide in 50 mM NaOH, was important for the preparation of Aβ monomers. The purity and stability of the starting material is critical, as it can affect the preparation of future Aβ aggregates. Next, I optimised the protocols for preparing Aβ in the oligomeric and fibrillary states. Protocols available in the literature were first used (Cerf *et al.*, 2009; Stine *et al.*, 2011), and the preparations were characterised using transmission electron microscopy and size exclusion chromatography. Experiments revealed that Aβ did not aggregate under the conditions described in the literature. I speculated that this was due to the high pH of the starting monomeric Aβ material, which meant that the optimal conditions for Aβ aggregations were not met. To account for the high pH of the starting material, a revised protocol using TBS buffer was derived. By manipulating the pH levels with HCl, optimal pH conditions for aggregation were reached. The aggregation rate of Aβ was further manipulated by controlling the temperature of the aggregates. Lower temperatures slow down the aggregation rates of Aβ, and therefore a two-week aggregation at 4°C was chosen for Aβ oligomers. Meanwhile, high temperatures promote faster aggregation rates, which meant that the fibrillary Aβ aggregates were achieved by peptide incubation at 37°C for 24 hours. The resulting peptide aggregates were extensively characterised using immunoblotting, transmission electron microscopy, thioflavin t assays, and size exclusion chromatography. This fulfilled the first aim of the study, which was to prepare distinct Aβ aggregation species *in vitro* for the use in future astrocyte treatments.

To characterise the astrocyte responses in Alzheimer's disease, I firstly chose a known disease stressor, oxidative stress, as a positive control for astrocyte injury. By inducing oxidative stress in astrocytes, I was able to optimise the cell treatments and timings of potential astrocyte responses. Fetal astrocytes are commercially available, well-characterised, robust, and fast and easy to grow in the laboratory environment. Therefore, duo to their ease of use, they were the chosen model for characterisation of astrocyte responses to oxidative stress, and to optimise any treatments prior to investigating the iAstrocytes. Treatment of fetal astrocytes with a high, but largely sublethal dose of $H_2O_2$ (100 μM) resulted in a rapid upregulation of DNA damage markers, specific to double-stranded DNA damage. Furthermore, oxidative stress caused a rapid formation of γH2AX-positive nuclear foci in astrocytes, further indicating that DNA damage and a DNA damage response takes place. After 24 hours of treatment, the astrocytes experience a decrease in cell viability.

In comparison, the highest physiological dose of Aβ oligomers or fibrils (1 μM) did not cause an upregulation in γH2AX-positive foci after 1 hour, 24 hours or 48 hours of treatment in fetal astrocytes. I then decided to investigate any potential morphological changes to astrocytes, by characterising the expression of vimentin. Harmony software analysis revealed that none of the chosen cell morphology parameters (mean cell area, cytoplasm region, mean cell length, mean cell width or mean cell roundness) changed as a response to the Aβ treatments at 1 hour, 24 hours, or 48 hours. The cell viability was also investigated, and this showed that the Aβ treatments did not cause any significant cell death after 24 hours or 48 hours of treatment in fetal astrocytes. As fetal astrocytes are young, they may not be entirely representative of an ageing brain. Therefore, the stress caused by Aβ treatments may not have been enough to cause the same effects as oxidative stress. Additionally, the full expression of DNA damage markers was not investigated in Aβ treatments, and therefore it is possible that Aβ may have caused less-lethal single stranded DNA breaks. These could be characterised by the upregulation of ATR and pChk1 proteins. The expression of these could be included in any future investigations to aid in the understanding of how Aβ treatments modulate astrocyte DNA damage response. Moreover, it is possible that Aβ does not cause any DNA damage in astrocytes. However, this does not mean that other cellular changes in molecular function are not present.

To fully characterise the astrocyte responses to Aβ in an ageing brain and in Alzheimer's disease, I switched the *in vitro* model to the use of iNPC-derived iAstrocytes. These astrocytes have been reprogrammed from the skin fibroblasts of donors and retain their ageing properties. Hence, they may be a more reliable and representative astrocyte model in Alzheimer's disease. 1μM Aβ oligomer and fibril treatments of iAstrocytes did not cause any significant upregulation of the DNA damage marker, γH2AX, specifically when investigating the formation of γH2AX-positive DNA foci, and when iAstrocyte cell lines were pooled together. Furthermore, the Aβ treatments did not cause any cell morphology changes as investigated by the expression of vimentin, using multiple measures of cell size and shape. This was comparable to the responses of fetal astrocytes. Similar to fetal astrocytes, the iAstrocytes did not show any cell viability changes to Aβ treatments, when iAstrocyte cell lines were pooled together. This showed that both fetal astrocytes and iAstrocytes showed a great resistance to Aβ-mediated DNA damage, and Aβ-mediated cell toxicity. However, when iAstrocyte cell lines were separated, the results indicated that, at least to some degree, there may be some individual responses to amyloid-beta. This is an interesting result, which could be investigated further. In the current age of research, it is more clear that there is a real need to develop more options to deliver therapeutics based on precision and personalised medicine.

In terms of both DNA damage and cytotoxicity, it would be interesting to investigate the dose response to Aβ treatments, by exceeding the peptide concentrations. However, the potential problem with this

could be that high Aβ concentrations are not physiological. Furthermore, even though Aβ treatments did not have an effect on astrocytes alone, they could have adverse effects on astrocytes in co-culture with neurons. As astrocyte main function is to support neurons, it is reasonable to assume that astrocytes in monoculture may focus on their own survival in the presence of disease stressors. Hence, astrocyte responses to Aβ treatments in co-culture would be an interesting avenue to explore in the future.

However, it is also possible that Aβ *in vitro* may not be as toxic as Aβ *in vivo,* namely in Alzheimer's disease brains. Therefore, prior to conducting further investigation of Aβ treatments in iAstrocytes, I focused on isolating and extracting Aβ from Alzheimer's disease brain homogenates. The extraction was successful and resulted in a physiological amount of Aβ isolation. The extracts were subsequently used in the treatments of iAstrocytes prior to RNAseq analysis.

RNAseq is a technique which allows for the analysis and characterisation of the transcriptome. The iAstrocytes were treated with Aβ oligomers, fibrils, and extracts; the RNA was isolated and subsequently sequenced commercially to investigate which genes were upregulated or downregulated as a response. The functional enrichment analysis, and differential gene expression pathway analysis revealed a number of genes which were significantly down- and up-regulated in iAstrocytes as a response to Aβ treatments.

The results indicated that Aβ treatments may cause heterogenic response of astrocytes, where astrocytes may have a varying molecular phenotype depending on which aggregation species, they are exposed to. When investigating the differentially expressed gene pathways, common themes were found. In particular, the IL-17 signalling pathway was a common inflammatory pathway in iAstrocytes treated with Aβ extracts, as well as $A\beta_{1\text{-}42}$ oligomers and fibrils. However, oligomer-treated iAstrocytes showed a mostly pro-inflammatory profile. Interferon-γ signalling pathway, NFκB signalling pathway, TNF signalling pathway, MAPK signalling pathway and acute inflammatory response were uniquely differentially expressed in oligomer-treated iAstrocytes, and not in other aggregation species treatment groups. This suggests that oligomers may elicit a proinflammatory profile in astrocytes, a response that is very different to Aβ fibrils and extracts. Furthermore, oligomers may be involved in differential expression of apoptotic signalling pathways in astrocytes, as well as elicit changes to the extracellular matrix. In comparison, Aβ fibrils and extracts did not elicit such profound responses; however, they were involved in neurotransmitter signalling changes (especially regarding glutamate), as well as in changes to the tight junctions. This could represent that in later stages of the disease, it may be the Aβ fibrils that may be the main contributors to astrocyte-mediated BBB breakdown.

The genes that were differentially expressed related to a release proinflammatory cytokines and chemokines, which may be implicated in neuroinflammation. Furthermore, astrocytes can be involved in synaptic impairments and impairments to neuronal communications, as genes encoding neurotransmitter receptors (NMDA receptors and GABA receptors) have been dysregulated. The dysregulation of neurotransmitter receptors could therefore impact synapses and neurons directly, leading to profound adverse effects in Alzheimer's disease. Lastly, Aβ treatments in iAstrocytes have produced a dysregulation of genes relating to the tight junctions, as well as metalloproteinases. Both protein groups can be implicated in BBB breakdown and dysfunction, which has also been reported in Alzheimer's disease. The results therefore show that Aβ-mediated astrocyte changes could have detrimental effects in Alzheimer's disease, modulating disease onset and progression. These results would need to be further validated. For example, a qPCR analysis would allow confirmation of the pathways and proteins that may be involved in Aβ-mediated astrocyte changes. Analysis of Aβ-treated iAstrocytes in co-culture with neurons would allow us to investigate their ability to support neurons, and whether they mediate neuronal loss directly. Lastly, the iAstrocytes used in this study were from healthy donors. It is possible to obtain and reprogram iAstrocytes which are derived from skin fibroblasts of Alzheimer's disease patients. The RNAseq analysis on such astrocytes could therefore give comparative results, allowing for the full characterisation of the role of Aβ and astrocytes in Alzheimer's disease. Validation in human tissue would also allow testing of the relevance of the *in vitro* results. The expression of key proteins could be investigated further in human Alzheimer's disease cases and compared with matched controls by immunohistochemistry. Double staining with astrocyte markers and amyloid beta deposits would help to localise the plaque burden and astrocytes in the Alzheimer's disease brain and would aid further evaluation of the target proteins.

In conclusion, Alzheimer's disease is a multifactorial disease where amyloid beta may play an important role in modulating various cell types, which includes astrocytes. The current study shows that amyloid beta-mediated astrocyte changes could contribute to neuroinflammation, BBB breakdown and synaptic impairment in Alzheimer's disease. These responses appear to be unique to different Aβ aggregation species, suggesting that different stages of Alzheimer's disease and/or different Aβ species may cause astrocytes to elicit a varying molecular profile changing their normal functions. Such changes in astrocytes could contribute to disease pathology. This implicates astrocytes as key players in the onset and progression of Alzheimer's disease. It also confirms the involvement of amyloid beta in Alzheimer's disease. However, further validation of potential mechanisms and genes of interest is needed.

# References


Abbas, N. *et al.* (2002) 'Up-regulation of the inflammatory cytokines IFN-γ and IL-12 and down-regulation of IL-4 in cerebral cortex regions of APPSWE transgenic mice', *Journal of Neuroimmunology*, 126(1–2), pp. 50–57. doi: 10.1016/S0165-5728(02)00050-4.

Abouelasrar Salama, S. *et al.* (2020) 'Serum Amyloid A1 (SAA1) Revisited: Restricted Leukocyte-Activating Properties of Homogeneous SAA1', *Frontiers in Immunology*, 11, p. 843. doi: 10.3389/FIMMU.2020.00843/BIBTEX.

Agarwal, A. *et al.* (2017) 'Transient opening of the mitochondrial permeability transition pore induces microdomain calcium transients in astrocyte processes', *Neuron*, 93(3), p. 587. doi: 10.1016/J.NEURON.2016.12.034.

Akama, K. T. *et al.* (1998) 'Amyloid β-peptide stimulates nitric oxide production in astrocytes through an NFκB-dependent mechanism', *Proc Natl Acad Sci U S A*, 95(10), pp. 5795–5800. Available at: http://dx.doi.org/.

Aleksis, R. *et al.* (2017) 'Structural studies of amyloid-beta peptides: Unlocking the mechanism of aggregation and the associated toxicity', *Biochimie*. 2017/07/29, 140, pp. 176–192. doi: 10.1016/j.biochi.2017.07.011.

Almeida, Z. L. and Brito, R. M. M. (2020) 'Structure and Aggregation Mechanisms in Amyloids', *Molecules*, 25(5). doi: 10.3390/MOLECULES25051195.

Alzheimer, A. *et al.* (1995) 'An English translation of Alzheimer's 1907 paper, "Uber eine eigenartige Erkankung der Hirnrinde"', *Clin Anat*. 1995/01/01, 8(6), pp. 429–431. doi: 10.1002/ca.980080612 10.1002/ca.980080612.

Anderson, M. A. *et al.* (2016) 'Astrocyte scar formation aids central nervous system axon regeneration', *Nature*, 532(7598), pp. 195–200. doi: 10.1038/NATURE17623.

Anderson, M. A., Ao, Y. and Sofroniew, M. V. (2014) 'Heterogeneity of reactive astrocytes', *Neuroscience letters*, 565, pp. 23–29. doi: 10.1016/J.NEULET.2013.12.030.

Anderson, V. L. and Webb, W. W. (2011) 'Transmission electron microscopy characterization of fluorescently labelled amyloid β 1-40 and α-synuclein aggregates', in *BMC Biotechnol*. School of Applied and Engineering Physics, Cornell University, Ithaca, NY, USA, p. 125. doi: 10.1186/1472-6750-11-125.

Arbel-Ornath, M. *et al.* (2017) 'Soluble oligomeric amyloid-β induces calcium dyshomeostasis that precedes synapse loss in the living mouse brain', in *Mol Neurodegener*. 0000 0004 0386 9924grid.32224.35Alzheimer Research Unit, Department of Neurology, Massachusetts General Hospital and Harvard Medical School, 114, 16th St., Charlestown, MA 02129 USA000000041936754Xgrid.38142.3cDepartment of Biostatistics, Harvard School o. doi: 10.1186/s13024-017-0169-9.

Arber, C., Lovejoy, C. and Wray, S. (2017) 'Stem cell models of Alzheimer's disease: progress and challenges', *Alzheimer's Research & Therapy 2017 9:1*, 9(1), pp. 1–17. doi: 10.1186/S13195-017-0268-4.

Arvanitakis, Z., Shah, R. C. and Bennett, D. A. (2019) 'Diagnosis and Management of Dementia: Review', *JAMA*, 322(16), pp. 1589–1599. doi: 10.1001/JAMA.2019.4782.

Atherton-Fessler, S. *et al.* (1994) 'Cell cycle regulation of the p34cdc2 inhibitory kinases.', *Molecular Biology of the Cell*, 5(9), p. 989. doi: 10.1091/MBC.5.9.989.

Baghallab, I. *et al.* (2018) 'Epitomic Characterization of the Specificity of the Anti-Amyloid Aβ Monoclonal Antibodies 6E10 and 4G8', *Journal of Alzheimer's Disease*, 66(3), p. 1235. doi: 10.3233/JAD-180582.

Banerjee, S. *et al.* (2017) 'Nanoscale Dynamics of Amyloid β-42 Oligomers As Revealed by High-Speed Atomic Force Microscopy', *ACS Nano*, 11(12), pp. 12202–12209. doi: 10.1021/acsnano.7b05434.

Bardehle, S. *et al.* (2013) 'Live imaging of astrocyte responses to acute injury reveals selective juxtavascular proliferation', *Nature neuroscience*, 16(5), pp. 580–586. doi: 10.1038/NN.3371.

Bartolini, M. *et al.* (2011) 'Kinetic characterization of amyloid-beta 1-42 aggregation with a multimethodological approach', *Anal Biochem*. 2011/03/26, 414(2), pp. 215–225. doi: 10.1016/j.ab.2011.03.020.

Bate, C. *et al.* (2006) 'Interferon-γ increases neuronal death in response to amyloid-β1-42', *Journal of Neuroinflammation*, 3(1), pp. 1–7. doi: 10.1186/1742-2094-3-7/TABLES/3.

Beeg, M. *et al.* (2016) 'Clusterin Binds to Aβ1–42 Oligomers with High Affinity and Interferes with Peptide Aggregation by Inhibiting Primary and Secondary Nucleation*', in *J Biol Chem*. From the Department of Molecular Biochemistry and Pharmacology, IRCCS–Istituto di Ricerche Farmacologiche Mario Negri, 20156 Milan, Italy, pp. 6958–6966. doi: 10.1074/jbc.M115.689539.

Beher, D. *et al.* (2002) 'Generation of C-terminally truncated amyloid-beta peptides is dependent on gamma-secretase activity', *J Neurochem*. 2002/08/03, 82(3), pp. 563–575. Available at: http://dx.doi.org/.

Behl, T. *et al.* (2021) 'Multifaceted Role of Matrix Metalloproteinases in Neurodegenerative Diseases: Pathophysiological and Therapeutic Perspectives', *International Journal of Molecular Sciences*, 22(3), pp. 1–27. doi: 10.3390/IJMS22031413.

Bell, K. F. S. *et al.* (2003) 'Structural involvement of the glutamatergic presynaptic boutons in a transgenic mouse model expressing early onset amyloid pathology', *Neuroscience Letters*, 353(2), pp. 143–147. doi: 10.1016/J.NEULET.2003.09.027.

Bell, K. F. S., Bennett, D. A. and Cuello, A. C. (2007) 'Neurobiology of Disease Paradoxical Upregulation of Glutamatergic Presynaptic Boutons during Mild Cognitive Impairment'. doi: 10.1523/JNEUROSCI.3269-07.2007.

Benilova, I., Karran, E. and De Strooper, B. (2012) 'The toxic Abeta oligomer and Alzheimer's disease: an emperor in need of clothes', *Nat Neurosci*. 2012/01/31, 15(3), pp. 349–357. doi: 10.1038/nn.3028.

Bensimon, A., Aebersold, R. and Shiloh, Y. (2011) 'Beyond ATM: the protein kinase landscape of the DNA damage response', *FEBS Lett*. 2011/05/17, 585(11), pp. 1625–1639. doi: 10.1016/j.febslet.2011.05.013.

Bi, J. *et al.* (2008) 'Protective effects of catalpol against H2O2-induced oxidative stress in astrocytes primary cultures', *Neuroscience Letters*, 442(3), pp. 224–227. doi: 10.1016/J.NEULET.2008.07.029.

Bibl, M. *et al.* (2012) 'Characterization of cerebrospinal fluid aminoterminally truncated and oxidized amyloid-beta peptides', *Proteomics Clin Appl*. 2012/04/26, 6(3–4), pp. 163–169. doi: 10.1002/prca.201100082 10.1002/prca.201100082.

Birben, E. *et al.* (2012) 'Oxidative Stress and Antioxidant Defense', *World Allergy Organ J*, 5(1), pp. 9–19. doi: 10.1097/WOX.0b013e3182439613.

Blackburn, D. *et al.* (2009) 'Astrocyte function and role in motor neuron disease: A future

therapeutic target?', *Glia*, 57(12), pp. 1251–1264. doi: 10.1002/GLIA.20848.

Blasko, I. *et al.* (2000) 'Costimulatory effects of interferon-gamma and interleukin-1beta or tumor necrosis factor alpha on the synthesis of Abeta1-40 and Abeta1-42 by human astrocytes', *Neurobiology of disease*, 7(6 Pt B), pp. 682–689. doi: 10.1006/NBDI.2000.0321.

Bloom, G. S. (2014) 'Amyloid-beta and tau: the trigger and bullet in Alzheimer disease pathogenesis', *JAMA Neurol*. 2014/02/05, 71(4), pp. 505–508. doi: 10.1001/jamaneurol.2013.5847.

Bourgade, K. *et al.* (2015) 'β-Amyloid peptides display protective activity against the human Alzheimer's disease-associated herpes simplex virus-1', *Biogerontology*, 16(1), pp. 85–98. doi: 10.1007/s10522-014-9538-8.

Bouter, Y. *et al.* (2013) 'N-truncated amyloid β (Aβ) 4-42 forms stable aggregates and induces acute and long-lasting behavioral deficits', *Acta Neuropathol*, 126(2), pp. 189–205. doi: 10.1007/s00401-013-1129-2.

Bouvier, D. S. *et al.* (2022) 'The Multifaceted Neurotoxicity of Astrocytes in Ageing and Age-Related Neurodegenerative Diseases: A Translational Perspective', *Frontiers in Physiology*, 13, p. 467. doi: 10.3389/FPHYS.2022.814889/BIBTEX.

Breijyeh, Z. and Karaman, R. (2020) 'Comprehensive Review on Alzheimer's Disease: Causes and Treatment', *Molecules*, 25(24). doi: 10.3390/MOLECULES25245789.

Bria, C. R. M. and Williams, S. K. R. (2016) 'Impact of asymmetrical flow field-flow fractionation on protein aggregates stability', *Journal of Chromatography A*, 1465, pp. 155–164. doi: 10.1016/J.CHROMA.2016.08.037.

Brigas, H. C. *et al.* (2021) 'IL-17 triggers the onset of cognitive and synaptic deficits in early stages of Alzheimer's disease', *Cell Reports*, 36(9), p. 109574. doi: 10.1016/J.CELREP.2021.109574.

Brothers, H. M., Gosztyla, M. L. and Robinson, S. R. (2018) 'The Physiological Roles of Amyloid-β Peptide Hint at New Ways to Treat Alzheimer's Disease', *Front Aging Neurosci*, 10. doi: 10.3389/fnagi.2018.00118.

Brown, A. M., Tekkök, S. B. and Ransom, B. R. (2004) 'Energy transfer from astrocytes to axons: the role of CNS glycogen', *Neurochemistry international*, 45(4), pp. 529–536. doi: 10.1016/J.NEUINT.2003.11.005.

Bruno, M. A. *et al.* (2009) 'Increased Matrix Metalloproteinase 9 Activity in Mild Cognitive Impairment', *J Neuropathol Exp Neurol*, 68(12), pp. 1309–1318. Available at: https://academic.oup.com/jnen/article/68/12/1309/2610044.

Buonfiglioli, A. *et al.* (2019) 'let-7 MicroRNAs Regulate Microglial Function and Suppress Glioma Growth through Toll-Like Receptor 7', *Cell Reports*, 29(11), pp. 3460-3471.e7. doi: 10.1016/J.CELREP.2019.11.029.

Busciglio, J. *et al.* (1995) 'beta-amyloid fibrils induce tau phosphorylation and loss of microtubule binding', *Neuron*. 1995/04/01, 14(4), pp. 879–888. Available at: http://dx.doi.org/.

Bushong, E. A., Martone, M. E. and Ellisman, M. H. (2004) 'Maturation of astrocyte morphology and the establishment of astrocyte domains during postnatal hippocampal development', *International journal of developmental neuroscience : the official journal of the International Society for Developmental Neuroscience*, 22(2), pp. 73–86. doi: 10.1016/J.IJDEVNEU.2003.12.008.

Butterfield, D. A., Swomley, A. M. and Sultana, R. (2013a) 'Amyloid β-Peptide (1–42)-Induced Oxidative Stress in Alzheimer Disease: Importance in Disease Pathogenesis and Progression', *Antioxid Redox Signal*, 19(8), pp. 823–835. doi: 10.1089/ars.2012.5027.

Butterfield, D. A., Swomley, A. M. and Sultana, R. (2013b) 'Amyloid β-Peptide (1–42)-Induced Oxidative Stress in Alzheimer Disease: Importance in Disease Pathogenesis and Progression', in *Antioxid Redox Signal*. Department of Chemistry, University of Kentucky, Lexington, Kentucky., pp. 823–835. doi: 10.1089/ars.2012.5027.

Cabezas, R. *et al.* (2014) 'Astrocytic modulation of blood brain barrier: perspectives on Parkinson's disease', *Frontiers in Cellular Neuroscience*, 8(AUG). doi: 10.3389/FNCEL.2014.00211.

Cacace, R., Sleegers, K. and Van Broeckhoven, C. (2016) 'Molecular genetics of early-onset Alzheimer's disease revisited', *Alzheimers Dement*. 2016/03/27, 12(6), pp. 733–748. doi: 10.1016/j.jalz.2016.01.012.

Cacquevel, M. *et al.* (2012) 'Alzheimer's disease-linked mutations in presenilin-1 result in a drastic loss of activity in purified gamma-secretase complexes', *PLoS One*. 2012/04/25, 7(4), p. e35133. doi: 10.1371/journal.pone.0035133 10.1371/journal.pone.0035133. Epub 2012 Apr 18.

Campbell, S. C. *et al.* (2020) 'Potassium and glutamate transport is impaired in scar-forming tumor-associated astrocytes', *Neurochemistry international*, 133. doi: 10.1016/J.NEUINT.2019.104628.

Cerf, E. *et al.* (2009) 'Antiparallel beta-sheet: a signature structure of the oligomeric amyloid beta-peptide', *Biochem J*. 2009/05/14, 421(3), pp. 415–423. doi: 10.1042/bj20090379.

Cheignon, C. *et al.* (2018) 'Oxidative stress and the amyloid beta peptide in Alzheimer's disease', *Redox Biol*. 2017/10/29, 14, pp. 450–464. doi: 10.1016/j.redox.2017.10.014.

Chen, C. H. *et al.* (2012) 'Increased NF-κB signalling up-regulates BACE1 expression and its therapeutic potential in Alzheimer's disease', *International Journal of Neuropsychopharmacology*, 15(1), pp. 77–90. doi: 10.1017/S1461145711000149.

Chen, W.-T. *et al.* (2012) 'Amyloid-beta (Aβ) D7H mutation increases oligomeric Aβ42 and alters properties of Aβ-zinc/copper assemblies', *PloS one*. 2012/04/30, 7(4), pp. e35807–e35807. doi: 10.1371/journal.pone.0035807.

Chen, Y. *et al.* (2001) 'Astrocytes protect neurons from nitric oxide toxicity by a glutathione-dependent mechanism', *Journal of neurochemistry*, 77(6), pp. 1601–1610. doi: 10.1046/J.1471-4159.2001.00374.X.

Chen, Y. *et al.* (2020) 'The role of astrocytes in oxidative stress of central nervous system: A mixed blessing', *Cell Proliferation*, 53(3), p. e12781. doi: 10.1111/CPR.12781.

Chiu, F. -C, Norton, W. T. and Fields, K. L. (1981) 'The cytoskeleton of primary astrocytes in culture contains actin, glial fibrillary acidic protein, and the fibroblast-type filament protein, vimentin', *Journal of neurochemistry*, 37(1), pp. 147–155. doi: 10.1111/J.1471-4159.1981.TB05302.X.

Cho, K. J. *et al.* (2015) 'MicroRNA-Let-7a regulates the function of microglia in inflammation', *Molecular and Cellular Neuroscience*, 68, pp. 167–176. doi: 10.1016/J.MCN.2015.07.004.

Cho, K. S. *et al.* (2010) 'The effects of IL-32 on the inflammatory activation of cultured rat primary astrocytes', *Biochemical and biophysical research communications*, 402(1), pp. 48–53. doi: 10.1016/J.BBRC.2010.09.099.

Choi, J. J. *et al.* (2007) 'Hydrogen peroxide induces the death of astrocytes through the down-regulation of the constitutive nuclear factor-kappaB activity', *Free radical research*, 41(5), pp. 555–562. doi: 10.1080/10715760601173010.

Chow, V. W. *et al.* (2010) 'An Overview of APP Processing Enzymes and Products', *Neuromolecular Med*, 12(1), pp. 1–12. doi: 10.1007/s12017-009-8104-z.

Chun, H. *et al.* (2020) 'Severe reactive astrocytes precipitate pathological hallmarks of Alzheimer's disease via H2O2− production', *Nature Neuroscience 2020 23:12*, 23(12), pp. 1555–1566. doi: 10.1038/s41593-020-00735-y.

Chung, W. S., Allen, N. J. and Eroglu, C. (2015) 'Astrocytes Control Synapse Formation, Function, and Elimination', *Cold Spring Harbor Perspectives in Biology*, 7(9). doi: 10.1101/CSHPERSPECT.A020370.

Cissé, M. *et al.* (2011) 'Reversing EphB2 depletion rescues cognitive functions in Alzheimer model', *Nature*. doi: 10.1038/nature09635.

Cizas, P. *et al.* (2010) 'Size-dependent neurotoxicity of β-amyloid oligomers', *Archives of Biochemistry and Biophysics*, 496(2), pp. 84–92. doi: 10.1016/j.abb.2010.02.001.

Clarke, L. E. *et al.* (2018) 'Normal aging induces A1-like astrocyte reactivity', *Proceedings of the National Academy of Sciences of the United States of America*, 115(8), pp. E1896–E1905. doi: 10.1073/PNAS.1800165115/-/DCSUPPLEMENTAL.

Cleary, J. P. *et al.* (2005) 'Natural oligomers of the amyloid-beta protein specifically disrupt cognitive function', *Nat Neurosci*. 2004/12/21, 8(1), pp. 79–84. doi: 10.1038/nn1372.

Cline, E. N. *et al.* (2018) 'The Amyloid-β Oligomer Hypothesis: Beginning of the Third Decade', *Journal of Alzheimer's disease : JAD*, 64(s1), pp. S567–S610. doi: 10.3233/JAD-179941.

Cobley, J. N., Fiorello, M. L. and Bailey, D. M. (2018) '13 reasons why the brain is susceptible to oxidative stress', *Redox Biol*, 15, pp. 490–503. doi: 10.1016/j.redox.2018.01.008.

Cohen, S. I. *et al.* (2013) 'Proliferation of amyloid-beta42 aggregates occurs through a secondary nucleation mechanism', *Proc Natl Acad Sci U S A*. 2013/05/25, 110(24), pp. 9758–9763. doi: 10.1073/pnas.1218402110 10.1073/pnas.1218402110. Epub 2013 May 23.

Cohen, S. I. A. *et al.* (2015) 'A molecular chaperone breaks the catalytic cycle that generates toxic Abeta oligomers', *Nat Struct Mol Biol*. 2015/02/17, 22(3), pp. 207–213. doi: 10.1038/nsmb.2971 10.1038/nsmb.2971. Epub 2015 Feb 16.

Colvin, M. T. *et al.* (2016) 'Atomic Resolution Structure of Monomorphic Aβ42 Amyloid Fibrils', *Journal of the American Chemical Society*. 2016/07/14, 138(30), pp. 9663–9674. doi: 10.1021/jacs.6b05129.

Conesa, A. *et al.* (2016) 'A survey of best practices for RNA-seq data analysis', *Genome biology*, 17(1). doi: 10.1186/S13059-016-0881-8.

Copani, A. *et al.* (2002) 'Beta-amyloid-induced synthesis of the ganglioside GD3 is a requisite for cell cycle reactivation and apoptosis in neurons', *The Journal of neuroscience : the official journal of the Society for Neuroscience*, 22(10), pp. 3963–3968. doi: 10.1523/JNEUROSCI.22-10-03963.2002.

Cregg, J. M. *et al.* (2014) 'Functional regeneration beyond the glial scar', *Experimental neurology*, 253, pp. 197–207. doi: 10.1016/J.EXPNEUROL.2013.12.024.

Cristiano, C. *et al.* (2019) 'Neutralization of IL-17 rescues amyloid-β-induced neuroinflammation and memory impairment', *British journal of pharmacology*, 176(18), pp. 3544–3557. doi: 10.1111/BPH.14586.

Csukly, G. *et al.* (2016) 'The differentiation of amnestic type MCI from the non-amnestic types by structural MRI', *Frontiers in Aging Neuroscience*, 8(MAR), p. 52. doi: 10.3389/FNAGI.2016.00052/BIBTEX.

Dahlgren, K. N. *et al.* (2002) 'Oligomeric and fibrillar species of amyloid-beta peptides differentially affect neuronal viability', *J Biol Chem*. 2002/06/12, 277(35), pp. 32046–32053. doi:

10.1074/jbc.M201750200 10.1074/jbc.M201750200. Epub 2002 Jun 10.

Dalva, M. B. *et al.* (2000) 'EphB receptors interact with NMDA receptors and regulate excitatory synapse formation', *Cell*, 103(6), pp. 945–956. doi: 10.1016/S0092-8674(00)00197-5.

DaRocha-Souto, B. *et al.* (2011) 'Brain oligomeric beta-amyloid but not total amyloid plaque burden correlates with neuronal loss and astrocyte inflammatory response in amyloid precursor protein/tau transgenic mice', *J Neuropathol Exp Neurol*. 2011/04/14, 70(5), pp. 360–376. doi: 10.1097/NEN.0b013e318217a118.

Das, H. *et al.* (2021) 'Subtle genomic DNA damage induces intraneuronal production of amyloid-β (1-42) by increasing β-secretase activity', *The FASEB Journal*, 35(5), p. e21569. doi: 10.1096/FJ.202001676RR.

Das, S. *et al.* (2020) 'Meta-analysis of mouse transcriptomic studies supports a context-dependent astrocyte reaction in acute CNS injury versus neurodegeneration', *Journal of neuroinflammation*, 17(1). doi: 10.1186/S12974-020-01898-Y.

Decourt, B., Lahiri, D. K. and Sabbagh, M. N. (2017) 'Targeting Tumor Necrosis Factor Alpha for Alzheimer's Disease', *Current Alzheimer research*, 14(4), p. 412. doi: 10.2174/1567205013666160930110551.

DeKosky, S. T. and Scheff, S. W. (1990) 'Synapse loss in frontal cortex biopsies in Alzheimer's disease: correlation with cognitive severity', *Annals of neurology*, 27(5), pp. 457–464. doi: 10.1002/ANA.410270502.

DeMattos, R. B. *et al.* (2002) 'Clusterin promotes amyloid plaque formation and is critical for neuritic toxicity in a mouse model of Alzheimer's disease', *Proc Natl Acad Sci U S A*. 2002/07/30, 99(16), pp. 10843–10848. doi: 10.1073/pnas.162228299 10.1073/pnas.162228299. Epub 2002 Jul 26.

Derkow, K. *et al.* (2018) 'Distinct expression of the neurotoxic microRNA family let-7 in the cerebrospinal fluid of patients with Alzheimer's disease'. doi: 10.1371/journal.pone.0200602.

Desagher, S., Glowinski, J. and Premont, J. (1996) 'Astrocytes protect neurons from hydrogen peroxide toxicity', *Journal of Neuroscience*, 16(8), pp. 2553–2562. doi: 10.1523/JNEUROSCI.16-08-02553.1996.

DiSabato, D. J., Quan, N. and Godbout, J. P. (2016) 'Neuroinflammation: The Devil is in the Details', *Journal of neurochemistry*, 139(Suppl 2), p. 136. doi: 10.1111/JNC.13607.

Doi, Yukiko *et al.* (2009) 'Microglia Activated with the Toll-Like Receptor 9 Ligand CpG Attenuate Oligomeric Amyloid β Neurotoxicity in in Vitro and in Vivo Models of Alzheimer's Disease', *The American Journal of Pathology*, 175(5), p. 2121. doi: 10.2353/AJPATH.2009.090418.

Doi, Y *et al.* (2009) 'Microglia Activated with the Toll-Like Receptor 9 Ligand CpG Attenuate Oligomeric Amyloid β Neurotoxicity in in Vitro and in Vivo Models of Alzheimer's Disease', *Am J Pathol*, 175(5), pp. 2121–2132. doi: 10.2353/ajpath.2009.090418.

Drake, J., Link, C. D. and Butterfield, D. A. (2003) 'Oxidative stress precedes fibrillar deposition of Alzheimer's disease amyloid beta-peptide (1-42) in a transgenic Caenorhabditis elegans model', *Neurobiol Aging*. 2003/02/26, 24(3), pp. 415–420. Available at: http://dx.doi.org/.

Dresselhaus, E. C. and Meffert, M. K. (2019) 'Cellular Specificity of NF-κB Function in the Nervous System', *Frontiers in Immunology*, 10(MAY). doi: 10.3389/FIMMU.2019.01043.

Driessens, N. *et al.* (2009) 'Hydrogen peroxide induces DNA single- and double-strand breaks in thyroid cells and is therefore a potential mutagen for this organ', *Endocr Relat Cancer*. 2009/06/11, 16(3), pp. 845–856. doi: 10.1677/erc-09-0020.

Driver, J. A. *et al.* (2012) 'Inverse association between cancer and Alzheimer's disease: Results from the Framingham Heart Study', *BMJ (Online)*, 344(7850), p. 19. doi: 10.1136/bmj.e1442.

Duits, F. H. *et al.* (2015) 'Matrix Metalloproteinases in Alzheimer's Disease and Concurrent Cerebral Microbleeds', *Journal of Alzheimer's Disease*, 48(3), pp. 711–720. doi: 10.3233/JAD-143186.

Dwir, D. *et al.* (2019) 'MMP9/RAGE pathway overactivation mediates redox dysregulation and neuroinflammation, leading to inhibitory/excitatory imbalance: a reverse translation study in schizophrenia patients', *Molecular Psychiatry 2019 25:11*, 25(11), pp. 2889–2904. doi: 10.1038/s41380-019-0393-5.

Edbauer, D. *et al.* (2003) 'Reconstitution of gamma-secretase activity', *Nat Cell Biol*. 2003/04/08, 5(5), pp. 486–488. doi: 10.1038/ncb960 10.1038/ncb960.

Elahy, M. *et al.* (2015) 'Blood-brain barrier dysfunction developed during normal aging is associated with inflammation and loss of tight junctions but not with leukocyte recruitment', *Immunity and Ageing*, 12(1), pp. 1–9. doi: 10.1186/S12979-015-0029-9/FIGURES/3.

Elmore, S. (2007) 'Apoptosis: A Review of Programmed Cell Death', *Toxicologic pathology*, 35(4), p. 495. doi: 10.1080/01926230701320337.

Escartin, C. *et al.* (2021) 'Reactive astrocyte nomenclature, definitions, and future directions', *Nature neuroscience*, 24(3), pp. 312–325. doi: 10.1038/S41593-020-00783-4.

Faller, P. and Hureau, C. (2021) 'Reproducibility Problems of Amyloid-β Self-Assembly and How to Deal With Them', *Frontiers in Chemistry*, 8, p. 1236. doi: 10.3389/FCHEM.2020.611227/BIBTEX.

Farris, W. *et al.* (2003) 'Insulin-degrading enzyme regulates the levels of insulin, amyloid beta-protein, and the beta-amyloid precursor protein intracellular domain in vivo', *Proc Natl Acad Sci U S A*. 2003/03/14, 100(7), pp. 4162–4167. doi: 10.1073/pnas.0230450100 10.1073/pnas.0230450100. Epub 2003 Mar 12.

Farris, W. *et al.* (2004) 'Partial Loss-of-Function Mutations in Insulin-Degrading Enzyme that Induce Diabetes also Impair Degradation of Amyloid β-Protein', *Am J Pathol*, 164(4), pp. 1425–1434. Available at: http://dx.doi.org/.

Faulkner, J. R. *et al.* (2004) 'Reactive astrocytes protect tissue and preserve function after spinal cord injury', *The Journal of neuroscience : the official journal of the Society for Neuroscience*, 24(9), pp. 2143–2155. doi: 10.1523/JNEUROSCI.3547-03.2004.

Di Fede, G. *et al.* (2009) 'A recessive mutation in the APP gene with dominant-negative effect on amyloidogenesis', *Science*. 2009/03/17, 323(5920), pp. 1473–1477. doi: 10.1126/science.1168979.

Feeney, C. J. *et al.* (2008) 'Vulnerability of glial cells to hydrogen peroxide in cultured hippocampal slices', *Brain research*, 1198, pp. 1–15. doi: 10.1016/J.BRAINRES.2007.12.049.

Fein, J. A. *et al.* (2008) 'Co-localization of amyloid beta and tau pathology in Alzheimer's disease synaptosomes', *Am J Pathol*. 2008/05/10, 172(6), pp. 1683–1692. doi: 10.2353/ajpath.2008.070829.

Fernandez-Perez, E. J. *et al.* (2021) 'Synaptic dysregulation and hyperexcitability induced by intracellular amyloid beta oligomers', *Aging Cell*, 20(9). doi: 10.1111/ACEL.13455.

Finder, V. H. *et al.* (2010) 'The recombinant amyloid-beta peptide Abeta1-42 aggregates faster and is more neurotoxic than synthetic Abeta1-42', *J Mol Biol*. 2009/12/23, 396(1), pp. 9–18. doi: 10.1016/j.jmb.2009.12.016.

van der Flier, W. M. *et al.* (2011) 'Early-onset versus late-onset Alzheimer's disease: the case of the missing APOE varepsilon4 allele', *Lancet Neurol*. 2010/12/28, 10(3), pp. 280–288. doi:

10.1016/s1474-4422(10)70306-9 10.1016/S1474-4422(10)70306-9. Epub 2010 Dec 22.

Florent, S. *et al.* (2006) 'Docosahexaenoic acid prevents neuronal apoptosis induced by soluble amyloid-beta oligomers', *Journal of neurochemistry*, 96(2), pp. 385–395. doi: 10.1111/J.1471-4159.2005.03541.X.

Forloni, G. (2020) 'Alzheimer's disease: from basic science to precision medicine approach', *BMJ Neurology Open*, 2(2), p. e000079. doi: 10.1136/BMJNO-2020-000079.

Franciosi, S. *et al.* (2005) 'IL-8 enhancement of amyloid-beta (Aβ1-42)-induced expression and production of pro-inflammatory cytokines and COX-2 in cultured human microglia', *Journal of Neuroimmunology*, 159(1–2), pp. 66–74. doi: 10.1016/j.jneuroim.2004.10.006.

Funamoto, S. *et al.* (2004) 'Truncated carboxyl-terminal fragments of beta-amyloid precursor protein are processed to amyloid beta-proteins 40 and 42', *Biochemistry*. 2004/10/20, 43(42), pp. 13532–13540. doi: 10.1021/bi049399k 10.1021/bi049399k.

Furlaneto, C. J. and Campa, A. (2000) 'A novel function of serum amyloid A: a potent stimulus for the release of tumor necrosis factor-alpha, interleukin-1beta, and interleukin-8 by human blood neutrophil', *Biochemical and biophysical research communications*, 268(2), pp. 405–408. doi: 10.1006/BBRC.2000.2143.

Furukawa, K. *et al.* (1996) 'Increased activity-regulating and neuroprotective efficacy of alpha-secretase-derived secreted amyloid precursor protein conferred by a C-terminal heparin-binding domain', *Journal of neurochemistry*, 67(5), pp. 1882–1896. doi: 10.1046/J.1471-4159.1996.67051882.X.

Gao, Y. *et al.* (2019) 'Mutation profile of APP, PSEN1, and PSEN2 in Chinese familial Alzheimer's disease', *Neurobiol Aging*. 2019/03/02, 77, pp. 154–157. doi: 10.1016/j.neurobiolaging.2019.01.018.

Garaschuk, O. and Verkhratsky, A. (2019) 'GABAergic astrocytes in Alzheimer's disease', *Aging (Albany NY)*, 11(6), p. 1602. doi: 10.18632/AGING.101870.

Garwood, C. J. *et al.* (2011) 'Astrocytes are important mediators of Abeta-induced neurotoxicity and tau phosphorylation in primary culture', *Cell Death Dis*. 2011/06/03, 2, p. e167. doi: 10.1038/cddis.2011.50.

Garwood, C. J. *et al.* (2017) 'Review: Astrocytes in Alzheimer's disease and other age-associated dementias: a supporting player with a central role', *Neuropathol Appl Neurobiol*. 2016/07/22, 43(4), pp. 281–298. doi: 10.1111/nan.12338.

Gatto, N. *et al.* (2021) 'Directly converted astrocytes retain the ageing features of the donor fibroblasts and elucidate the astrocytic contribution to human CNS health and disease', *Aging Cell*, 20(1). doi: 10.1111/ACEL.13281.

Gauthier, S. *et al.* (2006) 'Mild cognitive impairment', *Lancet (London, England)*, 367(9518), pp. 1262–1270. doi: 10.1016/S0140-6736(06)68542-5.

Geula, C. *et al.* (1998) 'Aging renders the brain vulnerable to amyloid beta-protein neurotoxicity', *Nature medicine*, 4(7), pp. 827–831. doi: 10.1038/NM0798-827.

Ghavami, M. *et al.* (2013) 'Physiological TemperatureHas a Crucial Role in AmyloidBeta in the Absence and Presence of Hydrophobic and Hydrophilic Nanoparticles', *ACS Chemical Neuroscience*, 4(3), p. 375. doi: 10.1021/CN300205G.

Ghosh, P. *et al.* (2016) 'Determination of critical nucleation number for a single nucleation amyloid-beta aggregation model', *Math Biosci*. 2016/01/17, 273, pp. 70–79. doi: 10.1016/j.mbs.2015.12.004 10.1016/j.mbs.2015.12.004. Epub 2016 Jan 7.

Glenner, G. G. and Wong, C. W. (1984) 'Alzheimer's disease: Initial report of the purification and characterization of a novel cerebrovascular amyloid protein', *Biochemical and Biophysical Research Communications*, 120(3), pp. 885–890. doi: 10.1016/S0006-291X(84)80190-4.

Goate, A. *et al.* (1991) 'Segregation of a missense mutation in the amyloid precursor protein gene with familial Alzheimer's disease', *Nature*. 1991/02/21, 349(6311), pp. 704–706. doi: 10.1038/349704a0.

Goel, P. *et al.* (2022) 'Neuronal cell death mechanisms in Alzheimer's disease: An insight', *Frontiers in Molecular Neuroscience*, 15. doi: 10.3389/FNMOL.2022.937133.

Gomez-Arboledas, A. *et al.* (2018) 'Phagocytic clearance of presynaptic dystrophies by reactive astrocytes in Alzheimer's disease', *Glia*, 66(3), pp. 637–653. doi: 10.1002/GLIA.23270.

Gong, L. *et al.* (2020) 'Interleukin 32: A novel player in perioperative neurocognitive disorders', *Medical Hypotheses*, 144, p. 110158. doi: 10.1016/J.MEHY.2020.110158.

González-Gualda, E. *et al.* (2021) 'A guide to assessing cellular senescence in vitro and in vivo', *The FEBS Journal*, 288(1), pp. 56–80. doi: 10.1111/FEBS.15570.

Gonzalez-Reyes, R. E. *et al.* (2017) 'Involvement of Astrocytes in Alzheimer's Disease from a Neuroinflammatory and Oxidative Stress Perspective', *Front Mol Neurosci*. 2018/01/10, 10, p. 427. doi: 10.3389/fnmol.2017.00427.

Gorina, R. *et al.* (2005) 'AG490 prevents cell death after exposure of rat astrocytes to hydrogen peroxide or proinflammatory cytokines: involvement of the Jak2/STAT pathway'. doi: 10.1111/j.1471-4159.2004.02878.x.

Gould, K. L. and Nurse, P. (1989) *Tyrosine phosphorylation of the fission yeast cdc2+ protein kinase regulates entry into mitosis*.

Gouras, G. K. *et al.* (2000) 'Short Communication Intraneuronal A42 Accumulation in Human Brain', *American Journal of Pathology*, 156(1).

Grimaldi, L. M. E. *et al.* (2000) 'Association of early-onset Alzheimer's disease with an interleukin-1α gene polymorphism', *Annals of Neurology*, 47, pp. 361–365.

Grontvedt, G. R. *et al.* (2018) 'Alzheimer's disease', *Curr Biol*. 2018/06/06, 28(11), pp. R645-r649. doi: 10.1016/j.cub.2018.04.080 10.1016/j.cub.2018.04.080.

Grosche, J. *et al.* (1999) 'Microdomains for neuron-glia interaction: parallel fiber signaling to Bergmann glial cells', *Nature neuroscience*, 2(2), pp. 139–143. doi: 10.1038/5692.

Guerreiro, R. *et al.* (2013) 'TREM2 Variants in Alzheimer's Disease', *N Engl J Med*, 368(2), pp. 117–127. doi: 10.1056/NEJMoa1211851.

Guo, J. tao *et al.* (2002) 'Inflammation-Dependent Cerebral Deposition of Serum Amyloid A Protein in a Mouse Model of Amyloidosis', *Journal of Neuroscience*, 22(14), pp. 5900–5909. doi: 10.1523/JNEUROSCI.22-14-05900.2002.

Gursky, O. and Aleshkov, S. (2000) 'Temperature-dependent β-sheet formation in β-amyloid Aβ1–40 peptide in water: uncoupling β-structure folding from aggregation', *Biochimica et Biophysica Acta (BBA) - Protein Structure and Molecular Enzymology*, 1476(1), pp. 93–102. doi: 10.1016/S0167-4838(99)00228-9.

Haass, C. *et al.* (2012) 'Trafficking and proteolytic processing of APP', *Cold Spring Harb Perspect Med*. 2012/05/04, 2(5), p. a006270. doi: 10.1101/cshperspect.a006270 10.1101/cshperspect.a006270.

Haber, M., Zhou, L. and Murai, K. K. (2006) 'Cooperative astrocyte and dendritic spine dynamics at hippocampal excitatory synapses', *The Journal of neuroscience : the official journal of the Society for Neuroscience*, 26(35), pp. 8881–8891. doi: 10.1523/JNEUROSCI.1302-06.2006.

Habib, A., Sawmiller, D. and Tan, J. (2017) 'Restoring sAPPα functions as a potential treatment for Alzheimer's disease', *J Neurosci Res*, 95(4), pp. 973–991. doi: 10.1002/jnr.23823 10.1002/jnr.23823.

Den Haese, G. J. *et al.* (1995) 'The Wee1 protein kinase regulates T14 phosphorylation of fission yeast Cdc2.', *Molecular Biology of the Cell*, 6(4), p. 371. doi: 10.1091/MBC.6.4.371.

Haidet-Phillips, A. M. *et al.* (2011) 'Astrocytes from Familial and Sporadic ALS Patients are Toxic to Motor Neurons', *Nature biotechnology*, 29(9), p. 824. doi: 10.1038/NBT.1957.

Hampel, H. *et al.* (2021) 'The Amyloid-β Pathway in Alzheimer's Disease', *Molecular psychiatry*, 26(10), pp. 5481–5503. doi: 10.1038/S41380-021-01249-0.

Hardy, J. A. and Higgins, G. A. (1992) 'Alzheimer's disease: the amyloid cascade hypothesis', *Science*. 1992/04/10, 256(5054), pp. 184–185. Available at: http://dx.doi.org/.

Hardy, J. and Selkoe, D. J. (2002) 'The amyloid hypothesis of Alzheimer's disease: Progress and problems on the road to therapeutics', *Science*, 297(5580), pp. 353–356. doi: 10.1126/SCIENCE.1072994/ASSET/C4ED1918-4F2B-4649-BA69-684D0145F32B/ASSETS/GRAPHIC/SE2820694002.JPEG.

Harold, D. *et al.* (2009) 'Genome-wide association study identifies variants at CLU and PICALM associated with Alzheimer's disease', *Nature Genetics 2009 41:10*, 41(10), pp. 1088–1093. doi: 10.1038/ng.440.

Hashioka, S. *et al.* (2009) 'Interferon-gamma-dependent cytotoxic activation of human astrocytes and astrocytoma cells', *Neurobiology of aging*, 30(12), pp. 1924–1935. doi: 10.1016/J.NEUROBIOLAGING.2008.02.019.

Hatip, F. F. B. *et al.* (2009) 'Reversal of temperature-induced conformational changes in the amyloid-beta peptide, Aβ40, by the β-sheet breaker peptides 16–23 and 17–24', *British Journal of Pharmacology*, 158(4), p. 1165. doi: 10.1111/J.1476-5381.2009.00384.X.

Hayden, M. S. and Ghosh, S. (2014) 'Regulation of NF-κB by TNF Family Cytokines', *Seminars in immunology*, 26(3), p. 253. doi: 10.1016/J.SMIM.2014.05.004.

He, Y. *et al.* (2012) 'Soluble oligomers and fibrillar species of amyloid beta-peptide differentially affect cognitive functions and hippocampal inflammatory response', *Biochem Biophys Res Commun*. 2012/11/14, 429(3–4), pp. 125–130. doi: 10.1016/j.bbrc.2012.10.129.

Hoe, H. S., Lee, H. K. and Pak, D. T. S. (2012) 'The Upside of APP at Synapses', *CNS Neuroscience & Therapeutics*, 18(1), p. 47. doi: 10.1111/J.1755-5949.2010.00221.X.

Hong, S. *et al.* (2014) 'Soluble Abeta oligomers are rapidly sequestered from brain ISF in vivo and bind GM1 ganglioside on cellular membranes', *Neuron*. 2014/04/02, 82(2), pp. 308–319. doi: 10.1016/j.neuron.2014.02.027.

Hou, B. *et al.* (2020) 'Inhibition of the NLRP3-inflammasome prevents cognitive deficits in experimental autoimmune encephalomyelitis mice via the alteration of astrocyte phenotype', *Cell Death & Disease 2020 11:5*, 11(5), pp. 1–16. doi: 10.1038/s41419-020-2565-2.

Hu, R. *et al.* (2017) 'Overexpression of EphB2 in hippocampus rescues impaired NMDA receptors trafficking and cognitive dysfunction in Alzheimer model', *Cell Death & Disease 2017 8:3*, 8(3), pp. e2717–e2717. doi: 10.1038/cddis.2017.140.

Huang, L. K., Chao, S. P. and Hu, C. J. (2020) 'Clinical trials of new drugs for Alzheimer disease', *J Biomed Sci*, 27. doi: 10.1186/s12929-019-0609-7.

Huang, W. J., Zhang, X. and Chen, W. W. (2016) 'Role of oxidative stress in Alzheimer's disease', *Biomed Rep*, 4(5), pp. 519–522. doi: 10.3892/br.2016.630.

Hunsberger, H. C. *et al.* (2019) 'The role of APOE4 in Alzheimer's disease: strategies for future therapeutic interventions', *Neuronal Signaling*, 3(2), p. 20180203. doi: 10.1042/NS20180203.

Ingelsson, M. *et al.* (2004) 'Early Abeta accumulation and progressive synaptic loss, gliosis, and tangle formation in AD brain', *Neurology*. 2004/03/24, 62(6), pp. 925–931. Available at: http://dx.doi.org/.

Ioannou, M. S. *et al.* (2019) 'Neuron-Astrocyte Metabolic Coupling Protects against Activity-Induced Fatty Acid Toxicity', *Cell*, 177(6), pp. 1522-1535.e14. doi: 10.1016/J.CELL.2019.04.001.

Ionescu-Tucker, A. and Cotman, C. W. (2021) 'Emerging roles of oxidative stress in brain aging and Alzheimer's disease', *Neurobiology of Aging*, 107, pp. 86–95. doi: 10.1016/J.NEUROBIOLAGING.2021.07.014.

Isik, A. T. (2010) 'Late onset Alzheimer's disease in older people', *Clin Interv Aging*, 5, pp. 307–311. doi: 10.2147/cia.s11718.

Ito, S. *et al.* (2007) 'Induction of matrix metalloproteinases (MMP3, MMP12 and MMP13) expression in the microglia by amyloid-beta stimulation via the PI3K/Akt pathway', *Experimental gerontology*, 42(6), pp. 532–537. doi: 10.1016/J.EXGER.2006.11.012.

Iwatsubo, T. *et al.* (1996) 'Full-length amyloid-beta (1-42(43)) and amino-terminally modified and truncated amyloid-beta 42(43) deposit in diffuse plaques', *Am J Pathol*, 149(6), pp. 1823–1830. Available at: http://dx.doi.org/.

Jack Jr., C. R. *et al.* (2010) 'Hypothetical model of dynamic biomarkers of the Alzheimer's pathological cascade', *Lancet Neurol*. 2010/01/20, 9(1), pp. 119–128. doi: 10.1016/s1474-4422(09)70299-6.

Jack, C. R. *et al.* (2013) 'Update on hypothetical model of Alzheimer's disease biomarkers', *Lancet neurology*, 12(2), p. 207. doi: 10.1016/S1474-4422(12)70291-0.

Jackson, M. P. and Hewitt, E. W. (2017) 'Why Are Functional Amyloids Non-Toxic in Humans?', *Biomolecules*, 7(4). doi: 10.3390/BIOM7040071.

Jain, M. *et al.* (2021) 'Role of JAK/STAT in the Neuroinflammation and its Association withNeurological Disorders', *Annals of Neurosciences*, 28(3–4), p. 191. doi: 10.1177/09727531211070532.

Jain, V., Langham, M. C. and Wehrli, F. W. (2010) 'MRI estimation of global brain oxygen consumption rate', *Journal of cerebral blood flow and metabolism : official journal of the International Society of Cerebral Blood Flow and Metabolism*, 30(9), pp. 1598–1607. doi: 10.1038/JCBFM.2010.49.

Jan, A. *et al.* (2011) 'Abeta42 neurotoxicity is mediated by ongoing nucleated polymerization process rather than by discrete Abeta42 species', *J Biol Chem*. 2010/12/16, 286(10), pp. 8585–8596. doi: 10.1074/jbc.M110.172411 10.1074/jbc.M110.172411. Epub 2010 Dec 14.

Janda, E., Boi, L. and Carta, A. R. (2018) 'Microglial Phagocytosis and Its Regulation: A Therapeutic Target in Parkinson's Disease?', *Front Mol Neurosci*, 11. doi: 10.3389/fnmol.2018.00144 10.3389/fnmol.2018.00144.

Jang, S. *et al.* (2019) 'Serum amyloid A1 is involved in amyloid plaque aggregation and memory decline in amyloid beta abundant condition', *Transgenic research*, 28(5–6), pp. 499–508. doi: 10.1007/S11248-019-00166-X.

Jang, W. Y. *et al.* (2017) 'Overexpression of serum amyloid a 1 induces depressive-like behavior in mice', *Brain Research*, 1654, pp. 55–65. doi: 10.1016/J.BRAINRES.2016.09.003.

Jarrett, J. T., Berger, E. P. and Lansbury Jr., P. T. (1993) 'The carboxy terminus of the beta amyloid protein is critical for the seeding of amyloid formation: implications for the pathogenesis of Alzheimer's disease', *Biochemistry*. 1993/05/11, 32(18), pp. 4693–4697. Available at: http://dx.doi.org/.

Jeong, J. S. *et al.* (2013) 'Novel mechanistic insight into the molecular basis of amyloid polymorphism and secondary nucleation during amyloid formation', *J Mol Biol*. 2013/02/19, 425(10), pp. 1765–1781. doi: 10.1016/j.jmb.2013.02.005 10.1016/j.jmb.2013.02.005. Epub 2013 Feb 13.

Ji, Y. *et al.* (2019) 'Effects of Microglial Cytokines on Alzheimer's Disease-Related Phenomena', *Journal of Alzheimer's disease : JAD*, 67(3), pp. 1021–1034. doi: 10.3233/JAD-180820.

Jin, M. *et al.* (2011) 'Soluble amyloid beta-protein dimers isolated from Alzheimer cortex directly induce Tau hyperphosphorylation and neuritic degeneration', *Proc Natl Acad Sci U S A*. 2011/03/23, 108(14), pp. 5819–5824. doi: 10.1073/pnas.1017033108.

Jo, D. H. *et al.* (2020) 'Intracellular amyloid-β disrupts tight junctions of the retinal pigment epithelium via NF-κB activation', *Neurobiology of Aging*, 95, pp. 115–122. doi: 10.1016/J.NEUROBIOLAGING.2020.07.013.

Jonsson, T. *et al.* (2012) 'A mutation in APP protects against Alzheimer's disease and age-related cognitive decline', *Nature*, 488(7409), pp. 96–99.

Jonsson, T. *et al.* (2013) 'Variant of TREM2 associated with the risk of Alzheimer's disease', *N Engl J Med*. 2012/11/16, 368(2), pp. 107–116. doi: 10.1056/NEJMoa1211103 10.1056/NEJMoa1211103. Epub 2012 Nov 14.

Kacem, K. *et al.* (1998) 'Structural organization of the perivascular astrocyte endfeet and their relationship with the endothelial glucose transporter: a confocal microscopy study', *Glia*, 1, pp. 1–10.

Kametani, F. (2008) 'Epsilon-secretase: reduction of amyloid precursor protein epsilon-site cleavage in Alzheimer's disease', *Curr Alzheimer Res*. 2008/04/09, 5(2), pp. 165–171. Available at: http://dx.doi.org/.

Kamphuis, W. *et al.* (2014) 'Glial fibrillary acidic protein isoform expression in plaque related astrogliosis in Alzheimer's disease', *Neurobiol Aging*. 2013/11/26, 35(3), pp. 492–510. doi: 10.1016/j.neurobiolaging.2013.09.035.

Karthick, C. *et al.* (2018) 'Time-dependent effect of oligomeric amyloid-beta (1-42)-induced hippocampal neurodegeneration in rat model of Alzheimer's disease', *Neurol Res*. 2018/11/21, pp. 1–12. doi: 10.1080/01616412.2018.1544745.

Katsouri, L. *et al.* (2020) 'Ablation of reactive astrocytes exacerbates disease pathology in a model of Alzheimer's disease', *Glia*, 68(5), pp. 1017–1030. doi: 10.1002/GLIA.23759.

Kayed, R. *et al.* (2003) 'Common structure of soluble amyloid oligomers implies common mechanism of pathogenesis', *Science*. 2003/04/19, 300(5618), pp. 486–489. doi: 10.1126/science.1079469 10.1126/science.1079469.

Kim, H. *et al.* (2009) 'Discriminative cytotoxicity assessment based on various cellular damages', *Toxicology letters*, 184(1), pp. 13–17. doi: 10.1016/J.TOXLET.2008.10.006.

Kim, H. J. *et al.* (2015) 'Elevation of the Plasma Aβ 40/Aβ 42 Ratio as a Diagnostic Marker of Sporadic Early-Onset Alzheimer's Disease', *Journal of Alzheimer's Disease*, 48(4), pp. 1043–1050. doi: 10.3233/JAD-143018.

Kimbrough, I. F. *et al.* (2015) 'Vascular amyloidosis impairs the gliovascular unit in a mouse model of Alzheimer's disease', *Brain : a journal of neurology*, 138(Pt 12), pp. 3716–3733. doi: 10.1093/BRAIN/AWV327.

Klein, A. M., Kowall, N. W. and Ferrante, R. J. (1999) 'Neurotoxicity and oxidative damage of beta amyloid 1-42 versus beta amyloid 1-40 in the mouse cerebral cortex', *Annals of the New York Academy of Sciences*, 893, pp. 314–320. doi: 10.1111/J.1749-6632.1999.TB07845.X.

Klement, K. *et al.* (2007) 'Effect of different salt ions on the propensity of aggregation and on the structure of Alzheimer's abeta(1-40) amyloid fibrils', *J Mol Biol*. 2007/10/02, 373(5), pp. 1321–1333. doi: 10.1016/j.jmb.2007.08.068 10.1016/j.jmb.2007.08.068. Epub 2007 Sep 7.

Kobayashi, S. *et al.* (2015) 'Dependence pH and proposed mechanism for aggregation of Alzheimer's disease-related amyloid-β(1–42) protein', *Journal of Molecular Structure*, 1094, pp. 109–117. doi: 10.1016/J.MOLSTRUC.2015.03.023.

Koffie, R. M. *et al.* (2009) 'Oligomeric amyloid beta associates with postsynaptic densities and correlates with excitatory synapse loss near senile plaques', *Proc Natl Acad Sci U S A*. 2009/02/21, 106(10), pp. 4012–4017. doi: 10.1073/pnas.0811698106.

Kok, J. R. *et al.* (2021) 'DNA damage as a mechanism of neurodegeneration in ALS and a contributor to astrocyte toxicity', 78, pp. 5707–5729. doi: 10.1007/s00018-021-03872-0.

Kollmer, M *et al.* (2019) 'Cryo-EM structure and polymorphism of Abeta amyloid fibrils purified from Alzheimer's brain tissue', *Nat Commun*. 2019/10/31, 10(1), p. 4760. doi: 10.1038/s41467-019-12683-8.

Kollmer, Marius *et al.* (2019) 'Cryo-EM structure and polymorphism of Aβ amyloid fibrils purified from Alzheimer's brain tissue', *Nature Communications*, 10(1), p. 4760. doi: 10.1038/s41467-019-12683-8.

Kostic, M. *et al.* (2017) 'IL-17 signalling in astrocytes promotes glutamate excitotoxicity: Indications for the link between inflammatory and neurodegenerative events in multiple sclerosis', *Multiple Sclerosis and Related Disorders*, 11, pp. 12–17. doi: 10.1016/j.msard.2016.11.006.

Kraft, A. W. *et al.* (2013) 'Attenuating astrocyte activation accelerates plaque pathogenesis in APP/PS1 mice', *FASEB journal : official publication of the Federation of American Societies for Experimental Biology*, 27(1), pp. 187–198. doi: 10.1096/FJ.12-208660.

Kuchibhotla, K. V. *et al.* (2009) 'Synchronous hyperactivity and intercellular calcium waves in astrocytes in Alzheimer mice', *Science (New York, N.Y.)*, 323(5918), pp. 1211–1215. doi: 10.1126/SCIENCE.1169096.

Kukurba, K. R. and Montgomery, S. B. (2015) 'RNA Sequencing and Analysis', *Cold Spring Harbor protocols*, 2015(11), p. 951. doi: 10.1101/PDB.TOP084970.

Kulijewicz-Nawrot, M. *et al.* (2012) 'Astrocytic cytoskeletal atrophy in the medial prefrontal cortex of a triple transgenic mouse model of Alzheimer's disease', *Journal of Anatomy*, 221(3), pp. 252–262. doi: 10.1111/J.1469-7580.2012.01536.X.

Kumar, L., Haque, R. and Nazir, A. (2016) 'Role of MicroRNA Let-7 in Modulating Multifactorial Aspect of Neurodegenerative Diseases: an Overview', *Mol Neurobiol*, 53, pp. 2787–2793. doi: 10.1007/s12035-015-9145-y.

Kumar, P., Nagarajan, A. and Uchil, P. D. (2018) 'Analysis of Cell Viability by the Lactate Dehydrogenase Assay', *Cold Spring Harb Protoc*. 2018/06/03, 2018(6). doi: 10.1101/pdb.prot095497.

Kummer, M. P. and Heneka, M. T. (2014) 'Truncated and modified amyloid-beta species', in *Alzheimers Res Ther*. Department of Neurology, University Hospital Bonn, Sigmund-Freud-Strasse 25, 53127 Bonn, Germany, p. 28. doi: 10.1186/alzrt258.

Kuo, L. J. and Yang, L. X. (2008) 'Gamma-H2AX - a novel biomarker for DNA double-strand breaks', *In Vivo*. 2008/07/10, 22(3), pp. 305–309. Available at: http://dx.doi.org/.

Lacor, P. N. *et al.* (2007) 'Abeta oligomer-induced aberrations in synapse composition, shape, and density provide a molecular basis for loss of connectivity in Alzheimer's disease', *J Neurosci*. 2007/01/26, 27(4), pp. 796–807. doi: 10.1523/jneurosci.3501-06.2007.

LaRocca, T. J. *et al.* (2021) 'Amyloid beta acts synergistically as a pro-inflammatory cytokine', *Neurobiology of Disease*, 159, p. 105493. doi: 10.1016/J.NBD.2021.105493.

Leake, A., Morris, C. M. and Whateley, J. (2000) 'Brain matrix metalloproteinase 1 levels are elevated in Alzheimer's disease', *Neuroscience Letters*, 291(3), pp. 201–203. doi: 10.1016/S0304-3940(00)01418-X.

Lee, J. *et al.* (2008) 'Adaptor Protein Sorting Nexin 17 Regulates Amyloid Precursor Protein Trafficking and Processing in the Early Endosomes*', *J Biol Chem*, 283(17), pp. 11501–11508. doi: 10.1074/jbc.M800642200.

Lee, K. H., Cha, M. and Lee, B. H. (2021) 'Crosstalk between Neuron and Glial Cells in Oxidative Injury and Neuroprotection', *International Journal of Molecular Sciences*, 22(24). doi: 10.3390/IJMS222413315.

Lee, S., Fernandez, E. J. and Good, T. A. (2007) 'Role of aggregation conditions in structure, stability, and toxicity of intermediates in the Aβ fibril formation pathway', *Protein Science : A Publication of the Protein Society*, 16(4), p. 723. doi: 10.1110/PS.062514807.

Lehmann, S. M. *et al.* (2012) 'An unconventional role for miRNA: let-7 activates Toll-like receptor 7 and causes neurodegeneration', *Nature Neuroscience 2012 15:6*, 15(6), pp. 827–835. doi: 10.1038/nn.3113.

LeVatte, M. A. *et al.* (2019) 'Preparation and characterization of a highly soluble Aβ1-42 peptide variant', *Protein Expression and Purification*, 164, p. 105480. doi: https://doi.org/10.1016/j.pep.2019.105480.

Levine, H. (1995) 'Soluble multimeric Alzheimer beta(1-40) pre-amyloid complexes in dilute solution', *Neurobiology of aging*, 16(5), pp. 755–764. doi: 10.1016/0197-4580(95)00052-G.

Levy-Lahad, E. *et al.* (1995) 'Candidate gene for the chromosome 1 familial Alzheimer's disease locus', *Science*. 1995/08/18, 269(5226), pp. 973–977. Available at: http://dx.doi.org/.

Li, D. *et al.* (2022) 'An evaluation of RNA-seq differential analysis methods', *PLoS ONE*, 17(9). doi: 10.1371/JOURNAL.PONE.0264246.

Li, K. *et al.* (2019) 'Reactive Astrocytes in Neurodegenerative Diseases', *Aging and Disease*, 10(3), p. 664. doi: 10.14336/AD.2018.0720.

Li, X. *et al.* (2015) 'Quality control of RNA-seq experiments', *Methods in Molecular Biology*, 1269, pp. 137–146. doi: 10.1007/978-1-4939-2291-8_8/FIGURES/5.

Li, Y. *et al.* (2022) 'Alzheimer's Amyloid-β Accelerates Human Neuronal Cell Senescence Which Could Be Rescued by Sirtuin-1 and Aspirin', *Frontiers in Cellular Neuroscience*, 16, p. 309. doi:

10.3389/FNCEL.2022.906270/BIBTEX.

Li, Yanfang *et al.* (2016) 'Implications of GABAergic Neurotransmission in Alzheimer's Disease'. doi: 10.3389/fnagi.2016.00031.

Lian, H. *et al.* (2015) 'NFκB-activated Astroglial Release of Complement C3 Compromises Neuronal Morphology and Function Associated with Alzheimer's Disease', *Neuron*, 85(1), pp. 101–115. doi: 10.1016/j.neuron.2014.11.018.

Lian, H. *et al.* (2016) 'Astrocyte-Microglia Cross Talk through Complement Activation Modulates Amyloid Pathology in Mouse Models of Alzheimer's Disease', *J Neurosci*, 36(2), pp. 577–589. doi: 10.1523/jneurosci.2117-15.2016.

Liang, J. shan *et al.* (1997) 'Evidence for local production of acute phase response apolipoprotein serum amyloid A in Alzheimer's disease brain', *Neuroscience Letters*, 225(2), pp. 73–76. doi: 10.1016/S0304-3940(97)00196-1.

Liddelow, S. A., Guttenplan, K. A., Clarke, L. E., Bennett, F. C., Bohlen, C. J., Schirmer, L., Bennett, M. L., Münch, A. E., *et al.* (2017) 'Neurotoxic reactive astrocytes are induced by activated microglia', *Nature*, 541(7638), pp. 481–487. doi: 10.1038/nature21029.

Liddelow, S. A., Guttenplan, K. A., Clarke, L. E., Bennett, F. C., Bohlen, C. J., Schirmer, L., Bennett, M. L., Munch, A. E., *et al.* (2017) 'Neurotoxic reactive astrocytes are induced by activated microglia', *Nature*. 2017/01/19, 541(7638), pp. 481–487. doi: 10.1038/nature21029.

Liddelow, S. A. and Barres, B. A. (2017) 'Reactive Astrocytes: Production, Function, and Therapeutic Potential', *Immunity*. 2017/06/22, 46(6), pp. 957–967. doi: 10.1016/j.immuni.2017.06.006.

Lightfoot, S., Salowsky, R. and Buhlmann, C. (2005) 'RNA integrity number: towards standardization of RNA quality assessment for better reproducibility and reliability of gene expression experiments', *Breast Cancer Research : BCR*, 7(Suppl 2), p. P7.05. doi: 10.1186/BCR1197.

Liguori, I. *et al.* (2018) 'Oxidative stress, aging, and diseases', *Clinical Interventions in Aging*, 13, p. 757. doi: 10.2147/CIA.S158513.

Limon, A., Reyes-Ruiz, J. M. and Miledi, R. (2012) 'Loss of functional GABA A receptors in the Alzheimer diseased brain', *Proceedings of the National Academy of Sciences of the United States of America*, 109(25), pp. 10071–10076. doi: 10.1073/PNAS.1204606109/SUPPL_FILE/PNAS.201204606SI.PDF.

Lin, X. *et al.* (2020) 'Contributions of DNA Damage to Alzheimer's Disease', *International journal of molecular sciences*, 21(5). doi: 10.3390/IJMS21051666.

Lin, Y.-T. *et al.* (2018) 'Correction APOE4 Causes Widespread Molecular and Cellular Alterations Associated with Alzheimer's Disease Phenotypes in Human iPSC-Derived Brain Cell Types'. doi: 10.1016/j.neuron.2018.06.011.

Linse, S. (2017) 'Monomer-dependent secondary nucleation in amyloid formation', *Biophys Rev*, 9(4), pp. 329–338. doi: 10.1007/s12551-017-0289-z 10.1007/s12551-017-0289-z.

Liu, C. C. *et al.* (2013) 'Apolipoprotein E and Alzheimer disease: risk, mechanisms, and therapy', *Nat Rev Neurol*, 9(2), pp. 106–118. doi: 10.1038/nrneurol.2012.263.

Liu, H. *et al.* (2021) 'Distinct conformers of amyloid beta accumulate in the neocortex of patients with rapidly progressive Alzheimer's disease', *The Journal of Biological Chemistry*, 297(5). doi: 10.1016/J.JBC.2021.101267.

Liu, M. *et al.* (2018) 'α-synuclein induces apoptosis of astrocytes by causing dysfunction of the

endoplasmic reticulum-Golgi compartment', *Molecular medicine reports*, 18(1), pp. 322–332. doi: 10.3892/MMR.2018.9002.

Lochhead, J. J. *et al.* (2020) 'Structure, Function, and Regulation of the Blood-Brain Barrier Tight Junction in Central Nervous System Disorders', *Frontiers in Physiology*, 11, p. 914. doi: 10.3389/FPHYS.2020.00914/BIBTEX.

Lu, J.-X. *et al.* (2013) 'Molecular structure of β-amyloid fibrils in Alzheimer's disease brain tissue', *Cell*, 154(6), pp. 1257–1268. doi: 10.1016/j.cell.2013.08.035.

Lührs, T. *et al.* (2005) '3D structure of Alzheimer's amyloid-beta(1-42) fibrils', *Proceedings of the National Academy of Sciences of the United States of America*. 2005/11/17, 102(48), pp. 17342–17347. doi: 10.1073/pnas.0506723102.

Maciotta, S. *et al.* (2013) 'The involvement of microRNAs in neurodegenerative diseases'. doi: 10.3389/fncel.2013.00265.

Madabhushi, R., Pan, L. and Tsai, L. H. (2014) 'DNA damage and its links to neurodegeneration', *Neuron*, 83(2), p. 266. doi: 10.1016/J.NEURON.2014.06.034.

Maezawa, I. *et al.* (2011) 'Amyloid-beta protein oligomer at low nanomolar concentrations activates microglia and induces microglial neurotoxicity', *J Biol Chem*. 2010/10/26, 286(5), pp. 3693–3706. doi: 10.1074/jbc.M110.135244.

Manning, R. R. *et al.* (2021) 'Analysis of Peptides using Asymmetrical Flow Field-flow Fractionation (AF4)', *Journal of Pharmaceutical Sciences*, 110(12), pp. 3969–3972. doi: 10.1016/J.XPHS.2021.09.036.

Mao, P. and Reddy, P. H. (2011) 'Aging and Amyloid beta-induced oxidative DNA damage and mitochondrial dysfunction in Alzheimer's Disease: Implications for early intervention and therapeutics', *Biochimica et biophysica acta*, 1812(11), p. 1359. doi: 10.1016/J.BBADIS.2011.08.005.

Marr, R. A. *et al.* (2003) 'Neprilysin gene transfer reduces human amyloid pathology in transgenic mice', *J Neurosci*. 2003/03/27, 23(6), pp. 1992–1996. Available at: http://dx.doi.org/.

Marr, R. A. and Hafez, D. M. (2014) 'Amyloid-beta and Alzheimer's disease: the role of neprilysin-2 in amyloid-beta clearance', *Front Aging Neurosci*, 6. doi: 10.3389/fnagi.2014.00187 10.3389/fnagi.2014.00187.

Martinez, I. *et al.* (2016) 'Induction of DNA double-strand breaks and cellular senescence by human respiratory syncytial virus', *Virulence*. 2016/01/27, 7(4), pp. 427–442. doi: 10.1080/21505594.2016.1144001.

Martins, S. G. *et al.* (2021) 'Linking Oxidative Stress and DNA Damage to Changes in the Expression of Extracellular Matrix Components', *Frontiers in Genetics*, 12, p. 1279. doi: 10.3389/FGENE.2021.673002/XML/NLM.

Matés, J. M. (2000) 'Effects of antioxidant enzymes in the molecular control of reactive oxygen species toxicology', *Toxicology*, 153. Available at: www.elsevier.com/locate/toxicol (Accessed: 6 September 2022).

Mathur, R. *et al.* (2015) 'A Reduced Astrocyte Response to β-Amyloid Plaques in the Ageing Brain Associates with Cognitive Impairment', in *PLoS One*. Sheffield Institute for Translational Neuroscience, University of Sheffield, Sheffield, England, United KingdomInstitute of Public Health, University of Cambridge, Cambridge, England, United KingdomMRC Biostatistics Unit, Cambridge, England, United Kingdo. doi: 10.1371/journal.pone.0118463.

Mattsson, N. *et al.* (2013) 'CSF biomarker variability in the Alzheimer's Association quality control

program', *Alzheimer's and Dementia*, 9(3), pp. 251–261. doi: 10.1016/j.jalz.2013.01.010.

Matuszyk, M. M. *et al.* (2022) 'Biological and methodological complexities of beta-amyloid peptide: Implications for Alzheimer's disease research', *Journal of Neurochemistry*, 160(4), pp. 434–453. doi: 10.1111/JNC.15538.

Mawuenyega, K. G. *et al.* (2010) 'Decreased clearance of CNS beta-amyloid in Alzheimer's disease', *Science*. 2010/12/15, 330(6012), p. 1774. doi: 10.1126/science.1197623 10.1126/science.1197623. Epub 2010 Dec 9.

Mclarnon, J. (2016) 'Chemokine Interleukin-8 (IL-8) in Alzheimer's and Other Neurodegenerative Diseases', *J Alzheimers Dis Parkinsonism*, 6, p. 273. doi: 10.4172/2161-0460.1000273.

Di Meco, A. and Vassar, R. (2021) 'Early detection and personalized medicine: Future strategies against Alzheimer's disease', *Progress in molecular biology and translational science*, 177, p. 157. doi: 10.1016/BS.PMBTS.2020.10.002.

Meda, L., Cassatella, M. A., *et al.* (1995) 'Activation of microglial cells by β-amyloid protein and interferon-γ', *Nature 1995 374:6523*, 374(6523), pp. 647–650. doi: 10.1038/374647a0.

Meda, L., Bonaiuto, C., *et al.* (1995) 'β-Amyloid(25–35) induces the production of interleukin-8 from human monocytes', *Journal of Neuroimmunology*, 59(1–2), pp. 29–33. doi: 10.1016/0165-5728(95)00021-S.

Melrose, J., Hayes, A. J. and Bix, G. (2021) 'The CNS/PNS Extracellular Matrix Provides Instructive Guidance Cues to Neural Cells and Neuroregulatory Proteins in Neural Development and Repair', *International Journal of Molecular Sciences*, 22(11). doi: 10.3390/IJMS22115583.

Meral, D. and Urbanc, B. (2013) 'Discrete Molecular Dynamics Study of Oligomer Formation by N-Terminally Truncated Amyloid β-Protein', *J Mol Biol*, 425(12), pp. 2260–2275. doi: 10.1016/j.jmb.2013.03.010.

Merlo, D. *et al.* (2016) 'DNA Double Strand Breaks: A Common Theme in Neurodegenerative Diseases', *Current Alzheimer research*, 13(11), pp. 1208–1218. doi: 10.2174/1567205013666160401114915.

Meyer-Luehmann, M. *et al.* (2006) 'Exogenous induction of cerebral beta-amyloidogenesis is governed by agent and host', *Science*. 2006/09/23, 313(5794), pp. 1781–1784. doi: 10.1126/science.1131864.

Meyer-Luehmann, M. *et al.* (2008) 'Rapid appearance and local toxicity of amyloid-b plaques in a mouse model of Alzheimer's disease', 451. doi: 10.1038/nature06616.

Meyer, K. *et al.* (2014) 'Direct conversion of patient fibroblasts demonstrates non-cell autonomous toxicity of astrocytes to motor neurons in familial and sporadic ALS', *Proc Natl Acad Sci U S A*. 2014/01/01, 111(2), pp. 829–832. doi: 10.1073/pnas.1314085111.

Michelucci, A. *et al.* (2009) 'Characterization of the microglial phenotype under specific pro-inflammatory and anti-inflammatory conditions: Effects of oligomeric and fibrillar amyloid-beta', *J Neuroimmunol*. 2009/03/10, 210(1–2), pp. 3–12. doi: 10.1016/j.jneuroim.2009.02.003.

Min, H. *et al.* (2015) 'TLR2-induced astrocyte MMP9 activation compromises the blood brain barrier and exacerbates intracerebral hemorrhage in animal models', *Molecular Brain*, 8(1), pp. 1–14. doi: 10.1186/S13041-015-0116-Z/FIGURES/8.

Miners, J. S., Clarke, P. and Love, S. (2017) 'Clusterin levels are increased in Alzheimer's disease and influence the regional distribution of Abeta', *Brain Pathol*. 2016/06/02, 27(3), pp. 305–313. doi: 10.1111/bpa.12392.

Mishizen-Eberz, A. J. *et al.* (2004) 'Biochemical and molecular studies of NMDA receptor subunits NR1/2A/2B in hippocampal subregions throughout progression of Alzheimer's disease pathology', *Neurobiology of Disease*, 15(1), pp. 80–92.

Misonou, H., Morishima-Kawashima, M. and Ihara, Y. (2000) 'Oxidative Stress Induces Intracellular Accumulation of Amyloid β-Protein (Aβ) in Human Neuroblastoma Cells', *Biochemistry*, 39(23), pp. 6951–6959. doi: 10.1021/BI000169P.

Mizoguchi, H. *et al.* (2009) 'Matrix metalloprotease-9 inhibition improves amyloid beta-mediated cognitive impairment and neurotoxicity in mice', *The Journal of pharmacology and experimental therapeutics*, 331(1), pp. 14–22. doi: 10.1124/JPET.109.154724.

Montagne, A. *et al.* (2015) 'Blood-brain barrier breakdown in the aging human hippocampus', *Neuron*. 2015/01/23, 85(2), pp. 296–302. doi: 10.1016/j.neuron.2014.12.032.

Montagne, A., Zhao, Z. and Zlokovic, B. V. (2017) 'Alzheimer's disease: A matter of blood–brain barrier dysfunction?', *The Journal of Experimental Medicine*, 214(11), p. 3151. doi: 10.1084/JEM.20171406.

Monterey, M. D. *et al.* (2021) 'The Many Faces of Astrocytes in Alzheimer's Disease', *Frontiers in Neurology*, 12, p. 1402. doi: 10.3389/FNEUR.2021.619626/BIBTEX.

Moulson, A. J. *et al.* (2021) 'Diversity of Reactive Astrogliosis in CNS Pathology: Heterogeneity or Plasticity?', *Frontiers in Cellular Neuroscience*, 15, p. 284. doi: 10.3389/FNCEL.2021.703810/BIBTEX.

Müller, U. C., Deller, T. and Korte, M. (2017) 'Not just amyloid: physiological functions of the amyloid precursor protein family', *Nature Reviews Neuroscience 2017 18:5*, 18(5), pp. 281–298. doi: 10.1038/nrn.2017.29.

Murphy, M. P. and LeVine, H. (2010) 'Alzheimer's Disease and the β-Amyloid Peptide', *J Alzheimers Dis*, 19(1), p. 311. doi: 10.3233/jad-2010-1221.

Nagele, R G *et al.* (2003) 'Astrocytes accumulate A beta 42 and give rise to astrocytic amyloid plaques in Alzheimer disease brains', *Brain Res*. 2003/04/23, 971(2), pp. 197–209. doi: 10.1016/s0006-8993(03)02361-8.

Nagele, Robert G. *et al.* (2003) 'Astrocytes accumulate A beta 42 and give rise to astrocytic amyloid plaques in Alzheimer disease brains', *Brain research*, 971(2), pp. 197–209. doi: 10.1016/S0006-8993(03)02361-8.

Nagele, R. G. *et al.* (2004) 'Contribution of glial cells to the development of amyloid plaques in Alzheimer's disease', *Neurobiol Aging*. 2004/06/03, 25(5), pp. 663–674. doi: 10.1016/j.neurobiolaging.2004.01.007.

Naslund, J. *et al.* (1994) 'Relative abundance of Alzheimer A beta amyloid peptide variants in Alzheimer disease and normal aging', *Proc Natl Acad Sci U S A*. 1994/08/30, 91(18), pp. 8378–8382. Available at: http://dx.doi.org/.

Naslund, J. *et al.* (2000) 'Correlation between elevated levels of amyloid beta-peptide in the brain and cognitive decline', *Jama*. 2000/03/29, 283(12), pp. 1571–1577. doi: 10.1001/jama.283.12.1571.

Näslund, J. *et al.* (1994) 'Relative abundance of Alzheimer Aβ amyloid peptide variants in Alzheimer disease and normal aging', *Proceedings of the National Academy of Sciences of the United States of America*, 91(18), pp. 8378–8382. doi: 10.1073/pnas.91.18.8378.

Navarrete, M. and Araque, A. (2014) 'The Cajal school and the physiological role of astrocytes: a way of thinking', *Frontiers in Neuroanatomy*, 8(MAY). doi: 10.3389/FNANA.2014.00033.

Newington, J. T., Harris, R. A. and Cumming, R. C. (2013) 'Reevaluating Metabolism in Alzheimer's Disease from the Perspective of the Astrocyte-Neuron Lactate Shuttle Model', *Journal of neurodegenerative diseases*, 2013, pp. 1–13. doi: 10.1155/2013/234572.

Newman, L. A., Korol, D. L. and Gold, P. E. (2011) 'Lactate produced by glycogenolysis in astrocytes regulates memory processing', *PloS one*, 6(12). doi: 10.1371/JOURNAL.PONE.0028427.

Nichols, M. R. *et al.* (2005) 'Amyloid-beta protofibrils differ from amyloid-beta aggregates induced in dilute hexafluoroisopropanol in stability and morphology', *J Biol Chem*. 2004/11/06, 280(4), pp. 2471–2480. doi: 10.1074/jbc.M410553200.

Nichols, M. R. *et al.* (2015) 'Biophysical comparison of soluble amyloid-beta(1-42) protofibrils, oligomers, and protofilaments', *Biochemistry*. 2015/03/11, 54(13), pp. 2193–2204. doi: 10.1021/bi500957g.

Nicolas, C. S. *et al.* (2013) 'The role of JAK-STAT signaling within the CNS', *JAK-STAT*, 2(1), p. e22925. doi: 10.4161/JKST.22925.

Niemi, K. *et al.* (2011) 'Serum amyloid A activates the NLRP3 inflammasome via P2X7 receptor and a cathepsin B-sensitive pathway', *Journal of immunology (Baltimore, Md. : 1950)*, 186(11), pp. 6119–6128. doi: 10.4049/JIMMUNOL.1002843.

Nitta, T. *et al.* (2003) 'Size-selective loosening of the blood-brain barrier in claudin-5-deficient mice', *The Journal of cell biology*, 161(3), pp. 653–660. doi: 10.1083/JCB.200302070.

Noorani, A. A. *et al.* (2020) 'High temperature promotes amyloid β-protein production and γ-secretase complex formation via Hsp90', *The Journal of Biological Chemistry*, 295(52), p. 18010. doi: 10.1074/JBC.RA120.013845.

Nortley, R. *et al.* (2019) 'Amyloid β oligomers constrict human capillaries in Alzheimer's disease via signaling to pericytes', *Science*, eaav9518. doi: 10.1126/science.aav9518.

Nussbaum, J. M. *et al.* (2012) 'Prion-like behaviour and tau-dependent cytotoxicity of pyroglutamylated amyloid-beta', *Nature*. 2012/06/05, 485(7400), pp. 651–655. doi: 10.1038/nature11060.

O'Brien, J. *et al.* (2018) 'Overview of microRNA biogenesis, mechanisms of actions, and circulation', *Frontiers in Endocrinology*, 9(AUG), p. 402. doi: 10.3389/FENDO.2018.00402/BIBTEX.

O'Brien, R. J. and Wong, P. C. (2011) 'Amyloid Precursor Protein Processing and Alzheimer's Disease', *Annu Rev Neurosci*, 34, pp. 185–204. doi: 10.1146/annurev-neuro-061010-113613 10.1146/annurev-neuro-061010-113613.

Oberheim, N. A. *et al.* (2009) 'Uniquely hominid features of adult human astrocytes', *J Neurosci*, 29(10), p. 3276. doi: 10.1523/jneurosci.4707-08.2009.

Oddo, S. *et al.* (2006) 'Temporal profile of amyloid-beta (Abeta) oligomerization in an in vivo model of Alzheimer disease. A link between Abeta and tau pathology', *J Biol Chem*. 2005/11/12, 281(3), pp. 1599–1604. doi: 10.1074/jbc.M507892200.

Ohsawa, I. *et al.* (1999) 'Amino-terminal region of secreted form of amyloid precursor protein stimulates proliferation of neural stem cells', *The European journal of neuroscience*, 11(6), pp. 1907–1913. doi: 10.1046/J.1460-9568.1999.00601.X.

Oksanen, M. *et al.* (2017) 'PSEN1 Mutant iPSC-Derived Model Reveals Severe Astrocyte Pathology in Alzheimer's Disease', *Stem Cell Reports*, 9(6), pp. 1885–1897. doi: 10.1016/J.STEMCR.2017.10.016.

Olson, M. J. (1988) 'DNA strand breaks induced by hydrogen peroxide in isolated rat hepatocytes', *J*

*Toxicol Environ Health*. 1988/01/01, 23(3), pp. 407–423. doi: 10.1080/15287398809531123.

Orre, M. *et al.* (2013) 'Reactive glia show increased immunoproteasome activity in Alzheimer's disease', *Brain*. 2013/04/23, 136(Pt 5), pp. 1415–1431. doi: 10.1093/brain/awt083.

Ortinski, P. I. *et al.* (2010) 'Selective induction of astrocytic gliosis generates deficits in neuronal inhibition', *Nature neuroscience*, 13(5), pp. 584–591. doi: 10.1038/NN.2535.

Ovod, V. *et al.* (2017) 'Amyloid beta concentrations and stable isotope labeling kinetics of human plasma specific to CNS amyloidosis', *Alzheimer's & dementia : the journal of the Alzheimer's Association*, 13(8), p. 841. doi: 10.1016/J.JALZ.2017.06.2266.

Pan, X. D. *et al.* (2011) 'Microglial phagocytosis induced by fibrillar beta-amyloid is attenuated by oligomeric beta-amyloid: implications for Alzheimer's disease', *Mol Neurodegener*. 2011/07/02, 6, p. 45. doi: 10.1186/1750-1326-6-45.

Di Paolo, N. C. and Shayakhmetov, D. M. (2016) 'r e v i e w interleukin 1α and the inflammatory process', *nature immunology*, 17. doi: 10.1038/ni.3503.

Paravastu, A. K. *et al.* (2008) 'Molecular structural basis for polymorphism in Alzheimer's beta-amyloid fibrils', *Proceedings of the National Academy of Sciences of the United States of America*. 2008/11/17, 105(47), pp. 18349–18354. doi: 10.1073/pnas.0806270105.

Parodi-Rullán, R. *et al.* (2020) 'Alzheimer's amyloid β heterogeneous species differentially affect brain endothelial cell viability, blood-brain barrier integrity, and angiogenesis', *Aging Cell*, 19(11), p. e13258. doi: 10.1111/acel.13258.

Pekny, M., Wilhelmsson, U. and Pekna, M. (2014) 'The dual role of astrocyte activation and reactive gliosis', *Neuroscience letters*, 565, pp. 30–38. doi: 10.1016/J.NEULET.2013.12.071.

Penney, J., Ralvenius, W. T. and Li-Huei, T. (2020) 'Modeling Alzheimer's disease with iPSC-derived brain cells', *Molecular Psychiatry*, 25, pp. 148–167. doi: 10.1038/s41380-019-0468-3.

Periole, X. *et al.* (2018) 'Energetics Underlying Twist Polymorphisms in Amyloid Fibrils', *The journal of physical chemistry. B*. 2018/01/05, 122(3), pp. 1081–1091. doi: 10.1021/acs.jpcb.7b10233.

Phatnani, H. and Maniatis, T. (2015) 'Astrocytes in neurodegenerative disease', *Cold Spring Harbor perspectives in biology*, 7(6), pp. 1–18. doi: 10.1101/CSHPERSPECT.A020628.

Pihlaja, R. *et al.* (2008) 'Transplanted astrocytes internalize deposited beta-amyloid peptides in a transgenic mouse model of Alzheimer's disease', *Glia*. 2007/11/16, 56(2), pp. 154–163. doi: 10.1002/glia.20599.

Pike, C. J. *et al.* (1994) 'Beta-amyloid-induced changes in cultured astrocytes parallel reactive astrocytosis associated with senile plaques in Alzheimer's disease', *Neuroscience*. 1994/11/01, 63(2), pp. 517–531. Available at: http://dx.doi.org/.

Pilié, P. G. *et al.* (2018) 'State-of-the-art strategies for targeting the DNA damage response in cancer', *Nature Reviews Clinical Oncology 2018 16:2*, 16(2), pp. 81–104. doi: 10.1038/s41571-018-0114-z.

Pizzino, G. *et al.* (2017) 'Oxidative Stress: Harms and Benefits for Human Health', *Oxid Med Cell Longev*, 2017. doi: 10.1155/2017/8416763.

Podhorecka, M., Skladanowski, A. and Bozko, P. (2010) 'H2AX Phosphorylation: Its Role in DNA Damage Response and Cancer Therapy', *J Nucleic Acids*, 2010. doi: 10.4061/2010/920161.

Potter, R. *et al.* (2013) 'Increased in vivo amyloid-beta42 production, exchange, and loss in presenilin mutation carriers', *Sci Transl Med*. 2013/06/14, 5(189), p. 189ra77. doi:

10.1126/scitranslmed.3005615 10.1126/scitranslmed.3005615.

Preman, P. *et al.* (2021) 'Human iPSC-derived astrocytes transplanted into the mouse brain undergo morphological changes in response to amyloid-β plaques', *Molecular Neurodegeneration*, 16(1), pp. 1–18. doi: 10.1186/S13024-021-00487-8/FIGURES/7.

Pujol-Pina, R. *et al.* (2015) 'SDS-PAGE analysis of Abeta oligomers is disserving research into Alzheimer s disease: appealing for ESI-IM-MS', *Sci Rep*. 2015/10/10, 5, p. 14809. doi: 10.1038/srep14809.

van Putten, M. J. A. M. *et al.* (2021) 'Dysregulation of Astrocyte Ion Homeostasis and Its Relevance for Stroke-Induced Brain Damage', *International Journal of Molecular Sciences*, 22(11). doi: 10.3390/IJMS22115679.

Qi-Takahara, Y. *et al.* (2005) 'Longer forms of amyloid beta protein: implications for the mechanism of intramembrane cleavage by gamma-secretase', *J Neurosci*. 2005/01/14, 25(2), pp. 436–445. doi: 10.1523/jneurosci.1575-04.2005 10.1523/JNEUROSCI.1575-04.2005.

Qian, Y. *et al.* (2010) 'IL-17 signaling in host defense and inflammatory diseases', *Cellular & molecular immunology*, 7(5), pp. 328–333. doi: 10.1038/CMI.2010.27.

Qiang, W. *et al.* (2017a) 'Structural variation in amyloid-beta fibrils from Alzheimer's disease clinical subtypes', *Nature*. 2017/01/05, 541(7636), pp. 217–221. doi: 10.1038/nature20814.

Qiang, W. *et al.* (2017b) 'Structural Variation in Amyloid-β Fibrils from Alzheimer's Disease Clinical Subtypes', *Nature*, 541(7636), pp. 217–221. doi: 10.1038/nature20814.

Qin, Q. *et al.* (2021) 'TREM2, microglia, and Alzheimer's disease', *Mechanisms of Ageing and Development*, (Epub), p. 195:111438.

Rahimi, F., Maiti, P. and Bitan, G. (2009) 'Photo-induced cross-linking of unmodified proteins (PICUP) applied to amyloidogenic peptides', *Journal of visualized experiments : JoVE*, (23), p. 1071. doi: 10.3791/1071.

Ramesh, G., Maclean, A. G. and Philipp, M. T. (2013) 'Cytokines and Chemokines at the Crossroads of Neuroinflammation, Neurodegeneration, and Neuropathic Pain', *Mediators of Inflammation*, 2013, p. 20. doi: 10.1155/2013/480739.

Ratcliffe, L. E. *et al.* (2018) 'Loss of IGF1R in Human Astrocytes Alters Complex I Activity and Support for Neurons', *Neuroscience*, 390, pp. 46–59. doi: 10.1016/J.NEUROSCIENCE.2018.07.029.

Ray, P. D., Huang, B. W. and Tsuji, Y. (2012) 'Reactive oxygen species (ROS) homeostasis and redox regulation in cellular signaling', *Cell Signal*, 24(5), pp. 981–990. doi: 10.1016/j.cellsig.2012.01.008.

Reiss, A. B. *et al.* (2018) 'Amyloid toxicity in Alzheimer's disease', *Reviews in the Neurosciences*, 29(6), pp. 613–627. doi: 10.1515/REVNEURO-2017-0063/ASSET/GRAPHIC/J_REVNEURO-2017-0063_FIG_002.JPG.

Ren, S. Q. *et al.* (2018) 'Amyloid β causes excitation/inhibition imbalance through dopamine receptor 1-dependent disruption of fast-spiking GABAergic input in anterior cingulate cortex', *Scientific Reports 2017 8:1*, 8(1), pp. 1–10. doi: 10.1038/s41598-017-18729-5.

Resende, R. *et al.* (2008) 'Neurotoxic effect of oligomeric and fibrillar species of amyloid-beta peptide 1-42: involvement of endoplasmic reticulum calcium release in oligomer-induced cell death', *Neuroscience*. 2008/07/16, 155(3), pp. 725–737. doi: 10.1016/j.neuroscience.2008.06.036 10.1016/j.neuroscience.2008.06.036. Epub 2008 Jun 19.

Rizor, A. *et al.* (2019) 'Astrocytic Oxidative/Nitrosative Stress Contributes to Parkinson's Disease

Pathogenesis: The Dual Role of Reactive Astrocytes', *Antioxidants*, 8(8). doi: 10.3390/ANTIOX8080265.

Robel, S. *et al.* (2015) 'Reactive Astrogliosis Causes the Development of Spontaneous Seizures', *The Journal of Neuroscience*, 35(8), p. 3330. doi: 10.1523/JNEUROSCI.1574-14.2015.

Rosengarten, B. *et al.* (2009) 'Neurovascular coupling in Alzheimer patients: effect of acetylcholine-esterase inhibitors', *Neurobiol Aging*. 2008/04/09, 30(12), pp. 1918–1923. doi: 10.1016/j.neurobiolaging.2008.02.017.

Russo, C. *et al.* (2000) 'Presenilin-1 mutations in Alzheimer's disease', *Nature*. 2000/06/13, 405(6786), pp. 531–532. doi: 10.1038/35014735.

Ryu, J. K. *et al.* (2015) 'Pharmacological antagonism of interleukin-8 receptor CXCR2 inhibits inflammatory reactivity and is neuroprotective in an animal model of Alzheimer's disease', *Journal of Neuroinflammation*, 12(1), pp. 1–13. doi: 10.1186/S12974-015-0339-Z/FIGURES/7.

Sachse, C. *et al.* (2006) 'Quaternary Structure of a Mature Amyloid Fibril from Alzheimer's Aβ(1-40) Peptide', *Journal of Molecular Biology*, 362(2), pp. 347–354. doi: https://doi.org/10.1016/j.jmb.2006.07.011.

Saggu, R. *et al.* (2016) 'Astroglial NF-kB contributes to white matter damage and cognitive impairment in a mouse model of vascular dementia.', *Acta Neuropathol Commun.*, 4(1), p. 76.

Saido, T. C. *et al.* (1995) 'Dominant and differential deposition of distinct beta-amyloid peptide species, A beta N3(pE), in senile plaques', *Neuron*. 1995/02/01, 14(2), pp. 457–466. Available at: http://dx.doi.org/.

Sakono, M. and Zako, T. (2010) 'Amyloid oligomers: formation and toxicity of Abeta oligomers', *The FEBS journal*, 277(6), pp. 1348–1358. doi: 10.1111/J.1742-4658.2010.07568.X.

Sánchez, K. and Maguire-Zeiss, K. (2020) 'MMP13 Expression Is Increased Following Mutant α-Synuclein Exposure and Promotes Inflammatory Responses in Microglia', *Frontiers in Neuroscience*, 14, p. 1235. doi: 10.3389/FNINS.2020.585544/BIBTEX.

Sang, W. S. *et al.* (2007) 'Zinc Inhibits Astrocyte Glutamate Uptake by Activation of Poly(ADP-ribose) Polymerase-1', *Molecular Medicine*, 13(7–8), p. 344. doi: 10.2119/2007-00043.SUH.

Schellenberg, G. D. and Montine, T. J. (2012) 'The genetics and neuropathology of Alzheimer's disease', *Acta Neuropathol*. 2012/05/24, 124(3), pp. 305–323. doi: 10.1007/s00401-012-0996-2 10.1007/s00401-012-0996-2. Epub 2012 May 23.

Schenk, D. *et al.* (1999) 'Immunization with amyloid-beta attenuates Alzheimer-disease-like pathology in the PDAPP mouse', *Nature*, 400(6740), pp. 173–177.

Schmidt, M. *et al.* (2015) 'Peptide dimer structure in an Aβ(1–42) fibril visualized with cryo-EM', *Proceedings of the National Academy of Sciences*, 112(38), pp. 11858–11863. doi: 10.1073/pnas.1503455112.

Schroeder, A. *et al.* (2006) 'The RIN: an RNA integrity number for assigning integrity values to RNA measurements', *BMC Molecular Biology*, 7, p. 3. doi: 10.1186/1471-2199-7-3.

Selkoe, Dennis J and Hardy, J. (2016) 'The amyloid hypothesis of Alzheimer's disease at 25 years', *EMBO Molecular Medicine*, 8, pp. 595–608. doi: 10.15252/emmm.201606210.

Selkoe, D J and Hardy, J. (2016) 'The amyloid hypothesis of Alzheimer's disease at 25 years', *EMBO Mol Med*. 2016/03/31, 8(6), pp. 595–608. doi: 10.15252/emmm.201606210.

Sengupta, U., Nilson, A. N. and Kayed, R. (2016) 'The Role of Amyloid-β Oligomers in Toxicity, Propagation, and Immunotherapy', *EBioMedicine*, 6, pp. 42–49. doi: 10.1016/j.ebiom.2016.03.035.

Serrano-Pozo, A. *et al.* (2011) 'Neuropathological Alterations in Alzheimer Disease', *Cold Spring Harb Perspect Med.*, 1(1), p. a006189. doi: 10.1101/cshperspect.a006189.

Serrano-Pozo, A. *et al.* (2013) 'A phenotypic change but not proliferation underlies glial responses in Alzheimer disease', *The American journal of pathology*, 182(6), pp. 2332–2344. doi: 10.1016/J.AJPATH.2013.02.031.

Shah, P. *et al.* (2010) 'Neuronal and axonal loss are selectively linked to fibrillar amyloid-{beta} within plaques of the aged primate cerebral cortex', *The American journal of pathology*, 177(1), pp. 325–333. doi: 10.2353/AJPATH.2010.090937.

Shanbhag, N. M. *et al.* (2019) 'Early neuronal accumulation of DNA double strand breaks in Alzheimer's disease', *Acta Neuropathologica Communications 2019 7:1*, 7(1), pp. 1–18. doi: 10.1186/S40478-019-0723-5.

Shandra, O. *et al.* (2019) 'Repetitive Diffuse Mild Traumatic Brain Injury Causes an Atypical Astrocyte Response and Spontaneous Recurrent Seizures', *The Journal of neuroscience : the official journal of the Society for Neuroscience*, 39(10), pp. 1944–1963. doi: 10.1523/JNEUROSCI.1067-18.2018.

Shankar, G. M. *et al.* (2007) 'Natural oligomers of the Alzheimer amyloid-beta protein induce reversible synapse loss by modulating an NMDA-type glutamate receptor-dependent signaling pathway', *J Neurosci*. 2007/03/16, 27(11), pp. 2866–2875. doi: 10.1523/jneurosci.4970-06.2007.

Shankar, G. M. *et al.* (2008) 'Amyloid-beta protein dimers isolated directly from Alzheimer's brains impair synaptic plasticity and memory', *Nat Med*. 2008/06/24, 14(8), pp. 837–842. doi: 10.1038/nm1782.

Shea, D. *et al.* (2019) 'α-Sheet secondary structure in amyloid β-peptide drives aggregation and toxicity in Alzheimer's disease', *Proceedings of the National Academy of Sciences of the United States of America*. 2019/04/19, 116(18), pp. 8895–8900. doi: 10.1073/pnas.1820585116.

Sheng, W. S. *et al.* (2013) 'Reactive Oxygen Species From Human Astrocytes Induced Functional Impairment and Oxidative Damage', *Neurochemical research*, 38(10), p. 2148. doi: 10.1007/S11064-013-1123-Z.

Sherrington, R. *et al.* (1995) 'Cloning of a gene bearing missense mutations in early-onset familial Alzheimer's disease', *Nature*. 1995/06/29, 375(6534), pp. 754–760. doi: 10.1038/375754a0 10.1038/375754a0.

Shibata, M. *et al.* (2000) 'Clearance of Alzheimer's amyloid-β1-40 peptide from brain by LDL receptor–related protein-1 at the blood-brain barrier', *J Clin Invest*, 106(12), pp. 1489–1499. Available at: http://dx.doi.org/.

Shirotani, K. *et al.* (2001) 'Neprilysin degrades both amyloid beta peptides 1-40 and 1-42 most rapidly and efficiently among thiorphan- and phosphoramidon-sensitive endopeptidases', *J Biol Chem*. 2001/03/30, 276(24), pp. 21895–21901. doi: 10.1074/jbc.M008511200 10.1074/jbc.M008511200. Epub 2001 Mar 6.

Sies, H. (2017) 'Hydrogen peroxide as a central redox signaling molecule in physiological oxidative stress: Oxidative eustress☆', *Redox Biol*, 11, pp. 613–619. doi: 10.1016/j.redox.2016.12.035.

Simonovitch, S. *et al.* (2016) 'Impaired Autophagy in APOE4 Astrocytes', *Journal of Alzheimer's disease : JAD*, 51(3), pp. 915–927. doi: 10.3233/JAD-151101.

Simpson, J. E. *et al.* (2011) 'Microarray analysis of the astrocyte transcriptome in the aging brain: relationship to Alzheimer's pathology and APOE genotype', *Neurobiol Aging*. 2011/06/28, 32(10), pp. 1795–1807. doi: 10.1016/j.neurobiolaging.2011.04.013.

Simpson, J. E. *et al.* (2015) 'A neuronal DNA damage response is detected at the earliest stages of Alzheimer's neuropathology and correlates with cognitive impairment in the Medical Research Council's Cognitive Function and Ageing Study ageing brain cohort', *Neuropathology and applied neurobiology*, 41(4), pp. 483–496. doi: 10.1111/NAN.12202.

Singh, D. *et al.* (2020) 'Sinomenine inhibits amyloid beta-induced astrocyte activation and protects neurons against indirect toxicity', *Molecular brain*, 13(1). doi: 10.1186/S13041-020-00569-6.

Sinha, S. *et al.* (1999) 'Purification and cloning of amyloid precursor protein beta-secretase from human brain', *Nature*, 402(6761), pp. 537–540. doi: 10.1038/990114.

Sinigaglia-Coimbra, R., Cavalheiro, E. A. and Coimbra, C. G. (2002) 'Postischemic hyperthermia induces Alzheimer-like pathology in the rat brain', *Acta neuropathologica*, 103(5), pp. 444–452. doi: 10.1007/S00401-001-0487-3.

Siracusa, R., Fusco, R. and Cuzzocrea, S. (2019) 'Astrocytes: Role and functions in brain pathologies', *Frontiers in Pharmacology*, 10(SEP), p. 1114. doi: 10.3389/FPHAR.2019.01114/BIBTEX.

Slanzi, A. *et al.* (2020) 'In vitro Models of Neurodegenerative Diseases', *Frontiers in cell and developmental biology*, 8. doi: 10.3389/FCELL.2020.00328.

Smith, J. *et al.* (2010) 'The ATM-Chk2 and ATR-Chk1 pathways in DNA damage signaling and cancer', *Adv Cancer Res*. 2010/11/03, 108, pp. 73–112. doi: 10.1016/b978-0-12-380888-2.00003-0.

Snyder, E. M. *et al.* (2005) 'Regulation of NMDA receptor trafficking by amyloid-b', *NATURE NEUROSCIENCE VOLUME*, 8(8). doi: 10.1038/nn1503.

Söllvander, S. *et al.* (2016) 'Accumulation of amyloid-β by astrocytes result in enlarged endosomes and microvesicle-induced apoptosis of neurons', *Mol Neurodegener*, 11. doi: 10.1186/s13024-016-0098-z.

Some, D. *et al.* (2019) 'Characterization of Proteins by Size-Exclusion Chromatography Coupled to Multi-Angle Light Scattering (SEC-MALS)', *JoVE (Journal of Visualized Experiments)*, 2019(148), p. e59615. doi: 10.3791/59615.

Sondag, C M, Dhawan, G. and Combs, C. K. (2009) 'Beta amyloid oligomers and fibrils stimulate differential activation of primary microglia', *J Neuroinflammation*, 6, p. 1. doi: 10.1186/1742-2094-6-1.

Sondag, Cindy M., Dhawan, G. and Combs, C. K. (2009) 'Beta amyloid oligomers and fibrils stimulate differential activation of primary microglia', *Journal of Neuroinflammation*, 6(1), pp. 1–13. doi: 10.1186/1742-2094-6-1/FIGURES/4.

Soscia, S. J. *et al.* (2010) 'The Alzheimer's disease-associated amyloid β-protein is an antimicrobial peptide', *PLoS ONE*, 5(3). doi: 10.1371/journal.pone.0009505.

Spanos, F. and Liddelow, S. A. (2020) 'An Overview of Astrocyte Responses in Genetically Induced Alzheimer's Disease Mouse Models', *Cells*, 9(11), pp. 1–33. doi: 10.3390/CELLS9112415.

Stamenkovic, I. (2003) 'Extracellular matrix remodelling: the role of matrix metalloproteinases', *The Journal of pathology*, 200(4), pp. 448–464. doi: 10.1002/PATH.1400.

Stine Jr., W. B. *et al.* (2003) 'In vitro characterization of conditions for amyloid-beta peptide oligomerization and fibrillogenesis', *J Biol Chem*. 2002/12/25, 278(13), pp. 11612–11622. doi:

10.1074/jbc.M210207200 10.1074/jbc.M210207200. Epub 2002 Dec 23.

Stine, W. B. *et al.* (2011) 'Preparing synthetic Abeta in different aggregation states', *Methods Mol Biol*. 2010/10/23, 670, pp. 13–32. doi: 10.1007/978-1-60761-744-0_2.

Storck, S. E. *et al.* (2016) 'Endothelial LRP1 transports amyloid-β1–42 across the blood-brain barrier', *J Clin Invest*, 126(1), pp. 123–136. doi: 10.1172/jci81108 10.1172/JCI81108.

Storck, S. E. *et al.* (2018) 'The concerted amyloid-beta clearance of LRP1 and ABCB1/P-gp across the blood-brain barrier is linked by PICALM', *Brain Behav Immun*. 2018/07/25, 73, pp. 21–33. doi: 10.1016/j.bbi.2018.07.017 10.1016/j.bbi.2018.07.017. Epub 2018 Jul 21.

Streit, W. J. *et al.* (2018) 'Microglial activation occurs late during preclinical Alzheimer's disease', *Glia*. 2018/11/13. doi: 10.1002/glia.23510.

Studer, L., Vera, E. and Cornacchia, D. (2015) 'PROGRAMMING AND REPROGRAMMING CELLULAR AGE IN THE ERA OF INDUCED PLURIPOTENCY', *Cell stem cell*, 16(6), p. 591. doi: 10.1016/J.STEM.2015.05.004.

Su, J.-L. *et al.* (2012) 'Function and regulation of let-7 family microRNAs', *MicroRNA (Shariqah, United Arab Emirates)*, 1(1), pp. 34–39. doi: 10.2174/2211536611201010034.

Su, J. H. *et al.* (1994) 'Immunohistochemical evidence for apoptosis in Alzheimer's disease.', *Neuroreport*, 5(18), pp. 2529–2533. doi: 10.1097/00001756-199412000-00031.

Su, Y. and Chang, P. T. (2001) 'Acidic pH promotes the formation of toxic fibrils from β-amyloid peptide', *Brain Research*, 893(1–2), pp. 287–291. doi: 10.1016/S0006-8993(00)03322-9.

Sun, E. *et al.* (2022) 'The Pivotal Role of NF-kB in the Pathogenesis and Therapeutics of Alzheimer's Disease', *International journal of molecular sciences*, 23(16). doi: 10.3390/IJMS23168972.

Sun, Y. *et al.* (2020) 'Modulation of the Astrocyte-Neuron Lactate Shuttle System contributes to Neuroprotective action of Fibroblast Growth Factor 21', *Theranostics*, 10(18), p. 8430. doi: 10.7150/THNO.44370.

Sun, Y. *et al.* (2021) 'Role of the Extracellular Matrix in Alzheimer's Disease', *Frontiers in Aging Neuroscience*, 13. doi: 10.3389/FNAGI.2021.707466.

Sweeney, M. D., Sagare, A. P. and Zlokovic, B. V. (2018) 'Blood-brain barrier breakdown in Alzheimer disease and other neurodegenerative disorders', *Nature reviews. Neurology*, 14(3), pp. 133–150. doi: 10.1038/NRNEUROL.2017.188.

Tabner, B. J. *et al.* (2005) 'Hydrogen peroxide is generated during the very early stages of aggregation of the amyloid peptides implicated in Alzheimer disease and familial British dementia', *The Journal of biological chemistry*, 280(43), pp. 35789–35792. doi: 10.1074/JBC.C500238200.

Takami, M. *et al.* (2009) 'gamma-Secretase: successive tripeptide and tetrapeptide release from the transmembrane domain of beta-carboxyl terminal fragment', *J Neurosci*. 2009/10/16, 29(41), pp. 13042–13052. doi: 10.1523/jneurosci.2362-09.2009 10.1523/JNEUROSCI.2362-09.2009.

Takasu, M. A. *et al.* (2002) 'Modulation of NMDA receptor-dependent calcium influx and gene expression through EphB receptors', *Science (New York, N.Y.)*, 295(5554), pp. 491–495. doi: 10.1126/SCIENCE.1065983.

Tampi, R. R., Forester, B. P. and Agronin, M. (2021) 'Aducanumab: evidence from clinical trial data and controversies', *Drugs in Context*, 10. doi: 10.7573/DIC.2021-7-3.

Terry, R. D. *et al.* (1991) 'Physical basis of cognitive alterations in Alzheimer's disease: synapse loss is

the major correlate of cognitive impairment', *Annals of neurology*, 30(4), pp. 572–580. doi: 10.1002/ANA.410300410.

Thadathil, N. *et al.* (no date) 'DNA double-strand breaks: a potential therapeutic target for neurodegenerative diseases'. doi: 10.1007/s10577-019-09617-x.

Thal, D. R. *et al.* (2000) 'Amyloid beta-protein (Abeta)-containing astrocytes are located preferentially near N-terminal-truncated Abeta deposits in the human entorhinal cortex', *Acta Neuropathol*. 2000/11/15, 100(6), pp. 608–617. Available at: http://dx.doi.org/.

Thinakaran, G. and Koo, E. H. (2008) 'Amyloid Precursor Protein Trafficking, Processing, and Function*', *J Biol Chem*, 283(44), pp. 29615–29619. doi: 10.1074/jbc.R800019200.

Tiiman, A. *et al.* (2015) 'In vitro fibrillization of Alzheimer's amyloid-β peptide (1-42)', *AIP Advances*, 5(9), p. 092401. doi: 10.1063/1.4921071.

Tong, X. *et al.* (2014) 'Astrocyte Kir4.1 ion channel deficits contribute to neuronal dysfunction in Huntington's disease model mice', *Nature neuroscience*, 17(5), p. 694. doi: 10.1038/NN.3691.

Tönnies, E. and Trushina, E. (2017) 'Oxidative Stress, Synaptic Dysfunction, and Alzheimer's Disease', *Journal of Alzheimer's disease : JAD*, 57(4), pp. 1105–1121. doi: 10.3233/JAD-161088.

Tornquist, M. *et al.* (2018) 'Secondary nucleation in amyloid formation', *Chem Commun (Camb)*. 2018/07/07, 54(63), pp. 8667–8684. doi: 10.1039/c8cc02204f.

Tougu, V., Tiiman, A. and Palumaa, P. (2011) 'Interactions of Zn(II) and Cu(II) ions with Alzheimer's amyloid-beta peptide. Metal ion binding, contribution to fibrillization and toxicity', *Metallomics*. 2011/03/02, 3(3), pp. 250–261. doi: 10.1039/c0mt00073f 10.1039/c0mt00073f. Epub 2011 Feb 25.

Tsukita, S., Tanaka, H. and Tamura, A. (2019) 'The Claudins: From Tight Junctions to Biological Systems', *Trends in Biochemical Sciences*, 44(2), pp. 141–152. doi: 10.1016/j.tibs.2018.09.008.

Tu, L.-L. *et al.* (2019) 'Upregulation of GABA receptor promotes long-term potentiation and depotentiation in the hippocampal CA1 region of mice with type 2 diabetes mellitus', *Experimental and Therapeutic Medicine*, 18(4), p. 2429. doi: 10.3892/ETM.2019.7868.

Tu, S. *et al.* (2014) 'Oligomeric Aβ-induced synaptic dysfunction in Alzheimer's disease', *Molecular Neurodegeneration*, 9, p. 48. doi: 10.1186/1750-1326-9-48.

Tyzack, G. E. *et al.* (2017) 'A neuroprotective astrocyte state is induced by neuronal signal EphB1 but fails in ALS models', *Nature communications*, 8(1). doi: 10.1038/S41467-017-01283-Z.

Tzioras, M. *et al.* (2019) 'Invited Review: APOE at the interface of inflammation, neurodegeneration and pathological protein spread in Alzheimer's disease', *Neuropathol Appl Neurobiol*. 2018/11/06, 45(4), pp. 327–346. doi: 10.1111/nan.12529.

Ulrich, D. (2015) 'Amyloid-β Impairs Synaptic Inhibition via GABAA Receptor Endocytosis', *Journal of Neuroscience*, 35(24), pp. 9205–9210. doi: 10.1523/JNEUROSCI.0950-15.2015.

Vafadari, B., Salamian, A. and Kaczmarek, L. (2016) 'MMP-9 in translation: from molecule to brain physiology, pathology, and therapy', *Journal of Neurochemistry*, 139, pp. 91–114. doi: 10.1111/JNC.13415.

Vallon, R. *et al.* (2001) 'Serum amyloid A (apoSAA) expression is up-regulated in rheumatoid arthritis and induces transcription of matrix metalloproteinases', *Journal of immunology (Baltimore, Md. : 1950)*, 166(4), pp. 2801–2807. doi: 10.4049/JIMMUNOL.166.4.2801.

Vandersteen, A. *et al.* (2012a) 'A comparative analysis of the aggregation behavior of amyloid-β

peptide variants', *FEBS Letters*, 586(23), pp. 4088–4093. doi: 10.1016/J.FEBSLET.2012.10.022.

Vandersteen, A. *et al.* (2012b) 'A comparative analysis of the aggregation behavior of amyloid-β peptide variants', *FEBS letters*, 586(23), pp. 4088–4093. doi: 10.1016/J.FEBSLET.2012.10.022.

Varcianna, A. *et al.* (2019) 'Micro-RNAs secreted through astrocyte-derived extracellular vesicles cause neuronal network degeneration in C9orf72 ALS', *EBioMedicine*, 40, pp. 626–635. doi: 10.1016/J.EBIOM.2018.11.067.

Vargas, M. R. *et al.* (2008) 'Nrf2 activation in astrocytes protects against neurodegeneration in mouse models of familial amyotrophic lateral sclerosis', *The Journal of neuroscience : the official journal of the Society for Neuroscience*, 28(50), pp. 13574–13581. doi: 10.1523/JNEUROSCI.4099-08.2008.

Vassar, R. (2014) 'BACE1 inhibitor drugs in clinical trials for Alzheimer's disease', *Alzheimers Res Ther*, 6. doi: 10.1186/s13195-014-0089-7 10.1186/s13195-014-0089-7.

Vekrellis, K. *et al.* (2000) 'Neurons regulate extracellular levels of amyloid beta-protein via proteolysis by insulin-degrading enzyme', *J Neurosci*. 2000/02/24, 20(5), pp. 1657–1665. Available at: http://dx.doi.org/.

Venkataraman, L. *et al.* (2022) 'Modeling neurodegenerative diseases with cerebral organoids and other three-dimensional culture systems: focus on Alzheimer's disease', *Stem Cell Reviews and Reports*, 18(2), p. 696. doi: 10.1007/S12015-020-10068-9.

Verkhratsky, A. and Nedergaard, M. (2018) 'Physiology of Astroglia', *Physiol Rev*. 2018/01/20, 98(1), pp. 239–389. doi: 10.1152/physrev.00042.2016.

Verma, M., Vats, A. and Taneja, V. (2015) 'Toxic species in amyloid disorders: Oligomers or mature fibrils', *Ann Indian Acad Neurol*, 18(2), pp. 138–145. doi: 10.4103/0972-2327.144284.

Vezzoli, E. *et al.* (2020) 'Ultrastructural Evidence for a Role of Astrocytes and Glycogen-Derived Lactate in Learning-Dependent Synaptic Stabilization', *Cerebral cortex (New York, N.Y. : 1991)*, 30(4), pp. 2114–2127. doi: 10.1093/CERCOR/BHZ226.

Vicente-Gutierrez, C. *et al.* (2019) 'Astrocytic mitochondrial ROS modulate brain metabolism and mouse behaviour', *Nature metabolism*, 1(2), pp. 201–211. doi: 10.1038/S42255-018-0031-6.

Vidal, R. *et al.* (1999) 'A stop-codon mutation in the BRI gene associated with familial British dementia', *Nature*, 399, p. 776. doi: 10.1038/21637.

Vitek, M. P. *et al.* (2020) 'Translational animal models for Alzheimer's disease: An Alzheimer's Association Business Consortium Think Tank', *Alzheimer's and Dementia: Translational Research and Clinical Interventions*, 6(1), p. e12114. doi: 10.1002/trc2.12114.

Wagner, M. *et al.* (2014) 'Asymmetric Flow Field-Flow Fractionation in the Field of Nanomedicine'. doi: 10.1021/ac501664t.

Walsh, D. M. *et al.* (1997) 'Amyloid beta-protein fibrillogenesis. Detection of a protofibrillar intermediate', *J Biol Chem*. 1997/08/29, 272(35), pp. 22364–22372. doi: 10.1074/jbc.272.35.22364.

Walsh, D. M. *et al.* (2002) 'Naturally secreted oligomers of amyloid beta protein potently inhibit hippocampal long-term potentiation in vivo', *Nature*. 2002/04/05, 416(6880), pp. 535–539. doi: 10.1038/416535a.

Wang, L., Eom, K. and Kwon, T. (2021) 'Different Aggregation Pathways and Structures for Aβ40 and Aβ42 Peptides', *Biomolecules*, 11(2), pp. 1–9. doi: 10.3390/BIOM11020198.

Wang, R. and Reddy, P. H. (2017) 'Role of glutamate and NMDA receptors in Alzheimer's disease', *Journal of Alzheimer's disease : JAD*, 57(4), p. 1041. doi: 10.3233/JAD-160763.

Wang, W. *et al.* (2019) 'Toxic amyloid-beta oligomers induced self-replication in astrocytes triggering neuronal injury', *EBioMedicine*. 2019/03/31, 42, pp. 174–187. doi: 10.1016/j.ebiom.2019.03.049.

Wang, Z. *et al.* (2017) 'Human Brain-Derived Aβ Oligomers Bind to Synapses and Disrupt Synaptic Activity in a Manner That Requires APP', *Journal of Neuroscience*, 37(49), pp. 11947–11966. doi: 10.1523/JNEUROSCI.2009-17.2017.

Wang, Z. Q. *et al.* (2020) 'MicroRNA Let-7i Is a Promising Serum Biomarker for Post-stroke Cognitive Impairment and Alleviated OGD-Induced Cell Damage in vitro by Regulating Bcl-2', *Frontiers in Neuroscience*, 14. doi: 10.3389/FNINS.2020.00215.

Wanner, I. B. *et al.* (2013) 'Glial scar borders are formed by newly proliferated, elongated astrocytes that interact to corral inflammatory and fibrotic cells via STAT3-dependent mechanisms after spinal cord injury', *The Journal of neuroscience : the official journal of the Society for Neuroscience*, 33(31), pp. 12870–12886. doi: 10.1523/JNEUROSCI.2121-13.2013.

Watts, M. E. *et al.* (2018) 'Brain Energy and Oxygen Metabolism: Emerging Role in Normal Function and Disease'. doi: 10.3389/fnmol.2018.00216.

Weggen, S. and Beher, D. (2012) 'Molecular consequences of amyloid precursor protein and presenilin mutations causing autosomal-dominant Alzheimer's disease', *Alzheimer's research & therapy*, 4(2). doi: 10.1186/ALZRT107.

Welburn, J. P. *et al.* (2007) 'How tyrosine 15 phosphorylation inhibits the activity of cyclin-dependent kinase 2-cyclin A', *J Biol Chem*. 2006/11/11, 282(5), pp. 3173–3181. doi: 10.1074/jbc.M609151200.

Weller, R. O. *et al.* (2008) 'Perivascular drainage of amyloid-beta peptides from the brain and its failure in cerebral amyloid angiopathy and Alzheimer's disease', *Brain Pathol*. 2008/03/28, 18(2), pp. 253–266. doi: 10.1111/j.1750-3639.2008.00133.x 10.1111/j.1750-3639.2008.00133.x.

Welty, S., Thathiah, A. and Levine, A. S. (2022) 'DNA Damage Increases Secreted Aβ40 and Aβ42 in Neuronal Progenitor Cells: Relevance to Alzheimer's Disease', *Journal of Alzheimer's disease : JAD*, 88(1), pp. 177–190. doi: 10.3233/JAD-220030.

Welzel, A. T. *et al.* (2014) 'Secreted amyloid beta-proteins in a cell culture model include N-terminally extended peptides that impair synaptic plasticity', *Biochemistry*. 2014/05/21, 53(24), pp. 3908–3921. doi: 10.1021/bi5003053.

White, J. A. *et al.* (2005) 'Differential effects of oligomeric and fibrillar amyloid-beta 1-42 on astrocyte-mediated inflammation', *Neurobiol Dis*. 2005/03/10, 18(3), pp. 459–465. doi: 10.1016/j.nbd.2004.12.013.

Willander, H. *et al.* (2012) 'BRICHOS domains efficiently delay fibrillation of amyloid beta-peptide', *J Biol Chem*. 2012/07/18, 287(37), pp. 31608–31617. doi: 10.1074/jbc.M112.393157 10.1074/jbc.M112.393157. Epub 2012 Jul 16.

Willard, S. S. and Koochekpour, S. (2013) 'Glutamate, Glutamate Receptors, and Downstream Signaling Pathways', *International Journal of Biological Sciences*, 9(9), p. 948. doi: 10.7150/IJBS.6426.

World Health Organization (WHO) (2017) 'Global action plan on the public health response to dementia 2017 - 2025', *Geneva: World Health Organization*, p. 27. Available at: http://www.who.int/mental_health/neurology/dementia/action_plan_2017_2025/en/ (Accessed: 31 March 2022).

Wyss-Coray, T. *et al.* (2003) 'Adult mouse astrocytes degrade amyloid-beta in vitro and in situ', *Nat*

*Med*. 2003/03/04, 9(4), pp. 453–457. doi: 10.1038/nm838.

Xia, M. *et al.* (1997) 'Interleukin-8 receptor B immunoreactivity in brain and neuritic plaques of Alzheimer's disease.', *The American Journal of Pathology*, 150(4), p. 1267. Available at: /pmc/articles/PMC1858175/?report=abstract (Accessed: 18 October 2022).

Xie, J., Hoecke, L. Van and Vandenbroucke, R. E. (2022) 'The Impact of Systemic Inflammation on Alzheimer’s Disease Pathology', *Frontiers in Immunology*, 12, p. Article 796867. doi: 10.3389/fimmu.2021.796867.

Xue, W. F., Homans, S. W. and Radford, S. E. (2008) 'Systematic analysis of nucleation-dependent polymerization reveals new insights into the mechanism of amyloid self-assembly', *Proc Natl Acad Sci U S A*. 2008/06/27, 105(26), pp. 8926–8931. doi: 10.1073/pnas.0711664105.

Yagi, T. *et al.* (2011) 'Modeling familial Alzheimer's disease with induced pluripotent stem cells', *Human Molecular Genetics*, 20(23), pp. 4530–4539. doi: 10.1093/hmg/ddr394.

Yamamoto, M. *et al.* (2007) 'Interferon-γ and Tumor Necrosis Factor-α Regulate Amyloid-β Plaque Deposition and β-Secretase Expression in Swedish Mutant APP Transgenic Mice', *The American Journal of Pathology*, 170(2), p. 680. doi: 10.2353/AJPATH.2007.060378.

Yamazaki, Y. *et al.* (2019) 'Selective loss of cortical endothelial tight junction proteins during Alzheimer's disease progression', *Brain*, 142, pp. 1077–1092. doi: 10.1093/brain/awz011.

Yang, C. M. *et al.* (2015) 'IL-1β Induces MMP-9-Dependent Brain Astrocytic Migration via Transactivation of PDGF Receptor/NADPH Oxidase 2-Derived Reactive Oxygen Species Signals', *Molecular Neurobiology*, 52(1), pp. 303–317. doi: 10.1007/S12035-014-8838-Y/FIGURES/7.

Yang, T. *et al.* (2017) 'Large Soluble Oligomers of Amyloid β-Protein from Alzheimer Brain Are Far Less Neuroactive Than the Smaller Oligomers to Which They Dissociate', *The Journal of neuroscience : the official journal of the Society for Neuroscience*, 37(1), pp. 152–163. doi: 10.1523/JNEUROSCI.1698-16.2016.

Yang, T., Hsu, C. and Kuo, Y. (2009) 'Cell-derived soluble oligomers of human amyloid-β peptides disturb cellular homeostasis and induce apoptosis in primary hippocampal neurons', *J Neural Transm*, 116, p. 1561.

Ye, B. *et al.* (2016) 'Dynamic monitoring of oxidative DNA double-strand break and repair in cardiomyocytes', *Cardiovasc Pathol*. 2016/01/15, 25(2), pp. 93–100. doi: 10.1016/j.carpath.2015.10.010.

Yeung, J. H. Y. *et al.* (2020) 'Amyloid-beta1-42 induced glutamatergic receptor and transporter expression changes in the mouse hippocampus', *Journal of neurochemistry*, 155(1), pp. 62–80. doi: 10.1111/JNC.15099.

Yoon, S. S. and Jo, S. A. (2012) 'Mechanisms of Amyloid-β Peptide Clearance: Potential Therapeutic Targets for Alzheimer's Disease', *Biomol Ther (Seoul)*, 20(3), pp. 245–255. doi: 10.4062/biomolther.2012.20.3.245 10.4062/biomolther.2012.20.3.245.

Yosef, R. *et al.* (2017) 'p21 maintains senescent cell viability under persistent DNA damage response by restraining JNK and caspase signaling', *EMBO J*, 36(15), pp. 2280–2295. doi: 10.15252/embj.201695553.

Youssef, I. *et al.* (2008) 'N-truncated amyloid-β oligomers induce learning impairment and neuronal apoptosis', *Neurobiology of Aging*, 29(9), pp. 1319–1333. doi: 10.1016/J.NEUROBIOLAGING.2007.03.005.

Yun, H. M. *et al.* (2015) 'Neuroinflammatory and Amyloidogenic Activities of IL-32β in Alzheimer's

Disease', *Molecular neurobiology*, 52(1), pp. 341–352. doi: 10.1007/S12035-014-8860-0.

Zamanian, J. L. *et al.* (2012) 'Genomic Analysis of Reactive Astrogliosis', *The Journal of Neuroscience*, 32(18), p. 6391. doi: 10.1523/JNEUROSCI.6221-11.2012.

Zannini, L., Delia, D. and Buscemi, G. (2014) 'CHK2 kinase in the DNA damage response and beyond', *J Mol Cell Biol*, 6(6), pp. 442–457. doi: 10.1093/jmcb/mju045.

Zeng, C. *et al.* (2005) 'Amyloid-beta peptide enhances tumor necrosis factor-alpha-induced iNOS through neutral sphingomyelinase/ceramide pathway in oligodendrocytes', *Journal of neurochemistry*, 94(3), pp. 703–712. doi: 10.1111/J.1471-4159.2005.03217.X.

Zhang, Y. *et al.* (2011) 'APP processing in Alzheimer's disease', *Mol Brain*, 4, p. 3. doi: 10.1186/1756-6606-4-3.

Zhao, J., O'Connor, T. and Vassar, R. (2011) 'The contribution of activated astrocytes to Abeta production: implications for Alzheimer's disease pathogenesis', *J Neuroinflammation*. 2011/11/04, 8, p. 150. doi: 10.1186/1742-2094-8-150.

Zhou, Z. *et al.* (2011) 'The roles of amyloid precursor protein (APP) in neurogenesis: Implications to pathogenesis and therapy of Alzheimer disease', *Cell adhesion & migration*. 2011/07/01, 5(4), pp. 280–292. doi: 10.4161/cam.5.4.16986.

Zhu, B. L. *et al.* (2019) 'MMP13 inhibition rescues cognitive decline in Alzheimer transgenic mice via BACE1 regulation', *Brain : a journal of neurology*, 142(1), pp. 176–192. doi: 10.1093/BRAIN/AWY305.

# Appendix

## 1. Ethical permission for the use of patient-derived cell lines

**The ethical approval details:**

Motor system genomics,

Study reference: STH16573

REC reference: 12/YH/0330

## 2. Ethical permission for the use of human brain tissue

**Sheffield Brain Tissue Bank**

**Management Board review of Application/Extension for Access to Tissue**

| | |
|---|---|
| Name and institution of researcher(s): | Miss Martyna Matuszyk, University of Sheffield |
| Project title: | Characterising the varying astrocyte responses to amyloid-beta in Alzheimer's disease |
| Date of request: | 01-09-21 |

| Table 1. Management Board - Internal Comments | |
|---|---|
| 1. Has the researcher:<br>a. provided adequate information in the *Application/Extension for Access to Data* for the Committee to form an opinion; **and**<br>b. Fully completed and signed the *Agreement for Data Use*? | Yes |
| 2. Does the research fit within the REC-approved research aims of the SBTB (outlined below)?<br>• Neurodegeneration, neurological disease, or normal ageing -related studies investigating the genetic causes and potential environmental predispositions of the disease.<br>• Neurodegeneration, neurological disease, or normal ageing -related studies that will facilitate and support the improvements in clinical care and advance the knowledge of clinicians and researchers in attempt to find new treatments and methods of improving life for patients.<br>• Studies looking for specific trends or correlations in the data, aiding in understanding of the disease progression and phenotype, and investigating potential therapeutic benefits or targets for future therapies.<br>• Studies to enable Biomathematicians to build probabilistic models that can link clinical data to environmental risk factors and genetic risk factors.<br><br>*If No, but the further review questions are favourable, it is possible for the researcher(s) to access tissue if project-specific REC approval is received. The SBTB must be in receipt of the REC approval and all associated documents before the Management Board can approve release of any tissue.* | Yes |
| 3. Will the research develop new scientific knowledge, which has the potential benefit to patients? | Yes |
| 4. Is there a potential conflict with any currently ongoing research?<br><br>If Yes, Please give details: | No |
| | |

5. Recommended outcome:
   a. Grant access to tissue as outlined in the Tissue Request Form.
   b. Does not fit within our REC-approval, but worthwhile research – grant access to tissue as outlined in the Tissue Request Form but the researcher will need to provide project-specific REC approval before the tissue is released.
   c. Reject request for access to tissue, or request material changes to the application before re-applying to the Management Board (provide reasons)

   Comments:

A

The Management Board is given a deadline of 10 working days to respond to the request.

A minimum of 4 responses are required (one of which is the **Tissue Bank Director or Deputy-Director**; and **one lay member**) for the review to be quorate; and all responding members must agree in order for the tissue request to be approved.
If any concerns or objections are raised, these must be discussed and resolved as a group, so that a collective decision is made. Where agreement cannot be reached, the Tissue Bank Director takes the final decision (as long as the minimum quorate is reached).

Review completed by:

| **Management Board Member** | **Present** *(or email response provided)* | **Signature to confirm agreed outcome** *(or secretary signature to confirm email correspondence has been filed to provide confirmation of responses)* |
|---|---|---|
| Dr Robin Highley | Yes / No | |
| Professor Stephen Wharton | Yes / No | |
| Dr Esther Hobbs | Yes / No | |
| Dr John Cooper-Knock | Yes / No | |
| Mr Kevin Corke | Yes / No | |
| Helen Wollff | Yes / ~~No~~ | *A Taylor* |
| Ms Lynne Baxter | Yes / No | |
| Professor Dame Pamela Shaw | Yes / ~~No~~ | *A Taylor* |
| Prof Oliver Bandmann | Yes / No | |
| Dr Dan Blackburn | Yes / No | |
| Dr Julie Simpson | Yes / No | |
| Mr Paul Heath | Yes / No | |
| Prof Raj N Kalaria | Yes / No | |
| Prof Stephen Gentleman | Yes / No | |
| Dr Aditya Shivane | Yes / No | |
| Dr Gemma Lace-Costigan | Yes / No | |
| Prof Delphine Boche | Yes / ~~No~~ | *A Taylor* |
| John Laxton – Lay member | Yes / No | |
| Liz Erett – Lay member | Yes / No | |
| Val Heap – Lay member | Yes / ~~No~~ | *A Taylor* |
| Gwyn Jones – Lay member | Yes / No | |

| | |
|---|---|
| **5.** Recommended outcome:<br>a. Grant access to tissue as outlined in the Tissue Request Form.<br>b. Does not fit within our REC-approval, but worthwhile research – grant access to tissue as outlined in the Tissue Request Form but the researcher will need to provide project-specific REC approval before the tissue is released.<br>c. Reject request for access to tissue, or request material changes to the application before re-applying to the Management Board (provide reasons)<br>Comments: | A |

The Management Board is given a deadline of 10 working days to respond to the request.

A minimum of **4 responses** are required (one of which is the **Tissue Bank Director or Deputy-Director**; and **one lay member**) for the review to be quorate; and **all** responding members must agree in order for the tissue request to be approved.
If any concerns or objections are raised, these must be discussed and resolved as a group, so that a collective decision is made. Where agreement cannot be reached, the Tissue Bank Director takes the final decision (as long as the minimum quorate is reached).

Review completed by:

| **Management Board Member** | **Present** *(or email response provided)* | **Signature to confirm agreed outcome** *(or secretary signature to confirm email correspondence has been filed to provide confirmation of responses)* |
|---|---|---|
| Dr Robin Highley | Yes / No | |
| Professor Stephen Wharton | Yes / No | |
| Dr Esther Hobbs | Yes / No | |
| Dr John Cooper-Knock | Yes / No | |
| Mr Kevin Corke | Yes / No | |
| Helen Wollff | Yes / ~~No~~ | *A Taylor* |
| Ms Lynne Baxter | Yes / No | |
| Professor Dame Pamela Shaw | Yes / ~~No~~ | *A Taylor* |
| Prof Oliver Bandmann | Yes / No | |
| Dr Dan Blackburn | Yes / No | |
| Dr Julie Simpson | Yes / No | |
| Mr Paul Heath | Yes / No | |
| Prof Raj N Kalaria | Yes / No | |
| Prof Stephen Gentleman | Yes / No | |
| Dr Aditya Shivane | Yes / No | |
| Dr Gemma Lace-Costigan | Yes / No | |
| Prof Delphine Boche | Yes / ~~No~~ | *A Taylor* |
| John Laxton – Lay member | Yes / No | |
| Liz Erett – Lay member | Yes / No | |
| Val Heap – Lay member | Yes / ~~No~~ | *A Taylor* |
| Gwyn Jones – Lay member | Yes / No | |

## 3. Statistical analysis of fetal astrocytes treated with $A\beta_{1-42}$ oligomers

### 3.1 γH2AX DNA foci analysis

**All damage**

| One-way ANOVA results | | | | | |
|---|---|---|---|---|---|
| | | | | | |
| **ANOVA summary** | | | | | |
| F | 0.9796 | | | | |
| P value | 0.474 | | | | |
| P value summary | ns | | | | |
| Significant diff. among means (P < 0.05)? | No | | | | |
| R squared | 0.2957 | | | | |
| | | | | | |
| **Brown-Forsythe test** | | | | | |
| F (DFn, DFd) | 1.017 (6, 14) | | | | |
| P value | 0.453 | | | | |
| P value summary | ns | | | | |
| Are SDs significantly different (P < 0.05)? | No | | | | |
| | | | | | |
| **Bartlett's test** | | | | | |
| Bartlett's statistic (corrected) | | | | | |
| P value | | | | | |
| P value summary | | | | | |
| Are SDs significantly different (P < 0.05)? | | | | | |
| | | | | | |
| **ANOVA table** | SS | DF | MS | F (DFn, DFd) | P value |
| Treatment (between columns) | 0.005649 | 6 | 0.0009415 | F (6, 14) = 0.9796 | P=.474 |
| Residual (within columns) | 0.01346 | 14 | 0.0009611 | | |
| Total | 0.0191 | 20 | | | |

**All damage**

| Bonferroni's multiple comparisons test | | | | | |
|---|---|---|---|---|---|
| | | | | | |
| **Bonferroni's multiple comparisons test** | **Mean Diff.** | **95.00% CI of diff.** | **Below threshold?** | **Summary** | **Adjusted P Value** |
| Control vs. 48h oligomer | -0.01449 | -0.09733 to 0.06836 | No | ns | >.999 |
| Control vs. 48h scrambled | 0.01001 | -0.07284 to 0.09285 | No | ns | >.999 |
| Control vs. 24h oligomer | 0.000995 | -0.08185 to 0.08384 | No | ns | >.999 |
| Control vs. 24h scrambled | 0.00794 | -0.07490 to 0.09078 | No | ns | >.999 |
| Control vs. 1h oligomer | 0.01508 | -0.06777 to 0.09792 | No | ns | >.999 |
| Control vs. 1h scrambled | -0.03636 | -0.1192 to 0.04648 | No | ns | >.999 |
| 48h oligomer vs. 48h scrambled | 0.02449 | -0.05835 to 0.1073 | No | ns | >.999 |
| 24h oligomer vs. 24h scrambled | 0.006945 | -0.07590 to 0.08979 | No | ns | >.999 |
| 1h oligomer vs. 1h scrambled | -0.05144 | -0.1343 to 0.03140 | No | ns | 0.554 |

**Low damage**

| One-way ANOVA results | | | | | |
|---|---|---|---|---|---|
| | | | | | |
| **ANOVA summary** | | | | | |
| F | 0.7193 | | | | |
| P value | 0.641 | | | | |
| P value summary | ns | | | | |
| Significant diff. among means (P < 0.05)? | No | | | | |
| R squared | 0.2356 | | | | |
| | | | | | |
| **Brown-Forsythe test** | | | | | |
| F (DFn, DFd) | 0.7870 (6, 14) | | | | |
| P value | 0.594 | | | | |
| P value summary | ns | | | | |
| Are SDs significantly different (P < 0.05)? | No | | | | |
| | | | | | |
| **Bartlett's test** | | | | | |
| Bartlett's statistic (corrected) | | | | | |
| P value | | | | | |
| P value summary | | | | | |
| Are SDs significantly different (P < 0.05)? | | | | | |
| | | | | | |
| **ANOVA table** | **SS** | **DF** | **MS** | **F (DFn, DFd)** | **P value** |
| Treatment (between columns) | 0.6288 | 6 | 0.1048 | F (6, 14) = 0.7193 | P=.641 |
| Residual (within columns) | 2.04 | 14 | 0.1457 | | |
| Total | 2.669 | 20 | | | |

**Low damage**

| Bonferroni's multiple comparisons test | | | | | |
|---|---|---|---|---|---|
| | | | | | |
| **Bonferroni's multiple comparisons test** | **Mean Diff.** | **95.00% CI of diff.** | **Below threshold?** | **Summary** | **Adjusted P Value** |
| Control vs. 48h oligomer | -0.3182 | -1.338 to 0.7018 | No | ns | >.999 |
| Control vs. 48h scrambled | -0.259 | -1.279 to 0.7610 | No | ns | >.999 |
| Control vs. 24h oligomer | -0.3561 | -1.376 to 0.6639 | No | ns | >.999 |
| Control vs. 24h scrambled | -0.01705 | -1.037 to 1.003 | No | ns | >.999 |
| Control vs. 1h oligomer | 0.006026 | -1.014 to 1.026 | No | ns | >.999 |
| Control vs. 1h scrambled | 0.1132 | -0.9068 to 1.133 | No | ns | >.999 |
| 48h oligomer vs. 48h scrambled | 0.05913 | -0.9609 to 1.079 | No | ns | >.999 |
| 24h oligomer vs. 24h scrambled | 0.339 | -0.6809 to 1.359 | No | ns | >.999 |
| 1h oligomer vs. 1h scrambled | 0.1072 | -0.9128 to 1.127 | No | ns | >.999 |

## High damage

| One-wy ANOVA results | | | | | |
|---|---|---|---|---|---|
| | | | | | |
| **ANOVA summary** | | | | | |
| F | 1.083 | | | | |
| P value | 0.418 | | | | |
| P value summary | ns | | | | |
| Significant diff. among means (P < 0.05)? | No | | | | |
| R squared | 0.3171 | | | | |
| | | | | | |
| **Brown-Forsythe test** | | | | | |
| F (DFn, DFd) | 0.6534 (6, 14) | | | | |
| P value | 0.688 | | | | |
| P value summary | ns | | | | |
| Are SDs significantly different (P < 0.05)? | No | | | | |
| | | | | | |
| **Bartlett's test** | | | | | |
| Bartlett's statistic (corrected) | | | | | |
| P value | | | | | |
| P value summary | | | | | |
| Are SDs significantly different (P < 0.05)? | | | | | |
| | | | | | |
| **ANOVA table** | **SS** | **DF** | **MS** | **F (DFn, DFd)** | **P value** |
| Treatment (between columns) | 0.1131 | 6 | 0.01885 | F (6, 14) = 1.083 | P=.418 |
| Residual (within columns) | 0.2436 | 14 | 0.0174 | | |
| Total | 0.3568 | 20 | | | |
| | | | | | |

## High damage

| Bonferroni's multiple comparisons test | | | | | |
|---|---|---|---|---|---|
| | | | | | |
| **Bonferroni's multiple comparisons test** | **Mean Diff.** | **95.00% CI of diff.** | **Below threshold?** | **Summary** | **Adjusted P Value** |
| Control vs. 48h oligomer | -0.01171 | -0.3642 to 0.3408 | No | ns | >.999 |
| Control vs. 48h scrambled | 0.08516 | -0.2673 to 0.4377 | No | ns | >.999 |
| Control vs. 24h oligomer | 0.05618 | -0.2963 to 0.4087 | No | ns | >.999 |
| Control vs. 24h scrambled | 0.06624 | -0.2863 to 0.4187 | No | ns | >.999 |
| Control vs. 1h oligomer | 0.1582 | -0.1944 to 0.5107 | No | ns | >.999 |
| Control vs. 1h scrambled | -0.08851 | -0.4410 to 0.2640 | No | ns | >.999 |
| 48h oligomer vs. 48h scrambled | 0.09688 | -0.2556 to 0.4494 | No | ns | >.999 |
| 24h oligomer vs. 24h scrambled | 0.01005 | -0.3424 to 0.3626 | No | ns | >.999 |
| 1h oligomer vs. 1h scrambled | -0.2467 | -0.5992 to 0.1058 | No | ns | 0.343 |

## 3.2 Cell morphology analysis

### Mean cytoplasm region

| ANOVA summary | | | | | | |
|---|---|---|---|---|---|---|
| F | 0.4792 | | | | | |
| P value | 0.813 | | | | | |
| P value summary | ns | | | | | |
| Significant diff. among means (P < 0.05)? | No | | | | | |
| R squared | 0.1704 | | | | | |
| | | | | | | |
| **Brown-Forsythe test** | | | | | | |
| F (DFn, DFd) | 1.101 (6, 14) | | | | | |
| P value | 0.409 | | | | | |
| P value summary | ns | | | | | |
| Are SDs significantly different (P < 0.05)? | No | | | | | |
| | | | | | | |
| **Bartlett's test** | | | | | | |
| Bartlett's statistic (corrected) | | | | | | |
| P value | | | | | | |
| P value summary | | | | | | |
| Are SDs significantly different (P < 0.05)? | | | | | | |
| | | | | | | |
| **ANOVA table** | **SS** | **DF** | **MS** | **F (DFn, DFd)** | **P value** | |
| Treatment (between columns) | 0.02981 | 6 | 0.004969 | F (6, 14) = 0.4792 | P=.813 | |
| Residual (within columns) | 0.1452 | 14 | 0.01037 | | | |
| Total | 0.175 | 20 | | | | |

| Bonferroni's multiple comparisons test | Mean Diff. | 95.00% CI of diff. | Below threshold? | Summary | Adjusted P Value |
|---|---|---|---|---|---|
| Control vs. 48h oligomer | -0.01318 | -0.2853 to 0.2589 | No | ns | >.999 |
| Control vs. 48h scrambled | 0.09939 | -0.1727 to 0.3715 | No | ns | >.999 |
| Control vs. 24h oligomer | 0.07751 | -0.1946 to 0.3496 | No | ns | >.999 |
| Control vs. 24h scrambled | 0.03765 | -0.2345 to 0.3098 | No | ns | >.999 |
| Control vs. 1h oligomer | 0.0163 | -0.2558 to 0.2884 | No | ns | >.999 |
| Control vs. 1h scrambled | 0.02597 | -0.2461 to 0.2981 | No | ns | >.999 |
| 48h oligomer vs. 48h scrambled | 0.1126 | -0.1595 to 0.3847 | No | ns | >.999 |
| 24h oligomer vs. 24h scrambled | -0.03986 | -0.3120 to 0.2322 | No | ns | >.999 |
| 1h oligomer vs. 1h scrambled | 0.009671 | -0.2624 to 0.2818 | No | ns | >.999 |

### Mean cell area

| ANOVA summary | | | | | | |
|---|---|---|---|---|---|---|
| F | 0.9177 | | | | | |
| P value | 0.511 | | | | | |
| P value summary | ns | | | | | |
| Significant diff. among means (P < 0.05)? | No | | | | | |
| R squared | 0.2823 | | | | | |
| | | | | | | |
| **Brown-Forsythe test** | | | | | | |
| F (DFn, DFd) | 0.6623 (6, 14) | | | | | |
| P value | 0.681 | | | | | |
| P value summary | ns | | | | | |
| Are SDs significantly different (P < 0.05)? | No | | | | | |
| | | | | | | |
| **Bartlett's test** | | | | | | |
| Bartlett's statistic (corrected) | | | | | | |
| P value | | | | | | |
| P value summary | | | | | | |
| Are SDs significantly different (P < 0.05)? | | | | | | |
| | | | | | | |
| **ANOVA table** | **SS** | **DF** | **MS** | **F (DFn, DFd)** | **P value** | |
| Treatment (between columns) | 0.01413 | 6 | 0.002355 | F (6, 14) = 0.9177 | P=.511 | |
| Residual (within columns) | 0.03593 | 14 | 0.002566 | | | |
| Total | 0.05006 | 20 | | | | |

| Bonferroni's multiple comparisons test | Mean Diff. | 95.00% CI of diff. | Below threshold? | Summary | Adjusted P Value |
|---|---|---|---|---|---|
| Control vs. 48h oligomer | 0.008172 | -0.1272 to 0.1435 | No | ns | >.999 |
| Control vs. 48h scrambled | -0.02125 | -0.1566 to 0.1141 | No | ns | >.999 |
| Control vs. 24h oligomer | -0.04726 | -0.1826 to 0.08811 | No | ns | >.999 |
| Control vs. 24h scrambled | -0.0596 | -0.1950 to 0.07577 | No | ns | >.999 |
| Control vs. 1h oligomer | 0.005743 | -0.1296 to 0.1411 | No | ns | >.999 |
| Control vs. 1h scrambled | -0.04429 | -0.1797 to 0.09108 | No | ns | >.999 |
| 48h oligomer vs. 48h scrambled | -0.02942 | -0.1648 to 0.1059 | No | ns | >.999 |
| 24h oligomer vs. 24h scrambled | -0.01234 | -0.1477 to 0.1230 | No | ns | >.999 |
| 1h oligomer vs. 1h scrambled | -0.05003 | -0.1854 to 0.08534 | No | ns | >.999 |

### Mean cell roundness

| ANOVA summary | | | | | | |
|---|---|---|---|---|---|---|
| F | 1.99 | | | | | |
| P value | 0.136 | | | | | |
| P value summary | ns | | | | | |
| Significant diff. among means (P < 0.05)? | No | | | | | |
| R squared | 0.4602 | | | | | |
| | | | | | | |
| **Brown-Forsythe test** | | | | | | |
| F (DFn, DFd) | 0.8980 (6, 14) | | | | | |
| P value | 0.523 | | | | | |
| P value summary | ns | | | | | |
| Are SDs significantly different (P < 0.05)? | No | | | | | |
| | | | | | | |
| **Bartlett's test** | | | | | | |
| Bartlett's statistic (corrected) | | | | | | |
| P value | | | | | | |
| P value summary | | | | | | |
| Are SDs significantly different (P < 0.05)? | | | | | | |
| | | | | | | |
| **ANOVA table** | **SS** | **DF** | **MS** | **F (DFn, DFd)** | **P value** | |
| Treatment (between columns) | 0.004027 | 6 | 0.0006711 | F (6, 14) = 1.990 | P=.136 | |
| Residual (within columns) | 0.004722 | 14 | 0.0003373 | | | |
| Total | 0.008749 | 20 | | | | |

| Bonferroni's multiple comparisons test | Mean Diff. | 95.00% CI of diff. | Below threshold? | Summary | Adjusted P Value |
|---|---|---|---|---|---|
| Control vs. 48h oligomer | 0.03114 | -0.01794 to 0.08021 | No | ns | 0.511 |
| Control vs. 48h scrambled | 0.0242 | -0.02488 to 0.07328 | No | ns | >.999 |
| Control vs. 24h oligomer | 0.0263 | -0.02278 to 0.07537 | No | ns | 0.912 |
| Control vs. 24h scrambled | 0.01798 | -0.03110 to 0.06706 | No | ns | >.999 |
| Control vs. 1h oligomer | -0.006968 | -0.05605 to 0.04211 | No | ns | >.999 |
| Control vs. 1h scrambled | 0.002027 | -0.04705 to 0.05110 | No | ns | >.999 |
| 48h oligomer vs. 48h scrambled | -0.006937 | -0.05601 to 0.04214 | No | ns | >.999 |
| 24h oligomer vs. 24h scrambled | -0.008317 | -0.05739 to 0.04076 | No | ns | >.999 |
| 1h oligomer vs. 1h scrambled | 0.008994 | -0.04008 to 0.05807 | No | ns | >.999 |

## Mean cell width

| ANOVA summary | | | | | | | Bonferroni's multiple comparisons test | Mean Diff. | 95.00% CI of diff. | Below threshold? | Summary | Adjusted P Value |
|---|---|---|---|---|---|---|---|---|---|---|---|---|
| F | 1.812 | | | | | | Control vs. 48h oligomer | 0.02264 | -0.04622 to 0.09149 | No | ns | >.999 |
| P value | 0.169 | | | | | | Control vs. 48h scrambled | -0.001025 | -0.06988 to 0.06783 | No | ns | >.999 |
| P value summary | ns | | | | | | Control vs. 24h oligomer | -0.02442 | -0.09327 to 0.04444 | No | ns | >.999 |
| Significant diff. among means (P < 0.05)? | No | | | | | | Control vs. 24h scrambled | -0.02572 | -0.09458 to 0.04313 | No | ns | >.999 |
| R squared | 0.4371 | | | | | | Control vs. 1h oligomer | -0.01646 | -0.08531 to 0.05240 | No | ns | >.999 |
| | | | | | | | Control vs. 1h scrambled | -0.03609 | -0.1049 to 0.03276 | No | ns | 0.975 |
| **Brown-Forsythe test** | | | | | | | 48h oligomer vs. 48h scrambled | -0.02366 | -0.09252 to 0.04519 | No | ns | >.999 |
| F (DFn, DFd) | 1.017 (6, 14) | | | | | | 24h oligomer vs. 24h scrambled | -0.001309 | -0.07016 to 0.06755 | No | ns | >.999 |
| P value | 0.453 | | | | | | 1h oligomer vs. 1h scrambled | -0.01964 | -0.08849 to 0.04922 | No | ns | >.999 |
| P value summary | ns | | | | | | | | | | | |
| Are SDs significantly different (P < 0.05)? | No | | | | | | | | | | | |
| | | | | | | | | | | | | |
| **Bartlett's test** | | | | | | | | | | | | |
| Bartlett's statistic (corrected) | | | | | | | | | | | | |
| P value | | | | | | | | | | | | |
| P value summary | | | | | | | | | | | | |
| Are SDs significantly different (P < 0.05)? | | | | | | | | | | | | |
| | | | | | | | | | | | | |
| **ANOVA table** | **SS** | **DF** | **MS** | **F (DFn, DFd)** | **P value** | | | | | | | |
| Treatment (between columns) | 0.007218 | 6 | 0.001203 | F (6, 14) = 1.812 | P=.169 | | | | | | | |
| Residual (within columns) | 0.009295 | 14 | 0.000664 | | | | | | | | | |
| Total | 0.01651 | 20 | | | | | | | | | | |

## Mean cell length

| ANOVA summary | | | | | | | Bonferroni's multiple comparisons test | Mean Diff. | 95.00% CI of diff. | Below threshold? | Summary | Adjusted P Value |
|---|---|---|---|---|---|---|---|---|---|---|---|---|
| F | 1.007 | | | | | | Control vs. 48h oligomer | -0.02722 | -0.1315 to 0.07706 | No | ns | >.999 |
| P value | 0.459 | | | | | | Control vs. 48h scrambled | -0.02545 | -0.1297 to 0.07883 | No | ns | >.999 |
| P value summary | ns | | | | | | Control vs. 24h oligomer | -0.02466 | -0.1289 to 0.07962 | No | ns | >.999 |
| Significant diff. among means (P < 0.05)? | No | | | | | | Control vs. 24h scrambled | -0.05223 | -0.1565 to 0.05205 | No | ns | >.999 |
| R squared | 0.3016 | | | | | | Control vs. 1h oligomer | 0.01831 | -0.08597 to 0.1226 | No | ns | >.999 |
| | | | | | | | Control vs. 1h scrambled | -0.009439 | -0.1137 to 0.09484 | No | ns | >.999 |
| **Brown-Forsythe test** | | | | | | | 48h oligomer vs. 48h scrambled | 0.001768 | -0.1025 to 0.1060 | No | ns | >.999 |
| F (DFn, DFd) | 0.7622 (6, 14) | | | | | | 24h oligomer vs. 24h scrambled | -0.02757 | -0.1319 to 0.07671 | No | ns | >.999 |
| P value | 0.611 | | | | | | 1h oligomer vs. 1h scrambled | -0.02775 | -0.1320 to 0.07653 | No | ns | >.999 |
| P value summary | ns | | | | | | | | | | | |
| Are SDs significantly different (P < 0.05)? | No | | | | | | | | | | | |
| | | | | | | | | | | | | |
| **Bartlett's test** | | | | | | | | | | | | |
| Bartlett's statistic (corrected) | | | | | | | | | | | | |
| P value | | | | | | | | | | | | |
| P value summary | | | | | | | | | | | | |
| Are SDs significantly different (P < 0.05)? | | | | | | | | | | | | |
| | | | | | | | | | | | | |
| **ANOVA table** | **SS** | **DF** | **MS** | **F (DFn, DFd)** | **P value** | | | | | | | |
| Treatment (between columns) | 0.009205 | 6 | 0.001534 | F (6, 14) = 1.007 | P=.459 | | | | | | | |
| Residual (within columns) | 0.02132 | 14 | 0.001523 | | | | | | | | | |
| Total | 0.03053 | 20 | | | | | | | | | | |

# 4. Statistical analysis of fetal astrocytes treated with $A\beta_{1-42}$ fibrils

## 4.1 γH2AX DNA foci analysis

### All damage

| ANOVA summary | | | | | | | Bonferroni's multiple comparisons test | Mean Diff. | 95.00% CI of diff. | Below threshold? | Summary | Adjusted P Value |
|---|---|---|---|---|---|---|---|---|---|---|---|---|
| F | 1.249 | | | | | | Control vs. 48h fibril | -0.1413 | -0.5145 to 0.2319 | No | ns | >.999 |
| P value | 0.34 | | | | | | Control vs. 48h scrambled | -0.2338 | -0.6070 to 0.1394 | No | ns | 0.536 |
| P value summary | ns | | | | | | Control vs. 24h fibril | -0.02228 | -0.3955 to 0.3509 | No | ns | >.999 |
| Significant diff. among means (P < 0.05)? | No | | | | | | Control vs. 24h scrambled | -0.001122 | -0.3743 to 0.3721 | No | ns | >.999 |
| R squared | 0.3487 | | | | | | Control vs. 1h fibril | -0.08887 | -0.4621 to 0.2843 | No | ns | >.999 |
| | | | | | | | Control vs. 1h scrambled | -0.002541 | -0.3758 to 0.3707 | No | ns | >.999 |
| **Brown-Forsythe test** | | | | | | | 48h fibril vs. 48h scrambled | -0.0925 | -0.4657 to 0.2807 | No | ns | >.999 |
| F (DFn, DFd) | 0.7370 (6, 14) | | | | | | 24h fibril vs. 24h scrambled | 0.02116 | -0.3521 to 0.3944 | No | ns | >.999 |
| P value | 0.629 | | | | | | 1h fibril vs. 1h scrambled | 0.08633 | -0.2869 to 0.4595 | No | ns | >.999 |
| P value summary | ns | | | | | | | | | | | |
| Are SDs significantly different (P < 0.05)? | No | | | | | | | | | | | |
| | | | | | | | | | | | | |
| **Bartlett's test** | | | | | | | | | | | | |
| Bartlett's statistic (corrected) | | | | | | | | | | | | |
| P value | | | | | | | | | | | | |
| P value summary | | | | | | | | | | | | |
| Are SDs significantly different (P < 0.05)? | | | | | | | | | | | | |
| | | | | | | | | | | | | |
| **ANOVA table** | **SS** | **DF** | **MS** | **F (DFn, DFd)** | **P value** | | | | | | | |
| Treatment (between columns) | 0.1462 | 6 | 0.02437 | F (6, 14) = 1.249 | P=.340 | | | | | | | |
| Residual (within columns) | 0.2731 | 14 | 0.01951 | | | | | | | | | |
| Total | 0.4193 | 20 | | | | | | | | | | |

### Low damage

| ANOVA summary | | | | | | | Bonferroni's multiple comparisons test | Mean Diff. | 95.00% CI of diff. | Below threshold? | Summary | Adjusted P Value |
|---|---|---|---|---|---|---|---|---|---|---|---|---|
| F | 0.7624 | | | | | | Control vs. 48h fibril | 0.2102 | -0.7397 to 1.160 | No | ns | >.999 |
| P value | 0.611 | | | | | | Control vs. 48h scrambled | 0.2633 | -0.6866 to 1.213 | No | ns | >.999 |
| P value summary | ns | | | | | | Control vs. 24h fibril | 0.001487 | -0.9484 to 0.9514 | No | ns | >.999 |
| Significant diff. among means (P < 0.05)? | No | | | | | | Control vs. 24h scrambled | -0.0019 | -0.9518 to 0.9480 | No | ns | >.999 |
| R squared | 0.2463 | | | | | | Control vs. 1h fibril | -0.08852 | -1.038 to 0.8614 | No | ns | >.999 |
| | | | | | | | Control vs. 1h scrambled | 0.3987 | -0.5512 to 1.349 | No | ns | >.999 |
| **Brown-Forsythe test** | | | | | | | 48h fibril vs. 48h scrambled | 0.05314 | -0.8968 to 1.003 | No | ns | >.999 |
| F (DFn, DFd) | 1.920 (6, 14) | | | | | | 24h fibril vs. 24h scrambled | -0.003386 | -0.9533 to 0.9465 | No | ns | >.999 |
| P value | 0.148 | | | | | | 1h fibril vs. 1h scrambled | 0.4872 | -0.4627 to 1.437 | No | ns | >.999 |
| P value summary | ns | | | | | | | | | | | |
| Are SDs significantly different (P < 0.05)? | No | | | | | | | | | | | |
| | | | | | | | | | | | | |
| **Bartlett's test** | | | | | | | | | | | | |
| Bartlett's statistic (corrected) | | | | | | | | | | | | |
| P value | | | | | | | | | | | | |
| P value summary | | | | | | | | | | | | |
| Are SDs significantly different (P < 0.05)? | | | | | | | | | | | | |
| | | | | | | | | | | | | |
| **ANOVA table** | SS | DF | MS | F (DFn, DFd) | P value | | | | | | | |
| Treatment (between columns) | 0.5781 | 6 | 0.09635 | F (6, 14) = 0.7624 | P=.611 | | | | | | | |
| Residual (within columns) | 1.769 | 14 | 0.1264 | | | | | | | | | |
| Total | 2.347 | 20 | | | | | | | | | | |

### High damage

| ANOVA summary | | | | | | | Bonferroni's multiple comparisons test | Mean Diff. | 95.00% CI of diff. | Below threshold? | Summary | Adjusted P Value |
|---|---|---|---|---|---|---|---|---|---|---|---|---|
| F | 2.072 | | | | | | Control vs. 48h fibril | -0.7277 | -2.087 to 0.6321 | No | ns | 0.916 |
| P value | 0.123 | | | | | | Control vs. 48h scrambled | -0.8068 | -2.167 to 0.5530 | No | ns | 0.653 |
| P value summary | ns | | | | | | Control vs. 24h fibril | -0.1414 | -1.501 to 1.218 | No | ns | >.999 |
| Significant diff. among means (P < 0.05)? | No | | | | | | Control vs. 24h scrambled | 0.1791 | -1.181 to 1.539 | No | ns | >.999 |
| R squared | 0.4704 | | | | | | Control vs. 1h fibril | 0.1779 | -1.182 to 1.538 | No | ns | >.999 |
| | | | | | | | Control vs. 1h scrambled | 0.1199 | -1.240 to 1.480 | No | ns | >.999 |
| **Brown-Forsythe test** | | | | | | | 48h fibril vs. 48h scrambled | -0.07915 | -1.439 to 1.281 | No | ns | >.999 |
| F (DFn, DFd) | 0.6654 (6, 14) | | | | | | 24h fibril vs. 24h scrambled | 0.3205 | -1.039 to 1.680 | No | ns | >.999 |
| P value | 0.679 | | | | | | 1h fibril vs. 1h scrambled | -0.05808 | -1.418 to 1.302 | No | ns | >.999 |
| P value summary | ns | | | | | | | | | | | |
| Are SDs significantly different (P < 0.05)? | No | | | | | | | | | | | |
| | | | | | | | | | | | | |
| **Bartlett's test** | | | | | | | | | | | | |
| Bartlett's statistic (corrected) | | | | | | | | | | | | |
| P value | | | | | | | | | | | | |
| P value summary | | | | | | | | | | | | |
| Are SDs significantly different (P < 0.05)? | | | | | | | | | | | | |
| | | | | | | | | | | | | |
| **ANOVA table** | **SS** | **DF** | **MS** | **F (DFn, DFd)** | **P value** | | | | | | | |
| Treatment (between columns) | 3.219 | 6 | 0.5366 | F (6, 14) = 2.072 | P=.123 | | | | | | | |
| Residual (within columns) | 3.625 | 14 | 0.2589 | | | | | | | | | |
| Total | 6.845 | 20 | | | | | | | | | | |

## 4.2 Cell morphology analysis

### Mean cytoplasm region

| ANOVA summary | | | | | | | Bonferroni's multiple comparisons test | Mean Diff. | 95.00% CI of diff. | Below threshold? | Summary | Adjusted P Value |
|---|---|---|---|---|---|---|---|---|---|---|---|---|
| F | 1.958 | | | | | | Control vs. 48h fibril | 0.01175 | -0.07066 to 0.09417 | No | ns | >.999 |
| P value | 0.141 | | | | | | Control vs. 48h scrambled | 0.004159 | -0.07826 to 0.08658 | No | ns | >.999 |
| P value summary | ns | | | | | | Control vs. 24h fibril | -0.03838 | -0.1208 to 0.04404 | No | ns | >.999 |
| Significant diff. among means (P < 0.05)? | No | | | | | | Control vs. 24h scrambled | -0.008921 | -0.09134 to 0.07349 | No | ns | >.999 |
| R squared | 0.4563 | | | | | | Control vs. 1h fibril | 0.04522 | -0.03720 to 0.1276 | No | ns | 0.848 |
| | | | | | | | Control vs. 1h scrambled | 0.004781 | -0.07763 to 0.08720 | No | ns | >.999 |
| **Brown-Forsythe test** | | | | | | | 48h fibril vs. 48h scrambled | -0.007595 | -0.09001 to 0.07482 | No | ns | >.999 |
| F (DFn, DFd) | 0.8883 (6, 14) | | | | | | 24h fibril vs. 24h scrambled | 0.02946 | -0.05296 to 0.1119 | No | ns | >.999 |
| P value | 0.529 | | | | | | 1h fibril vs. 1h scrambled | -0.04044 | -0.1229 to 0.04198 | No | ns | >.999 |
| P value summary | ns | | | | | | | | | | | |
| Are SDs significantly different (P < 0.05)? | No | | | | | | | | | | | |
| | | | | | | | | | | | | |
| **Bartlett's test** | | | | | | | | | | | | |
| Bartlett's statistic (corrected) | | | | | | | | | | | | |
| P value | | | | | | | | | | | | |
| P value summary | | | | | | | | | | | | |
| Are SDs significantly different (P < 0.05)? | | | | | | | | | | | | |
| | | | | | | | | | | | | |
| **ANOVA table** | **SS** | **DF** | **MS** | **F (DFn, DFd)** | **P value** | | | | | | | |
| Treatment (between columns) | 0.01118 | 6 | 0.001863 | F (6, 14) = 1.958 | P=.141 | | | | | | | |
| Residual (within columns) | 0.01332 | 14 | 0.0009512 | | | | | | | | | |
| Total | 0.02449 | 20 | | | | | | | | | | |

### Mean cell area

| ANOVA summary | | | | | | | Bonferroni's multiple comparisons test | Mean Diff. | 95.00% CI of diff. | Below threshold? | Summary | Adjusted P Value |
|---|---|---|---|---|---|---|---|---|---|---|---|---|
| F | 2.894 | | | | | | Control vs. 48h fibril | 0.0517 | -0.07031 to 0.1737 | No | ns | >.999 |
| P value | 0.048 | | | | | | Control vs. 48h scrambled | 0.01933 | -0.1027 to 0.1413 | No | ns | >.999 |
| P value summary | * | | | | | | Control vs. 24h fibril | -0.07821 | -0.2002 to 0.04380 | No | ns | 0.491 |
| Significant diff. among means (P < 0.05)? | Yes | | | | | | Control vs. 24h scrambled | -0.006645 | -0.1287 to 0.1154 | No | ns | >.999 |
| R squared | 0.5536 | | | | | | Control vs. 1h fibril | 0.04917 | -0.07284 to 0.1712 | No | ns | >.999 |
| | | | | | | | Control vs. 1h scrambled | -0.02162 | -0.1436 to 0.1004 | No | ns | >.999 |
| **Brown-Forsythe test** | | | | | | | 48h fibril vs. 48h scrambled | -0.03237 | -0.1544 to 0.08964 | No | ns | >.999 |
| F (DFn, DFd) | 0.3733 (6, 14) | | | | | | 24h fibril vs. 24h scrambled | 0.07157 | -0.05044 to 0.1936 | No | ns | 0.68 |
| P value | 0.884 | | | | | | 1h fibril vs. 1h scrambled | -0.07079 | -0.1928 to 0.05122 | No | ns | 0.705 |
| P value summary | ns | | | | | | | | | | | |
| Are SDs significantly different (P < 0.05)? | No | | | | | | | | | | | |
| | | | | | | | | | | | | |
| **Bartlett's test** | | | | | | | | | | | | |
| Bartlett's statistic (corrected) | | | | | | | | | | | | |
| P value | | | | | | | | | | | | |
| P value summary | | | | | | | | | | | | |
| Are SDs significantly different (P < 0.05)? | | | | | | | | | | | | |
| | | | | | | | | | | | | |
| **ANOVA table** | **SS** | **DF** | **MS** | **F (DFn, DFd)** | **P value** | | | | | | | |
| Treatment (between columns) | 0.0362 | 6 | 0.006033 | F (6, 14) = 2.894 | P=.048 | | | | | | | |
| Residual (within columns) | 0.02919 | 14 | 0.002085 | | | | | | | | | |
| Total | 0.06539 | 20 | | | | | | | | | | |

### Mean cell roundness

| ANOVA summary | | | | | | | Bonferroni's multiple comparisons test | Mean Diff. | 95.00% CI of diff. | Below threshold? | Summary | Adjusted P Value |
|---|---|---|---|---|---|---|---|---|---|---|---|---|
| F | 2.189 | | | | | | Control vs. 48h fibril | 0.01404 | -0.06618 to 0.09427 | No | ns | >.999 |
| P value | 0.107 | | | | | | Control vs. 48h scrambled | -0.02117 | -0.1014 to 0.05905 | No | ns | >.999 |
| P value summary | ns | | | | | | Control vs. 24h fibril | 0.02217 | -0.05806 to 0.1024 | No | ns | >.999 |
| Significant diff. among means (P < 0.05)? | No | | | | | | Control vs. 24h scrambled | -0.01229 | -0.09251 to 0.06794 | No | ns | >.999 |
| R squared | 0.4841 | | | | | | Control vs. 1h fibril | -0.05325 | -0.1335 to 0.02697 | No | ns | 0.427 |
| | | | | | | | Control vs. 1h scrambled | -0.02544 | -0.1057 to 0.05479 | No | ns | >.999 |
| **Brown-Forsythe test** | | | | | | | 48h fibril vs. 48h scrambled | -0.03521 | -0.1154 to 0.04501 | No | ns | >.999 |
| F (DFn, DFd) | 0.7457 (6, 14) | | | | | | 24h fibril vs. 24h scrambled | -0.03445 | -0.1147 to 0.04577 | No | ns | >.999 |
| P value | 0.623 | | | | | | 1h fibril vs. 1h scrambled | 0.02781 | -0.05241 to 0.1080 | No | ns | >.999 |
| P value summary | ns | | | | | | | | | | | |
| Are SDs significantly different (P < 0.05)? | No | | | | | | | | | | | |
| | | | | | | | | | | | | |
| **Bartlett's test** | | | | | | | | | | | | |
| Bartlett's statistic (corrected) | | | | | | | | | | | | |
| P value | | | | | | | | | | | | |
| P value summary | | | | | | | | | | | | |
| Are SDs significantly different (P < 0.05)? | | | | | | | | | | | | |
| | | | | | | | | | | | | |
| **ANOVA table** | **SS** | **DF** | **MS** | **F (DFn, DFd)** | **P value** | | | | | | | |
| Treatment (between columns) | 0.01184 | 6 | 0.001973 | F (6, 14) = 2.189 | P=.107 | | | | | | | |
| Residual (within columns) | 0.01262 | 14 | 0.0009014 | | | | | | | | | |
| Total | 0.02446 | 20 | | | | | | | | | | |

## Mean cell width

| ANOVA summary | | | | | | | Bonferroni's multiple comparisons test | Mean Diff. | 95.00% CI of diff. | Below threshold? | Summary | Adjusted P Value |
|---|---|---|---|---|---|---|---|---|---|---|---|---|
| F | 3.373 | | | | | | Control vs. 48h fibril | 0.07052 | -0.01720 to 0.1582 | No | ns | 0.178 |
| P value | 0.029 | | | | | | Control vs. 48h scrambled | 0.01535 | -0.07237 to 0.1031 | No | ns | >.999 |
| P value summary | * | | | | | | Control vs. 24h fibril | -0.03741 | -0.1251 to 0.05031 | No | ns | >.999 |
| Significant diff. among means (P < 0.05)? | Yes | | | | | | Control vs. 24h scrambled | 0.00247 | -0.08525 to 0.09019 | No | ns | >.999 |
| R squared | 0.5911 | | | | | | Control vs. 1h fibril | 0.004229 | -0.08349 to 0.09195 | No | ns | >.999 |
| | | | | | | | Control vs. 1h scrambled | -0.02734 | -0.1151 to 0.06038 | No | ns | >.999 |
| **Brown-Forsythe test** | | | | | | | 48h fibril vs. 48h scrambled | -0.05518 | -0.1429 to 0.03254 | No | ns | 0.528 |
| F (DFn, DFd) | 0.5571 (6, 14) | | | | | | 24h fibril vs. 24h scrambled | 0.03988 | -0.04784 to 0.1276 | No | ns | >.999 |
| P value | 0.757 | | | | | | 1h fibril vs. 1h scrambled | -0.03157 | -0.1193 to 0.05615 | No | ns | >.999 |
| P value summary | ns | | | | | | | | | | | |
| Are SDs significantly different (P < 0.05)? | No | | | | | | | | | | | |
| | | | | | | | | | | | | |
| **Bartlett's test** | | | | | | | | | | | | |
| Bartlett's statistic (corrected) | | | | | | | | | | | | |
| P value | | | | | | | | | | | | |
| P value summary | | | | | | | | | | | | |
| Are SDs significantly different (P < 0.05)? | | | | | | | | | | | | |
| | | | | | | | | | | | | |
| **ANOVA table** | **SS** | **DF** | **MS** | **F (DFn, DFd)** | **P value** | | | | | | | |
| Treatment (between columns) | 0.02181 | 6 | 0.003635 | F (6, 14) = 3.373 | P=.029 | | | | | | | |
| Residual (within columns) | 0.01509 | 14 | 0.001078 | | | | | | | | | |
| Total | 0.0369 | 20 | | | | | | | | | | |

## Mean cell length

| ANOVA summary | | | | | | | Bonferroni's multiple comparisons test | Mean Diff. | 95.00% CI of diff. | Below threshold? | Summary | Adjusted P Value |
|---|---|---|---|---|---|---|---|---|---|---|---|---|
| F | 1.958 | | | | | | Control vs. 48h fibril | 0.01175 | -0.07066 to 0.09417 | No | ns | >.999 |
| P value | 0.141 | | | | | | Control vs. 48h scrambled | 0.004159 | -0.07826 to 0.08658 | No | ns | >.999 |
| P value summary | ns | | | | | | Control vs. 24h fibril | -0.03838 | -0.1208 to 0.04404 | No | ns | >.999 |
| Significant diff. among means (P < 0.05)? | No | | | | | | Control vs. 24h scrambled | -0.008921 | -0.09134 to 0.07349 | No | ns | >.999 |
| R squared | 0.4563 | | | | | | Control vs. 1h fibril | 0.04522 | -0.03720 to 0.1276 | No | ns | 0.848 |
| | | | | | | | Control vs. 1h scrambled | 0.004781 | -0.07763 to 0.08720 | No | ns | >.999 |
| **Brown-Forsythe test** | | | | | | | 48h fibril vs. 48h scrambled | -0.007595 | -0.09001 to 0.07482 | No | ns | >.999 |
| F (DFn, DFd) | 0.8883 (6, 14) | | | | | | 24h fibril vs. 24h scrambled | 0.02946 | -0.05296 to 0.1119 | No | ns | >.999 |
| P value | 0.529 | | | | | | 1h fibril vs. 1h scrambled | -0.04044 | -0.1229 to 0.04198 | No | ns | >.999 |
| P value summary | ns | | | | | | | | | | | |
| Are SDs significantly different (P < 0.05)? | No | | | | | | | | | | | |
| | | | | | | | | | | | | |
| **Bartlett's test** | | | | | | | | | | | | |
| Bartlett's statistic (corrected) | | | | | | | | | | | | |
| P value | | | | | | | | | | | | |
| P value summary | | | | | | | | | | | | |
| Are SDs significantly different (P < 0.05)? | | | | | | | | | | | | |
| | | | | | | | | | | | | |
| **ANOVA table** | **SS** | **DF** | **MS** | **F (DFn, DFd)** | **P value** | | | | | | | |
| Treatment (between columns) | 0.01118 | 6 | 0.001863 | F (6, 14) = 1.958 | P=.141 | | | | | | | |
| Residual (within columns) | 0.01332 | 14 | 0.0009512 | | | | | | | | | |
| Total | 0.02449 | 20 | | | | | | | | | | |

# 5. Statistical analysis of induced Astrocytes treated with $A\beta_{1-42}$

## 5.1. LDH assay analysis

**Oligomer – all cell lines**

| ANOVA summary | | | | | | | Bonferroni's multiple comparisons test | Mean Diff. | 95.00% CI of diff. | Below threshold? | Summary | Adjusted P Value |
|---|---|---|---|---|---|---|---|---|---|---|---|---|
| F | 0.6988 | | | | | | Control vs. Oligomer 48h | 0.1111 | -0.7221 to 0.9444 | No | ns | >.999 |
| P value | 0.689 | | | | | | Control vs. Scrambled 48h | -0.0561 | -0.8893 to 0.7771 | No | ns | >.999 |
| P value summary | ns | | | | | | Control vs. Oligomer 24h | -0.1041 | -0.9374 to 0.7291 | No | ns | >.999 |
| Significant diff. among means (P < 0.05)? | No | | | | | | Control vs. Scrambled 24h | 0.04892 | -0.7843 to 0.8822 | No | ns | >.999 |
| R squared | 0.237 | | | | | | Control vs. Oligomer 2h | 0.1582 | -0.6751 to 0.9914 | No | ns | >.999 |
| | | | | | | | Control vs. Scrambled 2h | -0.3365 | -1.170 to 0.4967 | No | ns | >.999 |
| **Brown-Forsythe test** | | | | | | | Control vs. Oligomer 1h | 0.00465 | -0.8286 to 0.8379 | No | ns | >.999 |
| F (DFn, DFd) | 0.6982 (8, 18) | | | | | | Control vs. Scrambled 1h | -0.1609 | -0.9941 to 0.6724 | No | ns | >.999 |
| P value | 0.689 | | | | | | Oligomer 48h vs. Scrambled 48h | -0.1672 | -1.000 to 0.6660 | No | ns | >.999 |
| P value summary | ns | | | | | | Oligomer 24h vs. Scrambled 24h | 0.153 | -0.6802 to 0.9863 | No | ns | >.999 |
| Are SDs significantly different (P < 0.05)? | No | | | | | | Oligomer 2h vs. Scrambled 2h | -0.4947 | -1.328 to 0.3385 | No | ns | 0.808 |
| | | | | | | | Oligomer 1h vs. Scrambled 1h | -0.1655 | -0.9987 to 0.6677 | No | ns | >.999 |
| **Bartlett's test** | | | | | | | | | | | | |
| Bartlett's statistic (corrected) | | | | | | | | | | | | |
| P value | | | | | | | | | | | | |
| P value summary | | | | | | | | | | | | |
| Are SDs significantly different (P < 0.05)? | | | | | | | | | | | | |
| | | | | | | | | | | | | |
| **ANOVA table** | SS | DF | MS | F (DFn, DFd) | P value | | | | | | | |
| Treatment (between columns) | 0.5414 | 8 | 0.06767 | F (8, 18) = 0.6988 | P=.689 | | | | | | | |
| Residual (within columns) | 1.743 | 18 | 0.09684 | | | | | | | | | |
| Total | 2.284 | 26 | | | | | | | | | | |

**Oligomer – 155v2**

| ANOVA summary | | | | | | | Bonferroni's multiple comparisons test | Mean Diff. | 95.00% CI of diff. | Below threshold? | Summary | Adjusted P Value |
|---|---|---|---|---|---|---|---|---|---|---|---|---|
| F | 6.25 | | | | | | Control vs. Oligomer 48h | -0.008858 | -0.8549 to 0.8372 | No | ns | >.999 |
| P value | <.001 | | | | | | Control vs. Scrambled 48h | -0.268 | -1.114 to 0.5781 | No | ns | >.999 |
| P value summary | *** | | | | | | Control vs. Oligomer 24h | -0.1003 | -0.9463 to 0.7458 | No | ns | >.999 |
| Significant diff. among means (P < 0.05)? | Yes | | | | | | Control vs. Scrambled 24h | 0.0158 | -0.8302 to 0.8618 | No | ns | >.999 |
| R squared | 0.7353 | | | | | | Control vs. Oligomer 2h | 0.6754 | -0.1706 to 1.521 | No | ns | 0.209 |
| | | | | | | | Control vs. Scrambled 2h | -0.9056 | -1.752 to -0.05959 | Yes | * | 0.03 |
| **Brown-Forsythe test** | | | | | | | Control vs. Oligomer 1h | -0.4116 | -1.258 to 0.4344 | No | ns | >.999 |
| F (DFn, DFd) | 0.9073 (8, 18) | | | | | | Control vs. Scrambled 1h | -0.6681 | -1.514 to 0.1779 | No | ns | 0.222 |
| P value | 0.532 | | | | | | Oligomer 48h vs. Scrambled 48h | -0.2591 | -1.105 to 0.5869 | No | ns | >.999 |
| P value summary | ns | | | | | | Oligomer 24h vs. Scrambled 24h | 0.1161 | -0.7300 to 0.9621 | No | ns | >.999 |
| Are SDs significantly different (P < 0.05)? | No | | | | | | Oligomer 2h vs. Scrambled 2h | -1.581 | -2.427 to -0.7350 | Yes | *** | <.001 |
| | | | | | | | Oligomer 1h vs. Scrambled 1h | -0.2565 | -1.103 to 0.5895 | No | ns | >.999 |
| **Bartlett's test** | | | | | | | | | | | | |
| Bartlett's statistic (corrected) | | | | | | | | | | | | |
| P value | | | | | | | | | | | | |
| P value summary | | | | | | | | | | | | |
| Are SDs significantly different (P < 0.05)? | | | | | | | | | | | | |
| | | | | | | | | | | | | |
| **ANOVA table** | **SS** | **DF** | **MS** | **F (DFn, DFd)** | **P value** | | | | | | | |
| Treatment (between columns) | 4.992 | 8 | 0.624 | F (8, 18) = 6.250 | P<.001 | | | | | | | |
| Residual (within columns) | 1.797 | 18 | 0.09984 | | | | | | | | | |
| Total | 6.789 | 26 | | | | | | | | | | |

## Oligomer – CS-14

| ANOVA summary | | | | | | Bonferroni's multiple comparisons test | Mean Diff. | 95.00% CI of diff. | Below threshold? | Summary | Adjusted P Value |
|---|---|---|---|---|---|---|---|---|---|---|---|
| F | 0.3983 | | | | | Control vs. Oligomer 48h | 0.2192 | -0.7531 to 1.191 | No | ns | >.999 |
| P value | 0.907 | | | | | Control vs. Scrambled 48h | -0.04934 | -1.022 to 0.9229 | No | ns | >.999 |
| P value summary | ns | | | | | Control vs. Oligomer 24h | -0.1171 | -1.089 to 0.8551 | No | ns | >.999 |
| Significant diff. among means (P < 0.05)? | No | | | | | Control vs. Scrambled 24h | 0.1918 | -0.7804 to 1.164 | No | ns | >.999 |
| R squared | 0.1504 | | | | | Control vs. Oligomer 2h | -0.1127 | -1.085 to 0.8596 | No | ns | >.999 |
| | | | | | | Control vs. Scrambled 2h | 0.02107 | -0.9512 to 0.9933 | No | ns | >.999 |
| **Brown-Forsythe test** | | | | | | Control vs. Oligomer 1h | 0.1717 | -0.8005 to 1.144 | No | ns | >.999 |
| F (DFn, DFd) | 0.9783 (8, 18) | | | | | Control vs. Scrambled 1h | -0.0633 | -1.036 to 0.9090 | No | ns | >.999 |
| P value | 0.483 | | | | | Oligomer 48h vs. Scrambled 48h | -0.2685 | -1.241 to 0.7038 | No | ns | >.999 |
| P value summary | ns | | | | | Oligomer 24h vs. Scrambled 24h | 0.3089 | -0.6633 to 1.281 | No | ns | >.999 |
| Are SDs significantly different (P < 0.05)? | No | | | | | Oligomer 2h vs. Scrambled 2h | 0.1337 | -0.8385 to 1.106 | No | ns | >.999 |
| | | | | | | Oligomer 1h vs. Scrambled 1h | -0.235 | -1.207 to 0.7372 | No | ns | >.999 |
| **Bartlett's test** | | | | | | | | | | | |
| Bartlett's statistic (corrected) | | | | | | | | | | | |
| P value | | | | | | | | | | | |
| P value summary | | | | | | | | | | | |
| Are SDs significantly different (P < 0.05)? | | | | | | | | | | | |
| | | | | | | | | | | | |
| **ANOVA table** | **SS** | **DF** | **MS** | **F (DFn, DFd)** | **P value** | | | | | | |
| Treatment (between columns) | 0.4201 | 8 | 0.05251 | F (8, 18) = 0.3983 | P=.907 | | | | | | |
| Residual (within columns) | 2.373 | 18 | 0.1318 | | | | | | | | |
| Total | 2.793 | 26 | | | | | | | | | |

## Oligomer – 161

| ANOVA summary | | | | | | Bonferroni's multiple comparisons test | Mean Diff. | 95.00% CI of diff. | Below threshold? | Summary | Adjusted P Value |
|---|---|---|---|---|---|---|---|---|---|---|---|
| F | 4.025 | | | | | Control vs. Oligomer 48h | 0.1231 | -0.2251 to 0.4714 | No | ns | >.999 |
| P value | 0.007 | | | | | Control vs. Scrambled 48h | 0.149 | -0.1993 to 0.4972 | No | ns | >.999 |
| P value summary | ** | | | | | Control vs. Oligomer 24h | -0.09496 | -0.4432 to 0.2533 | No | ns | >.999 |
| Significant diff. among means (P < 0.05)? | Yes | | | | | Control vs. Scrambled 24h | -0.06086 | -0.4091 to 0.2874 | No | ns | >.999 |
| R squared | 0.6414 | | | | | Control vs. Oligomer 2h | -0.08822 | -0.4365 to 0.2600 | No | ns | >.999 |
| | | | | | | Control vs. Scrambled 2h | -0.125 | -0.4733 to 0.2232 | No | ns | >.999 |
| **Brown-Forsythe test** | | | | | | Control vs. Oligomer 1h | 0.2538 | -0.09444 to 0.6021 | No | ns | 0.336 |
| F (DFn, DFd) | 1.420 (8, 18) | | | | | Control vs. Scrambled 1h | 0.2489 | -0.09940 to 0.5971 | No | ns | 0.37 |
| P value | 0.254 | | | | | Oligomer 48h vs. Scrambled 48h | 0.02586 | -0.3224 to 0.3741 | No | ns | >.999 |
| P value summary | ns | | | | | Oligomer 24h vs. Scrambled 24h | 0.0341 | -0.3142 to 0.3824 | No | ns | >.999 |
| Are SDs significantly different (P < 0.05)? | No | | | | | Oligomer 2h vs. Scrambled 2h | -0.03682 | -0.3851 to 0.3114 | No | ns | >.999 |
| | | | | | | Oligomer 1h vs. Scrambled 1h | -0.004959 | -0.3532 to 0.3433 | No | ns | >.999 |
| **Bartlett's test** | | | | | | | | | | | |
| Bartlett's statistic (corrected) | | | | | | | | | | | |
| P value | | | | | | | | | | | |
| P value summary | | | | | | | | | | | |
| Are SDs significantly different (P < 0.05)? | | | | | | | | | | | |
| | | | | | | | | | | | |
| **ANOVA table** | **SS** | **DF** | **MS** | **F (DFn, DFd)** | **P value** | | | | | | |
| Treatment (between columns) | 0.5447 | 8 | 0.06809 | F (8, 18) = 4.025 | P=.007 | | | | | | |
| Residual (within columns) | 0.3045 | 18 | 0.01692 | | | | | | | | |
| Total | 0.8492 | 26 | | | | | | | | | |

## Fibrils – all cell lines

| ANOVA summary | | | | | | Bonferroni's multiple comparisons test | Mean Diff. | 95.00% CI of diff. | Below threshold? | Summary | Adjusted P Value |
|---|---|---|---|---|---|---|---|---|---|---|---|
| F | 1.13 | | | | | Control vs. 48h Fibril | -0.06702 | -0.4954 to 0.3613 | No | ns | >.999 |
| P value | 0.39 | | | | | Control vs. 48h Scrambled | -0.07525 | -0.5036 to 0.3531 | No | ns | >.999 |
| P value summary | ns | | | | | Control vs. 24h Fibril | 0.06919 | -0.3592 to 0.4975 | No | ns | >.999 |
| Significant diff. among means (P < 0.05)? | No | | | | | Control vs. 24h Scrambled | -0.1091 | -0.5375 to 0.3192 | No | ns | >.999 |
| R squared | 0.3342 | | | | | Control vs. 2h Fibril | 0.001745 | -0.4266 to 0.4301 | No | ns | >.999 |
| | | | | | | Control vs. 2h Scrambled | 0.005028 | -0.4233 to 0.4334 | No | ns | >.999 |
| **Brown-Forsythe test** | | | | | | Control vs. 1h Fibril | 0.2233 | -0.2050 to 0.6517 | No | ns | >.999 |
| F (DFn, DFd) | 0.7178 (8, 18) | | | | | Control vs. 1h Scrambled | 0.03263 | -0.3957 to 0.4610 | No | ns | >.999 |
| P value | 0.674 | | | | | 48h Fibril vs. 48h Scrambled | -0.008234 | -0.4366 to 0.4201 | No | ns | >.999 |
| P value summary | ns | | | | | 24h Fibril vs. 24h Scrambled | -0.1783 | -0.6067 to 0.2500 | No | ns | >.999 |
| Are SDs significantly different (P < 0.05)? | No | | | | | 2h Fibril vs. 2h Scrambled | 0.003283 | -0.4251 to 0.4316 | No | ns | >.999 |
| | | | | | | 1h Fibril vs. 1h Scrambled | -0.1907 | -0.6190 to 0.2377 | No | ns | >.999 |
| **Bartlett's test** | | | | | | | | | | | |
| Bartlett's statistic (corrected) | | | | | | | | | | | |
| P value | | | | | | | | | | | |
| P value summary | | | | | | | | | | | |
| Are SDs significantly different (P < 0.05)? | | | | | | | | | | | |
| | | | | | | | | | | | |
| **ANOVA table** | **SS** | **DF** | **MS** | **F (DFn, DFd)** | **P value** | | | | | | |
| Treatment (between columns) | 0.2313 | 8 | 0.02891 | F (8, 18) = 1.130 | P=.390 | | | | | | |
| Residual (within columns) | 0.4607 | 18 | 0.02559 | | | | | | | | |
| Total | 0.6919 | 26 | | | | | | | | | |

## Fibrils – 155v2

| ANOVA summary | | | | | | Bonferroni's multiple comparisons test | Mean Diff. | 95.00% CI of diff. | Below threshold? | Summary | Adjusted P Value |
|---|---|---|---|---|---|---|---|---|---|---|---|
| F | 11.53 | | | | | Control vs. 48h Fibril | -0.185 | -0.5246 to 0.1546 | No | ns | >.999 |
| P value | <.001 | | | | | Control vs. 48h Scrambled | -0.2909 | -0.6305 to 0.04867 | No | ns | 0.139 |
| P value summary | *** | | | | | Control vs. 24h Fibril | 0.1099 | -0.2297 to 0.4495 | No | ns | >.999 |
| Significant diff. among means (P < 0.05)? | Yes | | | | | Control vs. 24h Scrambled | -0.2544 | -0.5940 to 0.08516 | No | ns | 0.293 |
| R squared | 0.8367 | | | | | Control vs. 2h Fibril | 0.03141 | -0.3082 to 0.3710 | No | ns | >.999 |
| | | | | | | Control vs. 2h Scrambled | 0.0214 | -0.3182 to 0.3610 | No | ns | >.999 |
| **Brown-Forsythe test** | | | | | | Control vs. 1h Fibril | 0.4848 | 0.1453 to 0.8244 | Yes | ** | 0.002 |
| F (DFn, DFd) | 0.7156 (8, 18) | | | | | Control vs. 1h Scrambled | 0.2565 | -0.08311 to 0.5960 | No | ns | 0.281 |
| P value | 0.676 | | | | | 48h Fibril vs. 48h Scrambled | -0.1059 | -0.4455 to 0.2337 | No | ns | >.999 |
| P value summary | ns | | | | | 24h Fibril vs. 24h Scrambled | -0.3643 | -0.7039 to -0.02472 | Yes | * | 0.029 |
| Are SDs significantly different (P < 0.05)? | No | | | | | 2h Fibril vs. 2h Scrambled | -0.01001 | -0.3496 to 0.3296 | No | ns | >.999 |
| | | | | | | 1h Fibril vs. 1h Scrambled | -0.2284 | -0.5680 to 0.1112 | No | ns | 0.488 |
| **Bartlett's test** | | | | | | | | | | | |
| Bartlett's statistic (corrected) | | | | | | | | | | | |
| P value | | | | | | | | | | | |
| P value summary | | | | | | | | | | | |
| Are SDs significantly different (P < 0.05)? | | | | | | | | | | | |
| | | | | | | | | | | | |
| **ANOVA table** | **SS** | **DF** | **MS** | **F (DFn, DFd)** | **P value** | | | | | | |
| Treatment (between columns) | 1.484 | 8 | 0.1855 | F (8, 18) = 11.53 | P<.001 | | | | | | |
| Residual (within columns) | 0.2895 | 18 | 0.01608 | | | | | | | | |
| Total | 1.773 | 26 | | | | | | | | | |

## Fibrils – CS-14

| ANOVA summary | | | | | | Bonferroni's multiple comparisons test | Mean Diff. | 95.00% CI of diff. | Below threshold? | Summary | Adjusted P Value |
|---|---|---|---|---|---|---|---|---|---|---|---|
| F | 0.2711 | | | | | Control vs. 48h Fibril | 0.08433 | -0.8769 to 1.046 | No | ns | >.999 |
| P value | 0.967 | | | | | Control vs. 48h Scrambled | 0.02742 | -0.9338 to 0.9887 | No | ns | >.999 |
| P value summary | ns | | | | | Control vs. 24h Fibril | 0.1172 | -0.8441 to 1.078 | No | ns | >.999 |
| Significant diff. among means (P < 0.05)? | No | | | | | Control vs. 24h Scrambled | 0.09171 | -0.8696 to 1.053 | No | ns | >.999 |
| R squared | 0.1075 | | | | | Control vs. 2h Fibril | -0.009913 | -0.9712 to 0.9514 | No | ns | >.999 |
| | | | | | | Control vs. 2h Scrambled | 0.05441 | -0.9069 to 1.016 | No | ns | >.999 |
| **Brown-Forsythe test** | | | | | | Control vs. 1h Fibril | 0.3052 | -0.6561 to 1.266 | No | ns | >.999 |
| F (DFn, DFd) | 1.722 (8, 18) | | | | | Control vs. 1h Scrambled | -0.07755 | -1.039 to 0.8837 | No | ns | >.999 |
| P value | 0.161 | | | | | 48h Fibril vs. 48h Scrambled | -0.05692 | -1.018 to 0.9044 | No | ns | >.999 |
| P value summary | ns | | | | | 24h Fibril vs. 24h Scrambled | -0.02548 | -0.9867 to 0.9358 | No | ns | >.999 |
| Are SDs significantly different (P < 0.05)? | No | | | | | 2h Fibril vs. 2h Scrambled | 0.06433 | -0.8969 to 1.026 | No | ns | >.999 |
| | | | | | | 1h Fibril vs. 1h Scrambled | -0.3827 | -1.344 to 0.5785 | No | ns | >.999 |
| **Bartlett's test** | | | | | | | | | | | |
| Bartlett's statistic (corrected) | | | | | | | | | | | |
| P value | | | | | | | | | | | |
| P value summary | | | | | | | | | | | |
| Are SDs significantly different (P < 0.05)? | | | | | | | | | | | |
| | | | | | | | | | | | |
| **ANOVA table** | **SS** | **DF** | **MS** | **F (DFn, DFd)** | **P value** | | | | | | |
| Treatment (between columns) | 0.2795 | 8 | 0.03494 | F (8, 18) = 0.2711 | P=.967 | | | | | | |
| Residual (within columns) | 2.32 | 18 | 0.1289 | | | | | | | | |
| Total | 2.599 | 26 | | | | | | | | | |

## Fibrils – 161

| ANOVA summary | | | | | | Bonferroni's multiple comparisons test | Mean Diff. | 95.00% CI of diff. | Below threshold? | Summary | Adjusted P Value |
|---|---|---|---|---|---|---|---|---|---|---|---|
| F | 2.629 | | | | | Control vs. 48h Fibril | -0.185 | -0.4592 to 0.08917 | No | ns | 0.481 |
| P value | 0.042 | | | | | Control vs. 48h Scrambled | -0.2909 | -0.5651 to -0.01673 | Yes | * | 0.032 |
| P value summary | * | | | | | Control vs. 24h Fibril | -0.0195 | -0.2937 to 0.2547 | No | ns | >.999 |
| Significant diff. among means (P < 0.05)? | Yes | | | | | Control vs. 24h Scrambled | -0.1647 | -0.4389 to 0.1095 | No | ns | 0.773 |
| R squared | 0.5388 | | | | | Control vs. 2h Fibril | -0.01626 | -0.2904 to 0.2579 | No | ns | >.999 |
| | | | | | | Control vs. 2h Scrambled | -0.06072 | -0.3349 to 0.2134 | No | ns | >.999 |
| **Brown-Forsythe test** | | | | | | Control vs. 1h Fibril | -0.1201 | -0.3943 to 0.1541 | No | ns | >.999 |
| F (DFn, DFd) | 1.105 (8, 18) | | | | | Control vs. 1h Scrambled | -0.08101 | -0.3552 to 0.1932 | No | ns | >.999 |
| P value | 0.405 | | | | | 48h Fibril vs. 48h Scrambled | -0.1059 | -0.3801 to 0.1683 | No | ns | >.999 |
| P value summary | ns | | | | | 24h Fibril vs. 24h Scrambled | -0.1452 | -0.4194 to 0.1290 | No | ns | >.999 |
| Are SDs significantly different (P < 0.05)? | No | | | | | 2h Fibril vs. 2h Scrambled | -0.04447 | -0.3186 to 0.2297 | No | ns | >.999 |
| | | | | | | 1h Fibril vs. 1h Scrambled | 0.03909 | -0.2351 to 0.3133 | No | ns | >.999 |
| **Bartlett's test** | | | | | | | | | | | |
| Bartlett's statistic (corrected) | | | | | | | | | | | |
| P value | | | | | | | | | | | |
| P value summary | | | | | | | | | | | |
| Are SDs significantly different (P < 0.05)? | | | | | | | | | | | |
| | | | | | | | | | | | |
| **ANOVA table** | SS | DF | MS | F (DFn, DFd) | P value | | | | | | |
| Treatment (between columns) | 0.2205 | 8 | 0.02756 | F (8, 18) = 2.629 | P=.042 | | | | | | |
| Residual (within columns) | 0.1887 | 18 | 0.01048 | | | | | | | | |
| Total | 0.4092 | 26 | | | | | | | | | |

## 5.2 iAstrocyte ICC analysis as a response to $A\beta_{1-42}$ oligomers

**155v2– 1h**

All damage

| ANOVA summary | | | | | |
|---|---|---|---|---|---|
| F | 7.141 | | | | |
| P value | 0.026 | | | | |
| P value summary | * | | | | |
| Significant diff. among means (P < 0.05)? | Yes | | | | |
| R squared | 0.7042 | | | | |
| | | | | | |
| **Bonferroni's multiple comparisons test** | **Mean Diff.** | **95.00% CI of diff.** | **Below threshold?** | **Summary** | **Adjusted P Value** |
| Control vs. Oligomer | 0.2298 | -0.08351 to 0.5431 | No | ns | 0.157 |
| Control vs. Scrambled | -0.1253 | -0.4386 to 0.1881 | No | ns | 0.71 |
| Oligomer vs. Scrambled | -0.3551 | -0.6684 to -0.04176 | Yes | * | 0.029 |

Low damage

| ANOVA summary | | | | | |
|---|---|---|---|---|---|
| F | 2.798 | | | | |
| P value | 0.139 | | | | |
| P value summary | ns | | | | |
| Significant diff. among means (P < 0.05)? | No | | | | |
| R squared | 0.4826 | | | | |
| | | | | | |
| **Bonferroni's multiple comparisons test** | **Mean Diff.** | **95.00% CI of diff.** | **Below threshold?** | **Summary** | **Adjusted P Value** |
| Control vs. Oligomer | -0.02055 | -0.05906 to 0.01797 | No | ns | 0.39 |
| Control vs. Scrambled | 0.005838 | -0.03268 to 0.04436 | No | ns | >.999 |
| Oligomer vs. Scrambled | 0.02638 | -0.01213 to 0.06490 | No | ns | 0.196 |

**CS14– 1h**

High damage

| ANOVA summary | | | | | |
|---|---|---|---|---|---|
| F | 0.7817 | | | | |
| P value | 0.499 | | | | |
| P value summary | ns | | | | |
| Significant diff. among means (P < 0.05)? | No | | | | |
| R squared | 0.2067 | | | | |
| | | | | | |
| **Bonferroni's multiple comparisons test** | **Mean Diff.** | **95.00% CI of diff.** | **Below threshold?** | **Summary** | **Adjusted P Value** |
| Control vs. Oligomer | 0.03661 | -0.07835 to 0.1516 | No | ns | >.999 |
| Control vs. Scrambled | -0.002394 | -0.1174 to 0.1126 | No | ns | >.999 |
| Oligomer vs. Scrambled | -0.03901 | -0.1540 to 0.07595 | No | ns | 0.922 |

**CS14– 1h**

All damage

| ANOVA summary | | | | | |
|---|---|---|---|---|---|
| F | 0.3259 | | | | |
| P value | 0.734 | | | | |
| P value summary | ns | | | | |
| Significant diff. among means (P < 0.05)? | No | | | | |
| R squared | 0.09798 | | | | |
| | | | | | |
| **Bonferroni's multiple comparisons test** | **Mean Diff.** | **95.00% CI of diff.** | **Below threshold?** | **Summary** | **Adjusted P Value** |
| Control vs. Oligomer | 0.006162 | -0.04081 to 0.05314 | No | ns | >.999 |
| Control vs. Scrambled | -0.005365 | -0.05234 to 0.04161 | No | ns | >.999 |
| Oligomer vs. Scrambled | -0.01153 | -0.05850 to 0.03545 | No | ns | >.999 |

Low damage

| ANOVA summary | | | | | |
|---|---|---|---|---|---|
| F | 0.3306 | | | | |
| P value | 0.731 | | | | |
| P value summary | ns | | | | |
| Significant diff. among means (P < 0.05)? | No | | | | |
| R squared | 0.09925 | | | | |
| | | | | | |
| **Bonferroni's multiple comparisons test** | **Mean Diff.** | **95.00% CI of diff.** | **Below threshold?** | **Summary** | **Adjusted P Value** |
| Control vs. Oligomer | -0.2781 | -3.479 to 2.923 | No | ns | >.999 |
| Control vs. Scrambled | 0.503 | -2.698 to 3.704 | No | ns | >.999 |
| Oligomer vs. Scrambled | 0.7811 | -2.420 to 3.982 | No | ns | >.999 |

High damage

| ANOVA summary | | | | | |
|---|---|---|---|---|---|
| F | 0.6151 | | | | |
| P value | 0.597 | | | | |
| P value summary | ns | | | | |
| Significant diff. among means (P < 0.05)? | No | | | | |
| R squared | 0.2908 | | | | |
| | | | | | |
| **Bonferroni's multiple comparisons test** | **Mean Diff.** | **95.00% CI of diff.** | **Below threshold?** | **Summary** | **Adjusted P Value** |
| Control vs. Oligomer | -0.7145 | -7.642 to 6.213 | No | ns | >.999 |
| Control vs. Scrambled | -1.58 | -8.507 to 5.348 | No | ns | >.999 |
| Oligomer vs. Scrambled | -0.8652 | -7.793 to 6.063 | No | ns | >.999 |

## All cell lines– 1h

### All damage

| ANOVA summary | | | | | |
|---|---|---|---|---|---|
| F | 1.608 | | | | |
| P value | 0.335 | | | | |
| P value summary | ns | | | | |
| Significant diff. among means (P < 0.05)? | No | | | | |
| R squared | 0.5174 | | | | |
| | | | | | |
| **Bonferroni's multiple comparisons test** | **Mean Diff.** | **95.00% CI of diff.** | **Below threshold?** | **Summary** | **Adjusted P Value** |
| Control vs. Oligomer | 0.118 | -0.3852 to 0.6211 | No | ns | >.999 |
| Control vs. Scrambled | -0.06532 | -0.5685 to 0.4378 | No | ns | >.999 |
| Oligomer vs. Scrambled | -0.1833 | -0.6865 to 0.3199 | No | ns | 0.525 |

### Low damage

| ANOVA summary | | | | | |
|---|---|---|---|---|---|
| F | 1.595 | | | | |
| P value | 0.337 | | | | |
| P value summary | ns | | | | |
| Significant diff. among means (P < 0.05)? | No | | | | |
| R squared | 0.5154 | | | | |
| | | | | | |
| **Bonferroni's multiple comparisons test** | **Mean Diff.** | **95.00% CI of diff.** | **Below threshold?** | **Summary** | **Adjusted P Value** |
| Control vs. Oligomer | -0.1493 | -1.259 to 0.9608 | No | ns | >.999 |
| Control vs. Scrambled | 0.2544 | -0.8557 to 1.365 | No | ns | >.999 |
| Oligomer vs. Scrambled | 0.4037 | -0.7064 to 1.514 | No | ns | 0.527 |

### High damage

| ANOVA summary | | | | | |
|---|---|---|---|---|---|
| F | 0.4418 | | | | |
| P value | 0.662 | | | | |
| P value summary | ns | | | | |
| Significant diff. among means (P < 0.05)? | No | | | | |
| R squared | 0.1284 | | | | |
| | | | | | |
| **Bonferroni's multiple comparisons test** | **Mean Diff.** | **95.00% CI of diff.** | **Below threshold?** | **Summary** | **Adjusted P Value** |
| Control vs. Oligomer | -0.8979 | -4.110 to 2.315 | No | ns | >.999 |
| Control vs. Scrambled | -0.2809 | -3.494 to 2.932 | No | ns | >.999 |
| Oligomer vs. Scrambled | 0.6169 | -2.596 to 3.830 | No | ns | >.999 |

**155v2– 2h**

All damage

| ANOVA summary | | | | | |
|---|---|---|---|---|---|
| F | 0.7312 | | | | |
| P value | 0.52 | | | | |
| P value summary | ns | | | | |
| Significant diff. among means (P < 0.05)? | No | | | | |
| R squared | 0.196 | | | | |
| | | | | | |
| **Bonferroni's multiple comparisons test** | **Mean Diff.** | **95.00% CI of diff.** | **Below threshold?** | **Summary** | **Adjusted P Value** |
| Control vs. Oligomer | 0.05135 | -0.3247 to 0.4274 | No | ns | >.999 |
| Control vs. Scrambled | 0.1369 | -0.2391 to 0.5129 | No | ns | 0.829 |
| Oligomer vs. Scrambled | 0.08555 | -0.2905 to 0.4616 | No | ns | >.999 |

Low damage

| ANOVA summary | | | | | |
|---|---|---|---|---|---|
| F | 0.5794 | | | | |
| P value | 0.589 | | | | |
| P value summary | ns | | | | |
| Significant diff. among means (P < 0.05)? | No | | | | |
| R squared | 0.1619 | | | | |
| | | | | | |
| **Bonferroni's multiple comparisons test** | **Mean Diff.** | **95.00% CI of diff.** | **Below threshold?** | **Summary** | **Adjusted P Value** |
| Control vs. Oligomer | 0.01804 | -0.03879 to 0.07486 | No | ns | >.999 |
| Control vs. Scrambled | 0.00505 | -0.05178 to 0.06188 | No | ns | >.999 |
| Oligomer vs. Scrambled | -0.01298 | -0.06981 to 0.04384 | No | ns | >.999 |

High damage

| ANOVA summary | | | | | |
|---|---|---|---|---|---|
| F | 0.1071 | | | | |
| P value | 0.9 | | | | |
| P value summary | ns | | | | |
| Significant diff. among means (P < 0.05)? | No | | | | |
| R squared | 0.03446 | | | | |
| | | | | | |
| **Bonferroni's multiple comparisons test** | **Mean Diff.** | **95.00% CI of diff.** | **Below threshold?** | **Summary** | **Adjusted P Value** |
| Control vs. Oligomer | 0.004529 | -0.07555 to 0.08461 | No | ns | >.999 |
| Control vs. Scrambled | 0.0112 | -0.06888 to 0.09128 | No | ns | >.999 |
| Oligomer vs. Scrambled | 0.006674 | -0.07341 to 0.08675 | No | ns | >.999 |

## CS14– 2h

### All damage

| ANOVA summary | | | | | |
|---|---|---|---|---|---|
| F | 0.8924 | | | | |
| P value | 0.458 | | | | |
| P value summary | ns | | | | |
| Significant diff. among means (P < 0.05)? | No | | | | |
| R squared | 0.2293 | | | | |
| | | | | | |
| **Bonferroni's multiple comparisons test** | **Mean Diff.** | **95.00% CI of diff.** | **Below threshold?** | **Summary** | **Adjusted P Value** |
| Control vs. Oligomer | -0.000331 | -0.01724 to 0.01658 | No | ns | >.999 |
| Control vs. Scrambled | -0.00611 | -0.02302 to 0.01080 | No | ns | 0.839 |
| Oligomer vs. Scrambled | -0.005779 | -0.02269 to 0.01113 | No | ns | 0.913 |

### Low damage

| ANOVA summary | | | | | |
|---|---|---|---|---|---|
| F | 1.845 | | | | |
| P value | 0.237 | | | | |
| P value summary | ns | | | | |
| Significant diff. among means (P < 0.05)? | No | | | | |
| R squared | 0.3809 | | | | |
| | | | | | |
| **Bonferroni's multiple comparisons test** | **Mean Diff.** | **95.00% CI of diff.** | **Below threshold?** | **Summary** | **Adjusted P Value** |
| Control vs. Oligomer | -0.2067 | -1.291 to 0.8780 | No | ns | >.999 |
| Control vs. Scrambled | 0.4156 | -0.6691 to 1.500 | No | ns | 0.764 |
| Oligomer vs. Scrambled | 0.6223 | -0.4624 to 1.707 | No | ns | 0.325 |

## All cell lines– 2h

### High damage

| ANOVA summary | | | | | |
|---|---|---|---|---|---|
| F | 0.7001 | | | | |
| P value | 0.563 | | | | |
| P value summary | ns | | | | |
| Significant diff. among means (P < 0.05)? | No | | | | |
| R squared | 0.3182 | | | | |
| | | | | | |
| **Bonferroni's multiple comparisons test** | **Mean Diff.** | **95.00% CI of diff.** | **Below threshold?** | **Summary** | **Adjusted P Value** |
| Control vs. Oligomer | -0.4467 | -2.327 to 1.434 | No | ns | 0.997 |
| Control vs. Scrambled | -0.1349 | -2.015 to 1.746 | No | ns | >.999 |
| Oligomer vs. Scrambled | 0.3118 | -1.569 to 2.192 | No | ns | >.999 |

## All cell lines– 2h

### All damage

| ANOVA summary | | | | | |
|---|---|---|---|---|---|
| F | 0.5638 | | | | |
| P value | 0.62 | | | | |
| P value summary | ns | | | | |
| Significant diff. among means (P < 0.05)? | No | | | | |
| R squared | 0.2732 | | | | |
| | | | | | |
| **Bonferroni's multiple comparisons test** | **Mean Diff.** | **95.00% CI of diff.** | **Below threshold?** | **Summary** | **Adjusted P Value** |
| Control vs. Oligomer | 0.02551 | -0.2760 to 0.3270 | No | ns | >.999 |
| Control vs. Scrambled | 0.0654 | -0.2361 to 0.3669 | No | ns | >.999 |
| Oligomer vs. Scrambled | 0.03989 | -0.2616 to 0.3414 | No | ns | >.999 |

### Low damage

| ANOVA summary | | | | | |
|---|---|---|---|---|---|
| F | 1.333 | | | | |
| P value | 0.385 | | | | |
| P value summary | ns | | | | |
| Significant diff. among means (P < 0.05)? | No | | | | |
| R squared | 0.4704 | | | | |
| | | | | | |
| **Bonferroni's multiple comparisons test** | **Mean Diff.** | **95.00% CI of diff.** | **Below threshold?** | **Summary** | **Adjusted P Value** |
| Control vs. Oligomer | -0.09432 | -1.022 to 0.8336 | No | ns | >.999 |
| Control vs. Scrambled | 0.2103 | -0.7176 to 1.138 | No | ns | >.999 |
| Oligomer vs. Scrambled | 0.3046 | -0.6233 to 1.233 | No | ns | 0.627 |

## 155v2– 24h

### High damage

| ANOVA summary | | | | | |
|---|---|---|---|---|---|
| F | 1.017 | | | | |
| P value | 0.417 | | | | |
| P value summary | ns | | | | |
| Significant diff. among means (P < 0.05)? | No | | | | |
| R squared | 0.2531 | | | | |
| | | | | | |
| **Bonferroni's multiple comparisons test** | **Mean Diff.** | **95.00% CI of diff.** | **Below threshold?** | **Summary** | **Adjusted P Value** |
| Control vs. Oligomer | 0.4416 | -0.7700 to 1.653 | No | ns | 0.828 |
| Control vs. Scrambled | 0.4675 | -0.7441 to 1.679 | No | ns | 0.755 |
| Oligomer vs. Scrambled | 0.02588 | -1.186 to 1.237 | No | ns | >.999 |

**155v2– 24h**

All damage

| ANOVA summary | | | | | |
|---|---|---|---|---|---|
| F | 8.248 | | | | |
| P value | 0.019 | | | | |
| P value summary | * | | | | |
| Significant diff. among means (P < 0.05)? | Yes | | | | |
| R squared | 0.7333 | | | | |
| | | | | | |
| **Bonferroni's multiple comparisons test** | **Mean Diff.** | **95.00% CI of diff.** | **Below threshold?** | **Summary** | **Adjusted P Value** |
| Control vs. Oligomer | 0.381 | 0.05995 to 0.7021 | Yes | * | 0.024 |
| Control vs. Scrambled | 0.09498 | -0.2261 to 0.4161 | No | ns | >.999 |
| Oligomer vs. Scrambled | -0.2861 | -0.6071 to 0.03504 | No | ns | 0.079 |

Low damage

| ANOVA summary | | | | | |
|---|---|---|---|---|---|
| F | 8.117 | | | | |
| P value | 0.02 | | | | |
| P value summary | * | | | | |
| Significant diff. among means (P < 0.05)? | Yes | | | | |
| R squared | 0.7302 | | | | |
| | | | | | |
| **Bonferroni's multiple comparisons test** | **Mean Diff.** | **95.00% CI of diff.** | **Below threshold?** | **Summary** | **Adjusted P Value** |
| Control vs. Oligomer | -0.05901 | -0.1133 to -0.004761 | Yes | * | 0.035 |
| Control vs. Scrambled | -0.002969 | -0.05722 to 0.05128 | No | ns | >.999 |
| Oligomer vs. Scrambled | 0.05604 | 0.001791 to 0.1103 | Yes | * | 0.044 |

High damage

| ANOVA summary | | | | | |
|---|---|---|---|---|---|
| F | 0.2272 | | | | |
| P value | 0.803 | | | | |
| P value summary | ns | | | | |
| Significant diff. among means (P < 0.05)? | No | | | | |
| R squared | 0.07039 | | | | |
| | | | | | |
| **Bonferroni's multiple comparisons test** | **Mean Diff.** | **95.00% CI of diff.** | **Below threshold?** | **Summary** | **Adjusted P Value** |
| Control vs. Oligomer | 0.02711 | -0.1368 to 0.1911 | No | ns | >.999 |
| Control vs. Scrambled | 0.03077 | -0.1332 to 0.1947 | No | ns | >.999 |
| Oligomer vs. Scrambled | 0.003658 | -0.1603 to 0.1676 | No | ns | >.999 |

**CS14– 24h**

All damage

| ANOVA summary | | | | | |
|---|---|---|---|---|---|
| F | 1.278 | | | | |
| P value | 0.345 | | | | |
| P value summary | ns | | | | |
| Significant diff. among means (P < 0.05)? | No | | | | |
| R squared | 0.2987 | | | | |
| | | | | | |
| **Bonferroni's multiple comparisons test** | **Mean Diff.** | **95.00% CI of diff.** | **Below threshold?** | **Summary** | **Adjusted P Value** |
| Control vs. Oligomer | 0.002417 | -0.01652 to 0.02135 | No | ns | >.999 |
| Control vs. Scrambled | -0.006485 | -0.02542 to 0.01245 | No | ns | 0.909 |
| Oligomer vs. Scrambled | -0.008902 | -0.02783 to 0.01003 | No | ns | 0.519 |

Low damage

| ANOVA summary | | | | | |
|---|---|---|---|---|---|
| F | 1.052 | | | | |
| P value | 0.406 | | | | |
| P value summary | ns | | | | |
| Significant diff. among means (P < 0.05)? | No | | | | |
| R squared | 0.2596 | | | | |
| | | | | | |
| **Bonferroni's multiple comparisons test** | **Mean Diff.** | **95.00% CI of diff.** | **Below threshold?** | **Summary** | **Adjusted P Value** |
| Control vs. Oligomer | -0.5568 | -4.133 to 3.019 | No | ns | >.999 |
| Control vs. Scrambled | 1 | -2.576 to 4.576 | No | ns | >.999 |
| Oligomer vs. Scrambled | 1.557 | -2.019 to 5.133 | No | ns | 0.607 |

High damage

| ANOVA summary | | | | | |
|---|---|---|---|---|---|
| F | 0.6466 | | | | |
| P value | 0.584 | | | | |
| P value summary | ns | | | | |
| Significant diff. among means (P < 0.05)? | No | | | | |
| R squared | 0.3012 | | | | |
| | | | | | |
| **Bonferroni's multiple comparisons test** | **Mean Diff.** | **95.00% CI of diff.** | **Below threshold?** | **Summary** | **Adjusted P Value** |
| Control vs. Oligomer | 0.2344 | -0.9595 to 1.428 | No | ns | >.999 |
| Control vs. Scrambled | 0.2491 | -0.9447 to 1.443 | No | ns | >.999 |
| Oligomer vs. Scrambled | 0.01477 | -1.179 to 1.209 | No | ns | >.999 |

## All cell lines– 24h

### All damage

| ANOVA summary | | | | | |
|---|---|---|---|---|---|
| F | 0.7871 | | | | |
| P value | 0.531 | | | | |
| P value summary | ns | | | | |
| Significant diff. among means (P < 0.05)? | No | | | | |
| R squared | 0.3441 | | | | |
| | | | | | |
| **Bonferroni's multiple comparisons test** | **Mean Diff.** | **95.00% CI of diff.** | **Below threshold?** | **Summary** | **Adjusted P Value** |
| Control vs. Oligomer | 0.1917 | -0.5855 to 0.9689 | No | ns | 0.951 |
| Control vs. Scrambled | 0.04425 | -0.7329 to 0.8214 | No | ns | >.999 |
| Oligomer vs. Scrambled | -0.1475 | -0.9247 to 0.6297 | No | ns | >.999 |

### Low damage

| ANOVA summary | | | | | |
|---|---|---|---|---|---|
| F | 1.585 | | | | |
| P value | 0.339 | | | | |
| P value summary | ns | | | | |
| Significant diff. among means (P < 0.05)? | No | | | | |
| R squared | 0.5138 | | | | |
| | | | | | |
| **Bonferroni's multiple comparisons test** | **Mean Diff.** | **95.00% CI of diff.** | **Below threshold?** | **Summary** | **Adjusted P Value** |
| Control vs. Oligomer | -0.3079 | -2.528 to 1.912 | No | ns | >.999 |
| Control vs. Scrambled | 0.4985 | -1.722 to 2.719 | No | ns | >.999 |
| Oligomer vs. Scrambled | 0.8064 | -1.414 to 3.026 | No | ns | 0.528 |

## 155v2– 48h

### High damage

| ANOVA summary | | | | | |
|---|---|---|---|---|---|
| F | 0.7185 | | | | |
| P value | 0.525 | | | | |
| P value summary | ns | | | | |
| Significant diff. among means (P < 0.05)? | No | | | | |
| R squared | 0.1932 | | | | |
| | | | | | |
| **Bonferroni's multiple comparisons test** | **Mean Diff.** | **95.00% CI of diff.** | **Below threshold?** | **Summary** | **Adjusted P Value** |
| Control vs. Oligomer | 0.1612 | -2.148 to 2.470 | No | ns | >.999 |
| Control vs. Scrambled | -0.6351 | -2.944 to 1.674 | No | ns | >.999 |
| Oligomer vs. Scrambled | -0.7963 | -3.105 to 1.513 | No | ns | 0.901 |

**155v2– 48h**

All damage

| ANOVA summary | | | | | |
|---|---|---|---|---|---|
| F | 15.37 | | | | |
| P value | 0.004 | | | | |
| P value summary | ** | | | | |
| Significant diff. among means (P < 0.05)? | Yes | | | | |
| R squared | 0.8367 | | | | |
| | | | | | |
| **Bonferroni's multiple comparisons test** | **Mean Diff.** | **95.00% CI of diff.** | **Below threshold?** | **Summary** | **Adjusted P Value** |
| Control vs. Oligomer | 0.3444 | 0.08686 to 0.6020 | Yes | * | 0.014 |
| Control vs. Scrambled | -0.05702 | -0.3146 to 0.2006 | No | ns | >.999 |
| Oligomer vs. Scrambled | -0.4015 | -0.6591 to -0.1439 | Yes | ** | 0.007 |

Low damage

| ANOVA summary | | | | | |
|---|---|---|---|---|---|
| F | 47.41 | | | | |
| P value | <.001 | | | | |
| P value summary | *** | | | | |
| Significant diff. among means (P < 0.05)? | Yes | | | | |
| R squared | 0.9405 | | | | |
| | | | | | |
| **Bonferroni's multiple comparisons test** | **Mean Diff.** | **95.00% CI of diff.** | **Below threshold?** | **Summary** | **Adjusted P Value** |
| Control vs. Oligomer | -0.08266 | -0.1164 to -0.04889 | Yes | *** | <.001 |
| Control vs. Scrambled | 0.007451 | -0.02632 to 0.04122 | No | ns | >.999 |
| Oligomer vs. Scrambled | 0.09011 | 0.05634 to 0.1239 | Yes | *** | <.001 |

**CS14– 48h**

High damage

| ANOVA summary | | | | | |
|---|---|---|---|---|---|
| F | 4.323 | | | | |
| P value | 0.069 | | | | |
| P value summary | ns | | | | |
| Significant diff. among means (P < 0.05)? | No | | | | |
| R squared | 0.5903 | | | | |
| | | | | | |
| **Bonferroni's multiple comparisons test** | **Mean Diff.** | **95.00% CI of diff.** | **Below threshold?** | **Summary** | **Adjusted P Value** |
| Control vs. Oligomer | 0.01467 | -0.1564 to 0.1857 | No | ns | >.999 |
| Control vs. Scrambled | -0.1245 | -0.2956 to 0.04649 | No | ns | 0.161 |
| Oligomer vs. Scrambled | -0.1392 | -0.3102 to 0.03183 | No | ns | 0.11 |

## CS14– 48h

### All damage

| ANOVA summary | | | | | |
|---|---|---|---|---|---|
| F | 6 | | | | |
| P value | 0.037 | | | | |
| P value summary | * | | | | |
| Significant diff. among means (P < 0.05)? | Yes | | | | |
| R squared | 0.6667 | | | | |
| | | | | | |
| **Bonferroni's multiple comparisons test** | **Mean Diff.** | **95.00% CI of diff.** | **Below threshold?** | **Summary** | **Adjusted P Value** |
| Control vs. Oligomer | -0.002829 | -0.01751 to 0.01186 | No | ns | >.999 |
| Control vs. Scrambled | -0.01459 | -0.02928 to 9.578e-00 | No | ns | 0.051 |
| Oligomer vs. Scrambled | -0.01176 | -0.02645 to 0.002925 | No | ns | 0.117 |

### Low damage

| ANOVA summary | | | | | |
|---|---|---|---|---|---|
| F | 3.999 | | | | |
| P value | 0.079 | | | | |
| P value summary | ns | | | | |
| Significant diff. among means (P < 0.05)? | No | | | | |
| R squared | 0.5713 | | | | |
| | | | | | |
| **Bonferroni's multiple comparisons test** | **Mean Diff.** | **95.00% CI of diff.** | **Below threshold?** | **Summary** | **Adjusted P Value** |
| Control vs. Oligomer | 0.1671 | -0.5803 to 0.9146 | No | ns | >.999 |
| Control vs. Scrambled | 0.6212 | -0.1262 to 1.369 | No | ns | 0.102 |
| Oligomer vs. Scrambled | 0.4541 | -0.2933 to 1.202 | No | ns | 0.278 |

## All cell lines – 48h

### High damage

| ANOVA summary | | | | | |
|---|---|---|---|---|---|
| F | 2.628 | | | | |
| P value | 0.219 | | | | |
| P value summary | ns | | | | |
| Significant diff. among means (P < 0.05)? | No | | | | |
| R squared | 0.6366 | | | | |
| | | | | | |
| **Bonferroni's multiple comparisons test** | **Mean Diff.** | **95.00% CI of diff.** | **Below threshold?** | **Summary** | **Adjusted P Value** |
| Control vs. Oligomer | 0.08793 | -0.9653 to 1.141 | No | ns | >.999 |
| Control vs. Scrambled | -0.3798 | -1.433 to 0.6734 | No | ns | 0.534 |
| Oligomer vs. Scrambled | -0.4678 | -1.521 to 0.5855 | No | ns | 0.36 |

## All cell lines – 48h

All damage

| ANOVA summary | | | | | |
|---|---|---|---|---|---|
| F | 1.195 | | | | |
| P value | 0.415 | | | | |
| P value summary | ns | | | | |
| Significant diff. among means (P < 0.05)? | No | | | | |
| R squared | 0.4435 | | | | |
| | | | | | |
| **Bonferroni's multiple comparisons test** | **Mean Diff.** | **95.00% CI of diff.** | **Below threshold?** | **Summary** | **Adjusted P Value** |
| Control vs. Oligomer | 0.1708 | -0.5229 to 0.8645 | No | ns | 0.953 |
| Control vs. Scrambled | -0.03581 | -0.7295 to 0.6579 | No | ns | >.999 |
| Oligomer vs. Scrambled | -0.2066 | -0.9003 to 0.4871 | No | ns | 0.731 |

Low damage

| ANOVA summary | | | | | |
|---|---|---|---|---|---|
| F | 0.7954 | | | | |
| P value | 0.528 | | | | |
| P value summary | ns | | | | |
| Significant diff. among means (P < 0.05)? | No | | | | |
| R squared | 0.3465 | | | | |
| | | | | | |
| **Bonferroni's multiple comparisons test** | **Mean Diff.** | **95.00% CI of diff.** | **Below threshold?** | **Summary** | **Adjusted P Value** |
| Control vs. Oligomer | 0.04224 | -1.272 to 1.356 | No | ns | >.999 |
| Control vs. Scrambled | 0.3143 | -0.9996 to 1.628 | No | ns | 0.988 |
| Oligomer vs. Scrambled | 0.2721 | -1.042 to 1.586 | No | ns | >.999 |

## 155v2– repeated stress

High damage

| ANOVA summary | | | | | |
|---|---|---|---|---|---|
| F | 0.4368 | | | | |
| P value | 0.665 | | | | |
| P value summary | ns | | | | |
| Significant diff. among means (P < 0.05)? | No | | | | |
| R squared | 0.1271 | | | | |
| | | | | | |
| **Bonferroni's multiple comparisons test** | **Mean Diff.** | **95.00% CI of diff.** | **Below threshold?** | **Summary** | **Adjusted P Value** |
| Control vs. Oligomer | 0.7639 | -2.050 to 3.578 | No | ns | >.999 |
| Control vs. Scrambled | 0.5878 | -2.226 to 3.401 | No | ns | >.999 |
| Oligomer vs. Scrambled | -0.1761 | -2.990 to 2.638 | No | ns | >.999 |

## 155v2– repeated stress

### All damage

| ANOVA summary | | | | | |
|---|---|---|---|---|---|
| F | 0.7957 | | | | |
| P value | 0.494 | | | | |
| P value summary | ns | | | | |
| Significant diff. among means (P < 0.05)? | No | | | | |
| R squared | 0.2096 | | | | |
| | | | | | |
| **Bonferroni's multiple comparisons test** | **Mean Diff.** | **95.00% CI of diff.** | **Below threshold?** | **Summary** | **Adjusted P Value** |
| Control vs. Oligomer | 0.2269 | -0.4695 to 0.9234 | No | ns | 0.976 |
| Control vs. Scrambled | -0.0088 | -0.7053 to 0.6877 | No | ns | >.999 |
| Oligomer vs. Scrambled | -0.2357 | -0.9322 to 0.4607 | No | ns | 0.925 |

### Low damage

| ANOVA summary | | | | | |
|---|---|---|---|---|---|
| F | 1.328 | | | | |
| P value | 0.333 | | | | |
| P value summary | ns | | | | |
| Significant diff. among means (P < 0.05)? | No | | | | |
| R squared | 0.3069 | | | | |
| | | | | | |
| **Bonferroni's multiple comparisons test** | **Mean Diff.** | **95.00% CI of diff.** | **Below threshold?** | **Summary** | **Adjusted P Value** |
| Control vs. Oligomer | -0.04828 | -0.1672 to 0.07065 | No | ns | 0.691 |
| Control vs. Scrambled | 0.005178 | -0.1138 to 0.1241 | No | ns | >.999 |
| Oligomer vs. Scrambled | 0.05346 | -0.06547 to 0.1724 | No | ns | 0.57 |

## CS14– repeated stress

### High damage

| ANOVA summary | | | | | |
|---|---|---|---|---|---|
| F | 10.1 | | | | |
| P value | 0.012 | | | | |
| P value summary | * | | | | |
| Significant diff. among means (P < 0.05)? | Yes | | | | |
| R squared | 0.7709 | | | | |
| | | | | | |
| **Bonferroni's multiple comparisons test** | **Mean Diff.** | **95.00% CI of diff.** | **Below threshold?** | **Summary** | **Adjusted P Value** |
| Control vs. Oligomer | -0.1276 | -0.2432 to -0.01204 | Yes | * | 0.033 |
| Control vs. Scrambled | -0.1445 | -0.2601 to -0.02887 | Yes | * | 0.019 |
| Oligomer vs. Scrambled | -0.01683 | -0.1324 to 0.09876 | No | ns | >.999 |

## CS14– repeated stress

### All damage

| ANOVA summary | | | | | |
|---|---|---|---|---|---|
| F | 1.883 | | | | |
| P value | 0.232 | | | | |
| P value summary | ns | | | | |
| Significant diff. among means (P < 0.05)? | No | | | | |
| R squared | 0.3856 | | | | |
| | | | | | |
| **Bonferroni's multiple comparisons test** | **Mean Diff.** | **95.00% CI of diff.** | **Below threshold?** | **Summary** | **Adjusted P Value** |
| Control vs. Oligomer | 0.01011 | -0.02470 to 0.04492 | No | ns | >.999 |
| Control vs. Scrambled | -0.01044 | -0.04525 to 0.02437 | No | ns | >.999 |
| Oligomer vs. Scrambled | -0.02055 | -0.05536 to 0.01426 | No | ns | 0.301 |

### Low damage

| ANOVA summary | | | | | |
|---|---|---|---|---|---|
| F | 1.896 | | | | |
| P value | 0.23 | | | | |
| P value summary | ns | | | | |
| Significant diff. among means (P < 0.05)? | No | | | | |
| R squared | 0.3873 | | | | |
| | | | | | |
| **Bonferroni's multiple comparisons test** | **Mean Diff.** | **95.00% CI of diff.** | **Below threshold?** | **Summary** | **Adjusted P Value** |
| Control vs. Oligomer | -0.1754 | -1.437 to 1.087 | No | ns | >.999 |
| Control vs. Scrambled | 0.5417 | -0.7203 to 1.804 | No | ns | 0.624 |
| Oligomer vs. Scrambled | 0.7171 | -0.5450 to 1.979 | No | ns | 0.333 |

## All cell lines – repeated stress

### All damage

| ANOVA summary | | | | | |
|---|---|---|---|---|---|
| F | 1.3 | | | | |
| P value | 0.392 | | | | |
| P value summary | ns | | | | |
| Significant diff. among means (P < 0.05)? | No | | | | |
| R squared | 0.4643 | | | | |
| | | | | | |
| **Bonferroni's multiple comparisons test** | **Mean Diff.** | **95.00% CI of diff.** | **Below threshold?** | **Summary** | **Adjusted P Value** |
| Control vs. Oligomer | 0.1185 | -0.3114 to 0.5484 | No | ns | 0.819 |
| Control vs. Scrambled | -0.009618 | -0.4395 to 0.4203 | No | ns | >.999 |
| Oligomer vs. Scrambled | -0.1281 | -0.5581 to 0.3018 | No | ns | 0.731 |

### Low damage

| ANOVA summary | | | | | |
|---|---|---|---|---|---|
| F | 1.551 | | | | |
| P value | 0.345 | | | | |
| P value summary | ns | | | | |
| Significant diff. among means (P < 0.05)? | No | | | | |
| R squared | 0.5083 | | | | |
| | | | | | |
| **Bonferroni's multiple comparisons test** | **Mean Diff.** | **95.00% CI of diff.** | **Below threshold?** | **Summary** | **Adjusted P Value** |
| Control vs. Oligomer | -0.1118 | -1.205 to 0.9814 | No | ns | >.999 |
| Control vs. Scrambled | 0.2734 | -0.8198 to 1.367 | No | ns | 0.934 |
| Oligomer vs. Scrambled | 0.3853 | -0.7080 to 1.478 | No | ns | 0.557 |

**155v2– 1h**

High damage

| ANOVA summary | | | | | |
|---|---|---|---|---|---|
| F | 1.506 | | | | |
| P value | 0.295 | | | | |
| P value summary | ns | | | | |
| Significant diff. among means (P < 0.05)? | No | | | | |
| R squared | 0.3343 | | | | |
| | | | | | |
| **Bonferroni's multiple comparisons test** | **Mean Diff.** | **95.00% CI of diff.** | **Below threshold?** | **Summary** | **Adjusted P Value** |
| Control vs. Oligomer | -1.466 | -7.450 to 4.519 | No | ns | >.999 |
| Control vs. Scrambled | -3.157 | -9.141 to 2.827 | No | ns | 0.401 |
| Oligomer vs. Scrambled | -1.691 | -7.676 to 4.293 | No | ns | >.999 |

**All cell lines – 2h**

Mean cell roundness

| ANOVA summary | | | | | |
|---|---|---|---|---|---|
| F | 0.08223 | | | | |
| P value | 0.923 | | | | |
| P value summary | ns | | | | |
| Significant diff. among means (P < 0.05)? | No | | | | |
| R squared | 0.05197 | | | | |
| | | | | | |
| **Bonferroni's multiple comparisons test** | **Mean Diff.** | **95.00% CI of diff.** | **Below threshold?** | **Summary** | **Adjusted P Value** |
| Control vs. Oligomer | 0.0194 | -0.2591 to 0.2979 | No | ns | >.999 |
| Control vs. Scrambled | 0.02081 | -0.2577 to 0.2993 | No | ns | >.999 |
| Oligomer vs. Scrambled | 0.001413 | -0.2771 to 0.2799 | No | ns | >.999 |

Mean cell width

| ANOVA summary | | | | | |
|---|---|---|---|---|---|
| F | 6.021 | | | | |
| P value | 0.089 | | | | |
| P value summary | ns | | | | |
| Significant diff. among means (P < 0.05)? | No | | | | |
| R squared | 0.8006 | | | | |
| | | | | | |
| **Bonferroni's multiple comparisons test** | **Mean Diff.** | **95.00% CI of diff.** | **Below threshold?** | **Summary** | **Adjusted P Value** |
| Control vs. Oligomer | -0.1588 | -0.3814 to 0.06371 | No | ns | 0.121 |
| Control vs. Scrambled | -0.086 | -0.3085 to 0.1365 | No | ns | 0.472 |
| Oligomer vs. Scrambled | 0.07283 | -0.1497 to 0.2954 | No | ns | 0.631 |

**All cell lines – 2h**

Mean cytoplasm region

| ANOVA summary | | | | | |
|---|---|---|---|---|---|
| F | 1.165 | | | | |
| P value | 0.422 | | | | |
| P value summary | ns | | | | |
| Significant diff. among means (P < 0.05)? | No | | | | |
| R squared | 0.4373 | | | | |
| | | | | | |
| **Bonferroni's multiple comparisons test** | **Mean Diff.** | **95.00% CI of diff.** | **Below threshold?** | **Summary** | **Adjusted P Value** |
| Control vs. Oligomer | 0.01995 | -0.04572 to 0.08561 | No | ns | 0.71 |
| Control vs. Scrambled | 0.005367 | -0.06030 to 0.07103 | No | ns | >.999 |
| Oligomer vs. Scrambled | -0.01458 | -0.08024 to 0.05109 | No | ns | >.999 |

Mean cell area

| ANOVA summary | | | | | |
|---|---|---|---|---|---|
| F | 1.225 | | | | |
| P value | 0.408 | | | | |
| P value summary | ns | | | | |
| Significant diff. among means (P < 0.05)? | No | | | | |
| R squared | 0.4495 | | | | |
| | | | | | |
| **Bonferroni's multiple comparisons test** | **Mean Diff.** | **95.00% CI of diff.** | **Below threshold?** | **Summary** | **Adjusted P Value** |
| Control vs. Oligomer | -0.2118 | -0.8695 to 0.4460 | No | ns | 0.648 |
| Control vs. Scrambled | -0.114 | -0.7717 to 0.5438 | No | ns | >.999 |
| Oligomer vs. Scrambled | 0.09777 | -0.5600 to 0.7555 | No | ns | >.999 |

**24h- 155v2**

Mean cell length

| ANOVA summary | | | | | |
|---|---|---|---|---|---|
| F | 0.8181 | | | | |
| P value | 0.485 | | | | |
| P value summary | ns | | | | |
| Significant diff. among means (P < 0.05)? | No | | | | |
| R squared | 0.2143 | | | | |
| | | | | | |
| **Bonferroni's multiple comparisons test** | **Mean Diff.** | **95.00% CI of diff.** | **Below threshold?** | **Summary** | **Adjusted P Value** |
| Control vs. Oligomer | 0.03538 | -0.1278 to 0.1986 | No | ns | >.999 |
| Control vs. Scrambled | 0.06336 | -0.09984 to 0.2266 | No | ns | 0.747 |
| Oligomer vs. Scrambled | 0.02798 | -0.1352 to 0.1912 | No | ns | >.999 |

**24h- 155v2**

Mean cell roundness

| ANOVA summary | | | | | |
|---|---|---|---|---|---|
| F | 1.95 | | | | |
| P value | 0.223 | | | | |
| P value summary | ns | | | | |
| Significant diff. among means (P < 0.05)? | No | | | | |
| R squared | 0.3939 | | | | |
| | | | | | |
| **Bonferroni's multiple comparisons test** | **Mean Diff.** | **95.00% CI of diff.** | **Below threshold?** | **Summary** | **Adjusted P Value** |
| Control vs. Oligomer | -0.03731 | -0.1806 to 0.1059 | No | ns | >.999 |
| Control vs. Scrambled | -0.0858 | -0.2290 to 0.05745 | No | ns | 0.289 |
| Oligomer vs. Scrambled | -0.04849 | -0.1917 to 0.09476 | No | ns | 0.925 |

Mean cell width

| ANOVA summary | | | | | |
|---|---|---|---|---|---|
| F | 1.098 | | | | |
| P value | 0.392 | | | | |
| P value summary | ns | | | | |
| Significant diff. among means (P < 0.05)? | No | | | | |
| R squared | 0.268 | | | | |
| | | | | | |
| **Bonferroni's multiple comparisons test** | **Mean Diff.** | **95.00% CI of diff.** | **Below threshold?** | **Summary** | **Adjusted P Value** |
| Control vs. Oligomer | -0.002231 | -0.1466 to 0.1421 | No | ns | >.999 |
| Control vs. Scrambled | 0.05521 | -0.08915 to 0.1996 | No | ns | 0.766 |
| Oligomer vs. Scrambled | 0.05744 | -0.08692 to 0.2018 | No | ns | 0.716 |

**24h- 155v2**

Mean cytoplasm region

| ANOVA summary | | | | | |
|---|---|---|---|---|---|
| F | 0.5171 | | | | |
| P value | 0.621 | | | | |
| P value summary | ns | | | | |
| Significant diff. among means (P < 0.05)? | No | | | | |
| R squared | 0.147 | | | | |
| | | | | | |
| **Bonferroni's multiple comparisons test** | **Mean Diff.** | **95.00% CI of diff.** | **Below threshold?** | **Summary** | **Adjusted P Value** |
| Control vs. Oligomer | -0.007363 | -0.04768 to 0.03295 | No | ns | >.999 |
| Control vs. Scrambled | -0.0124 | -0.05271 to 0.02791 | No | ns | >.999 |
| Oligomer vs. Scrambled | -0.005036 | -0.04535 to 0.03528 | No | ns | >.999 |

Mean cell area

| ANOVA summary | | | | | |
|---|---|---|---|---|---|
| F | 0.4662 | | | | |
| P value | 0.648 | | | | |
| P value summary | ns | | | | |
| Significant diff. among means (P < 0.05)? | No | | | | |
| R squared | 0.1345 | | | | |
| | | | | | |
| **Bonferroni's multiple comparisons test** | **Mean Diff.** | **95.00% CI of diff.** | **Below threshold?** | **Summary** | **Adjusted P Value** |
| Control vs. Oligomer | 0.01321 | -0.2593 to 0.2857 | No | ns | >.999 |
| Control vs. Scrambled | 0.07498 | -0.1975 to 0.3475 | No | ns | >.999 |
| Oligomer vs. Scrambled | 0.06176 | -0.2107 to 0.3343 | No | ns | >.999 |

**24h –CS14**

Mean cell length

| ANOVA summary | | | | | |
|---|---|---|---|---|---|
| F | 0.6798 | | | | |
| P value | 0.542 | | | | |
| P value summary | ns | | | | |
| Significant diff. among means (P < 0.05)? | No | | | | |
| R squared | 0.1847 | | | | |
| | | | | | |
| **Bonferroni's multiple comparisons test** | **Mean Diff.** | **95.00% CI of diff.** | **Below threshold?** | **Summary** | **Adjusted P Value** |
| Control vs. Oligomer | 0.01555 | -0.1710 to 0.2022 | No | ns | >.999 |
| Control vs. Scrambled | 0.06349 | -0.1231 to 0.2501 | No | ns | 0.918 |
| Oligomer vs. Scrambled | 0.04794 | -0.1387 to 0.2345 | No | ns | >.999 |

**24h –CS14**

Mean cell roundness

| ANOVA summary | | | | | |
|---|---|---|---|---|---|
| F | 2.011 | | | | |
| P value | 0.215 | | | | |
| P value summary | ns | | | | |
| Significant diff. among means (P < 0.05)? | No | | | | |
| R squared | 0.4013 | | | | |
| | | | | | |
| **Bonferroni's multiple comparisons test** | **Mean Diff.** | **95.00% CI of diff.** | **Below threshold?** | **Summary** | **Adjusted P Value** |
| Control vs. Oligomer | -0.07431 | -0.2475 to 0.09889 | No | ns | 0.624 |
| Control vs. Scrambled | 0.02788 | -0.1453 to 0.2011 | No | ns | >.999 |
| Oligomer vs. Scrambled | 0.1022 | -0.07101 to 0.2754 | No | ns | 0.301 |

Mean cell width

| ANOVA summary | | | | | |
|---|---|---|---|---|---|
| F | 1.758 | | | | |
| P value | 0.251 | | | | |
| P value summary | ns | | | | |
| Significant diff. among means (P < 0.05)? | No | | | | |
| R squared | 0.3695 | | | | |
| | | | | | |
| **Bonferroni's multiple comparisons test** | **Mean Diff.** | **95.00% CI of diff.** | **Below threshold?** | **Summary** | **Adjusted P Value** |
| Control vs. Oligomer | -0.07649 | -0.2147 to 0.06174 | No | ns | 0.356 |
| Control vs. Scrambled | -0.02165 | -0.1599 to 0.1166 | No | ns | >.999 |
| Oligomer vs. Scrambled | 0.05484 | -0.08339 to 0.1931 | No | ns | 0.72 |

**24h –CS14**

Mean cytoplasm region

| ANOVA summary | | | | | |
|---|---|---|---|---|---|
| F | 0.6007 | | | | |
| P value | 0.578 | | | | |
| P value summary | ns | | | | |
| Significant diff. among means (P < 0.05)? | No | | | | |
| R squared | 0.1668 | | | | |
| | | | | | |
| **Bonferroni's multiple comparisons test** | **Mean Diff.** | **95.00% CI of diff.** | **Below threshold?** | **Summary** | **Adjusted P Value** |
| Control vs. Oligomer | 0.01025 | -0.02220 to 0.04270 | No | ns | >.999 |
| Control vs. Scrambled | 0.008124 | -0.02433 to 0.04058 | No | ns | >.999 |
| Oligomer vs. Scrambled | -0.002127 | -0.03458 to 0.03032 | No | ns | >.999 |

Mean cell area

| ANOVA summary | | | | | |
|---|---|---|---|---|---|
| F | 0.7936 | | | | |
| P value | 0.495 | | | | |
| P value summary | ns | | | | |
| Significant diff. among means (P < 0.05)? | No | | | | |
| R squared | 0.2092 | | | | |
| | | | | | |
| **Bonferroni's multiple comparisons test** | **Mean Diff.** | **95.00% CI of diff.** | **Below threshold?** | **Summary** | **Adjusted P Value** |
| Control vs. Oligomer | -0.08755 | -0.3217 to 0.1466 | No | ns | 0.795 |
| Control vs. Scrambled | -0.06082 | -0.2950 to 0.1733 | No | ns | >.999 |
| Oligomer vs. Scrambled | 0.02673 | -0.2074 to 0.2609 | No | ns | >.999 |

**All cell lines – 24h**

Mean cell length

| ANOVA summary | | | | | |
|---|---|---|---|---|---|
| F | 31.11 | | | | |
| P value | 0.01 | | | | |
| P value summary | ** | | | | |
| Significant diff. among means (P < 0.05)? | Yes | | | | |
| R squared | 0.954 | | | | |
| | | | | | |
| **Bonferroni's multiple comparisons test** | **Mean Diff.** | **95.00% CI of diff.** | **Below threshold?** | **Summary** | **Adjusted P Value** |
| Control vs. Oligomer | 0.02547 | -0.01384 to 0.06477 | No | ns | 0.154 |
| Control vs. Scrambled | 0.06343 | 0.02412 to 0.1027 | Yes | * | 0.013 |
| Oligomer vs. Scrambled | 0.03796 | -0.001342 to 0.07726 | No | ns | 0.055 |

**All cell lines – 24h**

Mean cell roundness

| ANOVA summary | | | | | |
|---|---|---|---|---|---|
| F | 0.654 | | | | |
| P value | 0.581 | | | | |
| P value summary | ns | | | | |
| Significant diff. among means (P < 0.05)? | No | | | | |
| R squared | 0.3036 | | | | |
| | | | | | |
| **Bonferroni's multiple comparisons test** | **Mean Diff.** | **95.00% CI of diff.** | **Below threshold?** | **Summary** | **Adjusted P Value** |
| Control vs. Oligomer | -0.05581 | -0.2928 to 0.1812 | No | ns | >.999 |
| Control vs. Scrambled | -0.02896 | -0.2660 to 0.2081 | No | ns | >.999 |
| Oligomer vs. Scrambled | 0.02685 | -0.2102 to 0.2639 | No | ns | >.999 |

Mean cell width

| ANOVA summary | | | | | |
|---|---|---|---|---|---|
| F | 0.8724 | | | | |
| P value | 0.503 | | | | |
| P value summary | ns | | | | |
| Significant diff. among means (P < 0.05)? | No | | | | |
| R squared | 0.3677 | | | | |
| | | | | | |
| **Bonferroni's multiple comparisons test** | **Mean Diff.** | **95.00% CI of diff.** | **Below threshold?** | **Summary** | **Adjusted P Value** |
| Control vs. Oligomer | -0.03936 | -0.2513 to 0.1725 | No | ns | >.999 |
| Control vs. Scrambled | 0.01678 | -0.1951 to 0.2287 | No | ns | >.999 |
| Oligomer vs. Scrambled | 0.05614 | -0.1558 to 0.2680 | No | ns | 0.865 |

**All cell lines – 24h**

Mean cytoplasm region

| ANOVA summary | | | | | |
|---|---|---|---|---|---|
| F | 0.05327 | | | | |
| P value | 0.949 | | | | |
| P value summary | ns | | | | |
| Significant diff. among means (P < 0.05)? | No | | | | |
| R squared | 0.03429 | | | | |
| | | | | | |
| **Bonferroni's multiple comparisons test** | **Mean Diff.** | **95.00% CI of diff.** | **Below threshold?** | **Summary** | **Adjusted P Value** |
| Control vs. Oligomer | 0.001444 | -0.05218 to 0.05507 | No | ns | >.999 |
| Control vs. Scrambled | -0.002137 | -0.05576 to 0.05149 | No | ns | >.999 |
| Oligomer vs. Scrambled | -0.003581 | -0.05720 to 0.05004 | No | ns | >.999 |

Mean cell area

| ANOVA summary | | | | | |
|---|---|---|---|---|---|
| F | 0.2371 | | | | |
| P value | 0.802 | | | | |
| P value summary | ns | | | | |
| Significant diff. among means (P < 0.05)? | No | | | | |
| R squared | 0.1365 | | | | |
| | | | | | |
| **Bonferroni's multiple comparisons test** | **Mean Diff.** | **95.00% CI of diff.** | **Below threshold?** | **Summary** | **Adjusted P Value** |
| Control vs. Oligomer | -0.03717 | -0.3724 to 0.2981 | No | ns | >.999 |
| Control vs. Scrambled | 0.007078 | -0.3282 to 0.3423 | No | ns | >.999 |
| Oligomer vs. Scrambled | 0.04425 | -0.2910 to 0.3795 | No | ns | >.999 |

**48h – 155v2**

Mean cell length

| ANOVA summary | | | | | |
|---|---|---|---|---|---|
| F | 1.386 | | | | |
| P value | 0.32 | | | | |
| P value summary | ns | | | | |
| Significant diff. among means (P < 0.05)? | No | | | | |
| R squared | 0.3161 | | | | |
| | | | | | |
| **Bonferroni's multiple comparisons test** | **Mean Diff.** | **95.00% CI of diff.** | **Below threshold?** | **Summary** | **Adjusted P Value** |
| Control vs. Oligomer | 0.04453 | -0.07070 to 0.1597 | No | ns | 0.753 |
| Control vs. Scrambled | 0.05494 | -0.06028 to 0.1702 | No | ns | 0.504 |
| Oligomer vs. Scrambled | 0.01042 | -0.1048 to 0.1256 | No | ns | >.999 |

**48h – 155v2**

Mean cell roundness

| ANOVA summary | | | | | |
|---|---|---|---|---|---|
| F | 1.264 | | | | |
| P value | 0.348 | | | | |
| P value summary | ns | | | | |
| Significant diff. among means (P < 0.05)? | No | | | | |
| R squared | 0.2965 | | | | |
| | | | | | |
| **Bonferroni's multiple comparisons test** | **Mean Diff.** | **95.00% CI of diff.** | **Below threshold?** | **Summary** | **Adjusted P Value** |
| Control vs. Oligomer | -0.02645 | -0.1042 to 0.05129 | No | ns | 0.918 |
| Control vs. Scrambled | -0.03637 | -0.1141 to 0.04137 | No | ns | 0.525 |
| Oligomer vs. Scrambled | -0.009917 | -0.08766 to 0.06782 | No | ns | >.999 |

Mean cell width

| ANOVA summary | | | | | |
|---|---|---|---|---|---|
| F | 4.853 | | | | |
| P value | 0.056 | | | | |
| P value summary | ns | | | | |
| Significant diff. among means (P < 0.05)? | No | | | | |
| R squared | 0.618 | | | | |
| | | | | | |
| **Bonferroni's multiple comparisons test** | **Mean Diff.** | **95.00% CI of diff.** | **Below threshold?** | **Summary** | **Adjusted P Value** |
| Control vs. Oligomer | 0.03758 | -0.07890 to 0.1541 | No | ns | 0.989 |
| Control vs. Scrambled | 0.1087 | -0.007809 to 0.2252 | No | ns | 0.066 |
| Oligomer vs. Scrambled | 0.07109 | -0.04539 to 0.1876 | No | ns | 0.275 |

**48h – 155v2**

Mean cytoplasm region

| ANOVA summary | | | | | |
|---|---|---|---|---|---|
| F | 4.837 | | | | |
| P value | 0.056 | | | | |
| P value summary | ns | | | | |
| Significant diff. among means (P < 0.05)? | No | | | | |
| R squared | 0.6172 | | | | |
| | | | | | |
| **Bonferroni's multiple comparisons test** | **Mean Diff.** | **95.00% CI of diff.** | **Below threshold?** | **Summary** | **Adjusted P Value** |
| Control vs. Oligomer | 0.02087 | -0.005569 to 0.04731 | No | ns | 0.123 |
| Control vs. Scrambled | 0.02237 | -0.004063 to 0.04881 | No | ns | 0.096 |
| Oligomer vs. Scrambled | 0.001506 | -0.02493 to 0.02794 | No | ns | >.999 |

Mean cell area

| ANOVA summary | | | | | |
|---|---|---|---|---|---|
| F | 5.629 | | | | |
| P value | 0.042 | | | | |
| P value summary | * | | | | |
| Significant diff. among means (P < 0.05)? | Yes | | | | |
| R squared | 0.6523 | | | | |
| | | | | | |
| **Bonferroni's multiple comparisons test** | **Mean Diff.** | **95.00% CI of diff.** | **Below threshold?** | **Summary** | **Adjusted P Value** |
| Control vs. Oligomer | 0.05669 | -0.1079 to 0.2213 | No | ns | 0.902 |
| Control vs. Scrambled | 0.1653 | 0.0007064 to 0.3298 | Yes | * | 0.049 |
| Oligomer vs. Scrambled | 0.1086 | -0.05598 to 0.2732 | No | ns | 0.219 |

**48h – CS14**

Mean cell length

| ANOVA summary | | | | | |
|---|---|---|---|---|---|
| F | 3.278 | | | | |
| P value | 0.109 | | | | |
| P value summary | ns | | | | |
| Significant diff. among means (P < 0.05)? | No | | | | |
| R squared | 0.5222 | | | | |
| | | | | | |
| **Bonferroni's multiple comparisons test** | **Mean Diff.** | **95.00% CI of diff.** | **Below threshold?** | **Summary** | **Adjusted P Value** |
| Control vs. Oligomer | -0.03373 | -0.1824 to 0.1149 | No | ns | >.999 |
| Control vs. Scrambled | -0.1128 | -0.2615 to 0.03587 | No | ns | 0.141 |
| Oligomer vs. Scrambled | -0.07907 | -0.2277 to 0.06960 | No | ns | 0.393 |

**48h – CS14**

Mean cell roundness

| ANOVA summary | | | | | |
|---|---|---|---|---|---|
| F | 3.972 | | | | |
| P value | 0.08 | | | | |
| P value summary | ns | | | | |
| Significant diff. among means (P < 0.05)? | No | | | | |
| R squared | 0.5697 | | | | |
| | | | | | |
| **Bonferroni's multiple comparisons test** | **Mean Diff.** | **95.00% CI of diff.** | **Below threshold?** | **Summary** | **Adjusted P Value** |
| Control vs. Oligomer | -0.2845 | -0.6499 to 0.08081 | No | ns | 0.129 |
| Control vs. Scrambled | -0.02883 | -0.3942 to 0.3365 | No | ns | >.999 |
| Oligomer vs. Scrambled | 0.2557 | -0.1096 to 0.6211 | No | ns | 0.183 |

Mean cell width

| ANOVA summary | | | | | |
|---|---|---|---|---|---|
| F | 0.5265 | | | | |
| P value | 0.616 | | | | |
| P value summary | ns | | | | |
| Significant diff. among means (P < 0.05)? | No | | | | |
| R squared | 0.1493 | | | | |
| | | | | | |
| **Bonferroni's multiple comparisons test** | **Mean Diff.** | **95.00% CI of diff.** | **Below threshold?** | **Summary** | **Adjusted P Value** |
| Control vs. Oligomer | 0.0755 | -0.2264 to 0.3774 | No | ns | >.999 |
| Control vs. Scrambled | 0.08659 | -0.2153 to 0.3885 | No | ns | >.999 |
| Oligomer vs. Scrambled | 0.01108 | -0.2908 to 0.3130 | No | ns | >.999 |

**48h – CS14**

Mean cytoplasm region

| ANOVA summary | | | | | |
|---|---|---|---|---|---|
| F | 2.107 | | | | |
| P value | 0.203 | | | | |
| P value summary | ns | | | | |
| Significant diff. among means (P < 0.05)? | No | | | | |
| R squared | 0.4126 | | | | |
| | | | | | |
| **Bonferroni's multiple comparisons test** | **Mean Diff.** | **95.00% CI of diff.** | **Below threshold?** | **Summary** | **Adjusted P Value** |
| Control vs. Oligomer | 0.02095 | -0.02985 to 0.07175 | No | ns | 0.672 |
| Control vs. Scrambled | -0.01015 | -0.06095 to 0.04065 | No | ns | >.999 |
| Oligomer vs. Scrambled | -0.0311 | -0.08190 to 0.01970 | No | ns | 0.272 |

Mean cell area

| ANOVA summary | | | | | |
|---|---|---|---|---|---|
| F | 0.4354 | | | | |
| P value | 0.666 | | | | |
| P value summary | ns | | | | |
| Significant diff. among means (P < 0.05)? | No | | | | |
| R squared | 0.1267 | | | | |
| | | | | | |
| **Bonferroni's multiple comparisons test** | **Mean Diff.** | **95.00% CI of diff.** | **Below threshold?** | **Summary** | **Adjusted P Value** |
| Control vs. Oligomer | 0.08258 | -0.3182 to 0.4833 | No | ns | >.999 |
| Control vs. Scrambled | 0.109 | -0.2917 to 0.5098 | No | ns | >.999 |
| Oligomer vs. Scrambled | 0.02645 | -0.3743 to 0.4272 | No | ns | >.999 |

**All cell lines – 48h**

Mean cell length

| ANOVA summary | | | | | |
|---|---|---|---|---|---|
| F | 0.1193 | | | | |
| P value | 0.892 | | | | |
| P value summary | ns | | | | |
| Significant diff. among means (P < 0.05)? | No | | | | |
| R squared | 0.0737 | | | | |
| | | | | | |
| **Bonferroni's multiple comparisons test** | **Mean Diff.** | **95.00% CI of diff.** | **Below threshold?** | **Summary** | **Adjusted P Value** |
| Control vs. Oligomer | 0.005396 | -0.3616 to 0.3724 | No | ns | >.999 |
| Control vs. Scrambled | -0.02893 | -0.3959 to 0.3381 | No | ns | >.999 |
| Oligomer vs. Scrambled | -0.03433 | -0.4013 to 0.3327 | No | ns | >.999 |

**All cell lines – 48h**

Mean cell roundness

| ANOVA summary | | | | | |
|---|---|---|---|---|---|
| F | 1.21 | | | | |
| P value | 0.412 | | | | |
| P value summary | ns | | | | |
| Significant diff. among means (P < 0.05)? | No | | | | |
| R squared | 0.4466 | | | | |
| | | | | | |
| **Bonferroni's multiple comparisons test** | **Mean Diff.** | **95.00% CI of diff.** | **Below threshold?** | **Summary** | **Adjusted P Value** |
| Control vs. Oligomer | -0.1555 | -0.6674 to 0.3564 | No | ns | 0.71 |
| Control vs. Scrambled | -0.0326 | -0.5445 to 0.4793 | No | ns | >.999 |
| Oligomer vs. Scrambled | 0.1229 | -0.3890 to 0.6348 | No | ns | 0.984 |

Mean cell width

| ANOVA summary | | | | | |
|---|---|---|---|---|---|
| F | 14.97 | | | | |
| P value | 0.027 | | | | |
| P value summary | * | | | | |
| Significant diff. among means (P < 0.05)? | Yes | | | | |
| R squared | 0.9089 | | | | |
| | | | | | |
| **Bonferroni's multiple comparisons test** | **Mean Diff.** | **95.00% CI of diff.** | **Below threshold?** | **Summary** | **Adjusted P Value** |
| Control vs. Oligomer | 0.05654 | -0.03048 to 0.1436 | No | ns | 0.153 |
| Control vs. Scrambled | 0.09763 | 0.01061 to 0.1846 | Yes | * | 0.036 |
| Oligomer vs. Scrambled | 0.04109 | -0.04593 to 0.1281 | No | ns | 0.317 |

**All cell lines – 48h**

Mean cytoplasm region

| ANOVA summary | | | | | |
|---|---|---|---|---|---|
| F | 1.311 | | | | |
| P value | 0.39 | | | | |
| P value summary | ns | | | | |
| Significant diff. among means (P < 0.05)? | No | | | | |
| R squared | 0.4665 | | | | |
| | | | | | |
| **Bonferroni's multiple comparisons test** | **Mean Diff.** | **95.00% CI of diff.** | **Below threshold?** | **Summary** | **Adjusted P Value** |
| Control vs. Oligomer | 0.02091 | -0.04358 to 0.08540 | No | ns | 0.64 |
| Control vs. Scrambled | 0.006112 | -0.05838 to 0.07060 | No | ns | >.999 |
| Oligomer vs. Scrambled | -0.0148 | -0.07929 to 0.04969 | No | ns | >.999 |

Mean cell area

| ANOVA summary | | | | | |
|---|---|---|---|---|---|
| F | 14.72 | | | | |
| P value | 0.028 | | | | |
| P value summary | * | | | | |
| Significant diff. among means (P < 0.05)? | Yes | | | | |
| R squared | 0.9075 | | | | |
| | | | | | |
| **Bonferroni's multiple comparisons test** | **Mean Diff.** | **95.00% CI of diff.** | **Below threshold?** | **Summary** | **Adjusted P Value** |
| Control vs. Oligomer | 0.06964 | -0.05312 to 0.1924 | No | ns | 0.211 |
| Control vs. Scrambled | 0.1372 | 0.01440 to 0.2599 | Yes | * | 0.037 |
| Oligomer vs. Scrambled | 0.06752 | -0.05524 to 0.1903 | No | ns | 0.227 |

**155v2– repeated stress**

Mean cell length

| ANOVA summary | | | | | |
|---|---|---|---|---|---|
| F | 0.2836 | | | | |
| P value | 0.763 | | | | |
| P value summary | ns | | | | |
| Significant diff. among means (P < 0.05)? | No | | | | |
| R squared | 0.08638 | | | | |
| | | | | | |
| **Bonferroni's multiple comparisons test** | **Mean Diff.** | **95.00% CI of diff.** | **Below threshold?** | **Summary** | **Adjusted P Value** |
| Control vs. Oligomer | -0.000202 | -0.1702 to 0.1698 | No | ns | >.999 |
| Control vs. Scrambled | -0.03383 | -0.2038 to 0.1362 | No | ns | >.999 |
| Oligomer vs. Scrambled | -0.03363 | -0.2036 to 0.1364 | No | ns | >.999 |

**155v2– repeated stress**

Mean cell roundness

| ANOVA summary | | | | | |
|---|---|---|---|---|---|
| F | 0.06062 | | | | |
| P value | 0.942 | | | | |
| P value summary | ns | | | | |
| Significant diff. among means (P < 0.05)? | No | | | | |
| R squared | 0.01981 | | | | |
| | | | | | |
| **Bonferroni's multiple comparisons test** | **Mean Diff.** | **95.00% CI of diff.** | **Below threshold?** | **Summary** | **Adjusted P Value** |
| Control vs. Oligomer | 0.01338 | -0.1611 to 0.1879 | No | ns | >.999 |
| Control vs. Scrambled | -0.004349 | -0.1788 to 0.1701 | No | ns | >.999 |
| Oligomer vs. Scrambled | -0.01773 | -0.1922 to 0.1567 | No | ns | >.999 |

Mean cell width

| ANOVA summary | | | | | |
|---|---|---|---|---|---|
| F | 2.991 | | | | |
| P value | 0.126 | | | | |
| P value summary | ns | | | | |
| Significant diff. among means (P < 0.05)? | No | | | | |
| R squared | 0.4993 | | | | |
| | | | | | |
| **Bonferroni's multiple comparisons test** | **Mean Diff.** | **95.00% CI of diff.** | **Below threshold?** | **Summary** | **Adjusted P Value** |
| Control vs. Oligomer | -0.06119 | -0.2312 to 0.1088 | No | ns | 0.844 |
| Control vs. Scrambled | 0.06525 | -0.1047 to 0.2352 | No | ns | 0.761 |
| Oligomer vs. Scrambled | 0.1264 | -0.04353 to 0.2964 | No | ns | 0.15 |

**155v2– repeated stress**

Mean cytoplasm region

| ANOVA summary | | | | | |
|---|---|---|---|---|---|
| F | 3.204 | | | | |
| P value | 0.113 | | | | |
| P value summary | ns | | | | |
| Significant diff. among means (P < 0.05)? | No | | | | |
| R squared | 0.5164 | | | | |
| | | | | | |
| **Bonferroni's multiple comparisons test** | **Mean Diff.** | **95.00% CI of diff.** | **Below threshold?** | **Summary** | **Adjusted P Value** |
| Control vs. Oligomer | -0.02213 | -0.05269 to 0.008441 | No | ns | 0.164 |
| Control vs. Scrambled | -0.004113 | -0.03468 to 0.02645 | No | ns | >.999 |
| Oligomer vs. Scrambled | 0.01801 | -0.01255 to 0.04858 | No | ns | 0.302 |

Mean cell area

| ANOVA summary | | | | | |
|---|---|---|---|---|---|
| F | 2.146 | | | | |
| P value | 0.198 | | | | |
| P value summary | ns | | | | |
| Significant diff. among means (P < 0.05)? | No | | | | |
| R squared | 0.417 | | | | |
| | | | | | |
| **Bonferroni's multiple comparisons test** | **Mean Diff.** | **95.00% CI of diff.** | **Below threshold?** | **Summary** | **Adjusted P Value** |
| Control vs. Oligomer | -0.139 | -0.4225 to 0.1446 | No | ns | 0.475 |
| Control vs. Scrambled | 0.0278 | -0.2557 to 0.3113 | No | ns | >.999 |
| Oligomer vs. Scrambled | 0.1668 | -0.1168 to 0.4503 | No | ns | 0.304 |

**CS14– repeated stress**

Mean cell length

| ANOVA summary | | | | | |
|---|---|---|---|---|---|
| F | 0.3101 | | | | |
| P value | 0.747 | | | | |
| P value summary | ns | | | | |
| Significant diff. among means (P < 0.05)? | No | | | | |
| R squared | 0.1103 | | | | |
| | | | | | |
| **Bonferroni's multiple comparisons test** | **Mean Diff.** | **95.00% CI of diff.** | **Below threshold?** | **Summary** | **Adjusted P Value** |
| Control vs. Oligomer | -0.06534 | -0.3801 to 0.2494 | No | ns | >.999 |
| Control vs. Scrambled | -0.05958 | -0.3743 to 0.2551 | No | ns | >.999 |
| Oligomer vs. Scrambled | 0.005763 | -0.2757 to 0.2873 | No | ns | >.999 |

**CS14– repeated stress**

Mean cell roundness

| ANOVA summary | | | | | |
|---|---|---|---|---|---|
| F | 0.5618 | | | | |
| P value | 0.602 | | | | |
| P value summary | ns | | | | |
| Significant diff. among means (P < 0.05)? | No | | | | |
| R squared | 0.1835 | | | | |
| | | | | | |
| **Bonferroni's multiple comparisons test** | **Mean Diff.** | **95.00% CI of diff.** | **Below threshold?** | **Summary** | **Adjusted P Value** |
| Control vs. Oligomer | -0.01384 | -0.1080 to 0.08029 | No | ns | >.999 |
| Control vs. Scrambled | 0.01138 | -0.08274 to 0.1055 | No | ns | >.999 |
| Oligomer vs. Scrambled | 0.02522 | -0.05897 to 0.1094 | No | ns | >.999 |

Mean cell width

| ANOVA summary | | | | | |
|---|---|---|---|---|---|
| F | 1.808 | | | | |
| P value | 0.257 | | | | |
| P value summary | ns | | | | |
| Significant diff. among means (P < 0.05)? | No | | | | |
| R squared | 0.4197 | | | | |
| | | | | | |
| **Bonferroni's multiple comparisons test** | **Mean Diff.** | **95.00% CI of diff.** | **Below threshold?** | **Summary** | **Adjusted P Value** |
| Control vs. Oligomer | -0.04116 | -0.4059 to 0.3236 | No | ns | >.999 |
| Control vs. Scrambled | 0.1288 | -0.2359 to 0.4936 | No | ns | 0.802 |
| Oligomer vs. Scrambled | 0.17 | -0.1563 to 0.4962 | No | ns | 0.375 |

**CS14– repeated stress**

Mean cytoplasm region

| ANOVA summary | | | | | |
|---|---|---|---|---|---|
| F | 0.5535 | | | | |
| P value | 0.607 | | | | |
| P value summary | ns | | | | |
| Significant diff. among means (P < 0.05)? | No | | | | |
| R squared | 0.1813 | | | | |
| | | | | | |
| **Bonferroni's multiple comparisons test** | **Mean Diff.** | **95.00% CI of diff.** | **Below threshold?** | **Summary** | **Adjusted P Value** |
| Control vs. Oligomer | 0.01259 | -0.04000 to 0.06517 | No | ns | >.999 |
| Control vs. Scrambled | 0.000102 | -0.05249 to 0.05269 | No | ns | >.999 |
| Oligomer vs. Scrambled | -0.01248 | -0.05952 to 0.03455 | No | ns | >.999 |

Mean cell area

| ANOVA summary | | | | | |
|---|---|---|---|---|---|
| F | 4.036 | | | | |
| P value | 0.09 | | | | |
| P value summary | ns | | | | |
| Significant diff. among means (P < 0.05)? | No | | | | |
| R squared | 0.6175 | | | | |
| | | | | | |
| **Bonferroni's multiple comparisons test** | **Mean Diff.** | **95.00% CI of diff.** | **Below threshold?** | **Summary** | **Adjusted P Value** |
| Control vs. Oligomer | -0.2972 | -0.8155 to 0.2210 | No | ns | 0.295 |
| Control vs. Scrambled | 0.05523 | -0.4630 to 0.5735 | No | ns | >.999 |
| Oligomer vs. Scrambled | 0.3525 | -0.1111 to 0.8160 | No | ns | 0.13 |

**All cell lines – repeated stress**

Mean cell length

| ANOVA summary | | | | | |
|---|---|---|---|---|---|
| F | 0.2137 | | | | |
| P value | 0.819 | | | | |
| P value summary | ns | | | | |
| Significant diff. among means (P < 0.05)? | No | | | | |
| R squared | 0.1247 | | | | |
| | | | | | |
| **Bonferroni's multiple comparisons test** | **Mean Diff.** | **95.00% CI of diff.** | **Below threshold?** | **Summary** | **Adjusted P Value** |
| Control vs. Oligomer | -0.003661 | -0.2704 to 0.2630 | No | ns | >.999 |
| Control vs. Scrambled | -0.03276 | -0.2995 to 0.2339 | No | ns | >.999 |
| Oligomer vs. Scrambled | -0.0291 | -0.2958 to 0.2376 | No | ns | >.999 |

**All cell lines – repeated stress**

Mean cell roundness

| ANOVA summary | | | | | |
|---|---|---|---|---|---|
| F | 4.783 | | | | |
| P value | 0.117 | | | | |
| P value summary | ns | | | | |
| Significant diff. among means (P < 0.05)? | No | | | | |
| R squared | 0.7613 | | | | |
| | | | | | |
| **Bonferroni's multiple comparisons test** | **Mean Diff.** | **95.00% CI of diff.** | **Below threshold?** | **Summary** | **Adjusted P Value** |
| Control vs. Oligomer | -0.03076 | -0.1208 to 0.05925 | No | ns | 0.587 |
| Control vs. Scrambled | 0.02651 | -0.06349 to 0.1165 | No | ns | 0.744 |
| Oligomer vs. Scrambled | 0.05727 | -0.03274 to 0.1473 | No | ns | 0.161 |

Mean cell width

| ANOVA summary | | | | | |
|---|---|---|---|---|---|
| F | 0.3677 | | | | |
| P value | 0.72 | | | | |
| P value summary | ns | | | | |
| Significant diff. among means (P < 0.05)? | No | | | | |
| R squared | 0.1969 | | | | |
| | | | | | |
| **Bonferroni's multiple comparisons test** | **Mean Diff.** | **95.00% CI of diff.** | **Below threshold?** | **Summary** | **Adjusted P Value** |
| Control vs. Oligomer | -0.08129 | -0.6145 to 0.4519 | No | ns | >.999 |
| Control vs. Scrambled | 0.000487 | -0.5327 to 0.5337 | No | ns | >.999 |
| Oligomer vs. Scrambled | 0.08178 | -0.4514 to 0.6150 | No | ns | >.999 |

**All cell lines – repeated stress**

Mean cytoplasm region

| ANOVA summary | | | | | |
|---|---|---|---|---|---|
| F | 5.332 | | | | |
| P value | 0.103 | | | | |
| P value summary | ns | | | | |
| Significant diff. among means (P < 0.05)? | No | | | | |
| R squared | 0.7804 | | | | |
| | | | | | |
| **Bonferroni's multiple comparisons test** | **Mean Diff.** | **95.00% CI of diff.** | **Below threshold?** | **Summary** | **Adjusted P Value** |
| Control vs. Oligomer | 0.008728 | -0.006889 to 0.02435 | No | ns | 0.219 |
| Control vs. Scrambled | -0.000692 | -0.01631 to 0.01493 | No | ns | >.999 |
| Oligomer vs. Scrambled | -0.00942 | -0.02504 to 0.006197 | No | ns | 0.183 |

Mean cell area

| ANOVA summary | | | | | |
|---|---|---|---|---|---|
| F | 0.9375 | | | | |
| P value | 0.483 | | | | |
| P value summary | ns | | | | |
| Significant diff. among means (P < 0.05)? | No | | | | |
| R squared | 0.3846 | | | | |
| | | | | | |
| **Bonferroni's multiple comparisons test** | **Mean Diff.** | **95.00% CI of diff.** | **Below threshold?** | **Summary** | **Adjusted P Value** |
| Control vs. Oligomer | -0.1734 | -0.8098 to 0.4630 | No | ns | 0.832 |
| Control vs. Scrambled | -0.0469 | -0.6833 to 0.5895 | No | ns | >.999 |
| Oligomer vs. Scrambled | 0.1265 | -0.5099 to 0.7629 | No | ns | >.999 |

**1h – 155v2**

Mean cell length

| ANOVA summary | | | | | |
|---|---|---|---|---|---|
| F | 0.4888 | | | | |
| P value | 0.636 | | | | |
| P value summary | ns | | | | |
| Significant diff. among means (P < 0.05)? | No | | | | |
| R squared | 0.1401 | | | | |
| | | | | | |
| **Bonferroni's multiple comparisons test** | **Mean Diff.** | **95.00% CI of diff.** | **Below threshold?** | **Summary** | **Adjusted P Value** |
| Control vs. Oligomer | 0.02677 | -0.1863 to 0.2399 | No | ns | >.999 |
| Control vs. Scrambled | 0.06382 | -0.1493 to 0.2769 | No | ns | >.999 |
| Oligomer vs. Scrambled | 0.03705 | -0.1761 to 0.2502 | No | ns | >.999 |

**1h – 155v2**

Mean cell roundness

| ANOVA summary | | | | | |
|---|---|---|---|---|---|
| F | 0.06937 | | | | |
| P value | 0.934 | | | | |
| P value summary | ns | | | | |
| Significant diff. among means (P < 0.05)? | No | | | | |
| R squared | 0.0226 | | | | |
| | | | | | |
| **Bonferroni's multiple comparisons test** | **Mean Diff.** | **95.00% CI of diff.** | **Below threshold?** | **Summary** | **Adjusted P Value** |
| Control vs. Oligomer | 0.01437 | -0.1678 to 0.1965 | No | ns | >.999 |
| Control vs. Scrambled | -0.005637 | -0.1878 to 0.1765 | No | ns | >.999 |
| Oligomer vs. Scrambled | -0.02001 | -0.2021 to 0.1621 | No | ns | >.999 |

Mean cell width

| ANOVA summary | | | | | |
|---|---|---|---|---|---|
| F | 0.6052 | | | | |
| P value | 0.576 | | | | |
| P value summary | ns | | | | |
| Significant diff. among means (P < 0.05)? | No | | | | |
| R squared | 0.1679 | | | | |
| | | | | | |
| **Bonferroni's multiple comparisons test** | **Mean Diff.** | **95.00% CI of diff.** | **Below threshold?** | **Summary** | **Adjusted P Value** |
| Control vs. Oligomer | 0.09481 | -0.2749 to 0.4645 | No | ns | >.999 |
| Control vs. Scrambled | 0.1162 | -0.2534 to 0.4859 | No | ns | >.999 |
| Oligomer vs. Scrambled | 0.02143 | -0.3482 to 0.3911 | No | ns | >.999 |

**1h – 155v2**

Mean cytoplasm region

| ANOVA summary | | | | | |
|---|---|---|---|---|---|
| F | 1.165 | | | | |
| P value | 0.374 | | | | |
| P value summary | ns | | | | |
| Significant diff. among means (P < 0.05)? | No | | | | |
| R squared | 0.2797 | | | | |
| | | | | | |
| **Bonferroni's multiple comparisons test** | **Mean Diff.** | **95.00% CI of diff.** | **Below threshold?** | **Summary** | **Adjusted P Value** |
| Control vs. Oligomer | -0.1857 | -0.6601 to 0.2887 | No | ns | 0.737 |
| Control vs. Scrambled | 0.009804 | -0.4646 to 0.4842 | No | ns | >.999 |
| Oligomer vs. Scrambled | 0.1955 | -0.2789 to 0.6699 | No | ns | 0.673 |

Mean cell area

| ANOVA summary | | | | | |
|---|---|---|---|---|---|
| F | 0.2414 | | | | |
| P value | 0.793 | | | | |
| P value summary | ns | | | | |
| Significant diff. among means (P < 0.05)? | No | | | | |
| R squared | 0.07448 | | | | |
| | | | | | |
| **Bonferroni's multiple comparisons test** | **Mean Diff.** | **95.00% CI of diff.** | **Below threshold?** | **Summary** | **Adjusted P Value** |
| Control vs. Oligomer | 0.03426 | -0.4851 to 0.5536 | No | ns | >.999 |
| Control vs. Scrambled | 0.1075 | -0.4119 to 0.6268 | No | ns | >.999 |
| Oligomer vs. Scrambled | 0.07319 | -0.4461 to 0.5925 | No | ns | >.999 |

**1h – CS14**

Mean cell length

| ANOVA summary | | | | | |
|---|---|---|---|---|---|
| F | 6.389 | | | | |
| P value | 0.033 | | | | |
| P value summary | * | | | | |
| Significant diff. among means (P < 0.05)? | Yes | | | | |
| R squared | 0.6805 | | | | |
| | | | | | |
| **Bonferroni's multiple comparisons test** | **Mean Diff.** | **95.00% CI of diff.** | **Below threshold?** | **Summary** | **Adjusted P Value** |
| Control vs. Oligomer | -0.1632 | -0.3301 to 0.003723 | No | ns | 0.055 |
| Control vs. Scrambled | -0.1504 | -0.3173 to 0.01653 | No | ns | 0.076 |
| Oligomer vs. Scrambled | 0.01281 | -0.1541 to 0.1797 | No | ns | >.999 |

**1h – CS14**

Mean cell roundness

| ANOVA summary | | | | | |
|---|---|---|---|---|---|
| F | 0.2988 | | | | |
| P value | 0.752 | | | | |
| P value summary | ns | | | | |
| Significant diff. among means (P < 0.05)? | No | | | | |
| R squared | 0.09058 | | | | |
| | | | | | |
| **Bonferroni's multiple comparisons test** | **Mean Diff.** | **95.00% CI of diff.** | **Below threshold?** | **Summary** | **Adjusted P Value** |
| Control vs. Oligomer | -0.003235 | -0.06383 to 0.05736 | No | ns | >.999 |
| Control vs. Scrambled | 0.0104 | -0.05019 to 0.07099 | No | ns | >.999 |
| Oligomer vs. Scrambled | 0.01363 | -0.04696 to 0.07423 | No | ns | >.999 |

Mean cell width

| ANOVA summary | | | | | |
|---|---|---|---|---|---|
| F | 0.5269 | | | | |
| P value | 0.615 | | | | |
| P value summary | ns | | | | |
| Significant diff. among means (P < 0.05)? | No | | | | |
| R squared | 0.1494 | | | | |
| | | | | | |
| **Bonferroni's multiple comparisons test** | **Mean Diff.** | **95.00% CI of diff.** | **Below threshold?** | **Summary** | **Adjusted P Value** |
| Control vs. Oligomer | -0.02863 | -0.1785 to 0.1212 | No | ns | >.999 |
| Control vs. Scrambled | -0.04637 | -0.1962 to 0.1035 | No | ns | >.999 |
| Oligomer vs. Scrambled | -0.01775 | -0.1676 to 0.1321 | No | ns | >.999 |

**1h – CS14**

Mean cytoplasm region

| ANOVA summary | | | | | |
|---|---|---|---|---|---|
| F | 1.229 | | | | |
| P value | 0.357 | | | | |
| P value summary | ns | | | | |
| Significant diff. among means (P < 0.05)? | No | | | | |
| R squared | 0.2907 | | | | |
| | | | | | |
| **Bonferroni's multiple comparisons test** | **Mean Diff.** | **95.00% CI of diff.** | **Below threshold?** | **Summary** | **Adjusted P Value** |
| Control vs. Oligomer | 0.01422 | -0.02576 to 0.05421 | No | ns | 0.86 |
| Control vs. Scrambled | 0.01812 | -0.02187 to 0.05811 | No | ns | 0.561 |
| Oligomer vs. Scrambled | 0.003894 | -0.03609 to 0.04388 | No | ns | >.999 |

Mean cell area

| ANOVA summary | | | | | |
|---|---|---|---|---|---|
| F | 2.338 | | | | |
| P value | 0.177 | | | | |
| P value summary | ns | | | | |
| Significant diff. among means (P < 0.05)? | No | | | | |
| R squared | 0.438 | | | | |
| | | | | | |
| **Bonferroni's multiple comparisons test** | **Mean Diff.** | **95.00% CI of diff.** | **Below threshold?** | **Summary** | **Adjusted P Value** |
| Control vs. Oligomer | -0.1697 | -0.4833 to 0.1439 | No | ns | 0.377 |
| Control vs. Scrambled | -0.1864 | -0.5000 to 0.1272 | No | ns | 0.295 |
| Oligomer vs. Scrambled | -0.01674 | -0.3303 to 0.2969 | No | ns | >.999 |

**All cell lines – 1h**

Mean cell length

| ANOVA summary | | | | | |
|---|---|---|---|---|---|
| F | 0.1744 | | | | |
| P value | 0.848 | | | | |
| P value summary | ns | | | | |
| Significant diff. among means (P < 0.05)? | No | | | | |
| R squared | 0.1042 | | | | |
| | | | | | |
| **Bonferroni's multiple comparisons test** | **Mean Diff.** | **95.00% CI of diff.** | **Below threshold?** | **Summary** | **Adjusted P Value** |
| Control vs. Oligomer | -0.06821 | -0.6359 to 0.4995 | No | ns | >.999 |
| Control vs. Scrambled | -0.04328 | -0.6110 to 0.5244 | No | ns | >.999 |
| Oligomer vs. Scrambled | 0.02493 | -0.5427 to 0.5926 | No | ns | >.999 |

**All cell lines – 1h**

Mean cell roundness

| ANOVA summary | | | | | |
|---|---|---|---|---|---|
| F | 0.1651 | | | | |
| P value | 0.855 | | | | |
| P value summary | ns | | | | |
| Significant diff. among means (P < 0.05)? | No | | | | |
| R squared | 0.09918 | | | | |
| | | | | | |
| **Bonferroni's multiple comparisons test** | **Mean Diff.** | **95.00% CI of diff.** | **Below threshold?** | **Summary** | **Adjusted P Value** |
| Control vs. Oligomer | 0.005568 | -0.04165 to 0.05279 | No | ns | >.999 |
| Control vs. Scrambled | 0.002381 | -0.04484 to 0.04960 | No | ns | >.999 |
| Oligomer vs. Scrambled | -0.003187 | -0.05041 to 0.04403 | No | ns | >.999 |

Mean cell width

| ANOVA summary | | | | | |
|---|---|---|---|---|---|
| F | 0.01189 | | | | |
| P value | 0.988 | | | | |
| P value summary | ns | | | | |
| Significant diff. among means (P < 0.05)? | No | | | | |
| R squared | 0.007862 | | | | |
| | | | | | |
| **Bonferroni's multiple comparisons test** | **Mean Diff.** | **95.00% CI of diff.** | **Below threshold?** | **Summary** | **Adjusted P Value** |
| Control vs. Oligomer | 0.005891 | -0.2486 to 0.2604 | No | ns | >.999 |
| Control vs. Scrambled | 0.007734 | -0.2468 to 0.2622 | No | ns | >.999 |
| Oligomer vs. Scrambled | 0.001843 | -0.2527 to 0.2564 | No | ns | >.999 |

**All cell lines – 1h**

Mean cytoplasm region

| ANOVA summary | | | | | |
|---|---|---|---|---|---|
| F | 0.8735 | | | | |
| P value | 0.502 | | | | |
| P value summary | ns | | | | |
| Significant diff. among means (P < 0.05)? | No | | | | |
| R squared | 0.368 | | | | |
| | | | | | |
| **Bonferroni's multiple comparisons test** | **Mean Diff.** | **95.00% CI of diff.** | **Below threshold?** | **Summary** | **Adjusted P Value** |
| Control vs. Oligomer | -0.08573 | -0.4824 to 0.3110 | No | ns | >.999 |
| Control vs. Scrambled | 0.01396 | -0.3827 to 0.4107 | No | ns | >.999 |
| Oligomer vs. Scrambled | 0.09969 | -0.2970 to 0.4964 | No | ns | 0.928 |

Mean cell area

| ANOVA summary | | | | | |
|---|---|---|---|---|---|
| F | 0.1085 | | | | |
| P value | 0.901 | | | | |
| P value summary | ns | | | | |
| Significant diff. among means (P < 0.05)? | No | | | | |
| R squared | 0.06745 | | | | |
| | | | | | |
| **Bonferroni's multiple comparisons test** | **Mean Diff.** | **95.00% CI of diff.** | **Below threshold?** | **Summary** | **Adjusted P Value** |
| Control vs. Oligomer | -0.06772 | -0.7770 to 0.6416 | No | ns | >.999 |
| Control vs. Scrambled | -0.03949 | -0.7488 to 0.6698 | No | ns | >.999 |
| Oligomer vs. Scrambled | 0.02822 | -0.6811 to 0.7375 | No | ns | >.999 |

**2h – 155v2**

Mean cell length

| ANOVA summary | | | | | |
|---|---|---|---|---|---|
| F | 0.1866 | | | | |
| P value | 0.834 | | | | |
| P value summary | ns | | | | |
| Significant diff. among means (P < 0.05)? | No | | | | |
| R squared | 0.05856 | | | | |
| | | | | | |
| **Bonferroni's multiple comparisons test** | **Mean Diff.** | **95.00% CI of diff.** | **Below threshold?** | **Summary** | **Adjusted P Value** |
| Control vs. Oligomer | 0.05802 | -0.3223 to 0.4383 | No | ns | >.999 |
| Control vs. Scrambled | -0.005942 | -0.3863 to 0.3744 | No | ns | >.999 |
| Oligomer vs. Scrambled | -0.06396 | -0.4443 to 0.3164 | No | ns | >.999 |

**2h – 155v2**

Mean cell roundness

| ANOVA summary | | | | | |
|---|---|---|---|---|---|
| F | 0.401 | | | | |
| P value | 0.686 | | | | |
| P value summary | ns | | | | |
| Significant diff. among means (P < 0.05)? | No | | | | |
| R squared | 0.1179 | | | | |
| | | | | | |
| **Bonferroni's multiple comparisons test** | **Mean Diff.** | **95.00% CI of diff.** | **Below threshold?** | **Summary** | **Adjusted P Value** |
| Control vs. Oligomer | -0.04767 | -0.3758 to 0.2805 | No | ns | >.999 |
| Control vs. Scrambled | 0.04165 | -0.2865 to 0.3698 | No | ns | >.999 |
| Oligomer vs. Scrambled | 0.08932 | -0.2388 to 0.4175 | No | ns | >.999 |

Mean cell width

| ANOVA summary | | | | | |
|---|---|---|---|---|---|
| F | 2.889 | | | | |
| P value | 0.132 | | | | |
| P value summary | ns | | | | |
| Significant diff. among means (P < 0.05)? | No | | | | |
| R squared | 0.4906 | | | | |
| | | | | | |
| **Bonferroni's multiple comparisons test** | **Mean Diff.** | **95.00% CI of diff.** | **Below threshold?** | **Summary** | **Adjusted P Value** |
| Control vs. Oligomer | -0.1214 | -0.3184 to 0.07559 | No | ns | 0.267 |
| Control vs. Scrambled | -0.1278 | -0.3249 to 0.06918 | No | ns | 0.231 |
| Oligomer vs. Scrambled | -0.006412 | -0.2034 to 0.1906 | No | ns | >.999 |

**2h – 155v2**

Mean cytoplasm region

| ANOVA summary | | | | | |
|---|---|---|---|---|---|
| F | 0.2667 | | | | |
| P value | 0.775 | | | | |
| P value summary | ns | | | | |
| Significant diff. among means (P < 0.05)? | No | | | | |
| R squared | 0.08163 | | | | |
| | | | | | |
| **Bonferroni's multiple comparisons test** | **Mean Diff.** | **95.00% CI of diff.** | **Below threshold?** | **Summary** | **Adjusted P Value** |
| Control vs. Oligomer | 0.004871 | -0.02507 to 0.03481 | No | ns | >.999 |
| Control vs. Scrambled | -0.001486 | -0.03142 to 0.02845 | No | ns | >.999 |
| Oligomer vs. Scrambled | -0.006357 | -0.03629 to 0.02358 | No | ns | >.999 |

Mean cell area

| ANOVA summary | | | | | |
|---|---|---|---|---|---|
| F | 0.9242 | | | | |
| P value | 0.447 | | | | |
| P value summary | ns | | | | |
| Significant diff. among means (P < 0.05)? | No | | | | |
| R squared | 0.2355 | | | | |
| | | | | | |
| **Bonferroni's multiple comparisons test** | **Mean Diff.** | **95.00% CI of diff.** | **Below threshold?** | **Summary** | **Adjusted P Value** |
| Control vs. Oligomer | -0.04964 | -0.4166 to 0.3173 | No | ns | >.999 |
| Control vs. Scrambled | -0.149 | -0.5160 to 0.2180 | No | ns | 0.691 |
| Oligomer vs. Scrambled | -0.09938 | -0.4664 to 0.2676 | No | ns | >.999 |

**2h – CS14**

Mean cell length

| ANOVA summary | | | | | |
|---|---|---|---|---|---|
| F | 0.6232 | | | | |
| P value | 0.568 | | | | |
| P value summary | ns | | | | |
| Significant diff. among means (P < 0.05)? | No | | | | |
| R squared | 0.172 | | | | |
| | | | | | |
| **Bonferroni's multiple comparisons test** | **Mean Diff.** | **95.00% CI of diff.** | **Below threshold?** | **Summary** | **Adjusted P Value** |
| Control vs. Oligomer | -0.1074 | -0.4988 to 0.2839 | No | ns | >.999 |
| Control vs. Scrambled | 0.014 | -0.3773 to 0.4053 | No | ns | >.999 |
| Oligomer vs. Scrambled | 0.1214 | -0.2699 to 0.5128 | No | ns | >.999 |

**2h – CS14**

Mean cell roundness

| ANOVA summary | | | | | |
|---|---|---|---|---|---|
| F | 1.326 | | | | |
| P value | 0.334 | | | | |
| P value summary | ns | | | | |
| Significant diff. among means (P < 0.05)? | No | | | | |
| R squared | 0.3065 | | | | |
| | | | | | |
| **Bonferroni's multiple comparisons test** | **Mean Diff.** | **95.00% CI of diff.** | **Below threshold?** | **Summary** | **Adjusted P Value** |
| Control vs. Oligomer | 0.08647 | -0.1151 to 0.2881 | No | ns | 0.625 |
| Control vs. Scrambled | -2.87E-05 | -0.2016 to 0.2016 | No | ns | >.999 |
| Oligomer vs. Scrambled | -0.08649 | -0.2881 to 0.1151 | No | ns | 0.624 |

Mean cell width

| ANOVA summary | | | | | |
|---|---|---|---|---|---|
| F | 1.239 | | | | |
| P value | 0.355 | | | | |
| P value summary | ns | | | | |
| Significant diff. among means (P < 0.05)? | No | | | | |
| R squared | 0.2922 | | | | |
| | | | | | |
| **Bonferroni's multiple comparisons test** | **Mean Diff.** | **95.00% CI of diff.** | **Below threshold?** | **Summary** | **Adjusted P Value** |
| Control vs. Oligomer | -0.1962 | -0.6262 to 0.2338 | No | ns | 0.553 |
| Control vs. Scrambled | -0.04416 | -0.4741 to 0.3858 | No | ns | >.999 |
| Oligomer vs. Scrambled | 0.1521 | -0.2779 to 0.5821 | No | ns | 0.867 |

**2h – CS14**

Mean cytoplasm region

| ANOVA summary | | | | | |
|---|---|---|---|---|---|
| F | 1.912 | | | | |
| P value | 0.228 | | | | |
| P value summary | ns | | | | |
| Significant diff. among means (P < 0.05)? | No | | | | |
| R squared | 0.3892 | | | | |
| | | | | | |
| **Bonferroni's multiple comparisons test** | **Mean Diff.** | **95.00% CI of diff.** | **Below threshold?** | **Summary** | **Adjusted P Value** |
| Control vs. Oligomer | 0.03502 | -0.02475 to 0.09479 | No | ns | 0.307 |
| Control vs. Scrambled | 0.01222 | -0.04755 to 0.07199 | No | ns | >.999 |
| Oligomer vs. Scrambled | -0.0228 | -0.08257 to 0.03697 | No | ns | 0.769 |

Mean cell area

| ANOVA summary | | | | | |
|---|---|---|---|---|---|
| F | 1.959 | | | | |
| P value | 0.221 | | | | |
| P value summary | ns | | | | |
| Significant diff. among means (P < 0.05)? | No | | | | |
| R squared | 0.395 | | | | |
| | | | | | |
| **Bonferroni's multiple comparisons test** | **Mean Diff.** | **95.00% CI of diff.** | **Below threshold?** | **Summary** | **Adjusted P Value** |
| Control vs. Oligomer | -0.3739 | -1.029 to 0.2807 | No | ns | 0.329 |
| Control vs. Scrambled | -0.07897 | -0.7336 to 0.5756 | No | ns | >.999 |
| Oligomer vs. Scrambled | 0.2949 | -0.3597 to 0.9495 | No | ns | 0.567 |

**All cell lines – 2h**

Mean cell length

| ANOVA summary | | | | | |
|---|---|---|---|---|---|
| F | 0.1046 | | | | |
| P value | 0.904 | | | | |
| P value summary | ns | | | | |
| Significant diff. among means (P < 0.05)? | No | | | | |
| R squared | 0.06521 | | | | |
| | | | | | |
| **Bonferroni's multiple comparisons test** | **Mean Diff.** | **95.00% CI of diff.** | **Below threshold?** | **Summary** | **Adjusted P Value** |
| Control vs. Oligomer | -0.02471 | -0.3552 to 0.3057 | No | ns | >.999 |
| Control vs. Scrambled | 0.00403 | -0.3264 to 0.3345 | No | ns | >.999 |
| Oligomer vs. Scrambled | 0.02874 | -0.3017 to 0.3592 | No | ns | >.999 |

## 5.3 iAstrocyte ICC analysis as a response to $A\beta_{1-42}$ fibrils

**155v2– repeated stress**

High damage

| ANOVA summary | | | | | |
|---|---|---|---|---|---|
| F | 0.8058 | | | | |
| P value | 0.49 | | | | |
| P value summary | ns | | | | |
| Significant diff. among means (P < 0.05)? | No | | | | |
| R squared | 0.2117 | | | | |
| | | | | | |
| **Bonferroni's multiple comparisons test** | **Mean Diff.** | **95.00% CI of diff.** | **Below threshold?** | **Summary** | **Adjusted P Value** |
| Control vs. Fibril | -0.8697 | -3.134 to 1.395 | No | ns | 0.761 |
| Control vs. Scrambled | -0.5138 | -2.778 to 1.751 | No | ns | >.999 |
| Fibril vs. Scrambled | 0.3559 | -1.908 to 2.620 | No | ns | >.999 |

**155v2– repeated stress**

All damage

| ANOVA summary | | | | | |
|---|---|---|---|---|---|
| F | 0.1422 | | | | |
| P value | 0.87 | | | | |
| P value summary | ns | | | | |
| Significant diff. among means (P < 0.05)? | No | | | | |
| R squared | 0.04526 | | | | |
| | | | | | |
| **Bonferroni's multiple comparisons test** | **Mean Diff.** | **95.00% CI of diff.** | **Below threshold?** | **Summary** | **Adjusted P Value** |
| Control vs. Fibril | 0.07197 | -0.3854 to 0.5294 | No | ns | >.999 |
| Control vs. Scrambled | 0.05163 | -0.4058 to 0.5090 | No | ns | >.999 |
| Fibril vs. Scrambled | -0.02034 | -0.4778 to 0.4371 | No | ns | >.999 |

Low damage

| ANOVA summary | | | | | |
|---|---|---|---|---|---|
| F | 0.1792 | | | | |
| P value | 0.84 | | | | |
| P value summary | ns | | | | |
| Significant diff. among means (P < 0.05)? | No | | | | |
| R squared | 0.05635 | | | | |
| | | | | | |
| **Bonferroni's multiple comparisons test** | **Mean Diff.** | **95.00% CI of diff.** | **Below threshold?** | **Summary** | **Adjusted P Value** |
| Control vs. Fibril | -0.01197 | -0.1032 to 0.07929 | No | ns | >.999 |
| Control vs. Scrambled | -0.01597 | -0.1072 to 0.07530 | No | ns | >.999 |
| Fibril vs. Scrambled | -0.003996 | -0.09526 to 0.08727 | No | ns | >.999 |

## 161– repeated stress

High damage

| ANOVA summary | | | | | |
|---|---|---|---|---|---|
| F | 0.1971 | | | | |
| P value | 0.826 | | | | |
| P value summary | ns | | | | |
| Significant diff. among means (P < 0.05)? | No | | | | |
| R squared | 0.06164 | | | | |
| | | | | | |
| **Bonferroni's multiple comparisons test** | **Mean Diff.** | **95.00% CI of diff.** | **Below threshold?** | **Summary** | **Adjusted P Value** |
| Control vs. Fibril | -0.03973 | -0.6168 to 0.5374 | No | ns | >.999 |
| Control vs. Scrambled | 0.06916 | -0.5079 to 0.6463 | No | ns | >.999 |
| Fibril vs. Scrambled | 0.1089 | -0.4682 to 0.6860 | No | ns | >.999 |

## 161– repeated stress

All damage

| ANOVA summary | | | | | |
|---|---|---|---|---|---|
| F | 0.1455 | | | | |
| P value | 0.868 | | | | |
| P value summary | ns | | | | |
| Significant diff. among means (P < 0.05)? | No | | | | |
| R squared | 0.04627 | | | | |
| | | | | | |
| **Bonferroni's multiple comparisons test** | **Mean Diff.** | **95.00% CI of diff.** | **Below threshold?** | **Summary** | **Adjusted P Value** |
| Control vs. Fibril | 0.01677 | -0.1907 to 0.2243 | No | ns | >.999 |
| Control vs. Scrambled | 0.03405 | -0.1734 to 0.2415 | No | ns | >.999 |
| Fibril vs. Scrambled | 0.01728 | -0.1902 to 0.2248 | No | ns | >.999 |

Low damage

| ANOVA summary | | | | | |
|---|---|---|---|---|---|
| F | 0.4031 | | | | |
| P value | 0.685 | | | | |
| P value summary | ns | | | | |
| Significant diff. among means (P < 0.05)? | No | | | | |
| R squared | 0.1184 | | | | |
| | | | | | |
| **Bonferroni's multiple comparisons test** | **Mean Diff.** | **95.00% CI of diff.** | **Below threshold?** | **Summary** | **Adjusted P Value** |
| Control vs. Fibril | -0.04864 | -0.3368 to 0.2395 | No | ns | >.999 |
| Control vs. Scrambled | -0.07791 | -0.3661 to 0.2103 | No | ns | >.999 |
| Fibril vs. Scrambled | -0.02926 | -0.3174 to 0.2589 | No | ns | >.999 |

**CS14– repeated stress**

High damage

| ANOVA summary | | | | | |
|---|---|---|---|---|---|
| F | 200.8 | | | | |
| P value | <.001 | | | | |
| P value summary | *** | | | | |
| Significant diff. among means (P < 0.05)? | Yes | | | | |
| R squared | 0.9853 | | | | |
| | | | | | |
| **Bonferroni's multiple comparisons test** | **Mean Diff.** | **95.00% CI of diff.** | **Below threshold?** | **Summary** | **Adjusted P Value** |
| Control vs. Fibril | 0.154 | 0.1230 to 0.1849 | Yes | *** | <.001 |
| Control vs. Scrambled | -0.01747 | -0.04842 to 0.01348 | No | ns | 0.339 |
| Fibril vs. Scrambled | -0.1714 | -0.2024 to -0.1405 | Yes | *** | <.001 |

**CS14– repeated stress**

All damage

| ANOVA summary | | | | | |
|---|---|---|---|---|---|
| F | 13.96 | | | | |
| P value | 0.006 | | | | |
| P value summary | ** | | | | |
| Significant diff. among means (P < 0.05)? | Yes | | | | |
| R squared | 0.8231 | | | | |
| | | | | | |
| **Bonferroni's multiple comparisons test** | **Mean Diff.** | **95.00% CI of diff.** | **Below threshold?** | **Summary** | **Adjusted P Value** |
| Control vs. Fibril | 0.05583 | 0.01572 to 0.09593 | Yes | * | 0.011 |
| Control vs. Scrambled | 0 | -0.04011 to 0.04011 | No | ns | >.999 |
| Fibril vs. Scrambled | -0.05583 | -0.09593 to -0.01572 | Yes | * | 0.011 |

Low damage

| ANOVA summary | | | | | |
|---|---|---|---|---|---|
| F | 7.537 | | | | |
| P value | 0.044 | | | | |
| P value summary | * | | | | |
| Significant diff. among means (P < 0.05)? | Yes | | | | |
| R squared | 0.7903 | | | | |
| | | | | | |
| **Bonferroni's multiple comparisons test** | **Mean Diff.** | **95.00% CI of diff.** | **Below threshold?** | **Summary** | **Adjusted P Value** |
| Control vs. Fibril | -7.824 | -16.51 to 0.8604 | No | ns | 0.07 |
| Control vs. Scrambled | 0.5258 | -11.76 to 12.81 | No | ns | >.999 |
| Fibril vs. Scrambled | 8.349 | -3.932 to 20.63 | No | ns | 0.164 |

High damage

| ANOVA summary | | | | | |
|---|---|---|---|---|---|
| F | 0.3675 | | | | |
| P value | 0.707 | | | | |
| P value summary | ns | | | | |
| Significant diff. among means (P < 0.05)? | No | | | | |
| R squared | 0.1091 | | | | |
| | | | | | |
| **Bonferroni's multiple comparisons test** | **Mean Diff.** | **95.00% CI of diff.** | **Below threshold?** | **Summary** | **Adjusted P Value** |
| Control vs. Fibril | -0.2518 | -1.225 to 0.7217 | No | ns | >.999 |
| Control vs. Scrambled | -0.154 | -1.128 to 0.8195 | No | ns | >.999 |
| Fibril vs. Scrambled | 0.09777 | -0.8757 to 1.071 | No | ns | >.999 |

**All cell lines – repeated stress**

All damage

| ANOVA summary | | | | | |
|---|---|---|---|---|---|
| F | 3.536 | | | | |
| P value | 0.097 | | | | |
| P value summary | ns | | | | |
| Significant diff. among means (P < 0.05)? | No | | | | |
| R squared | 0.541 | | | | |
| | | | | | |
| **Bonferroni's multiple comparisons test** | **Mean Diff.** | **95.00% CI of diff.** | **Below threshold?** | **Summary** | **Adjusted P Value** |
| Control vs. Fibril | 0.04819 | -0.01172 to 0.1081 | No | ns | 0.115 |
| Control vs. Scrambled | 0.02856 | -0.03135 to 0.08847 | No | ns | 0.504 |
| Fibril vs. Scrambled | -0.01963 | -0.07954 to 0.04028 | No | ns | 0.968 |

Low damage

| ANOVA summary | | | | | |
|---|---|---|---|---|---|
| F | 1.077 | | | | |
| P value | 0.398 | | | | |
| P value summary | ns | | | | |
| Significant diff. among means (P < 0.05)? | No | | | | |
| R squared | 0.2641 | | | | |
| | | | | | |
| **Bonferroni's multiple comparisons test** | **Mean Diff.** | **95.00% CI of diff.** | **Below threshold?** | **Summary** | **Adjusted P Value** |
| Control vs. Fibril | -2.628 | -9.620 to 4.364 | No | ns | 0.788 |
| Control vs. Scrambled | 0.144 | -6.848 to 7.136 | No | ns | >.999 |
| Fibril vs. Scrambled | 2.772 | -4.220 to 9.764 | No | ns | 0.721 |

**155v2– 1h**

High damage

| **ANOVA summary** | | | | | |
|---|---|---|---|---|---|
| F | 1.803 | | | | |
| P value | 0.244 | | | | |
| P value summary | ns | | | | |
| Significant diff. among means (P < 0.05)? | No | | | | |
| R squared | 0.3754 | | | | |
| | | | | | |
| **Bonferroni's multiple comparisons test** | **Mean Diff.** | **95.00% CI of diff.** | **Below threshold?** | **Summary** | **Adjusted P Value** |
| Control vs. Fibril | 0.2556 | -0.5685 to 1.080 | No | ns | >.999 |
| Control vs. Scrambled | 0.4756 | -0.3485 to 1.300 | No | ns | 0.32 |
| Fibril vs. Scrambled | 0.22 | -0.6041 to 1.044 | No | ns | >.999 |

**155v2– 1h**

All damage

| **ANOVA summary** | | | | | |
|---|---|---|---|---|---|
| F | 4.359 | | | | |
| P value | 0.068 | | | | |
| P value summary | ns | | | | |
| Significant diff. among means (P < 0.05)? | No | | | | |
| R squared | 0.5924 | | | | |
| | | | | | |
| **Bonferroni's multiple comparisons test** | **Mean Diff.** | **95.00% CI of diff.** | **Below threshold?** | **Summary** | **Adjusted P Value** |
| Control vs. Fibril | -0.2023 | -0.6621 to 0.2575 | No | ns | 0.594 |
| Control vs. Scrambled | 0.2106 | -0.2492 to 0.6704 | No | ns | 0.548 |
| Fibril vs. Scrambled | 0.413 | -0.04683 to 0.8727 | No | ns | 0.077 |

Low damage

| **ANOVA summary** | | | | | |
|---|---|---|---|---|---|
| F | 5.897 | | | | |
| P value | 0.038 | | | | |
| P value summary | * | | | | |
| Significant diff. among means (P < 0.05)? | Yes | | | | |
| R squared | 0.6628 | | | | |
| | | | | | |
| **Bonferroni's multiple comparisons test** | **Mean Diff.** | **95.00% CI of diff.** | **Below threshold?** | **Summary** | **Adjusted P Value** |
| Control vs. Fibril | 0.07819 | -0.08565 to 0.2420 | No | ns | 0.503 |
| Control vs. Scrambled | -0.09275 | -0.2566 to 0.07109 | No | ns | 0.336 |
| Fibril vs. Scrambled | -0.1709 | -0.3348 to -0.007102 | Yes | * | 0.042 |

**161– 1h**

High damage

| ANOVA summary | | | | | |
|---|---|---|---|---|---|
| F | 1.227 | | | | |
| P value | 0.357 | | | | |
| P value summary | ns | | | | |
| Significant diff. among means (P < 0.05)? | No | | | | |
| R squared | 0.2904 | | | | |
| | | | | | |
| **Bonferroni's multiple comparisons test** | **Mean Diff.** | **95.00% CI of diff.** | **Below threshold?** | **Summary** | **Adjusted P Value** |
| Control vs. Fibril | 0.1809 | -0.3282 to 0.6899 | No | ns | 0.861 |
| Control vs. Scrambled | -0.04961 | -0.5587 to 0.4595 | No | ns | >.999 |
| Fibril vs. Scrambled | -0.2305 | -0.7395 to 0.2786 | No | ns | 0.562 |

**161– 1h**

All damage

| ANOVA summary | | | | | |
|---|---|---|---|---|---|
| F | 1.581 | | | | |
| P value | 0.281 | | | | |
| P value summary | ns | | | | |
| Significant diff. among means (P < 0.05)? | No | | | | |
| R squared | 0.3451 | | | | |
| | | | | | |
| **Bonferroni's multiple comparisons test** | **Mean Diff.** | **95.00% CI of diff.** | **Below threshold?** | **Summary** | **Adjusted P Value** |
| Control vs. Fibril | 0.05811 | -0.1088 to 0.2251 | No | ns | 0.888 |
| Control vs. Scrambled | -0.03079 | -0.1977 to 0.1361 | No | ns | >.999 |
| Fibril vs. Scrambled | -0.08891 | -0.2558 to 0.07804 | No | ns | 0.392 |

Low damage

| ANOVA summary | | | | | |
|---|---|---|---|---|---|
| F | 1.218 | | | | |
| P value | 0.36 | | | | |
| P value summary | ns | | | | |
| Significant diff. among means (P < 0.05)? | No | | | | |
| R squared | 0.2887 | | | | |
| | | | | | |
| **Bonferroni's multiple comparisons test** | **Mean Diff.** | **95.00% CI of diff.** | **Below threshold?** | **Summary** | **Adjusted P Value** |
| Control vs. Fibril | -0.08133 | -0.3127 to 0.1501 | No | ns | 0.875 |
| Control vs. Scrambled | 0.02329 | -0.2081 to 0.2547 | No | ns | >.999 |
| Fibril vs. Scrambled | 0.1046 | -0.1268 to 0.3360 | No | ns | 0.563 |

**CS14– 1h**

High damage

| ANOVA summary | | | | | |
|---|---|---|---|---|---|
| F | 16.55 | | | | |
| P value | 0.004 | | | | |
| P value summary | ** | | | | |
| Significant diff. among means (P < 0.05)? | Yes | | | | |
| R squared | 0.8465 | | | | |
| | | | | | |
| **Bonferroni's multiple comparisons test** | **Mean Diff.** | **95.00% CI of diff.** | **Below threshold?** | **Summary** | **Adjusted P Value** |
| Control vs. Fibril | 0.0581 | 0.01247 to 0.1037 | Yes | * | 0.017 |
| Control vs. Scrambled | -0.01839 | -0.06402 to 0.02724 | No | ns | 0.7 |
| Fibril vs. Scrambled | -0.07649 | -0.1221 to -0.03086 | Yes | ** | 0.005 |

**CS14– 1h**

All damage

| ANOVA summary | | | | | |
|---|---|---|---|---|---|
| F | 11.4 | | | | |
| P value | 0.009 | | | | |
| P value summary | ** | | | | |
| Significant diff. among means (P < 0.05)? | Yes | | | | |
| R squared | 0.7916 | | | | |
| | | | | | |
| **Bonferroni's multiple comparisons test** | **Mean Diff.** | **95.00% CI of diff.** | **Below threshold?** | **Summary** | **Adjusted P Value** |
| Control vs. Fibril | 0.01665 | -0.0001008 to 0.0334( | No | ns | 0.051 |
| Control vs. Scrambled | -0.007037 | -0.02379 to 0.009716 | No | ns | 0.65 |
| Fibril vs. Scrambled | -0.02369 | -0.04044 to -0.006936 | Yes | * | 0.011 |

Low damage

| ANOVA summary | | | | | |
|---|---|---|---|---|---|
| F | 12.78 | | | | |
| P value | 0.018 | | | | |
| P value summary | * | | | | |
| Significant diff. among means (P < 0.05)? | Yes | | | | |
| R squared | 0.8647 | | | | |
| | | | | | |
| **Bonferroni's multiple comparisons test** | **Mean Diff.** | **95.00% CI of diff.** | **Below threshold?** | **Summary** | **Adjusted P Value** |
| Control vs. Fibril | -1.99 | -3.761 to -0.2201 | Yes | * | 0.034 |
| Control vs. Scrambled | 0.4194 | -2.084 to 2.923 | No | ns | >.999 |
| Fibril vs. Scrambled | 2.41 | -0.09389 to 4.914 | No | ns | 0.057 |

High damage

| ANOVA summary | | | | | |
|---|---|---|---|---|---|
| F | 0.7206 | | | | |
| P value | 0.524 | | | | |
| P value summary | ns | | | | |
| Significant diff. among means (P < 0.05)? | No | | | | |
| R squared | 0.1937 | | | | |
| | | | | | |
| **Bonferroni's multiple comparisons test** | **Mean Diff.** | **95.00% CI of diff.** | **Below threshold?** | **Summary** | **Adjusted P Value** |
| Control vs. Fibril | 0.1649 | -0.3172 to 0.6469 | No | ns | 0.912 |
| Control vs. Scrambled | 0.1359 | -0.3462 to 0.6180 | No | ns | >.999 |
| Fibril vs. Scrambled | -0.02899 | -0.5111 to 0.4531 | No | ns | >.999 |

**All cell lines– 1h**

All damage

| ANOVA summary | | | | | |
|---|---|---|---|---|---|
| F | 0.6094 | | | | |
| P value | 0.574 | | | | |
| P value summary | ns | | | | |
| Significant diff. among means (P < 0.05)? | No | | | | |
| R squared | 0.1688 | | | | |
| | | | | | |
| **Bonferroni's multiple comparisons test** | **Mean Diff.** | **95.00% CI of diff.** | **Below threshold?** | **Summary** | **Adjusted P Value** |
| Control vs. Fibril | -0.04252 | -0.3418 to 0.2567 | No | ns | >.999 |
| Control vs. Scrambled | 0.0576 | -0.2417 to 0.3569 | No | ns | >.999 |
| Fibril vs. Scrambled | 0.1001 | -0.1991 to 0.3994 | No | ns | 0.941 |

Low damage

| ANOVA summary | | | | | |
|---|---|---|---|---|---|
| F | 1.144 | | | | |
| P value | 0.379 | | | | |
| P value summary | ns | | | | |
| Significant diff. among means (P < 0.05)? | No | | | | |
| R squared | 0.2761 | | | | |
| | | | | | |
| **Bonferroni's multiple comparisons test** | **Mean Diff.** | **95.00% CI of diff.** | **Below threshold?** | **Summary** | **Adjusted P Value** |
| Control vs. Fibril | -0.6645 | -2.496 to 1.167 | No | ns | 0.834 |
| Control vs. Scrambled | 0.1166 | -1.715 to 1.948 | No | ns | >.999 |
| Fibril vs. Scrambled | 0.7812 | -1.051 to 2.613 | No | ns | 0.631 |

High damage

| ANOVA summary | | | | | |
|---|---|---|---|---|---|
| F | 0.1112 | | | | |
| P value | 0.897 | | | | |
| P value summary | ns | | | | |
| Significant diff. among means (P < 0.05)? | No | | | | |
| R squared | 0.03573 | | | | |
| | | | | | |
| **Bonferroni's multiple comparisons test** | **Mean Diff.** | **95.00% CI of diff.** | **Below threshold?** | **Summary** | **Adjusted P Value** |
| Control vs. Fibril | 0.07264 | -0.7829 to 0.9282 | No | ns | >.999 |
| Control vs. Scrambled | -0.04934 | -0.9049 to 0.8062 | No | ns | >.999 |
| Fibril vs. Scrambled | -0.122 | -0.9775 to 0.7336 | No | ns | >.999 |

**161– 2h**

All damage

| ANOVA summary | | | | | |
|---|---|---|---|---|---|
| F | 0.08461 | | | | |
| P value | 0.92 | | | | |
| P value summary | ns | | | | |
| Significant diff. among means (P < 0.05)? | No | | | | |
| R squared | 0.02743 | | | | |
| | | | | | |
| **Bonferroni's multiple comparisons test** | **Mean Diff.** | **95.00% CI of diff.** | **Below threshold?** | **Summary** | **Adjusted P Value** |
| Control vs. Fibril | 0.03292 | -0.2807 to 0.3465 | No | ns | >.999 |
| Control vs. Scrambled | -0.002042 | -0.3157 to 0.3116 | No | ns | >.999 |
| Fibril vs. Scrambled | -0.03496 | -0.3486 to 0.2787 | No | ns | >.999 |

Low damage

| ANOVA summary | | | | | |
|---|---|---|---|---|---|
| F | 0.1326 | | | | |
| P value | 0.878 | | | | |
| P value summary | ns | | | | |
| Significant diff. among means (P < 0.05)? | No | | | | |
| R squared | 0.04232 | | | | |
| | | | | | |
| **Bonferroni's multiple comparisons test** | **Mean Diff.** | **95.00% CI of diff.** | **Below threshold?** | **Summary** | **Adjusted P Value** |
| Control vs. Fibril | -0.02424 | -0.3994 to 0.3509 | No | ns | >.999 |
| Control vs. Scrambled | 0.03424 | -0.3409 to 0.4094 | No | ns | >.999 |
| Fibril vs. Scrambled | 0.05848 | -0.3167 to 0.4337 | No | ns | >.999 |

High damage

| ANOVA summary | | | | | |
|---|---|---|---|---|---|
| F | 0.0542 | | | | |
| P value | 0.948 | | | | |
| P value summary | ns | | | | |
| Significant diff. among means (P < 0.05)? | No | | | | |
| R squared | 0.01775 | | | | |
| | | | | | |
| **Bonferroni's multiple comparisons test** | **Mean Diff.** | **95.00% CI of diff.** | **Below threshold?** | **Summary** | **Adjusted P Value** |
| Control vs. Fibril | 0.06621 | -0.6040 to 0.7364 | No | ns | >.999 |
| Control vs. Scrambled | 0.02355 | -0.6466 to 0.6937 | No | ns | >.999 |
| Fibril vs. Scrambled | -0.04266 | -0.7128 to 0.6275 | No | ns | >.999 |

**155v2– 2h**

All damage

| ANOVA summary | | | | | |
|---|---|---|---|---|---|
| F | 0.1526 | | | | |
| P value | 0.862 | | | | |
| P value summary | ns | | | | |
| Significant diff. among means (P < 0.05)? | No | | | | |
| R squared | 0.04842 | | | | |
| | | | | | |
| **Bonferroni's multiple comparisons test** | **Mean Diff.** | **95.00% CI of diff.** | **Below threshold?** | **Summary** | **Adjusted P Value** |
| Control vs. Fibril | -0.02052 | -0.4574 to 0.4164 | No | ns | >.999 |
| Control vs. Scrambled | -0.07132 | -0.5082 to 0.3656 | No | ns | >.999 |
| Fibril vs. Scrambled | -0.0508 | -0.4877 to 0.3861 | No | ns | >.999 |

Low damage

| ANOVA summary | | | | | |
|---|---|---|---|---|---|
| F | 0.05421 | | | | |
| P value | 0.948 | | | | |
| P value summary | ns | | | | |
| Significant diff. among means (P < 0.05)? | No | | | | |
| R squared | 0.01775 | | | | |
| | | | | | |
| **Bonferroni's multiple comparisons test** | **Mean Diff.** | **95.00% CI of diff.** | **Below threshold?** | **Summary** | **Adjusted P Value** |
| Control vs. Fibril | -0.03073 | -0.3417 to 0.2803 | No | ns | >.999 |
| Control vs. Scrambled | -0.01093 | -0.3219 to 0.3001 | No | ns | >.999 |
| Fibril vs. Scrambled | 0.0198 | -0.2912 to 0.3308 | No | ns | >.999 |

High damage

| ANOVA summary | | | | | |
|---|---|---|---|---|---|
| F | 24.93 | | | | |
| P value | 0.001 | | | | |
| P value summary | ** | | | | |
| Significant diff. among means (P < 0.05)? | Yes | | | | |
| R squared | 0.8926 | | | | |
| | | | | | |
| **Bonferroni's multiple comparisons test** | **Mean Diff.** | **95.00% CI of diff.** | **Below threshold?** | **Summary** | **Adjusted P Value** |
| Control vs. Fibril | 0.09232 | 0.04026 to 0.1444 | Yes | ** | 0.003 |
| Control vs. Scrambled | -0.008497 | -0.06056 to 0.04356 | No | ns | >.999 |
| Fibril vs. Scrambled | -0.1008 | -0.1529 to -0.04875 | Yes | ** | 0.002 |

**CS14– 2h**

All damage

| ANOVA summary | | | | | |
|---|---|---|---|---|---|
| F | 20.31 | | | | |
| P value | 0.002 | | | | |
| P value summary | ** | | | | |
| Significant diff. among means (P < 0.05)? | Yes | | | | |
| R squared | 0.8713 | | | | |
| | | | | | |
| **Bonferroni's multiple comparisons test** | **Mean Diff.** | **95.00% CI of diff.** | **Below threshold?** | **Summary** | **Adjusted P Value** |
| Control vs. Fibril | 0.023 | 0.009485 to 0.03653 | Yes | ** | 0.004 |
| Control vs. Scrambled | 0.0006243 | -0.01290 to 0.01414 | No | ns | >.999 |
| Fibril vs. Scrambled | -0.02238 | -0.03590 to -0.00886( | Yes | ** | 0.005 |

Low damage

| ANOVA summary | | | | | |
|---|---|---|---|---|---|
| F | 15.3 | | | | |
| P value | 0.004 | | | | |
| P value summary | ** | | | | |
| Significant diff. among means (P < 0.05)? | Yes | | | | |
| R squared | 0.8361 | | | | |
| | | | | | |
| **Bonferroni's multiple comparisons test** | **Mean Diff.** | **95.00% CI of diff.** | **Below threshold?** | **Summary** | **Adjusted P Value** |
| Control vs. Fibril | -5.381 | -8.985 to -1.777 | Yes | ** | 0.008 |
| Control vs. Scrambled | -0.2684 | -3.872 to 3.335 | No | ns | >.999 |
| Fibril vs. Scrambled | 5.112 | 1.509 to 8.716 | Yes | * | 0.01 |

**All cell lines– 2h**

High damage

| ANOVA summary | | | | | |
|---|---|---|---|---|---|
| F | 13.71 | | | | |
| P value | 0.006 | | | | |
| P value summary | ** | | | | |
| Significant diff. among means (P < 0.05)? | Yes | | | | |
| R squared | 0.8205 | | | | |
| | | | | | |
| **Bonferroni's multiple comparisons test** | **Mean Diff.** | **95.00% CI of diff.** | **Below threshold?** | **Summary** | **Adjusted P Value** |
| Control vs. Fibril | 0.07705 | 0.01664 to 0.1375 | Yes | * | 0.017 |
| Control vs. Scrambled | -0.01143 | -0.07185 to 0.04899 | No | ns | >.999 |
| Fibril vs. Scrambled | -0.08848 | -0.1489 to -0.02806 | Yes | ** | 0.009 |

**All cell lines– 2h**

All damage

| ANOVA summary | | | | | |
|---|---|---|---|---|---|
| F | 1.23 | | | | |
| P value | 0.357 | | | | |
| P value summary | ns | | | | |
| Significant diff. among means (P < 0.05)? | No | | | | |
| R squared | 0.2907 | | | | |
| | | | | | |
| **Bonferroni's multiple comparisons test** | **Mean Diff.** | **95.00% CI of diff.** | **Below threshold?** | **Summary** | **Adjusted P Value** |
| Control vs. Fibril | 0.0118 | -0.06524 to 0.08885 | No | ns | >.999 |
| Control vs. Scrambled | -0.02424 | -0.1013 to 0.05280 | No | ns | >.999 |
| Fibril vs. Scrambled | -0.03605 | -0.1131 to 0.04100 | No | ns | 0.525 |

Low damage

| ANOVA summary | | | | | |
|---|---|---|---|---|---|
| F | 0.9839 | | | | |
| P value | 0.427 | | | | |
| P value summary | ns | | | | |
| Significant diff. among means (P < 0.05)? | No | | | | |
| R squared | 0.247 | | | | |
| | | | | | |
| **Bonferroni's multiple comparisons test** | **Mean Diff.** | **95.00% CI of diff.** | **Below threshold?** | **Summary** | **Adjusted P Value** |
| Control vs. Fibril | -1.812 | -6.609 to 2.985 | No | ns | 0.782 |
| Control vs. Scrambled | -0.08171 | -4.878 to 4.715 | No | ns | >.999 |
| Fibril vs. Scrambled | 1.73 | -3.066 to 6.527 | No | ns | 0.842 |

**161– 24h**

High damage

| ANOVA summary | | | | | |
|---|---|---|---|---|---|
| F | 0.1314 | | | | |
| P value | 0.879 | | | | |
| P value summary | ns | | | | |
| Significant diff. among means (P < 0.05)? | No | | | | |
| R squared | 0.04197 | | | | |
| | | | | | |
| **Bonferroni's multiple comparisons test** | **Mean Diff.** | **95.00% CI of diff.** | **Below threshold?** | **Summary** | **Adjusted P Value** |
| Control vs. Fibril | 0.09416 | -0.5361 to 0.7244 | No | ns | >.999 |
| Control vs. Scrambled | 0.07148 | -0.5587 to 0.7017 | No | ns | >.999 |
| Fibril vs. Scrambled | -0.02268 | -0.6529 to 0.6075 | No | ns | >.999 |

**161– 24h**

All damage

| ANOVA summary | | | | | |
|---|---|---|---|---|---|
| F | 0.05814 | | | | |
| P value | 0.944 | | | | |
| P value summary | ns | | | | |
| Significant diff. among means (P < 0.05)? | No | | | | |
| R squared | 0.01901 | | | | |
| | | | | | |
| **Bonferroni's multiple comparisons test** | **Mean Diff.** | **95.00% CI of diff.** | **Below threshold?** | **Summary** | **Adjusted P Value** |
| Control vs. Fibril | 0.001756 | -0.2153 to 0.2188 | No | ns | >.999 |
| Control vs. Scrambled | 0.02032 | -0.1968 to 0.2374 | No | ns | >.999 |
| Fibril vs. Scrambled | 0.01856 | -0.1985 to 0.2356 | No | ns | >.999 |

Low damage

| ANOVA summary | | | | | |
|---|---|---|---|---|---|
| F | 0.1052 | | | | |
| P value | 0.902 | | | | |
| P value summary | ns | | | | |
| Significant diff. among means (P < 0.05)? | No | | | | |
| R squared | 0.03389 | | | | |
| | | | | | |
| **Bonferroni's multiple comparisons test** | **Mean Diff.** | **95.00% CI of diff.** | **Below threshold?** | **Summary** | **Adjusted P Value** |
| Control vs. Fibril | -0.01068 | -0.3415 to 0.3202 | No | ns | >.999 |
| Control vs. Scrambled | -0.04424 | -0.3751 to 0.2866 | No | ns | >.999 |
| Fibril vs. Scrambled | -0.03356 | -0.3644 to 0.2973 | No | ns | >.999 |

**155v2– 24h**

High damage

| ANOVA summary | | | | | |
|---|---|---|---|---|---|
| F | 1.875 | | | | |
| P value | 0.233 | | | | |
| P value summary | ns | | | | |
| Significant diff. among means (P < 0.05)? | No | | | | |
| R squared | 0.3846 | | | | |
| | | | | | |
| **Bonferroni's multiple comparisons test** | **Mean Diff.** | **95.00% CI of diff.** | **Below threshold?** | **Summary** | **Adjusted P Value** |
| Control vs. Fibril | -0.01647 | -1.392 to 1.359 | No | ns | >.999 |
| Control vs. Scrambled | -0.7096 | -2.085 to 0.6655 | No | ns | 0.422 |
| Fibril vs. Scrambled | -0.6931 | -2.068 to 0.6820 | No | ns | 0.446 |

**155v2– 24h**

All damage

| ANOVA summary | | | | | |
|---|---|---|---|---|---|
| F | 5.237 | | | | |
| P value | 0.048 | | | | |
| P value summary | * | | | | |
| Significant diff. among means (P < 0.05)? | Yes | | | | |
| R squared | 0.6358 | | | | |
| | | | | | |
| **Bonferroni's multiple comparisons test** | **Mean Diff.** | **95.00% CI of diff.** | **Below threshold?** | **Summary** | **Adjusted P Value** |
| Control vs. Fibril | 0.06901 | -0.2277 to 0.3657 | No | ns | >.999 |
| Control vs. Scrambled | -0.2113 | -0.5080 to 0.08542 | No | ns | 0.173 |
| Fibril vs. Scrambled | -0.2803 | -0.5770 to 0.01641 | No | ns | 0.063 |

Low damage

| ANOVA summary | | | | | |
|---|---|---|---|---|---|
| F | 3.459 | | | | |
| P value | 0.1 | | | | |
| P value summary | ns | | | | |
| Significant diff. among means (P < 0.05)? | No | | | | |
| R squared | 0.5356 | | | | |
| | | | | | |
| **Bonferroni's multiple comparisons test** | **Mean Diff.** | **95.00% CI of diff.** | **Below threshold?** | **Summary** | **Adjusted P Value** |
| Control vs. Fibril | -0.000801 | -0.1487 to 0.1471 | No | ns | >.999 |
| Control vs. Scrambled | 0.1021 | -0.04582 to 0.2500 | No | ns | 0.191 |
| Fibril vs. Scrambled | 0.1029 | -0.04502 to 0.2508 | No | ns | 0.187 |

High damage

| ANOVA summary | | | | | |
|---|---|---|---|---|---|
| F | 98.47 | | | | |
| P value | <.001 | | | | |
| P value summary | *** | | | | |
| Significant diff. among means (P < 0.05)? | Yes | | | | |
| R squared | 0.9704 | | | | |
| | | | | | |
| **Bonferroni's multiple comparisons test** | **Mean Diff.** | **95.00% CI of diff.** | **Below threshold?** | **Summary** | **Adjusted P Value** |
| Control vs. Fibril | 0.1221 | 0.08804 to 0.1562 | Yes | *** | <.001 |
| Control vs. Scrambled | -0.00754 | -0.04165 to 0.02656 | No | ns | >.999 |
| Fibril vs. Scrambled | -0.1297 | -0.1638 to -0.09558 | Yes | *** | <.001 |

**CS14– 24h**

All damage

| ANOVA summary | | | | | |
|---|---|---|---|---|---|
| F | 23.11 | | | | |
| P value | 0.002 | | | | |
| P value summary | ** | | | | |
| Significant diff. among means (P < 0.05)? | Yes | | | | |
| R squared | 0.8851 | | | | |
| | | | | | |
| **Bonferroni's multiple comparisons test** | **Mean Diff.** | **95.00% CI of diff.** | **Below threshold?** | **Summary** | **Adjusted P Value** |
| Control vs. Fibril | 0.03077 | 0.01094 to 0.05060 | Yes | ** | 0.007 |
| Control vs. Scrambled | -0.008102 | -0.02793 to 0.01173 | No | ns | 0.684 |
| Fibril vs. Scrambled | -0.03887 | -0.05870 to -0.01904 | Yes | ** | 0.002 |

Low damage

| ANOVA summary | | | | | |
|---|---|---|---|---|---|
| F | 23.28 | | | | |
| P value | 0.001 | | | | |
| P value summary | ** | | | | |
| Significant diff. among means (P < 0.05)? | Yes | | | | |
| R squared | 0.8858 | | | | |
| | | | | | |
| **Bonferroni's multiple comparisons test** | **Mean Diff.** | **95.00% CI of diff.** | **Below threshold?** | **Summary** | **Adjusted P Value** |
| Control vs. Fibril | -4.361 | -6.924 to -1.798 | Yes | ** | 0.004 |
| Control vs. Scrambled | 0.4583 | -2.105 to 3.022 | No | ns | >.999 |
| Fibril vs. Scrambled | 4.819 | 2.256 to 7.383 | Yes | ** | 0.002 |

High damage

| ANOVA summary | | | | | |
|---|---|---|---|---|---|
| F | 1.026 | | | | |
| P value | 0.414 | | | | |
| P value summary | ns | | | | |
| Significant diff. among means (P < 0.05)? | No | | | | |
| R squared | 0.2549 | | | | |
| | | | | | |
| **Bonferroni's multiple comparisons test** | **Mean Diff.** | **95.00% CI of diff.** | **Below threshold?** | **Summary** | **Adjusted P Value** |
| Control vs. Fibril | 0.06661 | -0.6093 to 0.7425 | No | ns | >.999 |
| Control vs. Scrambled | -0.2152 | -0.8912 to 0.4607 | No | ns | >.999 |
| Fibril vs. Scrambled | -0.2818 | -0.9578 to 0.3941 | No | ns | 0.659 |

**All cell lines– 24h**

All damage

| ANOVA summary | | | | | |
|---|---|---|---|---|---|
| F | 1.368 | | | | |
| P value | 0.324 | | | | |
| P value summary | ns | | | | |
| Significant diff. among means (P < 0.05)? | No | | | | |
| R squared | 0.3132 | | | | |
| | | | | | |
| **Bonferroni's multiple comparisons test** | **Mean Diff.** | **95.00% CI of diff.** | **Below threshold?** | **Summary** | **Adjusted P Value** |
| Control vs. Fibril | 0.03385 | -0.1688 to 0.2364 | No | ns | >.999 |
| Control vs. Scrambled | -0.06635 | -0.2689 to 0.1362 | No | ns | 0.969 |
| Fibril vs. Scrambled | -0.1002 | -0.3028 to 0.1024 | No | ns | 0.465 |

Low damage

| ANOVA summary | | | | | |
|---|---|---|---|---|---|
| F | 1.129 | | | | |
| P value | 0.384 | | | | |
| P value summary | ns | | | | |
| Significant diff. among means (P < 0.05)? | No | | | | |
| R squared | 0.2734 | | | | |
| | | | | | |
| **Bonferroni's multiple comparisons test** | **Mean Diff.** | **95.00% CI of diff.** | **Below threshold?** | **Summary** | **Adjusted P Value** |
| Control vs. Fibril | -1.457 | -5.375 to 2.460 | No | ns | 0.801 |
| Control vs. Scrambled | 0.1721 | -3.745 to 4.089 | No | ns | >.999 |
| Fibril vs. Scrambled | 1.63 | -2.288 to 5.547 | No | ns | 0.661 |

**161– 48h**

High damage

| ANOVA summary | | | | | |
|---|---|---|---|---|---|
| F | 2.755 | | | | |
| P value | 0.142 | | | | |
| P value summary | ns | | | | |
| Significant diff. among means (P < 0.05)? | No | | | | |
| R squared | 0.4787 | | | | |
| | | | | | |
| **Bonferroni's multiple comparisons test** | **Mean Diff.** | **95.00% CI of diff.** | **Below threshold?** | **Summary** | **Adjusted P Value** |
| Control vs. Fibril | -0.1304 | -0.3947 to 0.1339 | No | ns | 0.468 |
| Control vs. Scrambled | 0.0529 | -0.2114 to 0.3172 | No | ns | >.999 |
| Fibril vs. Scrambled | 0.1833 | -0.08098 to 0.4476 | No | ns | 0.188 |

**161– 48h**

All damage

| ANOVA summary | | | | | |
|---|---|---|---|---|---|
| F | 1.188 | | | | |
| P value | 0.368 | | | | |
| P value summary | ns | | | | |
| Significant diff. among means (P < 0.05)? | No | | | | |
| R squared | 0.2837 | | | | |
| | | | | | |
| **Bonferroni's multiple comparisons test** | **Mean Diff.** | **95.00% CI of diff.** | **Below threshold?** | **Summary** | **Adjusted P Value** |
| Control vs. Fibril | -0.02567 | -0.1159 to 0.06452 | No | ns | >.999 |
| Control vs. Scrambled | 0.01627 | -0.07393 to 0.1065 | No | ns | >.999 |
| Fibril vs. Scrambled | 0.04194 | -0.04825 to 0.1321 | No | ns | 0.532 |

Low damage

| ANOVA summary | | | | | |
|---|---|---|---|---|---|
| F | 2.322 | | | | |
| P value | 0.179 | | | | |
| P value summary | ns | | | | |
| Significant diff. among means (P < 0.05)? | No | | | | |
| R squared | 0.4363 | | | | |
| | | | | | |
| **Bonferroni's multiple comparisons test** | **Mean Diff.** | **95.00% CI of diff.** | **Below threshold?** | **Summary** | **Adjusted P Value** |
| Control vs. Fibril | 0.05712 | -0.09069 to 0.2049 | No | ns | 0.753 |
| Control vs. Scrambled | -0.03923 | -0.1870 to 0.1086 | No | ns | >.999 |
| Fibril vs. Scrambled | -0.09635 | -0.2442 to 0.05146 | No | ns | 0.228 |

**155v2– 48h**

High damage

| ANOVA summary | | | | | |
|---|---|---|---|---|---|
| F | 0.2247 | | | | |
| P value | 0.805 | | | | |
| P value summary | ns | | | | |
| Significant diff. among means (P < 0.05)? | No | | | | |
| R squared | 0.06968 | | | | |
| | | | | | |
| **Bonferroni's multiple comparisons test** | **Mean Diff.** | **95.00% CI of diff.** | **Below threshold?** | **Summary** | **Adjusted P Value** |
| Control vs. Fibril | -0.1405 | -1.380 to 1.099 | No | ns | >.999 |
| Control vs. Scrambled | 0.1117 | -1.128 to 1.351 | No | ns | >.999 |
| Fibril vs. Scrambled | 0.2522 | -0.9873 to 1.492 | No | ns | >.999 |

**155v2– 48h**

All damage

| ANOVA summary | | | | | |
|---|---|---|---|---|---|
| F | 1.383 | | | | |
| P value | 0.321 | | | | |
| P value summary | ns | | | | |
| Significant diff. among means (P < 0.05)? | No | | | | |
| R squared | 0.3155 | | | | |
| | | | | | |
| **Bonferroni's multiple comparisons test** | **Mean Diff.** | **95.00% CI of diff.** | **Below threshold?** | **Summary** | **Adjusted P Value** |
| Control vs. Fibril | -0.01557 | -0.3801 to 0.3489 | No | ns | >.999 |
| Control vs. Scrambled | -0.1669 | -0.5314 to 0.1976 | No | ns | 0.549 |
| Fibril vs. Scrambled | -0.1513 | -0.5159 to 0.2132 | No | ns | 0.664 |

Low damage

| ANOVA summary | | | | | |
|---|---|---|---|---|---|
| F | 1.9 | | | | |
| P value | 0.23 | | | | |
| P value summary | ns | | | | |
| Significant diff. among means (P < 0.05)? | No | | | | |
| R squared | 0.3877 | | | | |
| | | | | | |
| **Bonferroni's multiple comparisons test** | **Mean Diff.** | **95.00% CI of diff.** | **Below threshold?** | **Summary** | **Adjusted P Value** |
| Control vs. Fibril | -0.002869 | -0.1154 to 0.1097 | No | ns | >.999 |
| Control vs. Scrambled | 0.0563 | -0.05623 to 0.1688 | No | ns | 0.453 |
| Fibril vs. Scrambled | 0.05916 | -0.05336 to 0.1717 | No | ns | 0.404 |

**CS14– 48h**

High damage

| ANOVA summary | | | | | |
|---|---|---|---|---|---|
| F | 2.572 | | | | |
| P value | 0.156 | | | | |
| P value summary | ns | | | | |
| Significant diff. among means (P < 0.05)? | No | | | | |
| R squared | 0.4616 | | | | |
| | | | | | |
| **Bonferroni's multiple comparisons test** | **Mean Diff.** | **95.00% CI of diff.** | **Below threshold?** | **Summary** | **Adjusted P Value** |
| Control vs. Fibril | -0.1551 | -0.4498 to 0.1396 | No | ns | 0.403 |
| Control vs. Scrambled | 0.03627 | -0.2584 to 0.3310 | No | ns | >.999 |
| Fibril vs. Scrambled | 0.1914 | -0.1033 to 0.4861 | No | ns | 0.23 |

**CS14– 48h**

All damage

| ANOVA summary | | | | | |
|---|---|---|---|---|---|
| F | 2.571 | | | | |
| P value | 0.156 | | | | |
| P value summary | ns | | | | |
| Significant diff. among means (P < 0.05)? | No | | | | |
| R squared | 0.4615 | | | | |
| | | | | | |
| **Bonferroni's multiple comparisons test** | **Mean Diff.** | **95.00% CI of diff.** | **Below threshold?** | **Summary** | **Adjusted P Value** |
| Control vs. Fibril | 0.007099 | -0.02167 to 0.03587 | No | ns | >.999 |
| Control vs. Scrambled | -0.0125 | -0.04127 to 0.01627 | No | ns | 0.61 |
| Fibril vs. Scrambled | -0.0196 | -0.04837 to 0.00917 | No | ns | 0.199 |

Low damage

| ANOVA summary | | | | | |
|---|---|---|---|---|---|
| F | 4.244 | | | | |
| P value | 0.071 | | | | |
| P value summary | ns | | | | |
| Significant diff. among means (P < 0.05)? | No | | | | |
| R squared | 0.5858 | | | | |
| | | | | | |
| **Bonferroni's multiple comparisons test** | **Mean Diff.** | **95.00% CI of diff.** | **Below threshold?** | **Summary** | **Adjusted P Value** |
| Control vs. Fibril | -0.6149 | -2.285 to 1.055 | No | ns | 0.815 |
| Control vs. Scrambled | 0.8583 | -0.8117 to 2.528 | No | ns | 0.426 |
| Fibril vs. Scrambled | 1.473 | -0.1968 to 3.143 | No | ns | 0.082 |

## All cell lines – 48h

High damage

| ANOVA summary | | | | | |
|---|---|---|---|---|---|
| F | 59.49 | | | | |
| P value | <.001 | | | | |
| P value summary | *** | | | | |
| Significant diff. among means (P < 0.05)? | Yes | | | | |
| R squared | 0.952 | | | | |
| | | | | | |
| **Bonferroni's multiple comparisons test** | **Mean Diff.** | **95.00% CI of diff.** | **Below threshold?** | **Summary** | **Adjusted P Value** |
| Control vs. Fibril | -0.142 | -0.2064 to -0.07771 | Yes | ** | 0.001 |
| Control vs. Scrambled | 0.06694 | 0.002619 to 0.1313 | Yes | * | 0.042 |
| Fibril vs. Scrambled | 0.209 | 0.1447 to 0.2733 | Yes | *** | <.001 |

## All cell lines – 48h

All damage

| ANOVA summary | | | | | |
|---|---|---|---|---|---|
| F | 0.7414 | | | | |
| P value | 0.516 | | | | |
| P value summary | ns | | | | |
| Significant diff. among means (P < 0.05)? | No | | | | |
| R squared | 0.1982 | | | | |
| | | | | | |
| **Bonferroni's multiple comparisons test** | **Mean Diff.** | **95.00% CI of diff.** | **Below threshold?** | **Summary** | **Adjusted P Value** |
| Control vs. Fibril | -0.01138 | -0.1663 to 0.1435 | No | ns | >.999 |
| Control vs. Scrambled | -0.05438 | -0.2093 to 0.1005 | No | ns | 0.877 |
| Fibril vs. Scrambled | -0.043 | -0.1979 to 0.1119 | No | ns | >.999 |

Low damage

| ANOVA summary | | | | | |
|---|---|---|---|---|---|
| F | 1.374 | | | | |
| P value | 0.323 | | | | |
| P value summary | ns | | | | |
| Significant diff. among means (P < 0.05)? | No | | | | |
| R squared | 0.3141 | | | | |
| | | | | | |
| **Bonferroni's multiple comparisons test** | **Mean Diff.** | **95.00% CI of diff.** | **Below threshold?** | **Summary** | **Adjusted P Value** |
| Control vs. Fibril | -0.1869 | -1.144 to 0.7700 | No | ns | >.999 |
| Control vs. Scrambled | 0.2918 | -0.6651 to 1.249 | No | ns | >.999 |
| Fibril vs. Scrambled | 0.4787 | -0.4783 to 1.436 | No | ns | 0.454 |

**155v2– repeated stress**

Mean cell length

| ANOVA summary | | | | | |
|---|---|---|---|---|---|
| F | 0.2797 | | | | |
| P value | 0.765 | | | | |
| P value summary | ns | | | | |
| Significant diff. among means (P < 0.05)? | No | | | | |
| R squared | 0.08527 | | | | |
| | | | | | |
| **Bonferroni's multiple comparisons test** | **Mean Diff.** | **95.00% CI of diff.** | **Below threshold?** | **Summary** | **Adjusted P Value** |
| Control vs. Fibril | -0.1194 | -1.103 to 0.8639 | No | ns | >.999 |
| Control vs. Scrambled | -0.2235 | -1.207 to 0.7598 | No | ns | >.999 |
| Fibril vs. Scrambled | -0.1041 | -1.087 to 0.8793 | No | ns | >.999 |

**155v2– repeated stress**

Mean cell roundness

| ANOVA summary | | | | | |
|---|---|---|---|---|---|
| F | 1.844 | | | | |
| P value | 0.238 | | | | |
| P value summary | ns | | | | |
| Significant diff. among means (P < 0.05)? | No | | | | |
| R squared | 0.3806 | | | | |
| | | | | | |
| **Bonferroni's multiple comparisons test** | **Mean Diff.** | **95.00% CI of diff.** | **Below threshold?** | **Summary** | **Adjusted P Value** |
| Control vs. Fibril | 0.1367 | -0.1967 to 0.4702 | No | ns | 0.679 |
| Control vs. Scrambled | 0.1885 | -0.1450 to 0.5219 | No | ns | 0.337 |
| Fibril vs. Scrambled | 0.05173 | -0.2817 to 0.3851 | No | ns | >.999 |

Mean cell width

| ANOVA summary | | | | | |
|---|---|---|---|---|---|
| F | 28.17 | | | | |
| P value | <.001 | | | | |
| P value summary | *** | | | | |
| Significant diff. among means (P < 0.05)? | Yes | | | | |
| R squared | 0.9038 | | | | |
| | | | | | |
| **Bonferroni's multiple comparisons test** | **Mean Diff.** | **95.00% CI of diff.** | **Below threshold?** | **Summary** | **Adjusted P Value** |
| Control vs. Fibril | -0.2725 | -0.4597 to -0.08520 | Yes | ** | 0.009 |
| Control vs. Scrambled | 0.1491 | -0.03813 to 0.3364 | No | ns | 0.119 |
| Fibril vs. Scrambled | 0.4216 | 0.2343 to 0.6089 | Yes | *** | <.001 |

**155v2– repeated stress**

Mean cytoplasm region

| ANOVA summary | | | | | |
|---|---|---|---|---|---|
| F | 0.4749 | | | | |
| P value | 0.643 | | | | |
| P value summary | ns | | | | |
| Significant diff. among means (P < 0.05)? | No | | | | |
| R squared | 0.1367 | | | | |
| | | | | | |
| **Bonferroni's multiple comparisons test** | **Mean Diff.** | **95.00% CI of diff.** | **Below threshold?** | **Summary** | **Adjusted P Value** |
| Control vs. Fibril | 0.2104 | -1.748 to 2.169 | No | ns | >.999 |
| Control vs. Scrambled | 0.5739 | -1.385 to 2.533 | No | ns | >.999 |
| Fibril vs. Scrambled | 0.3635 | -1.595 to 2.322 | No | ns | >.999 |

Mean cell area

| ANOVA summary | | | | | |
|---|---|---|---|---|---|
| F | 3.256 | | | | |
| P value | 0.11 | | | | |
| P value summary | ns | | | | |
| Significant diff. among means (P < 0.05)? | No | | | | |
| R squared | 0.5205 | | | | |
| | | | | | |
| **Bonferroni's multiple comparisons test** | **Mean Diff.** | **95.00% CI of diff.** | **Below threshold?** | **Summary** | **Adjusted P Value** |
| Control vs. Fibril | -0.4311 | -1.120 to 0.2580 | No | ns | 0.256 |
| Control vs. Scrambled | 0.0587 | -0.6304 to 0.7478 | No | ns | >.999 |
| Fibril vs. Scrambled | 0.4898 | -0.1993 to 1.179 | No | ns | 0.174 |

**CS14– repeated stress**

Mean cell length

| ANOVA summary | | | | | |
|---|---|---|---|---|---|
| F | 4.412 | | | | |
| P value | 0.066 | | | | |
| P value summary | ns | | | | |
| Significant diff. among means (P < 0.05)? | No | | | | |
| R squared | 0.5953 | | | | |
| | | | | | |
| **Bonferroni's multiple comparisons test** | **Mean Diff.** | **95.00% CI of diff.** | **Below threshold?** | **Summary** | **Adjusted P Value** |
| Control vs. Fibril | 0.06769 | -0.008180 to 0.143€ | No | ns | 0.079 |
| Control vs. Scrambled | 0.04326 | -0.03261 to 0.1191 | No | ns | 0.33 |
| Fibril vs. Scrambled | -0.02443 | -0.1003 to 0.05144 | No | ns | 0.992 |

**CS14– repeated stress**

Mean cell roundness

| ANOVA summary | | | | | |
|---|---|---|---|---|---|
| F | 4.688 | | | | |
| P value | 0.059 | | | | |
| P value summary | ns | | | | |
| Significant diff. among means (P < 0.05)? | No | | | | |
| R squared | 0.6098 | | | | |
| | | | | | |
| **Bonferroni's multiple comparisons test** | **Mean Diff.** | **95.00% CI of diff.** | **Below threshold?** | **Summary** | **Adjusted P Value** |
| Control vs. Fibril | -0.107 | -0.2218 to 0.007891 | No | ns | 0.067 |
| Control vs. Scrambled | -0.05176 | -0.1666 to 0.06309 | No | ns | 0.567 |
| Fibril vs. Scrambled | 0.0552 | -0.05965 to 0.1701 | No | ns | 0.496 |

Mean cell width

| ANOVA summary | | | | | |
|---|---|---|---|---|---|
| F | 4.506 | | | | |
| P value | 0.064 | | | | |
| P value summary | ns | | | | |
| Significant diff. among means (P < 0.05)? | No | | | | |
| R squared | 0.6003 | | | | |
| | | | | | |
| **Bonferroni's multiple comparisons test** | **Mean Diff.** | **95.00% CI of diff.** | **Below threshold?** | **Summary** | **Adjusted P Value** |
| Control vs. Fibril | -0.06957 | -0.1460 to 0.006825 | No | ns | 0.073 |
| Control vs. Scrambled | -0.03933 | -0.1157 to 0.03706 | No | ns | 0.424 |
| Fibril vs. Scrambled | 0.03024 | -0.04616 to 0.1066 | No | ns | 0.723 |

**CS14– repeated stress**

Mean cytoplasm region

| ANOVA summary | | | | | |
|---|---|---|---|---|---|
| F | 1.555 | | | | |
| P value | 0.286 | | | | |
| P value summary | ns | | | | |
| Significant diff. among means (P < 0.05)? | No | | | | |
| R squared | 0.3414 | | | | |
| | | | | | |
| **Bonferroni's multiple comparisons test** | **Mean Diff.** | **95.00% CI of diff.** | **Below threshold?** | **Summary** | **Adjusted P Value** |
| Control vs. Fibril | 0.00563 | -0.02813 to 0.03940 | No | ns | >.999 |
| Control vs. Scrambled | 0.01772 | -0.01604 to 0.05149 | No | ns | 0.405 |
| Fibril vs. Scrambled | 0.01209 | -0.02167 to 0.04586 | No | ns | 0.851 |

Mean cell area

| ANOVA summary | | | | | |
|---|---|---|---|---|---|
| F | 2.89 | | | | |
| P value | 0.132 | | | | |
| P value summary | ns | | | | |
| Significant diff. among means (P < 0.05)? | No | | | | |
| R squared | 0.4906 | | | | |
| | | | | | |
| **Bonferroni's multiple comparisons test** | **Mean Diff.** | **95.00% CI of diff.** | **Below threshold?** | **Summary** | **Adjusted P Value** |
| Control vs. Fibril | -0.0678 | -0.1678 to 0.03221 | No | ns | 0.202 |
| Control vs. Scrambled | -0.01016 | -0.1102 to 0.08984 | No | ns | >.999 |
| Fibril vs. Scrambled | 0.05764 | -0.04236 to 0.1576 | No | ns | 0.321 |

**All cell lines – repeated stress**

Mean cell length

| ANOVA summary | | | | | |
|---|---|---|---|---|---|
| F | 2.172 | | | | |
| P value | 0.261 | | | | |
| P value summary | ns | | | | |
| Significant diff. among means (P < 0.05)? | No | | | | |
| R squared | 0.5916 | | | | |
| | | | | | |
| **Bonferroni's multiple comparisons test** | **Mean Diff.** | **95.00% CI of diff.** | **Below threshold?** | **Summary** | **Adjusted P Value** |
| Control vs. Fibril | -0.171 | -0.7201 to 0.3781 | No | ns | 0.683 |
| Control vs. Scrambled | 0.0549 | -0.4942 to 0.6040 | No | ns | >.999 |
| Fibril vs. Scrambled | 0.2259 | -0.3232 to 0.7750 | No | ns | 0.419 |

**1h – 155v2**

Mean cell length

| ANOVA summary | | | | | |
|---|---|---|---|---|---|
| F | 3.148 | | | | |
| P value | 0.116 | | | | |
| P value summary | ns | | | | |
| Significant diff. among means (P < 0.05)? | No | | | | |
| R squared | 0.512 | | | | |
| | | | | | |
| **Bonferroni's multiple comparisons test** | **Mean Diff.** | **95.00% CI of diff.** | **Below threshold?** | **Summary** | **Adjusted P Value** |
| Control vs. Fibril | 0.2503 | -0.5848 to 1.085 | No | ns | >.999 |
| Control vs. Scrambled | -0.3824 | -1.217 to 0.4526 | No | ns | 0.549 |
| Fibril vs. Scrambled | -0.6327 | -1.468 to 0.2023 | No | ns | 0.141 |

**1h – 155v2**

Mean cell roundness

| ANOVA summary | | | | | |
|---|---|---|---|---|---|
| F | 1.6 | | | | |
| P value | 0.277 | | | | |
| P value summary | ns | | | | |
| Significant diff. among means (P < 0.05)? | No | | | | |
| R squared | 0.3478 | | | | |
| | | | | | |
| **Bonferroni's multiple comparisons test** | **Mean Diff.** | **95.00% CI of diff.** | **Below threshold?** | **Summary** | **Adjusted P Value** |
| Control vs. Fibril | -0.3041 | -0.8800 to 0.2718 | No | ns | 0.4 |
| Control vs. Scrambled | -0.08663 | -0.6626 to 0.4893 | No | ns | >.999 |
| Fibril vs. Scrambled | 0.2175 | -0.3584 to 0.7934 | No | ns | 0.782 |

Mean cell width

| ANOVA summary | | | | | |
|---|---|---|---|---|---|
| F | 0.9054 | | | | |
| P value | 0.453 | | | | |
| P value summary | ns | | | | |
| Significant diff. among means (P < 0.05)? | No | | | | |
| R squared | 0.2318 | | | | |
| | | | | | |
| **Bonferroni's multiple comparisons test** | **Mean Diff.** | **95.00% CI of diff.** | **Below threshold?** | **Summary** | **Adjusted P Value** |
| Control vs. Fibril | 0.1593 | -0.5378 to 0.8565 | No | ns | >.999 |
| Control vs. Scrambled | -0.1254 | -0.8225 to 0.5718 | No | ns | >.999 |
| Fibril vs. Scrambled | -0.2847 | -0.9818 to 0.4125 | No | ns | 0.684 |

**1h – 155v2**

Mean cytoplasm region

| ANOVA summary | | | | | |
|---|---|---|---|---|---|
| F | 0.07883 | | | | |
| P value | 0.925 | | | | |
| P value summary | ns | | | | |
| Significant diff. among means (P < 0.05)? | No | | | | |
| R squared | 0.0256 | | | | |
| | | | | | |
| **Bonferroni's multiple comparisons test** | **Mean Diff.** | **95.00% CI of diff.** | **Below threshold?** | **Summary** | **Adjusted P Value** |
| Control vs. Fibril | 0.1065 | -1.464 to 1.677 | No | ns | >.999 |
| Control vs. Scrambled | 0.1891 | -1.381 to 1.759 | No | ns | >.999 |
| Fibril vs. Scrambled | 0.0826 | -1.487 to 1.653 | No | ns | >.999 |

Mean cell area

| ANOVA summary | | | | | |
|---|---|---|---|---|---|
| F | 3.277 | | | | |
| P value | 0.109 | | | | |
| P value summary | ns | | | | |
| Significant diff. among means (P < 0.05)? | No | | | | |
| R squared | 0.5221 | | | | |
| | | | | | |
| **Bonferroni's multiple comparisons test** | **Mean Diff.** | **95.00% CI of diff.** | **Below threshold?** | **Summary** | **Adjusted P Value** |
| Control vs. Fibril | 0.2435 | -1.050 to 1.537 | No | ns | >.999 |
| Control vs. Scrambled | -0.7246 | -2.018 to 0.5687 | No | ns | 0.345 |
| Fibril vs. Scrambled | -0.9681 | -2.261 to 0.3252 | No | ns | 0.147 |

**1h – CS14**

Mean cell length

| ANOVA summary | | | | | |
|---|---|---|---|---|---|
| F | 1.705 | | | | |
| P value | 0.259 | | | | |
| P value summary | ns | | | | |
| Significant diff. among means (P < 0.05)? | No | | | | |
| R squared | 0.3624 | | | | |
| | | | | | |
| **Bonferroni's multiple comparisons test** | **Mean Diff.** | **95.00% CI of diff.** | **Below threshold?** | **Summary** | **Adjusted P Value** |
| Control vs. Fibril | -0.08643 | -0.2501 to 0.07725 | No | ns | 0.4 |
| Control vs. Scrambled | -0.01605 | -0.1797 to 0.1476 | No | ns | >.999 |
| Fibril vs. Scrambled | 0.07039 | -0.09330 to 0.2341 | No | ns | 0.622 |

**1h – CS14**

Mean cell roundness

| ANOVA summary | | | | | |
|---|---|---|---|---|---|
| F | 4.897 | | | | |
| P value | 0.055 | | | | |
| P value summary | ns | | | | |
| Significant diff. among means (P < 0.05)? | No | | | | |
| R squared | 0.6201 | | | | |
| | | | | | |
| **Bonferroni's multiple comparisons test** | **Mean Diff.** | **95.00% CI of diff.** | **Below threshold?** | **Summary** | **Adjusted P Value** |
| Control vs. Fibril | 0.1034 | -0.01484 to 0.2217 | No | ns | 0.085 |
| Control vs. Scrambled | 0.01319 | -0.1051 to 0.1315 | No | ns | >.999 |
| Fibril vs. Scrambled | -0.09023 | -0.2085 to 0.02803 | No | ns | 0.138 |

Mean cell width

| ANOVA summary | | | | | |
|---|---|---|---|---|---|
| F | 2.29 | | | | |
| P value | 0.182 | | | | |
| P value summary | ns | | | | |
| Significant diff. among means (P < 0.05)? | No | | | | |
| R squared | 0.4329 | | | | |
| | | | | | |
| **Bonferroni's multiple comparisons test** | **Mean Diff.** | **95.00% CI of diff.** | **Below threshold?** | **Summary** | **Adjusted P Value** |
| Control vs. Fibril | -0.06438 | -0.2314 to 0.1026 | No | ns | 0.756 |
| Control vs. Scrambled | 0.04367 | -0.1233 to 0.2107 | No | ns | >.999 |
| Fibril vs. Scrambled | 0.108 | -0.05893 to 0.2750 | No | ns | 0.233 |

**1h – CS14**

Mean cytoplasm region

| ANOVA summary | | | | | |
|---|---|---|---|---|---|
| F | 2.934 | | | | |
| P value | 0.129 | | | | |
| P value summary | ns | | | | |
| Significant diff. among means (P < 0.05)? | No | | | | |
| R squared | 0.4944 | | | | |
| | | | | | |
| **Bonferroni's multiple comparisons test** | **Mean Diff.** | **95.00% CI of diff.** | **Below threshold?** | **Summary** | **Adjusted P Value** |
| Control vs. Fibril | 0.04239 | -0.01514 to 0.09992 | No | ns | 0.155 |
| Control vs. Scrambled | 0.02116 | -0.03637 to 0.07865 | No | ns | 0.816 |
| Fibril vs. Scrambled | -0.02123 | -0.07876 to 0.03630 | No | ns | 0.812 |

Mean cell area

| ANOVA summary | | | | | |
|---|---|---|---|---|---|
| F | 5.514 | | | | |
| P value | 0.044 | | | | |
| P value summary | * | | | | |
| Significant diff. among means (P < 0.05)? | Yes | | | | |
| R squared | 0.6476 | | | | |
| | | | | | |
| **Bonferroni's multiple comparisons test** | **Mean Diff.** | **95.00% CI of diff.** | **Below threshold?** | **Summary** | **Adjusted P Value** |
| Control vs. Fibril | -0.2093 | -0.4474 to 0.02868 | No | ns | 0.083 |
| Control vs. Scrambled | -0.002263 | -0.2403 to 0.2358 | No | ns | >.999 |
| Fibril vs. Scrambled | 0.2071 | -0.03094 to 0.4451 | No | ns | 0.086 |

**All cell lines – 1h**

Mean cell length

| ANOVA summary | | | | | |
|---|---|---|---|---|---|
| F | 0.2982 | | | | |
| P value | 0.762 | | | | |
| P value summary | ns | | | | |
| Significant diff. among means (P < 0.05)? | No | | | | |
| R squared | 0.1658 | | | | |
| | | | | | |
| **Bonferroni's multiple comparisons test** | **Mean Diff.** | **95.00% CI of diff.** | **Below threshold?** | **Summary** | **Adjusted P Value** |
| Control vs. Fibril | 0.04747 | -0.5085 to 0.6034 | No | ns | >.999 |
| Control vs. Scrambled | -0.04085 | -0.5968 to 0.5151 | No | ns | >.999 |
| Fibril vs. Scrambled | -0.08832 | -0.6442 to 0.4676 | No | ns | >.999 |

**All cell lines – 1h**

Mean cell roundness

| ANOVA summary | | | | | |
|---|---|---|---|---|---|
| F | 1.013 | | | | |
| P value | 0.461 | | | | |
| P value summary | ns | | | | |
| Significant diff. among means (P < 0.05)? | No | | | | |
| R squared | 0.4032 | | | | |
| | | | | | |
| **Bonferroni's multiple comparisons test** | **Mean Diff.** | **95.00% CI of diff.** | **Below threshold?** | **Summary** | **Adjusted P Value** |
| Control vs. Fibril | 0.08193 | -0.9047 to 1.069 | No | ns | >.999 |
| Control vs. Scrambled | -0.1992 | -1.186 to 0.7874 | No | ns | >.999 |
| Fibril vs. Scrambled | -0.2812 | -1.268 to 0.7055 | No | ns | 0.781 |

Mean cell width

| ANOVA summary | | | | | |
|---|---|---|---|---|---|
| F | 0.1757 | | | | |
| P value | 0.847 | | | | |
| P value summary | ns | | | | |
| Significant diff. among means (P < 0.05)? | No | | | | |
| R squared | 0.1048 | | | | |
| | | | | | |
| **Bonferroni's multiple comparisons test** | **Mean Diff.** | **95.00% CI of diff.** | **Below threshold?** | **Summary** | **Adjusted P Value** |
| Control vs. Fibril | -0.1003 | -0.9322 to 0.7316 | No | ns | >.999 |
| Control vs. Scrambled | -0.03672 | -0.8686 to 0.7952 | No | ns | >.999 |
| Fibril vs. Scrambled | 0.06362 | -0.7683 to 0.8955 | No | ns | >.999 |

**All cell lines – 1h**

Mean cytoplasm region

| ANOVA summary | | | | | |
|---|---|---|---|---|---|
| F | 1.085 | | | | |
| P value | 0.442 | | | | |
| P value summary | ns | | | | |
| Significant diff. among means (P < 0.05)? | No | | | | |
| R squared | 0.4198 | | | | |
| | | | | | |
| **Bonferroni's multiple comparisons test** | **Mean Diff.** | **95.00% CI of diff.** | **Below threshold?** | **Summary** | **Adjusted P Value** |
| Control vs. Fibril | 0.07446 | -0.2820 to 0.4310 | No | ns | >.999 |
| Control vs. Scrambled | 0.1051 | -0.2514 to 0.4616 | No | ns | 0.742 |
| Fibril vs. Scrambled | 0.03068 | -0.3258 to 0.3872 | No | ns | >.999 |

Mean cell area

| ANOVA summary | | | | | |
|---|---|---|---|---|---|
| F | 0.7627 | | | | |
| P value | 0.54 | | | | |
| P value summary | ns | | | | |
| Significant diff. among means (P < 0.05)? | No | | | | |
| R squared | 0.3371 | | | | |
| | | | | | |
| **Bonferroni's multiple comparisons test** | **Mean Diff.** | **95.00% CI of diff.** | **Below threshold?** | **Summary** | **Adjusted P Value** |
| Control vs. Fibril | 0.01709 | -1.673 to 1.707 | No | ns | >.999 |
| Control vs. Scrambled | -0.3634 | -2.054 to 1.327 | No | ns | >.999 |
| Fibril vs. Scrambled | -0.3805 | -2.071 to 1.310 | No | ns | >.999 |

**2h – 155v2**

Mean cell length

| ANOVA summary | | | | | |
|---|---|---|---|---|---|
| F | 0.6003 | | | | |
| P value | 0.579 | | | | |
| P value summary | ns | | | | |
| Significant diff. among means (P < 0.05)? | No | | | | |
| R squared | 0.1667 | | | | |
| | | | | | |
| **Bonferroni's multiple comparisons test** | **Mean Diff.** | **95.00% CI of diff.** | **Below threshold?** | **Summary** | **Adjusted P Value** |
| Control vs. Fibril | 0.05397 | -0.8957 to 1.004 | No | ns | >.999 |
| Control vs. Scrambled | -0.2431 | -1.193 to 0.7066 | No | ns | >.999 |
| Fibril vs. Scrambled | -0.2971 | -1.247 to 0.6526 | No | ns | >.999 |

**2h – 155v2**

Mean cell roundness

| ANOVA summary | | | | | |
|---|---|---|---|---|---|
| F | 0.1926 | | | | |
| P value | 0.83 | | | | |
| P value summary | ns | | | | |
| Significant diff. among means (P < 0.05)? | No | | | | |
| R squared | 0.06033 | | | | |
| | | | | | |
| **Bonferroni's multiple comparisons test** | **Mean Diff.** | **95.00% CI of diff.** | **Below threshold?** | **Summary** | **Adjusted P Value** |
| Control vs. Fibril | 0.07755 | -0.3614 to 0.5165 | No | ns | >.999 |
| Control vs. Scrambled | 0.06409 | -0.3749 to 0.5030 | No | ns | >.999 |
| Fibril vs. Scrambled | -0.01345 | -0.4524 to 0.4255 | No | ns | >.999 |

Mean cell width

| ANOVA summary | | | | | |
|---|---|---|---|---|---|
| F | 0.3454 | | | | |
| P value | 0.721 | | | | |
| P value summary | ns | | | | |
| Significant diff. among means (P < 0.05)? | No | | | | |
| R squared | 0.1032 | | | | |
| | | | | | |
| **Bonferroni's multiple comparisons test** | **Mean Diff.** | **95.00% CI of diff.** | **Below threshold?** | **Summary** | **Adjusted P Value** |
| Control vs. Fibril | -0.03491 | -0.5069 to 0.4371 | No | ns | >.999 |
| Control vs. Scrambled | 0.08136 | -0.3906 to 0.5533 | No | ns | >.999 |
| Fibril vs. Scrambled | 0.1163 | -0.3557 to 0.5883 | No | ns | >.999 |

**2h – 155v2**

Mean cytoplasm region

| ANOVA summary | | | | | |
|---|---|---|---|---|---|
| F | 1.804 | | | | |
| P value | 0.243 | | | | |
| P value summary | ns | | | | |
| Significant diff. among means (P < 0.05)? | No | | | | |
| R squared | 0.3756 | | | | |
| | | | | | |
| **Bonferroni's multiple comparisons test** | **Mean Diff.** | **95.00% CI of diff.** | **Below threshold?** | **Summary** | **Adjusted P Value** |
| Control vs. Fibril | -1.819 | -5.055 to 1.416 | No | ns | 0.342 |
| Control vs. Scrambled | -0.5365 | -3.772 to 2.699 | No | ns | >.999 |
| Fibril vs. Scrambled | 1.283 | -1.953 to 4.518 | No | ns | 0.721 |

Mean cell area

| ANOVA summary | | | | | |
|---|---|---|---|---|---|
| F | 0.007917 | | | | |
| P value | 0.992 | | | | |
| P value summary | ns | | | | |
| Significant diff. among means (P < 0.05)? | No | | | | |
| R squared | 0.002632 | | | | |
| | | | | | |
| **Bonferroni's multiple comparisons test** | **Mean Diff.** | **95.00% CI of diff.** | **Below threshold?** | **Summary** | **Adjusted P Value** |
| Control vs. Fibril | 0.01911 | -1.007 to 1.045 | No | ns | >.999 |
| Control vs. Scrambled | 0.03927 | -0.9869 to 1.065 | No | ns | >.999 |
| Fibril vs. Scrambled | 0.02016 | -1.006 to 1.046 | No | ns | >.999 |

**2h – CS14**

Mean cell length

| ANOVA summary | | | | | |
|---|---|---|---|---|---|
| F | 0.06861 | | | | |
| P value | 0.934 | | | | |
| P value summary | ns | | | | |
| Significant diff. among means (P < 0.05)? | No | | | | |
| R squared | 0.02236 | | | | |
| | | | | | |
| **Bonferroni's multiple comparisons test** | **Mean Diff.** | **95.00% CI of diff.** | **Below threshold?** | **Summary** | **Adjusted P Value** |
| Control vs. Fibril | 0.009539 | -0.08145 to 0.1005 | No | ns | >.999 |
| Control vs. Scrambled | 0.001514 | -0.08947 to 0.0925( | No | ns | >.999 |
| Fibril vs. Scrambled | -0.008025 | -0.09901 to 0.0829( | No | ns | >.999 |

**2h – CS14**

Mean cell roundness

| ANOVA summary | | | | | |
|---|---|---|---|---|---|
| F | 0.005967 | | | | |
| P value | 0.994 | | | | |
| P value summary | ns | | | | |
| Significant diff. among means (P < 0.05)? | No | | | | |
| R squared | 0.001985 | | | | |
| | | | | | |
| **Bonferroni's multiple comparisons test** | **Mean Diff.** | **95.00% CI of diff.** | **Below threshold?** | **Summary** | **Adjusted P Value** |
| Control vs. Fibril | 0.001906 | -0.1195 to 0.1234 | No | ns | >.999 |
| Control vs. Scrambled | -0.002128 | -0.1236 to 0.1193 | No | ns | >.999 |
| Fibril vs. Scrambled | -0.004034 | -0.1255 to 0.1174 | No | ns | >.999 |

Mean cell width

| ANOVA summary | | | | | |
|---|---|---|---|---|---|
| F | 1.692 | | | | |
| P value | 0.261 | | | | |
| P value summary | ns | | | | |
| Significant diff. among means (P < 0.05)? | No | | | | |
| R squared | 0.3606 | | | | |
| | | | | | |
| **Bonferroni's multiple comparisons test** | **Mean Diff.** | **95.00% CI of diff.** | **Below threshold?** | **Summary** | **Adjusted P Value** |
| Control vs. Fibril | -0.0516 | -0.1522 to 0.04899 | No | ns | 0.428 |
| Control vs. Scrambled | -0.006345 | -0.1069 to 0.09424 | No | ns | >.999 |
| Fibril vs. Scrambled | 0.04526 | -0.05533 to 0.1458 | No | ns | 0.569 |

**2h – CS14**

Mean cytoplasm region

| ANOVA summary | | | | | |
|---|---|---|---|---|---|
| F | 0.3851 | | | | |
| P value | 0.696 | | | | |
| P value summary | ns | | | | |
| Significant diff. among means (P < 0.05)? | No | | | | |
| R squared | 0.1138 | | | | |
| | | | | | |
| **Bonferroni's multiple comparisons test** | **Mean Diff.** | **95.00% CI of diff.** | **Below threshold?** | **Summary** | **Adjusted P Value** |
| Control vs. Fibril | -0.01821 | -0.09251 to 0.05609 | No | ns | >.999 |
| Control vs. Scrambled | -0.002301 | -0.07660 to 0.07200 | No | ns | >.999 |
| Fibril vs. Scrambled | 0.01591 | -0.05839 to 0.09021 | No | ns | >.999 |

Mean cell area

| ANOVA summary | | | | | |
|---|---|---|---|---|---|
| F | 0.9761 | | | | |
| P value | 0.43 | | | | |
| P value summary | ns | | | | |
| Significant diff. among means (P < 0.05)? | No | | | | |
| R squared | 0.2455 | | | | |
| | | | | | |
| **Bonferroni's multiple comparisons test** | **Mean Diff.** | **95.00% CI of diff.** | **Below threshold?** | **Summary** | **Adjusted P Value** |
| Control vs. Fibril | -0.07544 | -0.2629 to 0.1120 | No | ns | 0.702 |
| Control vs. Scrambled | -0.01559 | -0.2030 to 0.1718 | No | ns | >.999 |
| Fibril vs. Scrambled | 0.05986 | -0.1276 to 0.2473 | No | ns | >.999 |

**All cell lines – 2h**

Mean cell length

| ANOVA summary | | | | | |
|---|---|---|---|---|---|
| F | 1.258 | | | | |
| P value | 0.401 | | | | |
| P value summary | ns | | | | |
| Significant diff. among means (P < 0.05)? | No | | | | |
| R squared | 0.4561 | | | | |
| | | | | | |
| **Bonferroni's multiple comparisons test** | **Mean Diff.** | **95.00% CI of diff.** | **Below threshold?** | **Summary** | **Adjusted P Value** |
| Control vs. Fibril | 0.03175 | -0.4612 to 0.5247 | No | ns | >.999 |
| Control vs. Scrambled | -0.1208 | -0.6138 to 0.3722 | No | ns | 0.959 |
| Fibril vs. Scrambled | -0.1526 | -0.6456 to 0.3404 | No | ns | 0.69 |

**All cell lines – 2h**

Mean cell roundness

| ANOVA summary | | | | | |
|---|---|---|---|---|---|
| F | 0.5174 | | | | |
| P value | 0.641 | | | | |
| P value summary | ns | | | | |
| Significant diff. among means (P < 0.05)? | No | | | | |
| R squared | 0.2565 | | | | |
| | | | | | |
| **Bonferroni's multiple comparisons test** | **Mean Diff.** | **95.00% CI of diff.** | **Below threshold?** | **Summary** | **Adjusted P Value** |
| Control vs. Fibril | 0.03973 | -0.1596 to 0.2391 | No | ns | >.999 |
| Control vs. Scrambled | 0.03098 | -0.1683 to 0.2303 | No | ns | >.999 |
| Fibril vs. Scrambled | -0.008743 | -0.2081 to 0.1906 | No | ns | >.999 |

Mean cell width

| ANOVA summary | | | | | |
|---|---|---|---|---|---|
| F | 2.459 | | | | |
| P value | 0.233 | | | | |
| P value summary | ns | | | | |
| Significant diff. among means (P < 0.05)? | No | | | | |
| R squared | 0.6211 | | | | |
| | | | | | |
| **Bonferroni's multiple comparisons test** | **Mean Diff.** | **95.00% CI of diff.** | **Below threshold?** | **Summary** | **Adjusted P Value** |
| Control vs. Fibril | -0.04325 | -0.2203 to 0.1338 | No | ns | 0.962 |
| Control vs. Scrambled | 0.03751 | -0.1395 to 0.2145 | No | ns | >.999 |
| Fibril vs. Scrambled | 0.08076 | -0.09625 to 0.2578 | No | ns | 0.34 |

**All cell lines – 2h**

Mean cytoplasm region

| ANOVA summary | | | | | |
|---|---|---|---|---|---|
| F | 0.7584 | | | | |
| P value | 0.541 | | | | |
| P value summary | ns | | | | |
| Significant diff. among means (P < 0.05)? | No | | | | |
| R squared | 0.3358 | | | | |
| | | | | | |
| **Bonferroni's multiple comparisons test** | **Mean Diff.** | **95.00% CI of diff.** | **Below threshold?** | **Summary** | **Adjusted P Value** |
| Control vs. Fibril | -0.9187 | -4.644 to 2.806 | No | ns | 0.951 |
| Control vs. Scrambled | -0.2694 | -3.994 to 3.455 | No | ns | >.999 |
| Fibril vs. Scrambled | 0.6493 | -3.075 to 4.374 | No | ns | >.999 |

Mean cell area

| ANOVA summary | | | | | |
|---|---|---|---|---|---|
| F | 0.4242 | | | | |
| P value | 0.688 | | | | |
| P value summary | ns | | | | |
| Significant diff. among means (P < 0.05)? | No | | | | |
| R squared | 0.2204 | | | | |
| | | | | | |
| **Bonferroni's multiple comparisons test** | **Mean Diff.** | **95.00% CI of diff.** | **Below threshold?** | **Summary** | **Adjusted P Value** |
| Control vs. Fibril | -0.02817 | -0.2449 to 0.1886 | No | ns | >.999 |
| Control vs. Scrambled | 0.01184 | -0.2049 to 0.2286 | No | ns | >.999 |
| Fibril vs. Scrambled | 0.04001 | -0.1767 to 0.2568 | No | ns | >.999 |

**24h- 155v2**

Mean cell length

| ANOVA summary | | | | | |
|---|---|---|---|---|---|
| F | 2.965 | | | | |
| P value | 0.127 | | | | |
| P value summary | ns | | | | |
| Significant diff. among means (P < 0.05)? | No | | | | |
| R squared | 0.497 | | | | |
| | | | | | |
| **Bonferroni's multiple comparisons test** | **Mean Diff.** | **95.00% CI of diff.** | **Below threshold?** | **Summary** | **Adjusted P Value** |
| Control vs. Fibril | 0.332 | -0.3359 to 0.9999 | No | ns | 0.46 |
| Control vs. Scrambled | -0.1516 | -0.8195 to 0.5163 | No | ns | >.999 |
| Fibril vs. Scrambled | -0.4836 | -1.152 to 0.1843 | No | ns | 0.164 |

**24h- 155v2**

Mean cell roundness

| ANOVA summary | | | | | |
|---|---|---|---|---|---|
| F | 1.351 | | | | |
| P value | 0.328 | | | | |
| P value summary | ns | | | | |
| Significant diff. among means (P < 0.05)? | No | | | | |
| R squared | 0.3104 | | | | |
| | | | | | |
| **Bonferroni's multiple comparisons test** | **Mean Diff.** | **95.00% CI of diff.** | **Below threshold?** | **Summary** | **Adjusted P Value** |
| Control vs. Fibril | -0.0721 | -0.5494 to 0.4052 | No | ns | >.999 |
| Control vs. Scrambled | 0.1609 | -0.3164 to 0.6383 | No | ns | 0.93 |
| Fibril vs. Scrambled | 0.233 | -0.2443 to 0.7104 | No | ns | 0.479 |

Mean cell width

| ANOVA summary | | | | | |
|---|---|---|---|---|---|
| F | 3.582 | | | | |
| P value | 0.095 | | | | |
| P value summary | ns | | | | |
| Significant diff. among means (P < 0.05)? | No | | | | |
| R squared | 0.5442 | | | | |
| | | | | | |
| **Bonferroni's multiple comparisons test** | **Mean Diff.** | **95.00% CI of diff.** | **Below threshold?** | **Summary** | **Adjusted P Value** |
| Control vs. Fibril | 0.07737 | -0.4464 to 0.6012 | No | ns | >.999 |
| Control vs. Scrambled | -0.3246 | -0.8484 to 0.1993 | No | ns | 0.263 |
| Fibril vs. Scrambled | -0.4019 | -0.9257 to 0.1219 | No | ns | 0.135 |

**24h- 155v2**

Mean cytoplasm region

| ANOVA summary | | | | | |
|---|---|---|---|---|---|
| F | 2.498 | | | | |
| P value | 0.163 | | | | |
| P value summary | ns | | | | |
| Significant diff. among means (P < 0.05)? | No | | | | |
| R squared | 0.4543 | | | | |
| | | | | | |
| **Bonferroni's multiple comparisons test** | **Mean Diff.** | **95.00% CI of diff.** | **Below threshold?** | **Summary** | **Adjusted P Value** |
| Control vs. Fibril | 0.7665 | -0.4179 to 1.951 | No | ns | 0.232 |
| Control vs. Scrambled | 0.1697 | -1.015 to 1.354 | No | ns | >.999 |
| Fibril vs. Scrambled | -0.5968 | -1.781 to 0.5876 | No | ns | 0.446 |

Mean cell area

| ANOVA summary | | | | | |
|---|---|---|---|---|---|
| F | 1.551 | | | | |
| P value | 0.286 | | | | |
| P value summary | ns | | | | |
| Significant diff. among means (P < 0.05)? | No | | | | |
| R squared | 0.3408 | | | | |
| | | | | | |
| **Bonferroni's multiple comparisons test** | **Mean Diff.** | **95.00% CI of diff.** | **Below threshold?** | **Summary** | **Adjusted P Value** |
| Control vs. Fibril | 0.2915 | -1.110 to 1.693 | No | ns | >.999 |
| Control vs. Scrambled | -0.4534 | -1.855 to 0.9480 | No | ns | 0.985 |
| Fibril vs. Scrambled | -0.7449 | -2.146 to 0.6565 | No | ns | 0.393 |

**24h –CS14**

Mean cell length

| ANOVA summary | | | | | |
|---|---|---|---|---|---|
| F | 1.359 | | | | |
| P value | 0.326 | | | | |
| P value summary | ns | | | | |
| Significant diff. among means (P < 0.05)? | No | | | | |
| R squared | 0.3118 | | | | |
| | | | | | |
| **Bonferroni's multiple comparisons test** | **Mean Diff.** | **95.00% CI of diff.** | **Below threshold?** | **Summary** | **Adjusted P Value** |
| Control vs. Fibril | 0.0225 | -0.04942 to 0.0944 | No | ns | >.999 |
| Control vs. Scrambled | -0.01316 | -0.08508 to 0.0587 | No | ns | >.999 |
| Fibril vs. Scrambled | -0.03566 | -0.1076 to 0.03626 | No | ns | 0.463 |

**24h –CS14**

Mean cell roundness

| ANOVA summary | | | | | |
|---|---|---|---|---|---|
| F | 1.98 | | | | |
| P value | 0.219 | | | | |
| P value summary | ns | | | | |
| Significant diff. among means (P < 0.05)? | No | | | | |
| R squared | 0.3976 | | | | |
| | | | | | |
| **Bonferroni's multiple comparisons test** | **Mean Diff.** | **95.00% CI of diff.** | **Below threshold?** | **Summary** | **Adjusted P Value** |
| Control vs. Fibril | -0.03565 | -0.1083 to 0.03696 | No | ns | 0.473 |
| Control vs. Scrambled | 0.004432 | -0.06818 to 0.0770 | No | ns | >.999 |
| Fibril vs. Scrambled | 0.04009 | -0.03252 to 0.1127 | No | ns | 0.358 |

Mean cell width

| ANOVA summary | | | | | |
|---|---|---|---|---|---|
| F | 1.127 | | | | |
| P value | 0.384 | | | | |
| P value summary | ns | | | | |
| Significant diff. among means (P < 0.05)? | No | | | | |
| R squared | 0.2731 | | | | |
| | | | | | |
| **Bonferroni's multiple comparisons test** | **Mean Diff.** | **95.00% CI of diff.** | **Below threshold?** | **Summary** | **Adjusted P Value** |
| Control vs. Fibril | -0.01763 | -0.1222 to 0.08696 | No | ns | >.999 |
| Control vs. Scrambled | 0.02963 | -0.07496 to 0.1342 | No | ns | >.999 |
| Fibril vs. Scrambled | 0.04726 | -0.05733 to 0.1518 | No | ns | 0.564 |

**24h –CS14**

Mean cytoplasm region

| ANOVA summary | | | | | |
|---|---|---|---|---|---|
| F | 2.635 | | | | |
| P value | 0.151 | | | | |
| P value summary | ns | | | | |
| Significant diff. among means (P < 0.05)? | No | | | | |
| R squared | 0.4676 | | | | |
| | | | | | |
| **Bonferroni's multiple comparisons test** | **Mean Diff.** | **95.00% CI of diff.** | **Below threshold?** | **Summary** | **Adjusted P Value** |
| Control vs. Fibril | 0.02995 | -0.01467 to 0.07456 | No | ns | 0.208 |
| Control vs. Scrambled | 0.00753 | -0.03709 to 0.05215 | No | ns | >.999 |
| Fibril vs. Scrambled | -0.02242 | -0.06703 to 0.02220 | No | ns | 0.449 |

Mean cell area

| ANOVA summary | | | | | |
|---|---|---|---|---|---|
| F | 0.4527 | | | | |
| P value | 0.656 | | | | |
| P value summary | ns | | | | |
| Significant diff. among means (P < 0.05)? | No | | | | |
| R squared | 0.1311 | | | | |
| | | | | | |
| **Bonferroni's multiple comparisons test** | **Mean Diff.** | **95.00% CI of diff.** | **Below threshold?** | **Summary** | **Adjusted P Value** |
| Control vs. Fibril | -0.04169 | -0.2256 to 0.1422 | No | ns | >.999 |
| Control vs. Scrambled | 0.007814 | -0.1761 to 0.1917 | No | ns | >.999 |
| Fibril vs. Scrambled | 0.04951 | -0.1344 to 0.2334 | No | ns | >.999 |

**All cell lines – 24h**

Mean cell length

| ANOVA summary | | | | | |
|---|---|---|---|---|---|
| F | 1.837 | | | | |
| P value | 0.301 | | | | |
| P value summary | ns | | | | |
| Significant diff. among means (P < 0.05)? | No | | | | |
| R squared | 0.5506 | | | | |
| | | | | | |
| **Bonferroni's multiple comparisons test** | **Mean Diff.** | **95.00% CI of diff.** | **Below threshold?** | **Summary** | **Adjusted P Value** |
| Control vs. Fibril | 0.1773 | -0.4950 to 0.8495 | No | ns | 0.871 |
| Control vs. Scrambled | -0.08239 | -0.7547 to 0.5899 | No | ns | >.999 |
| Fibril vs. Scrambled | -0.2596 | -0.9319 to 0.4126 | No | ns | 0.472 |

**All cell lines – 24h**

Mean cell roundness

| ANOVA summary | | | | | |
|---|---|---|---|---|---|
| F | 0.9716 | | | | |
| P value | 0.473 | | | | |
| P value summary | ns | | | | |
| Significant diff. among means (P < 0.05)? | No | | | | |
| R squared | 0.3931 | | | | |
| | | | | | |
| **Bonferroni's multiple comparisons test** | **Mean Diff.** | **95.00% CI of diff.** | **Below threshold?** | **Summary** | **Adjusted P Value** |
| Control vs. Fibril | 0.02086 | -0.6689 to 0.7106 | No | ns | >.999 |
| Control vs. Scrambled | -0.1601 | -0.8498 to 0.5297 | No | ns | >.999 |
| Fibril vs. Scrambled | -0.1809 | -0.8706 to 0.5088 | No | ns | 0.877 |

Mean cell width

| ANOVA summary | | | | | |
|---|---|---|---|---|---|
| F | 0.8044 | | | | |
| P value | 0.525 | | | | |
| P value summary | ns | | | | |
| Significant diff. among means (P < 0.05)? | No | | | | |
| R squared | 0.3491 | | | | |
| | | | | | |
| **Bonferroni's multiple comparisons test** | **Mean Diff.** | **95.00% CI of diff.** | **Below threshold?** | **Summary** | **Adjusted P Value** |
| Control vs. Fibril | 0.02987 | -0.6972 to 0.7569 | No | ns | >.999 |
| Control vs. Scrambled | -0.1475 | -0.8745 to 0.5796 | No | ns | >.999 |
| Fibril vs. Scrambled | -0.1773 | -0.9044 to 0.5497 | No | ns | 0.964 |

**All cell lines – 24h**

Mean cytoplasm region

| ANOVA summary | | | | | |
|---|---|---|---|---|---|
| F | 0.9222 | | | | |
| P value | 0.487 | | | | |
| P value summary | ns | | | | |
| Significant diff. among means (P < 0.05)? | No | | | | |
| R squared | 0.3807 | | | | |
| | | | | | |
| **Bonferroni's multiple comparisons test** | **Mean Diff.** | **95.00% CI of diff.** | **Below threshold?** | **Summary** | **Adjusted P Value** |
| Control vs. Fibril | 0.3982 | -1.097 to 1.894 | No | ns | 0.859 |
| Control vs. Scrambled | 0.08863 | -1.407 to 1.584 | No | ns | >.999 |
| Fibril vs. Scrambled | -0.3096 | -1.805 to 1.186 | No | ns | >.999 |

Mean cell area

| ANOVA summary | | | | | |
|---|---|---|---|---|---|
| F | 1.15 | | | | |
| P value | 0.426 | | | | |
| P value summary | ns | | | | |
| Significant diff. among means (P < 0.05)? | No | | | | |
| R squared | 0.4339 | | | | |
| | | | | | |
| **Bonferroni's multiple comparisons test** | **Mean Diff.** | **95.00% CI of diff.** | **Below threshold?** | **Summary** | **Adjusted P Value** |
| Control vs. Fibril | 0.1249 | -1.003 to 1.253 | No | ns | >.999 |
| Control vs. Scrambled | -0.2228 | -1.351 to 0.9053 | No | ns | >.999 |
| Fibril vs. Scrambled | -0.3477 | -1.476 to 0.7804 | No | ns | 0.694 |

**48h – 155v2**

Mean cell length

| ANOVA summary | | | | | |
|---|---|---|---|---|---|
| F | 1.824 | | | | |
| P value | 0.241 | | | | |
| P value summary | ns | | | | |
| Significant diff. among means (P < 0.05)? | No | | | | |
| R squared | 0.3781 | | | | |
| | | | | | |
| **Bonferroni's multiple comparisons test** | **Mean Diff.** | **95.00% CI of diff.** | **Below threshold?** | **Summary** | **Adjusted P Value** |
| Control vs. Fibril | -0.4207 | -1.268 to 0.4269 | No | ns | 0.462 |
| Control vs. Scrambled | -0.4321 | -1.280 to 0.4156 | No | ns | 0.434 |
| Fibril vs. Scrambled | -0.01133 | -0.8590 to 0.8363 | No | ns | >.999 |

**48h – 155v2**

Mean cell roundness

| ANOVA summary | | | | | |
|---|---|---|---|---|---|
| F | 5.463 | | | | |
| P value | 0.045 | | | | |
| P value summary | * | | | | |
| Significant diff. among means (P < 0.05)? | Yes | | | | |
| R squared | 0.6455 | | | | |
| | | | | | |
| **Bonferroni's multiple comparisons test** | **Mean Diff.** | **95.00% CI of diff.** | **Below threshold?** | **Summary** | **Adjusted P Value** |
| Control vs. Fibril | 0.334 | -0.01688 to 0.6850 | No | ns | 0.061 |
| Control vs. Scrambled | 0.2654 | -0.08548 to 0.6164 | No | ns | 0.142 |
| Fibril vs. Scrambled | -0.0686 | -0.4195 to 0.2823 | No | ns | >.999 |

Mean cell width

| ANOVA summary | | | | | |
|---|---|---|---|---|---|
| F | 0.5262 | | | | |
| P value | 0.616 | | | | |
| P value summary | ns | | | | |
| Significant diff. among means (P < 0.05)? | No | | | | |
| R squared | 0.1492 | | | | |
| | | | | | |
| **Bonferroni's multiple comparisons test** | **Mean Diff.** | **95.00% CI of diff.** | **Below threshold?** | **Summary** | **Adjusted P Value** |
| Control vs. Fibril | -0.3582 | -1.596 to 0.8796 | No | ns | >.999 |
| Control vs. Scrambled | -0.3043 | -1.542 to 0.9335 | No | ns | >.999 |
| Fibril vs. Scrambled | 0.05393 | -1.184 to 1.292 | No | ns | >.999 |

**48h – 155v2**

Mean cytoplasm region

| ANOVA summary | | | | | |
|---|---|---|---|---|---|
| F | 6.499 | | | | |
| P value | 0.032 | | | | |
| P value summary | * | | | | |
| Significant diff. among means (P < 0.05)? | Yes | | | | |
| R squared | 0.6842 | | | | |
| | | | | | |
| **Bonferroni's multiple comparisons test** | **Mean Diff.** | **95.00% CI of diff.** | **Below threshold?** | **Summary** | **Adjusted P Value** |
| Control vs. Fibril | -1.171 | -3.817 to 1.475 | No | ns | 0.588 |
| Control vs. Scrambled | -2.885 | -5.531 to -0.2388 | Yes | * | 0.035 |
| Fibril vs. Scrambled | -1.714 | -4.360 to 0.9323 | No | ns | 0.232 |

Mean cell area

| ANOVA summary | | | | | |
|---|---|---|---|---|---|
| F | 1.995 | | | | |
| P value | 0.217 | | | | |
| P value summary | ns | | | | |
| Significant diff. among means (P < 0.05)? | No | | | | |
| R squared | 0.3994 | | | | |
| | | | | | |
| **Bonferroni's multiple comparisons test** | **Mean Diff.** | **95.00% CI of diff.** | **Below threshold?** | **Summary** | **Adjusted P Value** |
| Control vs. Fibril | -1.483 | -4.113 to 1.147 | No | ns | 0.339 |
| Control vs. Scrambled | -1.257 | -3.886 to 1.373 | No | ns | 0.502 |
| Fibril vs. Scrambled | 0.2264 | -2.403 to 2.856 | No | ns | >.999 |

**48h – CS14**

Mean cell length

| ANOVA summary | | | | | |
|---|---|---|---|---|---|
| F | 0.4773 | | | | |
| P value | 0.642 | | | | |
| P value summary | ns | | | | |
| Significant diff. among means (P < 0.05)? | No | | | | |
| R squared | 0.1373 | | | | |
| | | | | | |
| **Bonferroni's multiple comparisons test** | **Mean Diff.** | **95.00% CI of diff.** | **Below threshold?** | **Summary** | **Adjusted P Value** |
| Control vs. Fibril | 0.005412 | -0.1040 to 0.1148 | No | ns | >.999 |
| Control vs. Scrambled | -0.02505 | -0.1344 to 0.08433 | No | ns | >.999 |
| Fibril vs. Scrambled | -0.03047 | -0.1398 to 0.07891 | No | ns | >.999 |

**48h – CS14**

Mean cell roundness

| ANOVA summary | | | | | |
|---|---|---|---|---|---|
| F | 14.37 | | | | |
| P value | 0.005 | | | | |
| P value summary | ** | | | | |
| Significant diff. among means (P < 0.05)? | Yes | | | | |
| R squared | 0.8273 | | | | |
| | | | | | |
| **Bonferroni's multiple comparisons test** | **Mean Diff.** | **95.00% CI of diff.** | **Below threshold?** | **Summary** | **Adjusted P Value** |
| Control vs. Fibril | -0.1042 | -0.1801 to -0.02821 | Yes | * | 0.012 |
| Control vs. Scrambled | 0.005971 | -0.06999 to 0.08193 | No | ns | >.999 |
| Fibril vs. Scrambled | 0.1101 | 0.03418 to 0.1861 | Yes | ** | 0.009 |

Mean cell width

| ANOVA summary | | | | | |
|---|---|---|---|---|---|
| F | 2.357 | | | | |
| P value | 0.176 | | | | |
| P value summary | ns | | | | |
| Significant diff. among means (P < 0.05)? | No | | | | |
| R squared | 0.44 | | | | |
| | | | | | |
| **Bonferroni's multiple comparisons test** | **Mean Diff.** | **95.00% CI of diff.** | **Below threshold?** | **Summary** | **Adjusted P Value** |
| Control vs. Fibril | -0.07034 | -0.1856 to 0.04494 | No | ns | 0.275 |
| Control vs. Scrambled | -0.009919 | -0.1252 to 0.1054 | No | ns | >.999 |
| Fibril vs. Scrambled | 0.06042 | -0.05486 to 0.1757 | No | ns | 0.407 |

**48h – CS14**

Mean cytoplasm region

| ANOVA summary | | | | | |
|---|---|---|---|---|---|
| F | 1.668 | | | | |
| P value | 0.265 | | | | |
| P value summary | ns | | | | |
| Significant diff. among means (P < 0.05)? | No | | | | |
| R squared | 0.3574 | | | | |
| | | | | | |
| **Bonferroni's multiple comparisons test** | **Mean Diff.** | **95.00% CI of diff.** | **Below threshold?** | **Summary** | **Adjusted P Value** |
| Control vs. Fibril | -0.01235 | -0.05803 to 0.03332 | No | ns | >.999 |
| Control vs. Scrambled | 0.01302 | -0.03265 to 0.05869 | No | ns | >.999 |
| Fibril vs. Scrambled | 0.02537 | -0.02030 to 0.07105 | No | ns | 0.353 |

Mean cell area

| ANOVA summary | | | | | |
|---|---|---|---|---|---|
| F | 2.061 | | | | |
| P value | 0.208 | | | | |
| P value summary | ns | | | | |
| Significant diff. among means (P < 0.05)? | No | | | | |
| R squared | 0.4073 | | | | |
| | | | | | |
| **Bonferroni's multiple comparisons test** | **Mean Diff.** | **95.00% CI of diff.** | **Below threshold?** | **Summary** | **Adjusted P Value** |
| Control vs. Fibril | -0.1086 | -0.2857 to 0.06851 | No | ns | 0.271 |
| Control vs. Scrambled | -0.04282 | -0.2199 to 0.1343 | No | ns | >.999 |
| Fibril vs. Scrambled | 0.06575 | -0.1113 to 0.2428 | No | ns | 0.804 |

**All cell lines – 48h**

Mean cell length

| ANOVA summary | | | | | |
|---|---|---|---|---|---|
| F | 0.5517 | | | | |
| P value | 0.625 | | | | |
| P value summary | ns | | | | |
| Significant diff. among means (P < 0.05)? | No | | | | |
| R squared | 0.2689 | | | | |
| | | | | | |
| **Bonferroni's multiple comparisons test** | **Mean Diff.** | **95.00% CI of diff.** | **Below threshold?** | **Summary** | **Adjusted P Value** |
| Control vs. Fibril | -0.2077 | -1.376 to 0.9607 | No | ns | >.999 |
| Control vs. Scrambled | -0.2286 | -1.397 to 0.9398 | No | ns | >.999 |
| Fibril vs. Scrambled | -0.0209 | -1.189 to 1.147 | No | ns | >.999 |

**All cell lines – 48h**

Mean cell roundness

| ANOVA summary | | | | | |
|---|---|---|---|---|---|
| F | 0.2472 | | | | |
| P value | 0.795 | | | | |
| P value summary | ns | | | | |
| Significant diff. among means (P < 0.05)? | No | | | | |
| R squared | 0.1415 | | | | |
| | | | | | |
| **Bonferroni's multiple comparisons test** | **Mean Diff.** | **95.00% CI of diff.** | **Below threshold?** | **Summary** | **Adjusted P Value** |
| Control vs. Fibril | 0.1149 | -0.8948 to 1.125 | No | ns | >.999 |
| Control vs. Scrambled | 0.1357 | -0.8740 to 1.145 | No | ns | >.999 |
| Fibril vs. Scrambled | 0.02077 | -0.9890 to 1.030 | No | ns | >.999 |

Mean cell width

| ANOVA summary | | | | | |
|---|---|---|---|---|---|
| F | 0.8715 | | | | |
| P value | 0.503 | | | | |
| P value summary | ns | | | | |
| Significant diff. among means (P < 0.05)? | No | | | | |
| R squared | 0.3675 | | | | |
| | | | | | |
| **Bonferroni's multiple comparisons test** | **Mean Diff.** | **95.00% CI of diff.** | **Below threshold?** | **Summary** | **Adjusted P Value** |
| Control vs. Fibril | -0.2143 | -1.031 to 0.6020 | No | ns | 0.876 |
| Control vs. Scrambled | -0.1571 | -0.9734 to 0.6592 | No | ns | >.999 |
| Fibril vs. Scrambled | 0.05718 | -0.7591 to 0.8735 | No | ns | >.999 |

**All cell lines – 48h**

Mean cytoplasm region

| **ANOVA summary** | | | | | |
|---|---|---|---|---|---|
| F | 0.6416 | | | | |
| P value | 0.586 | | | | |
| P value summary | ns | | | | |
| Significant diff. among means (P < 0.05)? | No | | | | |
| R squared | 0.2996 | | | | |
| | | | | | |
| **Bonferroni's multiple comparisons test** | **Mean Diff.** | **95.00% CI of diff.** | **Below threshold?** | **Summary** | **Adjusted P Value** |
| Control vs. Fibril | -0.5917 | -6.780 to 5.596 | No | ns | >.999 |
| Control vs. Scrambled | -1.436 | -7.624 to 4.752 | No | ns | >.999 |
| Fibril vs. Scrambled | -0.8442 | -7.032 to 5.344 | No | ns | >.999 |

Mean cell area

| **ANOVA summary** | | | | | |
|---|---|---|---|---|---|
| F | 0.6405 | | | | |
| P value | 0.587 | | | | |
| P value summary | ns | | | | |
| Significant diff. among means (P < 0.05)? | No | | | | |
| R squared | 0.2992 | | | | |
| | | | | | |
| **Bonferroni's multiple comparisons test** | **Mean Diff.** | **95.00% CI of diff.** | **Below threshold?** | **Summary** | **Adjusted P Value** |
| Control vs. Fibril | -0.7958 | -4.432 to 2.840 | No | ns | >.999 |
| Control vs. Scrambled | -0.6497 | -4.285 to 2.986 | No | ns | >.999 |
| Fibril vs. Scrambled | 0.1461 | -3.490 to 3.782 | No | ns | >.999 |

# 6. Disease ontology results for significant differentially pathways for oligomers vs control

| DOID | Description | GeneRatio | BgRatio | pvalue | padj | geneID | geneName | EntrezID | Count | Up | Up_Gene_names | Down | Down_Gene_names |
|---|---|---|---|---|---|---|---|---|---|---|---|---|---|
| DOID:229 | female reg | Jul-23 | 165/6929 | 6.80E-07 | 0.000301 | ENSG0000 | MMP1/PI3/N | 4312/5266 | 7 | 6 | ENSG0000 | 1 | ENSG00000187556 |
| DOID:005( | primary ba | Jul-23 | 191/6929 | 1.83E-06 | 0.000405 | ENSG0000 | MMP1/SAA1, | 4312/6288 | 7 | 7 | ENSG0000 | 0 | |
| DOID:289 | endometri | May-23 | 78/6929 | 4.56E-06 | 0.000553 | ENSG0000 | MMP1/MMP | 4312/4322 | 5 | 5 | ENSG0000 | 0 | |
| DOID:104 | bacterial ir | Jul-23 | 222/6929 | 4.99E-06 | 0.000553 | ENSG0000 | MMP1/SAA1, | 4312/6288 | 7 | 7 | ENSG0000 | 0 | |
| DOID:1172 | Lyme disea | Mar-23 | 15/6929 | 1.42E-05 | 0.001255 | ENSG0000 | MMP1/MMP | 4312/4322 | 3 | 3 | ENSG0000 | 0 | |
| DOID:3085 | chronic ob | Jun-23 | 193/6929 | 2.94E-05 | 0.002168 | ENSG0000 | MMP1/PI3/N | 4312/5266 | 6 | 6 | ENSG0000 | 0 | |
| DOID:399 | tuberculos | May-23 | 124/6929 | 4.40E-05 | 0.002784 | ENSG0000 | MMP1/IL1A/ | 4312/3552 | 5 | 5 | ENSG0000 | 0 | |
| DOID:15 | reproducti | Jul-23 | 321/6929 | 5.53E-05 | 0.003062 | ENSG0000 | MMP1/PI3/N | 4312/5266 | 7 | 6 | ENSG0000 | 1 | ENSG00000187556 |
| DOID:7148 | rheumatoi | Aug-23 | 465/6929 | 7.73E-05 | 0.003804 | ENSG0000 | MMP1/SAA1, | 4312/6288 | 8 | 8 | ENSG0000 | 0 | |
| DOID:403 | mouth dise | May-23 | 159/6929 | 0.000144 | 0.005862 | ENSG0000 | MMP1/MMP | 4312/4322 | 5 | 5 | ENSG0000 | 0 | |
| DOID:2320 | obstructive | Jun-23 | 257/6929 | 0.000146 | 0.005862 | ENSG0000 | MMP1/PI3/N | 4312/5266 | 6 | 6 | ENSG0000 | 0 | |
| DOID:37 | skin diseas | Jun-23 | 290/6929 | 0.000282 | 0.010189 | ENSG0000 | MMP1/DSP/I | 4312/1832 | 6 | 5 | ENSG0000 | 1 | ENSG00000096696 |
| DOID:850 | lung diseas | Jul-23 | 420/6929 | 0.0003 | 0.010189 | ENSG0000 | MMP1/PI3/N | 4312/5266 | 7 | 6 | ENSG0000 | 1 | ENSG00000141448 |
| DOID:005( | lower resp | Jul-23 | 429/6929 | 0.000341 | 0.010189 | ENSG0000 | MMP1/PI3/N | 4312/5266 | 7 | 6 | ENSG0000 | 1 | ENSG00000141448 |
| DOID:193( | atheroscle | Jun-23 | 305/6929 | 0.00037 | 0.010189 | ENSG0000 | MMP1/SAA1, | 4312/6288 | 6 | 6 | ENSG0000 | 0 | |
| DOID:2348 | arterioscle | Jun-23 | 306/6929 | 0.000377 | 0.010189 | ENSG0000 | MMP1/SAA1, | 4312/6288 | 6 | 6 | ENSG0000 | 0 | |
| DOID:377( | pulmonary | Apr-23 | 109/6929 | 0.000407 | 0.010189 | ENSG0000 | MMP1/IL1A/ | 4312/3552 | 4 | 3 | ENSG0000 | 1 | ENSG00000141448 |
| DOID:1337 | Kawasaki d | Mar-23 | 45/6929 | 0.000414 | 0.010189 | ENSG0000 | MMP1/MMP | 4312/4322 | 3 | 3 | ENSG0000 | 0 | |
| DOID:2345 | arterioscle | Jun-23 | 316/6929 | 0.000448 | 0.010443 | ENSG0000 | MMP1/SAA1, | 4312/6288 | 6 | 6 | ENSG0000 | 0 | |
| DOID:3386 | periodonta | Apr-23 | 115/6929 | 0.0005 | 0.010704 | ENSG0000 | MMP1/MMP | 4312/4322 | 4 | 4 | ENSG0000 | 0 | |
| DOID:1602 | lymphader | Mar-23 | 49/6929 | 0.000533 | 0.010704 | ENSG0000 | MMP1/MMP | 4312/4322 | 3 | 3 | ENSG0000 | 0 | |
| DOID:9942 | lymph nod | Mar-23 | 49/6929 | 0.000533 | 0.010704 | ENSG0000 | MMP1/MMP | 4312/4322 | 3 | 3 | ENSG0000 | 0 | |
| DOID:16 | integumen | Jun-23 | 331/6929 | 0.000574 | 0.010704 | ENSG0000 | MMP1/DSP/I | 4312/1832 | 6 | 5 | ENSG0000 | 1 | ENSG00000096696 |
| DOID:1485 | cystic fibrc | Apr-23 | 120/6929 | 0.000587 | 0.010704 | ENSG0000 | PI3/IL1A/MN | 5266/3552 | 4 | 4 | ENSG0000 | 0 | |
| DOID:1575 | respiratory | Jul-23 | 477/6929 | 0.000652 | 0.010704 | ENSG0000 | MMP1/PI3/N | 4312/5266 | 7 | 6 | ENSG0000 | 1 | ENSG00000141448 |
| DOID:1285 | keratocon | Feb-23 | Dec-29 | 0.000682 | 0.010704 | ENSG0000 | IL1A/MMP9 | 3552/4318 | 2 | 2 | ENSG0000 | 0 | |
| DOID:9368 | keratocon | Feb-23 | Dec-29 | 0.000682 | 0.010704 | ENSG0000 | IL1A/MMP9 | 3552/4318 | 2 | 2 | ENSG0000 | 0 | |
| DOID:9563 | bronchiect | Feb-23 | Dec-29 | 0.000682 | 0.010704 | ENSG0000 | MMP1/MMP | 4312/4318 | 2 | 2 | ENSG0000 | 0 | |
| DOID:1100 | ovarian dis | Mar-23 | 54/6929 | 0.00071 | 0.010704 | ENSG0000 | MMP1/NANC | 4312/3429 | 3 | 2 | ENSG0000 | 1 | ENSG00000187556 |
| DOID:2462 | retinal vas | Mar-23 | 55/6929 | 0.000749 | 0.010704 | ENSG0000 | MMP1/MMP | 4312/4318 | 3 | 3 | ENSG0000 | 0 | |
| DOID:8947 | diabetic re | Mar-23 | 55/6929 | 0.000749 | 0.010704 | ENSG0000 | MMP1/MMP | 4312/4318 | 3 | 3 | ENSG0000 | 0 | |
| DOID:1014 | dry eye syr | Feb-23 | 13/6929 | 0.000804 | 0.010794 | ENSG0000 | IL1A/MMP9 | 3552/4318 | 2 | 2 | ENSG0000 | 0 | |
| DOID:1400 | lacrimal ap | Feb-23 | 13/6929 | 0.000804 | 0.010794 | ENSG0000 | IL1A/MMP9 | 3552/4318 | 2 | 2 | ENSG0000 | 0 | |
| DOID:1091 | tooth disea | Apr-23 | 134/6929 | 0.00089 | 0.011597 | ENSG0000 | MMP1/MMP | 4312/4322 | 4 | 4 | ENSG0000 | 0 | |
| DOID:1015 | osteomyel | Feb-23 | 14/6929 | 0.000936 | 0.01185 | ENSG0000 | MMP1/IL1A | 4312/3552 | 2 | 2 | ENSG0000 | 0 | |
| DOID:3371 | chondrosa | Mar-23 | 62/6929 | 0.001064 | 0.012263 | ENSG0000 | MMP1/MMP | 4312/4322 | 3 | 3 | ENSG0000 | 0 | |
| DOID:9637 | stomatitis | Feb-23 | 15/6929 | 0.001078 | 0.012263 | ENSG0000 | IL1A/IL32 | 3552/9235 | 2 | 2 | ENSG0000 | 0 | |
| DOID:9675 | pulmonary | Feb-23 | 15/6929 | 0.001078 | 0.012263 | ENSG0000 | MMP1/MMP | 4312/4318 | 2 | 2 | ENSG0000 | 0 | |
| DOID:5844 | myocardia | May-23 | 247/6929 | 0.001098 | 0.012263 | ENSG0000 | MMP1/PI3/IL | 4312/5266 | 5 | 5 | ENSG0000 | 0 | |
| DOID:6364 | migraine | Mar-23 | 63/6929 | 0.001114 | 0.012263 | ENSG0000 | IL1A/MMP9/ | 3552/4318 | 3 | 3 | ENSG0000 | 0 | |
| DOID:2723 | dermatitis | Apr-23 | 143/6929 | 0.001135 | 0.012263 | ENSG0000 | IL1A/MMP9/ | 3552/4318 | 4 | 4 | ENSG0000 | 0 | |
| DOID:3082 | interstitial | Apr-23 | 146/6929 | 0.001226 | 0.012668 | ENSG0000 | MMP1/IL1A/ | 4312/3552 | 4 | 3 | ENSG0000 | 1 | ENSG00000141448 |
| DOID:1532 | pleural dis | Feb-23 | 16/6929 | 0.00123 | 0.012668 | ENSG0000 | MMP9/ICAM | 4318/3383 | 2 | 2 | ENSG0000 | 0 | |
| DOID:3302 | chordoma | Feb-23 | 17/6929 | 0.001391 | 0.013691 | ENSG0000 | MMP1/MMP | 4312/4318 | 2 | 2 | ENSG0000 | 0 | |
| DOID:3305 | notochord | Feb-23 | 17/6929 | 0.001391 | 0.013691 | ENSG0000 | MMP1/MMP | 4312/4318 | 2 | 2 | ENSG0000 | 0 | |
| DOID:1324 | Behcet's d | Mar-23 | 70/6929 | 0.001513 | 0.014571 | ENSG0000 | IL1A/MMP9/ | 3552/4318 | 3 | 3 | ENSG0000 | 0 | |
| DOID:3087 | gingivitis | Feb-23 | 18/6929 | 0.001561 | 0.014717 | ENSG0000 | IL1A/MMP9 | 3552/4318 | 2 | 2 | ENSG0000 | 0 | |
| DOID:936 | brain disea | Jun-23 | 408/6929 | 0.001719 | 0.015861 | ENSG0000 | GABRA1/IL1A | 2554/3552 | 6 | 5 | ENSG0000 | 1 | ENSG00000175899 |
| DOID:1575 | rheumatic | Apr-23 | 165/6929 | 0.001927 | 0.016452 | ENSG0000 | MMP1/IL1A/ | 4312/3552 | 4 | 4 | ENSG0000 | 0 | |
| DOID:418 | systemic s | Apr-23 | 165/6929 | 0.001927 | 0.016452 | ENSG0000 | MMP1/IL1A/ | 4312/3552 | 4 | 4 | ENSG0000 | 0 | |
| DOID:419 | sclerodern | Apr-23 | 165/6929 | 0.001927 | 0.016452 | ENSG0000 | MMP1/IL1A/ | 4312/3552 | 4 | 4 | ENSG0000 | 0 | |
| DOID:1400 | cerebral m | Feb-23 | 20/6929 | 0.001931 | 0.016452 | ENSG0000 | MMP1/ICAM | 4312/3383 | 2 | 2 | ENSG0000 | 0 | |
| DOID:8398 | osteoarthr | Apr-23 | 173/6929 | 0.002292 | 0.019161 | ENSG0000 | MMP1/MMP | 4312/4322 | 4 | 4 | ENSG0000 | 0 | |
| DOID:123( | malaria | Mar-23 | 82/6929 | 0.002385 | 0.019532 | ENSG0000 | MMP1/SAA1, | 4312/6288 | 3 | 3 | ENSG0000 | 0 | |
| DOID:854 | collagen di | Apr-23 | 176/6929 | 0.002441 | 0.019532 | ENSG0000 | MMP1/IL1A/ | 4312/3552 | 4 | 4 | ENSG0000 | 0 | |
| DOID:381 | arthropath | Mar-23 | 83/6929 | 0.002469 | 0.019532 | ENSG0000 | MMP1/SAA1, | 4312/6288 | 3 | 3 | ENSG0000 | 0 | |
| DOID:9471 | meningitis | Feb-23 | 23/6929 | 0.002556 | 0.019865 | ENSG0000 | MMP9/ICAM | 4318/3383 | 2 | 2 | ENSG0000 | 0 | |
| DOID:3395 | coronary a | May-23 | 303/6929 | 0.002716 | 0.020516 | ENSG0000 | MMP1/PI3/IL | 4312/5266 | 5 | 5 | ENSG0000 | 0 | |
| DOID:75 | lymphatic | Mar-23 | 86/6929 | 0.002732 | 0.020516 | ENSG0000 | MMP1/MMP | 4312/4322 | 3 | 3 | ENSG0000 | 0 | |
| DOID:1147 | osteoporo | Mar-23 | 87/6929 | 0.002824 | 0.02085 | ENSG0000 | MMP13/IL1A | 4322/3552 | 3 | 3 | ENSG0000 | 0 | |
| DOID:008( | bone reso | Mar-23 | 88/6929 | 0.002917 | 0.021186 | ENSG0000 | MMP13/IL1A | 4322/3552 | 3 | 3 | ENSG0000 | 0 | |
| DOID:114 | heart disea | Jun-23 | 458/6929 | 0.003097 | 0.021883 | ENSG0000 | MMP1/MMP | 4312/4322 | 6 | 5 | ENSG0000 | 1 | ENSG00000141448 |
| DOID:552 | pneumonia | Mar-23 | 91/6929 | 0.003209 | 0.021883 | ENSG0000 | MMP1/IL1A/ | 4312/3552 | 3 | 3 | ENSG0000 | 0 | |
| DOID:2600 | laryngeal c | Feb-23 | 26/6929 | 0.003264 | 0.021883 | ENSG0000 | MMP1/MMP | 4312/4318 | 2 | 2 | ENSG0000 | 0 | |
| DOID:2797 | idiopathic | Feb-23 | 26/6929 | 0.003264 | 0.021883 | ENSG0000 | MMP1/IL1A | 4312/3552 | 2 | 2 | ENSG0000 | 0 | |
| DOID:0066 | integumen | Mar-23 | 92/6929 | 0.00331 | 0.021883 | ENSG0000 | MMP1/MMP | 4312/4322 | 3 | 3 | ENSG0000 | 0 | |
| DOID:4155 | skin cance | Mar-23 | 92/6929 | 0.00331 | 0.021883 | ENSG0000 | MMP1/MMP | 4312/4322 | 3 | 3 | ENSG0000 | 0 | |
| DOID:1022 | dermatom | Feb-23 | 27/6929 | 0.003518 | 0.022916 | ENSG0000 | IL1A/MMP9 | 3552/4318 | 2 | 2 | ENSG0000 | 0 | |
| DOID:6000 | congestive | Apr-23 | 196/6929 | 0.003605 | 0.022937 | ENSG0000 | MMP1/MMP | 4312/4322 | 4 | 4 | ENSG0000 | 0 | |
| DOID:4985 | pancreatit | Mar-23 | 95/6929 | 0.003624 | 0.022937 | ENSG0000 | MMP9/ICAM | 4318/3383 | 3 | 2 | ENSG0000 | 1 | ENSG00000175899 |
| DOID:3905 | lung carcin | Jun-23 | 479/6929 | 0.003876 | 0.024186 | ENSG0000 | MMP1/SAA1, | 4312/6288 | 6 | 4 | ENSG0000 | 2 | ENSG00000170689/ENSG |
| DOID:865 | vasculitis | Mar-23 | 98/6929 | 0.003957 | 0.024346 | ENSG0000 | IL1A/MMP9/ | 3552/4318 | 3 | 3 | ENSG0000 | 0 | |
| DOID:824 | periodonti | Mar-23 | 99/6929 | 0.004072 | 0.024478 | ENSG0000 | MMP1/IL1A/ | 4312/3552 | 3 | 3 | ENSG0000 | 0 | |
| DOID:1885 | hepatitis C | Apr-23 | 203/6929 | 0.004089 | 0.024478 | ENSG0000 | SAA1/IL1A/M | 6288/3552 | 4 | 4 | ENSG0000 | 0 | |
| DOID:1686 | glaucoma | Mar-23 | 100/6929 | 0.004189 | 0.024523 | ENSG0000 | MMP1/IL1A/ | 4312/3552 | 3 | 3 | ENSG0000 | 0 | |
| DOID:1337 | temporal a | Feb-23 | 30/6929 | 0.004333 | 0.024523 | ENSG0000 | MMP9/ICAM | 4318/3383 | 2 | 2 | ENSG0000 | 0 | |
| DOID:1482 | gingival dis | Feb-23 | 30/6929 | 0.004333 | 0.024523 | ENSG0000 | IL1A/MMP9 | 3552/4318 | 2 | 2 | ENSG0000 | 0 | |
| DOID:525 | central ne | Feb-23 | 30/6929 | 0.004333 | 0.024523 | ENSG0000 | MMP9/ICAM | 4318/3383 | 2 | 2 | ENSG0000 | 0 | |
| DOID:1105 | urinary bla | Mar-23 | 102/6929 | 0.004428 | 0.024523 | ENSG0000 | MMP1/IL1A/ | 4312/3552 | 3 | 3 | ENSG0000 | 0 | |
| DOID:2785 | parasitic p | Mar-23 | 102/6929 | 0.004428 | 0.024523 | ENSG0000 | MMP1/SAA1, | 4312/6288 | 3 | 3 | ENSG0000 | 0 | |
| DOID:417 | hypersensi | Jun-23 | 494/6929 | 0.004518 | 0.02471 | ENSG0000 | MMP1/SAA1, | 4312/6288 | 6 | 6 | ENSG0000 | 0 | |
| DOID:3065 | astrocytor | Mar-23 | 104/6929 | 0.004677 | 0.025265 | ENSG0000 | MMP1/MMP | 4312/4318 | 3 | 3 | ENSG0000 | 0 | |
| DOID:1116 | pertussis | Feb-23 | 32/6929 | 0.004921 | 0.025952 | ENSG0000 | SAA1/ICAM1 | 6288/3383 | 2 | 2 | ENSG0000 | 0 | |
| DOID:1271 | newborn r | Feb-23 | 32/6929 | 0.004921 | 0.025952 | ENSG0000 | PI3/MMP9 | 5266/4318 | 2 | 2 | ENSG0000 | 0 | |
| DOID:201 | connective | May-23 | 356/6929 | 0.005437 | 0.027286 | ENSG0000 | MMP1/MMP | 4312/4322 | 5 | 5 | ENSG0000 | 0 | |
| DOID:1183 | myopia | Feb-23 | 34/6929 | 0.005543 | 0.027286 | ENSG0000 | MMP1/MMP | 4312/4318 | 2 | 2 | ENSG0000 | 0 | |
| DOID:1320 | proliferati | Feb-23 | 34/6929 | 0.005543 | 0.027286 | ENSG0000 | MMP9/ICAM | 4318/3383 | 2 | 2 | ENSG0000 | 0 | |
| DOID:2596 | larynx can | Feb-23 | 34/6929 | 0.005543 | 0.027286 | ENSG0000 | MMP1/MMP | 4312/4318 | 2 | 2 | ENSG0000 | 0 | |
| DOID:5158 | pleural car | Feb-23 | 34/6929 | 0.005543 | 0.027286 | ENSG0000 | PDZK1IP1/Mf | 10158/431 | 2 | 2 | ENSG0000 | 0 | |
| DOID:7474 | malignant | Feb-23 | 34/6929 | 0.005543 | 0.027286 | ENSG0000 | PDZK1IP1/Mf | 10158/431 | 2 | 2 | ENSG0000 | 0 | |
| DOID:005( | commensa | Feb-23 | 36/6929 | 0.0062 | 0.030184 | ENSG0000 | SAA1/ICAM1 | 6288/3383 | 2 | 2 | ENSG0000 | 0 | |
| DOID:1176 | bronchial c | Mar-23 | 120/6929 | 0.006967 | 0.033549 | ENSG0000 | MMP1/MMP | 4312/4318 | 3 | 3 | ENSG0000 | 0 | |
| DOID:8466 | retinal deg | Apr-23 | 238/6929 | 0.007183 | 0.034008 | ENSG0000 | MMP1/IL1A/ | 4312/3552 | 4 | 4 | ENSG0000 | 0 | |
| DOID:5157 | benign ple | Feb-23 | 39/6929 | 0.007249 | 0.034008 | ENSG0000 | PDZK1IP1/Mf | 10158/431 | 2 | 2 | ENSG0000 | 0 | |
| DOID:1398 | parasitic ir | Mar-23 | 122/6929 | 0.007293 | 0.034008 | ENSG0000 | MMP1/SAA1, | 4312/6288 | 3 | 3 | ENSG0000 | 0 | |
| DOID:8778 | Crohn's dis | Feb-23 | 40/6929 | 0.007615 | 0.03514 | ENSG0000 | MMP1/ICAM | 4312/3383 | 2 | 2 | ENSG0000 | 0 | |
| DOID:008( | bone remo | Mar-23 | 127/6929 | 0.008146 | 0.037205 | ENSG0000 | MMP13/IL1A | 4322/3552 | 3 | 3 | ENSG0000 | 0 | |
| DOID:1074 | kidney fail | Mar-23 | 128/6929 | 0.008324 | 0.037628 | ENSG0000 | MMP1/IL1A/ | 4312/3552 | 3 | 3 | ENSG0000 | 0 | |
| DOID:1055 | stomach c | Apr-23 | 252/6929 | 0.008765 | 0.039223 | ENSG0000 | MMP1/IL1A/ | 4312/3552 | 4 | 4 | ENSG0000 | 0 | |
| DOID:3480 | uveal disea | Feb-23 | 44/6929 | 0.009162 | 0.040586 | ENSG0000 | MMP1/ICAM | 4312/3383 | 2 | 2 | ENSG0000 | 0 | |
| DOID:8567 | Hodgkin's l | Feb-23 | 46/6929 | 0.009983 | 0.043788 | ENSG0000 | MMP9/ICAM | 4318/3383 | 2 | 2 | ENSG0000 | 0 | |
| DOID:0066 | musculosk | May-23 | 419/6929 | 0.010727 | 0.046588 | ENSG0000 | MMP1/MMP | 4312/4322 | 5 | 5 | ENSG0000 | 0 | |
| DOID:219 | colon canc | Apr-23 | 268/6929 | 0.010839 | 0.046618 | ENSG0000 | MMP13/MM | 4322/4318 | 4 | 3 | ENSG0000 | 1 | ENSG00000008516 |
| DOID:26 | pancreas c | Mar-23 | 142/6929 | 0.011053 | 0.04708 | ENSG0000 | MMP9/ICAM | 4318/3383 | 3 | 2 | ENSG0000 | 1 | ENSG00000175899 |
| DOID:438 | autoimmu | Feb-23 | 49/6929 | 0.011275 | 0.047571 | ENSG0000 | CACNA1S/Mf | 779/4318 | 2 | 2 | ENSG0000 | 0 | |
| DOID:9256 | colorectal | Apr-23 | 273/6929 | 0.011547 | 0.047993 | ENSG0000 | MMP13/MM | 4322/4318 | 4 | 3 | ENSG0000 | 1 | ENSG00000008516 |
| DOID:5672 | large intes | Apr-23 | 274/6929 | 0.011693 | 0.047993 | ENSG0000 | MMP13/MM | 4322/4318 | 4 | 3 | ENSG0000 | 1 | ENSG00000008516 |
| DOID:1116 | respiratory | Feb-23 | 50/6929 | 0.011721 | 0.047993 | ENSG0000 | PI3/MMP9 | 5266/4318 | 2 | 2 | ENSG0000 | 0 | |
| DOID:120 | female rep | May-23 | 429/6929 | 0.011812 | 0.047993 | ENSG0000 | MMP1/MMP | 4312/4322 | 5 | 5 | ENSG0000 | 0 | |
| DOID:1161 | polycystic | Mar-23 | 146/6929 | 0.011917 | 0.047993 | ENSG0000 | IL1A/MMP9/ | 3552/4318 | 3 | 2 | ENSG0000 | 1 | ENSG00000141448 |
| DOID:2377 | multiple sc | Mar-23 | 147/6929 | 0.012139 | 0.048447 | ENSG0000 | MMP9/ICAM | 4318/3383 | 3 | 2 | ENSG0000 | 1 | ENSG00000175899 |
| DOID:9970 | obesity | Apr-23 | 280/6929 | 0.012589 | 0.049541 | ENSG0000 | SAA1/IL1A/M | 6288/3552 | 4 | 4 | ENSG0000 | 0 | |
| DOID:1012 | corneal dis | Feb-23 | 52/6929 | 0.012637 | 0.049541 | ENSG0000 | MMP9/ICAM | 4318/3383 | 2 | 2 | ENSG0000 | 0 | |
| DOID:332 | amyotroph | Mar-23 | 150/6929 | 0.01282 | 0.049817 | ENSG0000 | CACNA1S/GA | 779/2554/ | 3 | 3 | ENSG0000 | 0 | |